University of Southampton

Faculty of Science

School of Ocean and Earth Science

High-resolution geochemical studies on the most recently-accumulated sapropel S1 in the eastern Mediterranean.

A thesis presented for the degree of Doctor of Philosophy

By

Domenico Carlo Mercone

Submitted: August 1999.

ABSTRACT

FACULTY OF SCIENCE
School of Ocean and Earth Science/Challenger Division for Seafloor Processes

DOCTOR OF PHILOSOPHY

High-resolution geochemical studies on the most recently-accumulated sapropel S1 in the eastern Mediterranean.

by
Domenico Carlo Mercone

The sediments of the eastern Mediterranean Sea contain Corg-rich layers, termed sapropels, interbedded with Corg-poor sediments which form by far the greater part of the sedimentary record. This research presents a high-resolution geochemical investigation on slowly- and rapidly-accumulated S1 units.

Mn, Fe, I and Se profiles in slowly-accumulated S1 units (5-10 $cm.kyr^{-1}$) have shown that these sapropels are affected by post-depositional oxidation following their formation which produces a much thinner sapropel than was originally deposited. In the slowly-accumulated examples investigated, up to 11.5 cm of the original sapropel has been lost through oxidation in as little as 6 kyr. Downward progression of the redox front causes the remobilisation and re-arrangement of redox-sensitive elements (As, Fe, I, Mn, Mo, Se, U and V) around the oxic/post-oxic boundary. Concentration-depth profiles of the redox-sensitive elements in S1 have shown that these elements are immobilised in oxic and post-oxic conditions or both. It is noted that I and Se form well-defined peaks at the top of S1, and it is suggested that these two elements may be reliable markers for defining the location of an active oxidation front in the absence of pore water measurements. During this research, it was discovered that Hg behaves similarly to I and Se at the oxic/post-oxic boundary, forming a well-defined peak in post-oxic conditions. In turbidite and sapropel examples, Hg is always closely associated with Se and it is suggested that Hg and Se become immobilised through the formation of the selenide mineral tiemannite (HgSe). The presence and persistence of Hg peaks in both recent and ancient sediments (up to 4 Ma) implies that Hg may be a useful diagnostic tool for defining the locations of both active and relict oxidation fronts.

Investigation of two rapidly-accumulated S1s from the Adriatic (MD 90-917) and Aegean Seas (LC21) has shown that these cores have suffered negligible post-depositional oxidation due to rapid accumulation rates. The validity of the Ba/Al ratio as a more reliable and persistent productivity index has been confirmed in both LC21 and MD 90-917 where Ba/Al is directly related to Corg content over the entire visual S1 units. In both cores S1 appears as a doublet. This doublet is centred on 7.5 kyr BP and geochemical and micropalaeontological evidence indicates that this "saddle" is best interpreted as an episode of improved reventilation and increased deep-water O_2 concentrations. A number of redox-sensitive elements are enriched (Cr, Mo, Ni, S, Se, U, V and Zn) in LC21 and MD 90-917, and exhibit double peaks in their concentration-depth profiles. The principal routes by which S1 develops high authigenic levels of redox-sensitive elements are: (i) pre-concentration in the water column by biological uptake followed by deposition at the sediment-water interface and/or (ii) diffusion from seawater through pore waters into sediments followed by reduction and immobilisation under more reducing conditions. Under more reducing conditions, redox-sensitive elements are immobilised through associations with Corg, pyrite, sulphides or form insoluble solid phases (e.g. U is precipitated and immobilised as $UO_{2(s)}$).

Palaeoproductivity estimates based on Ba/Al weight ratios indicate that productivity was up to 5 times higher during S1 formation compared with the present. It is suggested that high productivity was initiated by the formation of a deep chlorophyll maximum formed in response to an increased input of freshwater into the eastern Mediterranean. During S1 formation, the flux of Corg greatly exceeded the supply of dissolved O_2 to the bottom waters and so it is inferred that deposition of S1 occurred under anoxic conditions. Interpretations of geochemical parameters such as S/C criteria, I/Corg and V/(V+Ni) ratios and framboidal pyrite sizes all indicate that bottom waters were anoxic-non sulphidic rather than anoxic-sulphidic during S1 formation. The geochemical interpretation is in agreement with the benthic foraminiferal data, which show that the two S1 layers have an abundance of low-oxygen tolerant species. It is unclear whether anoxic conditions are induced by increased productivity alone or through a combination of increased productivity and reduction in deep-water formation. Evidence presented indicates that productivity and preservation are both necessary prerequisites for S1 deposition.

S1 initiation and cessation was investigated by AMS ^{14}C dating based upon the Ba/Al ratio criterion. AMS ^{14}C ages for slowly-accumulated sapropels indicate that S1 formation started at 10 kyr BP and ended by 5.3 kyr BP. For the rapidly-accumulated cores, the onset and termination of S1 is more variable although S1 was underway by 9.5kyr BP and complete by 6.0 kyr B.P. The offset in ages is attributed to bioturbation mixing artefacts affecting the Ba/Al signal in the slower-accumulated cores. Since rapidly-accumulated cores are not significantly affected by bioturbation, the best estimate for the duration of S1 is 9.5-6.0 kyr B.P.

Acknowledgements.

I would like to thank Drs. John Thomson (Challenger Division for Seafloor Processes) and Ian Croudace (School of Ocean and Earth Science) for their excellent supervision, guidance and support during my entire Ph.D; Darryl Green, Phil Warwick, Sharon Nixon and Cathy Ritchie are all thanked for showing me how to use all the wonderfully hi-tech instruments – you lot have the patience of saints. I would also like to thank Martine Paterne in Gif sur Yvette, France for providing me within additional sapropel material and data, and everyone aboard the R/V Urania who participated in the SAP-SINAPSI cruise to the eastern Mediterranean (Hilde, Caroline and Ivar). Thanks to Remi for keeping me sane whilst trying to squeeze pore waters in gale force winds, and also for being the only other person aboard ship who wasn't continually throwing up.

Thanks goes to all the post-grads at SOES especially, Danny, Julie, Barbs, Frank, Anneke, Gavin, Lawrence, Rachel C, Mikee and finally to Eta- for making life at the SOC bearable. I would also like to thank my housemates both past and present (Ali B, Deena, Lucy, Rich, Ali S, Andy, and Adam)- you all make me smile. I would like to make a special mention to Brian McG. - thank you for all of those 'quick pints' in the Dorchester Arms and providing a rather unique commentary on everyone we ever seem to meet. I will never tire of your stories about F.Y.E.O. Claire, your wild n' wicked ways and your revolving boyfriends is a constant source of amusement. Last, but by no means least, I would like to thank Craig Harris, an all round top-bloke and an exceptionally good friend.

Finally I would like to thank my family. Mum, Dad and sis- what can I say. Thank you so much for the love and support you have given me throughout my undergraduate and postgraduate studies. I owe you all more than you could ever possibly imagine.

Calvin and Hobbes ©, Homicidal Psycho Jungle Cat.
Bill Watterson (1994).

Declaration.

This study represents research conducted by myself. Some of the data presented, however (e.g. papers presented in chapters 1, 4 and 6), has resulted from collaboration with individuals within Southampton Oceanography Centre and from a number of European Universities. In all cases this has resulted in the publication in, or acceptance of papers in peer-reviewed journals. Where such collaboration has occurred, this clearly stated in the list of authors on the papers.

Contents.

Chapter 1:

Introduction.

1.1. Definition and general introduction to the nature of sapropels.

At present, extensive deep-water formation within the Adriatic and Aegean Seas ensures that the eastern Mediterranean is exceptionally well-ventilated and oxygenated to all depths (Schlitzer *et al.*, 1991, Roether *et al.*, 1996, and Malanotte-Rizzoli *et al.*, 1998). Furthermore, the anti-estuarine circulation of the eastern Mediterranean (i.e. inflow of freshwater at the surface and outflow of saline waters at depth) ensures that this basin is one of the most oligotrophic seas in the world (Bethoux, 1992). Recent estimates of primary productivity for the eastern Mediterranean have been placed between 12 – 26 gC m^{-2} yr^{-1}, significantly lower than for other open marine settings (Emeis *et al.*, 1995). A consequence of this unproductive and exceptionally well-ventilated eastern Mediterranean water column is that only 0.2% of the annual primary productivity (i.e. 0.033-0.037 gC m^{-2} yr^{-1}) actually survives oxic remineralisation to be deposited in the underlying sediments (Van Santvoort *pers comm.*). As a result, reported Corg concentrations for recently accumulated sediments of the eastern Mediterranean are exceptionally low, with concentrations typically in the range of 0.2-0.3 wt % (Van Santvoort *et al.*, 1996; 1997).

Extensive deep-sea coring during the 1947-1948 Swedish expedition of the Mediterranean (Kullenberg, 1952) and again during Leg 42A of the Deep Sea Drilling Project (DSDP) in 1977 (Kidd *et al.*, 1978), revealed the existence of discrete, centimetre-to-decimetre thick units with organic carbon concentrations from 2 - 20% (Calvert, 1983). The presence of organic-rich sediments, termed sapropels by Kidd *et al.* (1978), indicated that significant changes in either the circulation and/or primary productivity had periodically occurred in the eastern Mediterranean during the Late Quaternary (Bradley, 1938; Olausson, 1961; De Lange and Ten Haven, 1983; Calvert, 1983; Pedersen and Calvert, 1990 and Castradori, 1993).

Since their initial discovery in the late 1940s, up to 12 individual sapropel units have been recovered from the Holocene and Pliocene (Cita *et al.*, 1977). According to Kidd *et al.* (1978), sapropels are defined as "... discrete organic rich sediments greater than 1cm in thickness and having an organic carbon content greater than 2% by weight..." Sediments which contain 0.5-2% organic carbon and are >1cm in thickness are defined as being *sapropelic* (Kidd *et al.*, 1978). Over the past five decades, sapropels have been studied extensively in terms of their micropaleontology

(both benthic and planktonic foraminifera), sedimentology, timing and geochemistry. A number of general characteristics of sapropels can be described:

1) Sapropel S1 displays a significantly higher concentration of organic carbon in comparison to the intercalated pelagic sediments of the eastern Mediterranean (Calvert, 1983). This indicates that significant changes in either the bottom water oxygen (preservation) or productivity has occurred during the past 10,000 years.

2) Sapropel unit S1 contains an unusually high abundance of the low salinity planktonic foraminiferal species *Neoglobquadrina dutertrei* (Rohling, 1994) and either contain low O_2 tolerant benthic formainferas such as *Bolivinid* and *Rotaliid* species (Vismara-Schilling and Coulbourn, 1991) or are completely azoic (Jorissen, 1999).

3) S1 contains an abundance of planktonic foraminifera which show a marked depletion in the $\delta^{18}O$ isotope, indicating either reduced salinity or an increase in surface water temperature (Cita *et al.*, 1977; Vergnaud-Grazzini *et al.*, 1977; Tang and Stott, 1993; Aksu *et al.*, 1995).

4) The most recent sapropel, S1, displays elevated barium concentrations in a quasi-Gaussian distribution around the organic rich layer, indicating increased primary productivity (Thomson *et al.*, 1995; Van Santvoort *et al.*, 1996). Enhanced $\delta^{15}N$ isotope ratios from planktonic foraminifera also indicate significant productivity increases during sapropel formation (Calvert *et al.*, 1992).

5) The presence of sapropels are found to correlate with variations in the Earth's orbital parameters, particularly the eccentricity maximum (Rossignol- Strick *et al.*, 1982; Rossignol-Strick, 1985; Prell and Kutzbach, 1987).

6) Recent findings by Rohling *et al.* (1997) suggest that S1 formation was not continuous, but was interrupted for a period of 200 years.

All of the studies on sapropel units over the past 50 years have tried to describe the occurrence of these organic-rich sediments in terms of anoxia (Olausson, 1961; Cita *et al.*, 1977; Vergnaud-Grazzini *et al.*, 1977; Vergnaud-Grazzini *et al.*, 1985) or productivity (Calvert, 1983; Higgs *et al.*, 1994; Thomson *et al.*, 1995; Van Santvoort *et al.*, 1996), although more recently a number of authors (Sarmiento *et al.*, 1988; Rohling and Giesekes, 1989; Rohling, 1991ab; Rohling and Hilgen, 1991) have invoked a combination of both anoxia and productivity to explain sapropel

formation. The productivity *vs* anoxia debate is not only important for explaining sapropel formation but is also important for explaining the occurrence of other organic-rich sediments such as black shales, oil/petroleum source rocks, and ocean anoxic events (Wignall, 1994). An examination of the evidence for the anoxia and productivity hypotheses explaining sapropel formation is presented below.

1.2. Mechanisms proposed to explain sapropel formation.

1.2.1. The Anoxia Mechanism.

The discovery of sapropel units in 1947-1948 (Kullenberg, 1952), confirmed the hypothesis by Bradley (1938) that changes in Mediterranean circulation had induced severely-reducing conditions and had caused the deposition of reducing (organic-rich) sediments. Subsequent work on sapropel units, in terms of their sedimentology, micropalaeontology and geochemistry have also indicated that anoxia may have been a cause for sapropel formation.

Woolnough (1937) was amongst the first to suggest that organic carbon remineralisation under anoxic conditions was less efficient (when compared to oxic conditions), and so reasoned that anoxic environments preferentially aided the preservation of organic carbon in marine sediments. According to the anoxia mechanism, sapropels are formed in the eastern Mediterranean during stagnation episodes which are induced by excessive freshwater influxes (Olausson, 1961). The influx of freshwater was, according to a number of authors (Cita *et al.*, 1977; Vergnaud-Grazzini *et al.*, 1977; Vergnaud-Grazzini, 1985), sufficient to cause a permanent halo/pycnocline within the eastern Mediterranean, which inhibited deep water formation, leading to anoxia within the bottom waters (figure 1.1).

The anoxia mechanism for describing sapropel formation has received much support over the last 50 years (Cita and Grignani, 1982; Tang and Stott, 1993; Aksu *et al.*, 1995). Evidence to support it has come from a number of modern-day anoxic marine settings (e.g. the Black Sea, Cariaco Trench, oxygen minimum zones (OMZ)). Areas such as these are commonly cited as being modern analogues for explaining sapropel formation, since they all have low surface water productivities (like the modern day Mediterranean) but all display the preferential accumulation of Corg within their anoxic waters (Murray, 1991).

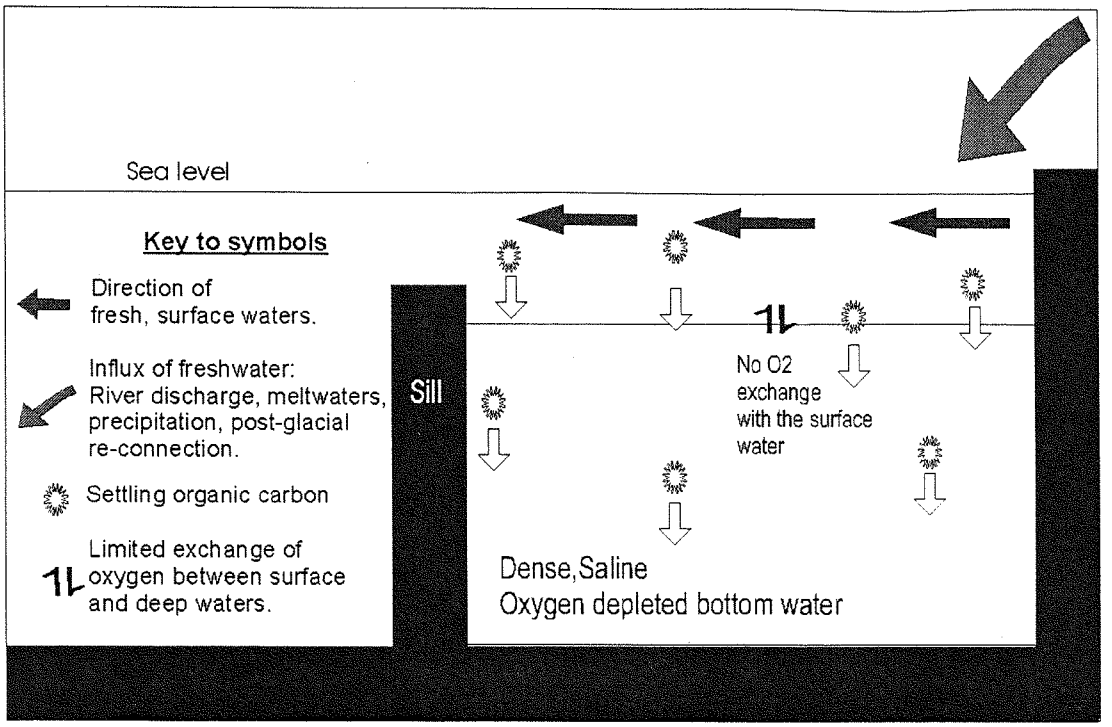

Figure 1.1: A schematic diagram of the anoxia mechanism for explaining sapropel formation. Input of freshwater from a number of sources causes stratification and isolation of bottom waters. Figure adapted from Emeis *et al.* (1995).

In the Black Sea for instance, work by Shimkus and Trimonis (1974) showed that although relatively unproductive, sediments that are accumulating beneath the oxic/anoxic interface at 75m have organic carbon values of up to 10% by weight. This value is approximately 4-5 times greater than the Corg content of Black Sea sediments that are being deposited within the oxic portion of the water column. Furthermore, work by Paropkari *et al.* (1992,1993) have shown that the highest Corg content of Arabian Sea sediments are those which are within the OMZ (150-1200m) and which have the lowest surface water productivities. Paropkari *et al.* (1993) suggest from this study that it is anoxia rather than productivity which controls the accumulation and preservation of organic-rich marine sediments. On the basis of such modern day analogues, proponents of the anoxia mechanism for sapropel formation claim that anoxia, rather than productivity, is the dominant mechanism controlling the formation and deposition of Corg rich sediments in the eastern Mediterranean (Rossignol-Strick *et al.*, 1982; Thunell *et al.*, 1983).

1.2.2. The possible cause(s) of anoxia in the eastern Mediterranean.

The anoxia mechanism for explaining sapropel formation was first proposed by Olausson (1961) who suggested that these deposits were formed during the periodic stagnation of the eastern Mediterranean as a result of an excess influx of freshwater. The source of this excess freshwater, however, has long been debated (Castradori, 1993; Rohling, 1994). Some authors suggest that it is derived from:-

(1) increased rainfall within the eastern Mediterranean region (Kullenberg, 1952; Fairbridge, 1972).

(2) an influx of excess freshwater from glacial meltwater input (Ryan 1972; Thunell *et al.*, 1977; Thunell and Williams, 1983).

(3) an increased inflow of less-saline Atlantic waters associated with sea-level rise (Muller, 1973; Vergnaud-Grazzini *et al.*, 1988).

Investigations on sapropel units over the past two decades, however, have concentrated on two principal source(s) of excess freshwater input. These are:-

(1) a spill-over of freshwater from the Black Sea in response to its reconnection with the eastern Mediterranean following post-glacial sea-level rise (Ryan, 1972; Thunell *et al.*, 1983; Lane-Serff *et al.*, 1997), and/or

(2) an increased freshwater inflow form the Nile river due to intensified African monsoonal activity over equatorial Africa (Street and Grove, 1979; Rossignol-Strick *et al.*, 1982; Rossignol-Strick, 1985, 1987; Howell and Thunell, 1992).

1.2.2.1. Freshwater input from the Black Sea.

The near coincidence of the deposition of the most recent sapropel S1, and the re-establishment of the Black and eastern Mediterranean Seas through the Bosporous Strait led Olausson (1961) to propose that excess freshwater from the Black Sea was responsible for initiating stagnation and sapropel deposition within the eastern Mediterranean. Recent dating of the onset of the most recent sapropel (S1) by Fontugne *et al.* (1994) and Thomson *et al.* (1995) has placed the start of sapropel formation at *ca.* 8.9 kyr BP. Work by Fairbanks (1989), however, has shown that the re-connection

between the Black and eastern Mediterranean Seas, occurred some 1200 years earlier at ~9900 yrs BP, so casting doubt as to the importance of freshwater input from the Black Sea. A hydraulic model of the Black Sea connection presented by Lane-Serff *et al.* (1997) demonstrated that there exists a 1200-1500 year time lag between the reconnection of the two seas and the onset of an influx of freshwater into the eastern Mediterranean. This model would then explain the time-lag between reconnection through the Bosporus at 9900 yr BP and the onset of S1 deposition in the eastern Mediterranean at ca 8700 yr BP (Lane-Serff *et al.,* 1997). These authors suggest that only after sea-level had risen to +10m above the sill freshwater displaced over from the Black Sea into the eastern Mediterranean, inhibiting deep-water formation and promoting deposition of sapropel S1 (Lane-Serff *et al.,* 1997). Estimates by Lane-Serff *et al.* (1997) demonstrate that the entire freshwater inventory of the Black Sea was drained in approximately 2500-3500 years. This modelled time span fits with the generally accepted chronology, that sapropel formation ended at around 6400 yr BP (Fontugne *et al.,* 1994), although some estimates by Higgs *et al.* (1994) and Thomson *et al.* (1995) place the end of S1 formation as late as 5300yrs BP.

1.2.2.2. Climatically-induced fluvial freshwater inputs.

The other dominant source of freshwater which has been invoked to produce anoxia in the eastern Mediterranean has been identified as coming from an enhanced freshwater input from the Nile river, following intensified monsoonal activity over equatorial Africa. Recently, correlations between variations in the Earth's orbital parameters (specifically the eccentricity maxima related to precession and insolation) and sapropel formation have been identified by Rossignol-Strick *et al.* (1982); Rossignol-Strick, (1983), Rossignol-Strick, (1985); Prell and Kutzbach, (1987); and Hilgen, (1991). These authors have shown that sapropel formation coincides with the minimum in the precessional cycle (which has a periodicity of ~21,000 years), with the last precessional minimum occurring at around 10,000 ^{14}C years BP (figure 1.2a,b).

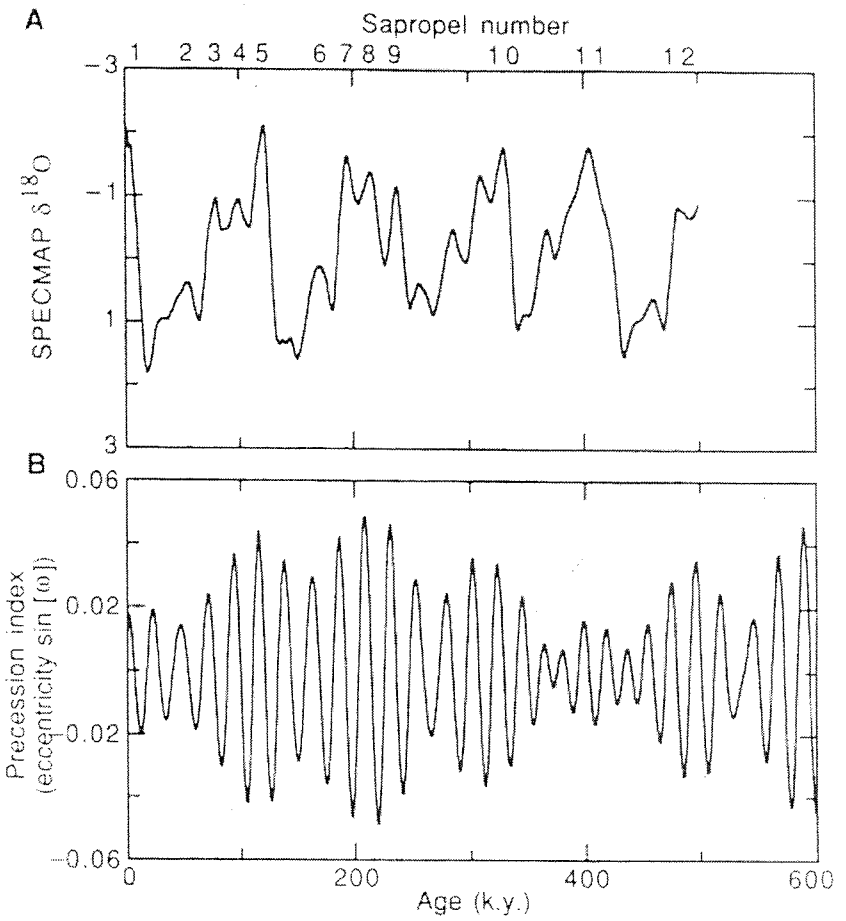

Figure 1.2. The correlation between sapropel occurrences (1.2a) and variations in the Earth's precession index (1.2b) during the last 600,000 years. Figure from Emeis *et al.* (1995).

At present, monsoon activity over equatorial Africa is driven by thermal gradients between the landmass and the surrounding ocean (Prell and Kutzbach, 1987). Owing to the large specific heat capacity of water, summer heating produces a greater temperature increase of the continent relative to the surrounding ocean. The strong heating of the atmosphere over the African continent produces ascending motion which causes an inflow of cool, moist air from the surrounding ocean. This inflow causes large-scale convergence of the surface winds over Africa, resulting in heavy precipitation (i.e. a monsoon).

Modelling of the Earth's climate at 9 kyr BP by Kutzbach and Guetter (1986ab); Prell and Kutzbach (1987); Kutzbach and Liu (1997) has demonstrated why sapropel occurrences coincide with the maximum in insolation. According to Kutzbach and Guetter (1986ab) Prell and Kutzbach (1987), and Kutzbach and Gallimore (1988), variations at 9 kyr BP in the Earth's orbital parameters were significantly different compared to the present day. For example, at 9 kyr BP, the

axial tilt of the Earth was 24.24°, (modern value is 23.44°), and perihelion occurred during Northern Hemisphere summer, whilst at present it occurs during the Northern Hemisphere winter (Street-Perrott and Perrott, 1993 figure 1.3.)

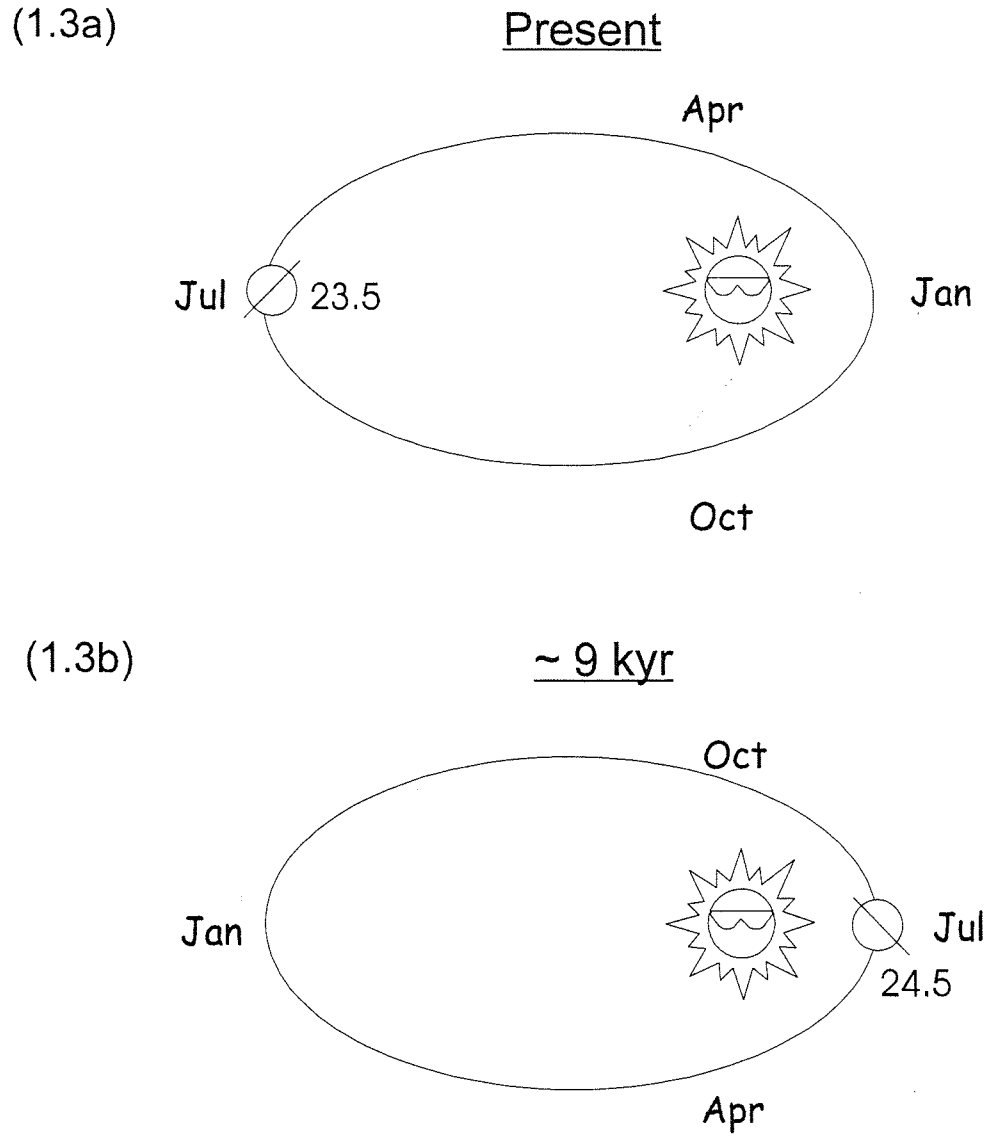

Figure 1.3. Earth-Sun geometry for 9ka and the present. During sapropel formation (fig.1.3b) perihelion occurs during July in the Northern Hemisphere whilst at present (fig. 1.3a) it occurs during the Northern Hemisphere winter. The resultant effect is an increase in insolation at 9ka and formation of S1 (as explained in text). The tilt of the earth during sapropel formation (~24.5°) is also greater than at present (~23.5°). Adapted from Kutzbach and Webb (1993) in 'Global climates since the last Glacial Maximum'.

According to Kutzbach and Guetter (1986ab), these changes in the Earth's orbital parameters had a dramatic effect upon the amount of solar radiation reaching the surface of the Earth. Modelling of the climate at 9000 years BP using the NCAR CCM model by Kutzbach and Guetter (1986) has demonstrated that, at the height of maximum insolation, the net radiation received over the African

continent was increased by 7%, corresponding to a temperature increase of 2-3°C. According to Street-Perrott *et al.* (1990), this led to a steepening of the thermal contrast between the land and ocean, resulting in an enhanced inflow of moist air from the surrounding ocean. In essence, during sapropel formation, orbital parameters were such that they only served to intensify the normal monsoon season experienced over equatorial Africa. The net result of intensified monsoonal activity was enhanced precipitation over Africa in a belt from 0-30 °N, and according to Kutzbach and Street-Perrott (1985), the mean annual precipitation increased by 236mm. This excess precipitation was drained via the Nile and its tributaries into the eastern Mediterranean, inducing stratification, anoxia and sapropel formation (Rossignol-Strick *et al.*, 1982; Rossignol-Strick, 1985; 1987).

Independent evidence in support of intensified monsoon activity during the Holocene over Africa has come from a number of geochemical, palaeolake level and biostratigraphic lines of evidence (Ritchie *et al.*, 1985; Finney and Johnson, 1991; Gasse *et al.*, 1994). For example, severely-depleted $\delta^{18}O$ isotopes from gastropods in north-central Sudan indicate that from 10,000 years BP this region of Africa had significantly less evaporation, whilst the extreme variability of the oxygen isotopes (up to 6-7 ppt PDB) in gastropod shells is consistent with the hypothesis that enhanced precipitation was seasonally controlled (Ayliffe *et al.*, 1996). Furthermore, compositional variations of terrigenous elements exemplified by ratios of Zr, Ti, K, Rb and Al reveal that an intensified freshwater discharge from the Zaire River occurred during the maximum in Northern hemisphere insolation 9500yr BP (Schneider *et al.*, 1997).

1.2.2.3. Enhanced precipitation over the eastern Mediterranean borderlands.

A review on the climate at the time of sapropel formation by Rohling and Hilgen, (1991) proposes that, during sapropel formation the climate over the northeastern Mediterranean borderlands (NBEM) was characterised by heavy precipitation induced by a low in atmospheric pressure. Rohling and Hilgen (1991) stipulated that excess freshwater from precipitation in the eastern Mediterranean was, in combination with excess water discharge from the Nile, responsible for inducing water column stratification and sapropel formation. Recently, Kallel *et al.* (1997) examined the oxygen isotope composition of two planktonic foraminifera species (*G.ruber* and *G.bulloides)* in 47 deep-sea cores from the eastern and western Mediterranean and found that not only was sea surface salinity reduced during S1 formation, but also it was homogenous throughout the entire basin. These authors indicated that the homogenous surface water salinities throughout the eastern Mediterranean could only have been caused by precipitation over the northern and eastern borderlands of the Mediterranean. Evidence to suggest that an increase in precipitation over

the borderlands of the Mediterranean has come from a number of sources. For example, Shaw and Evans (1984) and Cramp *et al.* (1988) demonstrated increased discharges from both Greek and Turkish rivers during S1 formation, whilst examination of the fluorescent rings of corals showed that exceptionally wet conditions prevailed at 9kyr BP in the Sinai Desert region (Klein *et al.*, 1990). Moreover, examination of the $\delta^{18}O$ isotopes from speleothems from Israel indicate enhanced rainfall from 10,000 to 7,000 years BP (Bar-Matthews *et al.*, 1997). Estimates by Bar-Matthews *et al.* (1997) indicate that the annual precipitation was ~1000 mm, almost double that of the modern-day value for this region.

Evidence from the eastern Mediterranean to suggest that a low-salinity surface water layer was present during sapropel formation has come from studies of planktonic and benthic foraminiferal, and sedimentological examinations. Cita *et al.* (1977); Vergnaud-Grazzini *et al.* (1977); Williams *et al.* (1978); Cita and Grignani (1982); Thunell *et al.* (1983); Thunell *et al.* (1984); Vergnaud-Grazzini, (1985); Thunell *et al.* (1987), Thunell and Williams, (1989); Tang and Stott, (1993), and Aksu *et al.* (1995) have all shown that all planktonic foraminifera from S1 display isotopically light $\delta\ ^{18}O$ signatures. This oxygen isotope excursion indicates that a low salinity surface layer was present during sapropel formation, although it does not discriminate the source of this freshwater. Isotopic examination of specific species of planktonic foraminifera by Tang and Stott (1993) indicated that this low salinity layer was highly seasonal and was only persistent throughout certain periods of the year (January-March). The presence of a low salinity surface water cap during January-March coincides with the times when winter cooling produces deep- and intermediate water formation within the eastern Mediterranean (Robinson *et al.*, 1991; Malanotte-Rizzoli and Hecht, 1988). From this it could be inferred that the low salinity layer could have induced stagnation of the bottom waters by inhibiting both deep and intermediate water formation.

Benthic foraminiferal successions in and around S1 demonstrate changes in water deep-water oxygen concentrations prior to sapropel formation. Jorissen (1999) found that the *Bolivina spathulata dilatlatissima* and *Bulimina costata* species of the pre-sapropel sediments were gradually replaced by deep infaunal taxa such as *Chilostomella spp* at the onset of sapropel formation, indicating a gradual transition from oxic to anoxic conditions within the water column. Furthermore, the absence of benthic foraminifera within S1 from shallow localities or the presence of low-oxygen tolerant *bolivinid* species in S1 from deeper sites, indicates that severely depleted oxygen conditions were present within the eastern Mediterranean during S1 (Vismara-Shilling and Coulbourn, 1991; Jorissen, 1999). It must be noted, however, that the presence of these low-O_2 tolerant species does not necessarily indicate that water column stratification was the cause of bottom water anoxia.

Interpretations of sedimentary sequences leading to sapropel development fit well with the interpretations derived from benthic foraminiferal successions. According to Stanley and Maldonado (1979) and Murat and Got (1987) typical sapropel sediment sequences from the eastern Mediterranean show the gradual transition from normal pelagic beige oozes to the grey/green colour of the protosapropel, passing up into the black/ dark grey of the sapropel proper and capped by an orange/red oxidised layer. The gradual transition in colour sequence from beige-green-grey-black indicates, according to Murat and Got (1987), the gradual depletion of oxygen within the bottom waters as a result of water column stagnation. Interpretations of the sediment sequence associated with sapropel formation has received much attention over the past two decades (Stanley and Maldonado, 1979; Anastakasis and Stanley, 1984; Murat and Got (1987) although often the interpretations have been independent of available geochemical data. For example, it has been observed that a grey region often underlies the sapropel proper (termed a protosapropel), and this layer has often been interpreted to mark the onset of oxygen depletion within the bottom waters and an increase in organic matter preservation (Murat and Got, 1987; Troelstra *et al.,* 1991). Geochemical interpretations of this 'protosapropel' by Passier *et al.* (1996), however, indicate it to be a diagenetic effect caused by the pyritisation of the sediment as downwards-diffusing HS^- and upwards-diffusing Fe^{2+} react beneath the sapropel to form pyrite. Whilst the interface at the base of the sapropel unit is transitional and not always clearly defined, the interface between the top of the sapropel and overlying sediment is exceptionally well marked. Previous suggestions by Murat and Got (1987) indicate that the transition from the sapropel to the overlying oxidised sediment indicated an almost instantaneous return of oxygen to the deep water following sapropel formation. The interpretation of the sediment sequence by Murat and Got (1987), however, does not readily explain why there was such a rapid return of oxygen to the deep water following sapropel formation, whilst the onset of sapropel formation was marked by a gradual depletion of oxygen in the bottom waters. Recent geochemical work by Higgs *et al.* (1994) and Thomson *et al.* (1995) suggests an alternative interpretation of the sharp upper contact between the sapropel and overlying sediment. According to Higgs *et al.* (1994) and Thomson *et al.* (1995), the upper contact represents the removal of the upper face of the sapropel unit by post-depositional oxidation from a downward-moving oxidation front following reventilation of the eastern Mediterranean below the depth of active bioturbation. It is probable that there was a similar (reverse) gradual transition in the sedimentary colour sequence following sapropel formation, however, post-depositional oxidation has effectively removed this upper sequence from the sedimentary record.

1.2.3. The Productivity Mechanism.

Recently, the anoxia mechanism proposed for the deposition of Corg-rich sediments has been challenged. In an extensive study on the formation of organic carbon rich sediments, Pedersen and Calvert (1990) found no evidence for the enhanced preservation of organic carbon in sediments that were underlying anoxic water columns. Calvert *et al.* (1987) and Pedersen and Calvert (1990) found that within anoxic settings such as Saanich Inlet and the Black Sea, the amount of organic carbon that was accumulating was comparable with the average Corg content accumulating within oxic environments such as Jervis Inlet. Moreover, Sarnthein *et al.* (1982) found that anoxia played a relatively unimportant role in the accumulation of organic rich sediments. In his study, Sarnthein *et al.* (1982) examined the Corg content of sediments from the northwest African slope, and found that organic-rich sediments were being deposited in a water depth from 1000-2000m, well below the OMZ situated at 400m. From this study they concluded that factors other than anoxia were important for accumulating Corg-rich sediments, and postulated that the supply of organic matter (productivity) was an important controlling mechanism. Experimental rate measurements using planktonic materials and radio-labelled organic tracers have recently demonstrated that anaerobic decomposition of organic matter in sediments occurs at rates which are comparable with, or even faster than, aerobic decomposition, implying that anoxic conditions do not directly enhance organic matter preservation in sediments (Westrich and Berner 1984; Heinrichs and Doyle 1986; Lee, 1992; Sun *et al.*, 1993). As a result, Calvert (1983) and Ten Haven and De Lange (1983) proposed that one of the fundamental controls on the accumulation of organic carbon in marine sediments, especially sapropels, was the amount of productivity in surface waters rather than the amount of dissolved oxygen.

Productivity as a mechanism for causing sapropel formation has been proposed by a number of authors (Schrader and Matherne, 1981; Thunell and Williams, 1982; Ten Haven *et al.*, 1991; Thomson *et al.*, 1995; Thomson *et al.*, 1999), who suggest that an increase in productivity within the eastern Mediterranean was sufficient to cause the formation of sapropel units. It must be noted that whilst these authors propose that productivity was the main cause of sapropel formation, they do not preclude anoxia development within the bottom waters. Within the productivity model, anoxia is merely a symptom of an exceedingly high oxygen demand as a result of high primary productivity levels. Evidence to suggest that productivity was increased during sapropel formation has come from a number of sources. For example Calvert *et al.* (1992) examined the nitrogen isotope ratio ($^{15}N/^{14}N$) of sedimentary organic matter from S1 in core collected from near the mouth of the Nile. They found that the sedimentary nitrogen ratios were isotopically lighter than the intercalated marl oozes, indicating that during S1 formation a greater fixation of nitrogen had occurred, and implying that greater primary productivity was present within the surface waters. The

results of Calvert *et al.* (1992) fit well with the study of Cd/Ca ratios in the foraminifera *G.ruber* by Boyle and Lea (1989), who found that Cd/Ca ratios were five-times higher both within and at the base of S1 than the intercalated pelagic sediments. From this study, Boyle and Lea (1989) concluded that increased nutrients within the surface water had existed during sapropel formation. Geochemical evidence from De Lange and Ten Haven (1983), Higgs *et al.* (1994), Thomson *et al.* (1995); and Van Santvoort *et al.* (1996), has shown elevated barium concentrations around S1. It is well known that a good correlation exists between the amounts of Corg and Ba present in sediments (Calvert, 1983; Calvert and Fontugne, 1988; Klinkhammer and Lambert, 1989) and also in sediment trap material (Dymond *et al.*, 1992). It was hypothesised by Dymond *et al.* (1992); Higgs *et al.* (1994); Thomson *et al.* (1995); Van Santvoort *et al.* (1996) that sedimentary barium concentration could be used as a palaeoproductivity proxy for estimating the waxing and waning of productivity during sapropel formation. The elevated barium concentrations in and above S1 led these authors to suggest that productivity had been significantly enhanced during sapropel formation. More recently, biological markers have helped to elucidate the origins of the organic matter from eastern Mediterranean sapropels (Bouloubassi *et al.*, 1998). According to Bouloubassi *et al.* (1998), extractable lipids such as alkandiols, alkanolones, alkenones and sterols dominate the organic matter of sapropels. The molecular composition of the organic matter implies that the origin of the organic matter was predominantly derived from marine algal sources, indicating that enhanced productivity had occurred during sapropel formation (Bouloubassi *et al.*, 1998). Organic geochemical data presented by Sutherland et al., (1984) for S1 from the Hellenic Outer Ridge, revealed $\delta^{13}C$ values in the range –18.5 ppt to –21.6 ppt, also indicative of a marine origin for the organic matter.

1.2.4. The Mixed Model Mechanism.

Recently, there has been strong evidence in support of both anoxia and productivity mechanisms, as discussed in sections 1.2.1 and 1.2.2. A number of authors (Sarmiento *et al.*, 1988; Rohling and Giesekes, 1989; Rohling, 1991ab; Rohling and Hilgen, 1991 and Kallel *et al.* 1997) have tried to combine the evidence to explain the formation of sapropels in a mixed model approach.

The first approach was proposed by Sarmiento *et al.* (1988), who explained the formation of sapropels in terms of a circulation reversal. In this study, Sarmiento *et al.* (1988) proposed that the influx of freshwater was sufficient to induce a circulation reversal within the eastern Mediterranean, with inflow at depth and outflow at the surface, i.e. an estuarine, nutrient trap circulation. At present, the eastern Mediterranean has a circulation pattern that is anti-estuarine and

as a result acts as a nutrient desert since nutrients are not returned to the surface because of a strong halo/pycnocline (figure 1.4).

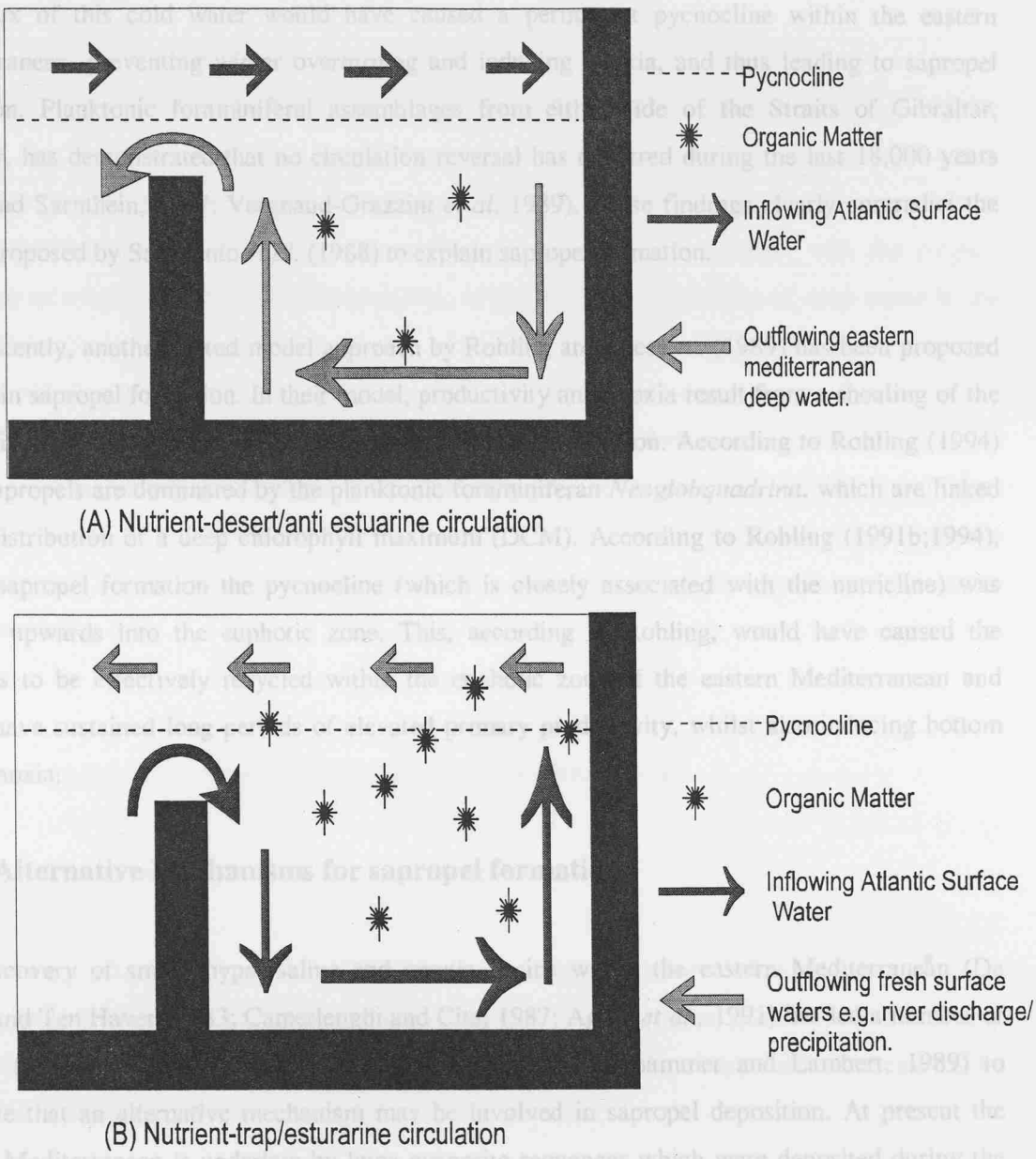

Figure 1.4. Schematic representations of (A) nutrient desert (present day) and (B) nutrient trap (proposed mechanism during sapropel formation) scenarios for the eastern Mediterranean. Figure adapted from Emeis *et al.* (1995).

Sarmiento *et al.* (1988) proposed that a circulation reversal could cause the eastern Mediterranean to become a nutrient trap, thereby inducing high levels of primary productivity. In this scenario, nutrients are continually recycled between the surface and deep waters. As a result this leads to high productivity and also bottom water anoxia which would explain both available proposals for sapropel formation. Moreover, data from Kallel *et al.* (1997) have shown that the influx of

freshwater from excess precipitation over the borderlands of the eastern Mediterranean was sufficient to cause the influx of cold intermediate water from the western Mediterranean (i.e. subsurface inflow which is equivalent to a circulation reversal). Kallel *et al.* (1997) reasoned that the influx of this cold water would have caused a permanent pycnocline within the eastern Mediterranean, preventing winter overturning and inducing anoxia, and thus leading to sapropel formation. Planktonic foraminiferal assemblages from either side of the Straits of Gibraltar, however, has demonstrated that no circulation reversal has occurred during the last 18,000 years (Zahn and Sarnthein, 1987; Vergnaud-Grazzini *et al.* 1989). These findings clearly contradict the model proposed by Sarmiento *et al.* (1988) to explain sapropel formation.

More recently, another mixed model approach by Rohling and Giesekes (1989) has been proposed to explain sapropel formation. In their model, productivity and anoxia result from a shoaling of the pycnocline into the euphotic zone at the time of sapropel formation. According to Rohling (1994) many sapropels are dominated by the planktonic foraminiferan *Neoglobquadrina*, which are linked to the distribution of a deep chlorophyll maximum (DCM). According to Rohling (1991b;1994), during sapropel formation the pycnocline (which is closely associated with the nutricline) was shoaled upwards into the euphotic zone. This, according to Rohling, would have caused the nutrients to be effectively recycled within the euphotic zone of the eastern Mediterranean and would have sustained long periods of elevated primary productivity, whilst also inducing bottom water anoxia.

1.2.5. Alternative Mechanisms for sapropel formation.

The discovery of small, hypersaline and anoxic basins within the eastern Mediterranean (De Lange and Ten Haven, 1983; Camerlenghi and Cita, 1987; Aghib *et al.*, 1991) has led a number of authors (Van Santvoort, 1996, De Lange *et al.*, 1990; Klinkhammer and Lambert, 1989) to postulate that an alternative mechanism may be involved in sapropel deposition. At present the eastern Mediterranean is underlain by huge evaporite sequences which were deposited during the Messinian Salinity Crisis (De Lange *et al.*, 1990). According to Klinkhammer and Lambert (1989), De Lange *et al.* (1990), and Van Santvoort *et al.* (1996); the possibility exists that exposure of these salt deposits within the eastern Mediterranean could (in combination with other factors) help to induce or intensify water column stability. Although work by Van Santvoort *et al.* (1996) and De Lange, (1990) has shown that the chloride flux from the Messinian deposits to the eastern Mediterranean is small relative to the input of chloride produced via evaporation, these authors suggest that, if for any reason the thermohaline circulation was reduced, then the flux of chloride from the salt deposits would be sufficient to increase the stability of the bottom waters by

increasing its salinity. According to De Lange *et al.* (1990), the dissolution of salt deposits could easily produce bottom waters with a salinity of 380 ppt as evidenced in the Bannock and Tyro Basins of the present-day eastern Mediterranean.

Whilst a very good correlation is observed between sapropel occurrence and the precessional cycle, it has been inferred from recent hydrographic surveys of the eastern Mediterranean that no drastic input of freshwater is needed to bring about major circulation changes within the eastern Mediterranean. For example, major changes in the source area of Eastern Mediterranean Deep Water (EMDW) are currently being observed in the eastern Mediterranean, with the Aegean becoming as important, (if not more important), as the Adriatic as a source of deep-water in the 1990s (Della Vedova *et al.*, 1995; Roether *et al.*, 1996). The effect of this has been to cause an uplift of old deep waters and to produce newer, more oxygen-rich deep waters (Roether *et al.*, 1996). These changes are induced within the modern day eastern Mediterranean without any major changes in either the freshwater input of the Mediterranean or the prevailing climatic conditions. This would therefore imply that the mechanisms proposed for sapropel formation may not require drastic changes in the freshwater input (e.g. Nile discharge, Black Sea spill over) to cause stagnation and anoxia.

1.3. Geology and bathymetry of the eastern Mediterranean.

1.3.1. Geological evolution of the eastern Mediterranean.

The geological history and evolution of the eastern Mediterranean, (here defined as being the body of water lying to the east of the Strait of Sicily), is exceptionally complex (Kennett, 1982) and only a brief discussion of the major points concerning the formation of the eastern Mediterranean will be addressed. Robertson (1998) presents a comprehensive review.

Interpretations regarding the origin of the eastern Mediterranean have stressed the importance of the interactions between the African and Eurasian continental plates (Hsu, 1977). What has become apparent over the last four decades is that the eastern Mediterranean is a complex area of collisional tectonics driven by the slow convergence of Africa and Europe (Fusi and Kenyon, 1996). There are three main explanations for the formation and evolution of the eastern Mediterranean, namely:

(1) the present-day Mediterranean is a remnant of the ancient Tethys Sea.

(2) the modern-day Mediterranean is a geologically new formation, created following the climax of the Paleogene Alpine folding event.

(3) the Mediterranean is a combination of both relic Tethys and neo-Tethys Seas (Hsu, 1977).

Recent drilling of the eastern Mediterranean during Leg 160 of the Ocean Drilling Program (ODP), confirmed the hypothesis that the modern eastern Mediterranean is a composite tectonic unit, combining a relic Tethys Sea with later basinal development associated with a neo-Tethys (Robertson, 1998). Seismic refraction (Woodside, 1977) and lithostratigraphic studies of ophiolites from northern Cyprus and Turkey (Robertson and Woodcock, 1979) indicate that the oceanic crust beneath the eastern Mediterranean is predominately of Mesozoic age, whilst the ophiolites represent the remnants of an emplaced southerly neo-Tethyian ocean basin (Robertson, 1998).

Hsu (1977) has carried out a synthesis of the tectonic evolution of the eastern Mediterranean. It is generally believed that the evolution of the modern-day eastern Mediterranean was associated with the formation and opening of the Atlantic Ocean (Kennett, 1982). During the early Jurassic, Pangea was split into northern and southern continents separated by the Tethys Sea. During this period, three micro-continents developed between Europe and Africa, namely the Alboran, the Italo-Dinaride and Bulgarian plates (Hsu, 1977). During the Jurassic and early Cretaceous, opening of the central Atlantic between North America and Africa resulted in an eastward movement of Africa relative to Europe. As the African plate moved eastwards during the late Jurassic, the three micro-continents separated from the African plate and moved northwards trapping the ancient Tethys (Kennett, 1982). During the second phase of rifting in the late Cretaceous to early Cenozoic, the north Atlantic opened up between North America and Europe faster than between North America and Africa. As a result, with respect to Europe, Africa had a predominantly westward motion. During the final phase of eastern Mediterranean evolution, it is believed that there was a northwards movement of the African plate towards the Eurasian plate, further compressing and restricting the eastern Mediterranean into its current configuration (Hsu, 1977; Kennett, 1982). The arcuate Mediterranean Ridge present throughout the entire eastern Mediterranean represents the subduction/compression of the African and Eurasian plates.

1.3.2. Bathymetry of the eastern Mediterranean.

The eastern Mediterranean is defined geographically as that part which lies to the east of the Straits of Sicily. The modern day eastern Mediterranean is split into four main physiographic areas, namely the Ionian and Levantine basins and Adriatic and Aegean Seas (figure 1.5).

Figure 1.5. Bathymetric chart of the eastern Mediterranean.

The Ionian basin extends from the Straits of Sicily to the west to the western edge of Crete. Communication of the Ionian with the Adriatic and Levantine Seas occurs through the Straits of Otranto and the Cretan Passage respectively. The Ionian basin, with an area of 616,000km^2, is the largest basin of the eastern Mediterranean and has a maximum recorded depth of 5093m. The Ionian is dominated by the presence of the Mediterranean Ridge, which stretches from the Calabrian Rise and extends over a distance of 1500km to the Florence Rise in the Levantine Basin (Limonov *et al.,* 1996). The width of the Mediterranean Ridge ranges from 150-300km and has an arcuate southward convex shape running almost parallel with the Hellenic Arc system, with an average water depth over the Ridge of 2.1-2.2km. The ridge topography is dominated by small closely-spaced depressions and ridges with a relief of 50-100m and which run parallel to the ridge trend. The majority of workers agree that the Mediterranean ridge is an accretionary complex (Cita and Camerlenghi, 1990; Fusi and Kenyon, 1996) which originated as a result of the subduction of the African plate under the Eurasian plate. It is believed that the ridge represents the accumulation of sediments that have been scraped off the down-going African plate, as it becomes subducted beneath the Eurasian plate (Limonov *et al.,* 1996). The other important features of the Ionian are the Sirte and Messina Rises and the Sicilia Basin. The Sirte Rise occupies the entire continental margin below the shelf in the Gulf of Sidra. The Sicilia Basin is delineated by the 3600m contour, and consists of a northern section bordered by the Messina Rise and the Mediterranean and Malta ridges, and a southern section bordered by the Sirte and Mediterranean Ridge.

The Levantine basin, with a volume of 7.5*10^6 km^3 is the second largest basin of the eastern Mediterranean. It is encircled by Asia Minor, the north-eastern African mainland and the Cretan Archipelago. Narrow passages such as the strait of Rhodes, Scarpathos and Kasos allows connection to the Aegean whilst communication of the Ionian and Levantine seas occurs through the Cretan Passage, which lies to the south of Crete (Ozsoy *et al.,* 1989; 1993). Topographically, the Levantine basin is dominated by the arcuate Mediterranean ridge, which extends for 350km from the middle of the Cretan Passage before terminating to the west of Cyprus. The Mediterranean Ridge effectively subdivides the Levantine Basin into two provinces, namely the northern and southern sub-basins. To the south of the Mediterranean Ridge, two important physiographic areas can be identified, the Herodotus Abyssal Plain and the Nile Cone. The Herodotus Abyssal Plain is delineated by the 2800-3000m isobath and attains a maximum depth of 3156m near its south-west end (Carter *et al.,* 1972). To the south east of the Herodotus Abyssal Plain lies the Nile Cone, an immense fan-shaped sedimentary deposit, with sediment sequences estimated to be as much as 3000m in thickness (McCoy, 1974). Geographically the Nile Cone can be divided into two fans; the Rosetta and Damietta fans that are separated from one another by north-south trending deeply dissected ridge (McCoy, 1974). North of the Mediterranean Ridge, the predominant topographic features of the Levantine Basin including the deep Rhodes Basin (4400m) the Antalya Basin, the

Cilician Basin to the north of Cyprus, the Cyprus Basin (a north-westerly sloping basin with a maximum depth of 2300m) and the Anaxamander and Erathosthenes seamounts (Robinson and Golnaraghi, 1993). The other prominent feature of the Levantine Basin is the arcuate Hellenic trench system. This trench system is a series of discontinuous deep basins, trenches and narrow ridges that extends from northern Greece to south-west Turkey. Two sub-parallel trenches lie to the south east of Crete and Karpathos, an outer (southern) Strabo Trench and an inner (northern) Pliny Trench. The Pliny Trench, the deeper of the two at 4384m extends for about 200km and has many small sediment-filled basins along its course (McCoy, 1974). The Strabo Trench lies 40km to the south of the Pliny Trench and has an average depth of 3000-3200m. A high ridge composed of several individual segments separates the Strabo trench from the Pliny trench.

The Aegean Sea is the third largest sea of the eastern Mediterranean, with an estimated volume of ~$7.4*10^4$ km^2. (Theocharis *et al.,* 1993), and is topographically more complex than any other region of the Mediterranean. The dominant features of the Aegean Sea are the Northern Aegean Trough (1600m deep), the Chios Basin which reaches a maximum depth of 1160m, and the Cretan Sea to the south which forms the largest basin of the Aegean (Theocharis *et al.,* 1993). Exchange of water between the Aegean and the Levantine Sea occurs through Rhodes Strait (350m), Karpathos Strait (850m) and Kasos Strait (1000m).

The Adriatic Sea is a rectangular-shaped, elongated basin, approximately 800km long and 200km wide orientated in a northwestly-southeasterly direction and is the smallest of the major sub-divisions of the eastern Mediterranean (Artegiani *et al.,* 1993). The Adriatic can be split into northern, middle and southern sub-basins. A continental shelf underlies the whole of the northern and middle sub-basins, with the northern continental shelf extending from the Gulf of Venice southeastward to the Mid-Adriatic depression. The northern sub-basin is gently sloping and also relatively shallow, attaining a maximum depth of only 100m towards its southern edge. The middle sub-basin is dominated by a depression termed the Jabuka Pit (Carter *et al.,* 1972), a NE-SW trending depression that reaches a maximum depth of 280m at its centre (Artegiani *et al.,* 1993). A broad, shallow channel delineated by the 160m isobath connects the Jabuka Pit with the southern Adriatic basin (Carter *et al.,* 1972; Ozsoy *et al.,* 1993), with the Palagruza Sill (170m deep) marking the onset of the southern sub-basin. The southern province is characterised by a circular depression, termed the southern Adriatic Pit, which reaches a maximum depth of 1230m at its centre. Communication of the Adriatic Sea with the Ionian Sea occurs through the Otranto Strait, a feature that attains an average depth of 325m over its 75km width.

1.4. Circulation of the Eastern Mediterranean.

The eastern Mediterranean Sea, defined as the body of water lying to the east of the Straits of Sicily (Robinson *et al.,* 1991), is composed of the Levantine and Ionian basins and the Adriatic and Aegean Seas (Malanotte-Rizzoli and Bergamsco, 1991). The Mediterranean as a whole is a concentration basin, i.e. a basin in which the total evaporative loss of water exceeds the input of freshwater from both run-off and precipitation (Malanotte-Rizzoli and Hecht, 1988;). Bethoux (1979) estimates that the evaporative loss of freshwater is ~ 1.60 m a^{-1} for the eastern basin, whilst the input of freshwater is only ~0.60 m a^{-1}. The resulting water budget deficit of 1.02m a^{-1} results in the circulation of the Mediterranean being driven by the conservation of salt and heat. This is achieved in the eastern Mediterranean by the inflow of relatively fresh surface waters, originating from the North Atlantic, entering through the straits of Gibraltar and Sicily (Magini and Schlosser, 1986; Malanotte-Rizzoli and Bergamasco, 1991).

Over recent years both the surface and thermohaline circulations of the eastern Mediterranean have received much attention (Ozsoy *et al.,* 1989; The Physical Oceanography of the Eastern Mediterranean (POEM) Group, 1992). Until recently the oceanography of the eastern Mediterranean had been considered simply as a rather static, anti-estuarine circulation regime. Work by the POEM Group (1992), however, has demonstrated that the circulation is far more complex with surficial sub-basin gyres (semi- and permanent types) being intimately connected by meandering jets. The circulation of the eastern Mediterranean is dominated by the budgets in salt, water and heat. As a result of excess evaporation in the eastern basin, relatively fresh surface waters from the Atlantic enter through the straits of Gibraltar and into the Ionian by way of the Straits of Sicily (Ozsoy *et al.,* 1989). This body of water, termed Modified Atlantic Water (MAW), can clearly be distinguished as a subsurface salinity minimum at the straits of Sicily, (θ=15°C, a salinity of 36.2 psu), confined to a depth of 0-~200m (Ozsoy *et al.,* 1989; Malanotte-Rizzoli *et al.,* 1997). The MAW passes through into the Ionian basin and is advected eastwards by the subsurface Atlantic-Ionian Stream (AIS) (Malanotte-Rizzoli *et al.,* 1997), until it reaches Crete, where the AIS joins the Mid-Mediterranean Jet (MMJ) which continues to advect MAW into the interior of the Levantine Basin through the Cretan Passage (Horton *et al.,* 1997). The major surface circulation features of the Mediterranean are shown in figure 1.6

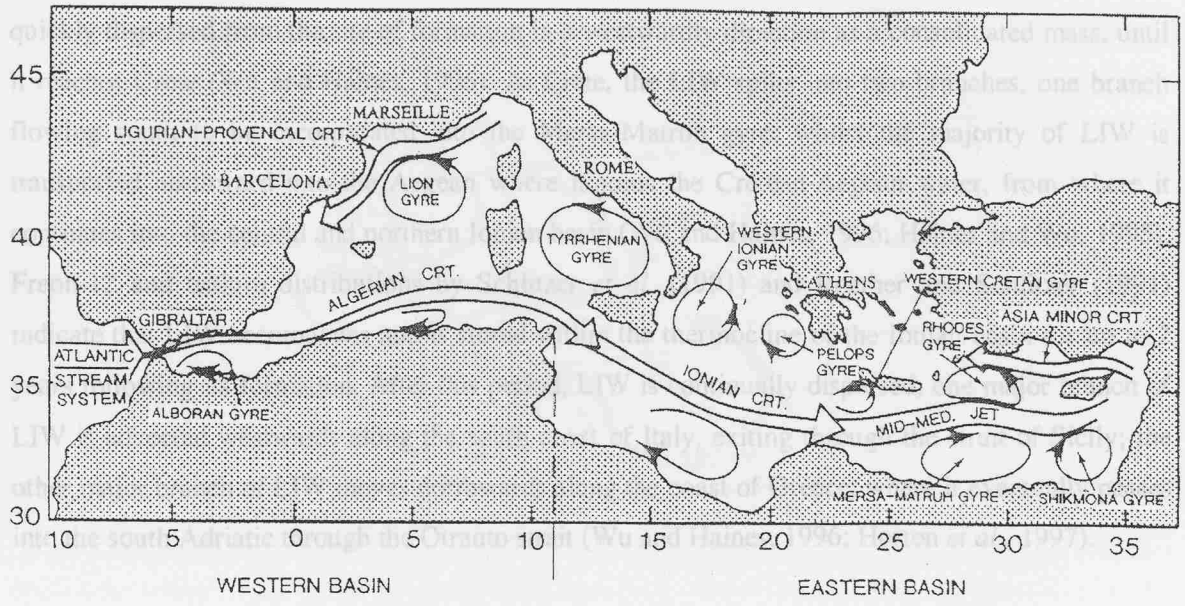

Figure 1.6. A schematic diagram showing the major surface water circulation features of the eastern (and western) Mediterranean Seas. Figure from Roussenov *et al.* (1995).

Within the Levantine basin the MAW enters into the permanent cyclonic Rhodes gyre (Wu and Haines, 1996; Haines and Wu, 1995), where it is transformed into Levantine Intermediate Water (LIW) through deep convective mixing during the winter months of February and March (Malanotte-Rizzoli and Hecht, 1988). The exact site of LIW formation has, over the past few years, been subject of much debate. Tracer and modelling work by Schlitzer *et al.* (1991) and Roether and Schlitzer (1991) have shown that LIW is present throughout the Levantine Basin, from which they imply numerous sites of LIW formation within the Levantine basin. Numerical modelling of LIW formation within the Levantine by Haines and Wu (1995), Wu and Haines (1996) and Lascaratos and Nittis (1998), however, clearly indicates that the cyclonic Rhodes gyre is the only major site for LIW formation. According to Lascaratos *et al.* (1993), Haines and Wu (1995), Wu and Haines (1996) and Lascaratos and Nittis (1998), the Rhodes gyre is important for the preconditioning of the waters in LIW formation. It is believed that, at the centre of the Rhodes gyre, doming of the isopycnals due to upwelling reduces the vertical stability of the water column and so facilitates the deepening of the mixed layer and subduction of LIW to intermediate depths (Lascaratos and Nittis, 1998). According to Malanotte- Rizzoli and Hecht (1988) and Lascaratos and Nittis (1998), LIW is formed during late February and March by continual evaporation of surface waters, induced by outbreaks of cold dry air blowing from the Eurasian land mass over the Rhodes gyre. During February and March, doming of the isopycnals reduces vertical stability within the centre of the Rhodes gyre, and LIW is subducted below the thermocline to a depth of 500m at a rate of 0.6±0.1 Sv (Stratford and Williams, 1997). Levantine intermediate water can clearly be distinguished within the Levantine Basin as a subsurface salinity maximum (from 200-600m) with salinities ranging from 38.95-39.05 (Malanotte-Rizzoli *et al.*, 1997). Following formation, the LIW is

quickly dispersed from the site of formation in a westwardly direction as a consolidated mass, until it reaches Crete (Wu and Haines, 1996). At Crete, the LIW splits into two branches, one branch flowing south to be incorporated into the Mersa-Matruh gyre, whilst the majority of LIW is transported northward into the Aegean where it joins the Cretean-Aegean water, from where it continues into the central and northern Ionian basin (Wu and Haines, 1996; Haines and Wu, 1995). Freon-12 and tritium distributions by Schlitzer *et al.* (1991) and Roether and Schlitzer (1991) indicate that LIW accumulates and is stored within the thermocline of the Ionian basin for up to 2 years following its formation. After this period, LIW is continually dispersed, one major branch of LIW is advected westwards along the south coast of Italy, exiting through the strait of Sicily; the other major branch of LIW moves northwards along the coast of Greece, where it eventually passes into the south Adriatic through the Otranto strait (Wu and Haines, 1996; Horton *et al.*, 1997).

Estimates from Haines and Wu (1995) suggest that the influx of LIW into the southern Adriatic is on the order of 0.4 Sv, and LIW can clearly be identified within the south Adriatic as a subsurface salinity maximum, underlying the fresh Adriatic surface waters (Artegiani *et al.*, 1997). Once in the Adriatic, the LIW circulates cyclonically round the south Adriatic, a process that makes the LIW more saline and which according to Wu and Haines (1996) preconditions this water mass for deep-water convection during the winter. During the winter, outbreaks of the Bora wind over the south Adriatic ensure that convective mixing occurs throughout the entire water column producing deep water (Horton *et al.*, 1997; Wu and Haines, 1996; Haines and Wu, 1995). This Adriatic deep water spills out over the western side of Otranto Strait, from where it sinks to depths of 700-1600m and is conventionally termed Eastern Mediterranean Deep Water (EMDW). EMDW passes out of the Otranto Strait, where it follows the isopycnals along the eastern coast of Italy before being moved eastwards along the African coastline, finally ending up in the Levantine Sea (POEM Group, 1992). Recently, oxygen distributions from the eastern Mediterranean have shown that EMDW dispersal also occurs along the eastern Hellenic trench at 39.5 °N, and which has been shown to follow the isobath contours along the western Greek coast (Malanotte-Rizzoli *et al.*, 1997). The two routes of EMDW dispersal converge and merge at 35-36 °N, producing a deep layer of EMDW that uniformly occupies the abyssal interior of the Ionian Sea (Malanotte-Rizzoli *et al.*, 1997). Uniform Freon-12 distributions in both the Levantine and Ionian Basins indicate the complete penetration of EMDW throughout the entire eastern Mediterranean (Roether and Schlitzer, 1991) and upwelling of the EMDW within the Levantine Sea completes the thermohaline cell of the eastern Mediterranean (Schlitzer *et al.*, 1991). Estimates by Roether and Schlitzer (1991) and Roether et al., (1991) suggest that the renewal time of the eastern Mediterranean is of the order of 126 years (figure 1.7).

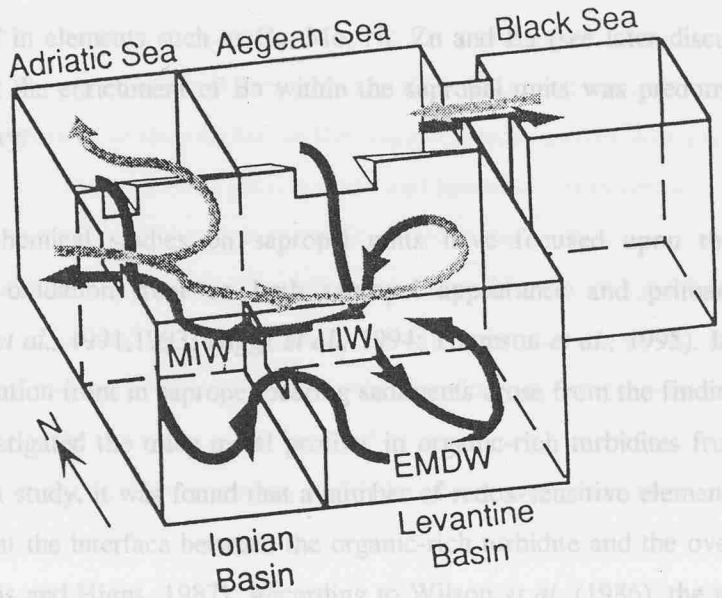

Figure 1.7. A schematic diagram of the thermohaline circulation within the eastern Mediterranean as discussed in the text. Figure from POEM Group (1992).

Over the past decade, however, another important source of deep-water formation has become apparent, namely the Aegean Sea (Theocharis *et al.,* 1998). Freon-12 and T/S data collected from recent cruises to the eastern Mediterranean (Roether *et al.,* 1996; Roether and Klein, 1998) have shown that a deeper, denser layer of water now exists beneath the EMDW and clearly has its origins in the Aegean Sea. Estimates by Roether *et al.* (1996) have shown that the formation of deep water from the Aegean has displaced up to 20% of the EMDW and moved it upwards in the water column. Also it has been noted that the formation of LIW has been affected (Roether *et al.,* 1996).

1.5. Previous inorganic geochemical investigations on sapropel, S1.

Although a number of studies have focused upon the micropaleontology and sedimentology of sapropel units over the past five decades, by comparison, the inorganic geochemisty of the most recent sapropel has been largely overlooked.

Calvert (1983) and Sutherland *et al.* (1984) performed the first comprehensive geochemical examinations of cores containing S1. In these rather low-resolution studies, major and trace elements as well as organic carbon and nitrogen were analysed. It was apparent that these organic-rich sediment layers were significantly enriched in trace metals by comparison with the intercalated pelagic, organic-poor sediments. For example, Calvert (1983) demonstrated that sapropel S1 was

significantly enriched in elements such as Cu, Mo, Ni, Zn and Ba (see later discussion). Calvert (1983) suggested that the enrichment of Ba within the sapropel units was predominately derived from biological activity.

More recently, geochemical studies on sapropel units have focused upon the effects of a downwards moving oxidation front on both sapropel appearance and primary geochemical signatures (Pruysers *et al.*, 1991,1993; Higgs *et al.*, 1994; Thomson *et al.*, 1995). Investigations of the effects of an oxidation front in sapropel-bearing sediments arose from the findings of Colley *et al.* (1984), who investigated the trace metal profiles in organic-rich turbidites from the Madeira Abyssal Plain. In that study, it was found that a number of redox-sensitive elements formed well-defined sharp peaks at the interface between the organic-rich turbidite and the overlying organic-poor sediments (Jarvis and Higgs, 1987). According to Wilson *et al.* (1986), the profiles of these metals could be explained in terms of the effects of a downwards-advancing oxidation front. An oxidation front is established within sediments in response to a change in either (1) sedimentation rate (2) Corg flux or (3) bottom water oxygen concentrations. With this in mind, it was suggested that a similar mechanism could be operating within eastern Mediterranean sediments, since it had long been established that changes in either the productivity (Schrader and Matherne, 1981; Thunell and Williams, 1982; Ten Haven *et al.*, 1991) and/or bottom water oxygen concentrations (Cita *et al.*, 1977; Vergnaud-Grazzini *et al.*, 1977; Vergnaud-Grazzini, 1985) had given rise to sapropel formation.

Ten Haven *et al.* (1987) and De Lange *et al.* (1989) were amongst the first to suggest that an oxidation front was active within S1-bearing sediments. Investigations by Ten Haven *et al.* (1987) revealed that whilst there was an exceptionally good correlation between bromine and organic carbon (as seen in other organic-rich sediments), the correlation was poorer between uranium and Corg. Examination of the U and Corg profiles in core 29 investigated by Ten Haven *et al.* (1987) showed that the majority of the uranium in the solid phase was concentrated towards the base of the sapropel unit. Ten Haven *et al.* (1987) suggested that this profile was the result of the remobilisation of U from the upper part the sapropel by the oxidation front, with re-precipitation of U at depth within the sapropel under more reducing conditions. Furthermore, De Lange *et al.* (1989) re-interpreted the sedimentary sequence for sapropel formation presented by Murat and Got (1987) in terms of a downward-moving oxidation front. De Lange *et al.* (1989) suggested that the sharp contact at the top of the sapropel was the result of a 'burn down' by an oxidation front following sapropel formation. Previously, Murat and Got (1987) had interpreted the sharp interface as marking a rapid return of oxygen to the bottom waters following sapropel formation.

The effect of the oxidation front on the primary geochemical signature of S1 has been examined by a number of authors (Pruysers *et al.*, 1991; Higgs *et al.*, 1994; Thomson *et al.*, 1995; Van Santvoort *et al.*, 1996). These authors have shown that, as the oxidation front moves downwards, it removes via oxidation reduced species such as organic carbon and sulphides from the sedimentary record, reducing the original thickness of the sapropel unit. Also, these authors have noted that, at the advancing oxidation front, redox sensitive elements such as Fe, Mn, As, Ni, Zn, V, Cr and Cu form well-defined peaks at the limit of oxygen penetration in the sediment. An additional feature noted for slowly-accumulated sapropels affected by an oxidation front is the presence of a double Mn peak, the lower peak thought to represent the locus of an active redox front based upon pore water Mn profiles (Higgs *et al.*, 1994; Thomson *et al.*, 1995; Van Santvoort *et al.*, 1996).

It has long been recognised that S1 is enriched in the element barium (Calvert, 1983). High-resolution studies of slowly-accumulated sediments by Thomson *et al.* (1995) and Van Santvoort *et al.* (1996) have demonstrated that Ba displays a quasi-Gaussian distribution within S1. Thomson *et al.* (1995) suggested that the Ba/Al profile demonstrated the variation in primary productivity during sapropel formation, given the closely-established relationship between Ba and productivity from sediment trap data (Dymond *et al.*, 1992; Francois *et al.*, 1995). Based on the Ba/Al weight ratio evidence, Thomson *et al.* (1995; 1999) proposed that sapropel formation occurred for a much longer period than had previously been suggested by dating the observed sediment colour change. Radiocarbon dating of the Ba/Al profile indicated that sapropel formation lasted until 5.2 kyr (Thomson *et al.*, 1995), whilst the established chronology implied that S1 terminated around 6.4kyr (Fontugne *et al.*, 1994).

1.6. Rationale for further geochemical work on the most recent sapropel, S1.

Whilst a number of inorganic geochemical studies on S1 have been reported, a number of key questions still remain regarding the geochemical nature and origin of the youngest sapropel S1.

As stated in section (1.5), it has been noted that sapropel sediments are enriched in a number of trace and major elements. Following sapropel formation, however, post-depositional oxidation of S1 has led to the attendant remobilisation and reallocation of redox sensitive elements around the oxic/post-oxic boundary and throughout the sapropel unit itself. Identification of the mechanism(s) which caused trace metal enrichment during sapropel formation has therefore been difficult since the primary geochemical signature of S1 is overlain by a secondary diagenetic signal. Work by Pruysers *et al.* (1991) and Thomson *et al.* (1995) identify organic carbon, sulphide formation and co-precipitation of elements with oxyhydroxides as important factors which control trace metal

enrichment and immobilisation within S1. Whether or not these phases were involved in the trace metal enrichment during sapropel formation is an issue that needs to be addressed. At present, detailed geochemical examinations have been restricted to slowly-accumulated sapropels, a consequence of which is that they are all affected by an oxidation front. Giant piston coring of the eastern Mediterranean during the 1995 Marion Dufresne Cruise (Rothwell, 1995), however, produced cores with exceptionally thick (>20cm) sapropel deposits. To date no detailed geochemical investigations on rapidly-accumulated S1 sapropel units have been published. It is envisaged that examination of these exceptionally thick S1 units will reduce/minimise the influence of post-depositional oxidation fronts, and so help to elucidate the primary geochemical nature of S1 i.e. which of the sulphide, organic carbon, or seawater phases controls the enrichment of trace metals in S1?

Even after five decades of sapropel research, one of the most contentious issues regarding sapropels is the mechanism by which they formed i.e. the productivity *vs* preservation debate. Establishing the mechanism that leads to sapropel formation will help explain the formation of other organic-rich sediments like black shales (Wignall, 1994). Detailed discussions of the productivity and preservation debates concerning sapropel formation are given in sections 1.2.1 and 1.2.2. In brief, what has become apparent over the last 50 years is that overwhelming amounts of evidence have been put forward for both anoxia and productivity as being the primary mechanism involved in sapropel formation. For example, the enrichment of $\delta^{15}N$ isotopes (Calvert *et al.*, 1992) during sapropel formation suggests enhanced productivity, whilst the C/S/Fe ratio from S1 examined by Passier *et al.* (1996) suggests that organic carbon deposition occurred under euxinic conditions. More recently, however, Thomson *et al.* (1995) and Van Santvoort *et al.* (1996) demonstrated that a quasi-Gaussian profile exists in the Ba/Al ratio around S1. According to Thomson *et al.* (1995), Ba/Al ratios could be used as a geochemical proxy for visualising the waxing and waning of productivity during sapropel formation. The accuracy of using Ba/Al ratios as a proxy for evaluating the role of productivity during sapropel formation, however, has not yet been established. At present certain key questions that arise concerning the use of Ba/Al usage are:-

1) are the Ba/Al profiles geochemically stable over long periods of time?

2) how accurate are the Ba/Al profiles in reconstructing the amount of Corg and its original profile in sapropel sediments that have been affected by oxidation fronts?

3) is it possible to quantify the amount of primary productivity occurring during sapropel formation based upon the Ba/Al profile?

4) was productivity continuous during sapropel formation?

5) can this information be used to assess the relative importance of both anoxia and productivity in controlling sapropel formation?

Again examination of rapidly-accumulated sapropels that have not undergone any post-depostional oxidation will allow for the accurate assessment of using the Ba/Al proxy in sapropel formation and in the reconstruction of partially-oxidised sapropels in more slowly-accumulated cores.

Another key question concerning sapropel formation is establishing an accurate chronology for both the onset and termination of S1. At present numerous radiocarbon datings of S1 have placed the onset of sapropel formation at ~8.97 kyr, whilst the termination of S1 is much more varied, ranging between 6.37 and 8.03 over the whole of the eastern Mediterranean (Fontugne *et al.*, 1994). Recent findings by Higgs *et al.* (1994) and Thomson *et al.* (1995) have suggested that the variation in ages for the end of S1 may in part, be due to the fact that dating of S1 has only been based upon the visual sapropel unit. To overcome this problem, Thomson *et al.* (1995) dated the onset and termination of S1 based on the Ba/Al profiles in three cores. Unlike previous studies, Thomson *et al.* (1995) found that there was a uniform age for the termination of S1, but more importantly, dating of the Ba/Al profile suggested that sapropel formation ended at 5.2kyr, much later than had previously been established. Based on these findings, a major aim of this research is to try and establish an accurate chronology for sapropel formation based on the Ba/Al criterion proposed by Thomson *et al.* (1995). Questions that need to be addressed are:-

1) how long did S1 formation actually last?

2) was sapropel formation synchronous over the entire eastern Mediterranean as implied by the datings of Thomson *et al.* (1995), or do variations in the sapropel ages (Fontugne *et al.*, 1994) suggest that the timing of S1 was different in different areas of the eastern Mediterranean?

3) is it possible to explain the ages for sapropel development in terms of circulation changes within the eastern Mediterranean?

During this research, a paper was published in *Marine Geology* regarding the current status of the inorganic geochemistry of S1. This paper is presented in section 1.7 at the end of this chapter.

1.7. Paper published in: *Marine Geology*, **153**, 77-89 (1999).

Review of recent advances in the interpretation of Eastern Mediterranean sapropel S1 from geochemical evidence.

J. Thomson*, D. Mercone*, G.J. de Lange+ and P.J.M. van Santvoort.

*Southampton Oceanography Centre, Empress Dock, Southampton SO14 3ZH, UK.

+Department of Geochemistry, Institute of Earth Sciences, University of Utrecht, P.O. Box 80.021, 3508 TA Utrecht, The Netherlands.

1.7.1. Abstract.

The sediments of the Eastern Mediterranean basin contain C_{org}-enriched layers (sapropels) interbedded with the C_{org}-poor sediments which form by far the greater part of the record. While it is generally appreciated that different surface ocean productivity and bottom water conditions are necessary for the formation and preservation of these two sediment types, less attention has been paid to diagenetic effects which are an expected consequence of transitions between dramatically different bottom water oxygenation levels. A geochemical interpretation has emerged of post-depositional oxidation of the most recent sapropel (S1), initially based on the relationship of the Mn, Fe, C_{org} and S concentration/depth profiles observed around S1, and the characteristic shapes of these elemental profiles known from other situations. This indicates that post-depositional oxidation has removed approximately half of the visual evidence of the sapropel (~6 cm from a total of ~12 cm in the deep basin). The oxidation interpretation from redox-sensitive element redistribution profiles has subsequently been consolidated with evidence from pore water (O_2, NO_3, Mn^{2+} and Fe^{2+}) studies, from characteristic solid phase Ba profiles which yield palaeoproductivity records, and from oxidation-sensitive indicator trace elements (I and Se). So far these geochemical observations have been concentrated in the deeper central parts of the basin, where sediment accumulation rates are lower than on the basin margins, and radiocarbon dating indicates that S1 formation occurred between 5.3 - 9.0 kyr BP (uncorrected conventional radiocarbon time). It remains to be demonstrated whether or not these times are applicable to the entire E. Mediterranean basin. The implications of these findings to guide sampling in future work on the S1 productivity episode and on older sapropels for palaeoenvironmental investigations are discussed.

1.7.2. Introduction.

Sapropels were defined by Kidd *et al.* (1978) as sharply-defined, dark-coloured sedimentary layers with a C_{org} content >2 wt. % and a thickness >1 cm. Besides C_{org}, such sediments are also enriched in S and a variety of redox-sensitive trace metals (Calvert, 1983). Recent ODP drilling found >80 such units in the sediments deposited in the E. Mediterranean basin since the Pliocene (Emeis *et al.* 1996). This review focuses on the contribution which inorganic geochemical investigations have made to the interpretation of sapropels in recent years, based on alteration effects caused by early diagenesis. It mainly concerns detailed investigations of the youngest (early Holocene) sapropel, as this unit contains the freshest geochemical evidence of its formation and recent diagenesis, and is amenable to radiocarbon dating. In the terminology of Hieke (1976), this is sapropel S1.

Understanding the mechanisms of sapropel formation and sapropel preservation is necessary for improved reconstructions of palaeoenvironmental conditions in the E. Mediterranean (Rossingnol-Strick *et al.* 1982; Rohling, 1994), but is also relevant to geochemical issues of wide importance. As recent, fine-grained, C_{org}-rich marine sediments, sapropels may be regarded as modern analogues for C_{org}-rich black shales, and there are similar uncertainties on the conditions and environments under which black shales and sapropels are formed and preserved (cf. review by Wignall, 1994). In the deep marine environment, the C_{org} content preserved in a sediment is primarily a balance between the input flux of organic matter and its oxidation by bottom water O_2 (Emerson and Hedges, 1988). Most marine sediments have C_{org} contents in the range 0.2 - 2%. The E. Mediterranean sedimentary record therefore comprises an intercalation of unusually C_{org}-rich sediments (the sapropels) within C_{org}-poor sediments (Ryan and Cita, 1977; Cita *et al.* 1977), caused by repeated fluctuations through time in either or both the C_{org} flux from surface ocean export production and bottom water O_2 levels.

The concepts which have been applied to the post-depositional diagenesis of sapropel S1 were initially developed from investigations of deep-sea turbidites, particularly C_{org}-rich turbidites (Wilson *et al.* 1985, 1986; Thomson *et al.* 1993). In such units oxidation of the upper part occurs after the turbidite's emplacement, as bottom water oxygen diffuses downwards into the newly-deposited sediment. One consequence is a sharp colour change in the turbidite sediment, which marks the limit of oxidation, caused by re-oxidation of the sediment C_{org} and other reduced species. Enrichment peaks of many redox-sensitive elements form in a particular sequence above and below the colour change (Thomson *et al.* 1993). On abyssal plains, turbidite emplacement is

the cause of the episodic changes in the nature of the sediment exposed to oxic bottom waters. In the E. Mediterranean, however, sediment accumulation is continuous and the changes are caused instead by fluctuations in C_{org} fluxes to the sediments and in bottom water O_2 levels. The strong parallels found in the geochemical evidence of the two different situations form the starting point for discussion of the early diagenesis of S1.

1.7.3. Discussion.

1.7.3.1. The visual evidence.

Interpretations of the environmental conditions leading to sapropel formation are based on the sedimentology, micropalaeontology and geochemistry of the dark-coloured layers and their enclosing sediments. Generalised sequences of sapropel formation, based on examination and interpretation of a large number of sapropel units and the sediments enclosing them, have been presented (e.g. Anastasakis and Stanley, 1984; Murat and Got, 1987). The interval of dark colour associated with a sapropel is often somewhat thicker than that defined by the >2% C_{org} criterion, and finer categorisations based on C_{org} content have been proposed (Anastasakis and Stanley, 1984) but are infrequently used. Three sharp colour changes are generally associated with S1; the upper and lower limits of the dark C_{org}-rich sapropel layer itself, (typically 6-8 cm thick in the central basin), and at the base of the grey "protosapropel" layer of variable thickness which underlies the sapropel layer. More diffuse dark brown bands 2-3 cm thick are often found, either or both immediately above and 6-8 cm above the upper surface of the sapropel. This brown colour is characteristic of Mn oxyhydroxide enrichments (Fig.1.8).

1.7.3.2. Evidence of post-depositional oxidation of S1 from oxygen, manganese, iron, organic carbon and sulphur profiles.

Post-depositional diagenesis acting on sapropel S1 was first postulated by Ten Haven *et al.* (1987) and de Lange *et al.* (1989), but was rebutted (Murat and Got, 1989). Comprehensive early diagenetic investigations to prove the hypothesis were not performed until recently (Pruysers *et al.* 1991,1993; Higgs *et al.* 1994; Thomson *et al.* 1995; van Santvoort *et al.* 1996). In contrast to earlier studies, these investigations have involved sampling at high-resolution (every cm or finer), in recognition of the fact that many early diagenetic signals are sharply localised and often located in close proximity to sediment colour changes. The following summary reviews the interlocking geochemical arguments which have emerged and their consequences. Sediment redistribution is common and complex in the tectonically-active Eastern Mediterranean basin (Stanley, 1985). In

order to avoid complications from downslope sediment movement, the work reported in this paper was undertaken in cores from local topographic highs in the central basin, between 16-25° E (east of Sicily to south of Crete).

Geochemists define sediments as *oxic* only as long as free O_2 is present in pore water solution (Berner, 1981), and the same sediments are termed *sediments laid down in oxic conditions* when all pore water O_2 has been consumed on deeper burial. At present the E. Mediterranean basin is oligotrophic (Bethoux, 1989; Antoine *et al.* 1995), with a well-mixed, warm (13°C) and well-oxygenated water column (Schlitzer *et al.* 1991). These conditions result in a low deposition flux of C_{org} to the sediment/water interface at the present time, and this flux is remineralised by oxic diagenesis to a low sediment C_{org} content. van Santvoort *et al.* (1996) presented the first comprehensive pore water evidence from E. Mediterranean sediments, crucially including O_2 and NO_3^- data, and demonstrated in three cores from different sites that the sediments were oxic from the sediment/water interface down to the upper face of sapropel S1 at ~25 cm depth. This proves that the available flux of O_2 into the sediments exceeds that necessary to consume the low fluxes of C_{org} currently deposited, and the excess O_2 diffuses downwards to oxidise C_{org} and other reduced species at depth in the underlying sapropel. If it were not for the presence of S1, the sediments would be oxic to a much greater depth.

The presence of oxic conditions above S1 had been inferred by Higgs *et al.* (1994) from analogy with turbidite studies. The downwards diffusion of bottom water oxygen in an oxidation front, as well as oxidising C_{org}, precipitates Mn and Fe as oxyhydroxides. Both of these elements are deposited in oxic sediments as oxyhydroxide coatings, but are reduced to soluble species (Mn^{2+} and Fe^{2+}) when buried into anoxic conditions. They are then re-oxidised and re-precipitated as oxyhydroxides (Mn^{4+} and Fe^{3+}) when they diffuse upwards and re-encounter oxic conditions (van Santvoort *et al.* 1996). If bottom water O_2 content suddenly increases from a low to a higher (constant) value, its rate of downwards diffusion into sediments will slow with time, as the diffusion distance to the oxidation front lengthens because of the increasing amount of sediment oxidised and the deposition of new sediment at the sediment/water interface. If their upward fluxes are also approximately constant, the resultant reprecipitation peaks of Mn and Fe oxyhydroxide achieve a characteristic shape with the amount of oxyhydroxide precipitated increasing with depth (Wilson *et al.* 1986). Exactly the expected profile shape is seen in Fe/Al profiles above S1 (between 15 and 22 cm depth in Figure 1.9). (Element/Al ratios rather than element concentrations are employed in Figure 1.9 to take account of fluctuations in sediment composition. The inherent assumptions are that detrital phases contain the element of interest at a fixed ratio with Al, that

$CaCO_3$ has a negligible content of the element of interest, and that diagenetic enhancements will be observed as increases above the constant detrital ratio. This procedure works well when the sediment can be considered as a two component clay/carbonate mixture, but is less satisfactory where the element of interest also occurs at appreciable concentration in a third phase. Thus although Mn/Al and Fe/Al are both at enhanced levels between 15 and 22 cm as oxyhydroxides in Figure 1.9, it is the presence of pyrite as a third phase that is the cause of the high Fe/Al values from 22-26 cm.)

In this oxidation front interpretation, high C_{org} and S values must initially have been present in the now oxidised region immediately above those still observed in the unoxidised dark S1 unit. Chemical consumption of O_2 by sapropel C_{org} and S oxidation is necessary to cause the slow migration of the oxidation front which leads to the development of the large Fe oxyhydroxide peak observed (Higgs *et al.* 1994). In the example shown (Figure 1.9), these enhanced S and C_{org} levels must originally have been present between 15 and 26 cm, so that 7 cm of C_{org}-rich sediment (15-22 cm) has already been oxidised to leave the remaining 4 cm of sapropel (22-26 cm).

Manganese is expected to behave similarly to Fe in response to an oxidation front, but Mn/Al profiles above S1 typically exhibit two peaks rather than one. In Figure 1.9, these peaks are centred on 15 cm and 22 cm. It is the lower peak which is in the anticipated oxidation front position analogous to Fe, and the significance of the upper Mn peak remains controversial. Pruysers *et al.* (1993) interpreted this peak as a consequence of a retreating oxidation front. This explanation is untenable for the examples studied by van Santvoort *et al.* (1996), who demonstrated by means of pore water data that it was the lower of the two Mn peaks which was actively forming. Cita and coworkers (Cita *et al.* 1989; De Capitani and Cita, 1996) identify the upper Mn peak as a hydrothermal emission linked with the Santorini eruption. An important factor in this interpretation was to provide an explanation of the very high Mn contents observed in the upper Mn peaks of a few, but by no means all, cores (the "Marker Bed", containing up to ~23%! Mn). The cores presented by De Capitani and Cita (1996) appear very similar to those on which diagenetic studies have been performed (cf. Fig. 1.8 here with Fig. 1 of De Capitani and Cita (1996)). It will be seen later that the sediments hosting the upper Mn peak in the cores investigated geochemically are in fact >1 ky older than the best estimate for the Santorini eruption (~3.6 ky B.P., Kuniholm *et al.* 1996). The third interpretation is that the upper Mn peak marks the point at which the oxidation front began to operate, which is consistent with the initiation of the Fe/Al peak (Thomson *et al.* 1995). In this case the upper Mn peak could either have been (i) the enhanced interface Mn concentration seen when sediments are anoxic but bottom waters are oxic, or (ii) Mn precipitated from an anoxic water column on reventilation (fig 1.10). This latter situation will occur when

Mn^{2+} builds up in an anoxic water column by diffusion out of anoxic sediments, followed by Mn precipitation as Mn oxyhydroxide when bottom waters are reventilated (Mangini *et al.* 1991). In either case, an increased bottom water reventilation rate at the level of the upper Mn peak is required to initiate the oxidation front which continues its downwards penetration at the present time (van Santvoort *et al.* 1996). The source of Mn to form the lower Mn peak is subsequent upwards diffusion of Mn^{2+} from anoxic sediments at depth, as confirmed by the pore water Mn^{2+} profiles reported by van Santvoort *et al.* (1996).

1.7.3.3. Barium as a palaeoproductivity indicator for definition of original sapropel thickness.

The Mn and Fe oxyhydroxide peaks on which the diagenetic "burn down" interpretation was based formed in oxic conditions above the residual S1 unit, and will redissolve through reduction on future burial into anoxic conditions. They are therefore unlikely to be reliable diagnostic indicators for sapropels older than S1. Other compositional parameters which would indicate the presence of oxidised sapropels are necessary for investigations of older units. Thomson *et al.* (1995) and van Santvoort *et al.* (1996) have demonstrated that the element Ba provides a quantitative proxy in the case of S1.

Barium has been employed as a palaeoproductivity indicator for some time (e.g. Bostrom *et al.* 1973). A correlation is observed between the settling fluxes of C_{org} and Ba intercepted by sediment traps, although the mechanism by which the association between the two elements forms in the water column remains poorly understood despite intensive investigation (Dymond *et al.* 1992; Francois *et al.* 1995; Dymond and Collier, 1996). Regardless of mechanism, however, Ba behaves in a highly systematic way in the vicinity of several S1 units investigated (Thomson *et al.* 1995; van Santvoort *et al.* 1996). In Figure 1.9, the Ba/Al data are consistent with a constant background Ba content (Ba/Al weight ratio = 35×10^{-4}) from 0-15 cm and from 28-50 cm. This background Ba/Al ratio is mainly detrital although it must include a small biogenic barite contribution from the oligotrophic conditions before and after sapropel formation. Between these zones, excess Ba is consistently present above this background level in a broad peak with a quasi-Gaussian shape. This excess Ba is present as discrete barite ($BaSO_4$) crystals <5 microns in size, and is inferred to be biogenic barite which accompanied the pulse of high productivity which formed S1 (Thomson *et al.* 1995).

The enhanced Ba levels from 15-28 cm are near-coincident with the sum of the zones with observed enhanced C_{org} content (22-26 cm) and with the diagenetic Fe/Al zone indicative of a slow moving front discussed above (15-22 cm). The excess Ba profile is therefore taken to

represent the entire period of high productivity which included the formation of S1. Six other cores have now been shown to exhibit quasi-Gaussian Ba/Al profiles similar to that in Figure 1.9 (Pruysers *et al.* 1991; Thomson *et al.* 1995; van Santvoort *et al.* 1996). In the examples studied, the Ba/Al reconstruction indicates oxidative removal of ~6-8 cm of visual evidence in the S1 units, which is comparable with the residual S1 thickness itself. van Santvoort *et al.* (1996) have demonstrated how Ba data may be used to reconstruct the amount of C_{org} oxidised. First the Ba:C_{org} relationship observed in unoxidised S1 sections is determined, then the oxidised C_{org} is estimated from the measured Ba in the oxidised sections (Figure 1.11).

It is known that barite dissolves at depth when pore water sulphate levels are drawn down to low levels by sulphide production (Brumsack, 1986; Torres *et al.* 1996), and van Os *et al.* (1991) have demonstrated that limited Ba migration and diagenesis may occur in sapropels. Nevertheless, Langereis *et al.* (1997) found that Ba profiles prove to be a reliable guide to sapropel position in E. Mediterranean sediments up to 1.1 My old, where they can reveal the positions of older, originally relatively thin sapropels in which the initial high C_{org} contents have been completely removed by oxidation.

1.7.3.4. Iodine and selenium as solid phase markers of oxidation front limits.

Because pore water investigations require immediate sampling with specialist facilities on board ship, diagnostic solid phase indicators for the oxidation front process described above would be a valuable tool for investigations of stored cores. The elements I and Se have promise for this purpose (Higgs *et al.* 1994; Thomson *et al.* 1995). Both I and Se are present at enhanced concentrations in sapropels relative to the detrital levels found in the C_{org}-poor enclosing sediments laid down in oxic conditions, and are presumably enriched in the sapropel organic matter (I and possibly Se) or sulphides (Se).

Higgs *et al.* (1994) noted that both I and Se exhibit an additional enrichment peak close to the inferred active oxic/post-oxic boundary at the top of the visual S1 unit. The large, narrow peaks for both elements considerably exceed detrital and sapropel values, implying a large mobile diagenetic component of both elements. Similar enrichment peaks with I above Se have been noted in turbidites containing an active oxidation front (Thomson *et al.* 1993), where it is clear that both peaks must continuously dissociate and reform to maintain the same relative positions with respect to the active oxic/post-oxic boundary. By analogy with this and other previous work, it is inferred that I is supplied as I^- from oxidation and remineralisation of C_{org} (including older sapropel C_{org}) at depth (Kennedy and Elderfield 1987; Price and Calvert, 1977). The solid phase I peak must be

composed of an I species more oxidised than I^- but less oxidised than IO_3^-, which is maintained in place by a critical low pore water O_2 concentration. The Se may be supplied from oxidation of sapropel C_{org} or sulphides and from seawater (Thomson *et al.* 1998), and the Se peak is inferred to form immediately where post-oxic (i.e. negligible pore water O_2) conditions are first encountered. Although the I and Se peaks are close together, therefore, the inferred sensitivity to pore water O_2 levels means that the I peak maximum will always be found just above the Se peak maximum (Figure 1.9).

In the case of sapropels, the concept is that if an I peak is found immediately above a Se peak, then oxidation is active and the limit of oxidation is located between the two peak maxima (Higgs *et al.* 1994; Thomson *et al.* 1995). This application is only likely to be useful for S1 units, because older sapropels should be buried too deeply to experience oxidation by bottom waters at the present time. In the case of an older sapropel which experienced an oxidation front at an earlier time, or an S1 unit which experienced some oxidation which has now ceased (e.g. because of rapid sediment accumulation at the site after S1 deposition), the I peak will no longer be stable and will dissociate. The Se peak should remain stable because it is not dependent on O_2 for its maintenance, however, and is expected to remain static. Thomson *et al.* (1998) demonstrated that oxidation front Se peaks in turbidites persist over at least 7 My. The contention is, therefore, that a large Se peak at the top of a sapropel is a permissible indication that the unit in question experienced post-depositional oxidation and must have originally been thicker. This application of Se as a marker peak for fossil oxidation fronts remains to be explored in older sapropel units.

1.7.3.5. "Protosapropels" are in fact diagenetic pyritisation features.

A distinct grey colouration lies immediately beneath the dark colouration of many sapropels, including most S1 examples. These grey layers generally have sharp contacts with the overlying sapropel and with the underlying C_{org}-poor sediments laid down in oxic conditions. This association and immediate proximity has led some workers to interpret the grey colouration as "protosapropel", i.e. as the sediments formed during the transition between deposition of C_{org}-poor and sapropel sediment (Anastasakis and Stanley, 1984; Murat and Got, 1987; Troelstra *et al.* 1991). While a transition of some duration obviously must occur between these two modes of sediment deposition, it is now highly unlikely that it is this transition which is signified by the grey layer.

Passier *et al.* (1996) have provided evidence that the grey colouration below sapropels is another diagenetic effect. It is a consequence of pyritisation of the sediment, caused by diffusion of sulfide (HS^-) downwards out of the sapropel unit to react with Fe^{2+} diffusing upwards from anoxic

conditions below to form pyrite. Thus these grey layers, unusually for C_{org}-poor sediments, are enriched in Fe and S in FeS_2 because of the downwards diagenetic export of S from the sapropel. The sharp lower interface of the grey layer marks the limit of sulfide diffusion (Passier *et al.* 1996). The grey colouration is generally much deeper than the level where the increase in the Ba/Al profile marks the onset of S1 productivity. In the example shown (Figure 1.9), the grey colouration is coincident with the slightly increased Fe/Al ratio from 22-36 cm, while the Ba/Al profile indicates the beginning of the productivity pulse which includes S1 at 28 cm. This interpretation is consistent with benthic faunal evidence where increased benthic productivity was observed to occur ~1 ky (equivalent to ~ 3cm in Fig. 1.9) before true sapropel formation (Rohling *et al.* 1997).

The fact that a similar grey pyritised zone is not observed *above* sapropels probably indicates either that (i) after sapropel formation, the presence of bottom water O_2 oxidises any upwards migrating HS^-, or (ii) by the time a sapropel is buried it is no longer generating sulfide, or at least is generating it at an insufficient rate, to produce excess sulfide available to diffuse out of the sapropel against the upwards pore water Fe^{2+} flux (Passier *et al.* 1996).

1.7.3.6. Radiocarbon ages for the initiation and cessation of S1.

S1 is the only E. Mediterranean sapropel within the time range where the radiocarbon dating method is precise and well calibrated. From earlier radiometric radiocarbon dating, its duration is usually quoted as 7-9 ky B.P. (Vergnaud-Grazzini *et al.* 1986). These are modal ages, and some earlier S1 radiometric analyses in the literature are likely to have been biased upwards by contamination with older carbonate or terrestrial organic carbon. This has been demonstrated by using the sensitive AMS radiocarbon analysis technique on small, hand-separated fractions which have a clear recent marine origin (Perissoratis and Piper, 1992). In the modern open ocean, the surface ocean reservoir has a radiocarbon age close to 400 conventional radiocarbon years (Bard, 1988; Austin *et al.* 1994). It is yet to be established if this open ocean correction is also applicable the restricted E. Mediterranean basin round which older carbonate rocks are being weathered. At present some workers impose a 400 y surface ocean correction on all radiocarbon ages when citing E. Mediterranean data, while others report the age without modification. The latter approach is taken here, and all subsequent ages quoted are in unmodified conventional radiocarbon years (Stuiver and Polach, 1977).

Fontugne *et al.* (1994) have summarised the large number of radiocarbon age determinations undertaken around S1 units. These workers find a reasonably consistent mean age of 8.97 conventional radiocarbon ky for the base of S1 over a wide area, but note a much wider spread for

the upper S1 interface, between 6.37 and 8.03 conventional radiocarbon ky. This spread in ages for the upper interface is at least in part be due to the oxidation of the upper reaches of S1 already discussed.

A critical geochemical level was identified earlier at which there is a coincidence of the upper Mn/Al peak maximum, the beginning of the downwards Fe/Al and lower Mn/Al oxidation front peaks, and the end of the productivity pulse indicated by the Ba/Al profile (15 cm depth in Fig. 1.9). Thomson *et al.* (1995) dated the sediments hosting this critical level in two different cores at 5.2 and 5.4 ky, and inferred that this was the time at which both deep water reventilation occurred and at which the S1 palaeoproductivity pulse ended (Fig. 1.10). This interpretation has been criticised by Rohling *et al.* (1997) who interpreted benthic foraminiferal evidence in an Adriatic core to place the end of anoxic bottom water conditions at 6.3 ky. These workers also noted, however, that benthic productivity values then remained high between 6.3 and 5.2 ky, after which well-oxygenated, oligotrophic conditions similar to the present were established. It appears in fact that the youngest ages so far determined on dark C_{org}-rich S1 material are ~6.3 ky (Perissoratis and Piper, 1992; Jorissen *et al.* 1993; Fontugne *et al.* 1994). While this is considerably younger than the Vergnaud-Grazzini *et al.* (1986) estimate for the end of S1 from radiometric data, it is not as young as that suggested by the geochemical interpretation.

The fact that the Ba/Al values remain aberrantly high between 6.3 and 5.3 ky in the central basin is good evidence that the sediments laid down during that period once contained high enhanced C_{org} contents (Figs. 1.9 and 1.11). It is unclear at present whether the major difference between the geochemical and micropalaeontological interpretations is a minor bioturbation effect (Thomson *et al.* 1995) or a real regional effect. To date, geochemical work has been undertaken at central basin locations where benthic foraminifera are rare in the sediments, presumably because of low C_{org} fluxes reaching the sea floor when conditions are oligotrophic and because of bottom water anoxia during sapropel times. The benthic foraminiferal work has been undertaken in marginal basins where sediment accumulation rates and C_{org} fluxes reaching the sea floor are higher and as a consequence benthic foraminifera are more abundant, although they are absent during sapropel formation when bottom waters are again inferred to be anoxic. The Adriatic Sea, where the Rohling *et al.* (1997) study was undertaken, is one of the E. Mediterranean deep water formation areas (Wust, 1961), and deep water reventilation may have penetrated progressively into the basin at the end of the sapropel formation episode. There is no certainty that the rates and times of initiation and cessation of sapropel formation of S1 were exactly simultaneous over the entire E. Mediterranean, and AMS radiocarbon dating potentially has the precision to resolve this problem in future work.

A final caveat for future radiocarbon dating of the S1 unit concerns sample selection. The dark colour of the visual S1 unit is often used to guide sample selection, on the assumption that it marks a clear change in the nature of the sediment deposited. Besides the effects of oxidation of the upper surface reviewed above, this colouration is not exactly coincident with either the > 2% C_{org} criterion of the Kidd *et al.* (1978) definition, nor with the enhanced Ba/Al values at the base of S1 which represent the initiation of the productivity pulse. The S1 Ba/Al profile may provide an objective criterion to resolve this uncertainty. If areal comparisons of the ages of the same stages of the productivity pulse producing S1 are sought, it would be better to sample for radiocarbon dating in future work with reference to the Ba palaeoproductivity profile, rather than to the C_{org} profile or residual visual S1 evidence.

1.7.3.7. Does productivity or preservation control sapropel formation?

It is a matter of contention whether the occurrence of C_{org}-rich marine sediments in the sedimentary record is primarily controlled by productivity (Pedersen and Calvert, 1990; Calvert and Pedersen 1992), or by preservation. The more traditional view is that enhanced preservation of C_{org} deposited under euxinic water columns is a dominant factor (Demaison and Moore, 1980).

Calvert (1983) pointed out that it was unlikely that the most C_{org}-rich sapropels could be formed at present-day C_{org} sedimentation fluxes, so that increased productivity is a prerequisite for sapropel formation. The quasi-Gaussian shape of the S1 Ba profile discussed above (Figures 1.9 and 1.11), along with ^{15}N evidence (Calvert *et al.* 1992), is taken as good evidence of enhanced productivity. On the other hand, Passier *et al.* (1996) demonstrated from C/S/Fe evidence that S1 had the characteristics expected of a sediment laid down in euxinic conditions. Laminations are present and benthic foraminifera absent in many S1 occurrences, suggesting complete bottom water anoxia rather than merely low oxygen conditions during at least part of the period of S1 formation (e.g. Rohling *et al.* 1997). The geochemical model for post-depositional modification of S1 also requires an anoxic or low O_2 water column during sapropel formation, followed by a reventilation to higher O_2 levels after 5.2 ky. The evidence is therefore consistent with both high productivity and bottom water anoxia during at least part of the period of sapropel formation.

The geochemical interpretation, supported by the pore water O_2 evidence of van Santvoort *et al.* (1996), implies that sapropel C_{org} must be readily oxidised by oxygen. The long persistence of sapropels during deeper burial, however, suggests the rate of remineralisation by less-efficient electron acceptors when buried into anoxic conditions must be lower. The initial rates of

remineralisation of freshly-deposited marine C_{org} are similar under oxic and sulphate reducing conditions, although Canfield (1994) believes that this is not necessarily the case with older C_{org} which may become more refractory through polymerisation or the buildup of metabolites. In the case of sapropels there is the further possibility that sulfidisation of the C_{org} may make it less reactive.

1.7.4. Conclusions

It has recently become evident that post-depositional oxic diagenesis exerts a major control in the modification and consequent appearance of S1 units. This results in the removal of the high C_{org} content evidence from the upper level of the original unit, and for extreme cases in the removal of all visual evidence of S1 (Thomson *et al.* 1995). The element Ba appears to act as a satisfactory proxy from which the original C_{org} profile can be reconstructed, so long as sulphate reduction does not draw down pore water sulphate levels below the critical barite solubility product value. By analogy, similar oxidation effects are likely to have affected older sapropel layers after deposition. Diagenetic peaks in I and Se are proposed as permissive indicators of an active oxidation front (likely in S1 only), and Se alone is suggested as a diagnostic tool to indicate the former action of an oxidation front in older sapropels. The grey "protosapropel" layer underlying S1 is also a diagenetic effect, caused by pyritisation rather than any productivity changes. Early diagenetic alterations must be taken into account when interpreting the significance of colour layering around a sapropel unit, and to guide sampling of the entire sapropel formation episode for dating and other investigations.

1.7.5. Acknowledgements.

The work reported here was supported by the European Union Marine Science and Technology programme, contracts 900022C and MAS2-CT93-0051. Preparation of this paper was enabled by British Council/NWO Joint Research Project 235, and the final version benefited from the comments of the two journal referees.

1.7.6. References.

Anastasakis G.C. and Stanley, D.J. (1984) Sapropels and organic-rich variants in the Mediterranean: sequence development and classification. In *Fine-Grained Sediments: Deep-Water Processes and Facies* (D.A.V Stow and D.J.W. Piper, Eds) Geological Society Special Publication No.15 497-510.

Antoine, D., Morel, A. and Andre, J.M. (1995). Algal pigment distribution and primary production in the eastern Mediterranean as derived from coastal zone color scanner observations. Journal of Geophysical Research, 100, 16193-16209.

Austin, W.E.N., Bard, E., Hunt, J.B., Kroon, D. and Peacock, J.D. (1994). The ^{14}C age of the Icelandic Vedde Ash: Implications for the Younger Dryas marine reservoir age correction. Radiocarbon 37, 53-62.

Bard, E. (1988). Correction of accelerator mass spectrometry ^{14}C ages measured in planktonic foraminifera: Paleoceanographic implications. Paleoceanography, 3, 635-645.

Berner, R.A. (1981) A new geochemical classification of sedimentary environments. J. Sediment. Petrol. 51, 359-365.

Bethoux, J.P. (1989). Oxygen consumption, new production, vertical advection and environmental evolution in the Mediterranean Sea. Deep-Sea Research, 36, 769-781.

Bostrom, K., Joensuu, O., Moore, C., Bostrom, B., Dalziel, M. and Horowitz, A. (1973) Geochemistry of barium in pelagic sediments. Lithos 6, 159-174.

Brumsack, H.J. (1986) The inorganic geochemistry of Cretaceous black shales (DSDP Leg 41) in comparison to modern upwelling sediments from the Gulf of California. In "North Atlantic Paleoceanography"(Eds. C.P. Summerhayes and N.J. Shackleton) Geol. Soc. Spec. Publ. No.21, pp. 447-462.

Calvert, S.E. (1983) Geochemistry of Pleistocene sapropels and associated sediments from the Eastern Mediterranean. Oceanologica Acta, 6, 255-267.

Calvert, S.E. and Pedersen, T.F. (1992) Organic carbon accumulation and preservation in marine sediments: How important is anoxia? In "Productivity, Accumulation and Preservation of Organic

Matter in Recent and Ancient Sediments." (eds. J.K. Whelan and J.W. Farrington) Columbia Univ. Press, New York, pp 231-263.

Calvert, S.E., Nielsen, B. and Fontugne, M. R. (1992) Evidence from nitrogen isotope ratios for enhanced productivity during formation of eastern Mediterranean sapropels. Nature, 359, 223-225.

Canfield, D.E. .(1994). Factors influencing organic carbon preservation in marine sediments. Chemical Geology, 114, 315-329.

Cita, M.B., Vergnaud-Grazzini, C., Robert, C., Chamley, H., Ciaranfi, N. and d'Onofrio, S. (1977). Paleoclimatic record of a long deep-sea core from the eastern Mediterranean. Quaternary Research, 8, 205-235.

Cita, M.B., Aghib, F., Arosio, S., Folco, E., Sarto L., Erba, E. and Rizzi, A. (1989). Bacterial colonies and manganese micronodules related to fluid escape on the crest of the Mediterranean Ridge. Riv. It. Paleontol. Stratigr., 95, 315-336.

De Capitani, L. and Cita, M.B. (1996). The 'marker-bed' of the Mediterranean Ridge diapiric belt: geochemical characteristics. Marine Geology, 132, 215-225.

De Lange, G.J., Middelburg, J.J. and Pruysers, P.A. (1989) Discussion: Middle and Late Quaternary depositional sequences and cycles in the eastern Mediterranean. Sedimentology, 36, 151-156.

Demaison, G.J. and Moore, G.T. (1980) Anoxic environments and oil source bed genesis. Bulletin of the American Association of Petroleum Geologists 64, 1179-1209.

Dymond, J. and Collier, R. (1996). Particulate barium fluxes and their relationships to biological productivity. Deep-Sea Research, II, 43, 1283-1308.

Dymond, J., Suess, E. and Lyle, M. (1992) Barium in deep-sea sediment: A geochemical proxy for paleoproductivity. Paleoceanography, 7, 163-181.

Emeis, K.-C., and the Shipboard Scientific Party, (1996). Paleoceanography and sapropel introduction. Proceedings of the Ocean Drilling Program, Initial Reports, 160, 21-28.

Emerson, S. and Hedges, J.I. (1988). Processes controlling the organic carbon content of open ocean sediments. Paleoceanography, 3, 621-634.

Fontugne, M., Arnold, M., Labeyrie, L., Paterne, M., Calvert, S.E. and Duplessy, J-C. (1994). Paleoenvironment, sapropel chronology and Nile River discharge during the last 20,000 years as indicated by deep-sea sediment records in the Eastern Mediterranean. In "Late Quaternary Chronology and Paleoclimates of the Eastern Mediterranean" (ed. O. Bar-Yosef and R.S. Kra); Radiocarbon, pp.75-88.

Francois, R., Honjo, S., Manganini, S.J. and Ravizza, G.E. (1995). Biogenic barium fluxes to the deep sea: implications for paleoproductivity reconstruction. Global Biogeochemical Cycles, 9, 289-303.

Hieke, W., (1976) Problems of eastern Mediterranean Late Quaternary stratigraphy - a critical re-evaluation of the literature. "Meteor" Forschungsergeb., Reihe C, 24, 68-88.

Higgs, N.C., Thomson, J., Wilson, T.R.S. and Croudace, I.W. (1994) Modification and complete removal of eastern Mediterranean sapropels by postdepositional oxidation. Geology 22, 423-426.

Jorissen, F.J., Asioli, A., Borsetti, A.M., Capotiondi, L., de Visser, J.P., Hilgen, F.J., Rohling, E.J., van der Borg, K., Vergnaud Grazzini, C. and Zachariasse, W.J. (1993) Late Quaternary central Mediterranean biochronology. Mar. Micropaleontol. 21, 169-189.

Kennedy, H.A. and Elderfield, H. (1987). Iodine diagenesis in non-pelagic deep-sea sediments. Geochim. Cosmochim. Acta, 51, 2505-2514.

Kidd, R.B., Cita, M.B. and Ryan, W.B.F. (1978). Stratigraphy of eastern Mediterranean sapropel sequences recovered during DSDP Leg42A and their paleoenvironmental significance. Initial Reports of the Deep Sea Drilling Project, Vol. 42A, 421-443.

Kuniholm, P.I., Kromer, B., Manning, S.W., Newton, M., Latini, C.E. and Bruce, M.J. Anatolian tree rings and the absolute chronology of the eastern Mediterranean, 2200-718 BC. Nature, 381, 780-783.

Langereis, C.G., Dekkers, M.J., van Santvoort, P.J.M. and de Lange, G.J. (1997). Magnetostratigraphy and astronomical calibration of the last 1.1 Myr from an eastern

Mediterranean piston core and dating of short events in the Brunhes. Geophysical Journal International, 129, 75-94.

Mangini, A., Eisenhauer, A. and Walter, P. (1991) A spike of CO_2 in the atmosphere at glacial-interglacial boundaries induced by rapid deposition of manganese in the oceans. Tellus, 43B, 97-105.

Murat, A. and Got, H. (1987) Middle and Late Quaternary depositional sequences and cycles in the eastern Mediterranean. Sedimentology, 34, 885-899.

Murat, A. and Got, H. (1989) Discussion: Middle and Late Quaternary depositional sequences and cycles in the eastern Mediterranean. Sedimentology, 36, 156-158.

Passier, H.F., Middelburg, J.J., van Os, B.J.H. and de Lange, G.J. (1996). Diagenetic pyritisation under eastern Mediterranean sapropels caused by downward sulphide diffusion. Geochimica et Cosmochimica Acta, 60, 751-763.

Pedersen, T.F. and Calvert, S.E. (1990) Anoxia vs. productivity: What controls the formation of organic-carbon-rich sediments and sedimentary rocks? American Association of Petroleum Geologists Bulletin 74, 454-466.

Perissoratis, C. and Piper, D.J.W. (1992) Age, regional variation, and shallowest occurrence of S1 sapropel in the Northern Aegean Sea. Geo-Marine Letters 12, 49-53.

Price, N.B. and Calvert, S.E. (1977) The contrasting geochemical behaviours of iodine and bromine in sediments from the Namibian Shelf. Geochim. Cosmochim. Acta, 41, 1769-1775.

Pruysers, P.A., de Lange, G.J. and Middelburg, J.J. (1991) Geochemistry of eastern Mediterranean sediments: Primary sediment composition and diagenetic alterations. Marine Geology, 100, 137-154.

Pruysers, P.A., de Lange, G.J., Middelburg, J.J. and Hydes, D.J. (1993) The diagenetic formation of metal-rich layers in sapropel-containing sediments in the eastern Mediterranean. Geochim. Cosmochim. Acta, 57, 527-536.

Rohling, E.J. (1994). Review and new aspects concerning the formation of eastern Mediterranean sapropels. Mar. Geol. 122, 1-28.

Rohling, E.J., Jorissen, F.J. and de Stigter, H.C. (1997). 200 year interruption of Holocene sapropel formation in the Adriatic Sea. J. Micropal., 16, 97-108.

Rossignol-Strick, M., Nesteroff, W., Olive, P. and Vergnaud-Grazzini, C. (1982). After the deluge: Mediterranean stagnation and sapropel formation. Nature 295, 105-110.

Ryan, W.B.F. and Cita, M.B. (1977) Ignorance concerning episodes of ocean-wide stagnation. Mar. Geol. 23, 197-215.

Schlitzer, R., Roether, W., Oster, H., Junghans, H-G., Hausmann, M., Johannsen, H. and Michelato, A. (1991). Chlorofluoromethane and oxygen in the eastern Mediterranean. Deep-Sea Research, 38A, 1531-1551.

Stanley, D.J. (1985) Mud redeposition and problems of assessing microfossil, isotopic and radiocarbon data in the Mediterranean. Mar. Geol., 62, 381-389.

Stuiver, M. and Polach, H.A. (1977), Discussion: Reporting of ^{14}C data. Radiocarbon, 19, 355-363.

Ten Haven, H.L., De Leeuw, J.W., Schenk, P.A. and Klaver, G.T. (1987) Geochemistry of Mediterranean sediments. Bromine/organic carbon and uranium/organic carbon ratios as indicators for different sources of input and post-depositional oxidation, respectively. Organic Geochem., 13, 255-261.

Thomson, J., Higgs, N.C., Croudace, I.W., Colley, S. and Hydes, D.J. (1993). Redox zonation of elements at an oxic/post-oxic boundary in deep-sea sediments. Geochim. Cosmochim. Acta, 57, 579-595.

Thomson, J., Higgs, N.C., Wilson, T.R.S., Croudace, I.W., De Lange, G.J. and van Santvoort, P.J.M. (1995). Redistribution and geochemical behaviour of redox-sensitive elements around S1, the most recent eastern Mediterranean sapropel. Geochim. Cosmochim. Acta 59, 3487-3501.

Thomson, J., Jarvis, I., Green, D.R.H. and Green, D.A. and Clayton, T. (1998). Mobility and immobility of redox-sensitive elements in deep-sea turbidites during shallow burial. Geochimica et Cosmochimica Acta, 62,643-656.

Torres, M.E., Brumsack, H.J., Bohrmann, G. and Emeis, K.C. (1996). Barite fronts in continental margin sediments: a new look at barium remobilization in the zone of sulfate reduction and formation of heavy barites in diagenetic fronts. Chemical Geology, 127, 125-139.

Troelstra, S.R., Ganssen, G.M., van der Borg, K. and de Jong, A.F.M. (1991). A Late Quaternary stratigraphic framework for Eastern Mediterranean sapropel S1 based on AMS ^{14}C dates and stable oxygen isotopes. Radiocarbon 33, 15-21.

van Os, B.J.H., Middelburg, J.J. and de Lange, G.J. (1991) Possible diagenetic mobilisation of barium in sapropelic sediment from the eastern Mediterranean. Mar. Geol., 100, 125-136.

van Santvoort , P.J.M., De Lange, G.J., Thomson, J., Cussen, H., Wilson, T.R.S., Krom, M.D. and Strohle, K. (1996). Active post-depositional oxidation of the most recent sapropel (S1) in sediments of the eastern Mediterranean Sea. Geochim. Cosmochim. Acta 60, 4007-4024.

Vergnaud Grazzini, C., Devaux, M. and Znaidi, J. (1986) Stable isotope "anomalies" in Mediterranean Pleistocene records. Marine Micropaleontology 10, 35-69.

Wignall, P.B. (1994). Black shales. (Oxford Monographs on Geology and Geophysics 30) Oxford: University of Oxford Press. 127pp.

Wilson, T.R.S., Thomson, J., Colley, S., Hydes, D.J., Higgs, N.C. and Sorensen, J. (1985) Early organic diagenesis: The significance of progressive subsurface oxidation fronts in pelagic sediments. Geochim. Cosmochim. Acta 49, 811-822.

Wilson, T.R.S., Thomson, J., Hydes, D.J., Colley, S., Culkin, F. and Sorensen, J. (1986) Oxidation fronts in pelagic sediments: Diagenetic formation of metal-rich layers. Science, 232, 972-975.

Wust, G. (1961). On the vertical circulation of the Mediterranean Sea. J. Geophys. Res. 66, 3261-3271.

Figure Captions.

Figure 1.8. Photograph of box core UM42 (from 1375 m water depth on Medina Rise at 34º57'N, 17º51'E). In this core, from the top down, the upper Mn-rich horizon is at 12-15 cm, the Fe- and second Mn-rich horizon is at 15-21 cm, the C_{org} -rich S1 horizon is at 21-23 cm and the grey underlying "protosapropel" horizon is present from 23cm to the base of the core at 38 cm.

Figure 1.9. Concentration versus depth data for C_{org}, S, Ba, Fe, Mn, I and Se in core MC12 (33º23.7'N, 25º01.3'E, 2211m; Thomson *et al.* 1995). Data except those for C_{org} and S are expressed as weight ratios to Al to minimise the effects of fluctuations in $CaCO_3$ content; and the ratios for Ba, I and Se have been multiplied by 10^4. The shaded area from 15-28 cm represents the inferred depth of the entire increased productivity episode which produced S1, based on the Ba profile. Note that the upper boundary of this zone coincides with the upper Mn peak maximum and the start of the downwards increase in the Fe/Al ratio (upper solid line). The horizontal line at 22 cm marks the present limit of oxidation, with higher Mn, Fe and I values above and higher C_{org}, S and Se values below. High C_{org}, S, Ba/Al and Fe/Al return to baseline values at around 28 cm (solid line). The visual dark S1 unit here is ~6 cm thick (22- ~28 cm), but only 4 cm (22-26 cm) exceeds the 2% C_{org} criterion. The grey "protosapropel" colouration occurs in this core from 28-36 cm and its base is marked (lowest solid line on the Fe/Al profile only).

Figure 1.10. Representation of post-depositional oxidation of S1 discussed in the text, in terms of the reactive fraction only of certain critical elements.

Left panel: 5.3 ky ago, the productivity pulse responsible for S1 has just ended, there is a Mn oxyhydroxide peak at the sediment/water interface, and the bottom water O_2 concentration has just increased from low to much higher values.

Middle panel: sediment accumulation has moved the sediment surface upwards, the upper Mn peak has been spread by bioturbation, and the higher (constant) bottom water O_2 level supports a downwards oxidation flux into the sediments which remineralises sapropel C_{org} and forms the lower Mn peak. Reactive fractions of I and Se form peaks immediately above and below the limit of oxidation, respectively.

Right panel: At present, accumulation continues to move the sediment/water interface upwards, the upper Mn peak is now unchanging below the level of bioturbation, but oxidation of sapropel C_{org} and formation of the lower Mn peak continues at a slower rate. The peaks of I and Se continue to move downwards to maintain the same relative positions with the oxidation front, with some augmentation from continued sapropel oxidation.

Figure 1.11. The use of S1 Ba profiles to reconstruct the original C_{org} levels in S1, as proposed by van Santvoort *et al.* (1996).

Upper panel: A similar quasi-Gaussian shape is seen in the Ba profiles observed in and above the present visual S1 unit in three different cores. The near-constant Ti profiles are consistent with an unchanging detrital phase in these cores.

Middle panel: Plot of corresponding C_{org} data against all Ba data from the three cores in the upper panel. Data in set 3 correspond to the increase in Ba observed along with C_{org} in S1, data in set 1 all correspond to samples above the visual S1 with high Ba but with low (oxidised) C_{org} values. The two points in set 2 are from mixed samples at the upper S1 interface with characteristics of sets 1 and 3.

Lower panel: Measured C_{org} in the three cores and "original level" S1 C_{org} values reconstructed from the Ba:C_{org} relationship of set 3 in the middle panel (dashed line).

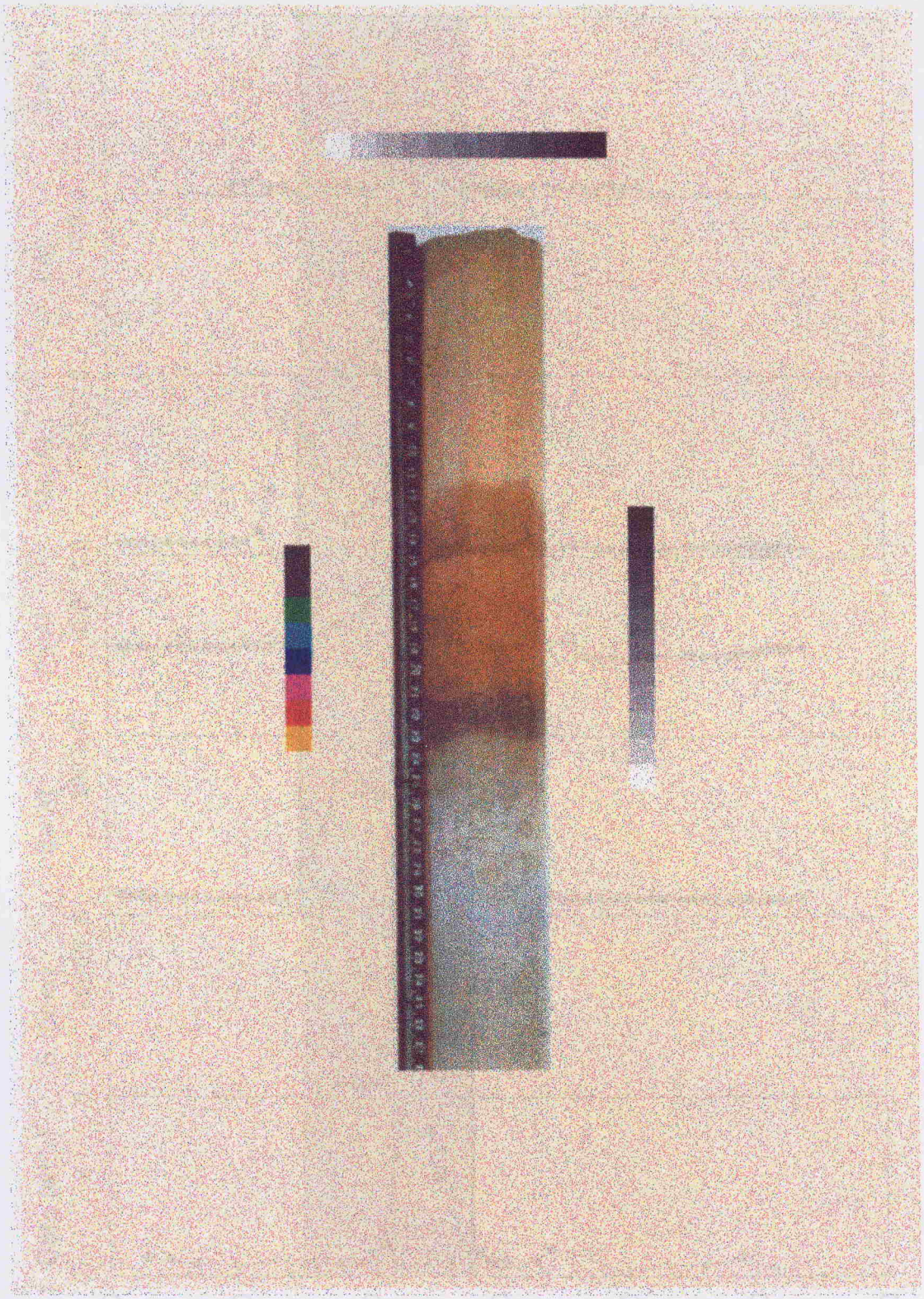

Figure 1.8

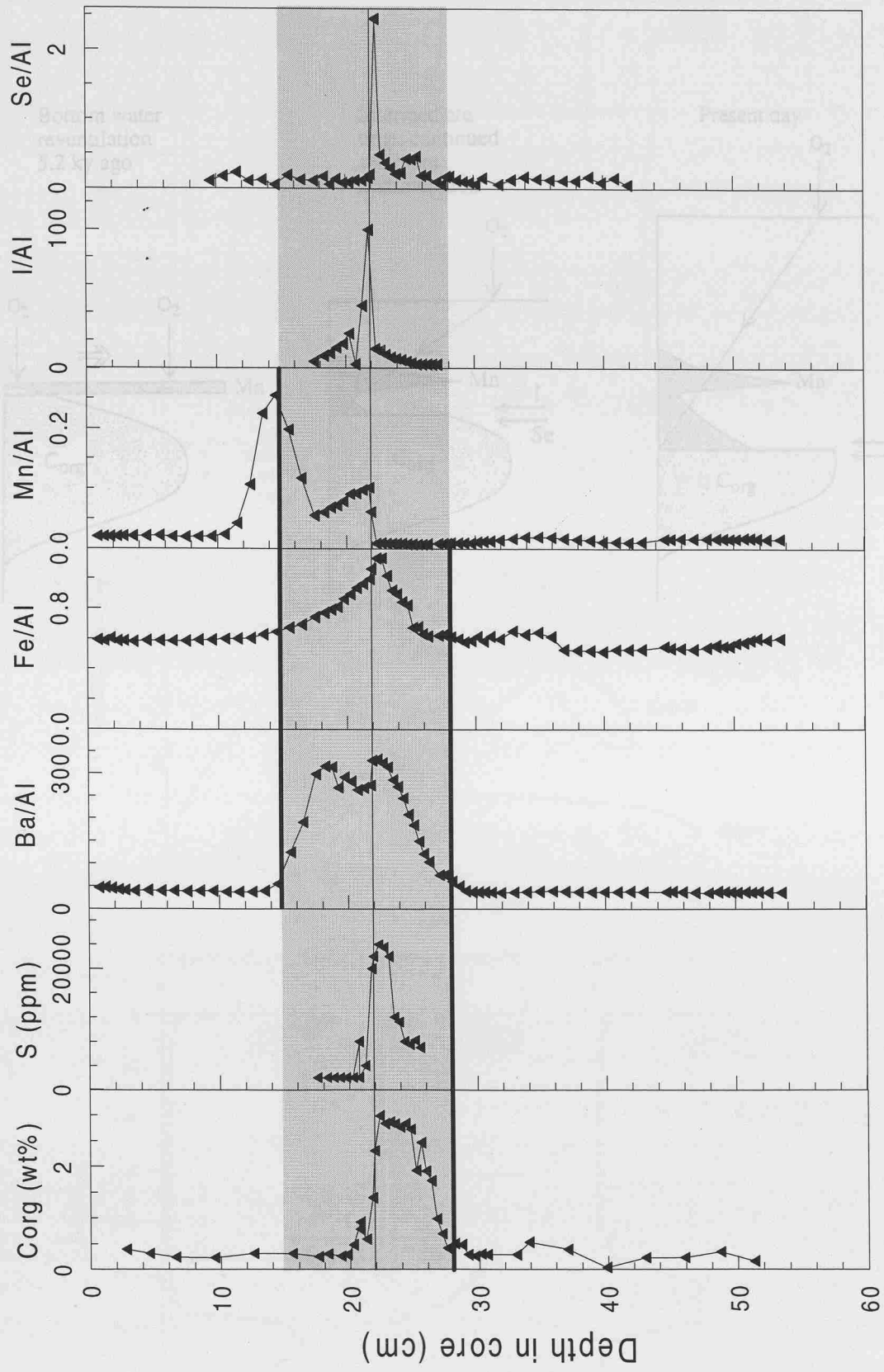
Corg (wt%)
0
2
S (ppm)
0
20000
Ba/Al
0
300
Fe/Al
0.0
0.8
Mn/Al
0.0
0.2
I/Al
0
100
Se/Al
0
2
0
10
20
30
40
50
60
Depth in core (cm)

Figure 1.9

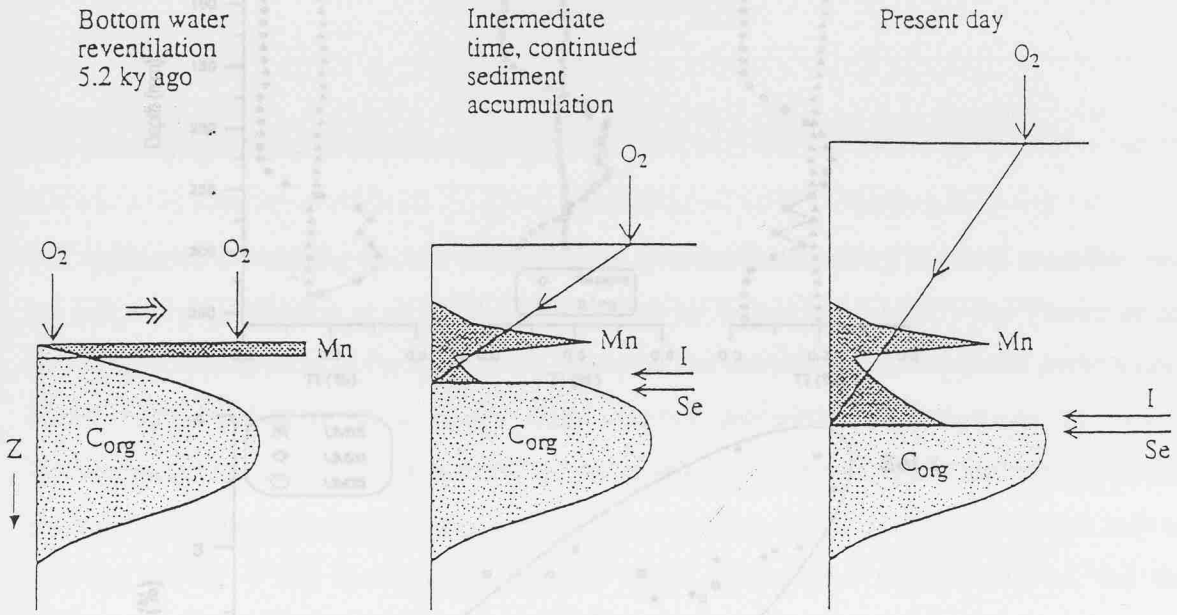
Bottom water reventilation 5.2 ky ago
Intermediate time, continued sediment accumulation
Present day
O2
O2
O2
O2
Mn
Mn
Mn
I
Se
I
Se
Z
Corg
Corg
Corg

Figure 1.10

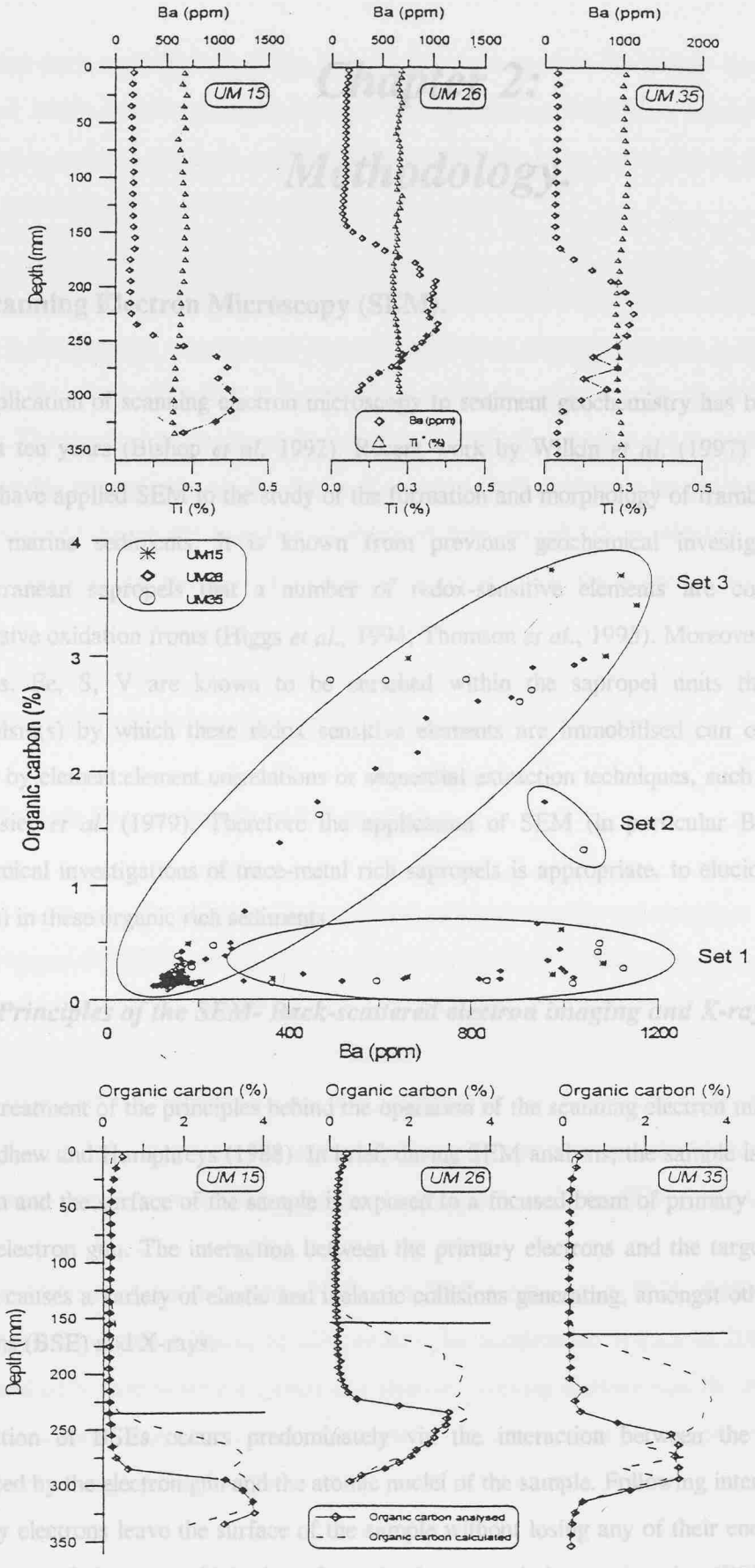
Ba (ppm)
UM 15
UM 26
UM 35
Depth (mm)
Ti (%)
Ba (ppm)
Ti * (%)
UM15
UM26
UM35
Set 3
Set 2
Set 1
Organic carbon (%)
Ba (ppm)
Organic carbon analysed
Organic carbon calculated

Figure 1.11

Chapter 2:
Methodology.

2.1. Scanning Electron Microscopy (SEM).

The application of scanning electron microscopy to sediment geochemistry has been extensive over the past ten years (Bishop *et al.* 1992). Recent work by Wilkin *et al.* (1997) and Passier *et al.* (1997) have applied SEM to the study of the formation and morphology of framboidal pyrite within anoxic marine sediments. It is known from previous geochemical investigations on eastern Mediterranean sapropels that a number of redox-sensitive elements are concentrated around progressive oxidation fronts (Higgs *et al.*, 1994; Thomson *et al.*, 1995). Moreover, elements such as Mo, As, Fe, S, V are known to be enriched within the sapropel units themselves, but the mechanism(s) by which these redox sensitive elements are immobilised can only be inferred at present by element:element correlations or sequential extraction techniques, such as those described by Tessier *et al.* (1979). Therefore the application of SEM (in particular BSEI and EDS) to geochemical investigations of trace-metal rich sapropels is appropriate, to elucidate the controlling phase(s) in these organic rich sediments.

2.1.2. Principles of the SEM- Back-scattered electron imaging and X-ray analysis.

A full treatment of the principles behind the operation of the scanning electron microscope are given in Goodhew and Humphreys (1988). In brief, during SEM analysis, the sample is placed into a high vacuum and the surface of the sample is exposed to a focused beam of primary electrons generated by an electron gun. The interaction between the primary electrons and the target atoms within the sample causes a variety of elastic and inelastic collisions generating, amongst others, back-scattered electrons (BSE) and X-rays.

Generation of BSEs occurs predominately via the interaction between the primary electrons generated by the electron gun and the atomic nuclei of the sample. Following interaction, some of the primary electrons leave the surface of the sample without losing any of their energy, and it is these back-scattered electrons which gives rise to back scattered electron imaging (BSEI). The number of BSEs produced in this way is a function of the number of collisions between the incident electrons and sample nuclei, which is fundamentally controlled by the mean atomic number of the element

composing the sample. Therefore, the greater the atomic number, the greater the numbers of BSEs produced, which leads to a brighter image. The application of BSEI to sapropel geochemistry is important in order to highlight or differentiate between the heavy metal phases (such as sulphides) and the organic matrix in which these phases are contained.

A further consequence of the bombardment of high-energy primary electrons with that of the sample surface is the potential to generate X-rays. If the incident electron transfers a sufficient amount of energy to the target atom then it is possible to ionise the atom via the ejection of an inner shell electron. The target atom, in this excited state, is intrinsically unstable and instantaneously decays to a more stable ground state via the decay of an outer shell electron to an inner orbital. The excess energy released during the transition of electrons between orbitals is released as X-rays, and the energy released is characteristic of a particular element. Using the generated X-rays, it is therefore possible to identify both the type of element present and also quantify how much of a particular element is present within the sample. It is hoped that the application of both the BSEI and X-ray analysis will discriminate how trace metals are enriched within the sapropel, S1.

2.1.3. Sample Preparation for SEM analysis.

In order to preserve the sediment fabric and also to limit/minimise any change in oxidation, samples were prepared for SEM analysis from wet sediment. After sectioning the core, wet samples were initially dried under vacuum for a period of 48 hours in a vacuum oven. Samples were then impregnated with epoxy resin and left to harden for a further 48 hours before being mounted on to frosted glass slides. The samples were then sectioned to give a specimen thickness of ~200μm, and given a final polish using 1μm diamond paste. Samples were then coated with carbon (~100Å thick) in a vacuum evaporator to minimise charges on the specimen during SEM analysis.

Samples were examined using the BSEI and EDS modes on a JEOL 6400 scanning electron microscope fitted with a Tracor II EDS system. An acceleration voltage of 20kV was used at all times, and EDS spectra were acquired at a standard working distance (i.e. the distance between the detector and sample) of 15mm, a take off angle of 30°, and a probe current of $6*10^{-10}$A. Each of the EDS spectra was acquired for 60s.

2.2. X-Ray Fluorescence Spectrometry (XRF).

X-ray fluorescence spectrometry (XRF) is a widely-used non-destructive technique for the routine determination of major and trace elements. An XRF spectrometer uses primary radiation from an X-ray tube to induce secondary X-ray emission (fluorescence) from the sample. Emission of an X-ray from a sample occurs when sufficiently energetic primary x-ray photons cause the ejection of an electron from the sample atom. The 'excited atom' is intrinsically unstable and returns to a more stable 'ground state' via the transition of electrons from the outer shells to inner ones. Each electron transfer represents a loss in potential energy of the atom, and this energy appears as a photon. In analytical determinations, the intensity of this characteristic secondary fluorescence radiation (after correction for enhancement/absorption effects) is proportional to the atomic concentration of the representative element. This allows for the quantitative determination of samples for most elements from Na to U in the concentration range of 1ppm to 100%.

2.2.1. Trace Element Determination.

Samples were prepared for trace element determination by XRF as pressed powder pellets. Work by Tertian and Claisse (1982) has demonstrated the effects of particle size on the determination of trace elements during XRF. Essentially, these workers have shown experimentally that when particles are smaller than a certain size, the sample behaves like an homogenous specimen of the same composition. The critical particle size at which the heterogeneity effects are minimised has been shown to be <30μm. Therefore, in order to minimise sample heterogeneity during XRF, samples were ground using a TEMA® tungsten carbide swing mill for five minutes to give a particle diameter of ~ 20μm.

Because of the limited availability of sample for XRF analysis in this work, approximately 3g of dried and ground sediment was used to make the pressed powder pellets. Pellets were made by quantitatively transferring the sample into a stainless steel mould and compacting the sediment (without binder) between two stainless steel dies under a pressure of 12 tons $inch^{-2}$ using a hydraulic pump. The compaction process produced powder pellets with a diameter of 35mm and thickness of 5-8 mm. The precision of trace element analysis was determined to be about 5% r.s.d (relative standard deviation), with detection limits between 1-5ppm for most trace elements under consideration (table 2.1).

2.2.2 Major Element Determination.

For the determination of major elements such as Al, Fe, K, Mn, Na, P, Si and Ti samples were prepared as fused glass discs. Essentially the fusion procedure consists of heating a mixture of sample and flux at a high temperature so that the flux melts and dissolves the sample.

Prior to fusion, samples were ignited in a furnace at a temperature of 1000°C for 12 hours in order to remove the volatile components such as water, carbon dioxide and sulphides from the sample, which would inevitably affect the summation of analytical results to 100%. Calcination of the samples prior to fusion ensures the removal of both organic matter and sulphides which are known to damage Pt-Au crucibles. Following ignition, 0.4000g of sample was well mixed with 4.0g of a eutectic flux (consisting of 80% lithium metaborate ($LiBO_2$) and 20% lithium tetraborate ($Li_2B_4O_7$)) in a fixed weight ratio of 1 part sample : 10 parts flux. The sample was fused in a non-wetting platinum alloy (Pt- 5% Au) crucible for 10 minutes with constant agitation to ensure complete mixing and dissolution. The resultant melt was poured into a Pt-Au mould to produce a glass disc for XRF analysis. The accuracy of the fusion method was ascertained by preparing the international standard reference material MAG-1 (marine mud from the USGS) and running it with the samples. For elements well above their detection limit the precision was found to be typically less than 1% r.s.d (relative standard deviation).

Both trace and major element determinations were performed using a Philips® PW1400 automatic sequential wavelength dispersive X-ray spectrometer. Matrix corrections (absorption/enhancement effects) were corrected for using equations by De Jong (1979) and also by those supplied by the manufacture (Philips®). The detection limit and counting times for the various elements determined by XRF during this study are shown in Table 2.1.

Element	X-Ray	Possible interferences	L.L.D. (ppm)
As	As Kβ		1
Ba	Ba Lβ	Ce, High As	10
Br	Br Kα		30
Cl	Cl Kα		50
Cr	Cr Kα	V	4
I	I Kα		4
Mo	Mo Kα		3
Ni	Ni Kα		1.5
Nb	Nb Kα	Y	1.5
P	P Kα		30
Pb	Pb Lβ	Bi	1.5
Rb	Rb Kα	High U	1.5
S	S Kα		50
Sr	Sr Kα		1.5
Th	Th Lα	High Pb	2
U	U Lα	High Rb	3
V	V Kα		4
Zn	Zn Kα		1.5
Zr	Zr Kα	Sr	1.5

Table 2.1: Detection limits of both major and trace elements using the Philips® PW1400 automatic sequential wavelength dispersive X-ray fluorescence spectrometer.

2.3. Coulometry.

Coulometry is a routinely-used method enabling the determination of both total organic carbon (Corg) and carbonate in marine sediments. The principle behind the coulometric determination of Corg and $CaCO_3$ is remarkably simple and is centred around measuring the carbon dioxide evolved from a sample either by combustion at 900°C or by acidification. High precision measurement of CO_2 occurs via a coulometer cell that is filled with an aqueous medium containing monoethanolamine and a coulometric pH indicator. A platinum cathode and a silver anode are positioned in the cell and the assembly positioned between a light source and a photodetector in the coulometer. As the CO_2 gas stream passes into the cell, the CO_2 is quantitatively absorbed, reacting with the monoethanolamine to form the titratable hydroxyethylcarbamic acid. This causes the colour indicator to fade from deep blue to colourless. Photodetection monitors the colour change in the solution as a percent transmittance (%T). As the transmittance increases, the titrant current is automatically activated to electrochemically generate base at a rate that is proportional to the %T, which is proportional to the CO_2 generated. When the solution returns to its original colour (original %T of ~29%), the current is switched off. A digital counter records the coulombs of charge required to obtain the original transmittance.

Calcium carbonate was determined in samples using the acidification module CM5130® supplied by UIC™. Approximately 25mg of sample was weighed into aluminium foil crucibles. Samples were then loaded into clean glass vials and acidified by the addition of 5ml of Analar Grade 10% v/v phosphoric acid (H_3PO_4). The calcium carbonate present within the sample reacts with the phosphoric acid generating a gaseous stream of carbon dioxide. The liberated CO_2 is then swept into the coulometer cell via a carrier gas (air, which has been pre-scrubbed using KI and KOH). The counts generated from each sample over a six-minute period were recorded and converted to weight % of $CaCO_3$ for each sediment sample analysed.

The total carbon content for a sample was quantified using the total carbon module CM5012® supplied by UIC™. Approximately 25mg of the sample was weighed into a nickel boat and combusted in a stream of oxygen at a temperature of 900°C for a period of 6 minutes. At this temperature, all of the carbon present (inorganic and organic) will combust to form a stream of CO_2. The CO_2 produced in this way is swept into the coulometer cell via the O_2 carrier gas, and the counts generated over a six-minute period were used to determine the amount of total carbon present. The difference between the CO_2 generated via combustion (i.e. the total carbon present) and that

generated by acidification was assumed to be equal to the amount of organic carbon present in the sediment.

The precision of the coulometric determination of both total carbon and calcium carbonate was assessed using an in-house sediment standard 10549#1K, a turbidite from the Maderia Abyssal Plain. The precision for calcium carbonate determinations was found to be 0.20% (r.s.d) and that of organic carbon to be better than 3%(r.s.d), see Table 2.2 below.

	Mean (n=19) (wt%)	**Relative Standard Deviation (r.s.d. %)**
Organic Carbon (Corg)	0.611 ± 0.07	3.0
Calcium carbonate ($CaCO_3$)	71.55 ± 0.02	0.20

Table 2.2. The precision (mean based on 19 samples and uncertainty at a confidence limit of 95%) of the coulometric method for the determination of $CaCO_3$ and organic carbon in sediments using the Challenger Division for Seafloor Processes in-house standard 10549#1K.

2.4. Atomic Fluorescence Spectroscopy (AFS).

2.4.1. Hydride Generation.

The application of hydride generation coupled with atomic fluorescence spectroscopy has become a powerful tool for the determination of elements such as As, Se, Te and Sb (Corns *et al.* 1993). The principle behind hydride generation relies upon the fact that many of the elements in Groups IVA, VA and VIA of the periodic table are capable of forming covalent, gaseous hydrides which are unstable at high temperatures (Green, 1996). Generation of elements as their hydride forms means that only those elements that are capable of forming hydrides are analysed, thereby removing virtually all matrix interference effects from the sample (Green, 1996). More importantly, removal of hydride elements from the matrix ensures that the spectrum is no longer complex thus making determination easier, and also increasing both the sensitivity and detection limit when compared to other spectrometric techniques.

An automated continuous flow hydride generation system (PSA 10.003 PS Analytical) was used to generate covalent gaseous hydrides. A schematic diagram of the instrumentation used for the determination of Se is shown in figure 2.1.

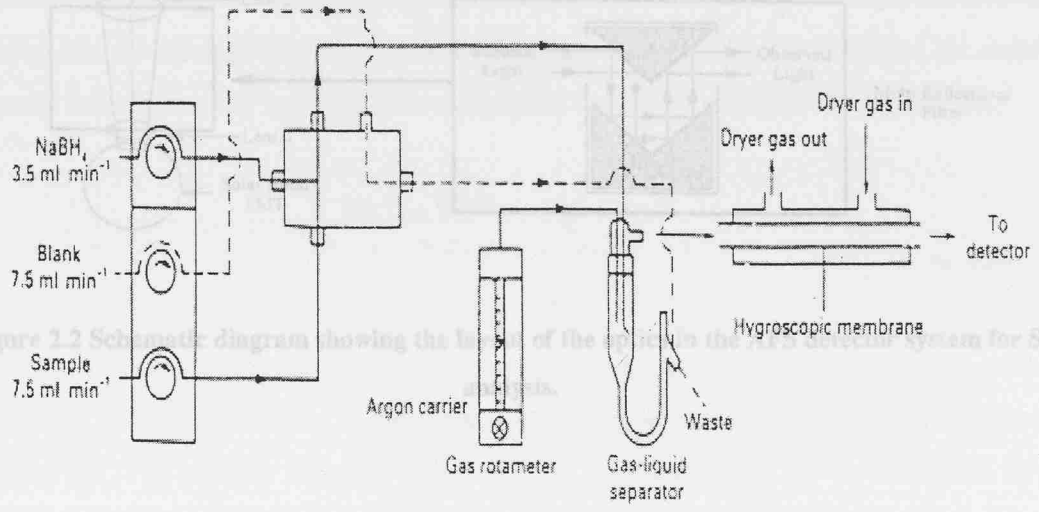

Figure 2.1. Schematic diagram showing how sample, reductant and blank are introduced into the mixing piece in order to generate selenium hydride (H_2Se) for Se analysis by AFS.

Generation of selenium as the hydride form occurs via the addition of the reductant sodium borohydride to an acidified sample (40% v/v HCl) in a mixing valve. A constant-speed peristaltic pump ensures a continual supply of $NaBH_4$ and therefore constant generation of Se as the hydride form. Within the mixing valve selenium as $Se^{IV}O_3^{2-}$ is transformed to covalent gaseous selenium hydride, H_2Se.

The reaction of $NaBH_4$ with HCl produces a steady stream of excess hydrogen gas which provides the fuel for the atom cell (i.e. the hydrogen flame). The solution containing H_2Se, HCl and $NaBH_4$ is passed into a gas/liquid separator and the selenium hydride and excess hydrogen are purged from the liquid phase by a stream of pure argon gas. The excess hydrogen is then flared off, and the H_2Se decomposes to elemental Se. A boosted hollow cathode discharge lamp (BHCDL) focused on the flame provides the excitation source (193nm) for the fluorescence of Se atoms, and a series of collimating lenses and photomultiplier tube orientated at 90° to the excitation source detects subsequent fluorescence (Corns *et al.,* 1993) (figure 2.2).

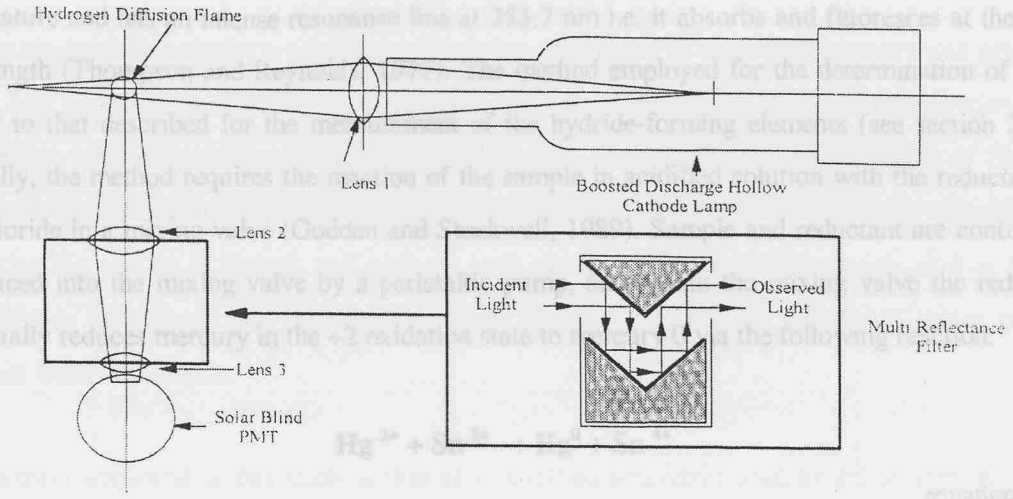

Figure 2.2 Schematic diagram showing the layout of the optics in the AFS detector system for Se analysis.

2.4.2. Cold Vapour- Atomic Fluorescence Spectrometry (CV-AFS).

Mercury determination was carried out using the Merlin Fluorescence detector (PSA 10.023 PS Analytical), and a schematic diagram of the layout of the instrument is shown in figure 2.3.

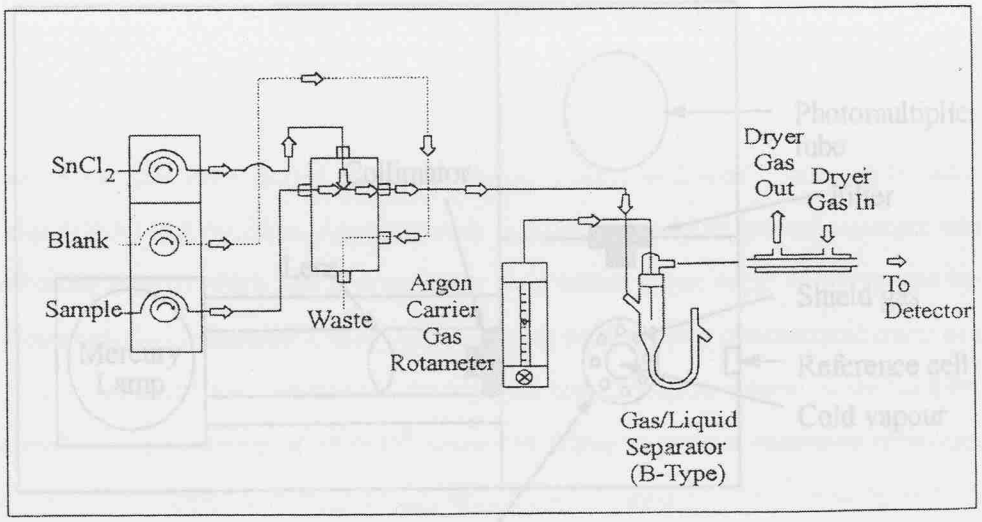

Figure 2.3 Diagram outlining how sample, reductant and blank are mixed in the mixing piece to generate Hg^0 for AFS detection.

Mercury is an ideal element for determination by AFS since elemental Hg is atomic at room temperature and has an intense resonance line at 253.7 nm i.e. it absorbs and fluoresces at the same wavelength (Thompson and Reynolds, 1971). The method employed for the determination of Hg is similar to that described for the measurement of the hydride-forming elements (see section 2.4.1). Basically, the method requires the reaction of the sample in acidified solution with the reductant tin (II) chloride in a mixing valve (Godden and Stockwell, 1989). Sample and reductant are continually introduced into the mixing valve by a peristaltic pump, and within the mixing valve the reductant continually reduces mercury in the +2 oxidation state to mercury 0 via the following reaction.

$$Hg^{2+} + Sn^{2+} \rightarrow Hg^{0} + Sn^{4+}$$

equation 2.1

Both tin(II) chloride solution and mercury vapour (Hg^0) are then immediately fed into a gas/liquid separator and the mercury vapour is separated from the liquid phase via purging with a stream of pure argon gas. The mercury vapour is then swept into the detector and Hg^0 is determined by non-dispersive AFS. The detector is similar to that described for the Excalibur system for the determination of Se, and consists of a high intensity mercury vapour discharge lamp, a series of collimating lenses to focus and collect the light, a 253nm interference filter to achieve wavelength isolation and a conventional photomultiplier tube at 90° to the excitation source (see diagram 2.4).

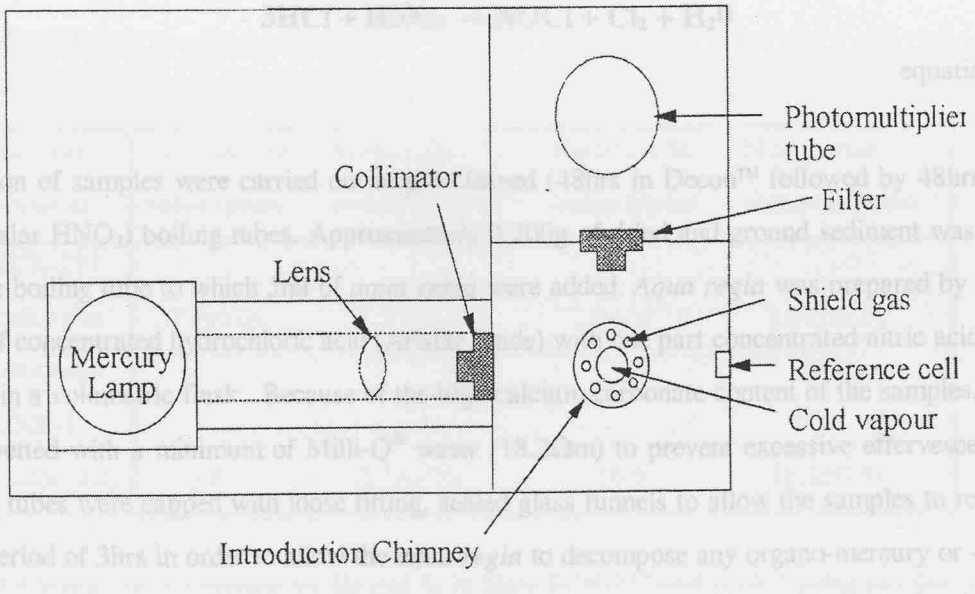

Figure 2.4 Optics layout in the mercury detector (PS Analytical model 10.023)

2.4.3. Sample Preparation.

Sample digestion constitutes a critical step in the determination of both total mercury and selenium. Errors can arise during digestion for example as a result of incomplete extraction of mercury, non-quantitative conversion of organo-selenium and mercury compounds and volatilisation of Hg from the sample as Hg^0. Because of the volatility of both selenium and mercury, the choice of method for extracting Hg and Se is limited, and methods such as dissolution with hydrofluoric acid or fusions with lithium metaborate are inappropriate since this would introduce significant losses of both elements from the sample.

The method employed in this study is that of a modified procedure used by PS Analytical for the determination of selenium and mercury in sediments and soils, and involves the use of *aqua regia* (3:1 HCl : HNO_3).

The effectiveness of an *aqua regia* leach for the extraction of both Se and Hg from marine sediments is thought to be due to the complexing power of the chloride ion and to the catalytic effect of Cl_2 and NOCl (see equation 2.2). Numerous studies in using *aqua regia* for extracting Se and Hg from sediment matrices have shown that this acid is highly effective.

$$\mathbf{3HCl + HNO_3 \rightarrow NOCl + Cl_2 + H_20}$$

equation 2.2

Digestion of samples were carried out in pre-cleaned (48hrs in Decon™ followed by 48hrs in 50% v/v Analar HNO_3) boiling tubes. Approximately 0.200g of dried and ground sediment was weighed into the boiling tube to which 5ml of *aqua regia* were added. *Aqua regia* was prepared by mixing 3 parts of concentrated hydrochloric acid (Aristar grade) with one part concentrated nitric acid (Aristar grade) in a volumetric flask. Because of the high calcium carbonate content of the samples, samples were wetted with a minimum of Milli-Q® water (18.2Ωm) to prevent excessive effervescence. The boiling tubes were capped with loose fitting, sealed glass funnels to allow the samples to reflux cold for a period of 3hrs in order to allow the *aqua regia* to decompose any organo-mercury or -selenium species present within the sample. Boiling tubes were then mounted into aluminium heating blocks and left to reflux at temperature of 80°C for a period of 18hrs. Samples were then left to cool, filtered through a 0.45μm polycarbonate membrane and diluted to 100ml with milli-Q water. This procedure produced solutions that contained 5% *aqua regia* at a dilution of 1/500.

Owing to the low concentrations of mercury in the samples it was found that the 1/500 solutions could be analysed on the Mercury Merlin Fluorescence Detector directly without any further dilution. The fluorescence detector was calibrated using synthetic standards of varying concentrations (prepared from Fisons 1000µg/ml Hg standard) in 5% (v/v) hydrochloric acid. The settings used for the determination of Hg are shown in Table 2.3.

Parameter	Value
$Sn(II)Cl_2$ concentration	2% m/v in 10% HCl
$Sn(II)Cl_2$ flow rate	3.5 ml min^{-1}
HCl concentration	5% HCl
HCl flow rate	7.0 ml min^{-1}
Argon carrier gas flow rate	0.3 l min^{-1}

Table 2.3 Instrument settings for the analysis of Hg using Merlin Atomic Fluorescence spectrometer (PS Analytical Model 10.023)

Precision was found to be better than 2% r.s.d, and the limit of detection (LOD) was 1ppt. International standard reference materials BCR-277 (estuarine sediment) and GXR-1 (jasperoid ore) were used to assess the accuracy of the *aqua regia* leach in the extraction of Hg from sediments. Based upon the SRM, *aqua regia* effectively recovers >98% of Hg in both BCR-277 and GXR-1 (see Table 2.4).

Reference Material	Certified Hg value (ppm)[1]	Mean value obtained (ppm)[1,2]	Certified Se value (ppm)[1]	Mean value obtained (ppm)[1,2]
BCR-277 (estuarine sediment)	1.77±0.06	1.75±0.1	2.04±0.18	2.06±0.28
GXR-1 (Jasperoid)	3.9	3.7±0.23	16.6	16.1±0.31

Table 2.4 Mean values obtained for Hg and Se in SRM BCR-277 and GXR-1 using an *aqua regia* attack and analysed using atomic fluorescence spectroscopy (AFS).[1] Uncertainty is taken as the 95% confidence limit of the mean. [2] Mean values based on 8 measurements.

Because hydride generation –AFS analysis of Se requires an excess of hydrogen to fuel the atom cell and also Se to be in an oxidation state of +4, 25ml of the 1/500 *aqua regia* solution was made up to 100ml with 40%HCl (Aristar grade) to produce a solution with a dilution factor of 1/2000. Within the 40% HCl, selenium initially present as Se^{+6} (due to the oxidising effects of *aqua regia*) is reduced to the +4 state, which is more conducive to forming the gaseous selenium hydride for AFS analysis.

The Excalibur instrument used to determine Se was calibrated using synthetic Se(IV) standards of varying concentrations prepared in 40% HCl to ensure matrix matching. Calibration was achieved by the method of least squares, and was linear over the concentration range concerned. International standard reference materials were run to assess the accuracy of the *aqua regia* method for extracting Se from marine sediments and Table 2.4 shows that the method employed in this study effectively recovered >98% of Se from BCR-277 and GXR-1. The detection limit using the Excalibur instrument was found to be better than 10ppt (parts per trillion). A standard of 5ppb was run after every 10 samples to check for instrumental drift. The settings of the instrument are shown in Table 2.5.

Parameter	Value
$NaBH_4$ concentration	1.5%m/v in 0.1mol^{-1} NaOH
$NaBH_4$ flow rate	3.5 ml min^{-1}
HCl concentration	40% v/v
HCl flow rate	7.5ml min^{-1}
Argon carrier gas flow rate	0.3 l min^{-1}
Dryer gas flow rate	2.6 l min^{-1}

Table 2.5: Instrumental settings used for the determination of Se using the PSA hydride generation model (10.003) Excalibur Atomic Fluorescence Spectrometer.

2.4.4. Assessment of mercury extraction from marine sediments.

As outlined earlier in section 2.4.3, sample preparation and sample digestion constitutes a critical step in the determination of mercury in marine sediments (DeGroot and Zschuppe, 1981). Owing to the high volatility of mercury, recommended procedures have been outlined for marine sediments for the quantitative determination of Hg. In this study, the samples analysed were never collected with Hg analysis in mind, an evaluation of sample preparation and digestion procedures was necessary to assess the loss(es) of Hg during each stage.

Numerous studies have outlined the importance of drying temperature upon the quantitative recovery of Hg from marine samples. The results however seem rather contradictory. For example Kennedy *et al.* (1971) found that oven drying samples at 110°C resulted in Hg concentrations being ~7% lower than samples that had been air-dried, whilst Crecelius (1975) and Applequist (1972) found no observable loss of Hg occurred at 80°, 90° or 100°C. Similar contradictory results have been obtained for sediments that have been freeze-dried. Clifton and Vivian (1975) and Pillay (1971) found no detectable loss in Hg, whereas Kennedy *et al.* (1971) found that freeze-drying sediment resulted in ~23% loss of Hg in sediments when compared to samples which were air-dried. In this investigation, samples were either freeze-dried or dried at 100°C.

To assess the effects of drying on the recovery of Hg, wet sediment from core LC25 was homogenised and sub-sampled into 1g splits. Individual sediment fractions were then dried at range of temperatures (40, 50, 60, 70, 80, 90 and 100°C) in a thermostatically-controlled oven until a constant dry weight had been achieved. The other remaining sediment fractions were freeze-dried and air-dried in a dessicator (for a period of 5 days) to provide a comparison with the Hg results from those samples that had been oven-dried. Samples were then digested using the *aqua regia* method as outlined in section 2.4.3. Table 2.6 shows the results of drying temperature upon mercury recovery.

No observable trend was observed between drying temperature and Hg recovery. No significant losses occur during freeze-drying or oven drying at 100°C. Therefore the method employed does not introduce significant Hg losses.

Drying Conditions	Sediment Weight/g	Concentration of Hg in solid phase/[ppb]	% recovery of Hg
40°C	0.2001	17.2	96
50°C	0.2003	17.5	97
60°C	0.1997	17.1	95
70°C	0.1999	17.5	97
80°C	0.1996	17.9	99
90°C	0.1999	16.9	94
100°C	0.2002	17.5	97
Wet sediment	0.2002	18	100
Freeze-dried	0.2000	17.8	99
Air-dried	0.2001	18.1	101

Table 2.6 Recovery of mercury from sediment dried under various conditions.

Another possible loss of Hg from sediments can occur during sample digestion. The effectiveness of the *aqua regia* leach comes from the oxidising nature of the NOCl and production of Cl_2 that could possibly volatilise Hg^0 from the sample. Also, because of the high $CaCO_3$ content of the samples, some loss of Hg may occur via release of CO_2. To assess the loss of Hg during *aqua regia* digestion, the following method was employed.

Silica was ignited in a thermostatically-controlled oven at 450°C overnight in order to remove any Hg present within the Si. The ignited Si was then ground and approximately 0.200g was accurately weighed into precleaned boiling tubes. The Si was spiked with a range of Hg concentrations prepared from synthetic Hg standards and 5ml of *aqua regia* was added. Samples were left to reflux overnight and then filtered and analysed the next day. Table 2.7 shows the effect of *aqua regia* upon the recovery of Hg in sediment.

Mass of Si/g	Mass of 50ng/g Hg added/g	[Hg]/ngg^{-1} in solid phase	[Hg]/ngg^{-1} in solution after digestion	% recovery of mercury
0.2006	0.0	0.0	0	N/A
0.1999	0.1969	49.25	47.5	96.3
0.1996	0.4042	101.25	95.5	94.3
0.2005	0.5071	126.46	122.23	96.5
0.2001	0.6068	151.62	144.53	94.9
0.2000	0.7113	177.83	170.5	95.9
0.2000	0.8069	201.73	195.03	96.7

Table 2.7 An assessment of the losses of Hg induced by the addition of *aqua regia*.

It can be seen that no significant loss of Hg occurs during the *aqua regia* leach. In order to ensure matrix matching, wet sediment from core LC25 was ignited at 450°C to remove any Hg present and the 0.200g of the ignited sediment was spiked with same concentrations of Hg as were used with the Si, and the same procedure employed (Table 2.8).

Mass of sediment /g	Mass of 50ng/g Hg added/g	[Hg]/ngg^{-1} in solid phase	[Hg]/ngg^{-1} in solution after digestion	% recovery of mercury
0.2005	0	0	0	0
0.1995	0.1989	49.85	47.43	95.15
0.1996	0.4012	100.50	98.02	97.53
0.1999	0.5036	125.96	124.12	98.54
0.2001	0.6008	150.12	148.42	98.86
0.2000	0.7015	175.38	173.21	98.76
0.2003	0.8007	199.88	197.87	98.99

Table 2.8 An assessment on the losses of mercury using *aqua regia* in sediment.

Again it can be seen that no observable loss of Hg occurs from the sample during *aqua regia* digestion. The >98% recovery of Hg in SRM BCR-277 and GXR-1 further suggests that no

significant loss of Hg occurs in digestion. Although this brief study indicates that no significant losses of Hg occurs during either sample preparation and digestion stages, the Hg values obtained must be taken as representing minimum concentrations since losses of mercury may have occurred during the period of core collection and storage (up to 10 years in some cases).

2.5. Radiocarbon Dating.

AMS radiocarbon analysis was performed on hand-picked planktonic foraminifera >150μm in size because they have an unequivocal surface ocean source and are the sediment size fraction least liable to post-depositional transport (Troelstra et al., 1991). Species differentiation was not attempted because the total sediment sample available (~3-5g) was often sufficient only to provide the 10-12 mg clean biogenic $CaCO_3$ in the desired size range necessary for a single AMS analysis. Samples were prepared as graphite targets at the NERC Radiocarbon Laboratory, East Kilbride and analysed at the Lawrence Livermore National Laboratory AMS Facility (CAAS- analyses), or at the Scottish Universities Research and Reactor Centre and analysed at the Arizona Radiocarbon Facility (AA-analyses). Further species specific (*Globigerinoides bulloides* or *G. ruber*) AMS radiocarbon analyses were available from LSCE for one core (GifA-analyses, Appendix 7). As in most previous AMS radiocarbon dating of sapropel S1, radiocarbon data (appendix 7) are quoted as unmodified radiocarbon convention ages in years before present (BP i.e. before 1950 A.D.).

2.6. Core Locations and descriptions.

2.6.1. Core Locations.

One of the objectives of this study is to determine whether S1 formation was contemporaneous over the entire eastern Mediterranean, or if deposition of these Corg-rich sediments occurred at different times within different regions of this semi-enclosed sea. To this end, cores containing S1 units were selected from each of the major eastern Mediterranean sub-basins. The locations of the sapropel S1 units investigated in this study are shown in table 2.9 and figure 2.5.

Core	Latitude °N	Longitude °E	Water Depth/m
UM41	34°57'	17°51'	1390
T87-26B	34°44'	16°48'	2415
MD81-LC25	32°36'	27°23'	3129
MD81-LC21	35°40'	26°35'	1522
MDVAL 95-02	34°46'	34°28'	860
MD 90-917	41°18'	17°37'	1010

Table 2.9. Locations of cores used in this study.

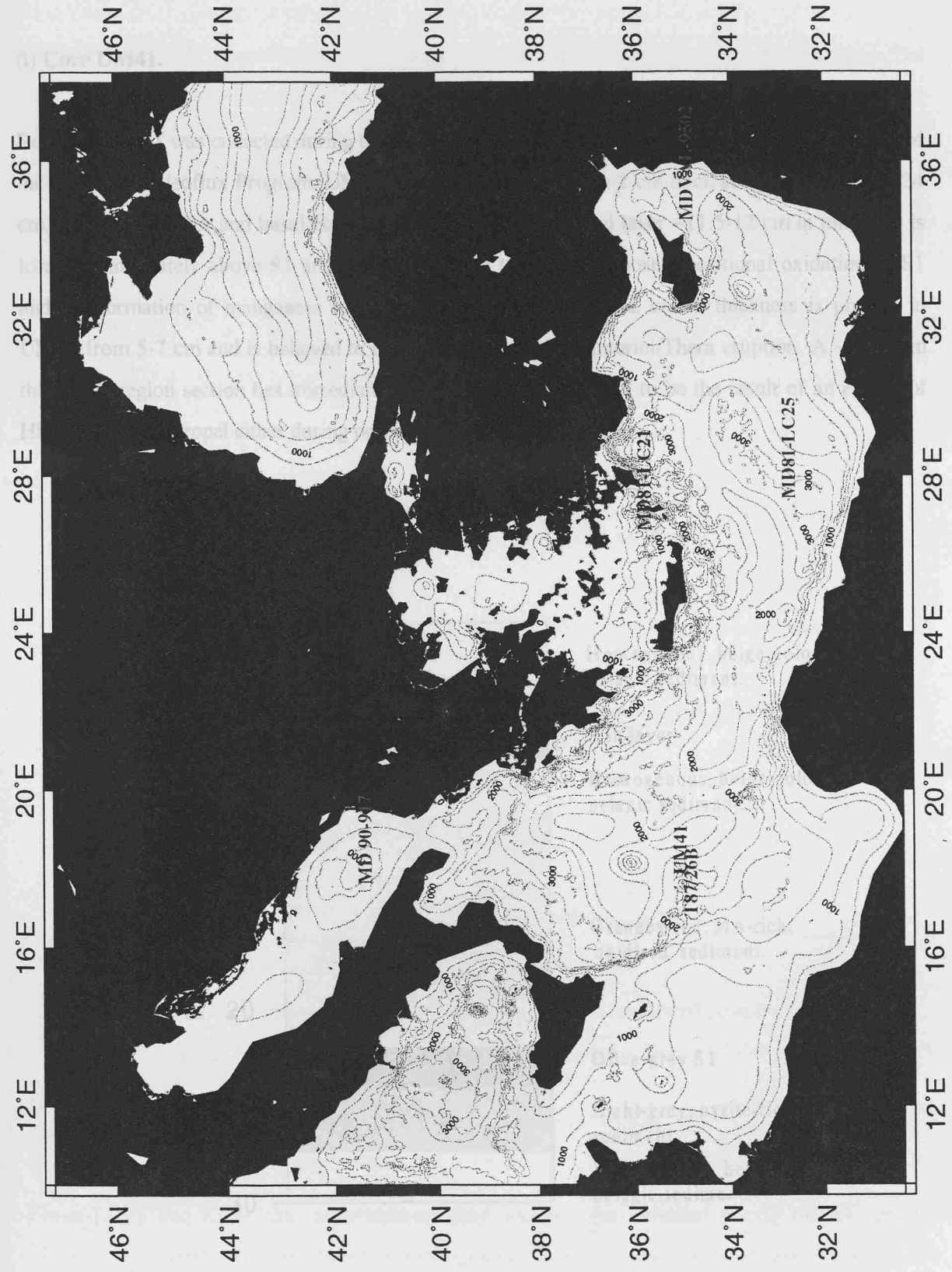

Figure 2.5. Map showing the eastern Mediterranean core positions.

2.6.2. Core descriptions.

(i) Core UM41.

Box core UM41 was collected during the 1994 Urania Cruise to the eastern Mediterranean as part of the MAST II Paleoflux Program. UM41 contains a representative 2 cm thick section of S1 at 22-24 cm, with sharp upper and basal contacts. A distinctive orange-red layer ~11.5-12 cm in thickness is located immediately above S1 and is believed to be the result of post-depositional oxidation of S1 and the formation of manganese oxyhydroxides. An ash layer, ~2 cm in thickness is present in UM41 from 5-7 cm and is believed to be deposited from the Santorini/Thera eruption. A ~ 3- 4 cm thick grey region section lies immediately below S1 and is believed to be the result of an export of HS^- out of the sapropel either during or after S1 formed (figure 2.6).

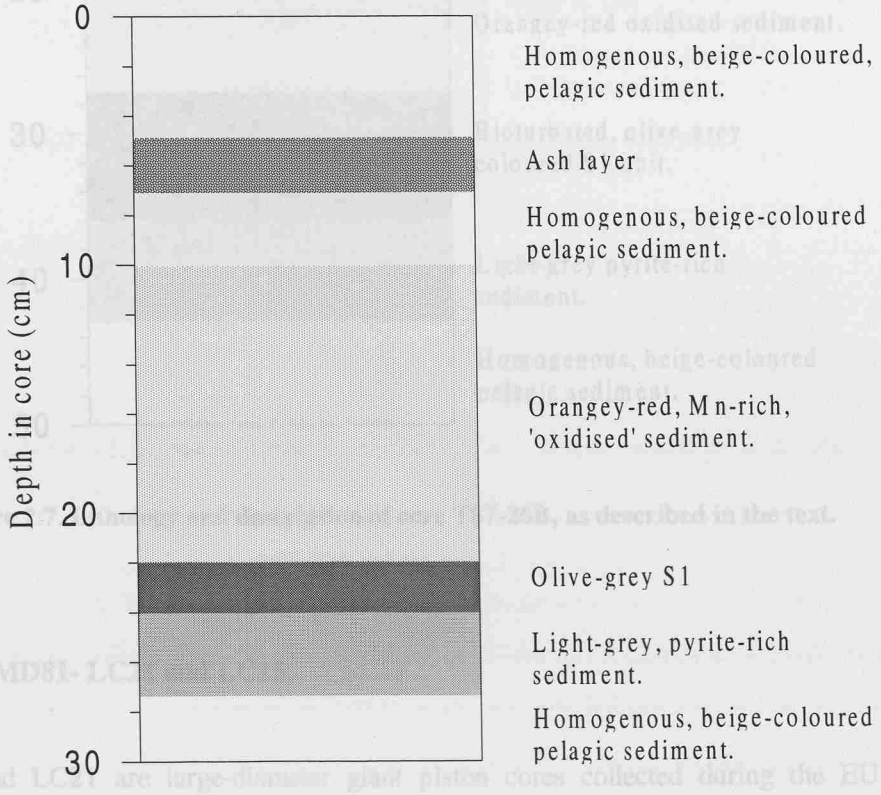

Figure 2.6. Lithology and description of core UM41, as described in the text.

(ii) Core T87-26B.

This is a Dutch box core collected on the Medina Rise and is the most easterly core examined. The core was collected in 1987 by the Dutch Tyro-expedition during T87/4. The core contains a visible sapropel from 27-36 cm, with a 10cm thick red 'oxidised layer' just above S1. The top of the oxidised layer consists of a 3cm thick black-speckled manganese layer, consisting of large Mn encrustations (figure 2.7). A light-grey region from 36-43 cm and rich in pyrite was located immediately below S1 (Troelstra *et al.*, 1991).

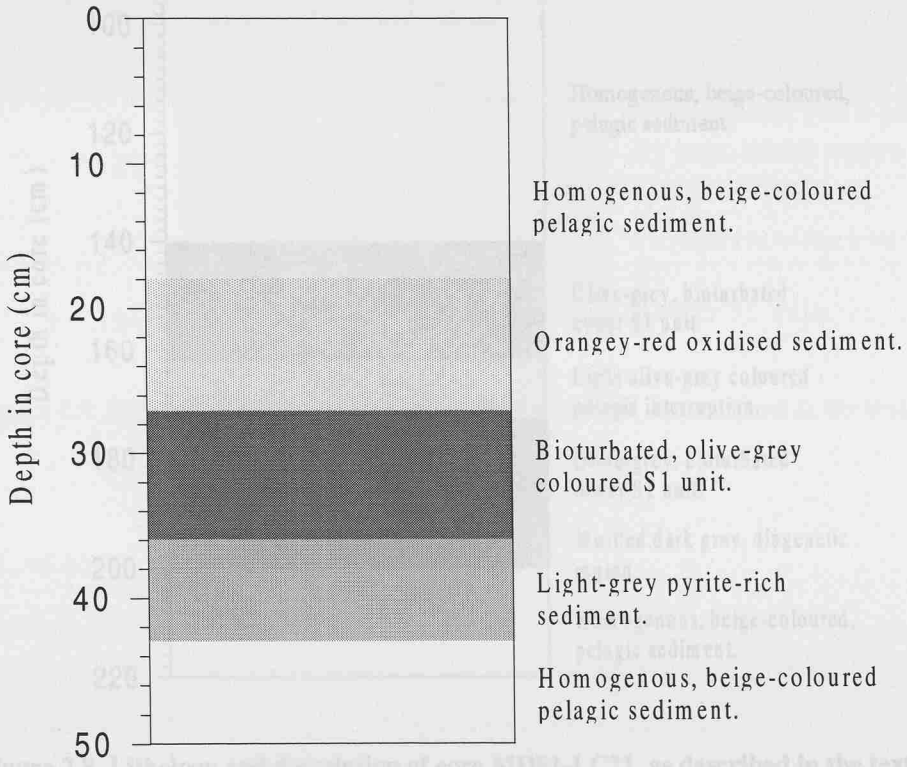

Figure 2.7. Lithology and description of core T87-26B, as described in the text.

(iii + iv) Cores MD81- LC21 and LC25.

Cores LC25 and LC21 are large-diameter giant piston cores collected during the EU project "Paleoflux" in 1995. LC21 is located on a topographic high situated to the north east of Crete in the northern half of the Aegean Sea. This core was selected because it has a rapid accumulation rate, so that the effects of post-depositional oxidation are expected to be minimal. The lithology of LC21 is dominated by two decimetre-thick pelagic, olive-grey sapropel units, interrupted by a 14 cm thick

light-coloured central section. Both sapropel units are thoroughly bioturbated and have sharp basal contacts but gradational/bioturabted upper contacts. A distinctive grey region ~ 9cm in thickness lies immediately beneath the lower sapropel unit and is thought to be the result of an export of HS^- out of S1 during or shortly after S1 formation. Above S1, a thick ash layer is present at 82-92 cm, suspected to have been deposited from the explosive eruption of the Santorini/Thera volcano (Hardy and Renfrew, 1990) because of the core location and the ash layer's position above the sapropel (figure 2.8).

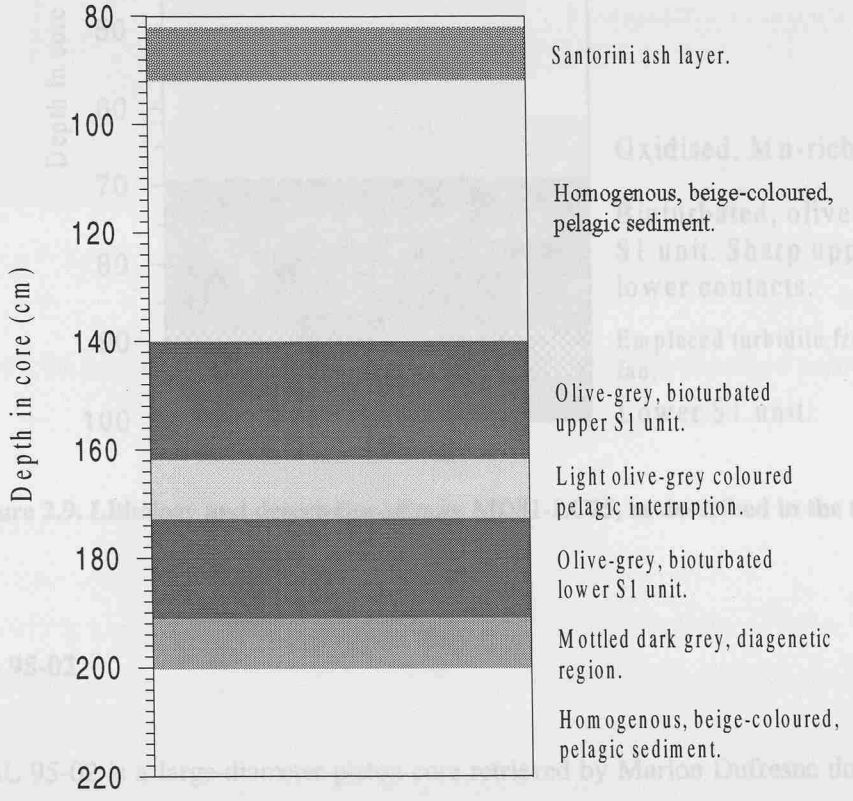

Figure 2.8. Lithology and description of core MD81-LC21, as described in the text.

Core LC25 collected from the Herodotus Abyssal Plain contains a visible olive-grey sapropel S1 unit from 69- 87cm and 94-100cm. The intervening section at 87-94 cm is clearly a turbidite based upon visual and compositional evidence and is derived from down-slope failures on the Nile fan. The base of S1 in this core was not located and is believed to have been removed from the sedimentary record when the underlying turbidite was emplaced. The upper face of the S1 unit at 61cm has a sharp contact with the orangey-red sediment (~8 cm in thickness) that lies immediately above the sapropel. This interval is thought to represent the partial oxidation of the upper face of S1 following its formation (figure 2.9).

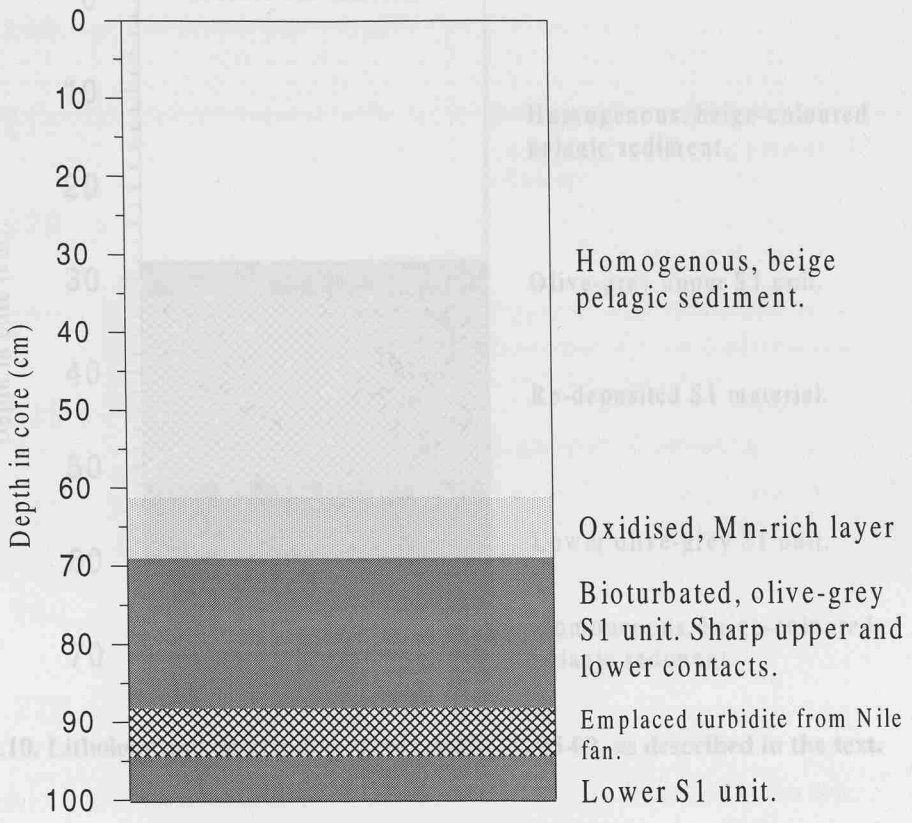

Figure 2.9. Lithology and description of core MD81-LC25, as described in the text.

(v) MDVAL 95-02.

Core MDVAL 95-02 is a large-diameter piston core retrieved by Marion Dufresne during the 1995 VALPAMED cruise in 1995. MDVAL 90-95 is located to the south east of Cyprus at a depth 860m and represents the most easterly core investigated during this study. This core contains a dark, bioturbated S1 unit from 28-55 cm and was sampled with expectation that it was a rapidly-accumulated sapropel. Whilst radiocarbon dating have confirmed that this sapropel is entirely of S1 age, the irregular progression of radiocarbon age with depth (chapter 6) suggests that this core is slowly accumulated with re-deposition of sapropel material in the centre of the dark unit from 32-52 cm (figure 2.10).

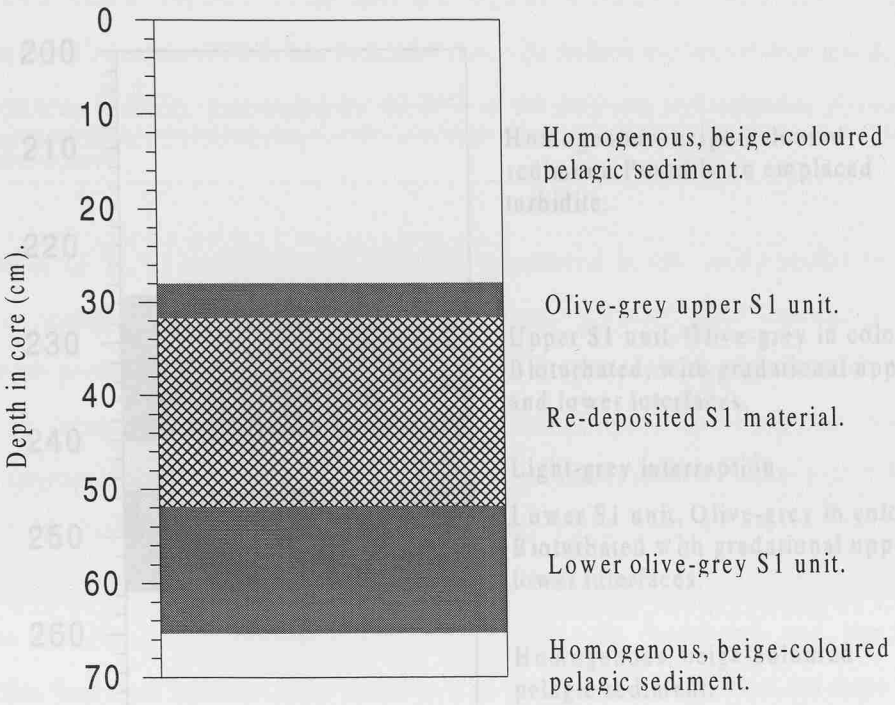

Figure 2.10. Lithology and description of core MDVAL 95-02, as described in the text.

(iv) MD 90-917.

Core MD 90-917 is a piston core collected during the PROMETE 90 cruise in 1990. This core was collected from the southern Adriatic pit in 1010m of water depth and like core MD81- LC21 contains two decimeter thick, bioturbated olive-grey S1 units. The visual upper and lower sapropel units are located from 225-240 and 245-255 cm in this core and an intervening light-coloured section ~5 cm in thickness separates the two sapropel units. Unlike MD81-LC21, both upper and basal contacts of the two S1 units are bioturbated and gradational (figure 2.11).

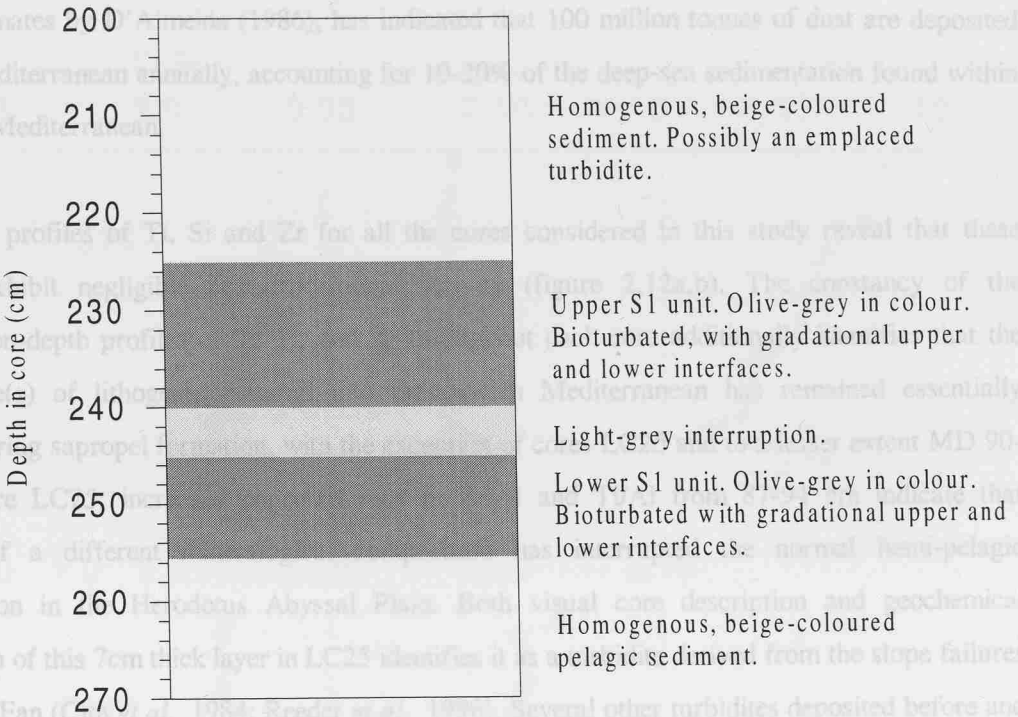

Figure 2.11. Lithology and description of core MD 90-917, as described in the text.

2.6.3. Core mineralogy.

A number of elements considered during this study are confined to lattice positions of lithogenic minerals (Shotyk *et al.,* 1990). In such lattice-bound positions these lithophile elements, which include Al, K, Si, Ti and Zr, exhibit little or no post-depositional re-distribution so that variations in their concentration-depth profiles originates from changes in the source/composition of the sedimentary material.

Over the past five decades, sedimentology within the eastern Mediterranean has been studied extensively (Stanley, 1972). It has become apparent that the composition of eastern Mediterranean sediments is controlled by the relative contributions of particulate matter derived from riverine, fluvial and atmospheric sources. For example, Krom *et al.,* (1999) has identified the importance of terrigenous material derived from riverine inputs in controlling the composition of sediments from the Ionian and Levantine basins, whilst Cita *et al.,* (1996) has indicated that a hydrothermal signal can be identified in sediments in close proximity to the mid-Mediterranean Ridge. Furthermore, it is recognised that the sedimentology of the eastern Mediterranean is strongly influenced by the

deposition of aeolian matter derived from the semi-arid regions of northern Africa (Guerzoni *et al.*, 1997). Estimates by D'Almeida (1986), has indicated that 100 million tonnes of dust are deposited over the Mediterranean annually, accounting for 10-20% of the deep-sea sedimentation found within the eastern Mediterranean.

Normalised profiles of Ti, Si and Zr for all the cores considered in this study reveal that these elements exhibit negligible post-depositional activity (figure 2.12a,b). The constancy of the concentration-depth profiles of Si, Ti, and Zr throughout each core additionally identifies that the input/source(s) of lithogenic material into the eastern Mediterranean has remained essentially constant during sapropel formation, with the exception of cores LC25 and to a lesser extent MD 90-917. In core LC25, increased concentrations in Zr/Al and Ti/Al from 87-94 cm indicate that sediment of a different mineralogical composition has interrupted the normal hemi-pelagic sedimentation in the Herodotus Abyssal Plain. Both visual core description and geochemical composition of this 7cm thick layer in LC25 identifies it as a turbidite derived from the slope failures on the Nile Fan (Cita *et al.*, 1984; Reeder *et al.*, 1998). Several other turbidites deposited before and after S1 are also present within LC25, one of which is 1.2m thick and has its top at 100cm in core. For core MD 90-917, near-uniform Si/Al, Ti/Al and Zr/Al profiles indicates that hemi-pelagic sedimentation within the southern Adriatic has been continuous during S1 formation, although it can be seen that a mineralogically distinct unit dominated by high Si/Al and Ti/Al (low Zr/Al values) ratios is present at the top of the upper S1 (figure 2.12b). It is known that sedimentation within the southern Adriatic is subject to re-depositional processes (Rohling *et al.*, 1997) and it is likely that reworked sediment has been emplaced after S1 formation.

Whilst the element/Al ratios within each individual core are essentially constant during sapropel S1 formation (except LC25), the mean ratios of each of the lithogenic elements display a degree of variability (table 2.10) indicating different sources of lithogenic material are supplied to the eastern Mediterranean. For example the core from the Aegean Sea (LC21) has systematically low Si/Al, Ti/Al and Zr/Al ratios in comparison with the core from the Adriatic Sea (MD 90-917) (table 2.10). Previous sedimentological studies in the Adriatic Sea have found that quartz (SiO_2) is the dominant component of the sediments, derived principally from the weathering of SiO_2-rich Paleogene and Eocene flysch deposits which surround this area (Ogorelec *et al.*, 1991). Aeolian deposition of terrigenous material originating from the semi-arid areas of northern Africa have been shown to be an important source of SiO_2 in Adriatic Sea sediments (Tomadin *et al.*, 1984). For core LC21, the mean Si/Al ratio is significantly lower than that of MD 90-917 reflecting the fact that the source rocks surrounding the Aegean Sea are depleted in SiO_2.

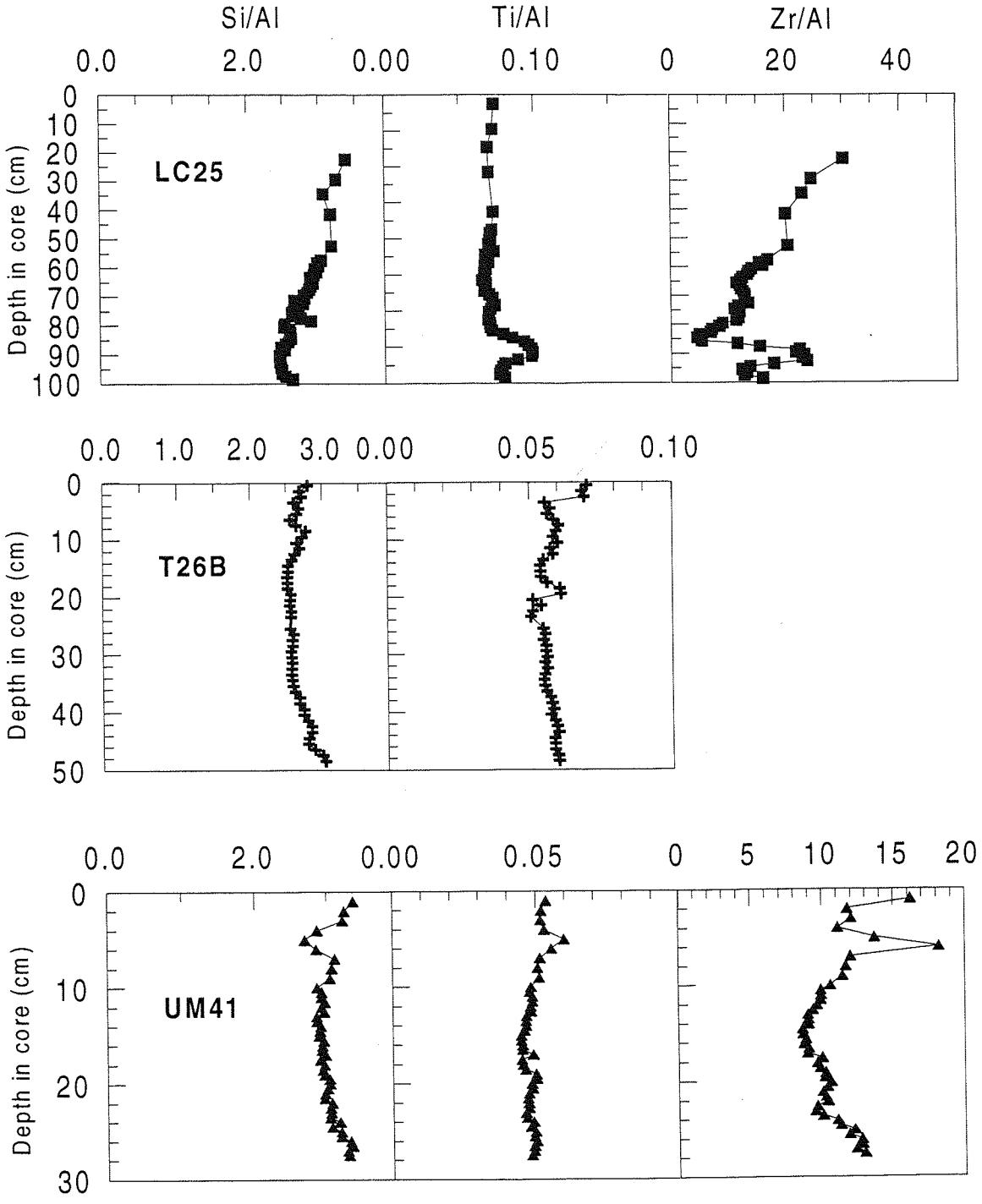

Figure 2.12a. Normalised depth-distributions of Si/Al, Ti/Al (wt%/wt%) and Zr/Al (ppm/wt%) in LC25, T26B and UM41. For T26B, Zr was not determined.

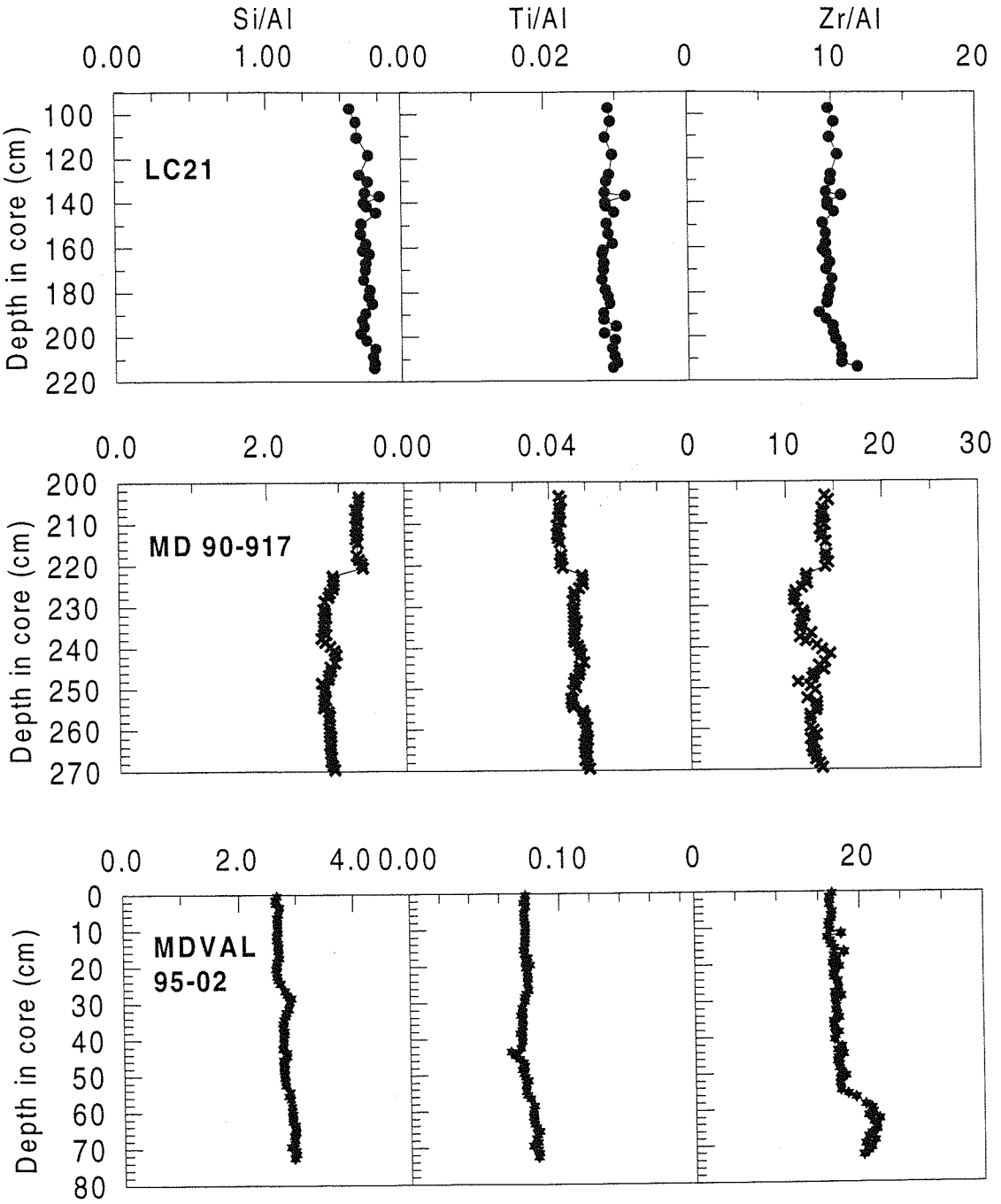

Figure 2.12b. Normalised depth-distributions of Si/Al, Ti/Al (wt%/wt%) and Zr/Al (ppm/wt%) in LC21, 90-917 and MDVAL 95-02.

Mineralogical analysis of the Psiloritis massif in central Crete suggests that quartz only makes up <5% of the host rock (Nihlen *et al.*, 1995), in contrast to the flysch deposits of the Adriatic which have SiO_2 concentrations between 20-40%. It is apparent that there is a high degree of variability in the Zr/Al ratios between the different cores. According to Shimmield (1992), Zr/Al ratios are indicators of the aeolian terrestrial fraction in marine sediments. It can observed that the cores with the highest Zr/Al ratios (LC25; MDVAL-9502) are those taken from the far eastern end of the Mediterranean which are closest in proximity to the arid areas of northern Africa (Sahara) and the Middle East (Negev Desert). This implies that cores MD81-LC25 and MDVAL 95-02 receive greater contributions of aeolian derived terrestrial matter in comparison to the other cores which are located further away from the sources of terrestrial particulate matter.

Core	Si/Al	Ti/Al	Zr/Al
UM41	3.02	0.049	10.78
T87-26B	2.66	0.057	n.d.
MD81-LC25	2.74	0.075	13.88
MDVAL-9502	2.79	0.077	18.15
MD81-LC21	1.67	0.029	9.96
MD 90-917	2.95	0.047	12.80

Table 2.10. Mean Si/Al, Ti/Al (wt%/wt%) and Zr/Al (ppm/wt%) for the S1-bearing cores examined during this investigation.

2.7. Manipulation and Treatment of Data.

2.7.1. Normalisation of data.

Normalisation of data is the attempt to compensate for the natural variability of trace elements in marine sediments caused through variations in the abundance of the detrital mineral phase or in order to overcome dilution effects caused through variations in the $CaCO_3$ content (Loring, 1991). Normalising the data provides an effective way of identifying authigenic and diagenetic signals in marine sediments, and geochemical normalisation procedures involve the ratioing of trace element data to geochemically inert elements that are representative of the detrital phase. Aluminium is commonly employed as the normalising agent in order to overcome the dilution effects of variable

$CaCO_3$ contents in deep-sea marine sediments (Thomson *et al.*, 1998) and is this procedure is used to represent the trace element data in this thesis.

2.7.2. Salinity Correction.

A number of elements discussed in this thesis are major constituents of seawater, and may therefore be present within the pore waters of marine sediments at significant concentrations. The contribution of iodine, bromine and sulphur in marine sediments derived from sea water can be assessed from the amount of chlorine present in the sample and from the known element/chlorine ratio found in sea water, according to equation 2.4. This procedure assumes that all of the Cl is derived from sea water. The symbol # is used to represent the data which have been corrected for a sea water component.

$$\mathbf{X\# = X_{tot} - (X/Cl_{sw} * Cl_{sample})}$$

equation 2.4

$\mathbf{X\#}$ = salinity-corrected element concentration ($\mu g\ g^{-1}$),

$\mathbf{X_{tot}}$ = total element concentration ($\mu g\ g^{-1}$),

$\mathbf{X/Cl_{sw}}$ = ratio of the element to chlorine in sea water,

$\mathbf{Cl_{sample}}$ = chlorine concentration in the sample (wt%).

2.7.3. Excess element concentration.

The geochemical composition of deep-sea marine sediments is dominated by detrital and authigenic signals (Chester, 1990). The detrital component is derived from the deposition of riverine, fluvial and aeolian particulate matter and this signal contains a wide range of elements that occupy the lattice sites of common sedimentary minerals. Identification of the detrital signature provides a useful indication for assessing the 'background' concentration of trace elements for a particular region. The authigenic signal (which is superimposed upon the detrital signal) represents the concentration of trace elements which are present in excess of 'background' concentrations. Authigenic signals in marine sediments are formed from the incorporation of trace elements that are deposited/associated with Corg, sulphides and oxyhydroxides (Chester, 1990). Identification of this signal allows the degree of enrichment of a particular element to be assessed and may also help to elucidate the mechanism(s) by which it is incorporated into the sedimentary phase. The authigenic signal can be

identified in marine sediments by calculating the amount of each element present relative to aluminium (as a proxy of the mineralogical composition) and identifying the value of the detrital (chiefly lattice-bound) element to aluminium ratio in these sediments. The detrital element concentration may then be determined and enable the calculation of the "excess" (non-lattice-bound) element concentration (equation 2.5). The detrital element signal for sapropel-bearing sediments from the eastern Mediterranean is assumed to be best represented by the element/aluminium ratios of the Corg-poor, pelagic sediments which lie above and below S1. The "excess" element concentration is denoted by the symbol * (e.g. Cr*).

$$\mathbf{X^* = X_{tot} - (R_{det} \times C_{al})}$$

equation 2.5

Where $\mathbf{X^*}$ = excess element concentration ($\mu g\ g^{-1}$),

$\mathbf{X_{tot}}$ = total element concentration ($\mu g\ g^{-1}$),

$\mathbf{R_{det}}$ = detrital ratio of the element to aluminium,

$\mathbf{C_{al}}$ = concentration of Al (wt%).

Chapter 3:

Trace element geochemistry of slowly-accumulated sapropels.

3.1 Early Diagenesis.

The concentration of trace elements in marine sediments reflects the geochemical processes controlling their supply to, distribution in, and removal from seawater. Of special interest is the geochemical behaviour of redox-sensitive elements which is tightly coupled to early diagenetic reactions involving the degradation of organic matter, the latter controlling the redox state of the sediment (Quednau *et al.*, 1997). The pathways by which organic matter is oxidised during early diagenesis are becoming increasingly well understood (Froelich *et al.*, 1979; Canfield *et al.*, 1993). There is a diverse population of micro-organisms utilising a variety of electron acceptors which are responsible for the oxidation of Corg in marine sediments (Luckge *et al.*, 1999). During early diagenesis, the sequence in which the terminal electron-accepting species are utilised is dependent upon the Gibbs free energy yield production per mole of organic carbon oxidised (Claypool and Kaplan, 1974; Froelich *et al.*, 1979; Bender and Heggie, 1984). Thus, as oxygen is exhausted, microbial organisms switch to a succession of alternative terminal electron acceptors in order of decreasing thermodynamic advantage. In marine sediments, the succession of electron acceptors utilised in the oxidation of Corg is thought to occur in the sequence: O_2 > nitrate ≥ manganese oxides > iron oxides > sulphate (Chester, 1990). In this diagenetic sequence it is assumed that the oxidants are limited i.e. each reaction involving the different electron acceptors proceeds to completion before the next one starts. According to Aller *et al.* (1983), possible half-reactions involving the reduction of suitable electron acceptors (in bold) can be written in the following manner:

1.	$\mathbf{O_2} + 4\,H^+ + 4\,e^- \rightarrow 2\,H_2O$	**(aerobic respiration)**
2.	$0.8\,\mathbf{NO_3^-} + 4.8\,H^+ + 4\,e^- \rightarrow 0.4\,N_2 + 2.4\,H_2O$	**(denitrification)**
3.	$2\,\mathbf{MnO_2} + 8\,H^+ + 4\,e^- \rightarrow 2\,Mn^{2+} + 4\,H_2O$	**(manganese reduction)**
4.	$4\,\mathbf{FeOOH} + 12\,H^+ + 4e^- \rightarrow 4\,Fe^{2+} + 8\,H_2O$	**(ferric iron reduction)**
5.	$0.5\,\mathbf{SO_4^{2-}} + 4.5\,H^+ + 4e^- \rightarrow 0.5\,HS^- + 2\,H_2O$	**(sulphate reduction)**

Under steady-state conditions, a series of well-developed diagenetic zones is set up in marine sediments where each process predominates (figure 3.1). The depth scales of these processes are controlled by factors such as the flux of Corg to the seafloor, bottom water oxygen concentration and the sedimentation rate. Investigation of deep-sea sediment pore water profiles of the common electron acceptors described above are often consistent with the zonation model depicted in figure 3.1.

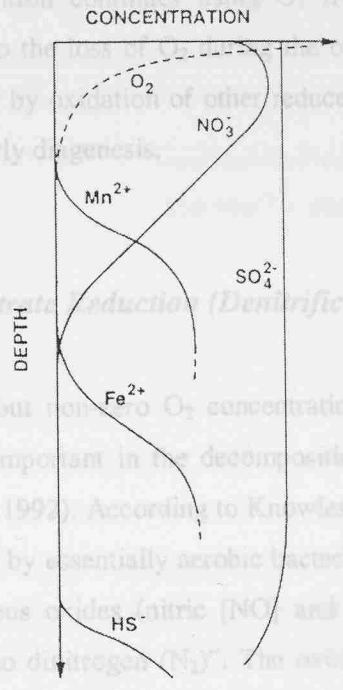

PROCESSES	ELECTRON ACCEPTOR	ΔG^0 (kJ/mol)
Aerobic Respiration	O_2	-3190
Denitrification	NO_3^-	-3030
Manganese Reduction	Mn(IV) (e.g., MnO_2)	-3090 to -2920
Iron Reduction	Fe(III) (e.g., FeOOH)	-1410 to -1330
Sulfate Reduction	SO_4^{2-}	-380

Figure 3.1. Hypothetical pore water profiles predicted by the successive utilisation of inorganic compounds as terminal electron acceptors in the remineralisation of sedimentary Corg (from Burdige, 1993).

3.1.1. Aerobic respiration.

During the initial stages of early diagenesis, the primary electron acceptor utilised in the oxidation of Corg is dissolved oxygen derived from interstitial pore waters (Van der Weijden, 1992). The organic matter that undergoes early diagenesis can be considered to have the Redfield composition i.e. $(CH_2O)_{106}(NH_3)_{16}(H_3PO_4)$. The oxidation of Corg by aerobic organisms can be represented by the equation proposed by Galoway and Bender (1982):

$$C_{106}H_{263}O_{110}N_{16}P + 138\ O_2 \rightarrow 106\ CO_2 + 16\ HNO_3 + H_3PO_4 + 122\ H_2O.$$

Equation 3.1

According to Bender and Heggie (1984), >90% of Corg that reaches the sea floor is oxidised by O_2. Oxygen may therefore be regarded as the primary oxidant involved in the destruction of Corg and in a closed system will continue until oxygen has been consumed to drive the redox potential low enough to favour the next most efficient oxidant. Thus, as oxygen becomes depleted, Corg decomposition continues using O_2 from secondary oxidant sources (sub-oxic diagenesis). In addition to the loss of O_2 during the oxidation of Corg, dissolved oxygen concentrations may be consumed by oxidation of other reduced species such as Mn^{+2}, Fe^{+2}, HS^-, H_2S and FeS_2 produced during early diagenesis.

3.1.2. Nitrate Reduction (Denitrification).

At low, but non-zero O_2 concentrations, dissimilatory reduction of nitrate and nitrite starts to become important in the decomposition of Corg (Froelich *et al.*, 1979; Berner, 1980; Van der Weijden, 1992). According to Knowles (1982), denitrification may be defined as "the dissimilatory reduction by essentially aerobic bacteria, of one or both ionic nitrogen oxides (nitrate or nitrite) to the gaseous oxides (nitric [NO] and nitrous [N_2O] oxides), which may themselves be further reduced to dinitrogen (N_2)". The oxidation of Corg by denitrification can be represented by the reactions:

$$C_{106}H_{263}O_{110}N_{16}P + 138\ O_2 + 94.4\ HNO_3 \rightarrow 106\ CO_2 + 55.2\ N_2 + H_3PO_4 + 177.2\ H_2O.$$

Equation 3.2a

or

$$C_{106}H_{263}O_{110}N_{16}P + O_2 + 84.8\ HNO_3 \rightarrow 106\ CO_2 + 42.4\ N_2 + 16\ NH_3 + H_3PO_4 + 148.4\ H_2O.$$

Equation 3.2b

According to Froelich *et al.* (1979), the fate of nitrogen has important consequences with respect to the sequence in which the oxidants are utilised. These authors argue that if all of the nitrogen is reduced to N_2, then the use of nitrate as a secondary oxidant overlaps with that of MnO_2, but if nitrogen is released as ammonia rather than N_2 then MnO_2 is reduced before nitrate.

3.1.3. Manganese Reduction.

In contrast to O_2 and nitrate, Mn oxides are present in sediments as a solid phase. Consequently, no additional supply of this oxidant can be derived from the downward diffusion of bottom waters so that the oxidising capacity of Mn oxides is primarily determined by the quantity of this phase incorporated into the sediment during deposition. Manganese oxides rarely display the ideal stoichiometry of MnO_2 and Mn is known to present in oxides as Mn(II), Mn(III) and Mn(IV) species (Van der Weijden, 1992). The higher valency states of Mn are exceptionally reactive oxidants, and the oxidation of Corg by Mn oxides can be described by the reaction:

$$C_{106}H_{263}O_{110}N_{16}P + 138\ O_2 + 236\ MnO_2 + 472\ H^+ \rightarrow$$
$$236\ Mn^{+2} + 106\ CO_2 + 8\ N_2 + H_3PO_4 + 366\ H_2O.$$

Equation 3.3

Reduction of manganese oxides during Corg remineralisation leads to the generation of and increase in pore water dissolved Mn^{+2} concentrations. Mn^{+2} ions are highly soluble and mobile and are capable of migrating both up and down depending upon the gradients set up within the sediment. According to Froelich *et al.* (1979), it is likely that the Gibbs free energy yield obtained from MnO_2 reduction is dependent upon the mineralogy of the Mn-oxide involved. The energy yield for MnO_2 and NO_3^- reduction are comparable (-51596 and – 53540 kJ $mole^{-1}$ Corg respectively) so that within marine sediments there is some degree of overlap in the utilisation of Mn-oxides and nitrate as electron acceptors.

3.1.4. Ferric Iron reduction.

Like Mn oxides, the capacity of iron oxides to act as an electron acceptor in the remineralisation of Corg is determined by the amount of Fe oxide incorporated into the sediment during burial, since it too is present as a solid phase. According to Froelich *et al.* (1979) only a small fraction of Fe(III) oxide present in the solid phase is available for reduction. The most reactive phases are those with the highest solubility, i.e. amorphous and poorly crystallised Fe-oxyhydroxides (Lovely and Phillips, 1986). Utilisation of Fe oxides produces highly soluble and mobile Fe^{2+} which is capable of migrating both up and down and re-precipitating in zones of higher oxygen concentrations. Reduction of Fe oxides can be described by:

$$C_{106}H_{263}O_{110}N_{16}P + 138\ O_2 + 212\ Fe_2O_3\ (\text{or } 424\ FeOOH) + 848\ H^+ \rightarrow$$
$$424\ Fe^{+2} + 106\ CO_2 + 16\ NH_3 + H_3PO_4 + 530\ H_2O\ (\text{or } 742\ H_2O).$$ **Equation 3.4**

3.1.5. Sulphate reduction.

After aerobic respiration, sulphate reduction is, on a global scale, the most important process in the diagenesis of Corg (Van der Weijden, 1992). Following the depletion of electron acceptors such as O_2, NO_3^-, MnO_2 and FeOOH, oxidation of Corg occurs via sulphate (SO_4^{2-}) reduction by sulphate-reducing bacteria such as *Desulfovibrio*. Sulphate reduction is common in environments with high sedimentation rates and high concentrations of Corg, where oxygen, nitrate and manganese and iron oxyhydroxides are quickly depleted. Sulphate reduction can be described by:

$$\mathbf{C_{106}H_{263}O_{110}N_{16}P + 53\ SO_4^{2-} \rightarrow}$$
$$\mathbf{106\ CO_2 + 16\ NH_3 + 53\ S^{2-} + H_3PO_4 + 106\ H_2O.}$$

Equation 3.5

3.2. Diagenetic Zonation.

As diagenesis proceeds via the sequence $O_2 > NO_3^- \geq$ Mn oxides > Fe oxides > sulphate, a number of diagenetic zones can be identified in marine sediments which can be related to the electron acceptor(s) used in the oxidation of Corg (table 3.1). Berner (1980) identified two main environments oxic and anoxic, the latter being sub-divided into non-sulphidic and sulphidic environments.

Diagenetic Zone	Oxidants
Oxic	O_2
Non-sulphidic post-oxic (Sub-oxic)	NO_3^- MnO_x Fe^{III}
Sulphidic	SO_4^{2-}

Table 3.1: Possible diagenetic zones in marine sediments resulting from the oxidation of Corg utilising different oxidants (after Berner, 1980).

3.2.1. Oxic environments.

In oxic environments where the concentration of dissolved oxygen is typically >6 μmole O_2 l^{-1}, early diagenesis of organic matter proceeds via aerobic respiration, with dissolved oxygen being utilised as the preferred electron acceptor. During aerobic respiration, >90% of Corg is oxidised, and in terms of the reactions given above, the diagenetic sequence only proceeds via equation 3.1.

3.2.2. Anoxic environments.

Anoxic environments develop when the continual consumption of Corg via aerobic respiration leads to a depletion in dissolved O_2 concentrations, such that when O_2 contents fall to ~5% of its concentration in aerated waters (or <6 μmole O_2 l^{-1}), diagenesis proceeds via secondary oxidants through anaerobic metabolism. Anoxic environments are subdivided into two types:

3.2.2.1. Non-sulphidic post-oxic environments.

In these environments pore waters contain negligible O_2 and no measurable dissolved sulphides, and such environments are commonly referred to as being **sub-oxic** or **post-oxic.** In order for sub-oxic diagenesis to develop, the supply of Corg to the seafloor is usually much greater than the supply of dissolved O_2 to the pore waters so that oxidants other than O_2 must be used in the oxidation of Corg. During sub-oxic diagenesis, nitrate and Mn- and Fe oxides are used as secondary oxidants, but the sequence does not proceed to the point where sulphate is utilised. In sub-oxic environments, oxidation of Corg occurs via the reactions given in 3.2ab, 3.3 and 3.4.

3.2.2.2. Sulphidic.

Complete consumption of the secondary oxidants leads to the point where bacterial populations reduce sulphate in order to oxidise Corg, producing H_2S and HS^- as by-products. If a sufficient supply of Corg is available for oxidation in marine sediments then sulphate reduction can be a common feature because of the availability of sulphate in both seawater and pore waters. In sulphate reducing environments, diagenesis proceeds via equation 3.5.

Factors controlling the extent to which the diagenetic zone sequence develops is largely governed by the amount of Corg deposited to the seafloor (which is determined by the amount of primary

productivity in the surface waters), the degree of water column oxygenation, and the rate at which the sediments accumulate; these factors determine the amount of Corg preserved in marine sediments and thus the extent to which the various electron acceptors are consumed.

3.3. Early diagenesis in slowly-accumulated sapropels.

A number of studies on the most recently accumulated sapropel S1 have shown that these Corg-rich units are affected by early diagenetic reactions following their formation. Following deposition, sapropels are subject to post-depositional diagenesis via a downward-moving oxidation front, a mechanism originally proposed to explain sharp colour changes and redox-sensitive metal profiles in Corg-rich distal turbidites from the north-east Atlantic (Wilson *et al.*, 1985; 1986).

Numerous studies on a variety of marine sediments have shown the importance of downward progressing oxidation fronts (Colley *et al.*, 1984; Wilson *et al.*, 1986; Thomson *et al.*, 1995; Van Santvoort *et al.*, 1996). According to Wilson *et al.* (1985), a progressive oxidation front (POF) is established when changes in depositional conditions allow oxygenated seawater to penetrate into anoxic or reducing sediments. In abyssal examples, periodic emplacement of Corg-rich turbidites is the main change in depositional characteristics and alters the exposure time to dissolved O_2. In sapropels however, sedimentation is continuous, so that changes in depositional conditions are achieved through fluctuations in both Corg accumulation and bottom water O_2 concentrations (Thomson *et al.*, 1999). Under these conditions, the downward flux of oxidants such as O_2 and NO_3^- exceeds the upward flux of reductants such as Fe^{2+} and Mn^{2+}. If this is the case, then the excess oxidants are consumed via the remineralisation of organic carbon and oxidation of reduced S complexes. Initially, the rate of advance of the POF is rapid, but it eventually slows as the diffusion path length increases and the oxidant flux falls (Higgs *et al.*, 1994). The rate at which the POF advances downwards in the sediments is governed primarily by the balance between the supply of oxidants and reductants and also by the reducing capacity of the sediments. The POF will eventually cease to move downwards within the sediment when the flux of oxidants is matched by an equal flux of reductants supplied from below. Other factors that influence the rate at which the POF advances within sediments are the oxygen content of the overlying sea water, the Corg content of surficial sediments and sediment accumulation rates (Wilson *et al.*, 1986; De Lange *et al.*, 1989; Higgs *et al.*, 1994).

A common observation in marine sediments affected by progressive oxidation fronts is the attendant rearrangement of redox-sensitive elements into sharp peaks at the advancing face of the

front (Wallace *et al.*, 1988; De Lange *et al.*, 1989; Pruysers *et al.*, 1993). At present, sapropel formation is regarded as a combination of both increased productivity and/or bottom water anoxia within the eastern Mediterranean (Chapter 1; Rohling, 1994). Following sapropel formation, the re-establishment of oxygenated bottom waters and oligotrophic surface waters allowed for the downward diffusion of oxidants (including O_2 and NO_3^-) from seawater into the underlying sediment, setting up an oxidation front. As such it is expected that the original geochemical signature of more slowly-accumulated sapropels will be over-printed by a secondary diagenetic signal induced by a combination of both the downwards advancement of the POF (oxic diagenesis) and early diagenetic reactions involving the oxidation of Corg (sub-oxic diagenesis).

3.4. Evidence for post-depositional oxidation.

3.4.1. Manganese and Iron.

Post-depositional oxidation of slowly-accumulated sapropels (S1) was initially proposed by Ten Haven (1987) and De Lange (1989), and was later inferred by Higgs *et al.* (1994) and Thomson *et al.* (1995) in order to explain the profiles of redox-sensitive elements (including Mn and Fe) in S1 sapropels. Van Santvoort *et al.* (1996) performed high-resolution pore water (including dissolved O_2 and nitrate) and solid-phase geochemistry on three cores collected from different geographical locations within the eastern Mediterranean. Pore water profiles of O_2 and NO_3^-, demonstrated that both dissolved oxygen and nitrate were present in significant quantities above the visual sapropel, and decreased to near-detection limit levels at the upper face of Corg-rich intervals. Oxic conditions immediately above S1 units investigated by Van Santvoort *et al.* (1996) reflect the fact that the present-day eastern Mediterranean is characterised by oligotrophic surface waters and a well-ventilated water column which is oxic to all depths. A consequence of low primary productivity and oxygenated bottom waters is that only 0.1-0.2% of Corg is actually deposited on the floor of the eastern Mediterranean (Van Santvoort *et al.*, 1997). As a result, the supply of oxidants to the bottom waters exceeds the flux of Corg to the seafloor so that O_2 and NO_3^- diffuse downward into the sediment along a concentration gradient, setting up a progressive oxidation front. Pore water O_2 and NO_3^- results presented by Van Santvoort *et al.* (1996) demonstrate conclusively that slowly-accumulated S1s are affected by post-depositional oxidation following their formation.

A conspicuous feature of cores LC25, T26B and UM41 is the presence of double Mn peaks situated immediately above the sapropel interval in oxic conditions (figure 3.2). Double manganese

peaks have been reported previously from a variety of pelagic and hemi-pelagic sediments (Gardner *et al.*, 1982; Berger *et al.*, 1983; Price and Froelich, 1987; Dean *et al.*, 1989; Mangini *et al.*, 1990) including sapropels (Anastasakis and Stanley, 1986; Murat and Got, 1987; De Lange *et al.*, 1989; Pruysers *et al.*, 1993), although their formation and interpretation have been the subject of much debate.

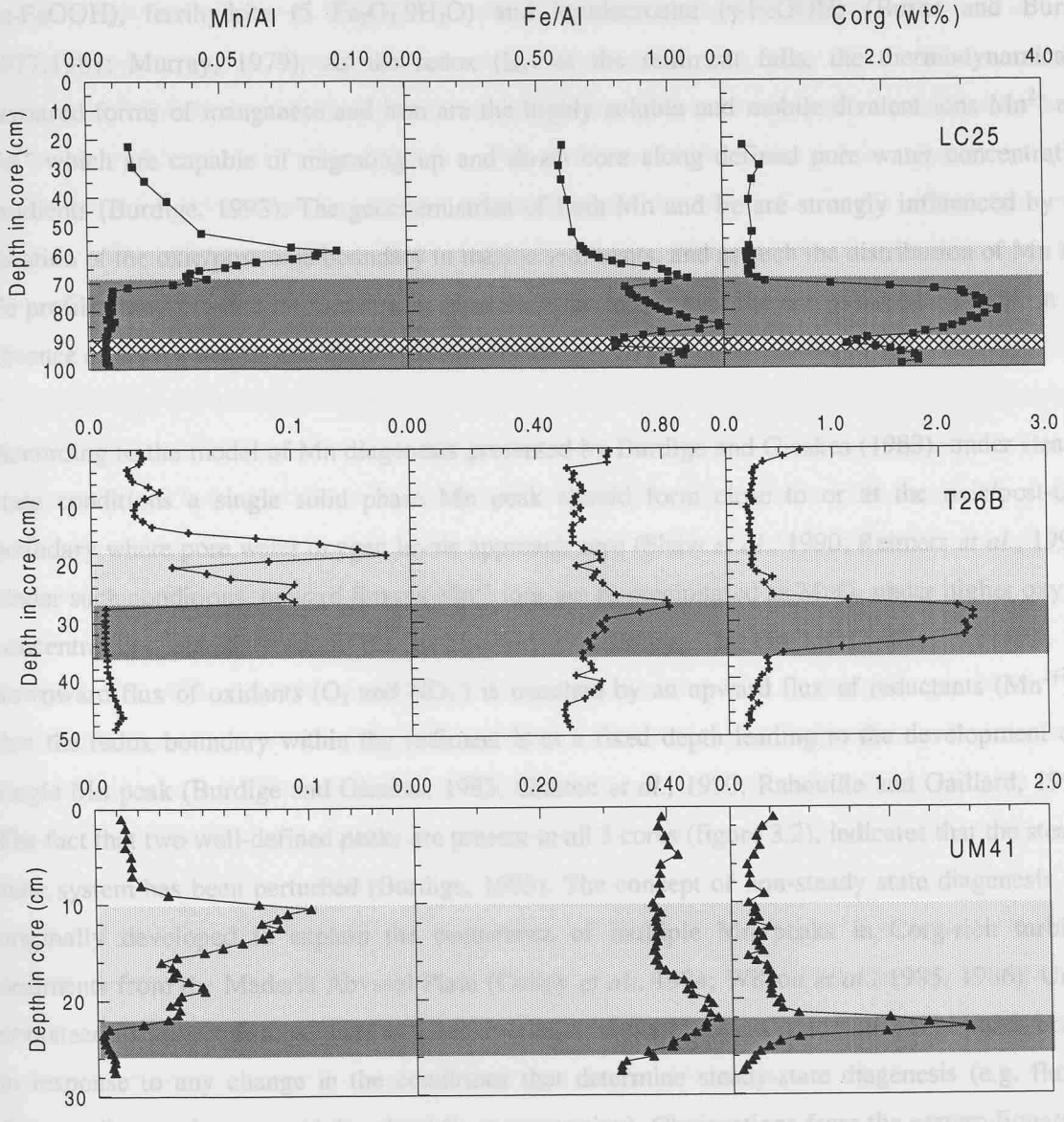

Figure 3.2. Depth-distribution of normalised excess Mn and Fe concentrations and Corg contents of LC25 (upper panel), T26B (middle panel) and UM41 (lower panel).

The geochemical behaviours of Mn and Fe are controlled primarily through changes in element oxidation states, which are governed by the redox status of the host sediment (Bruland, 1983). Under oxidising conditions, the thermodynamically-favoured forms of Mn and Fe are their respective (oxy)hydroxide phases (Stumm and Morgan, 1981). It is generally assumed that Mn is present as solid phase MnO_2 under oxidising conditions, although observations suggest that

manganese oxides are better represented by the formula MnOx, where X typically is >1 but <2 (Murray *et al.*, 1985; Gramm-Osipov, 1997). The non-stoichiometric formula implies that the average oxidation state of Mn in these oxide phases is a mixture of Mn(II), Mn(III) or Mn(IV) species. Similarly, a number of different iron phases are known to be present under more oxidising redox potentials, although the most commonly encountered oxides and oxyhydroxides are goethite (α-FeOOH), ferrihydrite (5 $Fe_2O_3.9H_2O$) and lepidocrocite (γ-FeOOH) (Burns and Burns, 1977;1981; Murray, 1979). As the redox (E_h) of the sediment falls, the thermodynamically favoured forms of manganese and iron are the highly soluble and mobile divalent ions Mn^{2+} and Fe^{2+} which are capable of migrating up and down core along defined pore water concentration gradients (Burdige, 1993). The geochemistries of both Mn and Fe are strongly influenced by the location of the oxic/post-oxic boundary in marine sediments, and as such the distribution of Mn and Fe profiles may provide information in regards to the location of the active oxidation front in the absence of pore water O_2 and nitrate measurements.

According to the model of Mn diagenesis presented by Burdige and Gieskes (1983), under steady-state conditions a single solid phase Mn peak should form close to or at the oxic/post-oxic boundary where pore water oxygen levels approach zero (Shaw *et al.*, 1990; Reimers *et al.*, 1992). Under such conditions, upward fluxing Mn^{2+} ions are re-precipitated as MnO_x under higher oxygen concentrations encountered at the oxic/post-oxic boundary. In the steady-state scenario, the downward flux of oxidants (O_2 and NO_3^-) is matched by an upward flux of reductants (Mn^{2+}) so that the redox boundary within the sediment is at a fixed depth leading to the development of a single Mn peak (Burdige and Gieskes, 1983; Gratton *et al.*, 1990; Rabouille and Gaillard, 1991). The fact that two well-defined peaks are present in all 3 cores (figure 3.2), indicates that the steady-state system has been perturbed (Burdige, 1993). The concept of non-steady state diagenesis was originally developed to explain the occurrence of multiple Mn peaks in Corg-rich turbidite sediments from the Maderia Abyssal Plain (Colley *et al.*, 1984; Wilson *et al.*, 1985, 1986). Under non-steady state conditions, there is a net migration of the oxic/post-oxic boundary, which occurs in response to any change in the conditions that determine steady-state diagenesis (e.g. flux of Corg, sedimentation rate and dissolved O_2 concentration). Observations from the eastern Equatorial Pacific indicate that the depth of the Mn^{+2}/Mn^{+4} redox boundary is inversely correlated with the flux in Corg, i.e. it occurs at a deeper level in the sediments under lower Corg rain (Finney *et al.*, 1988). In slowly-accumulated S1 examples, a downward shift in the depth of the oxic/post-oxic boundary has been recognised by Higgs *et al.* (1994) and Thomson *et al.* (1995) and is thought to occur in response to both an increase in bottom water O_2 concentrations and to a decrease in the Corg flux following sapropel formation.

Based on the assumption that Mn peaks form at depths close to where pore water O_2 concentrations reach zero levels, Higgs *et al.* (1994) and Thomson *et al.* (1995) interpreted the lower Mn peak as defining the location of the active oxidation front. Previous interpretations of the double Mn peaks by Pruysers *et al.* (1993) implied that the upper Mn peak was the site of the progressive oxidation front i.e. an upwards retreating oxic/post-oxic boundary. High-resolution pore water measurements made by Van Santvoort *et al.* (1996), demonstrated that at the depth of the lower Mn peak both O_2 and NO_3^- concentrations were approximately zero, indicating that lower Mn peaks are actively forming and define the oxic/post-oxic boundary in slowly-accumulating sapropels. Furthermore, the absence of Mn^{2+} and Fe^{2+} in the pore waters at the upper Mn peaks indicates that these upper peaks are not actively forming and so must represent the locus of a previous oxic/post-oxic boundary. By analogy with Mn, an iron peak will also form close to zero O_2 concentrations, since iron geochemistry is also dominated by sediment redox conditions. An iron peak is present in cores LC25, T26B and to a lesser extent in UM41, and it can be observed that these peaks are coincident with (T26B) or are located below the lower Mn peak (LC25) (figure 3.2). Based on the lower peaks in the Mn/Al and Fe/Al profiles, it can be inferred that an active oxidation front is present within all three cores and is located immediately above the visual sapropel. Above the lower Mn and Fe peaks, the sediments are oxic up to the sediment-water interface, and oxidation of the S1 units has occurred essentially under aerobic conditions, utilising O_2 and NO_3^- as electron acceptors.

Interpretation of the upper Mn peak has received much attention (Van Santvoort *et al.*, 1996). Prior to pore water measurements in S1-bearing sediments, the upper Mn peak was initially interpreted by Pruysers *et al.* (1993) as being diagenetic and was thought to represent the location of the progressive oxidation front. As discussed above, O_2 and NO_3^- profiles above S1 have shown that this peak is not actively forming and so can be disregarded as a plausible interpretation of this upper Mn peak. More recently, high concentrations of Mn have been found in sediments which are in close proximity to the Mid-Mediterranean Ridge (Varnavas *et al.*, 1988; De Capitani and Cita, 1996). According to De Capitani and Cita (1996), high sedimentary Mn concentrations (up to 23 wt%) were formed by hydrothermal activity in the eastern Mediterranean which was linked to the Santorini eruption. A hydrothermal origin for the upper Mn peak may be possible in some sediments close to the Mediterranean Ridge, but the presence of upper Mn peaks in cores collected from locations well away from hydrothermal inputs in the eastern Mediterranean suggest that a hydrothermal origin for the upper Mn peak is an unlikely interpretation. The third interpretation of the upper Mn peak is that it marks the point at which the oxidation front became active (Thomson *et al.*, 1995; Van Santvoort *et al.*, 1996; Thomson *et al.*, 1999). In one scenario proposed by Thomson *et al.* (1995), the upper Mn peak is thought to represent the fixation of Mn oxides in a surficial layer close to or at the sediment-water interface, when sediments were anoxic but bottom waters were still partially oxic. In such cases, Mn would continually precipitate out of solution in a

restricted layer at the oxic/post-oxic boundary poised at the sediment-water interface. Alternatively, Thomson *et al.* (1995) argued that the upper Mn peak might represent the re-oxygenation of eastern Mediterranean bottom waters following sapropel formation. At present, a number of workers have proposed that sapropel (S1) formation occurred under anoxic conditions in response to an excessive input of fresh water (*cf* chapter 1). By analogy with present-day settings which have anoxic water columns (e.g. Black Sea), the thermodynamically favoured form of Mn in the eastern Mediterranean during S1 formation would have been Mn^{2+} (Lewis and Landing, 1991; Mangini *et al.*, 1991). Upon the re-introduction of dissolved oxygen into the bottom waters, Mn^{2+} would have been oxidised to MnO_x, which would then settle at the sediment-water interface forming a well-defined Mn peak in the sediment (Mucci and Edenborn, 1992) (figure 3.2).

If the upper and lower Mn peaks do indeed represent the previous and current locations of an oxidation front respectively, then the distance between the two Mn peaks is a measure of how much post-depositional oxidation S1 has suffered following its formation. In LC25, T26B and UM41, 10, 8 and 11.5 cm of post-depositional oxidation has occurred, respectively. What these oxidation depths suggest is that significant quantities of the original sapropel have been lost after its formation through a downward-moving oxidation front. Therefore, it is inferred that S1 would have originally been much thicker than is suggested by visual evidence alone, with initially high Corg and S concentrations contained within the depths defined by the two Mn peaks.

Below the lower Mn and Fe peaks in LC25, T26B and UM41, Mn/Al concentration ratos are consistently and uniformly low within and below the visual sapropel, ranging from 0.005-0.02. It is known that above the sapropel, oxidation of Corg occurs via O_2 and NO_3^- reduction, and the lower peaks in Mn and Fe mark the locus of the oxic/post-oxic boundary. Below this depth, the appearance of Mn^{2+} and Fe^{+2} within the pore waters (Van Santvoort *et al.*, 1996) is coincident with uniformly low solid-phase Mn concentrations and suggests that, within and below the sapropel, oxidation of Corg occurs via Mn and Fe oxide reduction according to equations 3.3 and 3.4. Like Mn, it is expected that uniformly low Fe concentrations should be found below the redox front in sub-oxic conditions, considering that Fe oxides are thermodynamically unstable under more reducing conditions. The fact that relatively high Fe concentrations still persist below the redox boundary implies that Fe is not present as an oxide, but rather it is present as a solid phase which is stable under more reducing conditions. Considering that the Fe profile is similar to that of S implies that iron may exist as pyrite, and the immobilisation of both iron and sulphur under sub-oxic conditions will be discussed further in section 3.4.3.

3.4.2. Barium, Organic Carbon and Sulphur.

Further evidence consistent with the concept that the upper faces of slowly-accumulated sapropels have undergone post-depositional oxidation comes from the observations provided by the Ba/Al profiles in LC25, T26B and UM41. High-resolution investigation of three S1s by Thomson *et al.* (1995), revealed that the Ba/Al profiles exhibited a 'quasi-Gaussian' distribution in all three cores. From these observations, Thomson *et al.* (1995) proposed that Ba/Al profiles may be used as a proxy for defining not only the original thickness of S1 units but also for assessing the Corg content of the oxidised portions of the sapropel units.

The implicit assumption concerning the use of Ba/Al as a geochemical proxy in sapropel investigations relies upon numerous observations that Corg-rich sediments, including sapropels, often contain elevated Ba concentrations (Calvert, 1983; Klinkhammer and Lambert, 1989; Thomson *et al.*, 1995; 1999; Van Santvoort *et al.*, 1996). A positive correlation exists between the Ba (as the mineral barite) and Corg in both sediments and sediment trap material (Dehairs *et al.*, 1980; Dymond, 1981; Collier and Edmond, 1984; Dymond *et al.*, 1992; Dymond and Collier, 1996). This has led to the hypothesis that sedimentary Ba concentrations may be useful in reconstructing the productivity in older marine sediments (Dymond *et al.*, 1992; Francois *et al.*, 1995; Nijenhuis, 1999). Whilst the exact mechanism by which Ba and Corg are linked is unknown, it is believed by many authors that the barite formation occurs in reducing environments provided by specific (e.g. Acantharians, Bernstein *et al.*, 1998) and aspecific Corg-rich particles in the water column (Dehairs *et al.*, 1980; Collier and Edmond, 1984; Bishop, 1988), although a number of workers have proposed that barite formation occurs via active biological precipitation by specific planktonic species (Gooday and Nott, 1982).

As with other proxies, the accuracy and reliability of using Ba/Al ratios is dependent upon its stability and persistence within the sediment over long periods of time following sapropel formation. Investigations on the geochemistry of barite in sediments have shown that this mineral is capable of undergoing dissolution and remobilisation under sulphate reducing conditions (Brumsack, 1986; McManus *et al.*, 1994). During extensive sulphate depletion, barite dissolves producing Ba^{2+}, which is capable of migrating both up and down core. Upon encountering the sub-oxic/sulphate reduction boundary in sediments, Ba^{2+} has the capacity of re-precipitating out of solution as barite forming well-defined diagenetic 'barite fronts' (Torres *et al.*, 1996). Whilst it is accepted that the sulphate reduction occurred during S1, uniform $\delta^{34}S$ isotope data presented by Passier *et al.* (1996) indicates that pore water sulphate concentrations were never limiting, but had a continual influx of SO_4^{2-} from the overlying seawater into the sediment. Furthermore, pore water

profiles in combination with S speciation studies indicate that sulphate reduction was limited to periods during and just shortly after sapropel formation (Van Santvoort *et al.*, 1996; Passier and De Lange, 1998). As such it seems likely that no remobilisation of Ba has occurred either during or after S1 formation and is in agreement with the findings presented in chapter 5 that barium is a persistent and stable proxy. The Ba/Al profiles therefore offer an accurate and reliable tool in establishing the original thickness and Corg content of partially-oxidised sapropel units.

Whilst it has been recognised that some diagenetic remobilisation of Ba has occurred in some sapropel-bearing sediments (Van Os *et al.*, 1991), normalised Ba profiles reveal that barium behaves in a systematic way in all the cores examined (figure 3.3).

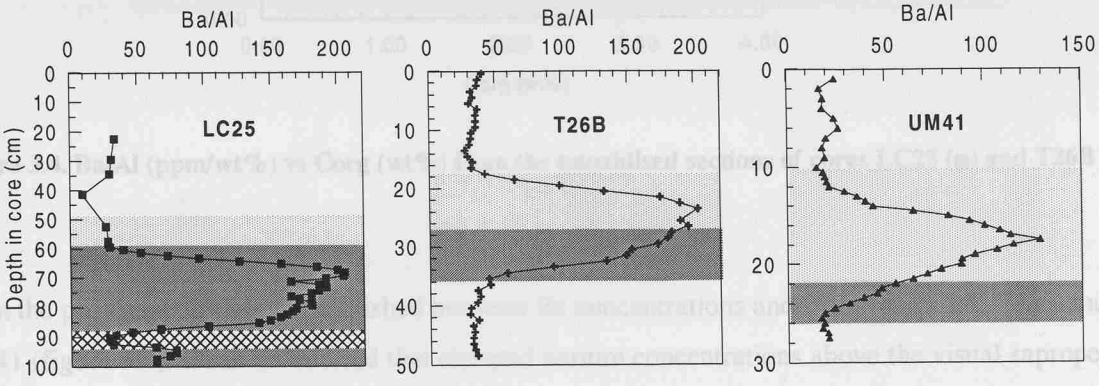

Figure 3.3. Depth distribution of Ba/Al (ppm/wt%) in LC25, T26B and UM41.

It is evident from figure 3.3 that the Ba/Al profiles exhibit a 'quasi-Gaussian' distribution previously noted for other slowly-accumulated sapropels (Thomson *et al.*, 1995; Van Santvoort *et al.*, 1996). In all the cores examined, the onset of elevated Ba concentrations coincides with the visual base of the S1 units (i.e. the onset of higher Corg concentrations) but terminates well above the visual top of the S1 unit and coincides with the upper Mn peak in all cases. Excess Ba concentrations between the base of the sapropel and the upper Mn peak is in the form of discrete, micron sized barite ($BaSO_4$) particles as revealed by SEM-EDS analysis of material collected from these intervals. Comparison of the Ba/Al profiles with those of Corg reveal that within the visual sapropel, high concentrations of barium tend to coincide with elevated levels Corg (which defines the depth of S1), implying that that Ba and Corg are geochemically linked during sapropel formation. Plotting excess Ba against Corg concentrations for the unoxidised portion the sediment from LC25, T26B and UM41 reveals that a high degree of correlation exists between organic carbon and barium (figure 3.4)

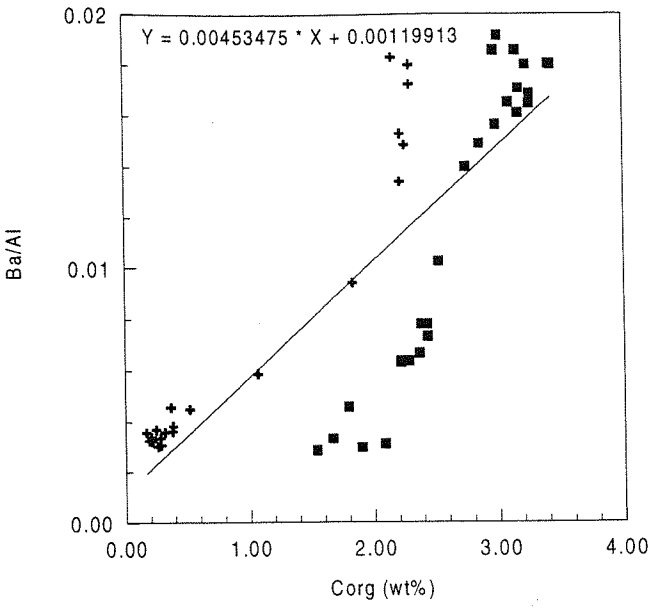

Figure 3.4. Ba/Al (ppm/wt%) vs Corg (wt%) from the unoxidised sections of cores LC25 (■) and T26B (✚).

From the positive correlation established between Ba concentrations and Corg for LC25, T26B and UM41 (figure 3.4), it can be inferred that elevated barium concentrations above the visual sapropel in all three cores represent the elevated Corg concentrations that were originally present between the two Mn peaks prior to oxidation by the progressive oxidation front. The fact that the Ba/Al concentrations return to 'background' levels at some considerable distance above the visual sapropel suggests that S1 (and Corg and S concentrations) must have originally been much thicker, as initially inferred by the presence of upper Mn peak in all the cores examined. Thus the difference between the lower Mn peak and the return of background Ba/Al concentrations (which coincide with the upper Mn peak) is therefore an indication of how much post-depositional oxidation S1 has suffered following its formation. Modelling the amount of post-depositional oxidation in S1-bearing sediments by Jung *et al.* (1997) demonstrates that the amount of oxidation is dependent upon the sedimentation accumulation rate of the cores. Sediment accumulation rates for cores LC25 and T26B are provided by AMS-^{14}C dating (see appendix 7) and according to the model presented by Jung *et al.* (1997), these cores should theoretically experience 8 and 9 cm of oxidation respectively, which is in good agreement with the estimates provided by the distance between the Mn peaks (10 and 8cm).

The effect of oxidation on the Corg and S profiles is evident in all 3 cores (figure 3.5). In all cases, only residual amounts of Corg and S are present with the most labile fractions of both organic carbon and sulphur having been oxidised during the introduction of O_2 and nitrate from the oxidation front, and only the most refractory components remaining above S1 in oxic conditions.

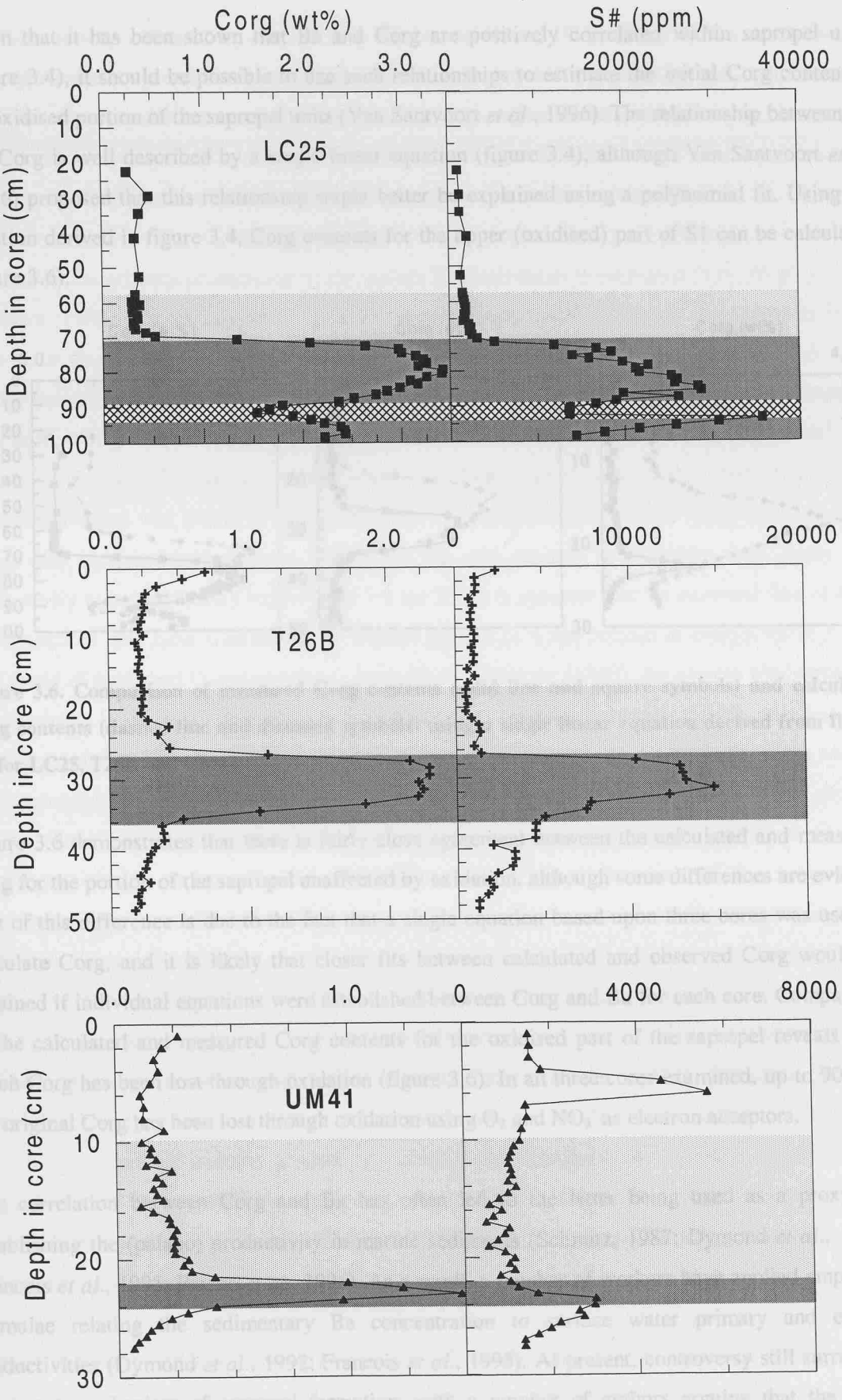

Figure 3.5. Depth distribution of Corg (wt%) and seawater corrected sulphur, S# (ppm) concentrations for LC25, T26B and UM41.

Given that it has been shown that Ba and Corg are positively correlated within sapropel units (figure 3.4), it should be possible to use such relationships to estimate the initial Corg content of the oxidised portion of the sapropel units (Van Santvoort *et al.*, 1996). The relationship between Ba and Corg is well described by a single linear equation (figure 3.4), although Van Santvoort *et al.* (1996) proposed that this relationship might better be explained using a polynomial fit. Using the equation derived in figure 3.4, Corg contents for the upper (oxidised) part of S1 can be calculated (figure 3.6).

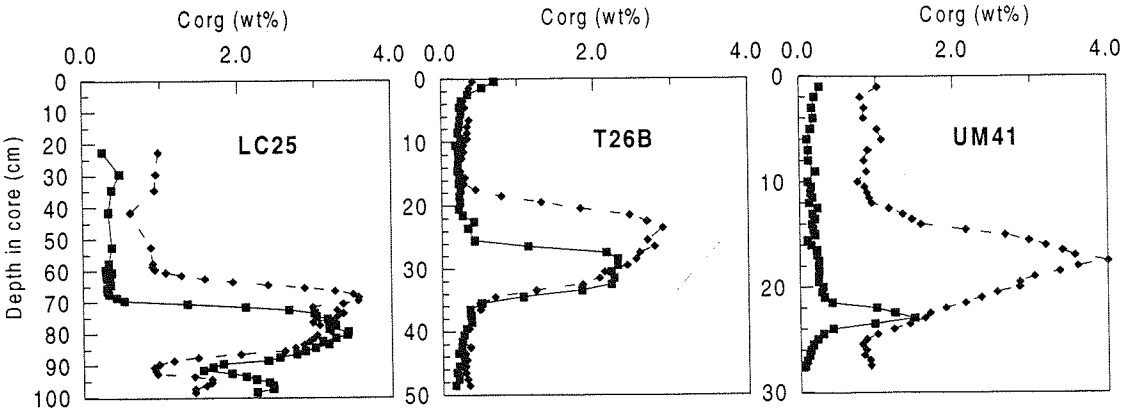

Figure 3.6. Comparison of measured Corg contents (solid line and square symbols) and calculated Corg contents (dashed line and diamond symbols) using a single linear equation derived from figure 3.4 for LC25, T26B and UM41.

Figure 3.6 demonstrates that there is fairly close agreement between the calculated and measured Corg for the portion of the sapropel unaffected by oxidation, although some differences are evident. Part of this difference is due to the fact that a single equation based upon three cores was used to calculate Corg, and it is likely that closer fits between calculated and observed Corg would be obtained if individual equations were established between Corg and Ba for each core. Comparison of the calculated and measured Corg contents for the oxidised part of the sapropel reveals how much Corg has been lost through oxidation (figure 3.6). In all three cores examined, up to 90% of the original Corg has been lost through oxidation using O_2 and NO_3^- as electron acceptors.

The correlation between Corg and Ba has often led to the latter being used as a proxy for establishing the (palaeo) productivity in marine sediments (Schmitz, 1987; Dymond *et al.*, 1992; Francois *et al.*, 1995; Paytan *et al.*, 1996). As a result, a number of workers have applied empirical formulae relating the sedimentary Ba concentration to surface water primary and export productivities (Dymond *et al.*, 1992; Francois *et al.*, 1995). At present, controversy still surrounds the exact mechanism of sapropel formation, with a number of authors arguing that the Corg concentrations within sapropels cannot be explained entirely in terms of enhanced preservation of Corg under anoxic conditions (chapter 1). Most methods of estimating palaeoproductivity within

sediments rely upon their Corg contents (e.g. Muller and Suess, 1979). Since Ba has not undergone any significant diagenetic remobilisation following sapropel formation, the Ba concentrations therefore represent the most reliable way of assessing surface water productivity in the eastern Mediterranean by applying equations which relate Ba to primary productivity. The equations used to estimate primary productivity during S1 formation can be found in chapter 5.

At present, the primary productivity of the eastern Mediterranean is estimated to be 26 gC m^{-2} yr^{-1} (Bethoux, 1989). Reconstruction of (palaeo) primary productivity values for the sapropels based upon their Ba contents indicates that during sapropel formation productivity was ~2-3.5 times greater than at present. These estimated productivity levels are comparable to those values found in high productivity areas such as the Atlantic Ocean off North West Africa (50-250 gC m^{-2} yr^{-1}, Muller and Suess, 1979) and are consistent with one of the main hypotheses that productivity rather than preservation was primarily responsible for the periodic deposition of Corg-rich sediments within the eastern Mediterranean. Whilst the Ba and primary productivity data imply that productivity was significantly increased at 9-5 kyr BP, it is apparent that an increased flux of Corg to the seafloor may have simultaneously induced periods of water column or bottom water anoxia as a result of increased O_2 consumption. According to Bethoux (1989), the eastern Mediterranean water column is oxic to all depths since the flux of Corg to the deep waters is significantly less than the supply of dissolved O_2. The present-day production and supply of dissolved O_2 to the eastern Mediterranean through deep-water formation in the Adriatic and Levantine seas is $1*10^{13}$ mol O_2 yr^{-1} (Bethoux, 1989). Comparison of newly produced and stored organic matter during S1 formation yields an oxygen demand of $3*10^{13}$ mol O_2 yr^{-1}, well in excess of that supplied by present day deep-water formation. This suggests that water column or bottom water anoxia could have been achieved within the eastern Mediterranean through the increased production of Corg during S1 formation without the need for any reduction in deep-water formation. It cannot be ruled out, however, that a reduction in deep-water formation occurred during S1 considering that sapropel deposition coincides with periods of intensified monsoonal activity (Rossignol-Strick *et al.*, 1982; Rossignol-Strick, 1985). It seems likely that S1 formation was initially induced by significant increases in primary productivity which then subsequently led to water column anoxia when the Corg flux exceeded the supply of O_2 to the bottom waters. Water column anoxia would have been promoted further if deep-water formation within the Adriatic/Levantine Seas had ceased or become reduced by comparison with the present day.

One of the most debated topics concerning S1 formation has centred upon the timing of its formation. Early radiocarbon dating of S1 has placed its duration from 7-9 kyr BP (Vergnaud-Grazzini *et al.*, 1986). Whilst the onset of sapropel deposition is fairly well constrained (8.97 kyr BP), the termination of S1 is varied with estimates placing the end of S1 formation between 6.37

and 8.03 kyr BP (Fontugne *et al.*, 1994). A primary cause of this variation is that previous investigations have not taken into consideration the removal of the upper face of S1 has occurred through post-depositional oxidation. As such, in slowly-accumulated sapropels, the visual top of S1 is not always the point at which sapropel formation ended. Whilst the onset of elevated Ba/Al and Corg concentrations are approximately coincident at the base of S1, the Ba/Al profile indicates that high productivity continued for a longer period than as suggested by the Corg profiles for all three cores. The discrepancy between the Ba/Al and Corg profiles for the top of S1 is due to the oxidation of Corg from the upper face of the sapropel unit. Since Ba/Al ratios and Corg have been shown to be well correlated and that Ba is a reliable proxy for visualising the waxing and waning of productivity (compared to Corg), then dating the points at which the barium concentrations rise and return to baseline values will provide a more accurate way of constraining the duration of S1. The use of Ba/Al ratios in constraining the chronology of S1 formation is explored further in chapter 6.

3.4.3. Iron and Sulphur.

It is evident from the Fe profiles in LC25, T26B and UM41 that under more oxidising conditions iron is immobilised as an iron oxyhydroxide phase, however, under more reducing conditions thermodynamics predict that the most favourable form of Fe is the soluble Fe^{+2} species. It is clear therefore, that enrichment of Fe below the redox front must involve a reduced Fe species that is stable and persistent under sub-oxic conditions (figure 3.7). The close correlation between Fe and S profiles suggests that these two elements are being immobilised under reducing conditions as an iron sulphide phase.

Plotting excess sulphur and Fe reveals that the data cluster around the regression line for pyrite (FeS_2) (figure 3.8), although a number of points from LC25 are intermediate between iron monosulphides and pyrite suggesting that iron species with mixed stoichiometries are present. A number of points plot well above the regression line for FeS_2 (core T26B) indicating that an excess of S relative to Fe is present. This suggests that other phases of S are present within the sapropel, and according to Passier (1998), may indicate the formation of organically-bound sulphur (OBS). It has been demonstrated that during sulphate reduction, if the supply of Fe^{+2} is limited relative to sulphide production then the excess HS^- is taken up by organic matter to form OBS (Raiswell *et al.*, 1993; Hartgers *et al.*, 1997).

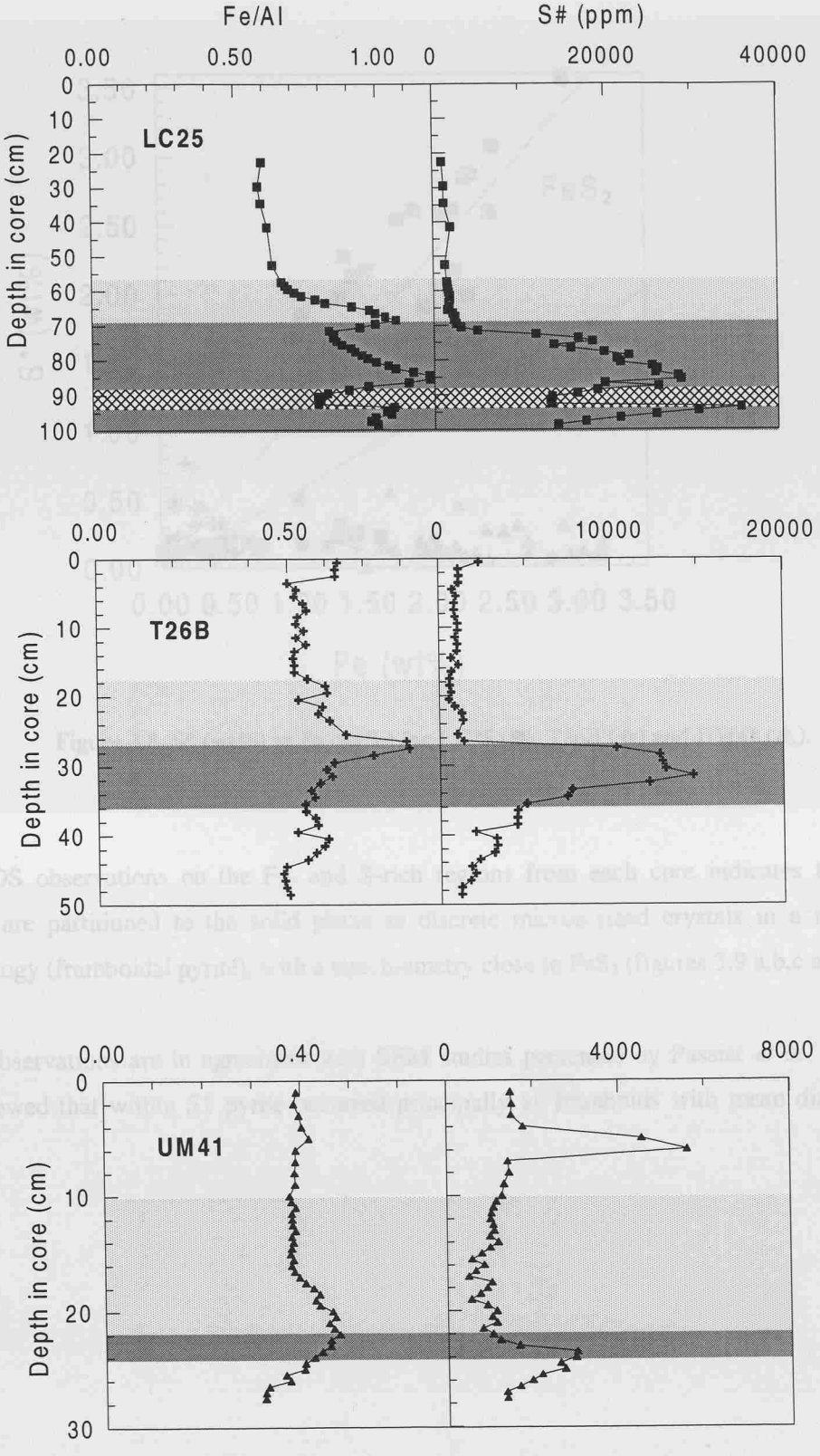

Figure 3.7. Depth distribution of Fe/Al (wt%/wt%) and sea water corrected sulphur concentrations (ppm) in LC25, T26B and UM41.

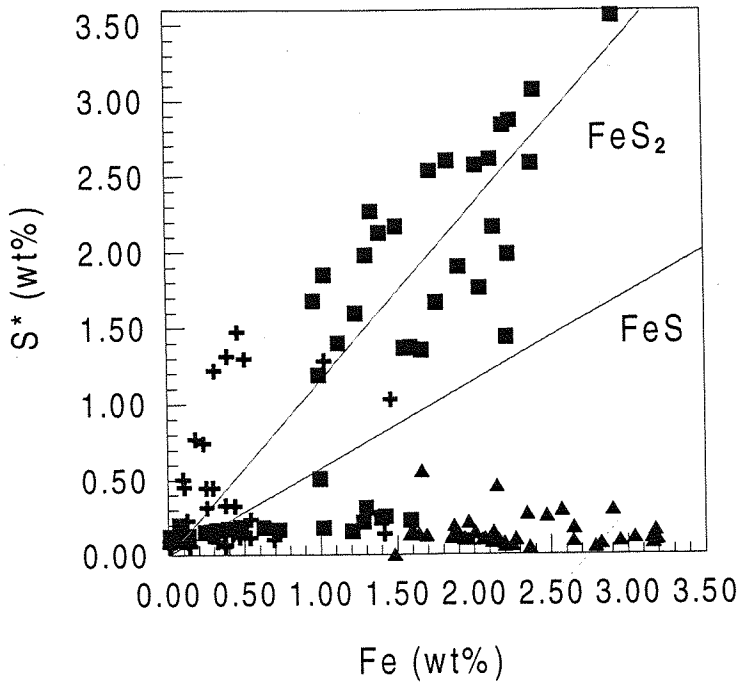

Figure 3.8. S* (wt%) vs Fe (wt%) for LC25 (■), T26B (✚) and UM41 (▲).

SEM-EDS observations on the Fe- and S-rich regions from each core indicates that iron and sulphur are partitioned to the solid phase as discrete micron-sized crystals in a raspberry-like morphology (framboidal pyrite), with a stoichiometry close to FeS_2 (figures 3.9 a,b,c and d).

These observations are in agreement with SEM studies presented by Passier *et al.* (1997; 1999) who showed that within S1 pyrite occurred principally as framboids with mean diameters of 5-10μm.

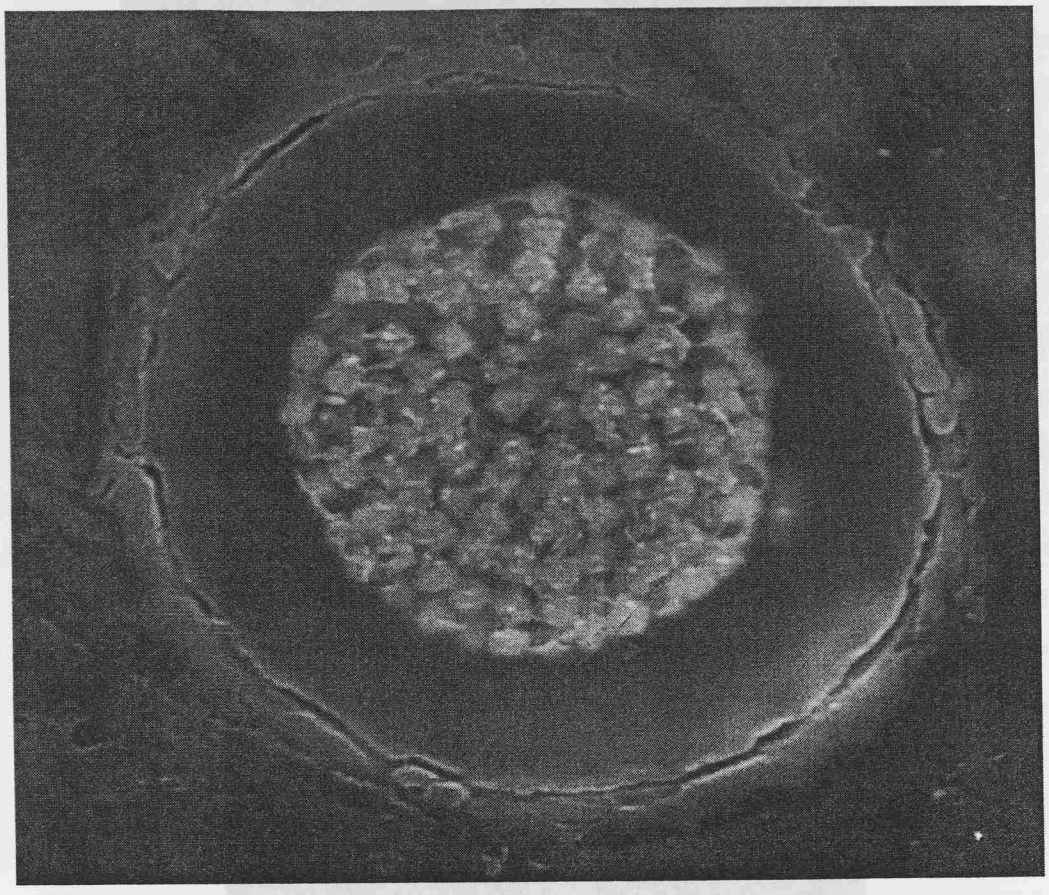

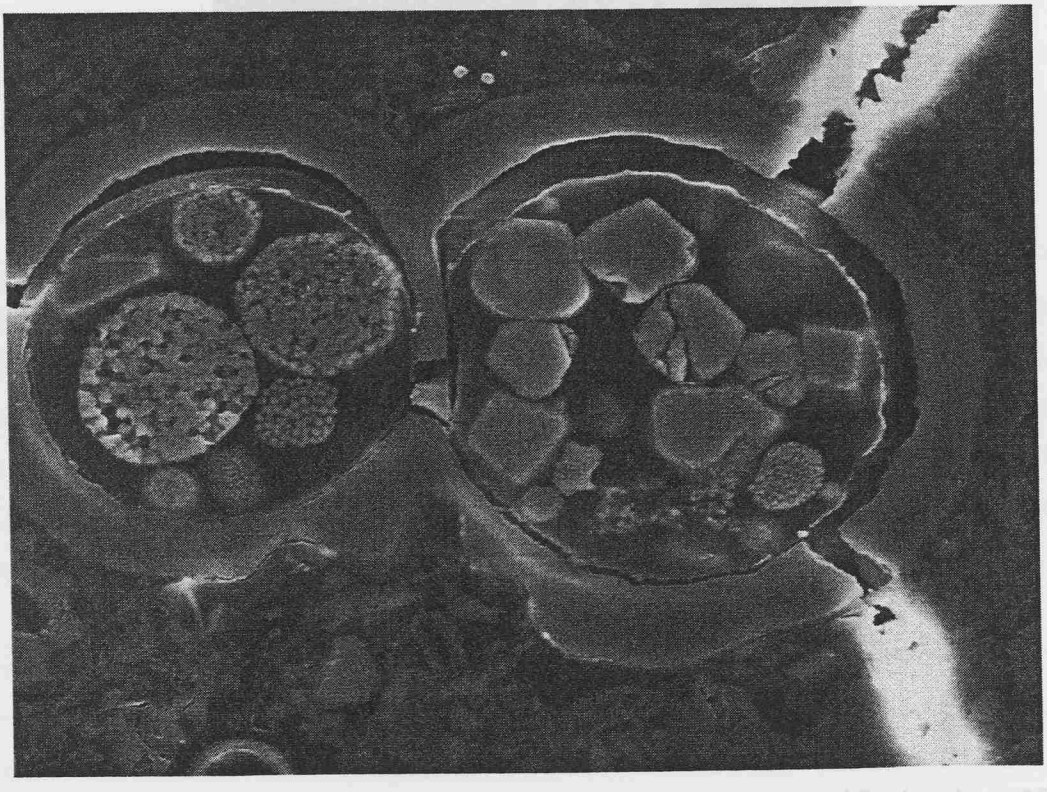

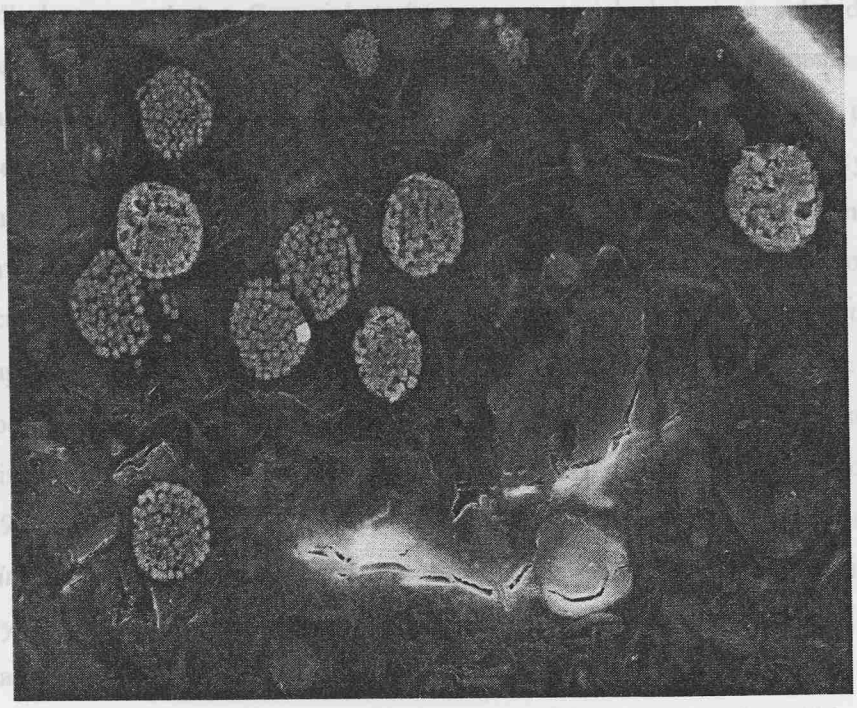

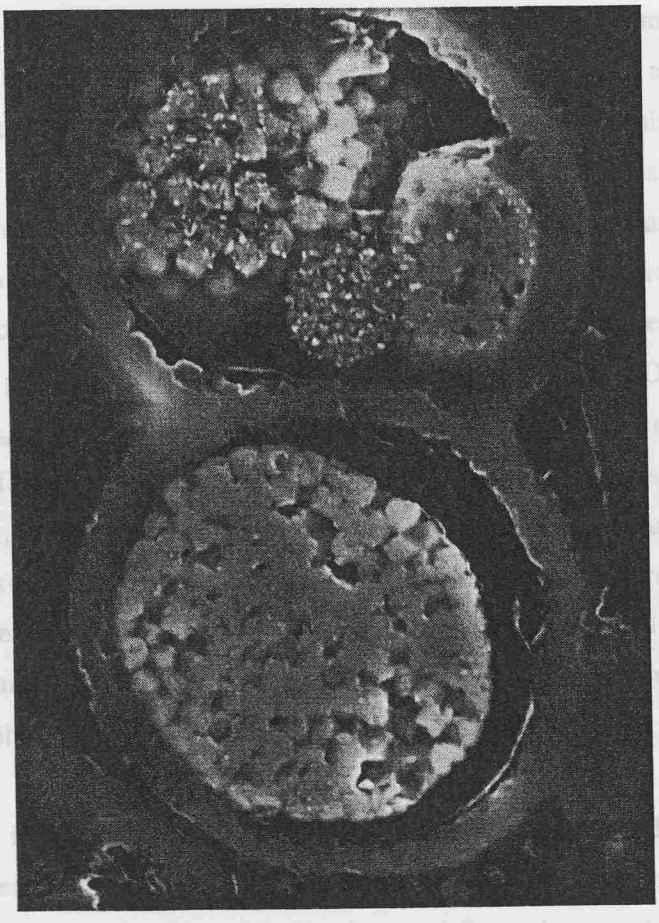

Figures 3.9 a, b, c and d. Examples of framboidal pyrite found within the un-oxidised regions of S1 in LC25 (a and b), T26B (c) and UM41 (d).

It has been well documented that Corg-rich sediments are enriched in iron sulphide phases (Raiswell and Berner, 1985; Calvert and Karlin, 1991; Calvert *et al.,* 1996). In sediments with high accumulation rates of Corg, diagenesis often proceeds down to sulphate reduction, producing dissolved sulphide as a by-product (see equation 3.5). There is still a degree of uncertainty over the exact mechanism by which pyrite forms, but it is generally believed that pyrite formation is a two-stage process involving (1) the reduction of sulphate and ferric iron to form iron monosulphides and (2) the reaction of iron monosulphides (greigite) with sulphur to form pyrite (Berner, 1970; Sweeny and Kaplan, 1973; Schoonen and Barnes, 1991a,b; Wilkin and Barnes, 1996). The $\delta^{34}S$ values of framboidal pyrite within a slowly-accumulated sapropel investigated by Passier *et al.* (1997; 1999) displayed fractionations of up to 57.7-70.2 ppt relative to seawater. According to Passier *et al.* (1997) this degree of fractionation is consistent with sulphate reduction and sulphide production *in situ* within S1, where SO_4^{2-} was derived principally from overlying seawater and so never limited pyrite formation. The presence of framboidal pyrite within S1 can be explained in terms of the relative production rates and mobilities of sulphide and Fe^{+2} (Berner, 1969; Passier *et al.*, 1997). According to Passier *et al.,* (1997), the formation of framboidal pyrite within S1 occurs when the production and supply of reactive Fe is well in excess of the HS^- that is generated by bacterial sulphate reduction in the Corg-rich layer (i.e. the high-Fe-content model proposed by Berner, 1969). As a result, Fe^{+2} continually diffuses upwards into the sapropel and reacts with the HS^- to produce pyrite. It is believed that the sources of Fe^{+2} are detrital Fe within the sapropel and the upward diffusion of Fe^{+2} released from sub-oxic sediments below S1 (Passier and De Lange, 1998). Insignificant amounts of acid-volatile sulphur (AVS), and S in organic polysulphudes ($S_{orgpoly}$), which are possible intermediates in pyrite formation (Luther and Church, 1992), are now found in S1 (Passier and De Lange, 1998). Since long-term accumulation of these intermediates is not possible, then the presence of these species are indicative of active SO_4^{2-} reduction. The absence of AVS and $S_{orgpoly}$ implies that no SO_4^{2-} reduction and no pyrite formation is presently occurring in S1. These findings are in agreement with pore water measurements of S1 investigated by Van Santvoort *et al.*, (1996), where it was demonstrated that diagenesis was proceeding at the sub-oxic stage. The close coincidence between the Fe and S profiles below the redox front suggests that these elements were being immobilised as the mineral pyrite, however, so that the formation of pyrite must have occurred either during or just shortly after S1 formation when diagenesis proceeded down to sulphate reduction.

A conspicuous feature in a number of slowly-accumulated cores, including T26B, is a sharply-defined grey colouration immediately below the sapropel. These grey regions are characterised by high sedimentary S levels but low Corg concentrations and form sharp contacts with the upper sapropel and lower, more oxic sediments beneath. According to sedimentological interpretations presented by Anastasakis and Stanley (1986), the grey colouration is thought to represent the onset

of restricted bottom water formation and circulation within the eastern Mediterranean prior to the deposition of the S1 proper. This feature has been termed the 'protosapropel' by a number of authors. More recently however, the 'protosapropel' interpretation has been challenged by Passier *et al.* (1996) who suggests that this feature is diagenetic in origin. SEM-EDS analysis and sequential leaching studies on the 'protosapropel' have shown that this region is dominated by euhedral pyrite crystals approximately 2-10μm in diameter (Passier *et al.*, 1997).

According to Passier *et al.* (1997), the presence of pyrite below the sapropel can again be explained in terms of the production and mobility of sulphide and reactive Fe. Experimental studies performed by Berner (1969) on the mobility of Fe and sulphide in Corg-rich sediments demonstrated that where the supply and/or generation of Fe^{+2} was low relative to sulphate reduction and HS^-, downward sulphidisation fronts developed with HS^- migrating out of Corg-rich layers, (Berner's low-Fe-content model). Sulphur isotope data from the 'protosapropel' indicates that HS^- was derived from sulphate reduction within the sapropel itself and supports the idea that sulphide has migrated out of S1 at some point. Considering that the 'protosapropel' is diagenetic and post-depositional in origin, it is likely that it formed shortly during or after S1 formation when the flux of Corg was sufficiently high to allow for the reduction of sulphate in the remineralisation of Corg. Passier (1998) suggests that 'protosapropel' should be more accurately termed synsapropel.

3.4.4. Uranium, Vanadium, Molybdenum and Arsenic.

3.4.4.1 Uranium.

Uranium is preferentially enriched in sub-oxic, Corg-rich marine sediments (Bernat and Church, 1989; Barnes and Cochran, 1993; Legeleux *et al.*, 1994). Normalised uranium-depth profiles in LC25, T26B and UM41 all display a stepped profile, with elevated concentrations confined to regions below the inferred limit of oxidation front (figure 3.10).

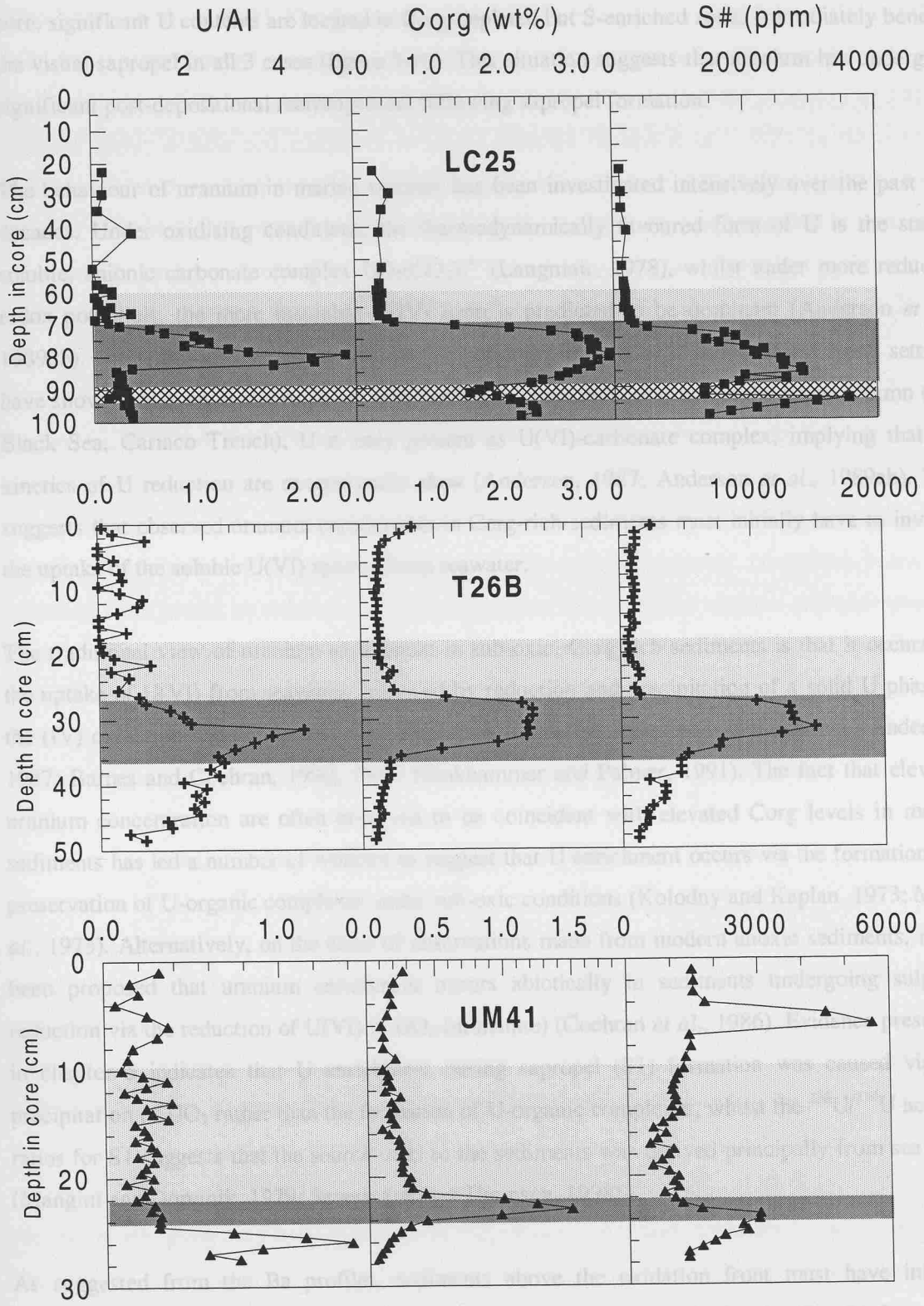

Figure 3.10. U/Al, Corg and S# in LC25, T26B and UM41.

Previous investigations on the behaviour of uranium in sapropel-bearing sediments have concluded that in general the U profile closely matches that of the Corg profile (cf chapter 5; Ten Haven *et al.*, 1987). Whilst high uranium concentrations are found within the Corg-rich sapropel units in each

core, significant U contents are located in Corg-depleted but S-enriched zones immediately beneath the visual sapropel in all 3 cases (figure 3.10). This situation suggests that uranium has undergone significant post-depositional rearrangement following sapropel formation.

The behaviour of uranium in marine systems has been investigated intensively over the past few decades. Under oxidising conditions, the thermodynamically favoured form of U is the stable, soluble, anionic carbonate complex $UO_2(CO_3)_3^{4-}$ (Langmuir, 1978), whilst under more reducing redox potentials, the more insoluble U(IV) form is predicted to be dominant (Anderson *et al.*, 1989ab). Numerous measurements on the U speciation in both oxic and anoxic marine settings have shown that even in environments undergoing sulphate reduction within the water column (e.g. Black Sea, Cariaco Trench), U is only present as U(VI)-carbonate complex, implying that the kinetics of U reduction are exceptionally slow (Anderson, 1987; Anderson *et al.*, 1989ab). This suggests that observed uranium enrichments in Corg-rich sediments must initially have to involve the uptake of the soluble U(VI) species from seawater.

The traditional view of uranium enrichment in sub-oxic, Corg-rich sediments is that it occurs via the uptake of U(VI) from seawater, followed by reduction and precipitation of a solid U phase in the (IV) oxidation state under reducing conditions below the sediment-water interface (Anderson, 1987; Barnes and Cochran, 1990; 1991; Klinkhammer and Palmer, 1991). The fact that elevated uranium concentration are often observed to be coincident with elevated Corg levels in marine sediments has led a number of workers to suggest that U enrichment occurs via the formation and preservation of U-organic complexes under sub-oxic conditions (Kolodny and Kaplan, 1973; Mo *et al.*, 1973). Alternatively, on the basis of observations made from modern anoxic sediments, it has been proposed that uranium enrichment occurs abiotically in sediments undergoing sulphate reduction via the reduction of U(VI) to UO_2 (uraninite) (Cochran *et al.*, 1986). Evidence presented in chapter 5 indicates that U enrichment during sapropel (S1) formation was caused via the precipitation of UO_2 rather than the formation of U-organic complexes, whilst the $^{238}U/^{234}U$ activity ratios for S1 suggests that the source of U to the sediments was derived principally from seawater (Mangini and Dominik, 1979; Severmann and Thomson, 1998).

As suggested from the Ba profiles, sediments above the oxidation front must have initially contained high Corg contents. As such, it is expected that during and shortly after S1 formation, high U concentrations would have been found between the upper and lower Mn peaks in all cores. The U/Al profiles for LC25, T26B and UM41 reveal that systematically low U concentrations are now found immediately above the oxidation front in all 3 cores (figure 3.10). Similar low U concentrations have been reported for Corg-rich turbidite and sapropel-bearing sediments affected by progressive oxidation fronts (Colley and Thomson, 1985; Wallace *et al.*, 1988; Colley *et al.*,

1989; Thomson *et al.*, 1993; Ten Haven *et al.*, 1987; Thomson *et al.*, 1995). By analogy with U reallocation patterns found in turbidite sediments, it is believed that following sapropel formation the introduction of O_2 into the sediments by the oxidation front caused the oxidation of UO_2 to form the highly soluble and mobile U-carbonate complex (Bruno *et al.*, 1988). In the oxidised sediments above the oxidation front only the detrital uranium content of the sapropel sediment now remains, with the U-carbonate complex migrating both up and down core according to pore water concentration gradients. Some of the remobilised U migrates up the core where it is eventually lost to the overlying seawater, whilst some portion of U is continuously relocated below the oxidation front to become re-reduced and immobilised as a solid phase in sub-oxic conditions.

Pore water, $\delta^{34}S$ and S speciation studies have demonstrated that the concentrations of reduced sulphur species such as HS^- and H_2S are negligible, indicating that sulphate reduction ended shortly after S1 formed (Van Santvoort *et al.*, 1996; Passier *et al.*, 1996; Passier, 1998). Accordingly, it seems unlikely that any downward migrating U(VI) entering sub-oxic conditions below the oxidation front would be reduced and immobilised as UO_2 given the absence and generation of reduced sulphur species. More recently however, it has been suggested that U can become immobilised (as UO_2) by bacterial populations that are responsible for Fe(III) reduction (Mohagheghi *et al.*, 1985; Gorby and Lovely, 1992). According to Cochran *et al.* (1986), uranium is utilised as an electron acceptor in the oxidation of Corg according to the reaction:-

$$\mathbf{CH_2O + 2\ UO_2(CO_3)_3^{4-} + H_2O \leftrightarrow 2\ UO_2 + 6\ HCO_3^- + CO_2} \quad \textbf{Equation 3.6}$$

Laboratory studies have shown that Fe(III) reducing bacteria can utilise U(VI) to gain enough energy so that U reduction and precipitation occurs after Mn reduction and starts almost simultaneously with Fe reduction (Lovely *et al.*, 1991; Klinkhammer and Palmer, 1992). Alternatively, it has been proposed that reduction of U immobilisation in recently-accumulated sediments can also occur via the metastable U(V) species (Kniewald and Branica, 1988;1990). It is likely that U(VI) migrating below the oxidation front is reduced and immobilised either during the oxidation of Corg (equation 3.6) rather than being directly precipitated as UO_2 from U(VI), given the lack of HS^- generation in S1. Evidence to suggest that U has been continuously relocated below the sapropel and immobilised by the prevailing redox conditions comes from the observation that there is marked differential behaviour between ^{234}U and ^{238}U in S1 (Mangini and Dominik, 1979; Severmann and Thomson, 1998). This isotopic disequilibrium is generally ascribed to the preferential diffusion of ^{234}U in the (VI) oxidation state produced *in situ* from ^{238}U in the (IV) oxidation state through radioactive decay.

3.4.4.2. Vanadium.

Like uranium, normalised vanadium profiles for LC25, T26B and UM41 display a stepped profile with elevated concentrations confined mainly to within and below the visual sapropel unit in LC25 and T26B, although some enrichment within the oxic region of UM41 can be identified (figure 3.11).

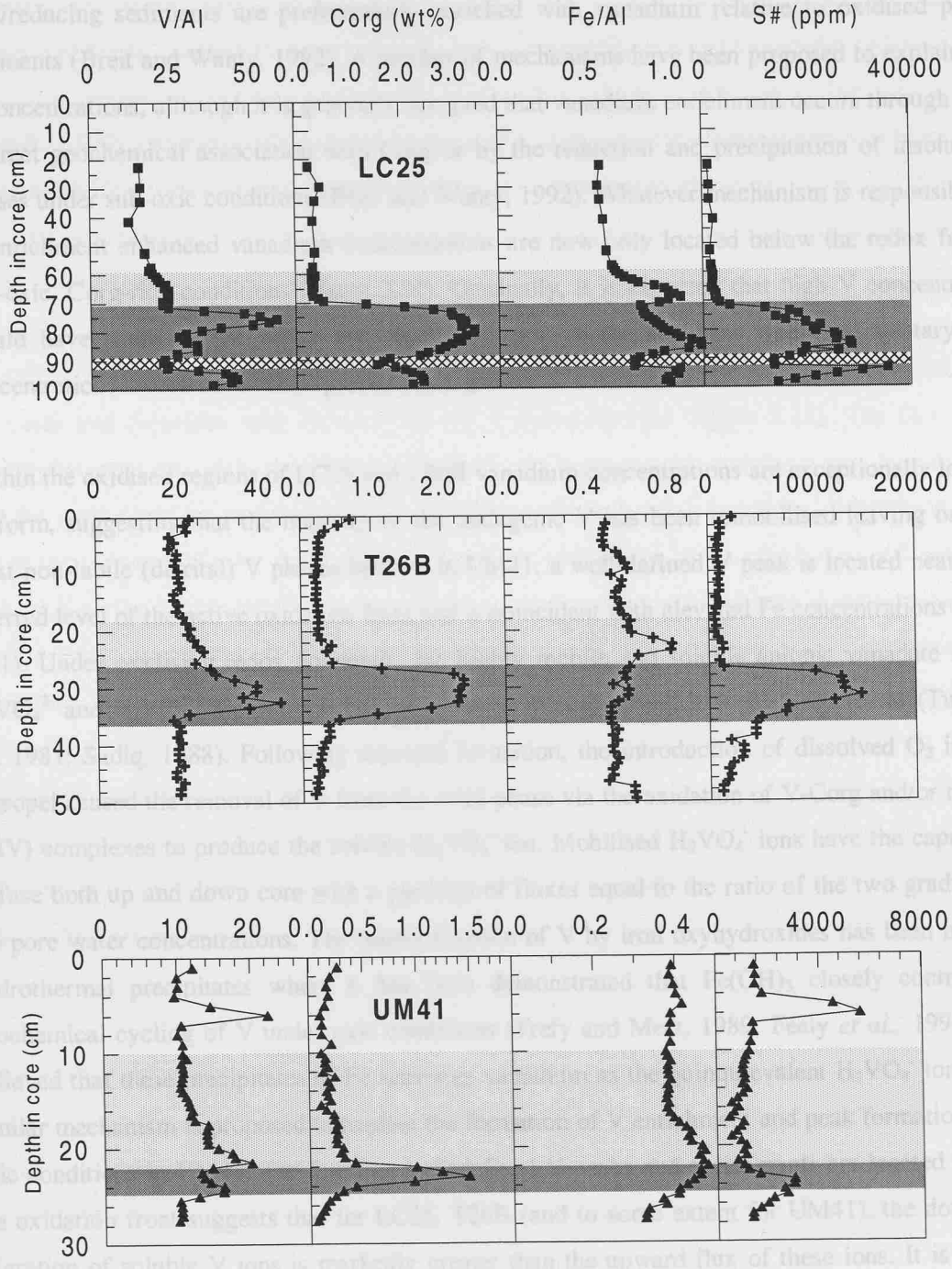

Figure 3.11. Concentration-depth profiles of V/Al (ppm/wt%), Corg (wt%), Fe/Al (wt%/wt%) and seawater corrected S (ppm) in LC25, T26B and UM41.

Whilst the uranium profiles display rather broad enrichments below the oxic/post-oxic boundary, vanadium is concentrated into better-defined peaks located immediately below the inferred location of the redox front, although a number of deeper V peaks in regions dominated by high S and Fe levels can be identified (figure 3.11).

Numerous studies on ancient and modern Corg-rich sediments have noted that these sub-oxic/reducing sediments are preferentially enriched with vanadium relative to oxidised pelagic sediments (Breit and Wanty, 1992). A number of mechanisms have been proposed to explain high V concentrations, although it is generally accepted that vanadium enrichment occurs through either a direct geochemical association with Corg or by the reduction and precipitation of insoluble V phases under sub-oxic conditions (Breit and Wanty, 1992). Whatever mechanism is responsible for V enrichment enhanced vanadium concentrations are now only located below the redox front in sub-oxic, Corg-rich conditions (figure 3.11). Originally, it is expected that high V concentrations would have been present within the oxidised region of the sediment when sedimentary Corg concentrations would have initially been much greater.

Within the oxidised regions of LC25 and T26B vanadium concentrations are exceptionally low and uniform, suggesting that the majority of the authigenic V has been remobilised leaving only the most non-labile (detrital) V phases behind. In UM41, a well-defined V peak is located near to the inferred level of the active oxidation front and is coincident with elevated Fe concentrations (figure 3.11). Under oxidising redox potentials, the highly mobile and soluble anionic vanadate species (HVO_4^{2-} and $H_2VO_4^-$) are predicted to be the most thermodynamically favoured forms (Turner *et al.*, 1981; Sadiq, 1988). Following sapropel formation, the introduction of dissolved O_2 into the sapropel caused the removal of V from the solid phase via the oxidation of V-Corg and/or reduced V(IV) complexes to produce the soluble $H_2VO_4^-$ ion. Mobilised $H_2VO_4^-$ ions have the capacity to diffuse both up and down core with a partition of fluxes equal to the ratio of the two gradients in the pore water concentrations. The immobilisation of V by iron oxyhydroxides has been noted in hydrothermal precipitates where it has been demonstrated that $Fe(OH)_3$ closely controls the geochemical cycling of V under oxic conditions (Trefy and Metz, 1989; Feely *et al.*, 1991). It is believed that these precipitates of Fe scavenge vanadium as the quinquievalent $H_2VO_4^-$ ion, and a similar mechanism is proposed to explain the formation of V enrichment and peak formation under oxic conditions in UM41. The fact that well-defined V peaks and enrichments are located beneath the oxidation front suggests that for LC25, T26B (and to some extent for UM41), the downward migration of soluble V ions is markedly greater than the upward flux of these ions. It is evident from the V/Al profiles that a small authigenic component of vanadium is continuously moved downwards in association with the oxidation front and partitions back into the solid phase below the depth of Mn and iron oxide reduction, consistent with the observation that reduced V species

are more insoluble and more particle reactive (Van der Sloot *et al.*, 1985; Wehrli and Stumm, 1989). It is unclear whether the source of vanadium is derived entirely from the oxidation of the sapropel unit itself, or whether there is some additional V component supplied to the redox front from the downward diffusion of V(V) from seawater. Furthermore, it remains unclear as to the exact mechanism by which soluble V ions below the oxidation front become partitioned back into the solid phase. The location of the V peak actually within the Corg-rich sapropel suggests that vanadium enrichment may occur via its association with organic matter. It is known that in the presence of humic substances, vanadate ions (V(V)) are readily reduced to vanadyl cations (V(IV)) which are capable of forming strong organic complexes (Szalay and Szilagyi, 1967; Wilson and Webber, 1979; Templeton III and Chasteen, 1980). Alternatively, thermodynamics predict that under sub-oxic conditions, enrichment of vanadium in the solid phase can occur by the redox-mediated reduction of V(V) to V(IV) which precipitates out as an insoluble vanadium hydroxide phase, $VO(OH)_2$ (Van der Sloot, *et al.*, 1985).

For LC25, T26B and UM41, it can be observed that vanadium enrichment is located deeper within the cores and coincides with elevated Fe and S concentrations (figure 3.11). The fact that V enrichment coincides with enrichments in both Fe and S implies that vanadium may be partitioned into the solid phase by its association/incorporation with iron sulphide phases. It has been shown that in the presence of pore water H_2S, V(IV) can be reduced to V(III) which then precipitates as V_2O_3 or $V(OH)_3$ (Wanty and Goldhaber, 1992). It is unknown whether deeper V enrichments occur via direct association with an iron sulphide phase or via the direct precipitation of insoluble V(III) complexes in the presence of H_2S. The lack of sulphate reduction (and hence H_2S production) within S1 (Passier *et al.*, 1996) makes the direct precipitation of V(III) complexes an unlikely mechanism for the fixation of downwards mobilised vanadium. It is apparent that the deeper V peaks are a combination of both the fixation of remobilised vanadium released during the oxidation of S1 and also the immobilisation of V under more reducing redox potentials during and shortly after S1 formation.

3.4.4.3. Molybdenum.

Whilst uranium and vanadium display little or no enrichment above the S1 unit in oxic conditions, Mo displays significant enrichments in oxic and sub-oxic regions of the sediment (figure 3.12).

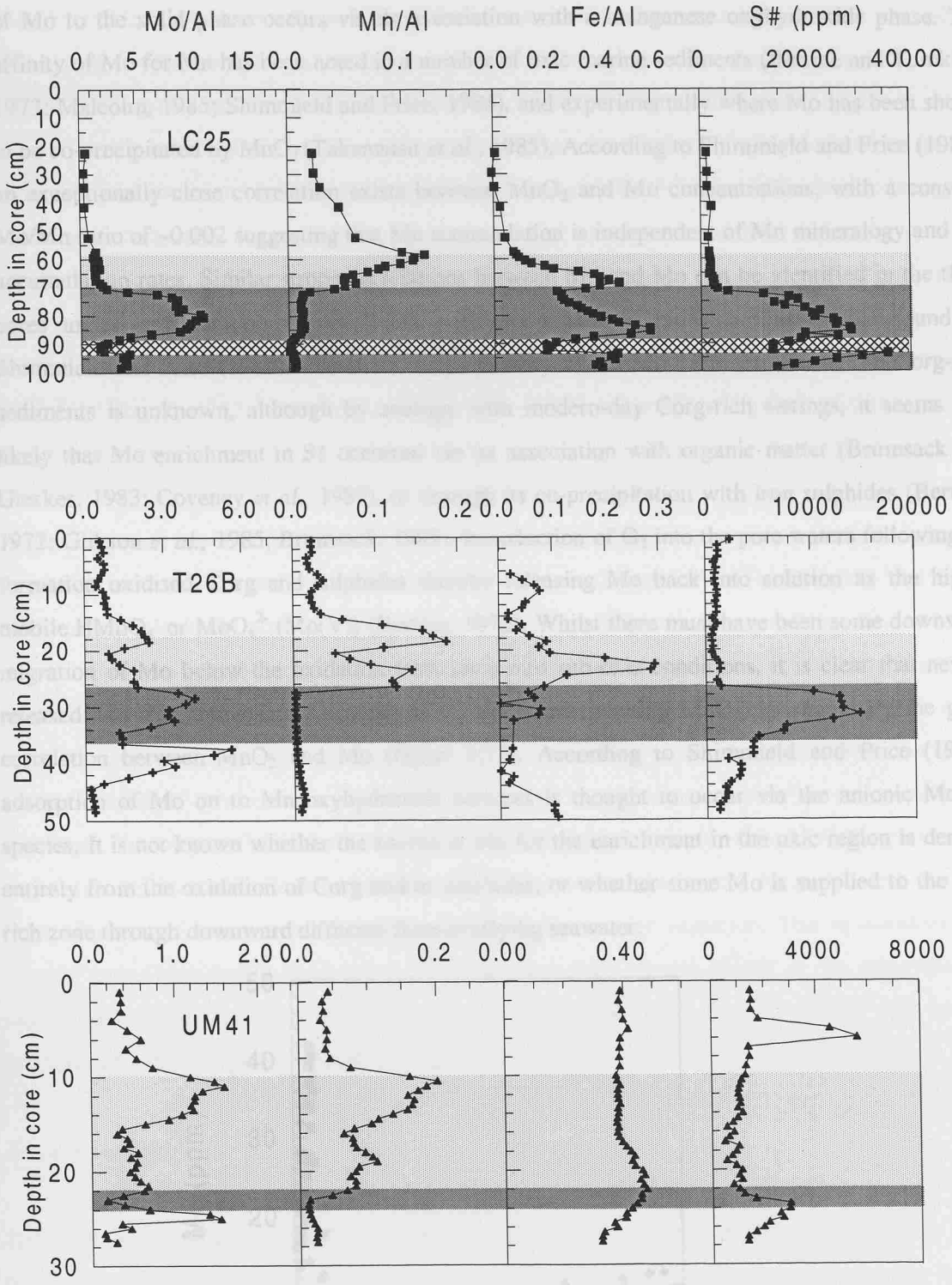

Figure 3.12. Depth-distribution of Mo/Al (ppm/wt%), Mn/Al, Fe/Al (wt%/wt%) and seawater corrected S (ppm) in cores LC25, T26B and UM41.

Under oxic conditions, the Mo profile broadly follows that of total Mn, implying that partitioning of Mo to the solid phase occurs via its association with a manganese oxyhydroxide phase. The affinity of Mo for Mn has been noted in a number of oxic marine sediments (Bertine and Turekian, 1973; Malcolm, 1985; Shimmield and Price, 1986), and experimentally where Mo has been shown to be co-precipitated by MnO_2 (Takematsu *et al.*, 1985). According to Shimmield and Price (1986), an exceptionally close correlation exists between MnO_2 and Mo concentrations, with a constant Mo/Mn ratio of ~0.002 suggesting that Mo accumulation is independent of Mn mineralogy and Mn accumulation rates. Similar strong correlations between Mn and Mo can be identified in the three cores under consideration (figure 3.13), with mean Mo/Mn ratios similar to that found by Shimmield and Price (1986). The exact mechanism by which Mo becomes enriched in Corg-rich sediments is unknown, although by analogy with modern-day Corg-rich settings, it seems that likely that Mo enrichment in S1 occurred via its association with organic matter (Brumsack and Gieskes, 1983; Coveney *et al.*, 1987), or through its co-precipitation with iron sulphides (Bertine, 1972; Glikson *et al.*, 1985; Brumsack, 1989). Introduction of O_2 into the pore waters following S1 formation oxidised Corg and sulphides thereby releasing Mo back into solution as the highly mobile $HMoO_4^-$ or MoO_4^{2-} (Mo(V)) (Bertine, 1972). Whilst there must have been some downward migration of Mo below the oxidation front back into sub-oxic conditions, it is clear that newly-released Mo was immediately scavenged by newly-precipitating MnO_2, as shown by the good correlation between MnO_2 and Mo (figure 3.12). According to Shimmield and Price (1986), adsorption of Mo on to Mn oxyhydroxide surfaces is thought to occur via the anionic MoO_4^{2-} species. It is not known whether the source of Mo for the enrichment in the oxic region is derived entirely from the oxidation of Corg and/or sulphides, or whether some Mo is supplied to the Mn-rich zone through downward diffusion from overlying seawater.

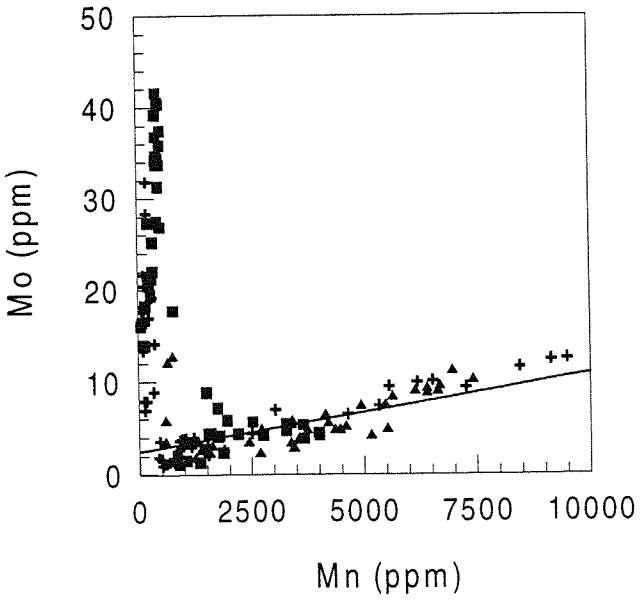

Figure 3.13. Molybdenum vs manganese (Mn*) in LC25 (■), T26B (✚) and UM41 (▲).

High Mo concentrations are present within and below the sapropel units, similar to those found for U and V. Whilst Mo is clearly partitioned back to the solid phase as an association with MnO_2 under oxic conditions, the controls under sub-oxic conditions are those provided by Corg and/or sulphides. Corg-rich sediments act as sinks for Mo enrichment (Brumsack, 1986; Legeleux, *et al.*, 1994; Crusius *et al.*, 1996), and according to Brumsack and Gieskes (1983) the decrease in pore water Mo concentrations in Corg-rich sediments from the Gulf of California basin is indicative of Mo-organic formation. Bertine (1972), noted that MoO_4^{2-} can be reduced to MoO_2^{+} under reducing conditions and is capable of being scavenged by negatively-charged particulates. Furthermore, the large concentration of Mo leached from the humic fraction of Corg-rich sediments (Nissenbaum and Swaine, 1976; Calvert and Morris, 1977) and the known ability of organic molecules to reduce MoO_4^{2-} (Szilagyi, 1967), suggests that re-mobilised Mo released during S1 oxidation has the capacity of being immobilsed below the oxidation front in regions of higher Corg concentration.

Examination of the Mo profiles reveals that enrichment below the oxic/post-oxic boundary correlates well with the profiles of both sulphur and iron (figure 3.12). This suggests that Mo is being partitioned back into the solid phase via its association with iron sulphides. Experimental evidence presented by Bertine (1972) has suggested that Mo is enriched in anoxic sediments via its co-precipitation with newly forming FeS. More recently, Helz *et al.* (1996) proposed that under reducing conditions, HS^- and thiols act as geochemical switches which change the behaviour of Mo so that it becomes more reactive to particles containing Fe and organic matter via the formation of S bridges. As seen with V, the Mo enrichment at depth must be the result of the preferential association of Mo with Fe sulphides and/or organic matter during S1 formation and also the immobilisation of downwards-migrating Mo released during S1 oxidation. This re-mobilised Mo has the capacity of being fixed either via association with organic matter or via adsorption on existing pyrite surfaces, but it is unlikely that the re-mobilised fraction of Mo will be co-precipitated with FeS given the lack of sulphate reduction in S1.

3.4.4.4. Arsenic.

Both oxic and anoxic sediments display elevated arsenic concentrations (Farmer and Lovell, 1986; Seyler and Martin, 1989; Legeleux *et al.*, 1994). Whilst it is generally accepted that in oxic marine sediments As enrichment is caused via its association with oxides and oxyhydroxides of iron and manganese (Pierce and Moore, 1982; Peterson and Carpenter, 1983; Belzile and Tessier, 1990), in sub- and anoxic settings As enrichment is believed to be caused by the formation of As minerals such as As_2S_3 (Agget and O'Brien, 1985), incorporation into pyrite (Belzile and Lebel, 1986; Huerta-Diaz and Morse, 1992; Morse, 1994) or through complexation/association with Corg (Van der Sloot *et al.*, 1990). From figure 3.14 it is apparent that elevated As concentrations are found

both above and below the sapropel in both oxic and sub-oxic sediments. The mechanism(s) by which As is partitioned to the solid phase in each setting is different and is dependent upon the redox state of the sediment.

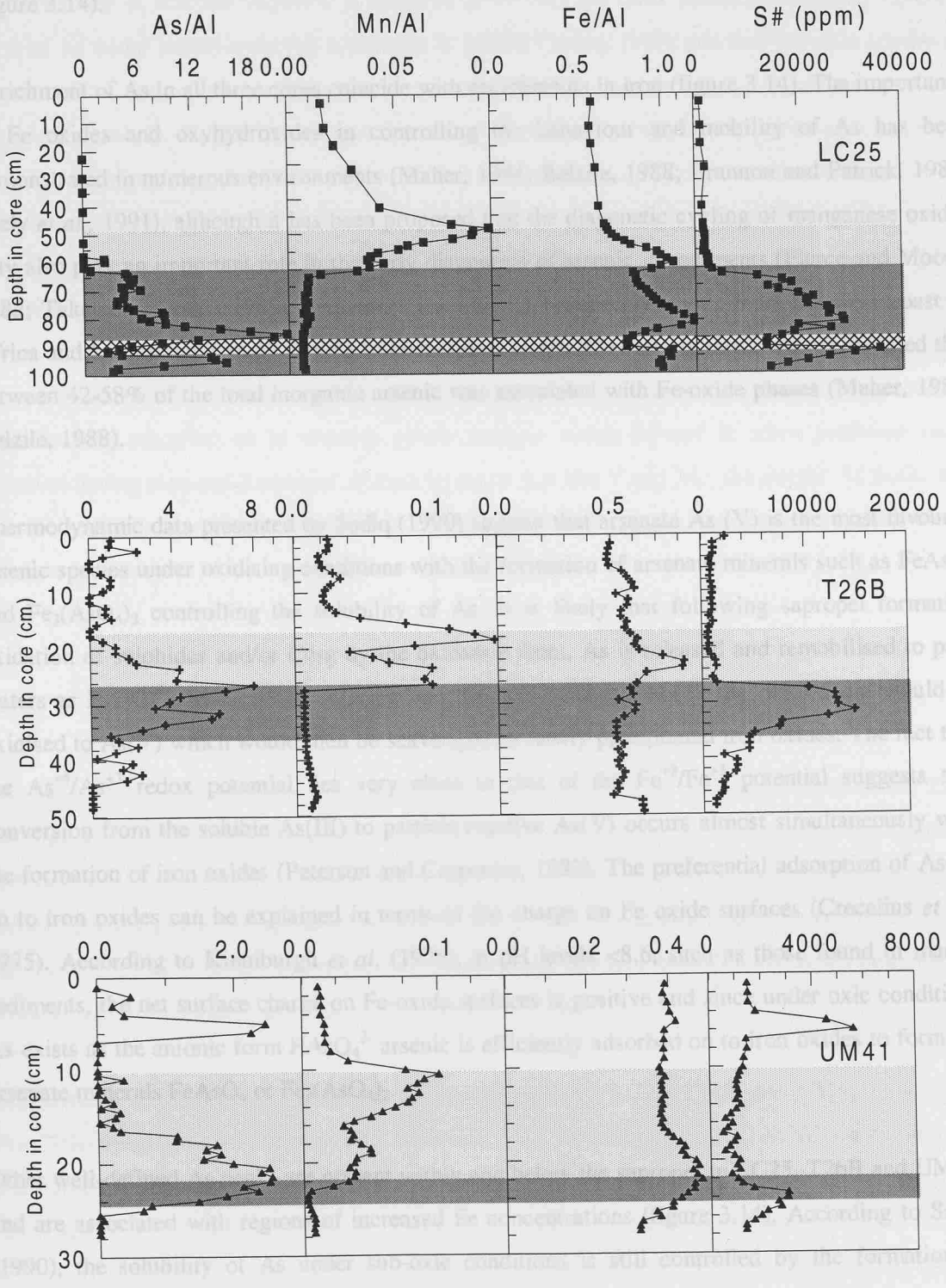

Figure 3.14. Depth profiles of normalised As (ppm/wt%), Mn and Fe concentrations (wt%/wt%) and seawater corrected sulphur (ppm) contents in LC25 (■), T26B (✚) and UM41 (▲).

Evidence presented in chapter 5 indicates that, during sapropel S1 formation As enrichment is derived through its incorporation with pyrite although the formation of As_2S_3 or As_2S_5 can not be discounted. Whilst As enrichments are still confined to Corg and S-rich regions within and below S1, additional arsenic enrichments within the oxic regions of T26B and UM41can be identified (figure 3.14).

Enrichment of As in all three cores coincide with enrichments in iron (figure 3.14). The importance of Fe oxides and oxyhydroxides in controlling the behaviour and mobility of As has been demonstrated in numerous environments (Maher, 1984; Belzile, 1988; Brannon and Patrick, 1987; Feely *et al.*, 1991), although it has been proposed that the diagenetic cycling of manganese oxides may also play an important role in the early diagenesis of arsenic in sediments (Pierce and Moore, 1982; Takamatsu *et al.*, 1985). Sequential leaching of pelagic sediments from the west coast of Africa and Laurentian Trough using a mild chemical attack (Chester-Hughes reagent) revealed that between 42-58% of the total inorganic arsenic was associated with Fe-oxide phases (Maher, 1984; Belzile, 1988).

Thermodynamic data presented by Sadiq (1990) suggest that arsenate As (V) is the most favoured arsenic species under oxidising conditions with the formation of arsenate minerals such as $FeAsO_4$ and $Fe_3(AsO_4)_2$ controlling the solubility of As. It is likely that following sapropel formation oxidation of sulphides and/or Corg by the oxidation front, As is released and remobilised to pore waters as $HAsO_4^{2-}$. Reduced As entering into the oxic zone just above the redox front would be oxidised to As(V) which would then be scavenged by newly precipitated iron oxides. The fact that the As^{+5}/As^{+3} redox potential lies very close to that of the Fe^{+2}/Fe^{+3} potential suggests that conversion from the soluble As(III) to particle reactive As(V) occurs almost simultaneously with the formation of iron oxides (Peterson and Carpenter, 1983). The preferential adsorption of As(V) on to iron oxides can be explained in terms of the charge on Fe oxide surfaces (Crecelius *et al.*, 1975). According to Kinniburgh *et al.* (1976), at pH levels <8.6, such as those found in marine sediments, the net surface charge on Fe-oxide surfaces is positive and since under oxic conditions As exists as the anionic form $HAsO_4^{2-}$ arsenic is efficiently adsorbed on to iron oxides to form the arsenate minerals $FeAsO_4$ or $Fe_3(AsO_4)_2$.

Other well-defined As peaks are present within and below the sapropel in LC25, T26B and UM41, and are associated with regions of increased Fe concentrations (figure 3.14). According to Sadiq (1990), the solubility of As under sub-oxic conditions is still controlled by the formation of arsenate minerals. Pore water profiles of slowly-accumulated sapropels presented by Van Santvoort *et al.* (1996) however, indicate increasing concentrations of Fe^{+2} beneath the visual sapropel, implying that iron reduction is occurring in these Corg-rich sediments. Detailed investigations on

pelagic and lake sediments indicates that increasing pore water arsenic concentrations are found associated with increased Fe^{+2} levels, suggesting that As is released back into solution upon the reduction of iron oxides in sub-oxic conditions (Edenborn *et al.*, 1986; Farmer and Lovelly, 1986; Belzile, 1988; Sullivan and Aller, 1996). As such, it is expected that within and below the sapropel, the formation of arsenate minerals is hindered given that the most thermodynamically favoured form of As under mildly-reducing conditions is As(III) (Sadiq, 1990) and that sub-oxic conditions do not allow Fe-oxides to form and/or persist either during or after S1 formation. Closer examination of the As profiles reveals that elevated concentrations coincide with enrichments in both S and Fe implying that As is co-precipitated with an iron sulphide phase. This mechanism has been used to explain increased solid phase As enrichments at depth in a number of pelagic marine sediments (Belzile and Lebel, 1986; Belzile, 1988) and the association of As with framboidal pyrite is believed to be responsible for As enrichment in Corg-rich sediments from a Norwegian fjord (Jacobs *et al.*, 1985). Morse (1994) has demonstrated that pyrite has a great affinity for As and so it is possible that under sub-oxic conditions, downwards mobilised As released during S1 oxidation is preferentially adsorbed on to existing pyrite surfaces which formed at some preferred redox potential during sapropel formation. It must be noted that like V and Mo, the deeper As peaks may have formed during and just shortly after S1 formation when pyrite was actively forming during sulphate reduction.

3.4.5. Bromine, Iodine, Selenium (and Mercury).

Bromine is known to form strong associations with Corg in marine sediments (Price *et al.*, 1970; Price and Calvert, 1977; Pedersen and Price, 1980; Ten Haven *et al.*, 1987). Previous investigations on Corg-rich sediments have shown that Br concentrations are positively correlated with organic carbon contents and are independent of the prevailing redox conditions (Pedersen and Price, 1980). This behaviour in Br is due to the fact that in sea water bromine exists solely as the conservative bromide ion (Br^-) in the –1 oxidation state (Brookins, 1980).

Examination of the total and corrected Br profiles in cores LC25, T26B and UM41 reveals that over 70% of the bromine in these cores is derived from sea water (figure 3.15). Above the sapropel in all cores, bromine enrichment is confined to regions of enhanced Corg concentrations within the visual sapropel (figure 3.17). The association of Br with Corg has been documented for a number of Corg-rich sediments and a good correlation can be established between Corg and Br for the unoxidised portion of the sapropel in all three cores (figure 3.15).

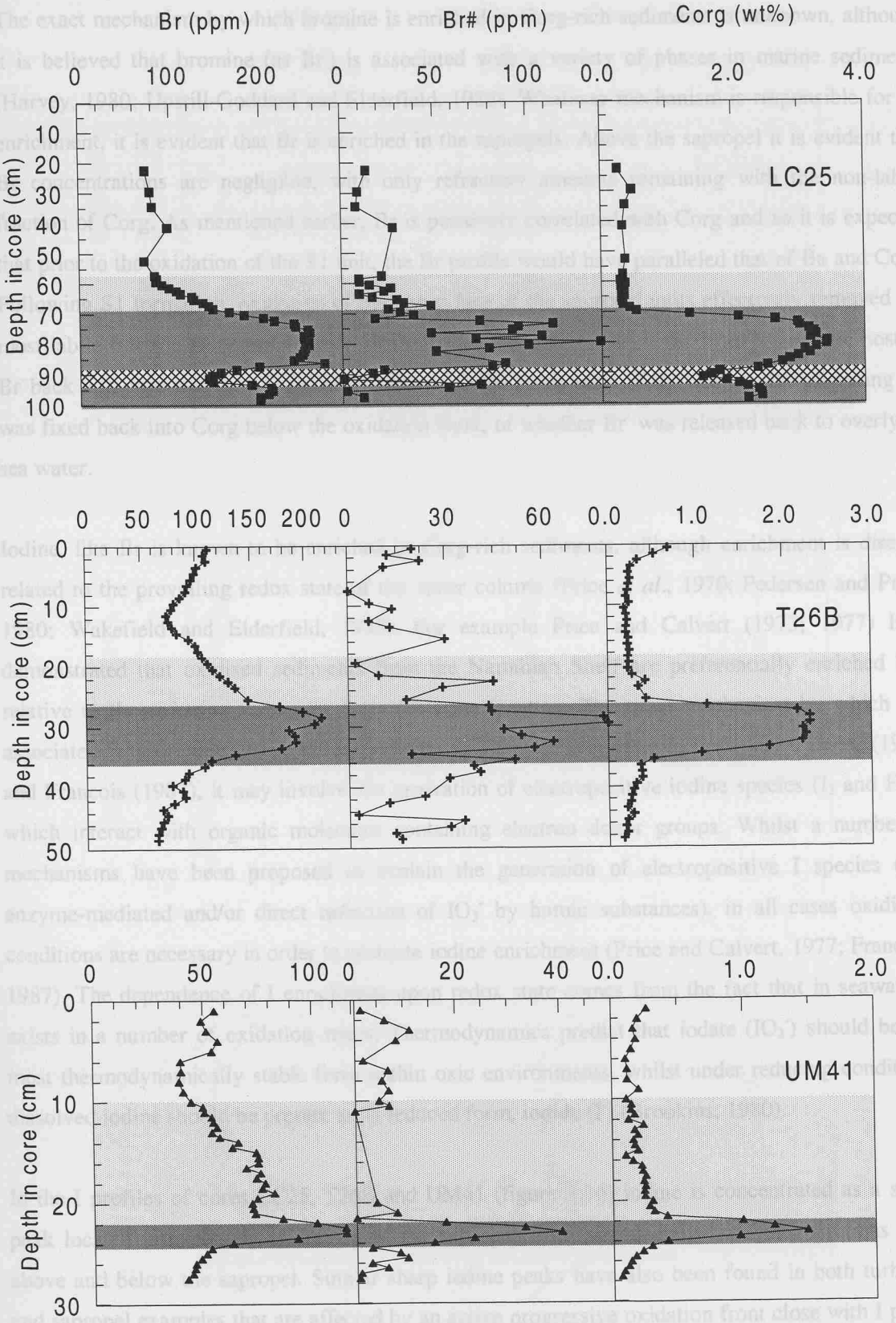

Figure 3.15. Comparison of the total, seawater corrected bromine concentrations (ppm) and Corg contents (wt%) in LC25 (■), T26B (✚) and UM41 (▲).

The exact mechanism by which bromine is enriched in Corg-rich sediments is unknown, although it is believed that bromine (as Br^-) is associated with a variety of phases in marine sediments (Harvey, 1980; Upstill-Goddard and Elderfield, 1988). Whatever mechanism is responsible for Br enrichment, it is evident that Br is enriched in the sapropels. Above the sapropel it is evident that Br concentrations are negligible, with only refractory amounts remaining with the non-labile fraction of Corg. As mentioned earlier, Br is positively correlated with Corg and so it is expected that prior to the oxidation of the S1 unit, the Br profile would have paralleled that of Ba and Corg. Following S1 formation, oxidation of the upper face of the sapropel units effectively removed the most labile fraction of organic carbon whilst simultaneously releasing Br from its organic host as Br^- back into pore waters. It is unknown whether some component of the downwards migrating Br^- was fixed back into Corg below the oxidation front, or whether Br^- was released back to overlying sea water.

Iodine, like Br is known to be enriched in Corg-rich sediments, although enrichment is directly related to the prevailing redox state of the water column (Price *et al.*, 1970; Pedersen and Price, 1980; Wakefield and Elderfield, 1985). For example Price and Calvert (1973; 1977) have demonstrated that oxidised sediments from the Namibian Shelf are preferentially enriched in I relative to the reducing sediments from the same location. The exact mechanism by which I is associated with organic matter remains unknown, although according to Price and Calvert, (1977) and Francois (1987), it may involve the generation of electropositive iodine species (I_2 and HOI) which interact with organic molecules containing electron donor groups. Whilst a number of mechanisms have been proposed to explain the generation of electropositive I species (e.g. enzyme-mediated and/or direct reduction of IO_3^- by humic substances), in all cases oxidising conditions are necessary in order to promote iodine enrichment (Price and Calvert, 1977; Francois, 1987). The dependence of I enrichment upon redox state comes from the fact that in seawater I exists in a number of oxidation states. Thermodynamics predict that iodate (IO_3^-) should be the most thermodynamically stable form within oxic environments, whilst under reducing conditions dissolved iodine should be present in its reduced form, iodide (I^-) (Brookins, 1980).

In the I profiles of cores LC25, T26B and UM41 (figure 3.16) iodine is concentrated as a sharp peak located immediately at the top of the sapropel, with consistently low concentrations both above and below the sapropel. Similar sharp iodine peaks have also been found in both turbidite and sapropel examples that are affected by an active progressive oxidation front close with I peaks forming close to the oxic/post-oxic boundary (Thomson *et al.*, 1993; Higgs *et al.*, 1994; Thomson *et al.*, 1995).

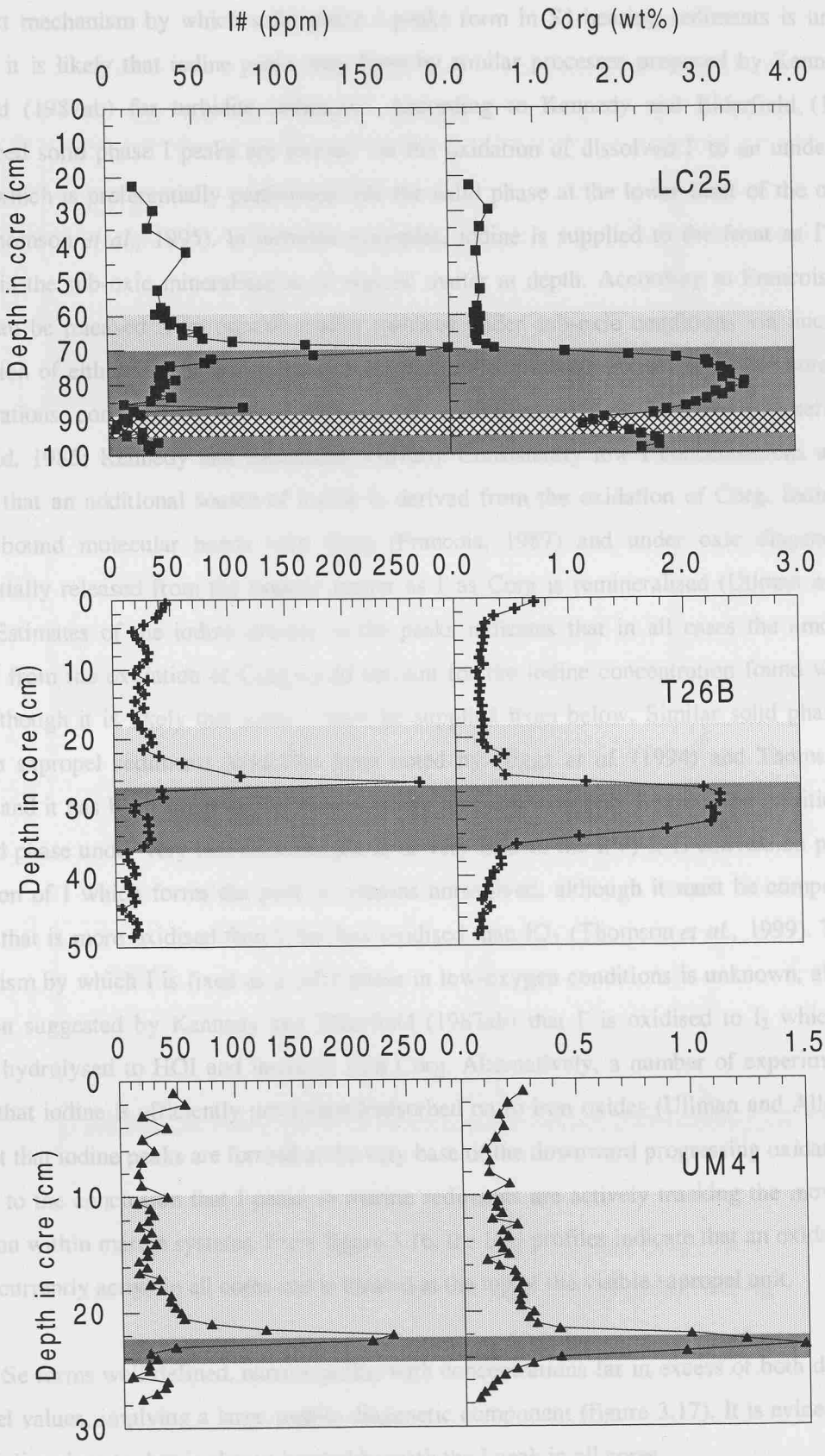

Figure 3.16. Seawater corrected I concentrations (ppm) and Corg contents (wt%) in LC25 (■), T26B (✚) and UM41 (▲).

The exact mechanism by which solid phase I peaks form in S1-bearing sediments is uncertain, although it is likely that iodine peaks may form by similar processes proposed by Kennedy and Elderfield (1987ab) for turbidite sediments. According to Kennedy and Elderfield (1987ab), pronounced solid phase I peaks are formed via the oxidation of dissolved I^- to an unidentified I species which is preferentially partitioned into the solid phase at the lower limit of the oxidation front (Thomson *et al.*, 1995). In turbidite examples, iodine is supplied to the front as I^- in pore waters via the sub-oxic mineralisation of organic matter at depth. According to Francois (1987), iodine can be released from organic matter matrices under sub-oxic conditions via nucleophilic substitution of either HS^- or $S_2O_3^{2-}$ ions. Oxidation of Corg results in an increase in pore water I concentrations concomitant with a decrease in solid-phase iodine contents (Wakefield and Elderfield, 1985; Kennedy and Elderfield, 1987ab). Consistently low I concentrations above S1 indicate that an additional source of iodine is derived from the oxidation of Corg. Iodine forms weakly bound molecular bonds with Corg (Francois, 1987) and under oxic diagenesis I is preferentially released from the organic matter as I^- as Corg is remineralised (Ullman and Aller, 1985). Estimates of the iodine content in the peaks indicates that in all cases the amount of I released from the oxidation of Corg could account for the iodine concentration found within the peak, although it is likely that some I must be supplied from below. Similar solid phase iodine peaks in sapropel sediments have also been noted by Higgs *et al.* (1994) and Thomson *et al.* (1995), and it has been suggested by these authors that iodine is only found to be partitioned into the solid phase under very low O2 tensions, at or very near to the I(V)-I(-I) conversion point. The speciation of I which forms the peak is remains unresolved, although it must be composed of a species that is more oxidised then I^- but less oxidised than IO_3^- (Thomson *et al.*, 1999). The exact mechanism by which I is fixed as a solid phase in low-oxygen conditions is unknown, although it has been suggested by Kennedy and Elderfield (1987ab) that I^- is oxidised to I_2 which is then rapidly hydrolysed to HOI and interacts with Corg. Alternatively, a number of experiments have shown that iodine is efficiently precipitated/adsorbed on to iron oxides (Ullman and Aller, 1985). The fact that iodine peaks are formed at the very base of the downward progressing oxidation front, has led to the conclusion that I peaks in marine sediments are actively tracking the movement of oxidation within marine systems. From figure 3.16, the I/Al profiles indicate that an oxidation front is now currently active in all cores and is located at the top of the visible sapropel unit.

Like I, Se forms well-defined, narrow peaks, with concentrations far in excess of both detrital and sapropel values, implying a large mobile diagenetic component (figure 3.17). It is evident that the Se peak lies close to, but is always located beneath the I peak in all cores.

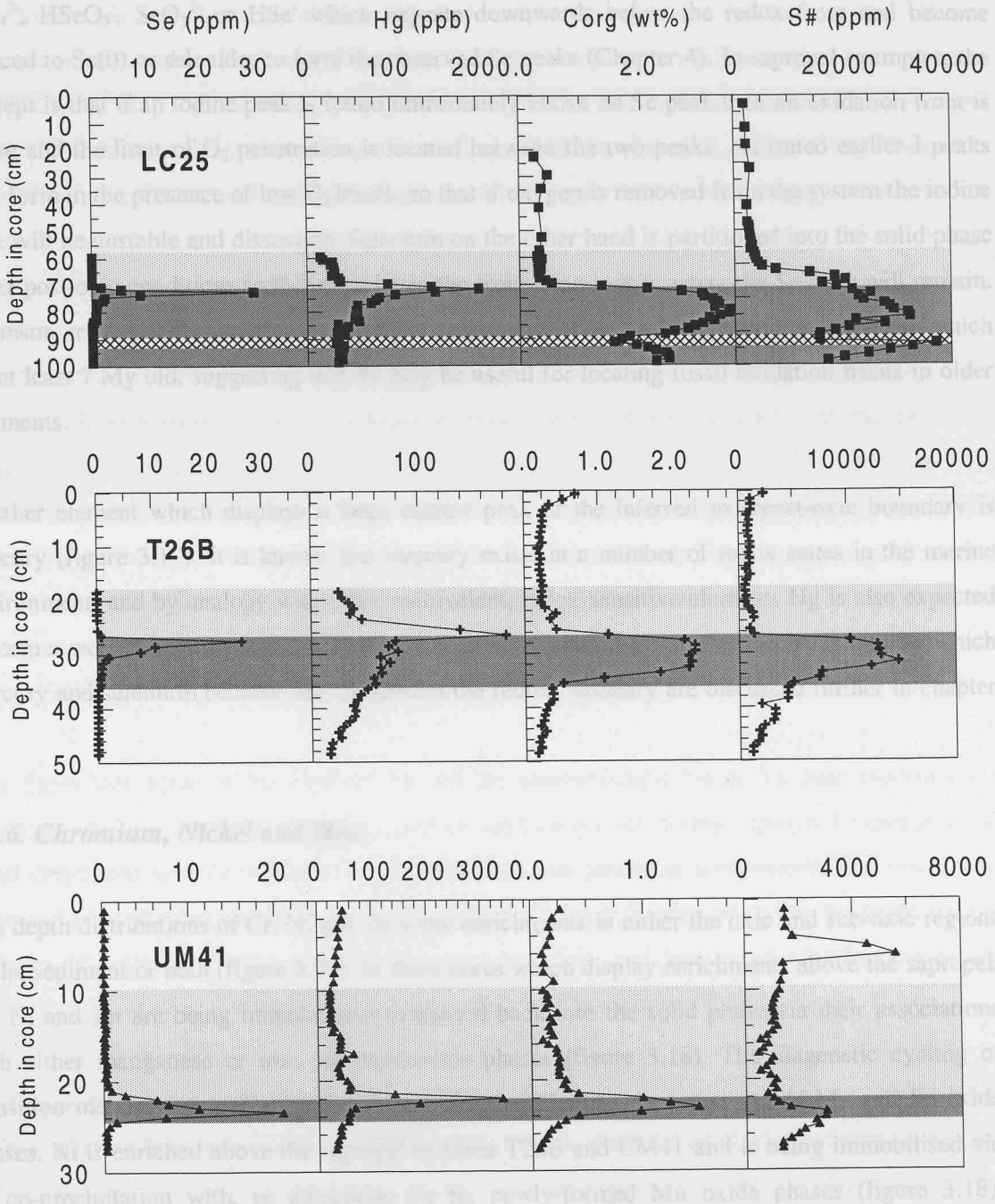

Figure 3.17. Depth-distribution of Se (ppm), Hg (ppb), Corg (wt%) and sea water corrected S (ppm) in LC25 (■), T26B (✚) and UM41 (▲).

Similar Se peaks have been found for Corg-rich turbidites and sapropels affected by progressive oxidation fronts and according to Thomson *et al.* (1995) may also help to define the location of an oxidation front in the absence of pore water O_2 measurements. Whilst iodine peaks are preferentially partitioned back into the solid phase under slightly oxic conditions, Se peaks are always found to be located in post-oxic conditions, suggesting that peak formation must involve a reduced, insoluble selenium species. Like, iodine the source of Se to the peak is derived from the

oxidation of Corg and sulphides and involves the release of highly mobile oxidised species such as SeO_4^{2-}, $HSeO_3^-$, SeO_3^{2-} or HSe^- which migrate downwards below the redox front and become reduced to Se(0) or selenides to form the observed Se peaks (Chapter 4). In sapropel examples, the concept is that if an iodine peak is found immediately above an Se peak then an oxidation front is active and the limit of O_2 penetration is located between the two peaks. As stated earlier I peaks only form in the presence of low O_2 levels, so that if oxygen is removed from the system the iodine peak will be unstable and dissociate. Selenium on the other hand is partitioned into the solid phase under post-oxic conditions so that even when the front is no longer active the Se peak will remain. Thomson *et al.* (1998) has demonstrated the persistence of Se peaks in turbidite sediments which are at least 7 My old, suggesting that Se may be useful for locating fossil oxidation fronts in older sediments.

Another element which displays a large narrow peak at the inferred oxic/post-oxic boundary is mercury (figure 3.17). It is known that mercury exists in a number of redox states in the marine environment, and by analogy with other multivalent, redox-sensitive elements Hg is also expected to form a well-defined peak in response to an active oxidation front. The mechanism(s) by which mercury and selenium become immobilised at the redox boundary are discussed further in chapter 4.

3.4.6. Chromium, Nickel and Zinc.

The depth distributions of Cr, Ni and Zn show enrichments in either the oxic and sub-oxic regions of the sediment or both (figure 3.18). In those cores which display enrichments above the sapropel, Cr, Ni and Zn are being immobilised/partitioned back into the solid phase via their associations with either manganese or iron (oxy)hydroxide phases (figure 3.18). The diagenetic cycling of transition metals such as Cr, Ni and Zn are closely linked to the behaviour of Mn and Fe oxide phases. Ni is enriched above the sapropel in cores T26B and UM41 and is being immobilised via its co-precipitation with, or adsorption on to, newly-formed Mn oxide phases (figure 3.18). Similarly, the close coincidence in zinc and Mn profiles in T26B and UM41 again suggests that Zn is partitioned back into the solid phase under more oxidising conditions.

Enrichment of Ni and Zn in Corg-rich, reducing sediments is evident from settings such as the Black Sea and Sannich Inlet (Francois, 1988). Thermodynamic considerations indicate that under oxidising conditions, Ni and Zn should be present as divalent cations (Ni^{+2} and Zn^{+2}), whilst in the presence of H_2S these elements are known to form stable sulphide complexes (Brookins, 1980). During S1 formation, it is likely that Ni and Zn were introduced into the sediment as their divalent

cation forms followed by sulphide formation within the sediment (Calvert and Pedersen, 1993). Oxidation of the sapropel released Ni and Zn from sulphide phases back into pore waters. Upward migration of the mobile Zn^{+2} and Ni^{+2} species into the oxic region of the core led to its removal from solution via co-precipitation/adsorption on to the surfaces of manganese and iron oxides (Hem, 1978; Hem *et al.*, 1989; Young and Harvey, 1992; Tessier *et al.*, 1985; 1996). There is a lack of Ni and Zn enrichment within the oxic region of LC25, even though this core has concentrations of Mn and Fe comparable to those found in both T26B and UM41. Furthermore, it is not known if the amount of Ni and Zn associated with Mn oxides above S1 is derived entirely from the oxidation of sulphides or that there is some downward supply from overlying seawater.

At depth, all three cores display some degree of enrichment in Ni and Zn suggesting that these two elements are being immobilised under more reducing conditions. Observations on sediments from the Black Sea, Framvaren and Sannich Inlet have shown that these Corg-rich sediments are enriched in Zn and Ni via the precipitation of these elements as their sulphide phases (ZnS and NiS) (Skei *et al.*, 1988; Calvert and Pedersen, 1993). The association of these two elements within the region of enhanced sedimentary sulphur concentrations in all three cores implies that both zinc and nickel are partitioned into the solid phase as NiS and ZnS.

It is likely that some of the elevated Ni and Zn concentrations below S1 must represent the formation of these elements as their respective sulphide phases during sapropel formation when redox conditions were favourable (i.e. when free H_2S was present in pore waters). The situation is complicated by the fact that downwards migrating Zn^{+2} and Ni^{+2} released during oxidation has the capacity of migrating below the oxic/post-oxic boundary and become re-adsorbed on to/into existing pyrite surfaces (Kornicker and Morse, 1991; Morse and Arakai, 1993; Morse, 1994).

For Cr, the situation is somewhat more complicated. Enrichment of Cr within the oxic region above S1 is evident only in core T26B, where its profile closely mimics that of MnO_2 (figure 3.18). It is not known why a similar Cr enrichment above S1 is not observed in UM41 or LC25, considering that both cores have had comparable amounts of post-depositional oxidation and also have similar solid-phase Mn concentrations. Unlike Ni and Zn which form sulphides under reducing conditions, Cr is predicted to be present as the particle reactive Cr(III) species and is quickly removed to the solid phase via adsorption onto particulate matter and/or Corg as the $Cr(OH)_2^+$ ion (Francois *et al.*, 1988; Sadiq, 1992). Whatever mechanism is responsible for Cr enrichment in Corg-rich sediments, it is evident that like Ni and Zn, Cr has been released from the solid phase as a mobile Cr species in a similar manner to Ni and Zn. In the case of T26B the upward migration of Cr into more oxidising condition has led to co-precipitation/adsorption on to MnO_2 surfaces.

For UM41, LC25 (and T26B), Cr enrichment is confined to the regions of the core that have high concentrations in both Corg and S (figure 3.18). Under more reducing conditions Cr is reduced to the particle reactive Cr(III) which exists primarily as the ion $Cr(OH)_2^+$ (Elderfield, 1970; Cranston, 1983). The reduced Cr(III) cation has a marked affinity for Corg and particle surfaces and so it is possible that downward migration of Cr ions produced during the oxidation of S1 are then re-reduced and subsequently scavenged below the redox boundary. It is feasible that some of the Cr enrichment below the redox front is that originally associated with Corg and particulates during sapropel formation when conditions were more reducing and so favoured the particle reactive Cr(III) species. In the case of LC25 and UM41 the downward fluxing component of Cr was presumably greater than that of the upward flux, so that the Cr released from S1 was preferentially partitioned back into the solid-phase under post-oxic conditions rather than being immobilised under oxic conditions.

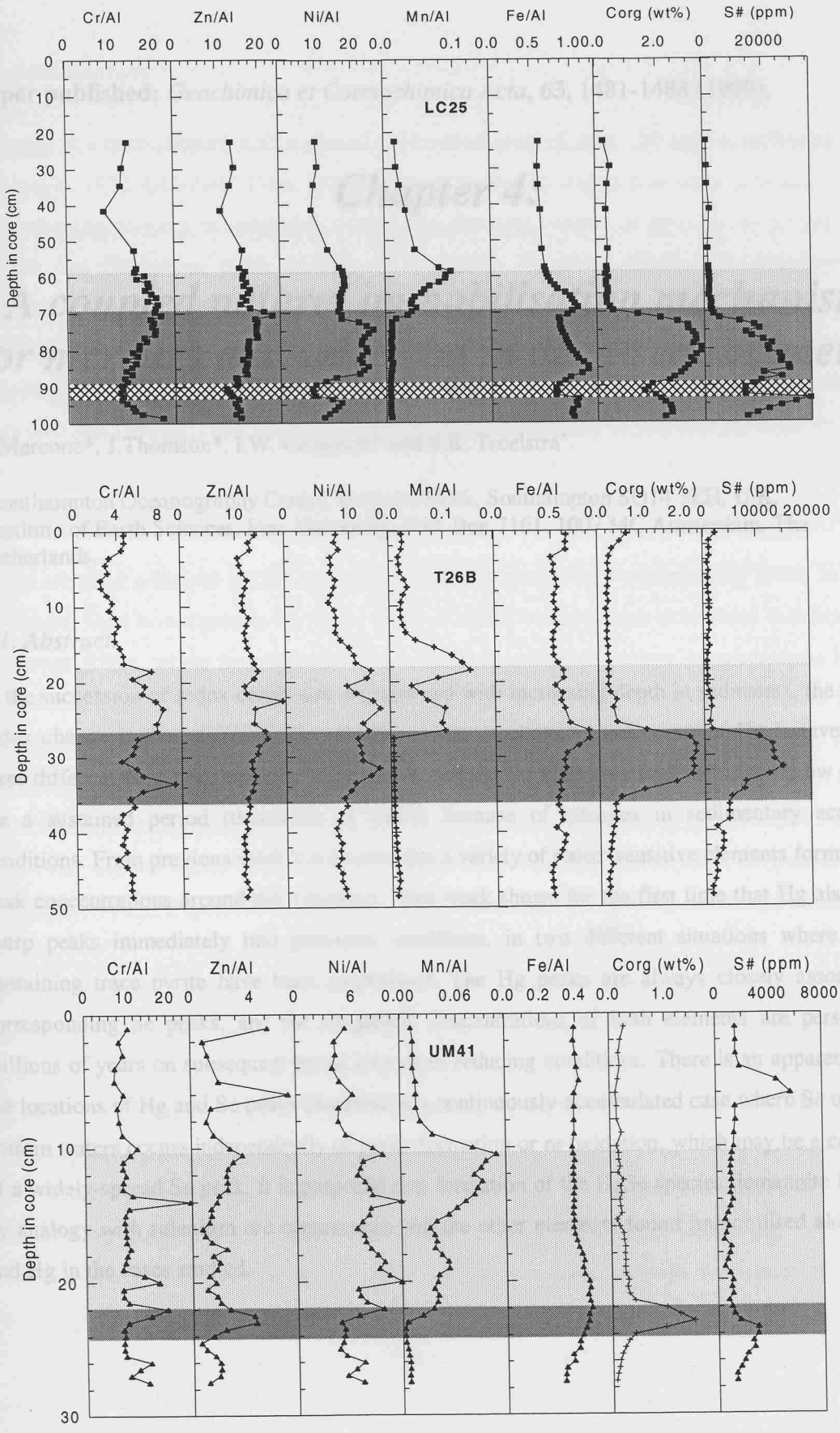

Figure 3.18. Depth distribution of Cr/Al, Zn/Al, Ni/Al (ppm/wt%), Mn/Al and Fe/Al (wt%/wt%) and Corg (wt%) and seawater corrected S (ppm) in LC25, T26B and UM41.

Paper published: *Geochimica et Cosmochimica Acta*, **63**, 1481-1488 (1999).

Chapter 4:

A coupled natural immobilisation mechanism for mercury and selenium in deep-sea sediments.

D.Mercone*, J.Thomson*, I.W. Croudace* and S.R. Troelstra[+].

*Southampton Oceanography Centre, Empress Dock, Southampton SO14 3ZH, U.K.
[+]Institute of Earth Sciences, Free University, P.O. Box 7161, 1007 MC Amsterdam, The Netherlands.

4.1. Abstract.

In the succession of redox conditions encountered with increasing depth in sediments, the first major redox change is the oxic/post-oxic boundary. The geochemical behaviour of Hg is investigated in three different deep-sea situations where this boundary has been localised within a narrow depth zone for a sustained period (thousands of years) because of changes in sedimentary accumulation conditions. From previous work it is known that a variety of redox-sensitive elements form diagenetic peak concentrations around this boundary. This work shows for the first time that Hg also develops sharp peaks immediately into post-oxic conditions, in two different situations where sediments containing trace pyrite have been re-oxidised. The Hg peaks are always closely associated with corresponding Se peaks, and the diagenetic concentrations of both elements are persistent over millions of years on subsequent burial into more reducing conditions. There is an apparent off-set in the locations of Hg and Se peaks observed in a continuously-accumulated case where Se uptake from bottom waters occurs independently of pyrite formation or re-oxidation, which may be a consequence of a widely-spread Se peak. It is proposed that formation of the HgSe species tiemannite is involved, by analogy with selenium ore occurrences and the other elements found immobilised along with Se and Hg in the cases studied.

4.2. *Introduction.*

Mercury is a trace element with a natural background level of only ~50 ppb in sediments (Jonasson and Boyle, 1972; GESAMP 1986, 1990), but its high toxicity makes it an environmental contaminant of continuing concern in industrial, mining and domestic wastes at ppm levels (Lindqvist, 1991; Watras and Huckabee, 1994; Porcella *et al.* 1995). Elemental Hg(0) and methylated Hg are neurotoxic while inorganic Hg salts are nephrotoxic (Magos and Webb, 1980). The methylated forms $CH_3Hg(II)$ and $(CH_3)_2Hg$ are of particular concern because they are readily produced from inorganic species in reducing sediments, and then concentrated up the marine food chain (Craig, 1980, 1986a; Bernhard and George, 1986; GESAMP 1986). The high volatility of Hg also prolongs the effects of anthropogenic releases through repeated atmospheric recycling to and from the land and sea (Nriagu, 1989; Mason *et al.* 1994).

There are three principal marine sedimentary environments where enhanced Hg levels in sediments are found. Most investigations have been made in coastal environments near major industrial or urban discharge points, where recent pollution can increase sediment mercury concentrations by three to four orders of magnitude (to 250,000 ppb; GESAMP, 1990) above natural background levels (e.g. Young *et al.* 1973; Skei and Paus, 1979). Second, naturally-enhanced Hg levels are also observed in sediments which are influenced by hydrothermal activity near mid-ocean ridges or other plate boundaries including the compressional type (Jonasson and Boyle, 1972; Bostrom and Fisher, 1969; Toth 1980; Kadko, 1980; Grousset and Donard, 1984). The third Hg-enriched environment is Corg-rich (Jonasson and Boyle, 1972) or pyritic (Huerta-Diaz and Morse, 1992) reducing sediments.

Mercury has three valency states (I, II and 0), and the ready interconversion of inorganic and organic forms, including the possibility of disproportionation reactions, means that the environmental behaviour of Hg is complex (Jonasson and Boyle, 1972; Craig, 1986b; Rasmussen, 1994). Continuing Hg loss from sediments decades after contaminating Hg inputs had ceased has been demonstrated by following the Hg levels in sediments (Bothner *et al.*. 1980; Gagnon *et al.* 1997) and biota (Locarnini and Presley, 1996) over time. Although HgS (cinnabar) has a very low solubility, it does not appear to control Hg geochemistry in reducing sediments (Bothner *et al.* 1980; Gagnon *et al.* 1997). Huerta-Diaz and Morse (1992) demonstrated that Hg develops a higher content in pyrite than in precursor early diagenetic Fe sulfides, an uptake which probably involves solution transfer of Hg. A consensus of recent investigations is that anoxic sedimentary environments with low sulfide concentrations are conducive to Hg(II) methylation and loss of Hg from sediments (Craig, 1986b; Gagnon *et al.* 1996).

This paper demonstrates that an efficient natural immobilisation mechanism for Hg exists immediately below the oxic/post-oxic boundary in certain deep-sea sediments. Berner (1981) differentiated the geochemical redox environments in sediments as the oxic, post-oxic, sulfidic and methanic zones, based on the zonal concentrations of oxygen and sulfide in sediment pore waters. The first major redox change encountered in this scheme is the contrast at the oxic/post-oxic boundary, where post-oxic is defined as the intermediate zone with negligible pore water O_2 or H_2S concentrations between oxic (free O_2 present) and sulfidic (or strongly-reducing; free H_2S present) conditions.

Changes in sediment accumulation conditions can cause the oxic/post-oxic boundary to be localised at a particular depth horizon for a prolonged period. When this occurs, it has been shown that an enrichment sequence of several redox-sensitive elements develops across the boundary, at slightly different depths dependent on elemental geochemistries (Jarvis and Higgs, 1987; Thomson *et al.* 1993, 1995, 1996). Here the behaviour and response of Hg at this boundary is investigated through study of three different modes of change in sediment accumulation. The first is in discontinuously-accumulated sediments (turbidites), and the second and third are in continuously-accumulated sediments where either the nature of the accumulated sediments has changed (Corg-rich sediments termed sapropels) or the rate of sediment accumulation has changed (transitional glacial/interglacial sediments).

4.3. Methods.

The sediments available for this study were not collected and processed with analysis for Hg in mind, but instead had been oven-dried at 100°C and ground in agate for major and trace element analysis. This treatment is anticipated to drive off volatile Hg species such as methyl or elemental Hg, so that the results here must be taken as minimum values. The dry powders (200 mg) were prepared for analysis by overnight reflux leach in 5 ml aqua regia (3 volumes c. HCl:1 volume c. HNO_3) at 80°C, filtered through a 0.45 μm polycarbonate filter and diluted to 100 ml with H_2O to give a 500:1 volume:mass solution. An aliquot of this digest was analysed directly for Hg by atomic fluorescence spectrometry, using an automated cold vapour generator (PSA Model 10.003). A further fourfold dilution of the digest solution in 40% HCl was analysed for Se by hydride-generation atomic fluorescence spectrometry, using an automated generator (PSA Model 10.001). The accuracy of the method was <2% for both elements when applied to USGS reference materials (marine sediment MAG-1, estuarine sediment BCR-277 and jasperoid rocks GXR-1 and GXR-2). The detection limit was 1 ppb in the sample.

Organic C (Corg) data were determined by coulometry, with $CaCO_3$ measured from the CO_2 liberated by 10% phosphoric acid, and Corg by subtraction of $CaCO_3$-CO_2 from the CO_2 liberated on total sample combustion at 900°C. Sulphur was measured by wave-length dispersive XRF on powder pellets.

4.4. Results.

The location of the oxic/post oxic boundary in the cores selected for this study of Hg behaviour has either been proved by pore water studies, or can be inferred because of clear similarities with such studies. In all cases, other compositional data have already been gathered as indicated in the selected cores which demonstrate that a range of other redox-sensitive elements form diagenetic peaks around the oxic/post-oxic boundary. The new Hg data have been collected in three situations.

4.4.1. Turbidites.

The effects of a downwards-migrating progressive oxidation front are particularly evident in organic-rich, distal deep-sea turbidites, because such units are vertically homogenous in composition on emplacement. At the low rates of sediment accumulation in the deep sea, oxidation acts on the upper surface of the turbidite after emplacement for a sustained period, typically tens of thousands of years, and the extent of this post-depositional oxidation by bottom waters is marked by a sharp colour contrast and change in Corg content below the top of the originally homogenous unit. Diagenetic enrichment peaks of redox-sensitive metals are found above and below this colour change, dependent on elemental geochemistry (Jarvis and Higgs, 1987; Thomson *et al.* 1993).

Mercury is now also shown to form a peak in this sequence (Figures 4.1 and 4.2). In the core 11805 turbidite (Figure 4.1), the oxidation front has been active for the past 250 ky up to the present (Thomson *et al*, 1993). By contrast, the core 157-950A-17H-3 turbidite (Figure 4.2) was recovered by ODP drilling from a depth of ~150 metres below the sea floor. In this case the oxidation front was active for the first few tens of thousands of years after emplacement, but since then the unit has been buried for ~ 4 My with the colour change persisting as a fossil trace of the oxidation front (Thomson *et al.* 1998). Elements which migrate into oxic conditions at an active front (Mn, I, Fe) are still in place in the core 11805 turbidite, but in the core 950A-17H unit the diagenetic enrichments of these elements have been lost by reduction on deeper burial. Other elements which form peaks in post-oxic conditions (e.g. Se, Cd, V, Sb and Tl) are present as sharply-defined concentration peaks in both units (Thomson *et al.* 1993, 1998).

4.4.2. Sapropels.

Sapropels are dark, unusually Corg-rich (>2 wt. %) sedimentary units, formed episodically in the sediments of the Eastern Mediterranean Sea (e.g. Rohling, 1994). They are found intercalated with Corg-poor sediments, and it is inferred that sapropels represent short episodes of high surface ocean productivity and/or bottom water anoxia in this restricted basin, which is otherwise oligotrophic, well-oxygenated and deposits Corg-poor sediments. Recent work has revealed that the upper faces of sapropels commonly experience post-depositional oxidation after productivity and bottom water oxygen levels return to the levels at which Corg-poor sediments accumulate (Thomson *et al.* 1995; van Santvoort *et al.* 1996; Jung *et al.* 1997). This process thins the original sapropel thickness by oxidation of Corg-rich sediment from the top downwards, and is responsible for the sharp visual upper boundary of the unit. Many of the same elements found to develop diagenetic enrichment peaks in deep-sea turbidites form similar peaks around the oxic/post-oxic boundary in sapropels, with the Mn, I and Fe peaks in oxic conditions and Se, V, Cd, U and Mo peaks in anoxic conditions (Thomson *et al.* 1995). Mercury also forms a peak at this oxidation interface, as shown in the two selected examples of the most recent sapropel, S1 (Figure 4.3 ab).

4.4.3. Glacial/interglacial transition sediments.

In the Atlantic Ocean, glacial sediments are generally found to accumulate more rapidly than interglacial sediments (e.g. Bacon, 1984). At glacial/interglacial transitions, as a consequence of the fall in the accumulation fluxes, a slow-moving oxidation front can develop downwards into the uppermost glacial sediments. Thomson *et al.* (1996) demonstrated that many of the elements which form diagenetic enrichment peaks at oxidation fronts in turbidites or sapropels also form similar peaks in such glacial/interglacial transition sediments. For the last two glacial/interglacial transitions, it was found that well-separated peaks of Mn, Fe, As and P were observed in oxic conditions in the sediments of the last transition where the oxic-post-oxic boundary was still actively maintained, but not at the previous transition where pore water conditions had become anoxic. In contrast, Se, Cd, V and U peaks were observed in post-oxic conditions at both of the last two glacial/interglacial transitions (Thomson *et al.* 1996). Although the Se peak at the active boundary in core CD63#9K is within a factor of 5 of the other Se peaks previously discussed, the x 2 enrichment of Hg is not exactly coincident with the peak Se values but rather the Hg maximum is located 7 cm above the Se maximum (Figure 4.4). This off-set will be considered further later.

4.5. Discussion.

Well-developed Hg peaks are observed close to the oxic/post-oxic boundary in all the turbidite and sapropel profiles studied. In three cases the oxidation front is currently active (Figures 4.1 and 4.3) but is inactive in one (Figure 4.2). This Hg peak formation occurs at a depth close to, but not exactly coincident with, the maxima of similar Se, Cd, Tl, Sb and Pt diagenetic peaks (Colodner *et al.* 1992; Rosenthal *et al.* 1995; Thomson *et al.* 1998). Within the resolution of sampling in all four examples, the Hg peak is either coincident with, or on the upper face of, a corresponding Se peak.

No persuasive Hg peak is observed at the active front in the glacial/interglacial profile coincident with the Se peak (CD63#9K; Figure 4.4, but see also below). The most obvious difference between the sediments in CD63#9K and the turbidite and sapropel examples is that the sediments in the last two cases contained trace pyrite before re-oxidation to source both the Hg and Se enrichments, whereas the first did not. The situation of a sapropel before oxidation is demonstrated by the elemental profiles of the S1 sapropel in core LC21 (Figure 4.5). Unlike the two S1 examples of figures 4.3ab, this example has suffered very little post-formation oxidation because it was accumulated at a rapid rate, ~20 cm.ky-1 (estimated from unpublished radiocarbon data). In core LC21 it is clear that Corg, S, Se and Hg are all well-correlated to a first approximation. Note, however, that even here there are slight enrichments in the Se and Hg profiles at 141-145 cm at the very top of the sapropel unit which are not present in the Corg and S profiles, consistent with a brief episode of oxidation. Mercury is one of the elements preferentially enriched in authigenic pyrite (Huerta-Diaz and Morse, 1992), and Se is also concentrated at greater or lesser levels of enhancement in pyrite (Simon *et al.* 1997), and this is believed to be the major source of Se in the sapropels and turbidites investigated. The Se peak observed in core CD63#9K, on the other hand, was developed without previous incorporation into sulfide, however, and instead it must have been supplied by downwards diffusion from bottom waters to have been immobilised by reduction. A bacterially-mediated reduction mechanism for Se to Se(0) has been demonstrated by Oremland *et al.* (1989) to occur in sediments. In effect it is similar to reduction mechanisms which enrich V and U from bottom waters into anoxic sediments, and indeed U and V enrichments are present deeper in core CD63#9K (Thomson *et al.* 1996). By inference, such a mechanism might also augment Se peaks on sulfide diagenesis in turbidites and sapropels. In core 11805 (Figure 4.1), the amount of Se estimated to be present in the peak (0.82 $\mu mol.cm^{-2}$ Se at an assumed dry bulk density of 0.75 $g.cm^{-3}$) slightly exceeds that estimated to have been released by oxidation from above the peak (0.77 $\mu mol.cm^{-2}$), consistent with a slight additional uptake of Se from bottom waters.

In the work cited above, it has been found that Se forms a peak immediately below that of Fe at stalled oxic/post-oxic boundaries. Elemental Se(0), FeSe and $FeSe_2$ (ferroselite) are the species predicted to control Se solubility in moderately-reducing conditions (Masscheleyn *et al.* 1991). Myneni *et al.* (1997) have found experimentally that Fe(II, III) "green rust" abiotically reduces Se(VI) to Se(0), but as noted above a similar reduction can be achieved bacterially in sediments (Oremland *et al.* 1989). The mechanism for Fe peak formation in the deep-sea sediments studied here is that Fe^{2+} diffusing upwards from reducing conditions at depth reacts with O_2 at the base of oxic conditions to form Fe oxyhydroxide. As a consequence such Fe(III) peaks are not persistent when the sediments are buried and become anoxic (Thomson *et al.* 1996). The Se peak on the other hand is persistent, as demonstrated by the 4 My old 950A-7H turbidite example (Figure 4.4). It is therefore inferred that Se is being immobilised in turbidites and sapropels as soon as post-oxic conditions are encountered (i.e. immediately below, and independent of, the corresponding Fe peak). If independent of Fe, this may involve the formation of Se(0) or selenides.

Two principal factors must be involved in the development of sharp enrichment peaks of Hg, Se and other redox-sensitive elements in the vicinity of localised oxic/post oxic boundaries. First, a redox gradient exists across the boundary, imposing thermodynamic controls on elemental speciation, which leads to the development of peaks at slightly different depth levels for different elemental geochemistries. Second, the prolonged (ky) maintenance of this redox gradient at more or less the same locus allows energetically-favoured reactions with slow kinetics to proceed towards completion. On this reasoning, the reduced Hg and Se species forming peaks must not only be highly unstable towards O_2 so that they are readily dissolved when overtaken by an advancing oxidation front, but must also be highly insoluble in anoxic (post-oxic) conditions to re-form solid phases immediately below the front. Migration must take place through an oxidised species released to pore water solution which is reduced and again immobilised in reducing conditions. In the case of the core 950A-17H turbidite (Figure 4.2), the well-developed Hg and Se peaks are still in place at the relict boundary of oxidation which can still be identified from the colour change and the Corg profile in the turbidite. This demonstrates the long-term stability of such peaks once formed, over 4 My and 150 m of burial, first in post-oxic and subsequently in sulphidic conditions on progressive burial and compaction (Thomson *et al.* 1998).

At the trace concentration levels of Hg and Se observed, the changes in chemical speciation which are involved in formation of the diagenetic enrichment peaks, and in their continuous dissolution and re-immobilisation when the oxidation front is active, cannot readily be determined directly but must instead be inferred from geochemical behaviour and thermodynamic predictions. Thermodynamic

stability predictions for most elements have been assembled by Brookins (1988). Simon and co-workers have recently investigated the stability fields of binary selenide minerals relative to the elements (Simon and Essene, 1996; Simon *et al.* 1997), but Simon and Essene (1996) point out that the thermodynamic properties and speciation of aqueous Se species remain uncertain. The predicted non-ionic forms of Hg at near-neutral pH values (as found in marine sediments) and around redox potential Eh ~ 0 volts (as found at the oxic/post-oxic boundary) are Hg(0) and HgS (Brookins 1988). The elemental Hg(0) form is both sparingly soluble and volatile, and appears unlikely to be the Hg species which forms the peaks in post-oxic conditions, particularly in view of its persistence as a sharp peak in the ODP turbidite unit over 4 My. Although post-oxic conditions are defined as having negligible O_2 and H_2S levels, it is possible that sufficient trace sulfide may be available to form HgS. This was the explanation advanced by Rosenthal *et al.* (1994) to explain similar diagenetic Cd peaks in turbidites. The problem for Cd is similar to that for Hg, i.e. to explain a large Cd peak when the thermodynamically-predicted insoluble form is CdS. Although HgS is highly insoluble, it does not appear to control the solubility of Hg, even in near-shore anoxic sulphidic sediments, and rather Hg is either incorporated into pyrite (Huerta-Diaz and Morse, 1992; Masscheleyn *et al.* 1991) or methylated (Gagnon *et al.* 1996, 1997). In fact, the description of geochemical conditions for Hg methylation by Gagnon *et al.* (1996) is similar to that inferred here in the formation of the Hg peaks.

An alternative and more likely explanation for the Hg profiles is that there is an interaction between Se and Hg rather than between S and Hg. This is suggested by the fact that, at the most detailed sampling resolution employed (cores 11805, UM41 and T87-26B, Figures 4.1 and 4.3), the Hg peak is always located on the upper face of the Se peak. Selenide minerals, including tiemannite (HgSe), are recognised in certain types of ore deposit (Simon and Essene, 1996; Simon *et al.* 1997), but such deposits are relatively rare because they require that the ore formation process separates Se from S in order to avoid the substitution of Se into sulfide minerals. Selenium minerals can also form in the weathering zone of Se-bearing minerals (Simon *et al.* 1997), a situation most similar to the cases studied in this work. Separation of Se from S is usually achieved by oxidation, and a large thermodynamic field exists in neutral pH conditions and low oxidation potential where the mobile species are SO_4^{2-} and HSe^- (Simon *et al.* 1997). In the turbidite and sapropel sediments studied here, it is re-oxidation of pre-existing sulfides (e.g. Fig. 4.5) which has been the principal source of Se and Hg to form the diagenetic peaks (e.g. Figs. 4.1, 4.2 and 4.3ab), rather than sea water. We speculate that, in the turbidites and sapropels, oxidation has released pyrite S as SO_4^{2-}, which has been lost back to bottom waters by diffusion because conditions are insufficiently reducing in the downwards direction to re-reduce SO_4^{2-} back to sulphides. In contrast, any Se released to solution (whether as SeO_4^{2-} or as less oxidised species $HSeO_3^-$, SeO_3^{2-} or as HSe^{2-}), must be efficiently reduced again (to

Se(0) or selenides) in the downwards direction in anoxic conditions. As noted above, the core CD63#9K Se peak also proves that post-oxic redox conditions can produce an uptake of Se from bottom waters (Oremland *et al.* 1989), independent of both S uptake by reduction from seawater SO_4^{2-}, and of oxidation of pre-existing sulphides.

In their investigation of selenium ore occurrences, Simon and Essene (1996) and Simon *et al.* (1997) have shown that a wide range of elements can form binary and more complex selenide minerals if sufficient separation from Se from S is achieved during formation. Dependent on degree of separation and the exact geochemical conditions at the time of formation, these minerals include diverse selenides of low abundance elements such as Ag, Au, Cd, Hg, Sb and Tl, as well as of more abundant chalcophile elements such as Cu, Ni and Zn. The former sets of elements appear to form selenides at lower Se and S fugacities than the latter set. The mineralogy and the amount of selenide formed from an oxidising fluid is a function of Se, S and O_2 fugacities and ultimately the solution Se concentration. In the turbidite examples (Figures 4.1 and 4.2), peaks of Cu, Co, Ni and Zn are formed below the oxidation front (Thomson *et al.* 1993), but these are mainly located below the Se peak. They cannot be binary selenide-associated because there is insufficient Se to balance the molar amount in the diagenetic peaks of these elements. Also these four elements clearly migrate over short distances on burial after the cessation of the oxidation front, unlike Se, Hg, Cd and Tl (Thomson *et al.* 1998).

Formation of selenides could also explain the Cd and Pt peaks previously reported in the core 11805 turbidite by Rosenthal *et al.* (1995) and Colodner *et al.* (1992), respectively (Figure 4.1). The active oxidation depth in this core is deep in the sediment at ~120 cm, and the redox gradient, as inferred from the spectrum of elements immobilised around the oxic/post-oxic boundary, is spread over several cm (Thomson *et al.* 1993). In this core there is clear evidence that S (as sulfides) in the turbidite is oxidised before Corg, and the Se peak is found entirely within with the intervening zone with low S but high Corg contents. In the turbidite cores studied, the elemental enrichments occurring with Se are zoned, consistent with some gradation of redox conditions across the Se peak. In all cores (including the sapropel examples), the diagenetic Hg enrichments are located mainly on the upper side of the corresponding Se peak. In cores 11805 and 950A-17H-3 (Figures 4.1 and 4.2), Pt is located over the entire Se peak while the Cd, Tl and Sb peaks occur at the base of the Se peak. Both Cd peaks are very sharp, but those of Pt, Tl and Sb are spread over a few cm. Selenium is a more abundant element than Hg, Cd, Pt, Tl or Sb, and the amount of diagenetic Se in the peaks is much greater than the molar sum of the concentrations of those individual elements inferred here to be immobilised as a selenide. Even at the large Cd peak in core 11805 where the concentration levels of

Cd and Se are similar, we estimate that the 1 cm sample with maximum Cd content contains 0.11 μmol/cm-2 Cd but 0.14 μmol cm^{-2} Se (Figure 4.1). It is not clear whether the additional Se not balanced by the trace elements identified in these peaks is present as Se(0) or whether it is complexed as selenides of other unidentified elements. It has only been possible to identify the redox-sensitive elements with a probable Se-association because (like Se itself) their diagenetic concentration is large compared with their detrital concentration.

The difference in elemental abundance may be the reason for the off-set between the smaller peaks observed for Se and Hg in core CD63#9K (Figure 4.4). The width of the redoxclines is in the order CD63#9K > turbidites > sapropels, and the magnitude of the elemental enrichment peaks is in the reverse order. It is possible that there is sufficient diagenetic (as opposed to detrital) Se on the upper side of the CD63#9K Se peak to react with the 20-30 ppb of diagenetic Hg, sufficient to form HgSe and hence produce the observed 7 cm peak off-set (Figure 4.4). Similar considerations apply to the downwards tail in the small Sb peak of in core 950A-17H-3, which appears to persist deeper than the corresponding Se peak (Figure 4.2).

Antagonistic biochemical reactions between Se and Hg and between Se and Cd are well-known in mammalian toxicology, to the extent that Se has been considered as an effective protection agent against the acute toxicities of both Hg and Cd (Magos and Webb, 1980; Byrne *et al.* 1995). A 1:1 atomic correlation between the contents of Se and Hg in certain organs (e.g. livers, brains) of marine mammals was first noted by Koeman *et al.* (1973), and has been verified by subsequent work (Pelletier, 1985; Palmisano *et al.* 1995; Nigro and Leonzio, 1996). This correlation is not inherited from the food source, because Hg is predominantly present in fish as $CH_3Hg(II)$. Formation of HgSe in mammals is therefore generally inferred to be the end result of a biochemical detoxification pathway involving Hg demethylation (Magos and Webb, 1980; Byrne *et al.* 1995). Martoja and Berry (1980) have unambiguously identified particles of the mineral tiemannite (HgSe) in cetacean livers.

An attempt was made in this work to identify tiemannite in selected sapropel samples with the highest Hg and Se contents. Freeze-dried, resin-impregnated and polished thin sections were examined by SEM using backscattered electron and EDS-XRF analysis. The backscatter electron technique is sensitive to variations in atomic number (Z), and it was hoped that micrometer-sized grains of tiemannite (if present) would stand out against the lower Z of background aluminosilicates. No such grains were identified, but it is possible that oxidative destruction of any such grains during section preparation might have occurred.

4.6. Conclusions.

Diagenetic redistribution peaks of Hg are reported from compositionally well-characterised deep-sea sediment cores. These are found at active and fossil occurrences of the oxic/post-oxic boundary in turbidites and sapropels where oxidation of pre-existing sulfides is involved, and less certainly in a continuously-accumulated section with an active oxic/post-oxic boundary where a Se peak is forming without accompanying sulfide formation. The Hg peaks are always coincident with the associated Se peaks, and by analogy with Se ore geochemistry it is proposed that formation of HgSe (tiemannite) occurs following Se separation from S after sulfide oxidation. This selenide formation mechanism following oxidation of precursor sulfides may apply to other trace elements such as Cd and Pt which also appear to form peaks in close association with Se.

Coupled Se and Hg peaks at the tops of sulfide-rich sedimentary units are therefore likely to be permissible indicators that post-depositional oxidation of the units has occurred. Sulfide wastes are often enriched in Hg, and their oxidation in the environment can give rise to environmental toxicity problems through release of associated elements (e.g. Morse, 1991; Cooper and Morse, 1998). The findings here suggest that Hg loss from oxidation of sulfides may be retarded so long as sufficient Se is present, and so long as sulfate reduction does not remain active in the waste (Di Toro *et al.* 1990).

4.7. Acknowledgements.

This work was partly supported by EU Marine Science and Technology project "Sapropels And Productivity" (SAP), MAS3-CT97-0137. We thank Phil Warwick and Darryl Green for their work on the set-up of the AFS Hg methods, and Robin Armstrong for discussions on Se geochemistry. Comments from the journal referees considerably improved the final manuscript.

4.8. References.

Bacon, M.P. (1984). Glacial to interglacial changes in carbonate and clay sedimentation in the Atlantic Ocean estimated from ^{230}Th measurements. *Isotope Geoscience,* **2**, 97-111.

Berner, R.A. (1981). A new geochemical classification of sedimentary environments. *J.Sediment.Petrol.,* **51**, 359-365.

Bernhard, M. and George, S.G. (1986). Importance of chemical species in uptake, loss and toxicity of elements in marine organisms. In *The Importance of Chemical "Speciation" in Environmental Processes* (eds. Bernhard, M., Brinckman, F.E. and Sadler, P.J.) Dahlem Konferenzen, 1986, Springer-Verlag, Berlin, pp. 385-422.

Bostrom, K. and Fisher, D.E. (1969). Distribution of mercury in East Pacific sediments. *Geochim. Cosmochim. Acta*, **33**, 743-745.

Bothner, M.H., Jahnke, R.A., Peterson, M.L. and Carpenter, R. (1980). Rate of mercury loss from contaminated estuarine sediments. *Geochim. Cosmochim. Acta,* **44**, 273-285.

Brookins, D.G. (1988). Eh-pH Diagrams for Geochemistry. Springer Verlag, Berlin, Heildelberg, pp.176.

Byrne, A.R., Skreblin, M., Al-Sabti, K., Stegnar, P. and Horvat, M. (1995) Mercury and selenium: Perspectives from Idrija. *Acta Chimica Slovenica,* **42**, 175-198.

Colodner, D.C., Boyle, E.A., Edmond, J.M. and Thomson, J. (1992). Post-depositional mobility of platinum, iridium and rhenium in marine sediments. *Nature*, **358**, 402-404.

Cooper, D.C. and Morse, J.W. (1998) Biogeochemical controls on trace metal cycling in anoxic marine sediments. *Environ. Sci. Technol.,* **32**, 327-330.

Corselli, C. (1994). Shipboard Report of R/V Urania Cruise 94/18, September 16 - October 3, 1994. Catania, Italy -Catania, Italy. 50pp with Appendix, unpublished manuscript.

Craig, P.J. (1980). Metal cycles and biomethylation. In*: "The Handbook of Environmental Chemistry,*

Volume 1 Part A, (Hutzinger, O. (ed.) The natural environment and the biogeochemical cycles" Springer Verlag, Berlin, pp. 169-227.

Craig, P.J. (1986a). Chemical species in industrial discharges and effluents. In: Bernhard, M., Brinckman, F.E. and Sadler, P.J. (eds.) The Importance of Chemical "Speciation" in Environmental Processes. Springer-Verlag, Berlin, pp. 443-464.

Craig, P.J. (1986b). *Organomercury compounds in the environment.* In: Craig, P.J. (ed) Organometallic componds in the environment. Longman, Harlow, pp. 65-110.

Di Toro, D.M., Mahony, J.D., Hansen, D.J., Scott, K.J., Hicks, M.B., Mayr, S.M. and Redmond, M.S. (1990). Toxicity of cadmium in sediments: the role of acid volatile sulfide. *Environ. Toxicol. Chem.*, **9**, 1487-1502.

Gagnon, C., Pelletier, E., Mucci, A. and Fitzgerald, W.F. (1996). Diagenetic behaviour of methyl mercury in organic-rich coastal sediments. *Limnol. Oceanogr.*, **41**, 428-434.

Gagnon, C., Pelletier, E. and Mucci, A. (1997). Behaviour of anthropogenic mercury in coastal marine sediments. *Mar. Chem.*, **59**, 159-176.

GESAMP 1986. (IMO/FAO/UNESCO/WMO/WHO/IAEA/UN/UNEP Joint Group of Experts on the Scientific Aspects of Marine Pollution), *Review of Potentially Harmful Substances: Arsenic, Mercury and Selenium.* Rep. Stud. GESAMP No.28, 172pp.

GESAMP 1990. (IMO/FAO/UNESCO/WMO/WHO/IAEA/UN/UNEP Joint Group of Experts on the Scientific Aspects of Marine Pollution), *The state of the marine environment.* Rep. Stud. GESAMP No.39, 111pp.

Grousset, F. and Donard, O. (1984). Enrichments in Hg, Cd, As and Sb in recent sediments of Azres-iceland Ridge. *Geo-Marine Lett.*, **4,** 117-124.

Huerta-Diaz, M.A. and Morse, J.W. (1992). Pyritisation of trace metals in anoxic marine sediments. *Geochimica et Cosmochimica Acta,* **56**, 2681-2702.

Jarvis, I. and Higgs. N.C. (1987) Trace-element mobility during early diagenesis in distal turbidites:

Late Quaternary of the Madeira Abyssal Plain, N. Atlantic. *In Geology and Geochemistry of Abyssal Plains* (eds. P.P.E. Weaver and J. Thomson); *Geological Society Special Publication No. 31.* pp 179-213.

Jonasson, I.R. and Boyle, R.W. (1972). Geochemistry of mercury and origins of natural contamination of the environment. *Can. Mining and Metall.Bull.,* **65,** 32-39.

Jung, M., Ilmberger, J., Mangini, A. and Emeis, K.-C. (1997). Why some Mediterranean sapropels survived burn-down (and others did not). *Mar. Geol.,* **141,** 51-60.

Kadko, D. (1980). A detailed study of some uranium series nuclides at an abyssal hill area near the East Pacific Rise at 8°45'N. *Earth Planet. Sci. Lett.,* **51,** 115-131.

Koeman, J.H., Peeters, W.H.M., Koudstaal-Hol, C.H.M., Tjioe, P.S. and De Goeu, J.J.M. (1973). Mercury selenium correlations in marine mammals. *Nature,* **245,** 385-386.

Lindqvist, O. (1991). Editor, papers from conference "Mercury as an environmental pollutant". *Water, Air and Soil Pollution,* **56,** 1-845.

Locarnini, S.J.P. and Presley, B.J. (1996) Mercury concentrations in benthic organisms from a contaminated estuary. *Marine Environmental Research,* **41**, 225-239.

Mason, R.P., Fitzgerald, W.F. and Morel, F.M.M. (1994). The biogeochemical cycling of elemental mercury: Anthropogenic influences. *Geochim. Cosmochim. Acta,* **58**, 3191-3198.

Magos, L. and Webb, M. (1980). The interactions of selenium with cadmium and mercury. *CRC Crit. Rev. Toxicol.,* **8**, 1-42

Masscheleyn, P.H., Delaune, R.D. and Patrick, W.H. Jnr. (1991). Biogeochemical behaviour of selenium in anoxic soils and sediments: An equilibrium thermodynamics approach. *J. Environ. Sci. Health,* **A26**, 555-573.

Martoja, R. and Berry, J.P. (1980). Identification of tiemannite as a probable product of demethylation of mercury by selenium in cetaceans. A complement to the scheme of the biological

cycle of mercury. *Vie Milieu*, **30,** 7-10.

Morse, J.W. (1991) Oxidation kinetics of sedimentary pyrite in seawater. *Geochim. Cosmochim. Acta*, **55,** 3665-3667.

Myneni, S.C.B., Tokunaga, T.K. and Brown, G.E. (1997). Abiotic selenium redox transformations in the presence of Fe(II,III) oxides. *Science,* **278**, 1106-1109.

Nigro, M. and Leonzio, C. (1996). Intracellular storage of mercury and selenium in different marine vertebrates. *Marine Ecology Progress Series,* **135,** 137-143.

Nriagu, J.O. (1989). A global assessment of natural sources of atmospheric trace metals. *Nature,* **338,** 47-49.

Oremland, R.S., Hollibaugh, J.T., Maest, A.S., Presser, T.S., Miller, L.G. and Culbertson, C.W. (1989). Selenate reduction to elemental selenium by anaeroboc bacteria in sediments and culture: Biogeochemical significance of a novel, sulfate-independent respiration. *Applied and Environmental Microbiology,* **55,** 2333-2343.

Palmisano, F., Cardellichio, N. and Zambonin, P.G. (1995). Speciation of mercury in dolphin liver: A two-stage mechanism for the demethylation accumulation process and role of selenium. *Marine Environmental Research,* **40,** 109-121.

Pelletier, E. (1985). Mercury-selenium interactions in aquatic organisms: a review. *Marine Environmental Research,* **18,** 111-132.

Porcella, D., Huckabee, J. and Wheatley, B. (1995). Editors, papers from conference "Mercury as a global pollutant". *Water, Air and Soil Pollution,* **80,** 1-1336.

Rasmussen, P.E. (1994). Current methods of estimating atmospheric mercury fluxes in remote areas. *Environmental Science and Technology,* **28,** 2233-2241.

Rohling, E.J. (1994). Review and new aspects concerning the formation of eastern Mediterranean sapropels. *Mar. Geol.,* **122,** 1-28.

Rosenthal, Y., Lam, P., Boyle, E.A., and Thomson, J. (1995).Authigenic cadmium enrichments in sub-oxic sediments: Precipitation and post-depositional mobility. *Earth Planet. Sci. Lett.*, **132,** 99-111.

Rothwell, R.G. (1995). Cruise report of Marion Dufresne cruise 81, 17 January - 9 February 1995; Marseille, France -Limassol, Cyprus. 70pp with Appendix, unpublished manuscript.

Simon, G. and Essene, E.J. (1996). Phase relations among selenides, sulfides, tellurides and oxides: I. Thermodynamic properties and calculated equilibria. *Econ. Geol.*, **91,** 1183-1208.

Simon, G., Kesler, S.E. and Essene, E.J. (1997). Phase relations among selenides, sulfides, tellurides and oxides: II. Applications to selenide-bearing ore deposits. *Econ. Geol.*, **99,** 468-484.

Skei, J. and Paus, P.E. (1979) Surface metal enrichment and partitioning of metals in a dated sediment core from a Norwegian fjord. *Geochim. Cosmochim. Acta,* **43,** 239-246.

Thomson, J., Higgs, N.C., Croudace I.W., Colley S. and Hydes, D.J. (1993). Redox zonation of elements at an oxic/post-oxic boundary in deep-sea sediments. *Geochim. Cosmochim. Acta,* **57,** 579-595.

Thomson, J., Higgs, N.C., Wilson, T.R.S., Croudace I.W., de Lange, G.J. and van Santvoort, P.J.M. (1995). Redistribution and geochemical behaviour of redox-sensitive elements around S1, the most recent Eastern Mediterranean sapropel. *Geochim. Cosmochim. Acta,* **59,** 3487-3501.

Thomson, J., Higgs, N.C. and Colley, S. (1996). Diagenetic redistributions of redox-sensitive elements in NE Atlantic glacial/interglacial sediments. *Earth Planet. Sci. Lett.*, **139,** 365-377.

Thomson, J., Jarvis, I., Green, D.R.H., Green, D.A. and Clayton, T. (1998). Mobility and immobility of redox-sensitive elements in deep-sea turbidites during shallow burial. *Geochim. Cosmochim. Acta.*, **62,** 643-656.

Toth, J.R. (1980). Deposition of submarine crusts rich in manganese and iron. *Geol. Soc. Amer. Bull.*, **91,** 44-54.

Troelstra, S.R., Ganssen, G.M., van der Borg, K. and de Jong, A.F.M. (1991). A Late Quaternary

stratigraphic framework for Eastern Mediterranean sapropel S1 based on AMS ^{14}C dates and stable oxygen isotopes. *Radiocarbon,* **33,** 15-21.

van Santvoort, P.J.M., de Lange, G.J., Thomson, J., Cussen, H., Wilson, T.R.S., Krom, M.D. and Strohle, K. (1996). Active post-depositional oxidation of the most recent sapropel (S1) in the eastern Mediterranean. *Geochim. Cosmochim. Acta.*, **60,** 4007-4024.

Watras, C.J. and Huckabee, J.W. (1994). Editors, *Mercury pollution: integration and synthesis,* 727 pp., CRC Press.

Young, D.R., Johnson, J.N., Soutar, A. and Isaacs, J.D. (1973). Mercury concentrations in dated varved marine sediments collected off Southern California. *Nature,* **244,** 273-275.

Figure Captions.

Figure 4.1. Concentration versus depth profiles for Corg, S, Se, Hg, Cd and Pt in the distal turbidite in core 11805K (25°39.8'N, 30°57.0'W; 6050 corrected m water depth). Organic C, S and Se data are from Thomson *et al.* (1993), Cd data are from Rosenthal *et al.* (1995) and Pt data from Colodner *et al.* (1992). An oxidation front is active at ~120cm depth below the sediment water interface in this core (Thomson *et al.* 1993). The lighter and darker tones represent the oxic and post-oxic sections of the same single turbidite unit, while the Se peak is contained within the shaded zone. The shaded zone lies between the step changes seen in the Corg and S profiles, is post-oxic, and is intermediate in colour between the overlying oxic and underlying post-oxic parts of this turbidite.

Figure 4.2. Concentration versus depth profiles for Corg, S, Se, Hg, Cd, Tl and Sb unit in the turbidite unit in ODP core 157-950A-17H-3 (31°9.01'N, 25°36.00'W; 5438 corrected m). Depths are cm in core section, but in fact this section is now 153 metres below the sea floor (Thomson *et al.* 1998). An oxidation front was active in this unit ~ 4 My ago. Data except Hg are from Thomson *et al.* (1998). The lighter and darker tones represent the sections of the same sapropel unit which were oxic or anoxic during the short period when the oxidation front was active, while the shaded area highlights the Se peak zone.

Figure 4.3 ab. Concentration versus depth profiles for Corg, S, Se and Hg in two cores containing the most recent Eastern Mediterranean sapropel, S1. (a) Core UM41 is at 34°57.26'N, 17°51.37'E; 1390 m (Corselli, 1994), while (b) core T87-26B is at 33°38'N, 28°26'E; 3295 m (Troelstra *et al.* 1991). In this case the lighter shading represents the amount of S1 oxidised since deposition, while the dark shading represents the remaining unoxidised S1 unit.

Figure 4.4. Concentration versus depth profiles for Se and Hg in core CD63#9K (46°23.8'N, 12°32.8'W; 3849 m). Although this core exhibits a diagenetic Se peak which has been developed just below the active oxic/post-oxic boundary by downwards diffusion from bottom waters (Thomson *et al.* 1996), the corresponding Hg peak, if real, is off-set by 7 cm upwards. See text.

Figure 4.5. Concentration versus depth profiles for Corg, S, Se and Hg in eastern Mediterranean core LC21 (35°39.71'N, 26°34.96'E; 1522 corrected m; Rothwell (1995)). Unlike the cores in figures 4.3 ab, the S1 sapropel in this core has been little affected by post-depositional oxic diagenesis because of its rapid accumulation rate (~20 $cm.ky^{-1}$, from unpublished radiocarbon data). As a result, a good

correlation is still retained between all four elements within the Corg-rich unit between 140-191 cm in core (shaded). Note, however, that even here there are higher Hg and Se values at the very top of the sapropel unit (140-145 cm), consistent with *trace* post-depositional oxidation.

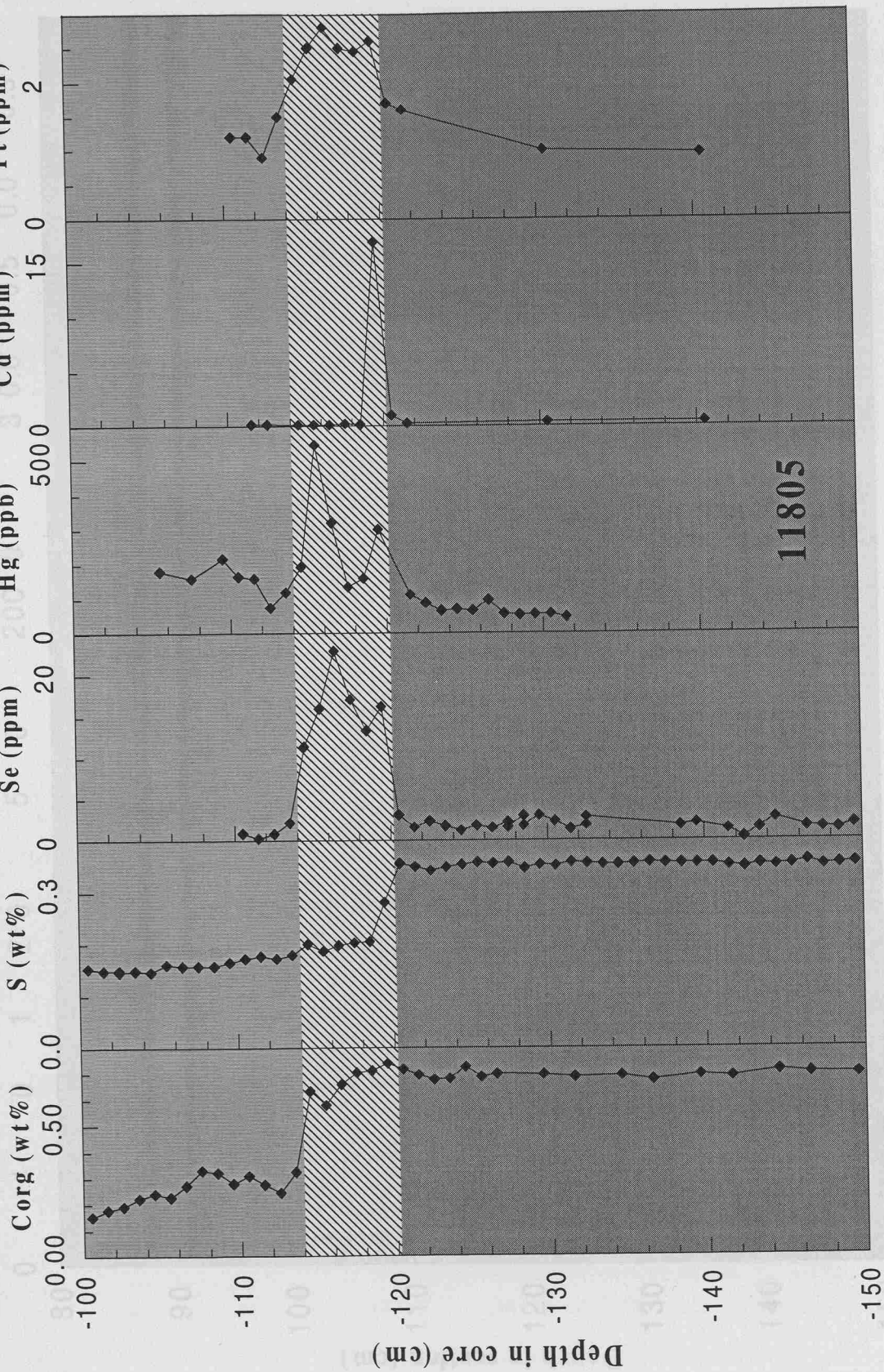
Corg (wt%)
0.00
0.50
S (wt%)
0.0
0.3
Se (ppm)
0
20
Hg (ppb)
0
5000
Cd (ppm)
0
15
Pt (ppm)
0
2
11805
-100
-110
-120
-130
-140
-150
Depth in core (cm)

Figure 4.1

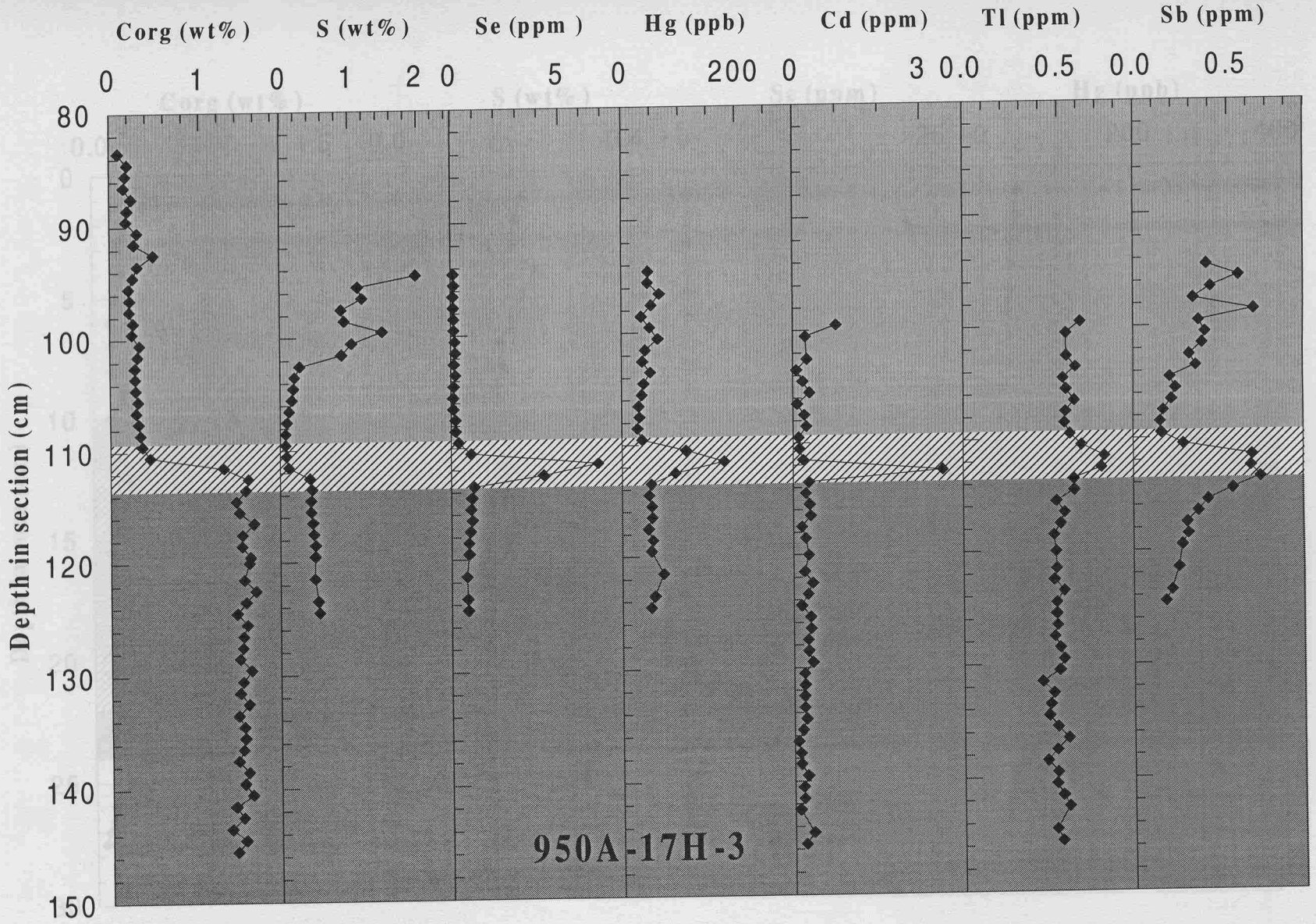
Corg (wt%)
S (wt%)
Se (ppm)
Hg (ppb)
Cd (ppm)
Tl (ppm)
Sb (ppm)
0
1
0
1
2
0
5
0
200
0
3
0.0
0.5
0.0
0.5
80
90
100
110
120
130
140
150
Depth in section (cm)
950A-17H-3

Figure 4.2

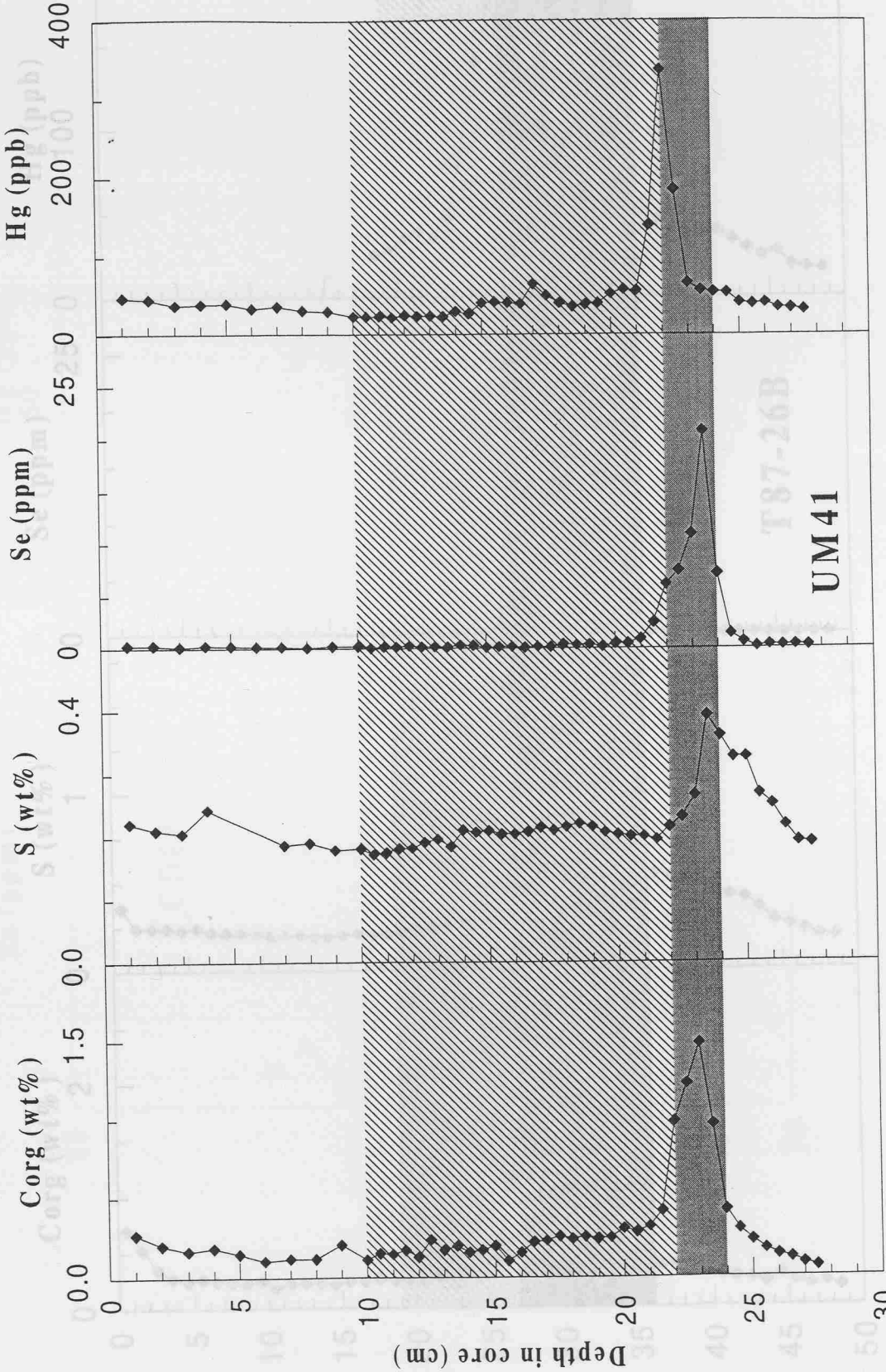
Corg (wt%)
0.0
1.5
S (wt%)
0.0
0.4
Se (ppm)
0
25
Hg (ppb)
0
200
400
Depth in core (cm)
0
5
10
15
20
25
30
UM41

Figure 4.3a

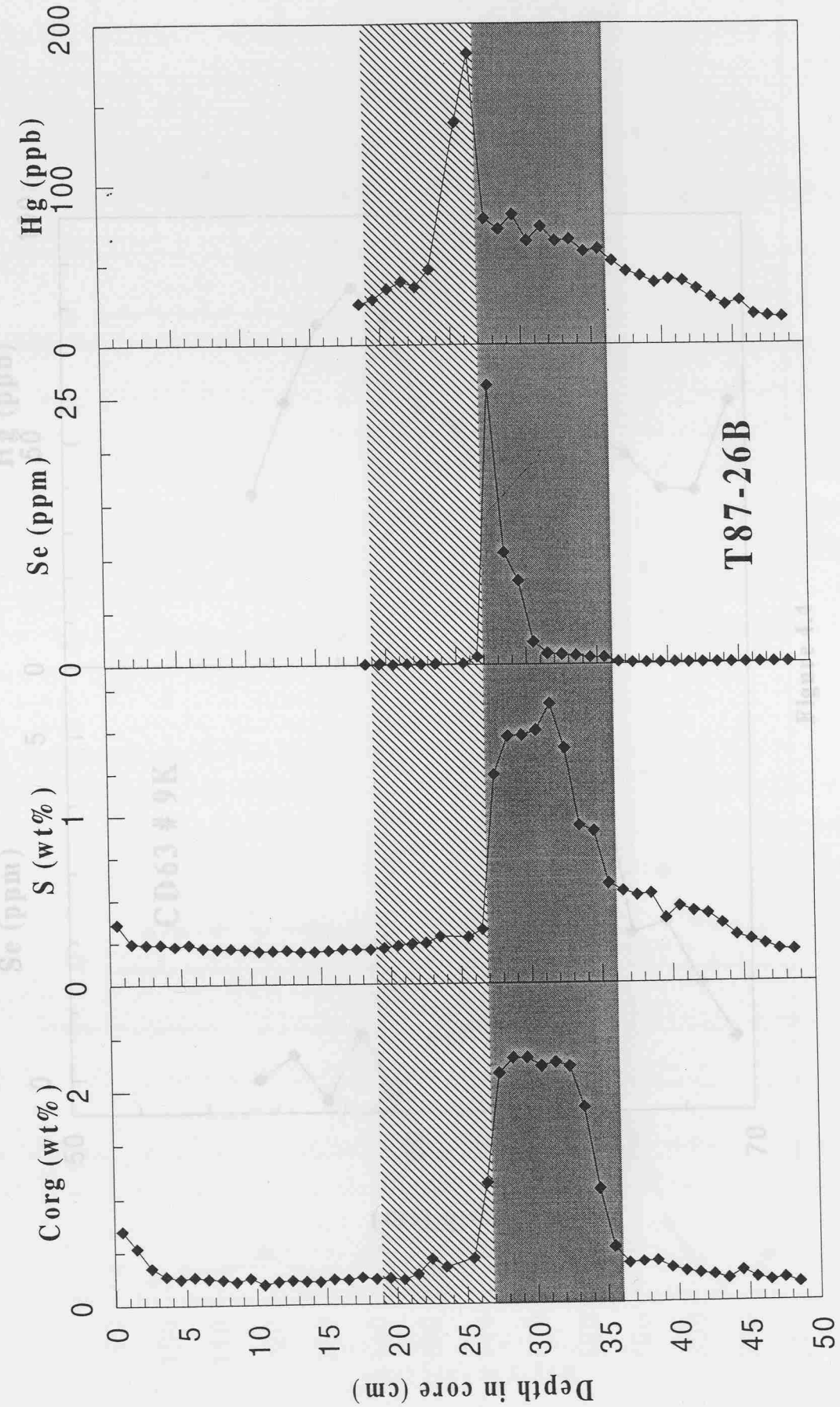
Depth in core (cm)
0
5
10
15
20
25
30
35
40
45
50
Corg (wt%)
0
2
S (wt%)
0
1
Se (ppm)
0
25
Hg (ppb)
0
100
200
T87-26B

Figure 4.3b

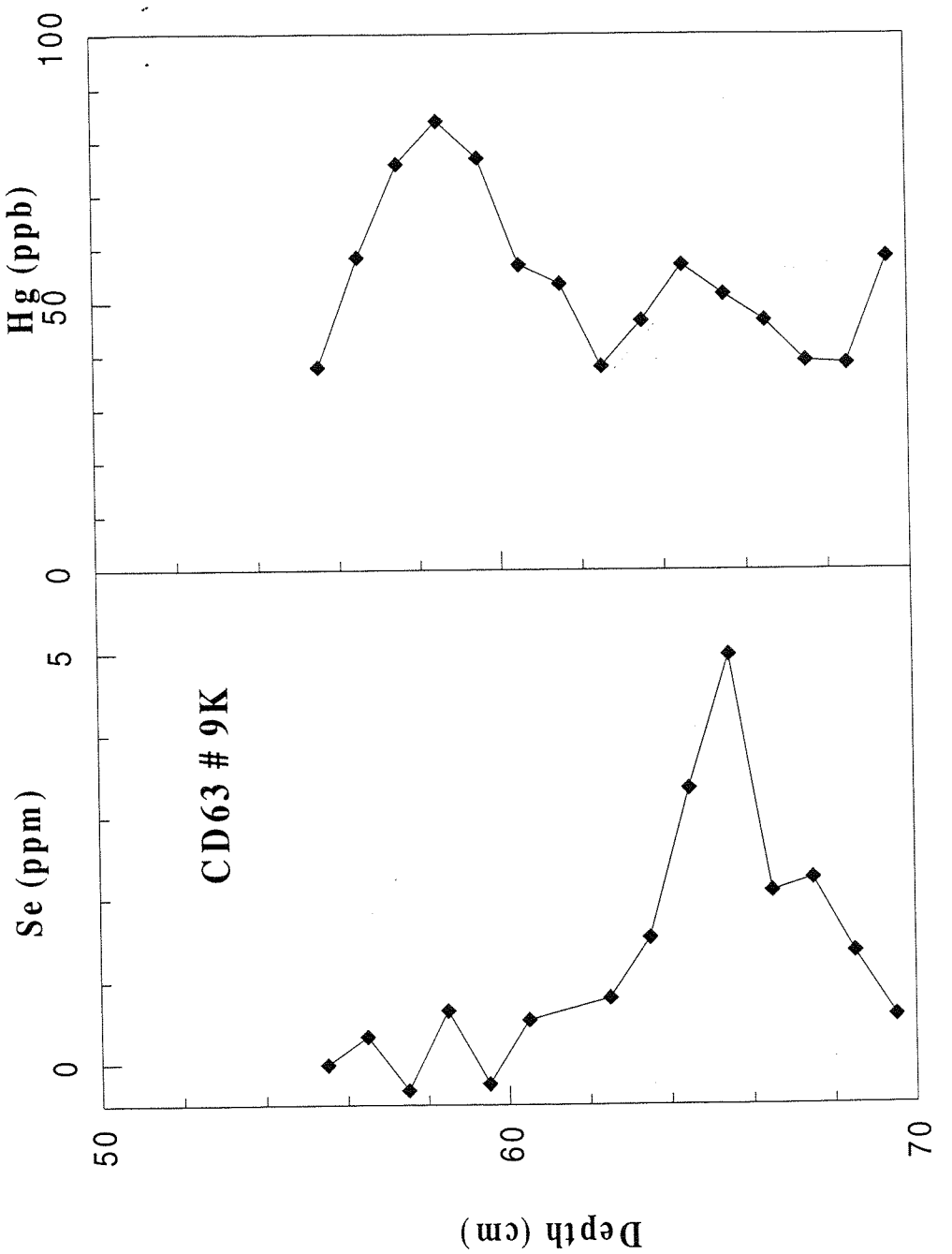

Figure 4.4

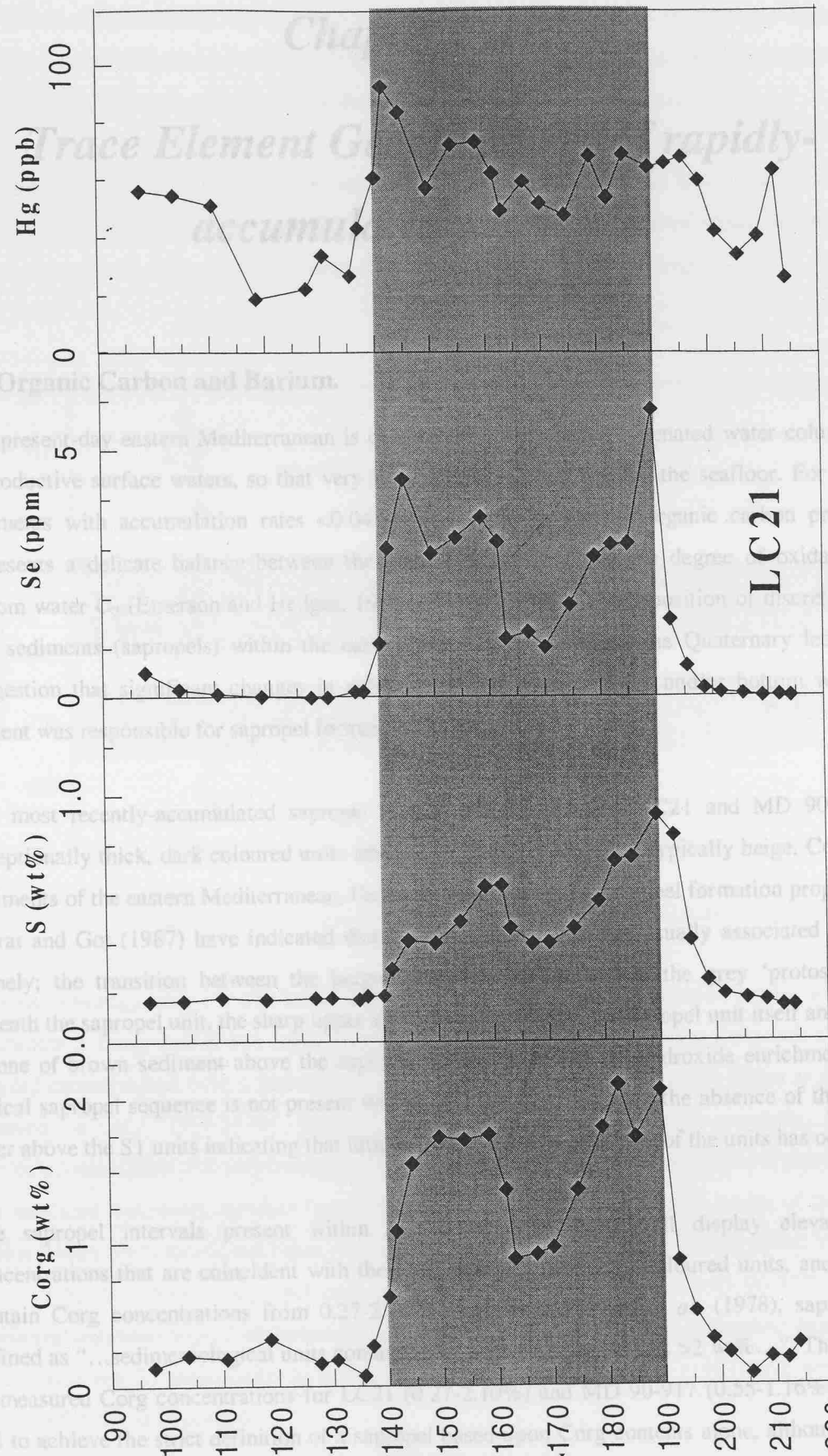
Hg (ppb)
0
100
Se (ppm)
0
5
S (wt%)
0.0
1.0
2
Corg (wt%)
0
1
LC21
Depth in core (cm)
90
100
110
120
130
140
150
160
170
180
190
200
210
220

Figure 4.5

Chapter Five:

Trace Element Geochemistry of rapidly-accumulated sapropels.

5.1 Organic Carbon and Barium.

The present-day eastern Mediterranean is characterised by a well-oxygenated water column and unproductive surface waters, so that very little organic carbon reaches the seafloor. For marine sediments with accumulation rates <0.04 $gcm^{-2}yr^{-1}$, the amount of organic carbon preserved represents a delicate balance between the input flux of Corg and the degree of oxidation by bottom water O_2 (Emerson and Hedges, 1988; Canfield, 1994). The deposition of discrete Corg-rich sediments (sapropels) within the eastern Mediterranean during the Quaternary led to the suggestion that significant changes in either the primary productivity and/or bottom water O_2 content was responsible for sapropel formation (Rohling, 1994).

The most recently-accumulated sapropel (S1) is present in cores LC21 and MD 90-917 as exceptionally thick, dark coloured units intercalated between the more typically beige, Corg-poor sediments of the eastern Mediterranean. Generalised sequences of sapropel formation proposed by Murat and Got (1987) have indicated that three colour changes are usually associated with S1 namely; the transition between the beige Corg-poor sediments and the grey 'protosapropel' beneath the sapropel unit, the sharp upper and lower contacts of the sapropel unit itself and finally a zone of brown sediment above the sapropel indicative of Mn oxyhydroxide enrichment. This typical sapropel sequence is not present within S1 in these cores, with the absence of the brown layer above the S1 units indicating that little post-depositional oxidation of the units has occurred.

The sapropel intervals present within LC21 and MD 90-917 all display elevated Corg concentrations that are coincident with the visual extent of the dark coloured units, and typically contain Corg concentrations from 0.27-2.10%. According to Kidd *et al.* (1978), sapropels are defined as "...sedimentological units containing organic carbon contents >2 wt%...". The majority of measured Corg concentrations for LC21 (0.27-2.10%) and MD 90-917 (0.55-1.16%) therefore fail to achieve the strict definition of a sapropel based upon Corg contents alone, although Calvert (1983) proposed that the >2 wt% criterion is only an approximate guide to the Corg content needed to develop the dark sapropel colour. Recently, Van Santvoort *et al.* (1996) proposed that a sapropel

could be better defined as "...distinct sediment layers with a Corg content significantly higher than that of the surrounding hemi-pelagic sediment and deposited in an open marine environment". This more liberal definition is adopted here to define the presence of sapropel units.

Based on the Corg contents of LC21 and MD 90-917, it appears that S1 formation was not continuous, but rather occurred in two distinct pulses separated by an interval characterised with a Corg content approaching those of present-day eastern Mediterranean sediments (figure 5.1).

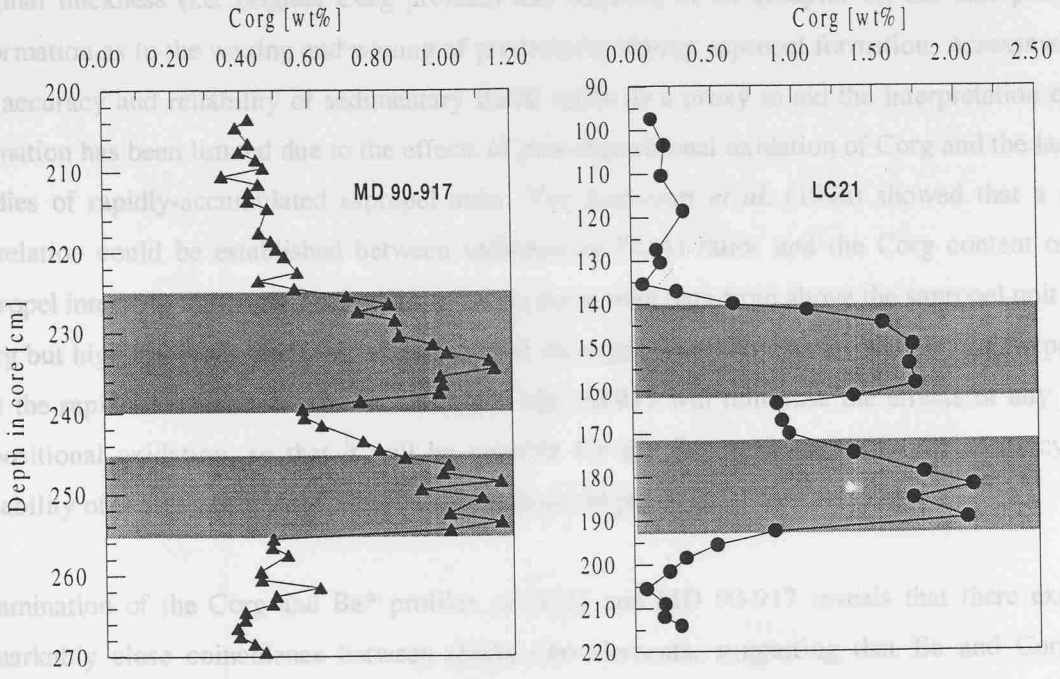

Figure 5.1 Distribution of Corg (wt%) in MD 90-917 and LC21.

Previous investigations on S1 formation have been based primarily upon cores with slow accumulation rates, and it has been assumed that the deposition of these Corg-rich sediments occurred uninterrupted over a period lasting from 5-9 kyr BP (Calvert, 1983; Higgs *et al.*, 1994; Thomson *et al.*, 1995;1999; Van Santvoort *et al.*, 1996). More recently however, micropalaeontological and sedimentological studies of S1 units from the Aegean and Adriatic Seas have indicated that recent sapropel formation was discontinuous within some basins of the eastern Mediterranean (Perissoratis and Piper, 1992; Rohling *et al.*, 1997). It has been suggested by Stanley et al. (1978) that 'double' sapropel units (such as those found in LC21, MD 90-917) represent significant sedimentological disturbances during S1 formation, although alternative explanations for the observed S1 interruption have been proposed by Rohling *et al.* (1997) and will also be discussed further in Chapter 6.

It has been recognised that slowly-accumulated cores are subject to extensive post-depositional alteration via downwards progressing oxidation fronts (Chapter 3), which effectively removes labile Corg from the upper face of the sapropel unit, significantly reducing its original thickness. Thomson *et al.* (1995), proposed that the Corg criterion established by Kidd *et al.* (1978) for the recognition of sapropel units within marine sediments was unreliable since organic carbon was not persistent over relatively short periods of geological time. As a result, Thomson *et al.* (1995) proposed that sedimentary Ba/Al ratios were a more reliable proxy for visualising not only the original thickness (i.e. original Corg profiles) and duration of S1 (chapter 6), but also provided information as to the waxing and waning of productivity during sapropel formation. Assessment of the accuracy and reliability of sedimentary Ba/Al ratios as a proxy to aid the interpretation of S1 formation has been limited due to the effects of post-depositional oxidation of Corg and the lack of studies of rapidly-accumulated sapropel units. Van Santvoort *et al.* (1996) showed that a good correlation could be established between sedimentary Ba/Al ratios and the Corg content of the sapropel intervals, although the correlation broke down with data from above the sapropel unit (low Corg but high Ba due to preferential oxidation of the organic carbon). As a corollary, it is expected that the rapid accumulation rates of LC21 and MD 90-917 will minimise the effects of any post-depositional oxidation, so that it will be possible for the first time to assess the accuracy and reliability of sedimentary Ba/Al ratios as a geochemical proxy in S1 formation.

Examination of the Corg and Ba* profiles in LC21 and MD 90-917 reveals that there exists a remarkably close coincidence between theses two elements, suggesting that Ba and Corg are coupled during sapropel formation (figure 5.2).

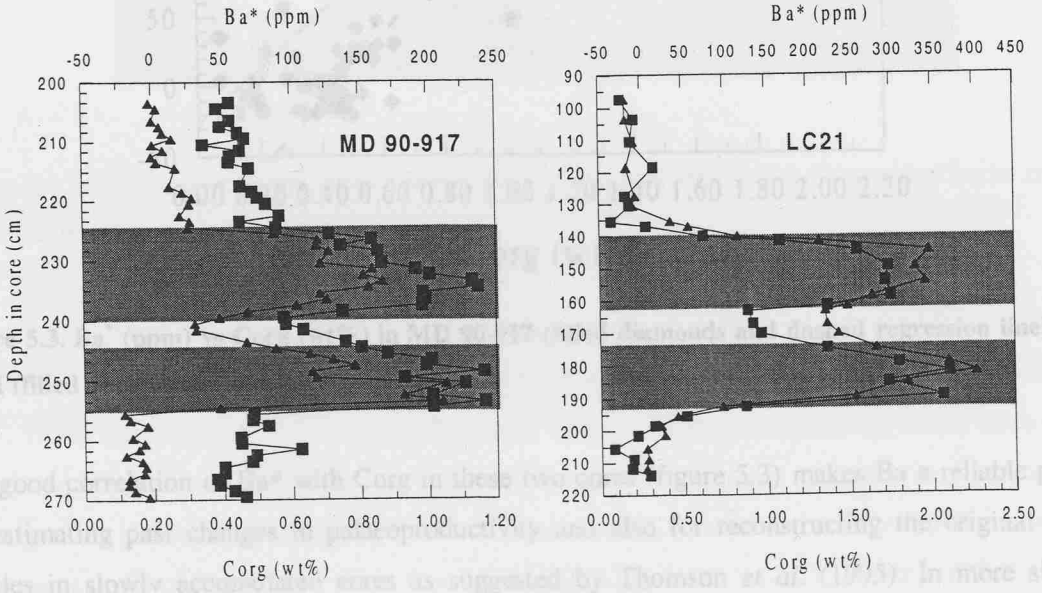

Figure 5.2 Comparison of Ba* (ppm) (top scale, filled triangles) and Corg (wt%) contents (bottom scale, filled squares) in MD 90-917 and LC21.

The positive correlation between Ba* and Corg throughout the entire sapropel units (LC21 r^2= 0.93; MD 90-917 r^2= 0.85) suggests little or no post-depositional oxidation of Corg in these cores (figure 5.3). The fact that the Ba* and Corg relationship is retained is likely due to the rapid accumulation rates of these cores having limited the penetration depth of oxygen into these sediments. Modelled O_2 penetration depths (Tromp *et al.*, 1995) indicate that in LC21 and MD 90-917, oxygen penetration would be limited to within the top 1-2 cm of the core. Moreover, continued high sedimentation rates coupled with reducing bottom waters during and shortly after S1 formation would have further aided the preservation of Corg and Ba* relationship by rapidly removing the sapropel units from any return of dissolved O_2 into the eastern Mediterranean deep-waters.

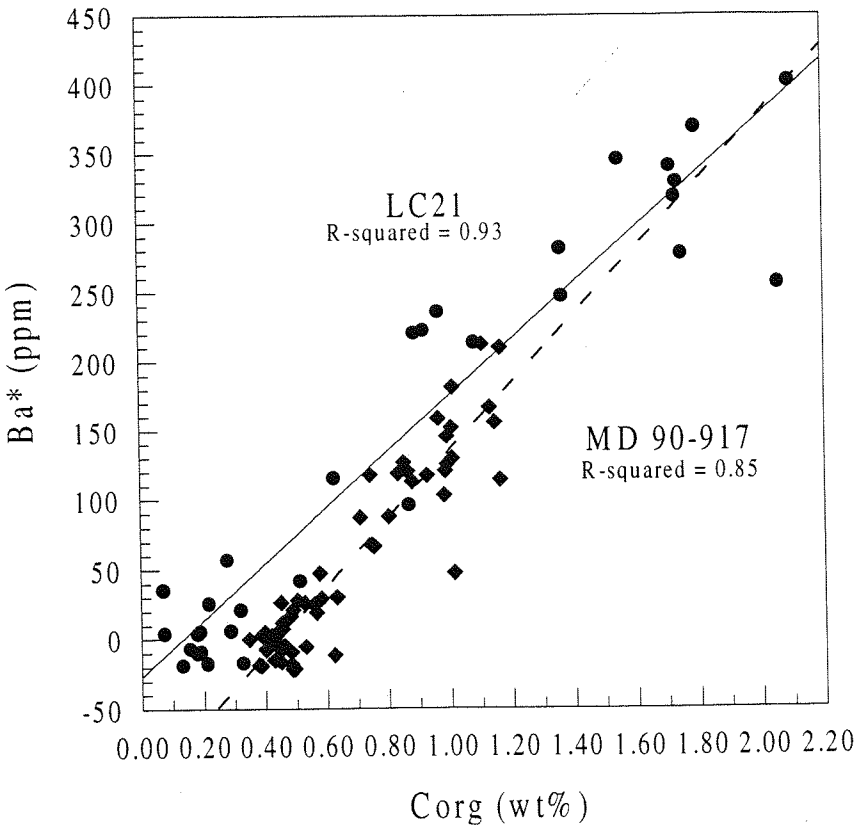

Figure 5.3. Ba* (ppm) vs Corg (wt%) in MD 90-917 (filled diamonds and dashed regression line) and LC21 (filled circles and solid regression line).

The good correlation of Ba* with Corg in these two cores (figure 5.3) makes Ba a reliable proxy for estimating past changes in palaeoproductivity and also for reconstructing the original Corg profiles in slowly accumulated cores as suggested by Thomson *et al.* (1995). In more slowly accumulated cores such as those examined by Thomson *et al.* (1995), the quasi-Gaussian Ba/Al profile indicated that sapropel formation was a continuous event, but from the rapid accumulation

rates of MD 90-917 and LC21 it is clear that S1 formation was more variable than previously thought. In figure 5.2, the Ba* data and Corg profiles are consistent with the fact that enhanced productivity occurred in these eastern Mediterranean areas in two distinct pulses, separated by an interval of reduced productivity rather than oligotrophic conditions as the background Ba* and Corg values are much lower than those found within the "saddle". The excess Ba* within these two zones occurs primarily as discrete ovoid, barite ($BaSO_4$) crystals typically <3μm in size, inferred to be biogenic barite which accompanied the pulses of high productivity which formed S1 (see figure 5.4).

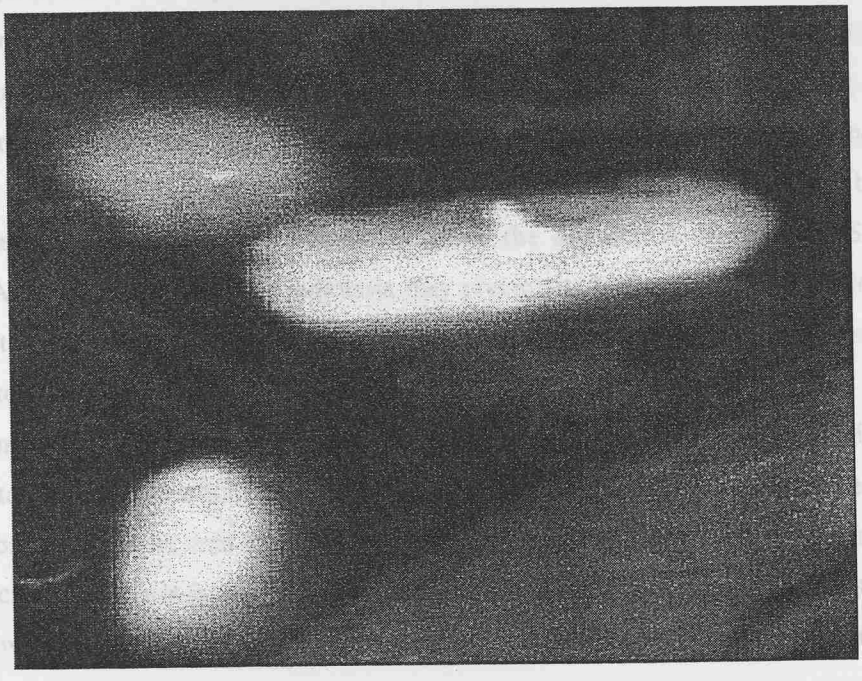

Figure 5.4. SEM image of barite crystals found within LC21 and MD 90-917. The central barite crystal is 2 μm in length.

A close association between Corg and Ba has been recognised in material collected from sediment traps and in marine sediments underlying highly productive regions of the world's oceans (Dehairs *et al.*, 1980; Dymond, 1981; Collier and Edmond, 1984). The mechanism(s) by which barium (as barite) and Corg are coupled within the water column however, remains unknown despite intensive investigations (Dymond *et al.*, 1992; Francois *et al.*, 1995; Dymond and Collier, 1996). Although seawater is undersaturated with respect to barite ($BaSO_4$), studies have demonstrated that a large fraction of the particulate barium in oceanic waters is present as barite crystals (Dehairs *et al.*, 1980; Bishop, 1988; Gingele and Dahmke, 1994). At present three mechanisms are hypothesised to

explain barite formation and its association with Corg. According to Bishop (1988), barite formation occurs within reducing microenvironments provided by biogenic aggregates settling from the euphotic zone. Within these Corg-rich environments, re-oxidation of sulphides significantly increases the concentration of dissolved sulphate thus allowing for the precipitation of $BaSO_4$. Observed correlations between barite, dissolved oxygen and the pCO_2 maximum within the water column of the Southern Ocean further suggests that a relationship exists between the remineralisation of biogenic aggregates and barite formation (Dehairs *et al* 1990; 1991). More recently it has been proposed that barite formation may be biologically mediated by a number of marine organisms. Recent investigations have shown that certain specific organisms such as the *Xenophyphoria* and the marine microplanktonic algae *Exanthemachrysis gayraliae* and *Pavlova sp* form barite crystals intracellularly (Gooday and Nott, 1982). The exact biological function of barite within these organisms is not known, although it is believed that barite crystals tend to function as statoliths (Schmitz, 1987; Bertram and Cowen, 1997). Comparison of the morphology and size of biologically-precipitated barite with those crystals found within marine sediments and sediment trap material bear a striking similarity suggesting that barite formation may be biologically mediated. Alternatively, it has been hypothesised that the dissolution of celestite ($SrSO_4$) tests produced by Acantharia and siliceous radiolaria may precipitate barite (Dymond and Collier *et al.*, 1996). Celestite tests are enriched in Ba and sulphate relative to their concentrations in seawater, so that upon dissolution, both Ba^{2+} and SO_4^{2-} are released. If dissolution of $SrSO_4$ occurs in reducing microenvironments of acantharia or within organic aggregates then barite may precipitate, in a similar way to the abiotic mechanism described previously. Regardless of the mechanism of formation of barite, it can be seen that the close coupling between Corg and Ba arises from the fact that a Corg-rich environment is needed to provide suitable conditions for barite precipitation. Thus it seems that with increasing productivity, more barite will form in response to greater abundance of Corg-rich environments.

The accuracy and reliability of using barium as a proxy in estimating changes in productivity during sapropel formation is based upon the assumption that barite is sufficiently persistent over short and long periods of geological time. Recent investigations on rapidly-accumulated continental margin sediments from Peru have shown that barite is capable of undergoing dissolution and remobilization under reducing conditions (Brumsack, 1986; Torres *et al.*, 1996). Furthermore, work on the most recently accumulated sapropel has shown that barium may form a well-defined peak (barite front) at the limit of sulphate reduction in sediments in some circumstances (Van Os *et al.*, 1991). There are two lines of evidence however, to suggest that little or no post-depositional rearrangement of Ba has occurred within the sapropels of LC21 or MD 90-917. Firstly, in studies where barite has undergone remobilisation, barite fronts form well-defined peaks at the region where sulphate reduction occurs, decoupling the relationship between Corg and Ba (Van Os *et al.*,

1991). In LC21 and MD 90-917 however, it can be clearly seen that the Ba* and the Corg contents of both cores are exceptionally well correlated indicating that the barite has not undergone any dissolution and remobilisation either during or after sapropel formation (figures 5.2 and 5.3). Secondly, the stability of barite in marine sediments is controlled by the concentrations of dissolved sulphate and barium in the pore waters (Gingele and Dahmke, 1994). In oxic and sub-oxic sediments, sulphate and barium are supersaturated with respect to the pore waters so that little/no dissolution of barite occurs. Under anoxic conditions however, where bacterially-mediated sulphate reduction reduces pore water sulphate levels close to zero, barite becomes undersaturated with respect to the interstitial waters and so begins to dissolve. Whilst sulphate reduction has occurred within LC21 and MD 90-917, as indicated by the presence of framboidal pyrite (see section 5.2), recent work by Passier *et al.* (1996) has indicated that during sapropel formation sulphate within the pore waters was never limiting within these sediments. Sulphur isotope data from S1 sediments presented by Passier *et al.* (1997) indicates that during sapropel formation sulphate ions continually influxed into the sediment (along a diffusion gradient) from the overlying seawater, thus preventing barite dissolution. Although the sediments of LC21 and MD 90-917 remained sub-oxic even after sapropel formation, the lack of pyrite formation after S1 had ended implies that sulphate reduction was negligible and that barite did not undergo any further dissolution. It can therefore be concluded that Ba has not undergone diagenetic remobilisation, thus the productivity signal encoded in the Ba* profile is retained and can be accurately and reliably used as a proxy for estimating (palaeo) productivity during S1 formation.

According to Dymond and Collier (1996), during transit through the water column Ba/Corg systematically increases with increasing water depth as Corg is preferentially oxidised relative to barite. Comparison of the Ba*/Corg ratios in LC21 and MD 90-917 reveal that on average the ratios are higher in MD90-917 (average 442) relative to LC21 (average 303). This result is somewhat surprising considering that in most marine environments the amount of Corg preserved is inversely related to the water depth (Muller and Suess, 1979). In LC21 however, the Corg content is consistently greater than that found in MD 90-917 and is in agreement with the observations of Murat *et al.* (1990) who found that Corg contents of S1 linearly increase with water-depth from 1% at 1000m to 3% at 3000m. The influence of water depth on the Ba/Al and Corg contents of LC21 and MD 90-917 is secondary to the effects of sediment accumulation rates which tends to dilute sedimentary components. The fact that the sediment accumulation rate in LC21 (~15 cm kyr) is slower than that of MD 90-917 (~20 cm kyr), indicates that more slowly-accumulated cores from deeper parts of the eastern Mediterranean are less diluted, producing systematically higher Ba* and Corg contents than their counter-parts from shallower locations (see chapter 6).

The close correlation between Corg and Ba has led to the latter element being used as a proxy for estimating changes in productivity in both recent and ancient sediments (Murray and Leinen, 1993; Gingele and Dahmke, 1994; Francois *et al.*, 1995). One of the most debated topics concerning sapropel formation is the mechanism of formation i.e. productivity and/or anoxia. In all the cores examined so far, including the slowly-accumulated cores referred to in chapter 3, total barium concentrations are well in excess of detrital (background) levels. Since Ba has been linked to variations in productivity (Bishop, 1988; Dehairs *et al.*, 1990; Dymond *et al.*, 1992), the 5 fold increases in barium concentrations within the Corg-rich sapropel intervals is indicative of increased productivity during S1 formation. More recently, algorithms have been applied to sedimentary barium contents in which the biogenic barium concentration is related to both export and primary productivities. Biogenic barium (Ba_{bio}) is calculated according to:

$$\mathbf{Ba_{bio} = Ba_{total} - (Al^{*} (Ba/Al)_{detrital})} \qquad \textbf{Equation 5.1}$$

Where $(Ba/Al)_{detrital}$ represents the Ba/Al ratio of the detrital fraction (0.00213-0.00228), Ba_{total} and Al are the total barium and aluminium contents of the sediment in μg/g and Ba_{bio} is the biogenic barium content of the sapropels in μg/g. The accumulation rate of Ba_{bio} which drives the biogenic barium flux (F_{bioBa}) is calculated from:

$$\mathbf{Ba_{bio\text{-}acc} = Ba_{bio}{}^{*}\rho{}^{*}AR} \qquad \textbf{Equation 5.2}$$

Where ρ is the dry sediment density of the sediment in g cm^{-3} (0.5) and AR is the accumulation rate of the sediment in cm yr^{-1}. The biogenic barium flux (F_{bioBa}) is obtained using an equation of Dymond *et al.* (1992):

$$\mathbf{F_{bioBa} = Ba_{bio\text{-}acc} / [(0.209{*}\log(MAR) - 0.213]} \qquad \textbf{Equation 5.3}$$

F_{bioBa} is in μg cm^{-2} yr^{-1} and MAR is the mass accumulation rate also in μg cm^{-2} yr^{-1}. The export (or new) production can be calculated using the equation of Francois *et al* (1995):

$$\mathbf{EP = 1.95{*}(F_{bioBa})^{1.41}} \qquad \textbf{Equation 5.4}$$

EP is the export productivity in gC m^{-2} yr^{-1}. Finally the EP can be related to primary productivity (PP) in units of gC m^{-2} yr^{-1}, using an equation developed by Berger *et al.* (1989):

$$\mathbf{EP = (PP^{2}/400) - (PP^{3}/340000)} \qquad \textbf{Equation 5.5}$$

Using these equations, during sapropel formation, primary productivity within all three cores ranged from 26 gC m^{-2} yr^{-1} at the start of S1 formation (similar to the present day value) up to a maximum of 120 gC m^{-2} yr^{-1} in MD 90-917. These values are approximately 5 times higher than the current day level of primary productivity within the eastern Mediterranean and are similar to estimates of S1 productivity calculated by Passier (1998) who suggests a mean palaeoproductivity of 118gC m^{-2} yr^{-1} based on empirical formulae proposed by Sarnthein *et al.* (1992) and Dymond *et al.* (1992). The calculated palaeoproductivities for LC21 and MD 90-917 suggest that primary productivity within the eastern Mediterranean was equivalent to modern day upwelling settings such as those found off the north-west African margin (50-250 $gCm^{-2}yr^{-1}$, Muller and Suess, 1979). The palaeoproductivity values for the 'saddle' in both LC21 and MD 90-917 are consistent with the interpretation provided by the Ba* profiles that productivity levels were reduced during this period, rather than indicating a return to pre-sapropel productivity levels. These simple calculations indicate that increased productivity was important in sapropel formation, although the actual values must be treated with some caution because the equations which were developed to relate Ba to palaeoproductivity and export productivity are based on field observations taken from oxic marine settings and may not be applicable during S1 formation. Whilst this establishes that increased productivity was likely to have been prevalent during sapropel formation, is there any indication that an increase in preservation aided Corg preservation within the eastern Mediterranean during S1? Comparison of the export productivity values of the sapropels with the Corg accumulation rate within these sediments gives an indication of the amount of export productivity that is preserved within the sediments and so provides an insight to the degree of water anoxia. Calculations suggest that within the sapropel intervals of LC21 and MD 90-917, the preservation factors (PF) range from 8-26% which are much greater than the equivalent PFs for the non-sapropel sediments that lie above and below the "double" sapropel units. Although the calculated PFs for LC21 and MD 90-917 are slightly less than the average PFs established for the euxinic Black Sea (30%), it can be seen that preservation is also likely to have been important in governing Corg accumulation during S1 formation. Both preservation and productivity are therefore likely to have been necessary to account for the observed Corg concentrations, and it is likely that the reducing water column is primarily a response to increased Corg utilising all of the dissolved O_2. According to Bethoux (1989), at present, the flux of Corg to the seafloor within the eastern Mediterranean is less than the supply of dissolved O_2 to the bottom waters of this basin. As a result, very little Corg accumulates within the sediments and the eastern Mediterranean remains oxic. However, Strohle and Krom (1997) stipulate that with increasing Corg production, the eastern Mediterranean water column could become reducing in a relatively short time (~200yrs). With the productivity levels estimated above, it can be seen that sustained productivity from 5-9 kyr BP years would have ensured a reducing water column, thus increasing the preservation and accumulation of Corg. Furthermore, cessation/reduction of deep-water formation during sapropel formation (Rohling, 1994), coupled

with substantial increases in primary productivity would have ensured that reducing bottom waters (favourable to the preservation of Corg) would have been achieved even faster than by increased productivity alone.

5.2. Sulphur and Iron Geochemistry.

Organic-rich sediments, including sapropels, usually contain elevated sulphur and iron concentrations. Elevated sulphur concentrations arise either from the incorporation of S compounds into organic matter or from the immobilisation of reduced sulphur as discrete iron sulphide minerals, such as pyrite (Berner, 1984; Henneke *et al.*, 1997). According to Canfield (1994), sediment accumulation rate is one of the most important parameters influencing the preservation of organic carbon in marine sediments. As in section 5.1, average accumulation rates for LC21 and MD 90-917 are 0.011 and 0.015 g cm^{-2} yr^{-1} respectively, and estimated oxygen penetration depths are exceptionally small (<2cm), suggesting that reducing conditions were prevalent in both cores at/near the sediment-water interface (SWI). As such, diagenetic reactions involving organic carbon occur principally via anaerobic mechanisms in which electron acceptors other than dissolved oxygen are used in the oxidation of Corg. Recent work by Passier *et al.* (1996) has shown that during S1 formation, oxidation of Corg occurred via sulphate reduction, with sulphate ions being supplied to the pore waters from seawater down a concentration gradient. During sulphate reduction (equation 5.6), sulphide is generated, and reactions involving this reduced species have important implications in controlling the geochemistry and cycling of both Fe and S in marine sediments.

$$C_{106}H_{263}O_{110}N_{16}P + 53\ SO_4^{2-} \rightarrow 106\ CO_2 + 16\ NH_3 + 53\ S^{2-} + H_3PO_4 + 106\ H_2O.$$

Equation 5.6

A schematic diagram (figure 5.5) shows the principal pathways and reactions of dissolved sulphide following its generation during sulphate reduction. Once sulphide has been generated, it has the potential to migrate into more oxidising conditions where it may undergo incomplete oxidation to form polysulphides, elemental sulphur or thiosulphates, or if sufficient oxidants are present, H_2S may be completely regenerated back to sulphate ion. As figure 5.5 shows, the two other important pathways of H_2S are its interaction with organic matter forming organically bound sulphur (OBS), or with detrital Fe forming pyrite. The relative importance of both mechanisms will be discussed below.

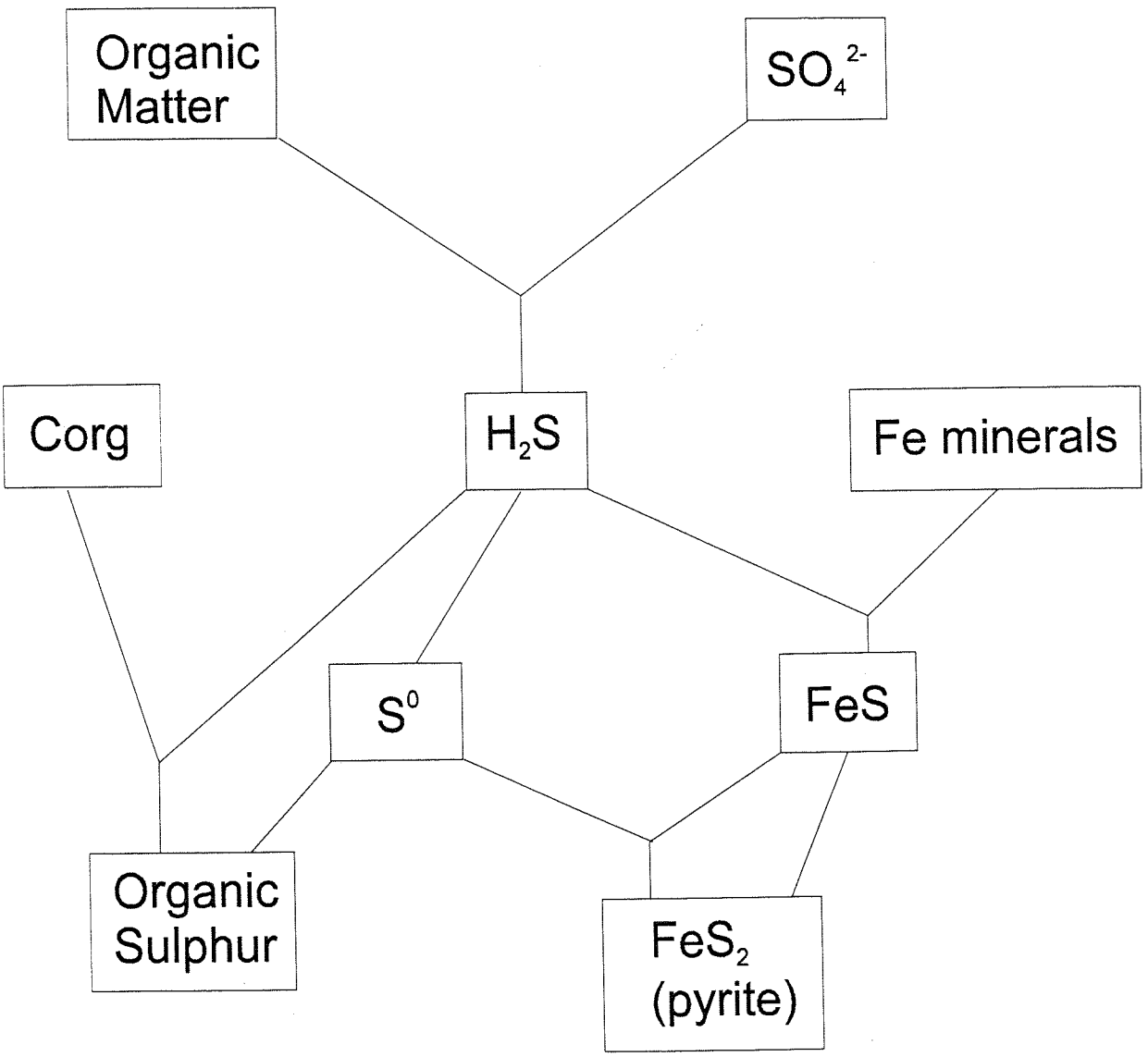

Figure 5.5. Schematic diagram summarising the pathways of H_2S in anoxic sediments, from Henneke *et al.* (1997).

5.2.1. Pyrite Formation.

Apart from the interactions of sulphide with organic matter, H_2S has the capacity of reacting with reactive iron within sediments to produce pyrite (FeS_2). Production of pyrite not only controls the cycling and geochemistry of both sulphur and iron within marine sediments, but is also known to affect the mobility and behaviour of trace metals including As and Mo (Huerta-Diaz and Morse, 1992).

Recent work on the youngest sapropel (S1) has revealed that the majority (82%) of sulphur within these organic-rich sediments is in the form of pyritic S, with the remainder in the form of other reduced S species, including organic S (section 5.2.2) (Henneke *et al.*, 1997). Examination of the excess iron (Fe*) and sulphur (S#) profiles in cores LC21 and MD 90-917 reveals that there is good correlation between these two elements suggesting that Fe* and S# are being immobilised as iron sulphide minerals, with a stoichiometry close to pyrite (FeS_2), (figure 5.6).

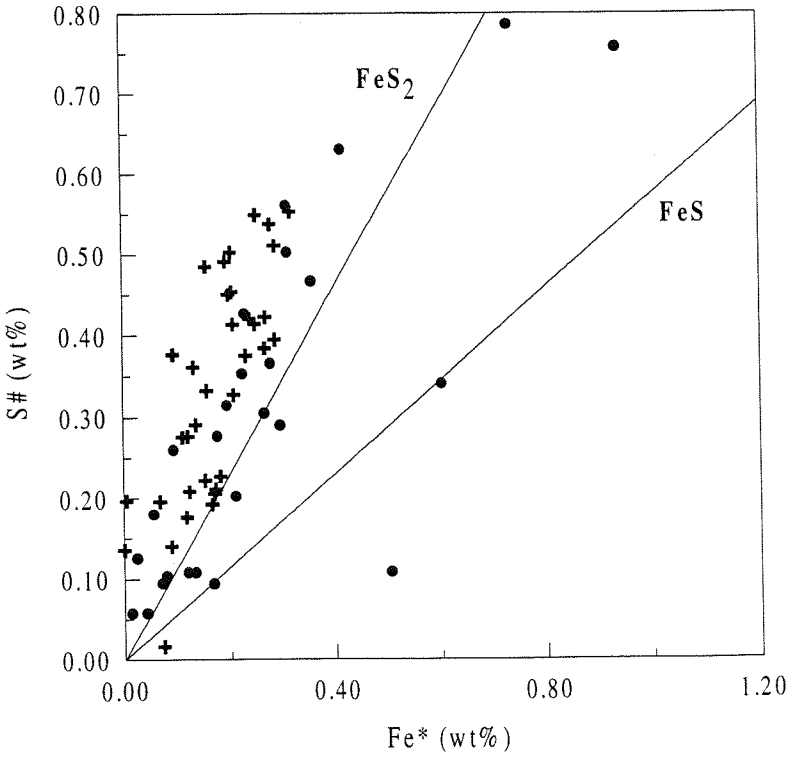

Figure 5.6. S# (wt%) vs Fe* (wt%) in LC21 (circles) and MD 90-917 (crosses). The regression lines for FeS_2 and FeS (iron monosulphides) are shown for clarity.

Further evidence that pyrite formation was immobilising and controlling the sulphur and iron geochemistries in both LC21 and MD 90-917 comes from SEM examination of thin sections from

both the upper and lower sapropel units. Scanning electron microscopy revealed that within these organic-rich intervals pyrite was present in the form of micron-sized crystals in a raspberry-like morphology (framboidal pyrite), with a stoichiometry of FeS_2. Framboidal pyrite within LC21 and MD 90-917 is mainly confined to the interiors of foraminferal tests, with framboidal diameters in the range of 8-15μm, with the diameter of the microcrystals <1μm (figure 5.7). The size distribution of the framboidal pyrite and microcrystals is similar to that found in S1 from box core UM26, examined by Passier *et al.* (1997), suggesting a common mechanism for framboidal pyrite formation during S1 deposition.

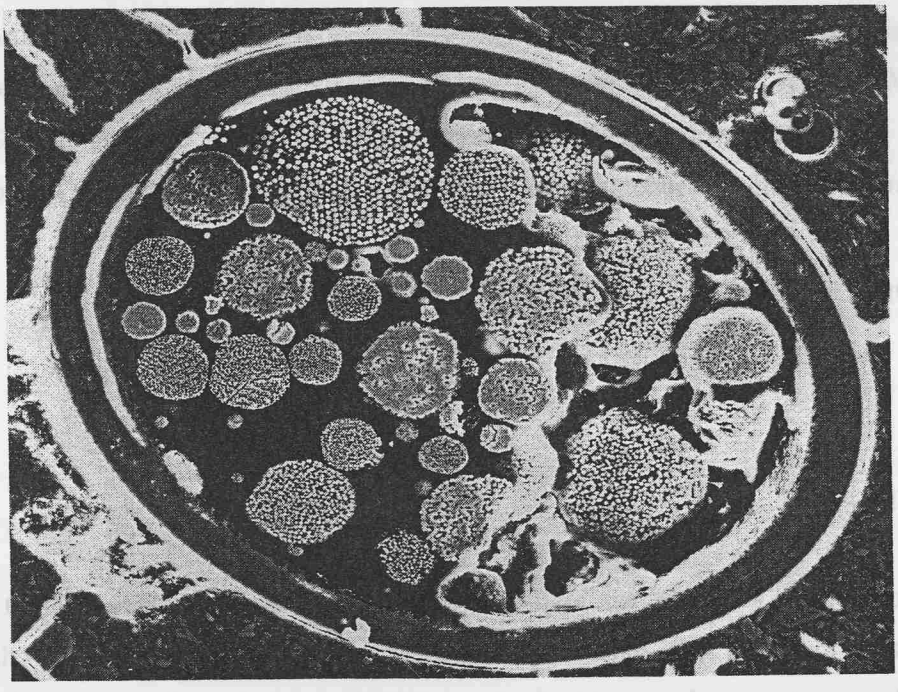

Figure 5.7. Example of framboidal pyrite found within LC21 and MD 90-917. Pyrite diameters are between 8 and 15 μm.

The presence of framboidal pyrite within the sapropel unit itself is consistent with the mechanisms proposed by Passier *et al.* (1997) for pyrite formation and can be explained in terms of the production and supply of Fe and sulphide during sapropel formation (Sweeny and Kaplan, 1973; Wang and Morse, 1996; Rickard, 1997; Wilkin and Barnes, 1997). According to Passier *et al.* (1997), during the deposition of S1 Fe was supplied to the sapropel from a combination of detrital iron sources present within the sapropel and also from upward diffusion of Fe^{2+} from sub-oxic sediments from beneath. Within the sapropel units, oxidation of organic matter proceeded via

sulphate reduction generating sulphide species that reacted *in situ* with Fe^{2+} to produce framboidal pyrite. In this scenario, the supply of Fe was much greater than the generation of sulphide so that all of the generated sulphide was consumed by reactions involving pyrite formation within the sapropel. If Fe were limited relative to sulphide formation during S1, then HS^- would have migrated downwards and would have formed euhedral pyrite (rather than framboidal pyrite) below the sapropel. The presence of framboidal pyrite within LC21 and MD 90-917 (and the absence of any pyrite peaks below the sapropels) suggests that in these rapidly accumulated sapropels the supply of reactive iron was much greater than sulphide generation. The actual formation of pyrite with framboidal morphology is generally believed to occur in aqueous solutions highly supersaturated with respect to both iron monosulphides and pyrite, in which reaction kinetics favour the formation of Fe monosulphides such as greigite prior to pyrite (Sweeny and Kaplan, 1973; Rickard, 1997). Experimental evidence has suggested that pyrite formation occurs via the following sequence:- disordered mackinawite → mackinawite →greigite →pyrite (Wilkin and Barnes, 1997). Relative to pyrite, greigite is thermodynamically unstable and so is rapidly converted to FeS_2 via interaction with either H_2S or zero valent sulphur according to the reactions:-

$$\mathbf{Fe_3S_4 + 2H_2S \leftrightarrow 3FeS_2 + 4H^+} \qquad \textbf{equation 5.7}$$

or

$$\mathbf{Fe_3S_4 + 2S^0 \leftrightarrow 3FeS_2} \qquad \textbf{equation 5.8}$$

Relative to the $\delta^{34}S$ content of eastern Mediterranean waters, the δS values for framboidal pyrite within S1 show a high degree of fractionation of 57.9 ppt-70.2ppt. This degree of fractionation is consistent with the fact that sulphate reduction occurred within marine porewaters which had a readily-available supply of SO_4^{2-} from the overlying seawater. These data tend to support the hypothesis that pyrite formation occurred *in situ* within the sediments rather than in the water column as is found in the modern Black Sea (Canfield *et al.*, 1996).

5.2.2. Organically Bound Sulphur (OBS).

From the previous discussion it is apparent that Fe* and S# are immobilised within sapropel units as pyrite, although it can be seen from figure 5.6 that there is an excess of sulphur in relation to the amount of Fe present in both cores. As such, this excess sulphur has the capacity of interacting with Corg to form organically bound sulphur (OBS) as demonstrated in figure 5.5.

Examination of the excess sulphur profiles in cores LC21 and MD 90-917 reveals that they display a remarkably close correlation with the distribution of Corg (figure 5.8), suggesting that there may be some chemical association/interaction between organic carbon and sulphur in these sediments.

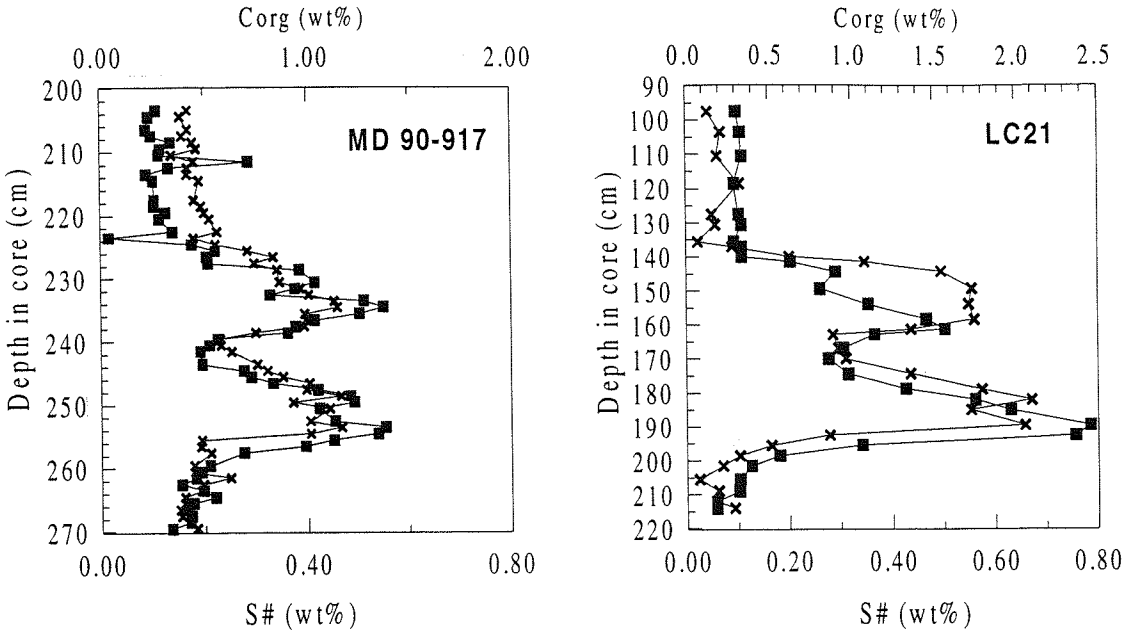

Figure 5.8. Distribution of Corg (crosses, upper scale) and S# (filled squares, lower scale) in MD 90-917 and LC21.

Kohen *et al.* (1989) has shown that during early diagenesis S is incorporated into organic matter. This incorporation of S is controlled by the availability of reactive Fe within the sediment, since organic matter competes with reactive Fe for reduced S especially when the amount of reactive Fe is limited (Passier *et al.*, 1997). In organic-rich sediments where the supply of organic matter is adequate to ensure sulphate reduction (as is the case during S1 formation) dissolved sulphide concentrations within the pore waters increase dramatically so that organic matter becomes an important sink for reduced S species (Francois, 1987a,b; Raiswell *et al.*, 1993; Hartgers *et al.*, 1997). It is assumed that reduced species such as H_2S, S_x^{2-} and $S_2O_3^{2-}$ (Luther *et al.*, 1986; Vairavamurthy and Mopper, 1987) become incorporated into organic matter via interactions with specific functional groups such as aldehydes and ketones found on organic matter, producing inter- and intramolecular sulphur-sulphur and sulphur-carbon bonds (Hartgers *et al.*, 1997). Assessment of the percentage uptake of reduced S into organic matter can be obtained by plotting S# concentrations against Corg contents for the sapropel sediments in LC21 and MD 90-917 (figure 5.9). It is clear from figure 5.9 that between 5-20% of the S produced is incorporated within organic matter during sapropel formation, although it is clear that more OBS was formed in MD 90-917 (10-20%) relative to LC21 (5-10%).

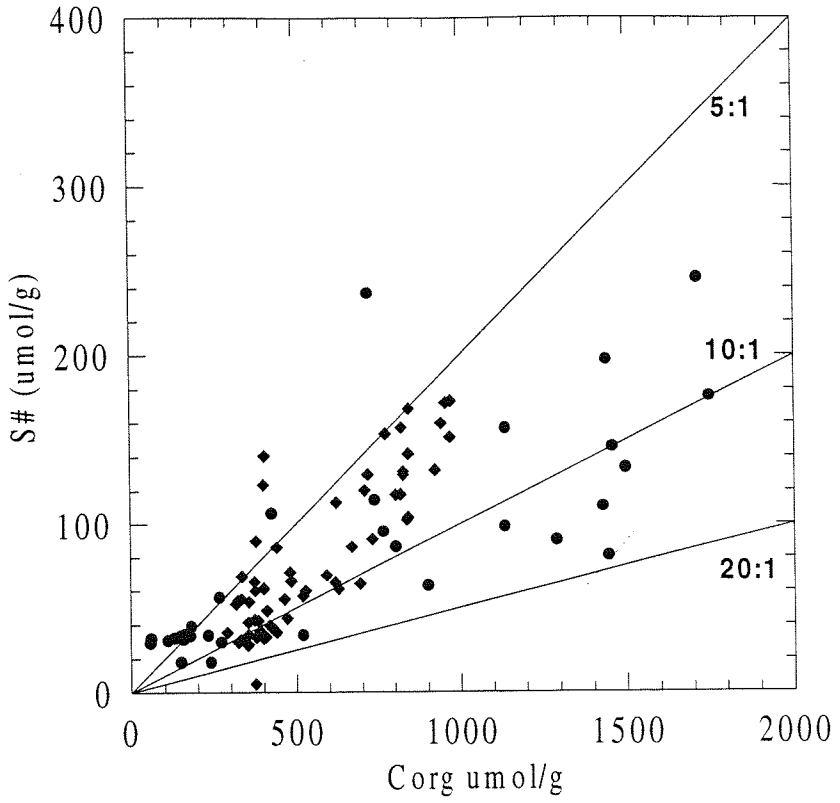

Figure 5.9. Proportion of excess S (μmol/g) that is incorporated into Corg (μmol/g) during sapropel formation in LC21 (filled circles) and MD 90-917 (filled squares).

Estimates of OBS in LC21 and MD 90-917 are similar to those measured for the anoxic-Corg-rich sediments from the Bannock and Tyro Basins (12-40%; Henneke *et al.*, 1997). Assuming an intermediate OBS concentration of 12%, the $(S/C)_{org}$ ratios for LC21 and MD 90-917 range from 0.009-0.042, which are similar to the reported ratios found for eastern Mediterranean sapropels and other organic-rich sedimentary and marine rocks (table 5.1). The fact that the S_{org} content correlates well with the Corg content, coupled with the fact that the $(S/C)_{org}$ ratios for both LC21 and MD 90-917 are much greater than the ratios obtained for marine plankton (0.004-0.010) suggests that there is an uptake of sulphur into organic matter following its deposition at the sediment-water interface. The positive correlation between Corg and S represents the fact that with increasing amounts of Corg, more sulphide is produced due to the increased availability of metabolizable organic matter, which is then available to become incorporated into organic matter when reactive iron is limited.

MATERIAL	ATOMIC S/C RANGE	REFERENCE
Marine plankton	0.004-0.010	Francois, 1987b
Californian Basins	0.006-0.015	Nissenbaum and Kaplan, 1972
Jervis Inlet, BC	0.011-0.019	Francois, 1987b
Peru Margin	0.011-0.056	Mossmann *et al.*, 1991
Cretaceous carbonates	0.04-0.38	Bein *et al.*, 1990
Jurassic marine shales	0.012-0.019	Raiswell *et al.*, 1993
E. Mediterranean anoxic basins	0.038-0.204	Henneke *et al.*, 1997
E. Mediterranean sapropels	0.005-0.038	Passier *et al.*, in press
LC21 and MD 90-917	0.009-0.042	This study

Table 5.1. Comparison of the atomic $(S/C)_{org}$ ratios of marine plankton and Corg-rich marine and sedimentary rocks with those obtained for the two eastern Mediterranean sapropels, LC21 and MD 90-917.

5.2.3 Corg and S Relationships.

Relationships between Corg and S are often used to characterise the environment of deposition of organic-rich sediments (Middelburg, 1991). Conventionally, S *vs* Corg plots are used to distinguish between the deposition of sediments under normal marine conditions (i.e. oxygenated bottom waters), euxinic-marine (i.e. H_2S within the water column) and freshwater environments (Berner and Raiswell, 1983; 1984).

In normal marine waters i.e. oxygenated bottom waters, there is a close correlation between Corg and S with a constant ratio of 1/2.8 (Berner, 1984; Goldhaber and Kaplan, 1974). According to Berner (1984), this constant ratio arises from the fact that when sulphate is reduced and Corg is oxidised a proportional amount of sulphide (FeS_2) is fixed within the sediment.

A close correlation between Corg and S occurs in the Corg-rich sediments of both LC21 and MD 90-917 (figure 5.10). The line for sediments deposited under normal marine conditions is shown for clarity, but it is obvious is that the majority of points plot above this line, indicating that S1 formation occurred under conditions which were more reducing than at present. According to Passier *et al.* (1996) however, S *vs* Corg plots for other S1s show data that plot above the normal marine line, and these authors infer that sapropel deposition occurred under euxinic conditions i.e. free H_2S within the water column. In modern, euxinic environments such as the Black Sea or Baltic

Sea, there is no significant correlation between Corg and S since the formation of iron sulphide is not limited by the presence of organic matter when water column H_2S is present (Lyons and Berner, 1992). This leads to significant intercepts on the S axis on C/S plots showing that 'excess' sulphide is added to the sediment during water column iron sulphide formation (Morse and Berner, 1995). In LC21 and MD 90-917, insignificant intercepts on the S axis (~0.07 wt%) for both cores indicate that during S1 formation, conditions were sub-oxic and that the supply of Corg limited the formation of pyrite (figure 5.10). Points that plot below the regression line for normal marine sediments are those from LC21 and are confined to the C and S data from within the 'saddle'. This tends to suggest that more oxidising conditions were present during this interval relative to times of sapropel deposition.

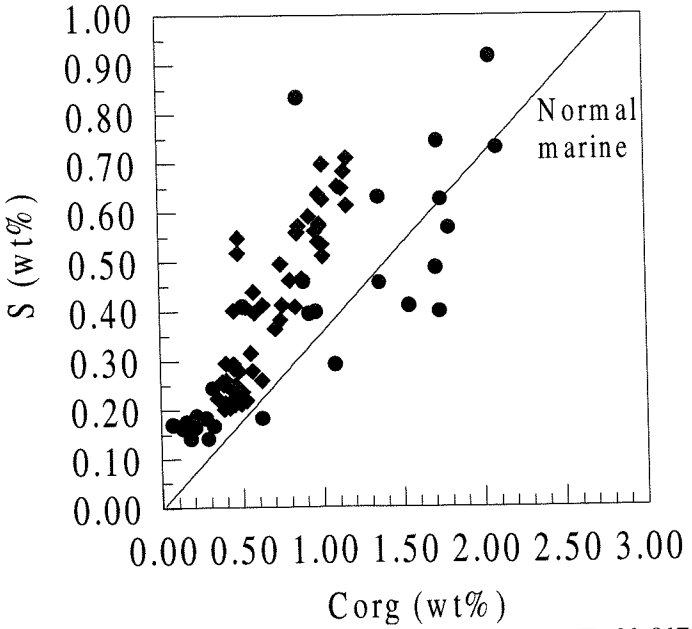

Figure 5.10. S (wt%) vs Corg (wt%) in LC21 (filled circles) and MD 90-917 (filled diamonds). The relationship between S and Corg for normal marine settings is shown for clarity (black regression line).

Further evidence to indicate that the water column of the eastern Mediterranean was sub-oxic rather than euxinic comes from the size distribution of the framboidal pyrite. In a review of the size distribution of framboidal pyrite diameters, Wilkin *et al.* (1996; 1997) demonstrated that framboids formed in euxinic conditions had significantly smaller diameters than those formed within the sediments which were overlain by sub-oxic waters. Although the number of framboidal pyrite diameters measured in this study was limited, the fact that the average pyrite diameters in LC21 and MD 90-917 (10-12μm) are comparable to those found in sediments overlain by sub-oxic waters would suggest that only mildly reducing waters were present during S1 formation (Wilkin *et al.*, 1996; 1997).

It seems that the close similarity in the Corg and S profiles results from a combination of factors. Firstly the S/C ratios indicates that there is preferential uptake of S into Corg during early diagenesis suggesting that part of the close correlation between S and Corg results from the fact that there is some organically bound sulphur present. However, pyrite formation is the second (and main) reason why the S profile parallels the Corg closely in both LC21 and MD 90-917. It is believed that increasing S concentrations relate positively with increasing Corg contents because organic matter is the controlling factor which generates sulphate reduction, sulphide formation, and hence pyrite formation. The S *vs* Corg plots, and the presence and size distribution of framboidal pyrite for both LC21 and MD 90-917 all tend to indicate that during S1 formation the waters were reducing/suboxic rather than euxinic. It is not possible to quantify the extent of this reducing water i.e. whether it was confined to a few metres above the sediment-water interface or extended throughout the entire water column itself.

5.3. Bromine and Iodine Geochemistry.

5.3.1. Bromine Geochemistry.

Based on thermodynamic considerations, bromine exists in the marine environment only as the bromide ion (Br^-) in the –1 oxidation state (Brookins, 1980). The oceanic distribution of bromine has shown that it behaves conservatively within seawater and has rather uniform concentrations, typically between 67-70ppm (Libes, 1992). Examination of recently accumulated sediments from different marine environments has shown that the behaviour and concentration of Br is controlled almost exclusively by the concentration of organic carbon and the early diagenetic processes that affect its preservation in sediments (Price *et al.*, 1970; Price and Calvert, 1977; Pedersen and Price, 1980). Moreover, the behaviour of Br is independent of the prevailing redox state of either the water column or underlying sediment, since Br exists only as the bromide ion (Pedersen and Price, 1980). Investigations of Corg-rich sediments underlying highly productive surface waters (e.g. Panama Basin and Namibian Shelf) have shown that these sediments are significantly enriched in Br (Price and Calvert, 1977; Pedersen and Price, 1980). As a corollary it is expected that the organic-rich sapropel units within the eastern Mediterranean will also display elevated Br concentrations.

Concentration-depth profiles of total and corrected Br concentrations show between 60-90% of the Br found within the sapropels is derived from seawater, a fact confirmed by the good correlation between Br and Cl (also an element derived from seawater, figure 5.11).

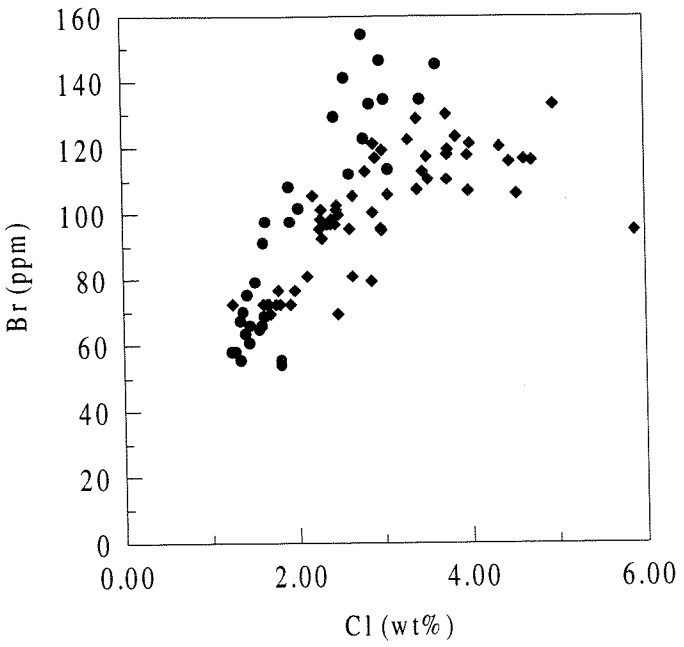

Figure 5.11. Br (ppm) vs Cl (wt%) in MD 90-917 (filled blue symbols) and LC21 (filled red symbols).

Comparison of salt corrected Br concentrations and Corg profiles in both LC21 and MD 90-917 shows that no significant Br enrichment occurs within the Corg-rich sapropel units in either core (figures 5.12). These results are somewhat surprising given that it has been widely reported that Br concentrations are positively correlated with Corg contents in marine sediments. The control of Corg on Br contents however, has been based primarily upon sediments with Corg contents significantly greater than those found in either LC21 or MD 90-917. For example, positive correlations between Br and Corg were reported by Price and Calvert (1977) for the Namibian Shelf where Corg concentrations typically reached 10%, ~5 times greater than those found within the sapropels. In LC21 and MD 90-917, it is likely that the smaller amounts of Corg deposited at the sediment-water interface were insufficient to cause any significant removal of Br from seawater during sapropel formation.

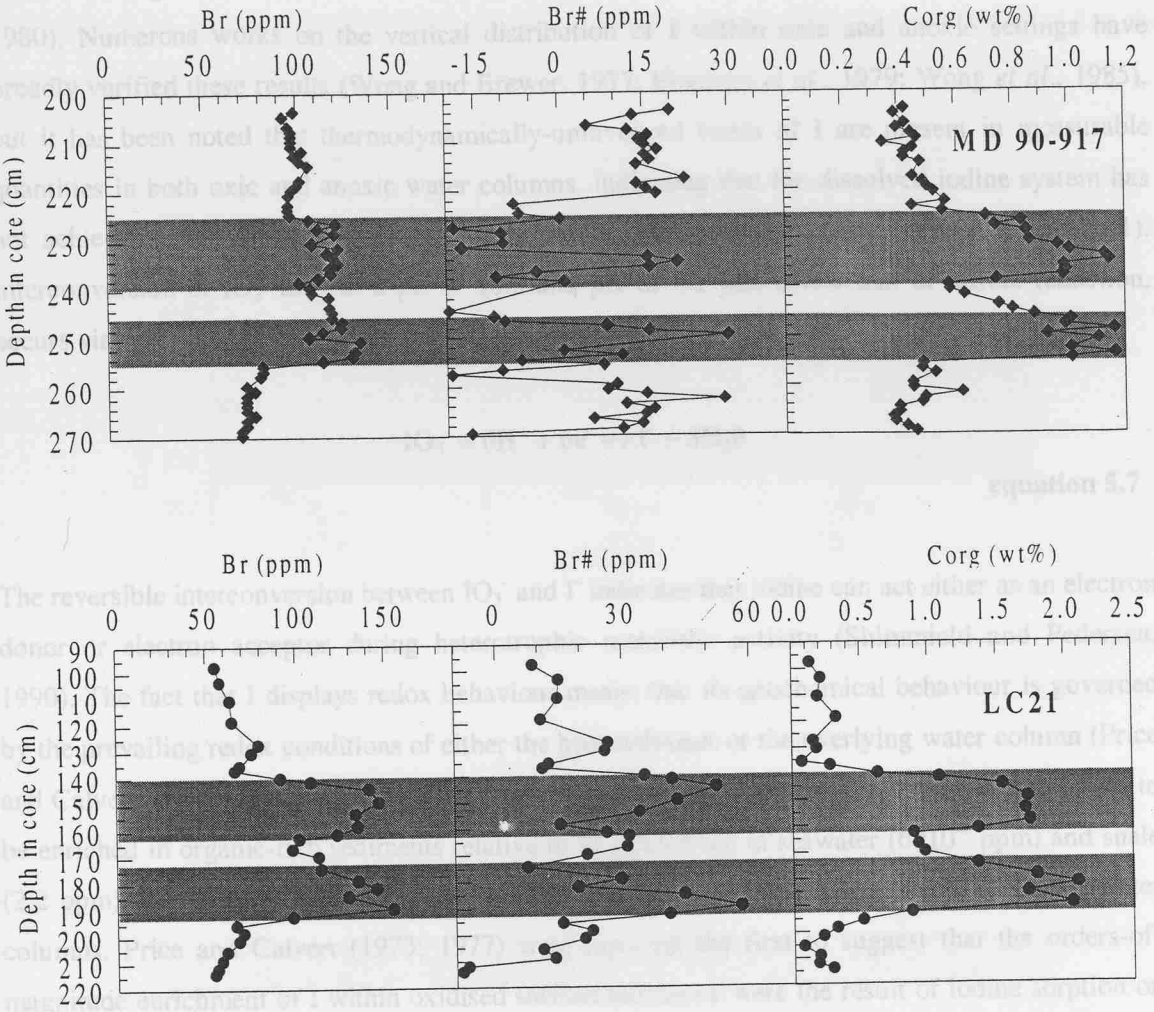

Figure 5.12. Concentration-depth profiles of total Br, Br# (ppm) and Corg (wt%) in MD 90-917 and LC21.

5.3.2. Iodine Geochemistry.

Unlike bromine, which only occurs in seawater as the bromide ion, iodine is known to be present in a number a number of oxidation states (Wong, 1991). Previous work on the behaviour of iodine in seawater has shown this element to biophillic in nature, displaying a nutrient-like distribution within the water column i.e. depletion of total I concentrations within surface waters and enrichment at depth (Elderfield and Truesdale, 1980). Water column measurements of dissolved I concentrations have shown that within the pE and pH range of marine waters, the speciation of iodine is dominated by iodate (IO_3^-) and iodide (I^-), although a number of intermediate I forms are known to exist i.e. organic I, hypoiodous acid (HIO) etc. Thermodynamic considerations predict that iodate should be the most thermodynamically stable form within oxic environments, whilst

under reducing conditions dissolved iodine should be present in its reduced form, iodide (Brookins, 1980). Numerous works on the vertical distribution of I within oxic and anoxic settings have broadly verified these results (Wong and Brewer, 1977; Emerson *et al.*, 1979; Wong *et al.*, 1985), but it has been noted that thermodynamically-unfavoured forms of I are present in measurable quantities in both oxic and anoxic water columns, indicating that the dissolved iodine system has not achieved equilibrium with the prevailing redox conditions (Chapman, 1983; Wong, 1991). Interconversion of IO_3^- to I^- at a pE of 10.5 and pH of 8.1 just below that of nitrate reduction, occurs via reaction:

$$\mathbf{IO_3^- + 6H^+ + 6e^- \leftrightarrow I^- + 3H_20}$$

equation 5.7

The reversible interconversion between IO_3^- and I^- indicates that iodine can act either as an electron donor or electron acceptor during heterotrophic metabolic activity (Shimmield and Pedersen, 1990). The fact that I displays redox behaviour means that its geochemical behaviour is governed by the prevailing redox conditions of either the host sediment or the overlying water column (Price and Calvert, 1973; Ullman and Aller, 1985; Francois, 1987). Like bromine, iodine is also found to be enriched in organic-rich sediments relative to its abundance in seawater ($6*10^{-2}$ ppm) and shale (2.2 ppm) with higher I concentrations in those sediments accumulating beneath oxidising water columns. Price and Calvert (1973; 1977) were amongst the first to suggest that the orders-of-magnitude enrichment of I within oxidised surface sediments were the result of iodine sorption on to seston at the sediment water interface. Francois (1987) performed a series of experiments that showed that enrichment of I on to organics occurs via the direct reduction of IO_3^- to electropositive iodine species (I_2 and HOI) by marine humic compounds followed by electrophilic substitution on to organic molecules. Alternatively, Price and Calvert (1977) proposed that electropositive species could be produced by other processes, including the oxidation of iodide to I_2 by aerobic bacteria and also by enzymatically mediated oxidation of I to I_2 by iodide oxidase, an enzyme present in the degradation products of plankton. Elemental I produced in this way would then quickly hydrolyse to form HOI which would then react with organic molecules because of its strong electrophilic nature. What is evident from these studies is that the production of I species which adsorb on to organic molecules only proceeds under oxic conditions, thus explaining the lack of I enrichment under more reducing conditions (Price and Calvert, 1973; 1977). As a result, the relative enrichment of I within marine sediments can provide a useful diagnostic tool for indicating the redox status of the water column at the time of sediment deposition and also for the source of organic matter. Since cores LC21 and 90-917 have undergone little/no post-depositional oxidation since burial, the iodine profiles in both cores should therefore provide some insight into the degree of water column oxygenation during sapropel formation and the source of organic matter.

Relative to the iodine concentration of average shale (~ 2.2 ppm), I# is enriched by up to 15-35 and 15-25 times for LC21 and 90-917 respectively, indicating that the detrital contribution of I to the sapropels at the time of formation was negligible (figure 5.13).

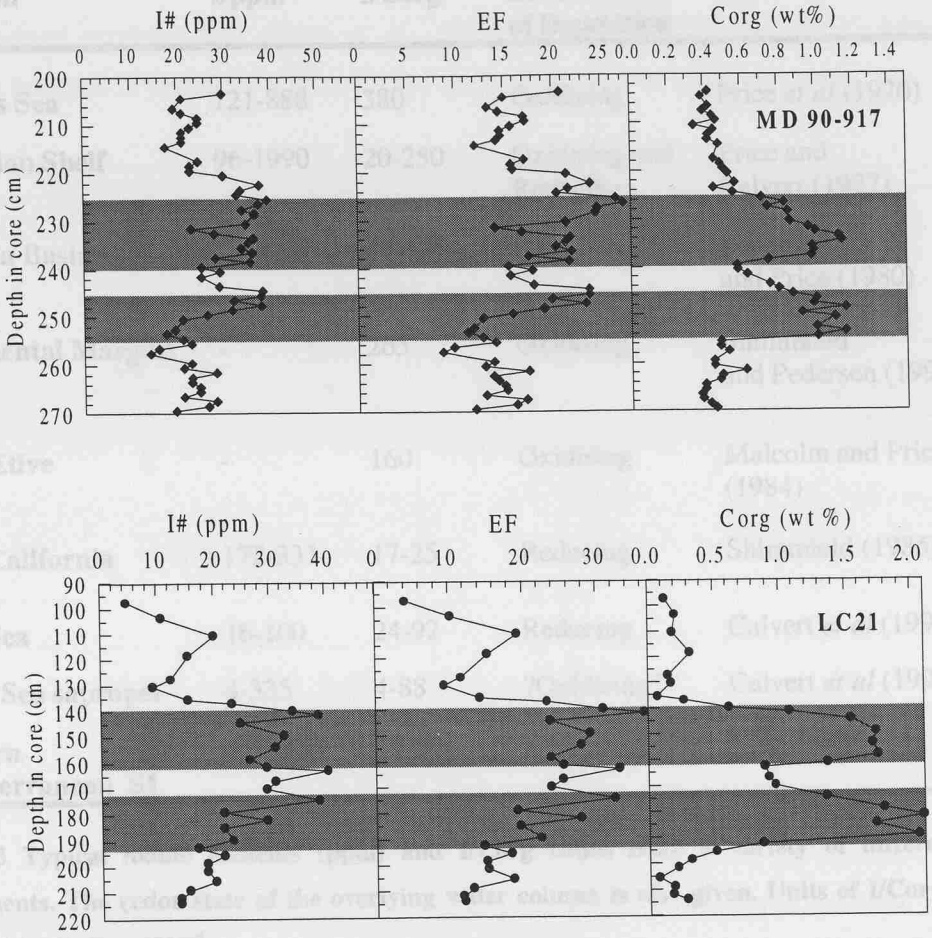

Figure 5.13. Distribution of I # (ppm), Corg (wt %) and iodine enrichment factors (EF) for cores MD 90-917 and LC21.

On average I# concentrations of LC21 (~20ppm) are slightly lower than those of 90-917 (~ 30ppm), however, the observed I# contents are significantly lower than the I concentrations of surficial sediments of the eastern Mediterranean (~ 50-55 ppm) reflecting the difference in bottom water oxygenation at the time of sapropel formation compared to the present day.

The present day eastern Mediterranean is characterised by a water column that is oxic to all depths, which is conducive to I enrichment within surface sediments. However, the ~46-64% decrease in sedimentary I concentrations of the organic-rich sapropel units in 90-917 and LC21 (relative to surface sediment I concentrations) is indicative of the fact that accumulation of sediments during sapropel formation occurred within a reducing water column. Direct comparison of the iodine

concentrations for LC21 and 90-917 indicates that iodine concentrations within the sapropels are significantly lower than those found in both oxidised and reduced sediments (table 5.3).

Location	I/ppm	I/Corg	Environment of Deposition	Reference
Barents Sea	121-888	380	Oxidising	Price *et al* (1970)
Namibian Shelf	96-1990	20-250	Oxidising and Reducing	Price and Calvert (1977)
Panama Basin	77-420	50-395	Oxidising	Pedersen and Price (1980)
Continental Margins	-	265	Oxidising	Shimmield and Pedersen (1990)
Loch Etive	-	160	Oxidising	Malcolm and Price (1984)
Baja California	172-333	17-25	Reducing	Shimmield (1985)
Sulu Sea	16-100	24-92	Reducing	Calvert *et al* (1993)
Black Sea sapropel	4-335	4-88	?Oxidising?	Calvert *et al* (1991)
Eastern Mediterranean S1	15-38	15-50	Reducing	This Study

Table 5.3 Typical iodine contents (ppm) and I/Corg ratios from a variety of different marine environments. The redox state of the overlying water column is also given. Units of I/Corg are (ppm halogen) / (wt% Corg)*10^{-4}.

Direct comparison of absolute I concentrations of different marine sediments is somewhat misleading since the concentration of iodine in sediments is governed primarily by the amount of dissolved iodate present within the surface waters, the amount incorporated into plankton (dependent upon type and quantity of organism present), level of primary productivity and efficiency and burial of planktonic detritus. As such it is difficult to ascertain the extent of bottom water oxygenation at the time of sapropel formation solely from the iodine concentrations in LC21 and 90-917. However, what has become apparent from numerous studies on the contrasting behaviour of I in anoxic and oxic environments is the relative decrease in iodine levels between sediments which are accumulating under reducing conditions compared with those from more oxidising environments (Price and Calvert, 1973; 1977). For example these authors have shown a ~40 % decrease in I concentrations between oxidising and reducing cores from the Namibian Shelf. A similar decrease (~ 46%) in the amount of I within the sapropels of LC21 and MD 90-917 and

that found in surficial sediments of the eastern Mediterranean suggests that sapropel formation had occurred under reducing conditions bottom waters.

Iodine, like bromine is also found to be closely associated with sedimentary Corg concentrations within oxidised environments (Price *et al.*, 1970). In MD 90-917 and LC21 however, the correlation between I# and Corg is poor (figure 5.14).

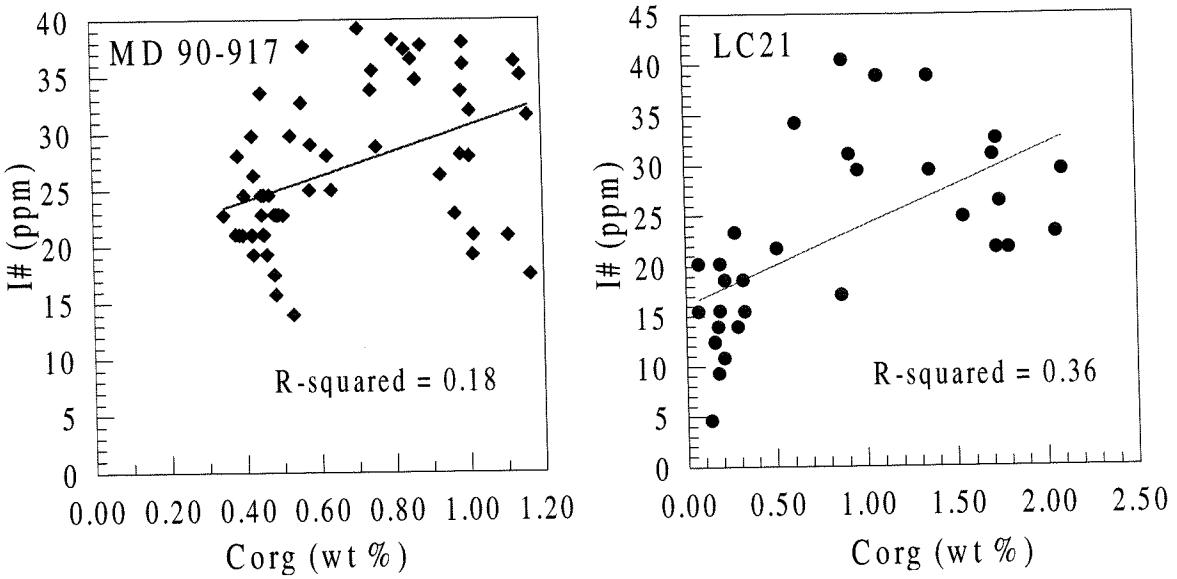

Figure 5.14. I# (ppm) vs Corg (wt%) in cores MD 90-917 and LC21 .

The lack of correlation suggests either that some I has been preferentially lost from the organic matter during shallow burial under sub-oxic conditions or that the conditions needed to produce a strong I-Corg associations were not present during sapropel formation (i.e. conditions were reducing rather than oxic) reflecting the influence of porewater redox state upon I speciation and behaviour in marine sediments (Francois, 1987; Shimmield and Pedersen, 1990; Wong, 1991). Similar poor correlations between Corg and I have been reported for surficial sediments from the Namibian and Californian Shelves, both of which have reducing bottom waters.

5.3.3. I/Corg Ratios.

Halogen/carbon ratios of sediments provide an insight into the early diagenesis of the element under consideration (Price and Calvert, 1977). Reported I/Corg ratios for sediments have shown that there is a general exponential decrease in the I/Corg ratio with depth indicating the preferential release of I relative to Corg (Price *et al.*, 1970; Price and Calvert, 1973,1977). Examination of

I/Corg ratios by Francois (1987) suggests that the decrease in I/Corg ratios results from the displacement of iodine by substitution by nucleophilic species such as HS^- and $S_2O_3^-$, however, the I#/Corg profile for core 90-917 and LC21 reveals no systematic decrease with depth through the sapropels (figure 5.15).

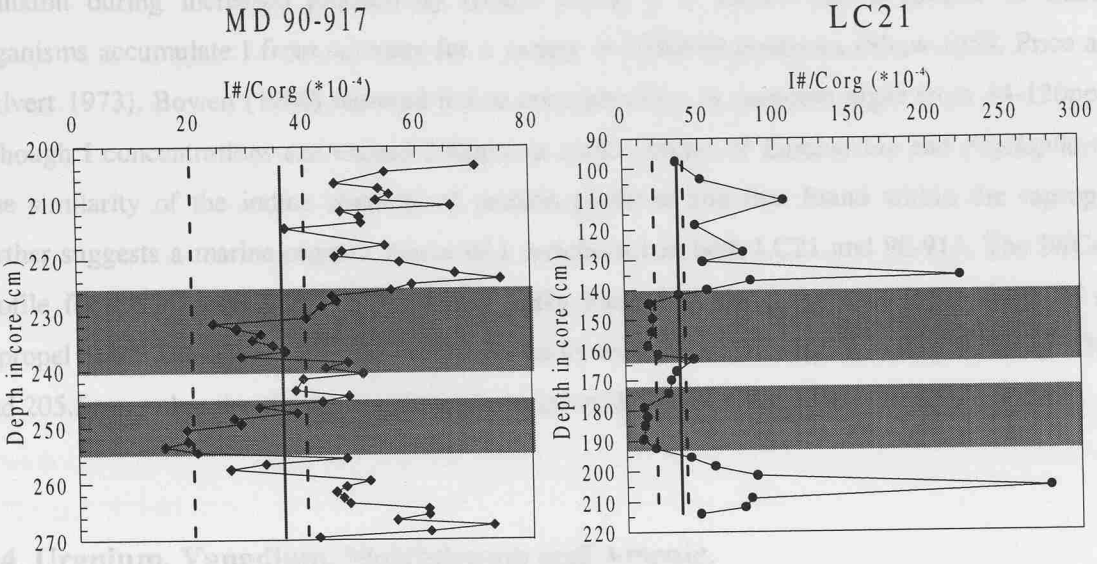

Figure 5.15. I#/Corg ratios for cores MD 90-917 and LC21. The vertical dashed lines indicate the range of I/Corg ratios reported in the literature for sediments accumulating under reducing bottom waters (table 5.3), whilst the solid vertical line indicates the mean I/Corg ratio for plankton (Ullman and Aller, 1985).

Comparison of the I/Corg ratios of marine sediments with those found in cores MD 90-917 and LC21 reveals that the observed ratios within the sapropel units are comparable to those I/Corg values obtained for sediments that are accumulating under reducing conditions (e.g. the Sulu sea, Baja (California) and the reducing sediments of the Namibian Shelf) (table 5.3). The close similarity in the I#/Corg ratios obtained for the sapropel units and those from other reducing environments further indicates a reducing depositional environment for LC21 and 90-917.

Under oxidising conditions the iodine content of sediment is governed by the Corg concentrations of the host sediment (Price *et al.* 1970). Plots of I# vs Corg for 90-917 and LC21 reveals no significant correlation (figure 5.14) suggesting that factors other than Corg content control the observed I levels. Although the concentrations of I in 90-917 and LC21 are lower than those found in other reducing environments, iodine is significantly enriched within both cores, relative to its content in normal shale. Because the evidence presented so far has indicated that both LC21 and 90-917 were deposited under reducing conditions then the observed enrichment must be derived

from the deposition and preservation of I associated with plankton from the euphotic zone, rather than by adsorption on to Corg at the sediment-water interface. Reported I/Corg ratios for plankton (1.06-13.7 ppm/wt%) and planktonic detritus (17-36 ppm/wt%) (Ullman and Aller, 1985) are similar to those ratios found within the sapropels indicating that the primary source of elevated iodine concentrations within these two cores was derived from the deposition and preservation of plankton during increased productivity (figure 5.15). It is known that a number of marine organisms accumulate I from seawater for a variety of different processes (Shaw 1959, Price and Calvert 1973). Bowen (1966) reported iodine concentrations in common algae from 44-120ppm, although I concentrations can exceed 200ppm in some species of *Laminariae* and *Phyllophorae*. The similarity of the iodine contents of modern plankton and that found within the sapropels further suggests a marine organic source of I enrichment in both LC21 and 90-917. The I#/Corg profile for LC21 reveals two well-defined peaks located at the upper and lower faces of the sapropel units. These two peaks are caused primarily by the anomalously low Corg values at 135.5 and 205.5cm, rather than indicating the preferential oxidation of Corg relative to I.

5.4. Uranium, Vanadium, Molybdenum and Arsenic.

Unlike iodine and bromine which are known to be enriched in organic-rich sediments via their associations with organic sedimentary components (section 5.3), a number of redox sensitive elements, including uranium, vanadium, arsenic and molybdenum, also display elevated sedimentary concentrations with respect to their abundances in seawater. Organic-rich sediments deposited under reducing or anoxic conditions often display a remarkably close correlation between the Corg and total sulphur concentrations (see section 5.1 and 5.2) however, and so it is often difficult to identify which phase (i.e. organic or sulphide) actually causes the elemental enrichment.

Previous investigations on the distribution of U, V, As and Mo within sapropel S1 sediments have found that these elements either form well-defined peaks at the advancing side of downwards-moving oxidation fronts or are remobilised both up and downcore to become re-associated either with the sulphide/organic matter phases at depth or with oxyhydroxides in the oxidised portion above the front (Higgs *et al.*, 1994; Thomson *et al.*, 1995; Quednau *et al.*, 1997).

5.4.1 Uranium.

At the pE-pH ranges of oxidising seawater, uranium is predicted to be present in the +6 oxidation state as the soluble uranyl tricarbonate complex $UO_2(CO_3)_3^{4-}$ (Langmuir, 1978). The strong

association of uranium with the carbonate ion in oxic seawater makes U biochemically unreactive, resulting in uniform concentrations (3.3 μg/L) in open-ocean seawater (Anderson, 1982). Based on thermodynamic considerations, uranium is predicted to be present entirely in the +4 oxidation state under more reducing conditions (Shimmield and Pedersen, 1990).

Anoxic and sub-oxic organic-rich sediments are proposed as major sinks controlling the oceanic uranium budget (Degens *et al.*, 1977; Bernat and Church, 1989; Barnes and Cochran, 1993). Estimates suggest that, globally, reducing Corg-rich sediments which cover ~10% of the ocean floor contain up to 45% of the total sedimentary U budget (Barnes and Cochran, 1990; Klinkhammer and Palmer, 1991). Previous investigations on the uranium contents of the most recently accumulated sapropel unit (S1) has shown significant enrichments relative to the U concentration found in shale (3.7ppm). Excess uranium concentrations (U*) within the sapropel units of LC21 (1.0 –5.8 ppm) and MD 90-917 (0.5-3.0 ppm) represent enrichments of 1.3 –2.0 times and 0.5-1.1 times respectively, and are lower in comparison to U values found in the Cariaco Trench and Sannich Inlet sediments (table 5.4), suggesting minor authigenic uranium enrichment in LC21 and MD 90-917.

	BLACK SEA[1]	SANNICH INLET[1]	FRAMVAREN FJORD[1]	CARIACO TRENCH[1]	LC21	MD 90-917	SHALE
U (μg/g)	16	7	13	14	1-6	0.5-3.0	3.7
U/Al (10^4)	3.3	1.4	8.1	2.2	0.2-1.50	0.08-0.48	0.4
EF	8.2	3.5	20.2	5.5	0.5-2.0	0.2-1.2	-

Table 5.4 Comparison of the U concentrations and EF in MD 90-917 and LC21 with those found in modern-day anoxic, Corg-rich marine settings. EF calculated as $(U/Al_{sap}) / (U/Al_{shale})$. [1] Data for tables from Pedersen and Calvert 1993.

It is evident from the concentration-depth distribution of uranium within the sapropel units of both LC21 and MD 90-917 that the highest U* concentrations are coincident with the highest levels of sedimentary Corg (figure 5.16).

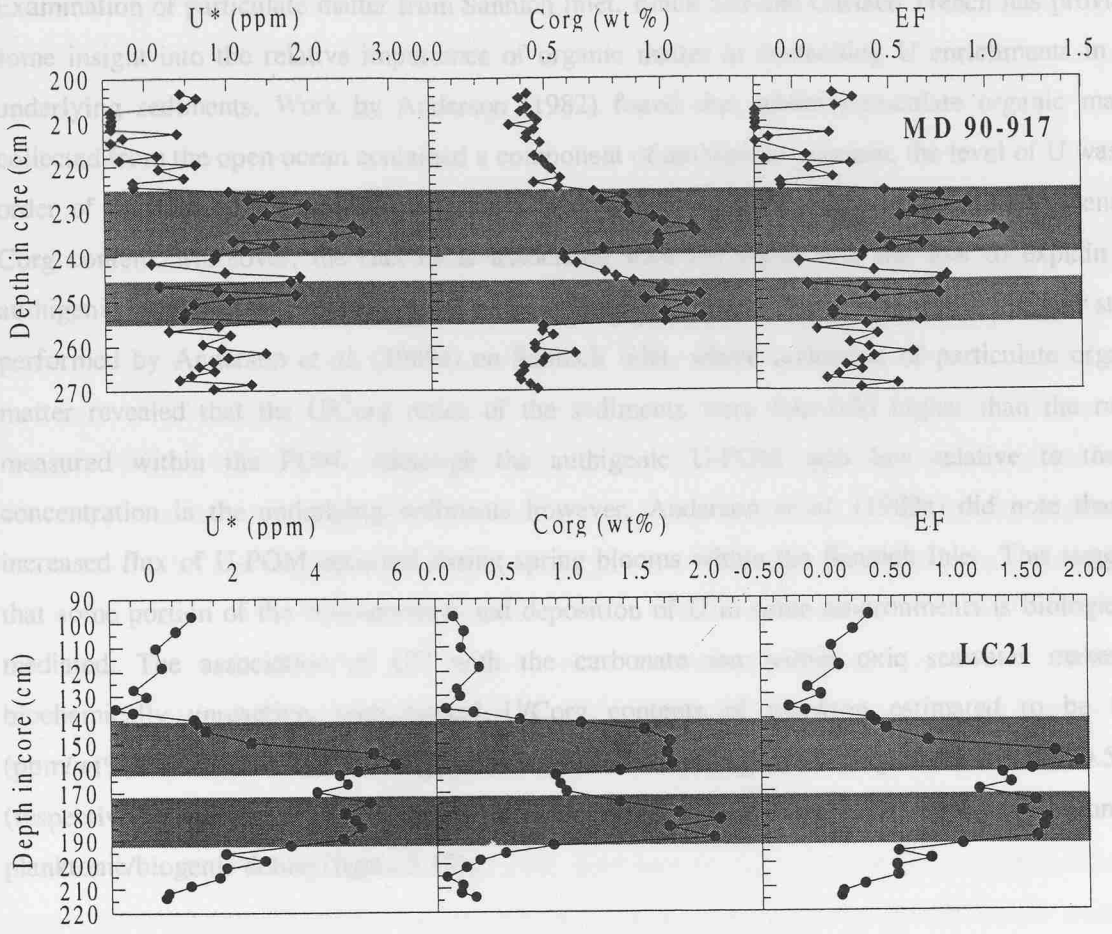

Figure 5.16. Distribution of U* (ppm), Corg (wt%) and uranium enrichment factors in LC21 and MD 90-917.

A relationship has been observed between sedimentary U and Corg contents of organic-rich marine sediments, including the most recently accumulated sapropel units of the eastern Mediterranean (Kolodny and Kaplan, 1973; Mo *et al.*, 1973; Mangini and Dominik, 1979; Colley and Thomson, 1985; Sarkar *et al.*, 1993). Similar authigenic U* enrichments coincide with elevated Corg concentrations in both cores (figure 5.16), suggesting that organic carbon is an important parameter in controlling the uptake of U from seawater. On the basis of the strong relationship found between Corg and U in a number of organic-rich sediments, it has been inferred that the process of uranium deposition involves the association/complexation of dissolved U^{+6} with particulate organic matter (POM) (Kolodny and Kaplan, 1973; Anderson *et al.*, 1989ab). Two proposed mechanisms for the association of U with Corg are (1) Active biological uptake of U by planktonic organisms followed by deposition and preservation under reducing conditions and (2) Chemical adsorption/complexation of dissolved U^{+6} by particulate organic matter, which eventually settles to the seafloor where the U-Corg complex is preserved in the sediment under anoxic conditions (Kochenov *et al.*, 1965; Bautrin *et al.*, 1971; Kolodny and Kaplan, 1973; Degens *et al.*, 1977).

Examination of particulate matter from Sannich Inlet, Black Sea and Cariaco Trench has provided some insight into the relative importance of organic matter in controlling U enrichments in the underlying sediments. Work by Anderson (1982) found that whilst particulate organic matter collected from the open ocean contained a component of authigenic uranium, the level of U was an order of magnitude less than the uranium concentration found associated with the sedimentary Corg content. Moreover, the flux of U associated with the POM was too low to explain the authigenic uranium enrichment within the sediments. These results are in keeping with a later study performed by Anderson *et al.* (1989a) on Sannich Inlet, where collection of particulate organic matter revealed that the U/Corg ratios of the sediments were four-fold higher than the ratios measured within the POM. Although the authigenic U-POM was low relative to the U concentration in the underlying sediments however, Anderson *et al.* (1989a) did note that an increased flux of U-POM occurred during spring blooms within the Sannich Inlet. This suggests that some portion of the concentration and deposition of U in some environments is biologically mediated. The association of U^{+6} with the carbonate ion within oxic seawater makes U biochemically unreactive, with typical U/Corg contents of plankton estimated to be 0.08 (ppm/wt%) (Bowen, 1966). For LC21 and 90-917 the U*/Corg ratios range from 2-6 and 0.5-2.5 (respectively) which is 6-75 times greater than that estimated by the deposition of planktonic/biogenic debris (figure 5.17).

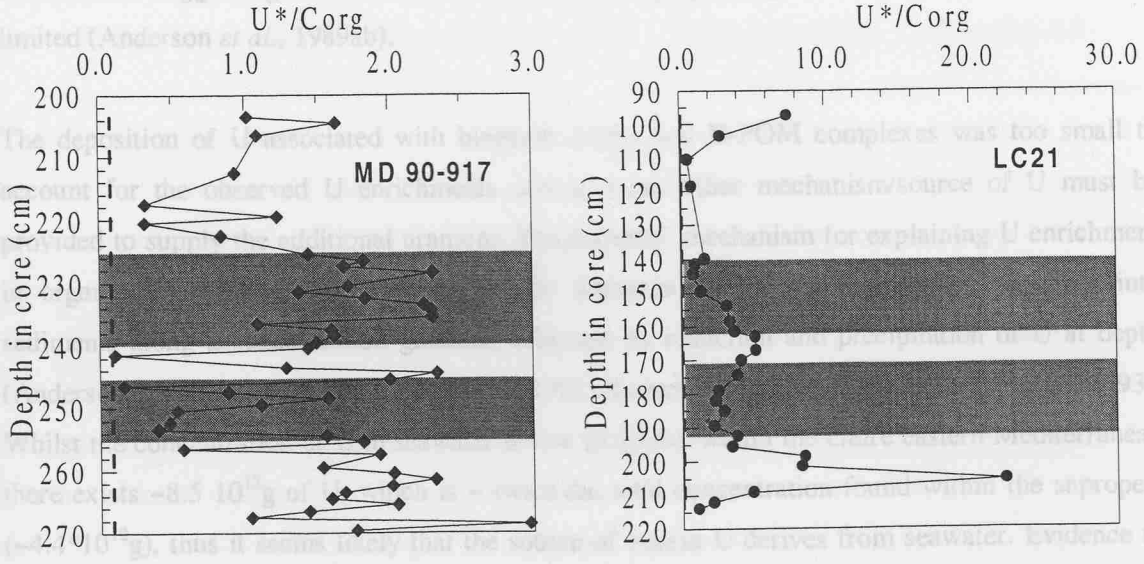

Figure 5.17. U*/Corg in MD 90-917 and LC21. The dashed vertical line in MD 90-917 indicates the U/Corg ratio for plankton. Units are (ppm / wt%).

It is highly unlikely that increase in the U*/Corg ratios seen in the sapropels is the result of partial oxidation of the Corg relative to the adsorbed U, thus it seems likely that the enrichment/association of U with organic matter occurs after the deposition of Corg at the

sediment-water interface. These results are in agreement with particulate matter collected from the Black Sea, where $^{238}U/^{230}Th$ and $^{238}U/^{232}Th$ ratios indicate that U associated with particulate organic matter is almost entirely lithogenic in origin suggesting little or no biological fixation of U within surface waters (Anderson *et al.*, 1989b).

Under more reducing conditions uranium is predicted to occur in the U^{+4} oxidation state. By analogy with other tetravalent actinides such as Th^{+4} and Pu^{+4}, U^{+4} is strongly hydrolysed and is reactive with respect to scavenging and adsorption by particulate matter (Cochran, 1982; Bacon and Anderson, 1982; Anderson *et al.*, 1983). Furthermore, the solubility of U^{+4} in equilibrium with uraninite $UO_2(c)$ is two orders of magnitude lower than the concentration of uranium dissolved in seawater, therefore the chemical reduction of U^{+6} to U^{+4} in reducing seawater should lead to the removal of U by scavenging or precipitation (Langmuir, 1978). Data presented in sections 5.1 and 5.2 have strongly indicated that S1 formation occurred under a reducing water column. Work on the distribution of U speciation within anoxic marine waters of the Black Sea, Sannich Inlet and Cariaco Trench however, have shown that even in the presence of H_2S, the dominant form of U is still the U^{+6} carbonate complex, indicating that the reduction of U^{+6} to U^{+4} is kinetically slow (Anderson, 1987; McKee and Todd, 1993). Furthermore, dissolved U concentrations within the Sannich Inlet and Black Sea show negligible decreases in concentration with depth within the anoxic zone suggesting that the mechanism of scavenging/adsorption on to particulate matter is limited (Anderson *et al.*, 1989ab).

The deposition of U associated with biogenic debris and U-POM complexes was too small to account for the observed U enrichments and so some other mechanism/source of U must be provided to supply the additional uranium. The preferred mechanism for explaining U enrichment in organic-rich sediments is the downwards diffusion of U^{+6} from overlying seawater into sediments along a concentration gradient, followed by reduction and precipitation of U at depth (Anderson, 1987; Klinkhammer and Palmer, 1991; Barnes and Cochran, 1993; Sarkar *et al.*, 1993). Whilst the concentration of U in seawater is low (3.3ppb), within the entire eastern Mediterranean there exists ~8.5 10^{12}g of U, which is ~ twice the total concentration found within the sapropels (~$4.4*10^{12}$g), thus it seems likely that the source of excess U derives from seawater. Evidence to support the hypothesis that U is supplied to sapropel sediments from overlying seawater comes from studies on the $^{234}U/^{238}U$ ratio of these sediments which has demonstrated that the isotopic ratio of the sapropels is identical to that of seawater (1.14) (Mangini and Dominik, 1979; Severman and Thomson, 1998). It is unclear as to why uranium is so readily reduced within reducing sediments as opposed to within reducing seawater, considering that the difference in redox potential between reducing seawater and sediments is only 0.02V (Anderson, 1987). According to Kochenov *et al.* (1977), reduction of U^{+6} to U^{+4} in laboratory experiments could only proceed when U^{+6} was first

adsorbed on to mineral surfaces. It seems therefore that an inadequate supply of specific mineral surfaces within the water column prohibits any reduction of U^{+6} to U^{+4}. More recently however, it has been realised that within reducing sediments, U^{+6} is reduced to U^{+4} close to redox potential of Fe^{+3}-Fe^{+2}, and it has been suggested that specific bacterial populations which are responsible for the reduction of Fe^{+3} to Fe^{+2} may participate in the reduction of U^{+6} to U^{+4} (Mohagheghi *et al.*, 1985; Gorby and Lovley, 1992). According to Cochran *et al* (1986), U^{+6} may become reduced during the oxidation of organic matter at depth with U being used as an electron acceptor via the reaction: -

$$CH_2O + 2UO_2(CO_3)_3^{4-} + H_2O \leftrightarrow 2UO_2 + 6HCO_3^- + CO_2 \qquad \textbf{Equation 5.8}$$

The energy yield from this reaction is intermediate between Mn and Fe reduction, and experiments by Lovley *et al.* (1991) indicate that dissimilatory Fe^{+3} reducing micro-organisms can obtain enough energy by reducing U^{+6} to U^{+4}. Moreover the sulphate reducing bacteria *Desulfovibrio desulfuricans* has been shown to reduce both U^{+6} and sulphate (Lovley and Philips, 1992) which is consistent with the pore water observations that the onset of U reduction in sediments occurs at the same depth as the reduction in dissolved Fe^{2+} concentrations (i.e. sulphate reduction) (Klinkhammer and Palmer, 1991). The proposed reaction for reducing and precipitating U^{+6} to U^{+4} within sediments during sulphate reduction is:

$$4UO_2(CO_3)_3^{4-} + HS^- + 15H^+ \leftrightarrow 4UO_2(c) + SO_4^{2-} + 12CO_2(g) + 8H_20. \qquad \textbf{Equation 5.9}$$

This reaction indicates that the immobilisation and enrichment of U occurs inorganically, but it is initiated by the microbially-mediated reduction of sulphate. This would also explain why there is a close association between U* and Corg (figure 5.16), since only in the most organic-rich sediments is the oxidation of organic matter sufficient to proceed down to utilising sulphate as an electron acceptor. Kniewald and Branica (1988) have proposed that reduction of U^{+6} to U^{+4} occurs via the metastable U^{+5} intermediate in recently accumulated sediments, which then disproportionates to form the stable U^{+4} complexes. According to Cochran *et al.* (1986), the formation of U^{+5} can occur via the oxidation of organic matter using U^{+6} as the oxidation source via the reaction:

$$CH_2O + 4UO_2(CO_3)_3^{4-} + H_2O + 8H^+ \leftrightarrow 4UO_2^+ + 6HCO_3^- + CO_2. \qquad \textbf{Equation 5.10}$$

The close similarity between the Corg and U* profile suggests that very little post-depositional remobilisation of U has occurred in LC21 and 90-917 and according to Thomson *et al.* (1990) the close similarity in U and Corg represents a steady-state diffusion mechanism for U enrichment in sediments. For cores LC21 and MD 90-917, the observed enrichment in uranium is consistent with

the commonly-proposed mechanism of U immobilisation in other organic-rich sediments, one of downwards diffusion of U^{+6} from the overlying seawater, followed by microbially-mediated reduction and precipitation at depth in the sediments. The close correlation observed between Corg and U* does not imply any chemical association between these two elements, but rather it indicates the influence of Corg in controlling the reducing conditions needed for U reduction and immobilisation (i.e. the production of H_2S through the oxidation of Corg during SO_4^{2-} reduction).

5.4.2 Vanadium.

Whilst it is recognised that carbon-rich sediments and rocks act as significant sinks for the accumulation of vanadium (Breit and Wanty, 1992), the exact mechanism(s) by which authigenic V enrichment occurs is often obscured by the fact that vanadium has a relatively high detrital content (~130μg/g).

Excess vanadium (V*) concentration-depth profiles for LC21 and MD 90-917 indicate that maximum V concentrations and enrichments coincide with the highest Corg contents in both cores (figure 5.18). Similar V enrichments in other Corg-rich sediments have been noted for a variety of different marine and black shales, and it has been inferred that this relationship either reflects an affinity of dissolved V for organic matter or that the conditions which favour the preservation of Corg in marine sediments also favours the partitioning of V from the dissolved to the solid phase (Breit and Wanty, 1992).

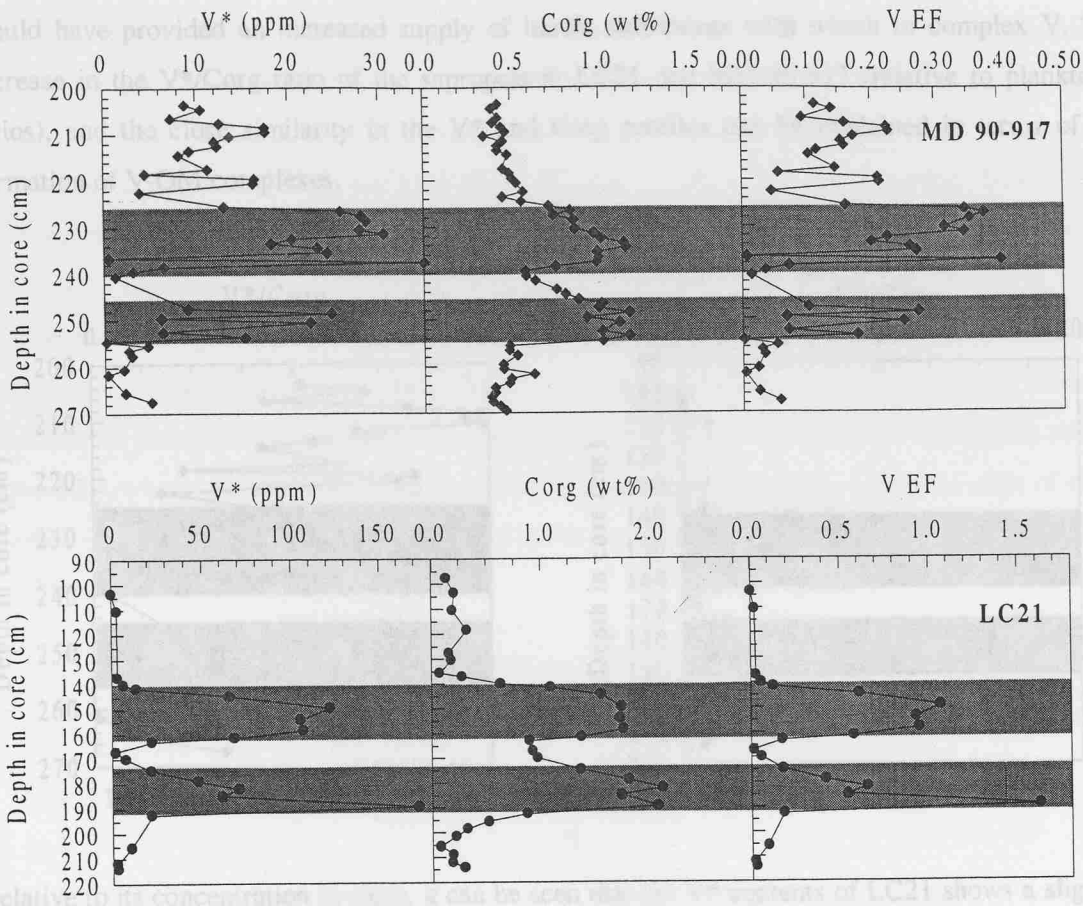

Figure 5.18. Distribution of V* (ppm), Corg (wt%) and EF in MD 90-917 and LC21.

Recent observations on the behaviour of V in the marine environment have shown that it displays a nutrient-like distribution (i.e. surface depletion and enrichment at depth), indicating that it is actively taken up by organisms within the euphotic zone (Jeandel *et al.*, 1987; Sherrell and Boyle, 1988). It is known that certain species take up V from seawater for a variety of biological functions (Quinby-Hunt and Wilde, 1994). Evidence presented in section 5.1 indicates that S1 formation was marked by a five-fold increase in productivity, indicating that the association between V* and Corg (figure 5.18) might in part have been the result of the deposition and preservation of V associated with planktonic detritus. The V/Corg content of plankton is estimated to be 0.05 (ppm/wt%) (Bowen, 1966), whilst that for LC21 and MD 90-917 ranges from 25-80 and 5-40 respectively (figure 5.19), suggesting that the vanadium contribution from the preservation of settling biogenic debris was limited during sapropel formation. A geochemical association between Corg and V has often been reported for marine sediments (Brumsack and Gieskes, 1983). Experimentally it has been demonstrated that vanadate ions ($H_2VO_4^-$) can be reduced to vanadyl cations (VO^{2+}) by humic substances, producing vanadyl organic complexes (Szalay and Szilagyi, 1967; Wilson and Weber, 1979; Templeton III and Chasteen, 1980). It is conceivable that such reactions could have occurred

during sapropel formation considering that S1 was dominated by high primary productivity and so would have provided an increased supply of humic substances with which to complex V. The increase in the V*/Corg ratio of the sapropels in LC21 and MD 90-917 (relative to planktonic ratios), and the close similarity in the V* and Corg profiles can be explained in terms of the formation of V-OM complexes.

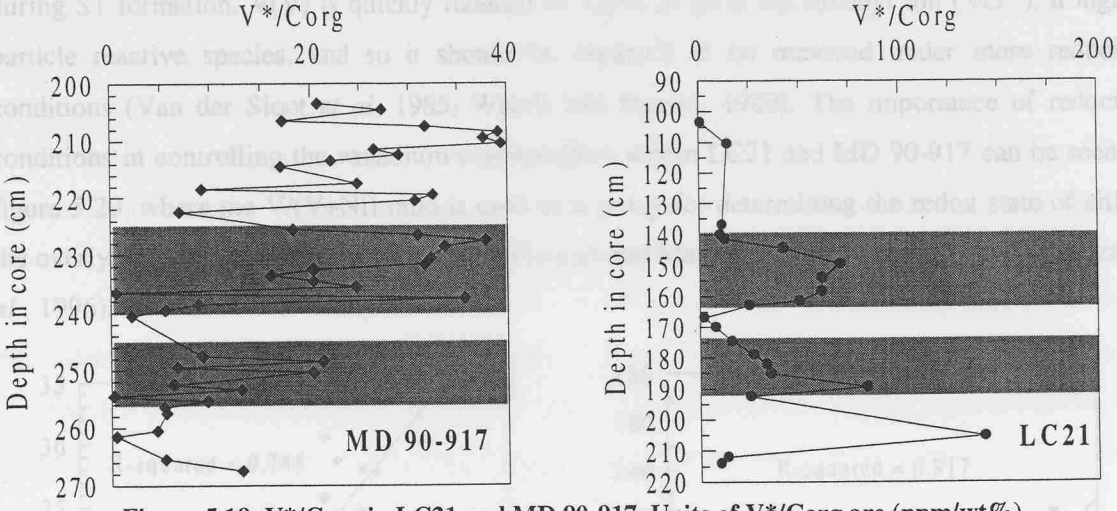

Figure 5.19. V*/Corg in LC21 and MD 90-917. Units of V*/Corg are (ppm/wt%).

Relative to its concentration in shale, it can be seen that the V* contents of LC21 shows a slight to moderate degree of enrichment which is comparable with vanadium enrichments found for other Corg-rich settings (table 5.5). The vanadium concentration in MD 90-917 is consistently lower than in LC21 primarily as a result of a combination lower Corg contents and higher accumulation rates (i.e. a more diluted authigenic V signal). Although vanadium enrichments in MD 90-917 are low relative to the modern-day Corg-rich settings, the higher concentrations of V within the Corg- and S-rich double sapropel units of both LC21 and MD 90-917 indicate these reducing sediments represent sinks for V accumulation.

	BLACK SEA[1]	SANNICH INLET[1]	FRAMVAREN FJORD[1]	CARIACO TRENCH[1]	LC21	MD 90-917	SHALE
V(μg/g)	141	141	43	229	13-172	5-45	130
V/Al (10^4)	28.1	27.6	26.9	35.8	2-44	0.5-7.0	14.8
EF	1.9	1.9	1.8	2.4	0.14-3.0	0.03-0.5	

Table 5.5 Comparison of the average V* (ppm) and enrichment factors (EF) of the sapropel units LC21 and MD90-917 with those found in modern day anoxic basins. EF calculated as (V/Al_{sap}) / (V/Al_{shale}). [1] Data for table from Pedersen and Calvert, 1993.

The preferential accumulation of V under reducing conditions is consistent with the fact that the behaviour of vanadium is closely controlled by its oxidation state which is ultimately governed by the prevailing redox state (Premovic *et al.*, 1993). Within oxic marine waters, vanadium exists primarily as the vanadate (V (V)) anionic species (HVO_4^{2-} and $H_2VO_4^-$) which are quickly hydrolysed to form $VO(OH)_3^-$ or $VO(OH_3)_2^-$ (Turner *et al.*, 1981; Sadiq 1988). Under more reducing conditions however, as experienced within the water column or sedimentary pore-waters during S1 formation, V(V) is quickly reduced to V(IV) to form the vanadyl ion (VO^{2+}), a highly particle reactive species, and so it should be expected to be removed under more reducing conditions (Van der Sloot *et al*, 1985; Wehrli and Stumm, 1989). The importance of reducing conditions in controlling the vanadium concentration within LC21 and MD 90-917 can be seen in figure 5.20, where the V/(V+Ni) ratio is used as a proxy for determining the redox state of either the overlying water column and/or sediment (Lewan and Maynard, 1982; Lewan, 1984; Bellanca *et al.*, 1996).

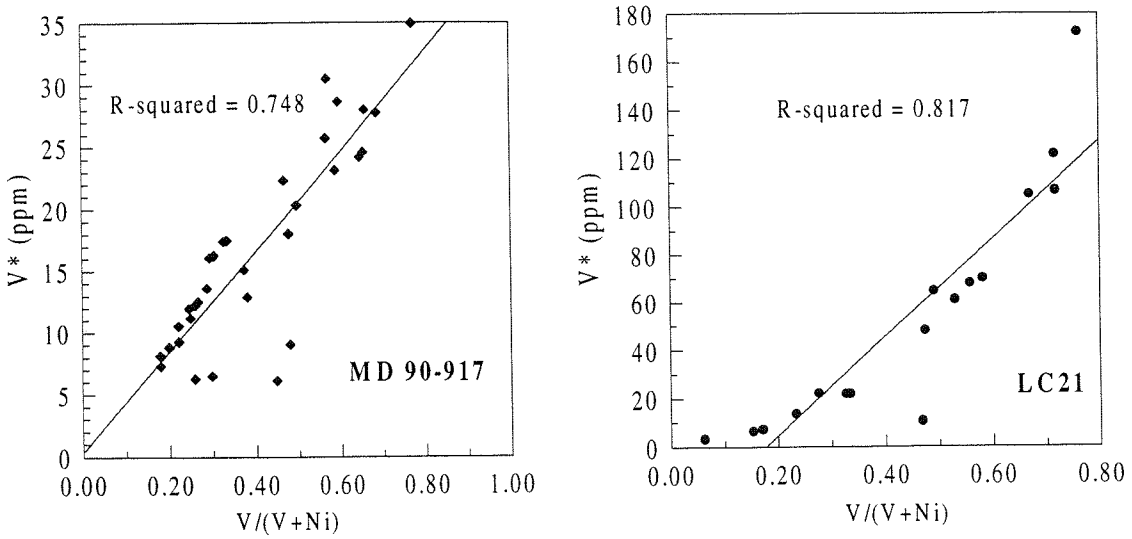

Figure 5.20. V* (ppm) vs V/(V+Ni) ratios in MD 90-917 and LC21.

According to Hatch and Leventhal (1992) values of V/(V+Ni) ratios of ~0.5 are characteristic of reducing water column/sediment, with progressively higher ratios indicating more reducing conditions. The V/(V+Ni) ratios calculated for MD 90-917 and LC21 (figure 5.20) are consistent with the fact that during sapropel formation the sediments were reducing in nature and that they were accumulating under a reducing water column. As such, during sapropel formation, it is likely that the speciation of vanadium would have been dominated by the presence of V(IV). It seems likely that during sapropel formation, V enrichment occurred via a combination of reduction, adsorption and complexation to inorganic and organic substrates (Brumsack and Gieskes, 1983; Brumsack, 1986; Breit and Wanty, 1992). A similar mechanism has been proposed by Fowler and Knauer (1986) to explain the decreases in dissolved V concentrations in anoxic waters of the Gulf

of Mexico. It is not clear whether the association of V(IV) to particulate organic matter occurred within the water column or at the sediment-water interface during sapropel formation, although according to Fowler and Knauer (1986), particles settling through the sub-oxic waters of the Gulf of Mexico had significantly more associated V in comparison to those particles collected within more oxidising conditions, consistent with the idea of passive uptake of V on to particulate matter under reducing conditions.

An alternative mechanism for explaining V enrichments in LC21 and MD 90-917 is one similarly proposed for U (section 5.4), in that there was a downwards diffusion of V into the sediment followed by reduction and immobilisation at depth (Jarvis and Higgs, 1987; Francois, 1988). Studies on pore water V concentrations in the reducing sediments of the Gulf of California have shown a significant decrease in the V content from the top of the core to the base, indicating that it was being reduced to V^{+4} and partitioned to the solid phase within the reducing sediments rather than within the water column (Brumsack, 1986). According to Brumsack (1986), the reduction in dissolved V concentrations can be attributed to the reduction of V^{+5} by organic ligands followed by subsequent adsorption on to sedimentary Corg, thus explaining the close association between Corg and V seen in figure 5.18.

Sulphur-rich sediments often display elevated vanadium concentrations, and it has been suggested that the V enrichment occurs via complexation to organic sulphur ligands attached to organic matter (Baker and Louda, 1986; Breit and Wanty, 1991). Examination of the V* and S# profiles in LC21 and MD 90-917 reveals distinct differences between the upper and lower units (figure 5.21). For example within the lower sapropel unit of LC21 (and to a lesser extent in MD 90-917) the profiles of V* and S# match more closely than in the upper units, where the vanadium profiles more closely resemble those of organic carbon (figure 5.21). According to Lewan (1984) formation of organic sulphur compounds occurs via the interaction of H_2S with organic matter during sulphate reduction. Recent work on the sulphur isotope composition of S1 by Passier *et al.* (1996) and evidence presented in section 5.2 has shown that the pore waters of LC21 and MD 90-917 were dominated by H_2S generated through bacterially-derived sulphate reduction. The close similarity between Corg and S# in both cores suggests that some of the V is associated with organic S ligands attached to organic matter, which is consistent with the findings presented in section 5.2.1, that organically-bound sulphur was important during S1 formation.

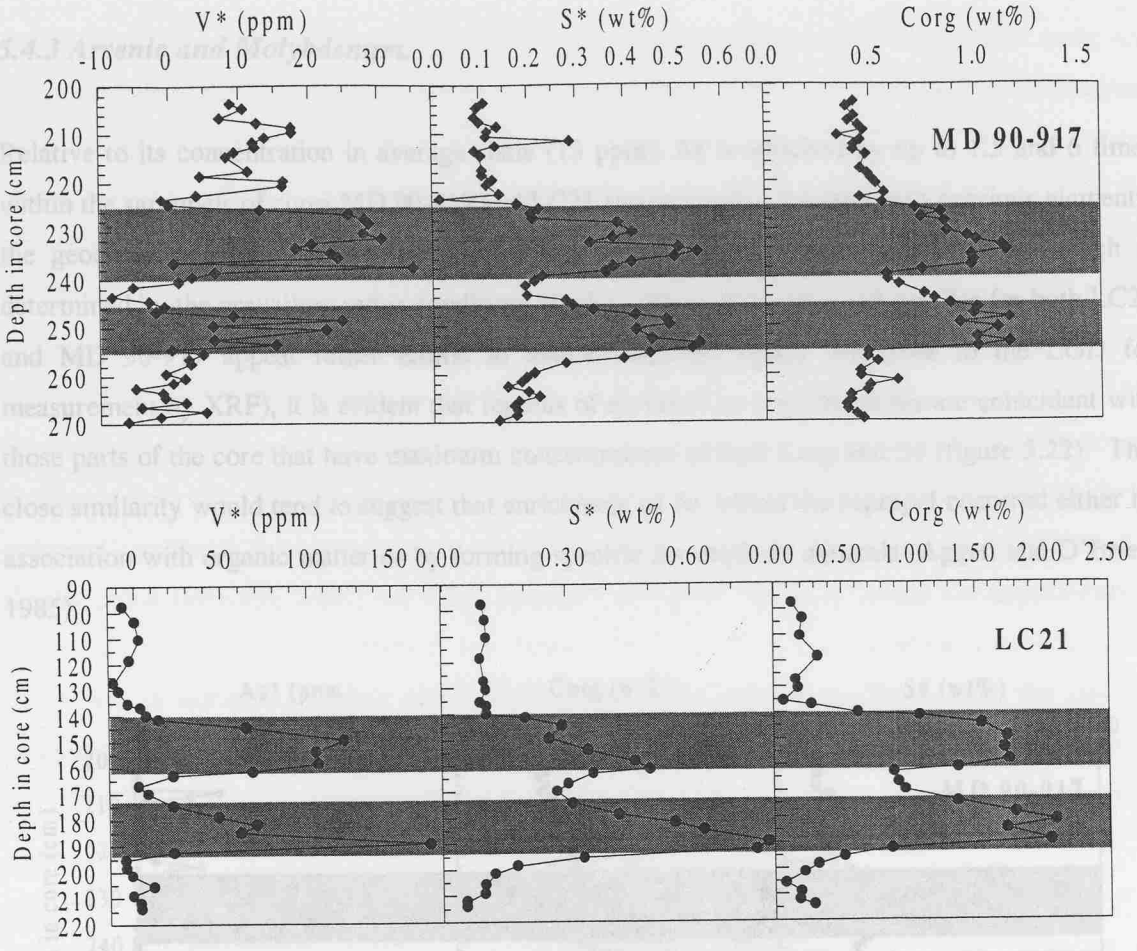

Figure 5.21. Depth distributions of V* (ppm), S# (wt%) and Corg (wt%) in MD 90-917 and LC21.

It seems therefore, that the accumulation of V within the sapropels represents a combination of a number of processes. It is likely that a significant portion of the V was delivered to the seafloor via complexation with organic matter within the water column or at the sediment-water interface, with the reducing bottom waters aiding the preservation of such complexes. Alternatively, some of the observed V enrichment seen in LC21 and MD 90-917 is derived from the downwards diffusion of V from seawater followed by its reduction and complexation with organic matter at depth within the sediment. These two mechanisms result in the close covariance between Corg and V* (figure 5.18), although it is not possible to quantify the importance of each process in the accumulation of V during sapropel formation. Furthermore, the close similarity between S# and V* (especially within the lower sapropel units of both cores) is indicative of the incorporation of V with organic S ligands which formed during sulphate reduction during sapropel formation (figure 5.21).

5.4.3 Arsenic and Molybdenum.

Relative to its concentration in average shale (13 ppm), As is enriched by up to 1.5 and 6 times within the sapropels of cores MD 90-917 and LC21 (respectively). As seen with previous elements, the geochemical mobility and behaviour of As is governed by its oxidation state, which is determined by the prevailing redox conditions (Sadiq, 1990). Whilst the As* profiles for both LC21 and MD 90-917 appear rather erratic in nature (reported values are close to the LOD for measurement by XRF), it is evident that regions of elevated As concentrations are coincident with those parts of the core that have maximum concentrations of both Corg and S# (figure 5.22). This close similarity would tend to suggest that enrichment of As within the sapropel occurred either by association with organic matter or by forming specific As sulphide minerals (Aggett and O'Brien, 1985).

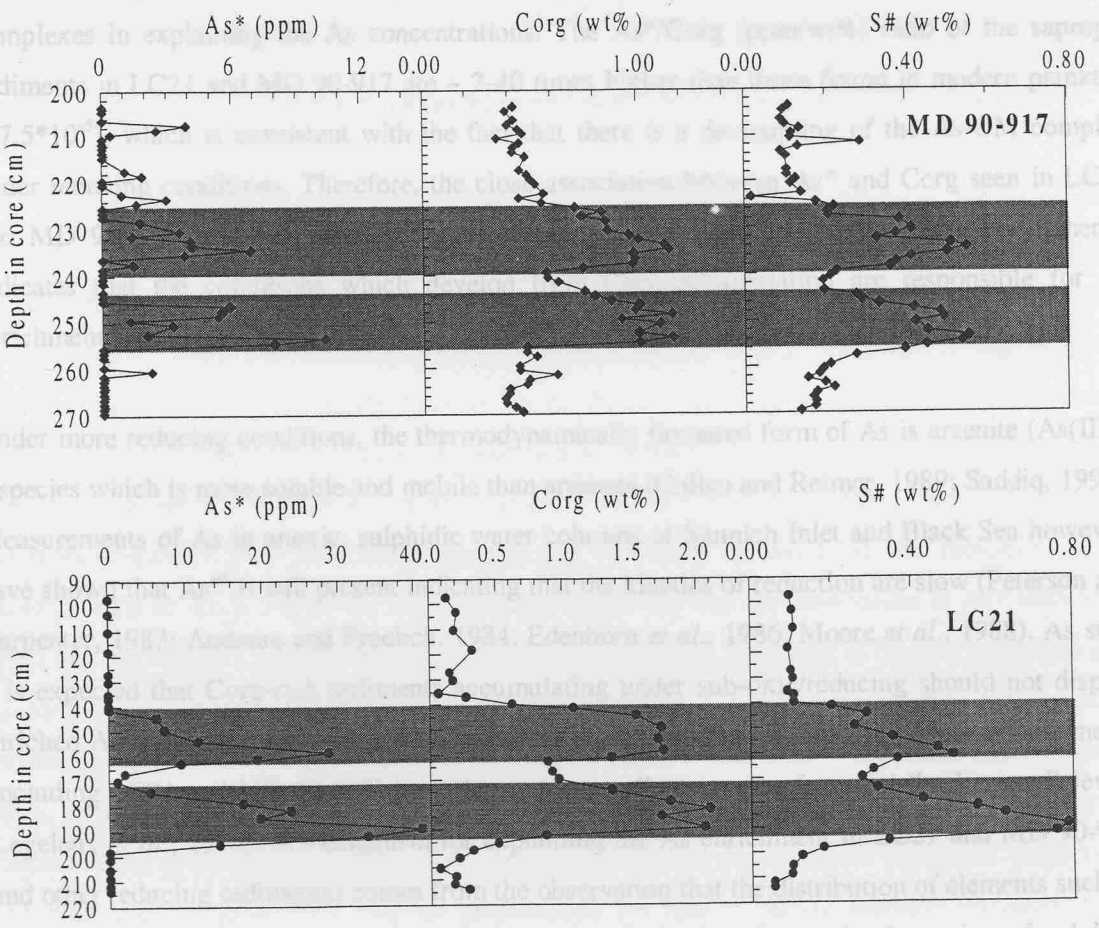

Figure 5.22. Distribution of As* (ppm), Corg (wt%) and S# (wt%) in MD 90-917 and LC21.

Based on thermodynamic considerations, under more oxidising conditions, arsenic is known to occur primarily as arsenate (As(V)), although it has been reported that arsenite (As(III)) occurs in oxidising environments produced through biological activity (Cutter, 1991). In the marine

environment, As is known to be actively taken up by phytoplankton within the euphotic zone, and often displays a vertical distribution which closely matches phosphate (Andreae, 1979; Andreae and Klumpp, 1979; Minami and Kato, 1997). It is believed that some combination of water column anoxia coupled with increased productivity was responsible for the formation of S1. As such, the possibility exists that preferential uptake of As(V) occurred within the surface waters during periods of high productivity followed by deposition and preservation of the As-organic matter complexes to account for the close association of As* and Corg in both LC21 and MD 90-917. Examination of the distribution of dissolved As at the oxic-anoxic interface of the Tyro and Bannock Basins however, has revealed a dramatic increase in dissolved As concentrations, consistent with the fact that As (as As(V)) is preferentially released from organic matter under reducing conditions (van der Sloot *et al.*, 1990). During sapropel formation, the existence of a similar redox boundary within the water column would have similarly caused the degradation of particulate organic matter (releasing As), limiting the contribution of organically associated As complexes in explaining the As concentrations. The As*/Corg (ppm/wt%) ratio of the sapropel sediments in LC21 and MD 90-917 are ~ 2-40 times higher than those found in modern plankton ($\sim 7.5*10^{-5}$), which is consistent with the fact that there is a de-coupling of the As-OM complex under reducing conditions. Therefore, the close association between As* and Corg seen in LC21 and MD 90-917 does not indicate any chemical immobilisation of As by Corg, but rather it indicates that the conditions which develop from Corg accumulation are responsible for As enrichment (i.e. reducing conditions).

Under more reducing conditions, the thermodynamically favoured form of As is arsenite (As(III)), a species which is more soluble and mobile than arsenate (Cullen and Reimer, 1989; Saddiq, 1990). Measurements of As in anoxic, sulphidic water columns of Sannich Inlet and Black Sea however, have shown that As^{+5} is still present indicating that the kinetics of reduction are slow (Peterson and Carpenter, 1983; Andreae and Froelich, 1984; Edenborn *et al.*, 1986; Moore *et al.*, 1988). As such it is expected that Corg-rich sediments accumulating under sub-oxic/reducing should not display enriched As concentrations, which is in contradiction to the observations that Corg-rich sediments (including LC21 and MD 90-917) have As contents well in excess of normal 'background' levels (Legeleux *et al.*, 1994). A mechanism for explaining the As enrichment in LC21 and MD 90-917 (and other reducing sediments) comes from the observation that the distribution of elements such as As, Mo, Ni and Zn within anoxic settings are controlled primarily by the formation of sulphide minerals (Jacobs and Emerson, 1982; Jacobs *et al.*, 1985; Jacobs *et al.*, 1987). The close covariance between the S# and As* profiles in LC21 and MD 90-917 would suggest that sulphide formation may be responsible for enriched As concentrations in both cores (figure 5.23).

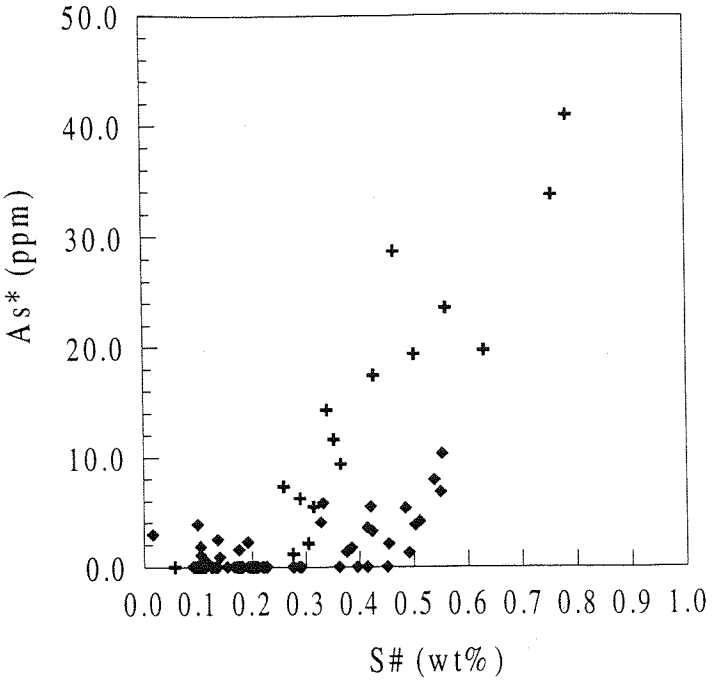

Figure 5.23. As* (ppm) vs S# (wt%) in MD 90-917 (diamonds) and LC21 (crosses).

The observed decrease in As concentrations within the anoxic water columns of the Oslo Fjord, Baltic Sea and Sannich Inlet suggests that removal of arsenic from the dissolved to the solid phase (as a sulphide As_2S_3) occurred within the water column rather than within the sediment (Peterson and Carpenter, 1983; Andreae and Froelich, 1984; Abdullah *et al.*, 1995). According to Cutter (1991) a necessary prerequisite for forming As sulphides within the water column is the presence and availability of dissolved H_2S. Data presented in section 5.2.3 indicated that during sapropel formation the eastern Mediterranean water column was sub-oxic rather than anoxic in nature. It therefore seems unlikely that As removal to the sediments occurred via the formation of As minerals such as As_2S_3 within the water column, suggesting that the association of As* with S# in LC21 and MD 90-917 must occur *in situ* within the sediments. Evidence to support the removal of As to the solid phase within reducing sediments comes from observation that a solid phase enrichment in As coincides with decreasing dissolved As concentrations (Peterson and Carpenter, 1986; Belzile, 1988; Moore *et al.*,1988). These authors ascribed the reduction in pore water As concentrations to the incorporation of As into iron sulphides during pyrite formation. Arguments presented above suggest As^{+3} was the predominant As species during sapropel formation, so it seems plausible that arsenite could have diffused down into the sediment along a concentration gradient where it was subsequently immobilised as a sulphide phase. Conditions in LC21 and MD 90-917 were sufficiently reducing to allow for the formation of framboidal pyrite (i.e. production of H_2S, section 5.2). As such, the possibility exists that interactions between H_2S and As produced arsenic sulphides such as As_2S_3, or more likely As was co-precipitated/incorporated into an iron

sulphide phase during framboidal pyrite formation, as proposed by Belzile and Lebel (1986) and Huerta-Diaz and Morse (1992).

Molybdenum (Mo*), like arsenic, shows increased concentrations within LC21 and MD 90-917 in association with increasing levels of both Corg and S# associated with the double sapropel units (figure 5.24).

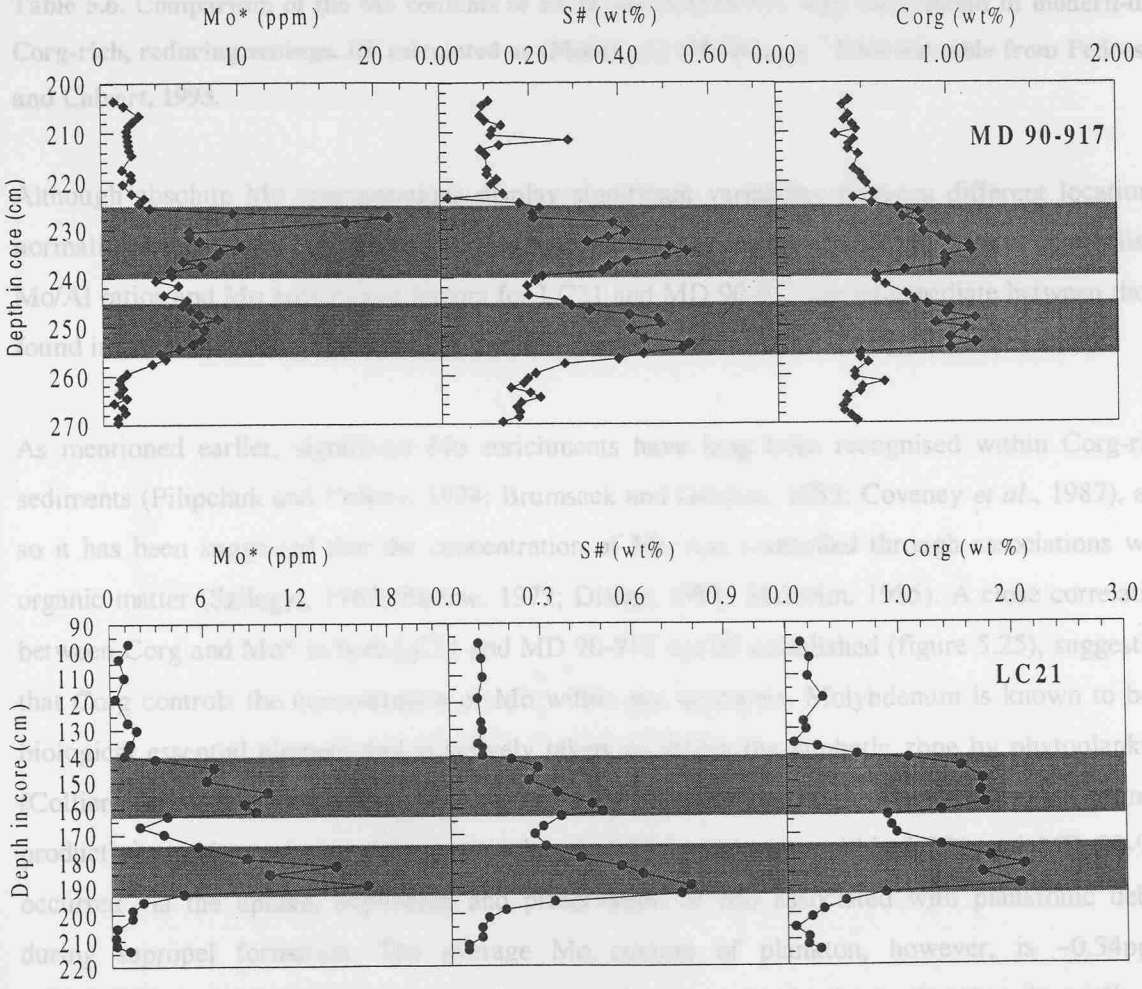

Figure 5.24. Distribution of Mo* (ppm), S# (wt%) and Corg (wt%) in MD 90-917 and LC21.

Corg-rich sediments, including those from the Black Sea, Sannich Inlet and Black Shales have Mo concentrations well in excess of those found in average shale (~2.3ppm). Table 5.5 presents the relative Mo contents of modern anoxic, Corg-rich sediments in comparison with that of the most recently accumulated sapropel S1 in LC21 and MD 90-917.

	BLACK SEA[1]	SANNICH INLET[1]	FRAMVAREN FJORD[1]	CARIACO TRENCH[1]	LC21	MD 90-917	SHALE
Mo (μg/g)	21	92	160	71	7.51	4.67	2.6
Mo/Al(*10^4)	4.3	18.0	100.0	11.1	1.33	1.50	0.3
EF	14.3	60.3	33.3	3.70	4.33	4.54	

Table 5.6. Comparison of the Mo contents of LC21 and MD 90-917 with those found in modern-day Corg-rich, reducing settings. EF calculated as (Mo/Al_{sap}) / (Mo/Al_{shale}). [1] Data for table from Pedersen and Calvert, 1993.

Although absolute Mo concentrations display significant variability between different locations, normalised Mo/Al concentrations are fairly uniform (except for the Framvaren Fjord). Normalised Mo/Al ratios and Mo enrichment factors for LC21 and MD 90-917 are intermediate between those found in the euxinic Black Sea and the Cariaco Trench.

As mentioned earlier, significant Mo enrichments have long been recognised within Corg-rich sediments (Pilipchuk and Volkov, 1974; Brumsack and Gieskes, 1983; Coveney *et al.*, 1987), and so it has been suggested that the concentration of Mo was controlled through associations with organic matter (Szilagyi, 1967; Bertine, 1972; Disnar, 1981; Malcolm, 1985). A close correlation between Corg and Mo* in both LC21 and MD 90-917 can be established (figure 5.25), suggesting that Corg controls the concentration of Mo within the sapropels. Molybdenum is known to be a biological essential element and is actively taken up within the euphotic zone by phytoplankton (Collier, 1985). It is known that sapropel formation was marked by periods of increased primary productivity and anoxia, so it is conceivable that Mo enrichment within LC21 and MD 90-917 occurred via the uptake, deposition and preservation of Mo associated with planktonic debris during sapropel formation. The average Mo content of plankton, however, is ~0.34ppm, significantly less than that found within the sapropel units, so mechanisms other than the settling of planktonic debris must be responsible for the observed Mo enrichment. Within the marine environment Mo is known to present as the molybdate (VI) ion (MoO_4^{2-}) under oxidising conditions (Emerson and Huested, 1991). However, in the presence of humic and fulvic acids, these organic ligands are known to reduce Mo(VI) to Mo(V) which is then scavenged/complexed by organic matter (Szilagyi, 1967). Certainly the reducing water column within the eastern Mediterranean at the time of S1 formation coupled with an abundance of organic ligands would be conducive to a passive scavenging mechanism of Mo on to particulate organic matter, which would then explain the close association between Corg and Mo in the sapropel units. Recent work on the Mo content of particulate organic matter collected from Sannich Inlet has shown that relative to the underlying sediments however, the POM is depleted in molybdenum, suggesting that the

mechanism/association of Mo with Corg must occur after the deposition of POM either at the sediment-water interface or *in situ* within the sediments (Francois, 1988). Recent work on the distribution of Mo in the pore waters of Corg-rich has shown that a positive correlation exists between dissolved humic substances and Mo concentrations (Contreras *et al.*, 1978; Brumsack and Gisekes, 1983; Malcolm, 1985; Calvert *et al.*, 1985). These authors suggest that within organic-rich sediments, Mo may become complexed by humic substances, by the prior reduction of Mo(VI) to $Mo(V)O_4^+$ ion by organic substrates. These data fit well with the observations that organic matter from Corg-rich sediments which are leached using organic solvents yield significant quantities of authigenic Mo (Nissenbaum and Swaine, 1976; Volkov and Fomina, 1974).

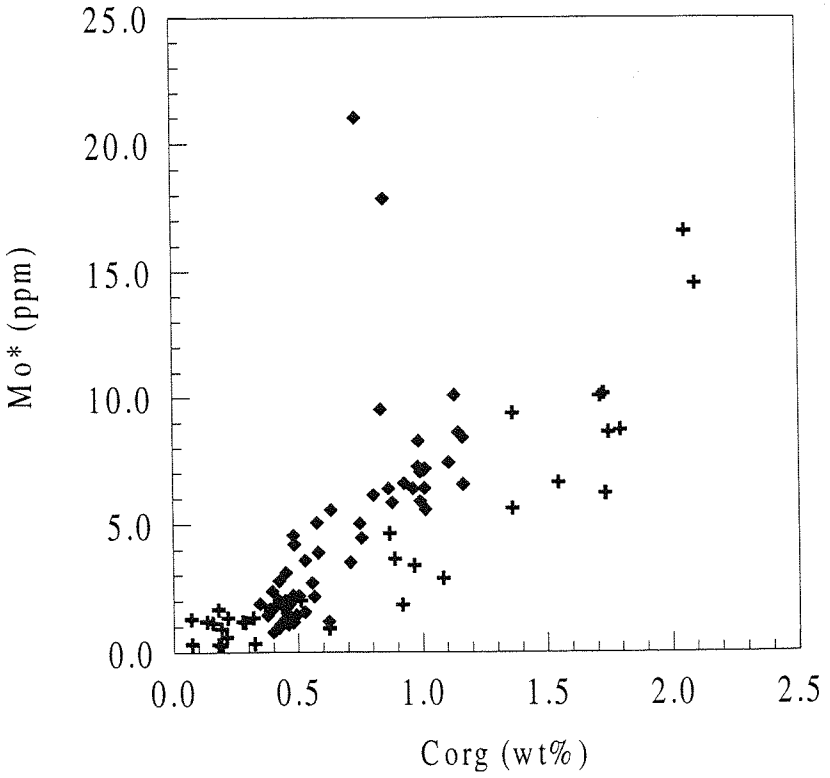

Figure 5.25. Mo* (ppm) vs Corg (wt%) in MD 90-917 (diamonds) and LC21 (crosses).

An alternative mechanism for explaining Mo enrichment within Corg-rich sediments has been proposed by a number of workers who found that there was a significant correlation between Mo and S contents of marine sediments (Glikson *et al.*, 1985; Brumsack, 1989). Similar close correlations exist between Mo* and S# in LC21 and MD 90-917 (figure 5.26), indicating that sedimentary sulphur may exert some control over the Mo contents of these cores, in a similar way that sulphur did with As* (see previous discussion). For example, van der Weijden *et al.* (1990)

showed the removal of Mo from the anoxic water columns of the Tyro and Bannock Basins, either via the direct precipitation of MoS_2 or via its incorporation into an iron sulphide phase.

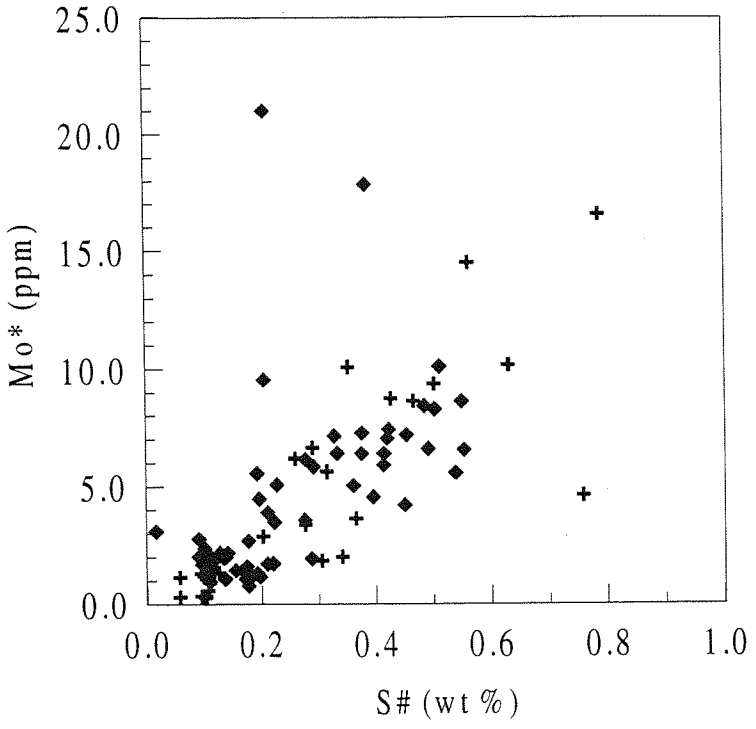

Figure 5.26. Mo* (ppm) *vs* S# (wt%) in MD 90-917 (diamonds) and LC21 (crosses).

According to Bertine (1972) Mo can be removed from solution under reducing conditions by the co-precipitation of MoS_3 on to iron sulphides by the reaction:

$$FeS_{amorphous} + MoO_2S_2^{2-} + H_2S + 2H^+ = FeS.MoS_{amorphous} + 2H_2O;$$

Based on the evidence presented in section 5.2.3, the absence of pyrite formation within the eastern Mediterranean water column during sapropel formation would have meant that removal of Mo to solid phase must have occurred *in situ* i.e. within the sediments. This is in agreement with the findings of Crusius *et al.* (1996) who found that Mo removal only occurred *in situ* within sediments undergoing sulphate reduction rather than within the water column. In LC21 and MD 90-917, it is plausible that the production of H_2S during sulphate reduction of Corg could have allowed for the immobilisation of Mo via its reduction and co-precipitation with pyrite formation as suggested by Bertine (1972). Certainly, the presence of framboidal pyrite within LC21 and MD 90-917 at the same depths as maximum enrichments in Mo concentration lends further support to the idea of Mo incorporation into iron sulphide minerals. More recently, an examination of the mechanisms by which Mo was incorporated into Black Shales was examined by Helz *et al.* (1996). These authors

proposed that under reducing conditions, HS^- acts as geochemical switch that prepares Mo for removal via its conversion from MoO_4^{2-} to $MoS_4^{2-}/MoO_2S_2^-$, a highly particle reactive species, which is capable of adsorbing/complexing with sites provided by organic matter. Again, it is expected that within the sediments of both LC21 and MD 90-917, the concentration of HS^- was sufficiently high to ensure the conversion of MoO_4^{2-} to $MoS_4^{2-}/MoO_2S_2^-$, followed by its uptake on to organic matter during sapropel formation.

For MD 90-917 and LC21, there are a number of points of enhanced Mo concentrations which cannot be explained by the immobilisation of Corg or sulphide formation. It can be seen from figure 5.27 that the region of enhanced Mo concentrations are coincident with maximum levels in sedimentary Mn concentrations, although the effect is more pronounced in MD 90-917 due to the greater Mn concentrations in this core relative to LC21.

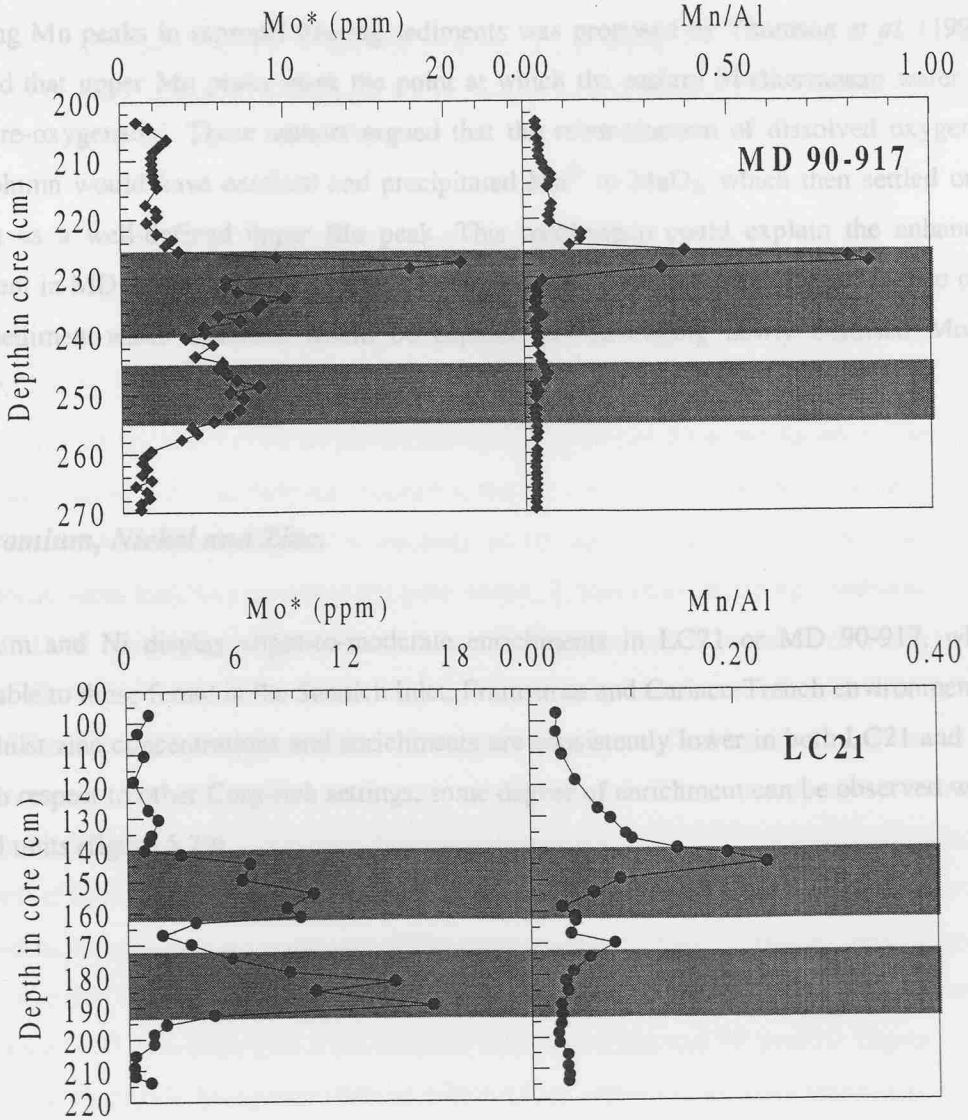

Figure 5.27. Depth-distribution of Mo* (ppm) and Mn/Al (ppm/ppm) in MD 90-917 and LC21.

The influence of Mn oxyhydroxides on controlling/immobilising Mo in sediments has been recognised (Berrang and Grill, 1974; Shimmield and Price, 1986). There are two likely explanations for the pronounced Mn peak at the top of the upper sapropel unit in MD 90-917 and in LC21. One explanation involves the partial oxidation of the upper sapropel unit following its formation in response to the re-establishment of oxygenated bottom waters. In such a scenario, downwards diffusing O_2 would have the capacity to oxidise Mo associated with either organic matter and/or sulphides and also simultaneously precipitate Mn^{2+} to MnO_2 which would then be capable of adsorbing/scavenging the released Mo^{+6} (Shimmield and Price, 1986). Examination of the Ba and Corg profiles (section 5.1 figure 5.2) however, indicates minor oxidation of the upper face of the upper sapropel units has occurred, and moreover if partial oxidation had occurred then it would be expected that a number of other redox-sensitive elements would also form well-defined peaks at this depth, but there appears to be no evidence for this. An alternative mechanism for explaining Mn peaks in sapropel bearing sediments was proposed by Thomson *et al.* (1995) who suggested that upper Mn peaks mark the point at which the eastern Mediterranean water column became re-oxygenated. These authors argued that the reintroduction of dissolved oxygen to the water column would have oxidised and precipitated Mn^{2+} to MnO_2, which then settled on to the sediment as a well-defined upper Mn peak. This mechanism could explain the enhanced Mo enrichment in MD 90-917 (and to a lesser extent in LC21), since an increased abundance of MnO_2 at the sediment-water interface would be capable of scavenging newly oxidised Mo^{+6} from seawater.

5.5 Chromium, Nickel and Zinc.

Chromium and Ni display slight-to-moderate enrichments in LC21 or MD 90-917, which are comparable to those found in the Sannich Inlet, Framvaren and Cariaco Trench environments (table 5.7). Whilst zinc concentrations and enrichments are consistently lower in both LC21 and MD 90-917 with respect to other Corg-rich settings, some degree of enrichment can be observed within the sapropel units (figure 5.29).

	BLACK SEA[1]	SANNICH INLET[1]	FRAMVAREN FJORD[1]	CARIACO TRENCH[1]	LC21	MD 90-917	SHALE
Cr (μg/g)	138	79	13	86	4-41	6-30	90
Cr/Al (*10^4)	28.2	15.5	8.1	13.4	1.02-6.12	1.02-5.1	10.2
EF	2.8	1.5	0.8	1.3	0.1-0.6	0.1-0.5	
Ni (μg/g)	97	38	145	37	11-70	2-26	68
Ni/Al (*10^4)	19.8	7.4	90.6	5.8	1.54-9.24	0.4-0.6	7.7
EF	2.6	1.0	11.8	0.8	0.2-1.2	0.05-0.6	
Zn (μg/g)	57	182	1740	104	1.6-12	3-22	95
Zn/Al (*10^4)	11.6	35.7	1090	16.2	0.22-1.6	0.54-4.3	10.8
EF	1.1	3.3	100.0	1.5	0.02-0.15	0.05-0.4	

Table 5.7. Comparison of the Cr, Ni and Zn contents of the sapropels in LC21 and MD 90-917 with those found in other Corg-rich sediments. EF calculated as (Element/Al_{sap}) / (Element/Al_{shale}). [1] Data for table from Pedersen and Calvert, 1993.

Under oxidising conditions, Cr exists primarily as the chromate (VI) anion (CrO_4^{2-}) and also to a lesser extent as the cationic (III) aquahydroxy species $Cr(OH)^{2+}(H_2O)_4$ (Elderfield, 1970; Cranston and Murray, 1978). Vertical distributions imply that this element is actively taken up within the euphotic zone by phytoplankton and regenerated at depth (Calvert and Pedersen, 1993). Recent measurements on the Cr content of particulate matter collected from the Sannich Inlet, however, shows that relative to the underlying sediments, the Cr content in the POM is depleted (Francois, 1988). This would tend to suggest that mechanisms for the enrichment of Cr must occur either at the sediment water interface or within the pore waters. Under more reducing conditions, Cr (VI) is rapidly reduced to Cr(III), a highly particle-reactive species which is removed from solution as $Cr(OH)_2^+$ (Emerson *et al.*, 1979). Within Sannich Inlet, it has been shown that Cr is correlated with Corg and Francois (1988) suggested that this relationship was derived by the adsorption of Cr on to organic matter at the sediment-water interface or that it resulted from incorporation into sediment in relation to the amount of Corg being deposited. Reduction of Cr (VI) to Cr(III) occurs just before the reduction of Mn(IV) to Mn(II), so that it is conceivable that this reduction could have occurred either within the reducing water column of the eastern Mediterranean during S1 deposition or more likely it occurred within the reducing sediments of LC21 and MD 90-917. For LC21 it can be seen that enhanced Cr* concentrations are coincident with both Corg and S# profiles (figure 5.28). This suggests that Cr (III) is being immobilised within LC21 either via its association with Corg or by the reducing conditions which Corg-rich sediments generate. The lack of any significant relationship between Cr* and Corg (or S#) in MD 90-917 implies that Cr enrichment within this

core does not occur by complexation with organic matter, but rather it is immobilised on to particle surfaces under reducing conditions generated by enhanced Corg deposition (figure 5.28).

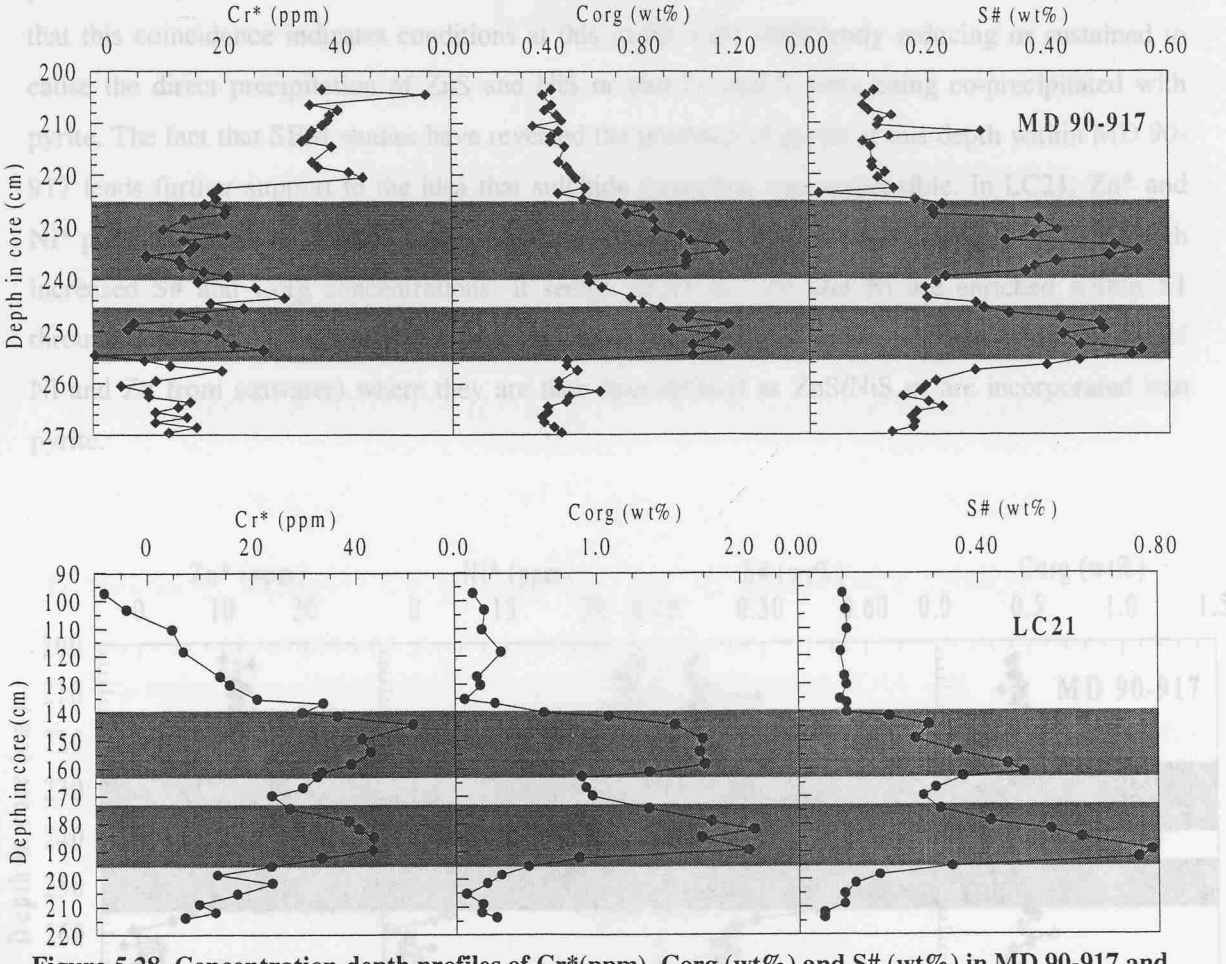

Figure 5.28. Concentration-depth profiles of Cr*(ppm), Corg (wt%) and S# (wt%) in MD 90-917 and LC21.

Both zinc and nickel are known to be chalcophilic elements, concentrated as disseminated sulphides within organic-rich deposits such as black shales (Calvert and Pedersen, 1993). In core MD 90-917 and LC21, both Ni* and Zn* display elevated concentrations within the sapropel units although there is little correlation between with either Corg or S# (figure 5.29). This would suggest that the influence of Corg/S in controlling the content of Ni and Zn is fairly limited. Under more oxidising conditions, Ni and Zn exist as divalent ions (Brookins, 1980), and are thought to be involved in uptake from surface waters analogous to the uptake of silicate by plankton (Bruland, 1983). Under reducing conditions however, thermodynamics and observations indicate that Ni and Zn are removed from solution as their respective sulphide phases (NiS and ZnS) (Haraldson and Westerlund, 1988; 1991; Jacobs *et al.*, 1987). For Zn and Ni, as stated earlier, removal from solution only occurs in the presence of free H_2S. It is unlikely that free H_2S existed within the water

column at the time of sapropel formation, so that it seems more plausible that enrichment of Zn occurred *in situ* within the sediment where H_2S was present within the pore waters. Closer examination of the Zn* and Ni* profiles in MD 90-917 (figure 5.29) reveals that there is a pronounced peak located at 252-254cm, coincident with elevated S concentrations. It is possible that this coincidence indicates conditions at this depth were sufficiently reducing or sustained to cause the direct precipitation of ZnS and NiS or that Ni and S were being co-precipitated with pyrite. The fact that SEM studies have revealed the presence of pyrite at this depth within MD 90-917 lends further support to the idea that sulphide formation was responsible. In LC21, Zn* and Ni* profiles generally display enrichments over the entire depth of the sapropels, coincident with increased S# and Corg concentrations. It seems likely that Zn and Ni are enriched within S1 through their associations with Corg or are removed from pore waters (from downward diffusion of Ni and Zn from seawater) where they are then immobilised as ZnS/NiS or are incorporated into pyrite.

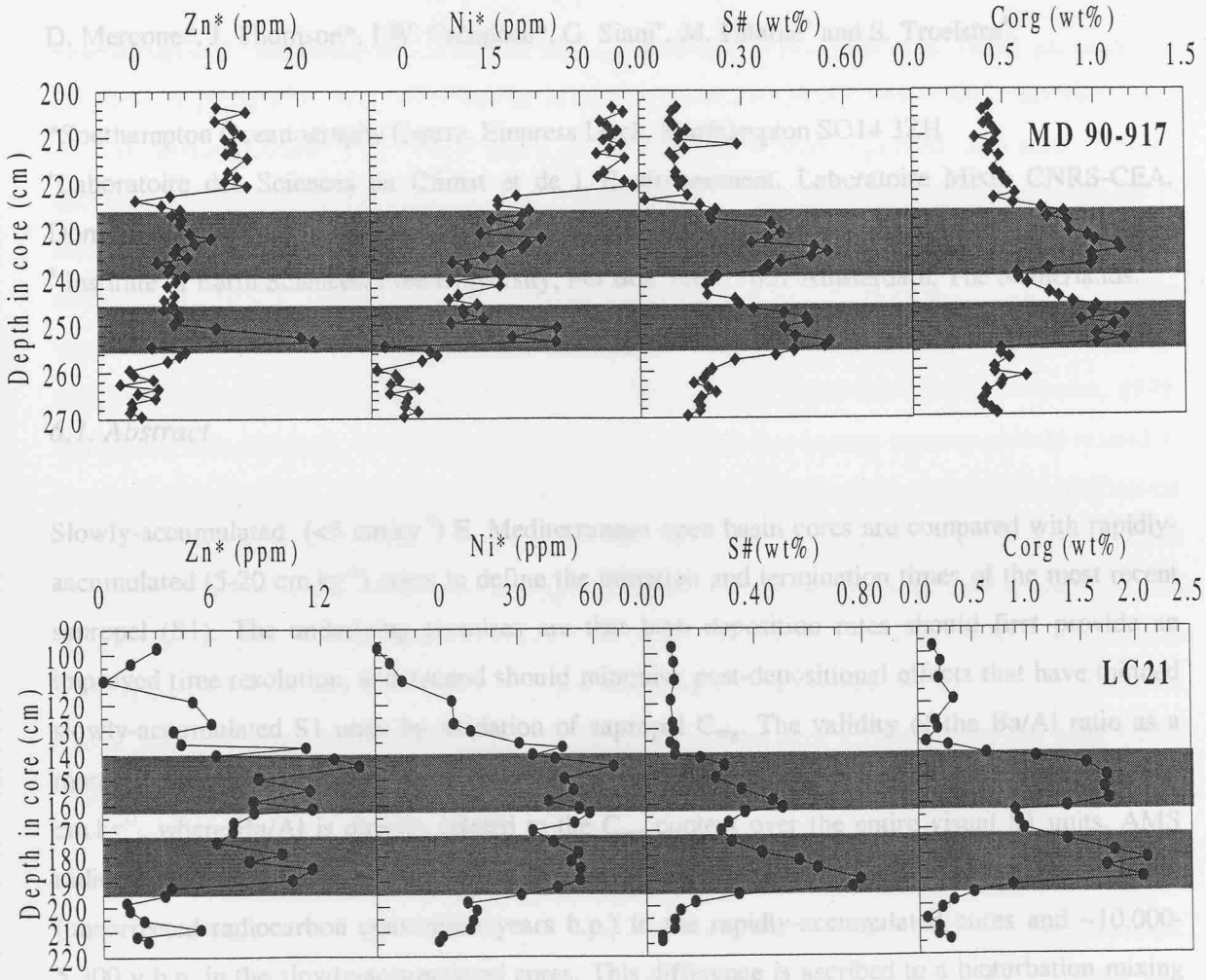

Figure 5.29. Distribution of Zn*, Ni* (ppm), S# (wt%) and Corg (wt%) in MD 90-917 and LC21.

Paper accepted for publication in: Paleoceanography.

Chapter 6:

Duration of S1, the most recent Eastern Mediterranean sapropel, as indicated by AMS radiocarbon and geochemical evidence.

D. Mercone*, J. Thomson*, I.W. Croudace*, G. Siani[+], M. Paterne[+] and S. Troelstra[#].

*Southampton Oceanography Centre, Empress Dock, Southampton SO14 3ZH

[+]Laboratoire des Sciences du Climat et de L'Environnement, Laboratoire Mixte CNRS-CEA, Domaine du CNRS, F-91198 Gif-sur-Yvette, Cedex France.

[#] Institute of Earth Sciences, Free University, PO Box 7161, 1007 Amsterdam, The Netherlands.

6.1. Abstract.

Slowly-accumulated (<5 cm.ky^{-1}) E. Mediterranean open basin cores are compared with rapidly-accumulated (5-20 cm.ky^{-1}) cores to define the initiation and termination times of the most recent sapropel (S1). The underlying premises are that high deposition rates should first provide an improved time resolution, and second should minimise post-depositional effects that have thinned slowly-accumulated S1 units by oxidation of sapropel C_{org}. The validity of the Ba/Al ratio as a more persistent productivity index than C_{org} is confirmed in two S1 units accumulated at >15 cm.ky^{-1}, where Ba/Al is directly related to the C_{org} content over the entire visual S1 units. AMS radiocarbon dating indicates a maximum duration for increased S1 Ba/Al levels from ~9,500-6,000 (uncorrected radiocarbon convention years b.p.) in the rapidly-accumulated cores and ~10,000-5,300 y b.p. in the slowly-accumulated cores. This difference is ascribed to a bioturbation mixing artifact affecting the slower-accumulated cores. By comparison with modern sediment trap Ba/Al versus C_{org} systematics, S1 formation can be explained by either a modest productivity increase or

by improved C_{org} preservation during settling through the water column and at the sea floor. In the two most rapidly-accumulated units, at water depths <1500 m from the Adriatic Sea and the SE Aegean, there is a "saddle" of lower values in both the C_{org} and Ba/Al profiles which makes the visual S1 unit appear as a doublet. This doublet is situated approximately in the middle of the S1 pulse and centered on 7500 radiocarbon yr b.p. Geochemical and micropalaeontological evidence indicates that this intervening period is best interpreted as an episode of increased water column oxygenation at intermediate depth rather than an interruption to sapropel formation, as the Ba/Al index does not fall to the low levels which preceded and post-dated S1. Like other reported Adriatic cores, the Adriatic S1 example has a distinctly shorter duration (8300-6300 radiocarbon y b.p.) than in any other S1 studied, consistent with new deep water affecting sapropel formation and preservation.

6.2. Introduction.

Sharply-defined, dark-coloured units, with high C_{org} contents (>2%, Kidd *et al.* 1978) and high S in the form of pyrite (Calvert, 1983; Passier *et al.* 1996), occur episodically in the otherwise C_{org} - poor E. Mediterranean sedimentary record. Such units are termed sapropels, and their repeated occurrence demonstrates the sensitivity of sedimentation in this topographically-isolated basin to climatic changes (e.g. Emeis *et al.* 1996). There is no agreement on the precise mechanism or sequence of events which leads to sapropel formation, however, principally because of the uncertainty on the relative roles of productivity and preservation in the development of high sediment C_{org} contents (Thunell and Williams, 1989; Calvert, 1983; Calvert and Pedersen, 1992; Bethoux, 1993; Rohling, 1994). Sapropel formation nevertheless always appears closely related to times of planetary N. hemisphere summer insolation maxima and resultant monsoon intensification (Rossignol-Strick *et al.* 1982; Lourens *et al.* 1996). These wet periods are believed to drive enhanced water column stability and perhaps increased surface ocean productivity, and the more isolated deep water column may then develop anoxia (or at least low oxygen levels), which may in turn lead to improved preservation of C_{org}. Improved records of sapropel deposition may constrain cause, effect and timing interpretations, and such records are most accessible for the most recent sapropel (S1; Hieke, 1976) because it is within the radiocarbon dating range.

Geochemical studies of S1 (Higgs *et al.* 1994; Thomson *et al.* 1995, 1999; van Santvoort *et al.* 1996) have revealed that although this unit is <10 ky old, it has already suffered extensive post-depositional alteration which has oxidised C_{org} from the upper reaches of the original S1 unit. This carries implications for micropalaeontological, sedimentological and palaeoenvironmental as well as for geochemical studies, because it means that the true duration of sapropel formation is not

coincident with the visual evidence in the sediments but rather occurs over a longer sediment interval. Thomson *et al.* (1999) proposed that the Ba/Al ratio was a more persistent criterion than colour or C_{org} content for the study of sapropel productivity pulses, and this contention has been borne out in older sapropels (van Santvoort *et al.* 1997). This paper uses a combination of the Ba/Al ratio and AMS radiocarbon data to study the development of S1 in cores from widely-separated E. Mediterranean basin locations, with different accumulation rates and from different water depths.

6.3. Material and methods.

Box and piston cores samples from the various E. Mediterranean localities were obtained from core archives at Free University, Amsterdam, Laboratoire des Sciences du Climat et de L'Environnement, Gif-sur-Yvette and BOSCOR, SOC (Table 6.1; Figure 6.1). Cores were sub-sampled at 1 cm resolution with sufficient sediment taken to give a dry weight of >3g. All samples were freeze-dried, or oven dried at 105°C, then ground and homogenised using a tungsten carbide swing mill. Aluminium, Ba, Mn and S were determined using a Philips PW1400 automatic sequential wavelength dispersive X-ray spectrometer on samples prepared either as pressed powder pellets or as lithium meta-tetraborate fusion discs. Accuracy and precision were ascertained by running the international standard reference material MAG-1 (marine mud); the precision for trace element determination was 5% relative standard deviation (r.s.d), whilst for major element analyses it was typically <1% r.s.d. Organic carbon (C_{org}) and $CaCO_3$ were determined coulometrically via the release of CO_2. Calcium carbonate was determined by the generation of CO_2 evolved by the addition of 10%(v/v) H_3PO_4, and C_{org} by subtraction of the CO_2 evolved from $CaCO_3$ from the CO_2 derived from total sample combustion at 900°C. Precision for both $CaCO_3$ and C_{org} analyses were determined by replicate analysis of an in-house standard (a deep-sea carbonate sediment) at <1% r.s.d. for $CaCO_3$ and <3% r.s.d for C_{org} measurements, respectively.

Planktonic foraminifera >150μm in size were hand-picked for AMS radiocarbon analysis because they have an unequivocal surface ocean source and are the sediment size fraction least liable to post-depositional transport (Troelstra *et al.* 1991). Species differentiation was not attempted because the total sediment sample available (~5 g wet) was often sufficient only to provide the 10-12 mg clean biogenic $CaCO_3$ in the desired size range necessary for a single AMS analysis. Samples were prepared as graphite targets at the NERC Radiocarbon Laboratory and analysed at the Lawrence Livermore National Laboratory AMS Facility (CAMS- analyses), or at the Scottish

Universities Research and Reactor Centre and analysed at the Arizona Radiocarbon Facility (AA- analyses). Further species specific (*Globigerinoides bulloides* or *G. ruber*) AMS radiocarbon analyses were available from LSCE for one core (GifA- analyses, Table 6.2).

6.4. Results and discussion.

Primary production of C_{org} and its preservation in the sediments are separated by remineralisation by oxic or anoxic mechanisms during sinking through the water column and after deposition at the sea floor. Although sapropel S1 is the sediment record of a sustained phase of either or both increased surface ocean productivity and improved C_{org} preservation, it is not yet clear whether the either the start or finish of S1 can be regarded as exactly synchronous across the entire E. Mediterranean basin (Troelstra *et al.* 1991; Fontugne *et al.* 1994; Strohle and Krom, 1997). Vergnaud-Grazzini *et al.* (1986) estimated the duration of S1 at 9000-7000 y from a review of early radiometric radiocarbon analyses. The compilation by Fontugne *et al.* (1994), which included newer AMS radiocarbon data, also returned a modal value of 9000-7000 y, although outlier values in the range 15000-4000 y were encountered. Based on the Ba/Al criterion discussed below and AMS radiocarbon data from deeper water, central basin cores, Thomson *et al.* (1995) proposed that S1 formation lasted until as late as 5300 years. This value has been criticised by Rohling *et al.* (1997) who prefer a duration of 6300-8300 years for S1 on the basis of data from a micropalaeontological, sedimentological and AMS radiocarbon dating investigation of a single Adriatic core.

Sapropel S1 is evident in most cores as a single, dark, C_{org} -rich horizon up to ~10 cm thick. The visual S1 units in certain cores studied are therefore unusually thick, and in some the dark colouration is in two parts (Table 1). "Double" S1 units have been reported before from various E. Mediterranean localities (see listing by Rohling *et al.* 1997), but implicitly or explicitly these have often been ascribed to sedimentological disturbances. High mean accumulation rates can be the result of high surface ocean productivity or land-derived detrital fluxes, but they can also result from downslope redeposition of sediment, or from a current-driven augmentation of accumulation in the form of drift deposits or contourites. Redeposition from turbidites will produce a discontinuous sediment record, while contourite formation may produce continuous but irregular records reflecting the waxing and waning of current strength through time. Sediment redeposition is certainly a common process in the Mediterranean basin, and Stanley *et al.* (1985) estimate that two thirds of the volume of recent basin sediments are affected by downslope mass flow. It is therefore necessary to establish whether or not redeposition has affected the studied cores, and in particular to validate the accumulation records containing double sapropels. This involves assessment of whether either or both sections are of S1 age, whether both dark sections represent

continuous accumulation, and the nature of the central lighter zone. This is achieved by defining S1 in terms of the Ba/Al productivity index rather than C_{org} content or colour and by using multiple AMS radiocarbon ages to confirm that the units are consistently of S1 age.

6.4.1. The productivity records from Ba/Al and C_{org} .

The element Ba is central to the geochemical interpretation of the productivity fluctuations recorded by S1. From the work of Dymond and coworkers (Dymond *et al.* 1992, Dymond and Collier, 1996), it is well established that settling material from surface ocean organic productivity develops a Ba enrichment during its descent through the water column before deposition. At times of high productivity, this flux of biogenic Ba becomes sufficiently large that it may be readily identified against detrital Ba in the sediments through increases in the sediment Ba/Al ratio. Normalisation to Al is necessary because of the dilution effects of $CaCO_3$ content, on the assumption that detrital phases have fairly constant Al and Ba contents which dominate the trace Ba content of $CaCO_3$. Barium has been used in this manner as a palaeoproductivity indicator for many years, but the precise mechanism by which biogenic Ba (Ba_{bio}) is progressively enriched in settling C_{org}, and therefore its quantification, remain elusive (Dymond and Collier, 1996).

In S1 examples previously investigated (Thomson *et al.* 1995; van Santvoort *et al.* 1996, 1997), the presence of high Ba but low C_{org} levels immediately above visual S1 units has been taken as evidence that post-depositional oxidation of S1 has remineralised C_{org} but has not affected biogenic Ba. This pattern is again observed in core T87-26B, where the Ba/Al ratio profile relative to the C_{org} and S profiles (both of which suffer oxidation loss) indicates that ~9 cm of oxidation has occurred (lighter shaded area of Figure 6.2). A corollary of this interpretation from slowly-accumulated S1 Ba/Al and C_{org} profiles is that less-oxidised, and consequently less-altered, examples ought to exist in areas of rapid accumulation, but this has not been demonstrated until now. Cores MD81-LC21 and MD90-917 are the most rapidly accumulated among those studied (15 and 20 $cm.ky^{-1}$, respectively, see below), and these two cores are used to test the prediction of an initial correspondence between the Ba/Al ratio and C_{org} contents in the absence of post-depositional oxidation.

The Ba/Al ratio and C_{org} contents of the dark intervals in MD81-LC21 and MD90-917 are consistently higher than in the enclosing sediments, both profiles have a similar double-peak shape (Figure 6.3), and there is a good correlation between Ba/Al and C_{org} (Figure 6.4). Both the maximum C_{org} and Ba/Al levels in LC21 consistently exceed those of core 90-917, although the slope of the Ba/Al:C_{org} relationship is similar in the two cores (Figure 6.4). Most of the C_{org} values in both cores fail to achieve the >2% Corg criterion proposed by Kidd *et al.* (1978) to define a

sapropel, but this criterion appears to be only an approximate guide to the C_{org} content necessary to develop the dark sapropel colour (Calvert, 1983). In low accumulation rate cores, Thomson *et al.* (1995) and van Santvoort *et al.* (1996) noted that the S1 Ba/Al ratio depth profile is quasi-Gaussian in shape, but the improved resolution provided by the rapid accumulation rates of MD81-LC21 and MD90-917 shows central "saddle" sections in both cores within the Ba/Al and C_{org} profile shapes which is responsible for the double sapropel feature. Although values in these central sections are markedly lower than those in the over- and underlying dark units, they are also markedly higher than the "background" levels which pre- and post-date the S1 productivity pulse where Ba/Al <0.004 and C_{org} <0.5 wt. %. The significance of this central section in these two cores will be discussed further below.

6.4.2. Rates of accumulation from radiocarbon data.

As in most previous AMS radiocarbon dating of sapropel S1, radiocarbon data (Table 6.2) are quoted throughout this paper as unmodified radiocarbon convention ages in years before present (b.p. *i.e.* before 1950 A.D.). On this basis, the quoted ages are neither corrected for the surface ocean reservoir effect, which in the present-day open ocean is ~ 400 y (Bard, 1988; Delebrias, 1989; Siani *et al.* 1999), nor for the time-varying difference between calibrated (dendrochronological) time and radiocarbon convention time, which amounts to +700 to +900 y in the radiocarbon convention time range 5000-9000 y b.p. (Stuiver and Becker, 1993; Kromer and Becker, 1993). As a combined result of these two effects, the marine radiocarbon convention ages used here are expected to underestimate calibrated time by 300-600 y in the marine radiocarbon time range 5000-9000 y b.p. (Stuiver and Braziunas, 1993).

To achieve a common basis with which to compare the different S1 units, a chronology for the sapropel region in each core is derived by fitting a linear regression of marine radiocarbon convention age on depth. In some cores, the radiocarbon data show clearly that whole core rates of accumulation have been irregular through time, and in such cases age values immediately above, within and immediately below the S1 unit are preferred for construction of local floating regressions in the vicinity of the units. The explicit assumption in selective omission of data points is that any redeposition process must introduce sediment with a radiocarbon age older than newly-deposited sediment; and such ages are therefore expected to exceed the regression lines through selected data.

6.4.2.1. Low (< 5cm. ky^{-1}) accumulation rate cores: (i) T87-26B.

Several AMS radiocarbon analyses are available for this box core (Troelstra *et al.* 1991), and the Ba/Al profile (Figure 6.2) was determined to extend the data base for comparison between slowly- and rapidly-accumulated cores. Unlike the remainder of the cores, all the AMS radiocarbon data for T26B were regressed on depth to give a whole core accumulation rate (Figure 6.5a). The accumulation rate for this core (4.3 cm.ky^{-1}) is slower than those for the cores discussed below, but on the same order as those for radiocarbon-dated multicores MC12 and MC07S (3.1 and 2.2 cm.ky^{-1}, respectively) reported by Thomson *et al.* (1995).

6.4.2.2. Low (< 5cm. ky^{-1}) accumulation rate cores: (ii) MDVAL95-02.

This core from the far east of the Mediterranean basin contains a dark visual unit from 28-65 cm, and it was sampled with the expectation that it was a rapidly-accumulated S1 unit. Although the radiocarbon data confirm that the dark unit is entirely of S1 age, however, the progression of radiocarbon age on depth is irregular, and this core is now interpreted as a slowly-accumulated unit with re-deposition of sapropel material with higher Ba/Al values in the centre of the dark unit. Unlike the other cores where re-deposition is inferred, compositional data do not indicate unequivocally the precise depths of the re-deposited section in this core because the redeposited material is also sapropelic. The depositional record is estimated from the extrapolations of the lines between the upper and lower data point pairs as shown (Figure 6.5a). The section from 32-52 cm is then inferred to be redeposited and disregarded in subsequent discussion. Note that the line between the upper two points intercepts the origin on extrapolation (Figure 6.5a). This is probably the least secure interpretation of all the cores studied.

6.4.2.3. Intermediate (5-10 cm.ky^{-1}) accumulation rate cores: (i) MD81-LC25

Based on the Ba/Al criterion, S1 is present in this Herodotus Abyssal Plain piston core from 61-87 cm and 94-100 cm. The intervening section at 87-94 cm is clearly a turbidite on visual and compositional evidence (Figure 6.5b). Several other turbidites deposited before and after S1 are also present in this core, one of which is 1.2 m thick and has its top at 100 cm in core. From the dark colour and mineralogy, both turbidites emplaced during S1 time (turbidites *c* and *d* in the terminology of Reeder *et al.* 1998) have been interpreted to derive from slope failures on the Nile fan (Cita *et al.* 1984; Reeder *et al.* 1998). The regression line (8.9 cm.ky^{-1}) to establish accumulation rate was determined from the upper four radiocarbon analyses in the section with high Ba/Al values, and extrapolated into the section at depths 94-100 cm by subtraction of 7 cm to

account for the presence of the smaller turbidite at 87-94 cm (Figure 6.5b). It was not possible to locate the base of S1in this core, because the pelagic sample at 225 cm underlying the larger turbidite at 100-224 cm had background Ba/Al levels and its radiocarbon age clearly pre-dated S1 (Table 6.2).

6.4.2.4. Rapid (>10 cm. ky^{-1}) accumulation rate cores: (i) MD81-LC21

All the radiocarbon data available for this SE Aegean piston core do not conform to a straight line, indicating that its accumulation rate has been variable in time (Figure 6.5b). Besides containing a double S1 unit, this core contains a thick, grey ash layer from 82-92 cm. This ash was suspected to have been deposited from the explosive eruption of the Santorini/Thera volcano (Hardy and Renfrew, 1990), because of the core location and the ash layer's position above the sapropel. Recent estimates based on AMS radiocarbon data place the Santorini event around 1650±50 B.C. (Guichard *et al.* 1993), and a more precise time of 1627/1628 B.C. has been proposed from dendrochronological investigations (Kuniholm *et al.* 1996). These calibrated times imply a radiocarbon convention age of ~3300-3400 years b.p. (Stuiver and Becker, 1993) for the Santorini explosion, so that the best estimate for the corresponding marine radiocarbon convention age is ~3700-3800 years b.p. The actual radiocarbon determinations 32 cm above and 3 cm below the ash layer in MD81-LC21 are 3370 and 4290 radiocarbon years, respectively, which by interpolation indicates an age of 4210 years for the ash level. This straddling of the probable Santorini age estimate by the data is taken as confirmation that the ash layer in core MD81-LC21 is in fact from Santorini, even though the interpolated layer age is ~450 years older than expected. The effects of bioturbation in the surface sediment mixed layer are expected to have increased the radiocarbon age of surficial sediment blanketed by the ash fall (Trauth *et al.* 1997).

From the eight AMS radiocarbon analyses available for this core, the four analyses spanning the depth range 137-191 cm were selected to estimate a mean accumulation rate of 14.9 cm.ky^{-1} by linear regression (Figure 6.5b). The duration of the light-coloured central section (160-174 cm) by this regression is estimated at 5840-8120 y.

6.4.2.5. Rapid (>10 cm. ky^{-1}) accumulation rate cores: (ii) MD 90-917.

Additional monospecific foraminiferal AMS ages are available from above and below the C_{org} - enriched S1 unit from Siani *et al.* (1999), who found that the the sapropelic sediments accumulated more rapidly than the sediments which precede and post-dated them. Only ages immediately above, in and below the S1 unit from Sianni *et al.* (1999) are included in Table 6.2 and Figure 6.5c.

The regression of all nine AMS radiocarbon analyses within the C_{org} -enriched unit on depth (221-253 cm) yields a sediment accumulation rate of ~19.5 cm.ky^{-1}. This regression estimates the duration of the light-coloured central section (240-245 cm) at 7520-7780 y.

6.4.3. S1 development in slowly-accumulated cores.

The fits to the radiocarbon data derived above allow the Ba/Al records of all cores to be compared directly as a function of time, by conversion of sample depth to radiocarbon convention years with the individual regression equations. When the Ba/Al profiles of cores T87-26B (Troelstra *et al.* 1991; Figure 6.5a), MC07S and MC12 (Thomson *et al.* 1995) are compared as a function of radiocarbon time over 4000-10000 y, a striking agreement is found between the three slowly-accumulated core records (Figure 6.6a). In all cases the increase in productivity indicted by the Ba/Al ratio increase begins at ~10000 years and ends at ~5300 years, considerably longer than the 9000-7000 y interval usually quoted for S1 (Vergnaud-Grazzini *et al.* 1985; Fontugne *et al.* 1994).

6.4.4. S1 development in rapidly-accumulated cores.

When the Ba/Al indexes of the cores accumulated at 10-20 cm.ky^{-1} and of MDVAL9502 are plotted as a function of radiocarbon time, a less coherent picture of the S1 high productivity episode emerges than was seen in the slowly-accumulated cores (Figure 6.6b). The initiation of high Ba/Al ratio values and hence S1 formation is clearly underway in all cores by 9000 years except for Adriatic core 90-917. High Ba/Al values in this latter core start later and end earlier (8200-6300 years) so that they are present over a much more restricted time interval than in any other core. The high Ba/Al values of the S1 pulse are completed by 6000 y in all the rapidly-accumulated cores except MD81-LC21, several hundred years earlier than the end of high productivity indicated in the slowly-accumulated cores. Few radiocarbon ages <6000 years have been reported previously for C_{org} -rich S1 material (Perissoratis and Piper, 1992), but the value of 5590±60 years at the C_{org}-enriched 137-138 cm interval in core MD81-LC21 is on-trend with the remainder of the S1 data in this core (Figure 6.5b).

At face value, the differences in time between the slowly- and rapidly-accumulated Ba/Al core profiles might represent a slightly earlier start and later end to sapropel formation in the slowly-accumulated cores. As the three box cores are generally from greater water depths than the rapidly-accumulated cores (Table 6.1), it is conceivable that water column anoxia might have been developed earlier and maintained longer the deeper parts of the basin. This is contrary to the

arguments of Strohle and Krom (1997) who envisaged S1 formation occurring first in a mid-water oxygen minimum zone which subsequently expanded downwards. The Herodotus Abyssal Plain core MD81-LC25 is critical to the water depth argument because it is from the deepest water depth of the available cores. High productivity in that core begins before 9000 y b.p. and is completed by 6100 y b.p. (Figure 6.6b), so that it does not appear as if the off-sets in S1 time can be related simply to water depth.

A different possibility is that the difference between the slowly- and rapidly-accumulated cores is a function of bioturbative mixing affecting both the AMS radiocarbon ages and the Ba/Al ratio values before and after sapropel formation in the slowly-accumulated cores. Thomson *et al.* (1995) have demonstrated by means of $^{210}Pb_{excess}$ distributions that the present-day sediment surface mixed layer (SML) in deep basin cores is <3 cm deep on the 100 year time-scale, a low value in comparison with most open ocean deep-sea cores (9.8±4.5 cm according to Boudreau 1994; 1998), and corresponding to a mixing of up to 1000 years of deposition in these slowly-accumulated sediments. Thin SMLs are most likely a consequence of a low flux of C_{org} reaching the present-day sea floor in the Eastern Mediterrranean, because this is what is observed in oligotrophic regions elsewhere (Trauth *et al.* 1997; Legeleux *et al.* 1994). Bioturbation may have been more intense immediately before and after S1 formation when bottom water oxygen content was still finite but the surficial sediments had high C_{org} contents. On this view, the chronology from the rapidly-accumulated cores must be preferred over those from the slowly-accumulated cores, because the former are less sensitive to bioturbation artefacts. Our best estimate for the duration of S1 based on the Ba/Al ratio is therefore 9500-6000 radiocarbon years (Figure 6.7). Rossignol-Strick (1995) proposed a duration of 9000-6000 y for the period of high summer moisture and mild winters around the E. Mediterranean, based on a reinterpretation of several marine and land pollen records.

6.4.5. Productivity versus preservation?

The magnitudes of the S1 Ba/Al values in the slowly-accumulated cores are consistently higher than those in the rapidly-accumulated cores (Figures 6.5 and 6.6). Given that Ba/Al has been shown above to be related to initial C_{org}, and that the slower-accumulated cores are from deeper water depths, this Ba/Al observation is reminiscent of the report by Murat *et al.* (1990) that maximum S1 C_{org} contents consistently and near-linearly increase with water depth, from 1% at 1000m to 3% at 3000m. A similar increase of maximum S1 Ba/Al occurs with water depth (Figure 6.7). According to Dymond and Collier (1996), sediment trap investigations show that Ba_{bio}/ C_{org} ratios increase systematically with water depth, but the ratio is largely (75%) set at depths <1200 m with the additional 25% added between 1200-3800 m. Recognising this fact, the Ba/Al data for all

cores may be modelled to a first approximation as a constant biogenic Ba (Ba_{bio}) flux of 1000-1500 $\mu g.cm^{-2}.\ ky^{-1}$ superimposed on a variable background flux with a constant Al content of 49000 ppm (average Al content of all data in all cores), a Ba/Al weight ratio of 0.0035 (the background value suggested by Figure 6.5a-c) and a dry bulk density of 0.5 $g.cm^{-3}$ (Figure 6.9). It may be significant that the deepest and shallowest cores studied fall above and below the model lines, respectively, compared with the remainder of the cores, consistent with the approximation of a constant Ba_{bio} flux (Figure 6.9). It may be concluded that any effect of water depth to Ba/Al or C_{org} content is secondary to flux dilution, *i.e.* high Ba/Al or C_{org} values in S1 are primarily a result of slower sediment accumulation rates and consequently less dilution in deeper, more remote parts of the basin.

The background Ba/Al ratio of 0.0035 adopted in Figure 6.9 will exceed the detrital Ba/Al ratio alone, because it is estimated from conditions which preceded and post-dated S1, and so will presumably include a small biogenic Ba contribution from these times. The constant Ba_{bio} flux applied to S1 times is therefore the excess productivity of sapropel times compared with the productivity levels which pre- and post-dated S1. From modern sediment trap studies at 1500 m water depth, 1000-1500 $\mu g.cm^{-2}.ky^{-1}$ is a modest Ba_{bio} flux which would be expected to be associated with a settling flux of ~0.05-0.075 $gC_{org}.cm^{-2}.ky^{-1}$(Dymond and Collier, 1996). By means of the relationship established by Francois *et al.* (1995) from empirical world ocean systematics on Ba_{bio}/ C_{org} in settling particulate matter and the remineralisation of C_{org} as functions of water depth, a Ba_{bio} flux of 1000-1500 $\mu g.cm^{-2}.ky^{-1}$ corresponds to a somewhat higher additional export production of 0.21-0.38 $gC_{org}.\ cm^{-2}.ky^{-1}$ in sapropel times over non-sapropel times. Thus, if the relationships between C_{org} and Ba_{bio} and the remineralisation kinetics of C_{org} established in the modern open (oxidised) ocean hold good for the Eastern Mediterranean during sapropel times (when water column oxygen levels were likely to be depressed), the S1 Ba data are consistent with only a very modest increase in export production and enhanced preservation is implied. Calvert (1983) contended that it was not possible to produce a sapropel with a C_{org} content of more than a few per cent without a productivity increase, but the Ba/Al evidence is that in the case of S1 improved preservation between primary production and burial in the sediments would be sufficient. It may well be that higher productivity is required to produce sapropel contents as high as 20% observed by Calvert (1983) in some older sapropels,.

If the Ba/Al data from sapropel S1 requires only a slight increase in export production, the question may be posed as to why the present-day productivity produces sediments of such low C_{org} and Ba/Al content. Calvert and Karlin (1998) explained the changing C_{org} content of Black Sea sediments over time by changes in the fluxes of other sedimentary components ($CaCO_3$ and clay),

an explanation similar to that advanced for variations in Ba/Al magnitude within different S1 sapropels accumulated at different rates. This explanation is unlikely for S1, because changes in overall accumulation rate in many of these cores over the past 10 ky is not dramatic, *e.g.* a single rate is applicable to all of core T26B (Figure 6.5a).

The most significant difference between the modern ocean and the E. Mediterranean in sapropel times is likely to have been the lower (or absent) water column oxygen levels in sapropel times. Estimates of primary productivity in the E. Mediterranean basin from recent satellite data show a decrease in primary productivity from ~ 100 $gC.m^{-2}.y^{-1}$ at the Adriatic Sea in the NE to <65 $g.m^{-2}.y^{-1}$ in the South Levantine basin in the SE (Plate 4 of Antoine *et al.* 1995). Such values are similar or somewhat higher than those measured experimentally (e.g. Bethoux, 1989; Azov, 1991). Dugdale and Wilkerson (1988) adopt a mean primary productivity value of 26 $g.m^{-2}.y^{-1}$ for the entire E. Mediterranean basin, and Bethoux (1989; 1993) calculates from nutrient and oxygen budgets that the resultant mean export productivity is ~12 $g.m^{-2}.y^{-1}$. This level of export activity is producing sediments with a C_{org} content below the SML of 0.25-0.5% (Figure 6.2). The flux of C_{org} reaching the sea floor is low and the C_{org} content of the sediments is further remineralised in the SML (Figure 2; Jung *et al.* 1997). Present-day productivity levels, together with the high O_2 utilisation rates associated with the warm (13°C), well-oxygenated water column (Schlitzer *et al.* 1991) result in rapid remineralisation of C_{org} and low C_{org} sediments which are typical of oligotrophic conditions (Trauth *et al.* 1997; Legeleux *et al.* 1994).

6.4.6. Reventilation of the Eastern Mediterranean during S1 times?

The differences in the timing of the S1 records above might be a function a well-organised regional patchiness in surface ocean productivity, or they may be consequences of different oxygenation histories of the water column in different parts of the basin. Two salient features of the Ba/Al profiles as a function of time are first, the saddle in the Ba/Al ratio (corresponding to the double sapropel phenomenon) in the shallow depth cores MD81-LC21 (1522 m), MD90-917 (1000 m) and to a lesser extent in MC12 (2211 m). The minimum Ba/Al values are centered at 7500 y b.p. in all three cores. There is no such feature at this time in any other core, which are either from deeper water depths (87-26B, MC07S and MC12), or from the southern half of the E. Mediterranean basin (LC25), or from shallower water depth in the far east of the basin (MDVAL9502). Second, the duration of the enhanced Ba/Al pulse in MD90-917 is markedly shorter than in any of the other cores.

Double S1 sapropel units have been reported frequently in the southern Adriatic Sea (van Straaten,

1966, 1972; Fontugne *et al.* 1989) and the northern Aegean Sea (Perissoratis and Piper, 1992). Rohling *et al.* (1997) interpreted the central section of one Adriatic core (core IN 68-9, 1234m) as a "200 year interruption to sapropel deposition". Despite the visual evidence of two separated dark units, however, the geochemical evidence is that the central section with lower Ba/Al values does not record a return to conditions as oligotrophic as those which preceded and followed sapropel deposition (Figures 6.3).

Estimates of total S1 duration from the Adriatic are shorter (e.g. 8300-6300 y; Jorissen *et al.* 1993; Rohling *et al.* 1997) than those from the Aegean (e.g. 9200-6400 y; Perissoratis and Piper, 1992). The thermohaline circulation of the Eastern Mediterranean is complex, but is driven by the formation of new deep water by increases in salinity or by cooling, or both. At present the well-ventilated condition of E. Mediterranean deep water (>1000m) is maintained by a seasonal (winter) down-welling of denser, oxygenated water in the north of the basin from sources in the Adriatic and Aegean Seas (Wust, 1961; Malanotte-Rizzoli and Hecht, 1988; Schlitzer *et al.* 1991; Bethoux, 1993; Roether *et al.* 1996). Times of sapropel formation are correlated convincingly with maxima in northern hemisphere insolation which produces monsoon conditions and high run-off into the E. Mediterranean. The resultant wetter and warmer conditions are believed to cause enhanced water column stabilisation and hence limited winter reventilation during times of sapropel formation (Rossignol-Strick *et al.* 1984; Mangini and Schlosser, 1986; Bethoux, 1993; Rohling 1994).

If the S1 sapropel has an unusually short duration in the Adriatic Sea area compared with the remainder of the basin, it appears likely that re-ventilation may not have been shut down completely during sapropel formation, but rather may have been intermittent or present at a reduced level which was insufficient to oxygenate the deep water column of the entire basin. This is opposite to the contention of Fontugne *et al.* (1989) who interpret a very late resumption of reventilation from what may be a later diagenetic feature. It is implicit in this explanation that oxic deep waters will cause more remineralisation of the C_{org} flux through the water column and on the sea floor, contrary to the interpretation of Calvert and coworkers (Calvert, 1983; Calvert and Pedersen, 1992). By extension of this explanation, the double sapropel observed in both the Adriatic and Aegean Seas may represent an episode of improved ventilation in both basins during S1 times. This improved deep water re-ventilation is centred at 7500 y marine radiocarbon years b.p., which corresponds to a calibrated time of ~7900 cal y B.P., although it begins a few hundred years earlier (Figure 6.6a-b). A Holocene excursion in climate close to this time is seen in many paleoclimatic records from diverse marine and terrestrial localities at 8200 B.P. (Alley *et al.* 1997). The cause of this short interval remains unknown, but it shares cold, dry and windy characteristics with the last glacial and Younger Dryas periods, although all palaeoproxy parameters are less intense during the 8.2 ky event. It may be therefore that this cooler and less humid interval enables

some increase in reventilation during the S1 period when reventilation has been much reduced by monsoonal conditions. Specifically, Rossignol-Strick (1995) noted a brief interruption of dry/cold conditions at ~8000 y in pollen records during the moist/warm 9000-6000 y period.

Thomson *et al.* (1995) have argued that a prominent Mn peak coincident with the top of many S1 Ba/Al profiles is evidence of bottom water reventilation at the end of S1 formation. In slowly-accumulated S1 examples, a second underlying Mn peak occurs within the high Ba/Al region which marks the extent of post-depositional oxidation of S1 (van Santvoort *et al.* 1996). A different (small) secondary Mn peak is present at the base of the Ba/Al and C_{org} saddle in the two cores with well-developed double sapropels (Figure 6.10), but there is no corresponding feature in any other core. In a similar manner to the argument that (larger) Mn peaks mark a return to higher bottom water oxygen levels, these smaller Mn peaks in cores MD81-LC21 and MD90-917 are consistent with the argument that the saddle feature represents a short period of improved deep water oxygenation within S1 times The Mn oxyhydroxide forming these small Mn peaks must now be metastable in anoxic conditions, so that they probably had higher Mn contents on formation. This contention of a temporarily-increased bottom water oxygen content in the Ba/Al saddle section compared with the remainder of the S1 episode is also compellingly substantiated by Rohling *et al.* (1997). These workers found that while the two lobes of S1 with high C_{org} contents in another Adriatic core were barren or had low benthic foraminiferan contents, the intervening saddle section contained a re-establishment of benthic foraminifera which necessitated some level of bottom water reoxygenation in the middle of S1.

6.5. Conclusions.

A re-evaluation of the duration of the most recent Mediterranean sapropel has been made, using AMS radiocarbon dating and the Ba/Al productivity index to define the timings of S1 formation. The most rapidly-accumulated cores (>10 $cm.ky^{-1}$) are demonstrably unaffected by substantial post-depositional oxidation because the Ba/Al index correlates with C_{org} through the S1 units. Low accumulation rate (< 5 $cm.ky^{-1}$) cores consistently indicate a duration between 10,000 and 5300 uncorrected marine radiocarbon convention years b.p. Generally the more rapidly-accumulated cores indicate a somewhat shorter duration between ~9500 and 6000 y. b.p. for S1. This difference is interpreted as an artifact of bioturbation on either or both the Ba/Al index and the dated foraminifera in the slowly-accumulated cores, rather than a water depth effect.

The Adriatic Sea core has a shorter S1 duration than any other core, which is interpreted to mean that, while reventilation was much reduced during the S1 episode, it may not have been fully or

continuously shut down. In this core and another rapidly-accumulated, shallow water depth (1000-2200 m) core from the north of the basin, a decrease in C_{org} and Ba_{bio} (still well in excess of present-day productivity levels) occurred just before 7500 radiocarbon y. b.p. It is suggested that this is a regional effect, caused by a temporary increase in intermediate-depth water ventilation in the Adriatic Sea in the north of the basin, during the brief interval of global cooling in the middle of S1 time.

6.6. Acknowledgments.

Samples for this work were obtained from the core repositories at Free University of Amsterdam, Southampton Oceanography Centre (BOSCOR) and Gif-sur-Yvette. IFRTP is gratefully acknowledged for the recovery of many of the cores studied from their vessel *Marion Dufresne*. Twenty radiocarbon analyses were undertaken by the NERC Radiocarbon Laboratory through allocation 674/1296. This work was partly supported by the EU Marine Science and Technology SAP (MAS3-CT97-0137) and CLIVAMP (MAS3-CT95-0043) programmes.

Figure Captions.

Figure 6.1. Map showing the E. Mediterranean core positions.

Figure 6.2. Profiles of C_{org}, S (weight %) and Ba/Al (weight) ratio (right-hand scale) in the slowly-accumulated core T87-26B (Troelstra *et al.* 1991). The upper portion of the original S1 inferred to have been oxidised is shown in lighter shading, while the residual C_{org} -rich unit is indicated by darker shading. Similar profiles have been described previously by Thomson *et al.* (1995) and van Santvoort *et al.* (1996).

Figure 6.3. Profiles of C_{org} (weight %) content (open symbols; right-hand scales) and Ba/Al (weight) ratio (filled symbols; left-hand scales) as a function of depth in the rapidly-accumulated cores MD81-LC21 (left panel) and MD90-917 (right panel). Note that there is a good coincidence between the Ba/Al and C_{org} profiles shapes in these cases, unlike the case in Figure 6.2.

Figure 6.4. Correlations between the Ba/Al and C_{org} data for the cores MD81-LC21 (filled circles) and MD90-917 (open squares) displayed in Figure 6.3. The lines shown are regressions of Ba/Al on C_{org} for each core.

Figure 6.5a. Uncorrected radiocarbon convention ages for >150 μm planktonic foraminifera fractions and Ba/Al ratio as a function of depth in cores T87-26B and MDVAL 95-02.The shaded area in core MD9502 is inferred to be redeposited sediment of some kind, and data from this section are omitted to form Figure 6.6b. The lines are regressions of radiocarbon age on depth which yield the accumulation rates shown.

Figure 6.5b. Uncorrected radiocarbon convention ages for >150 μm planktonic foraminifera fractions and Ba/Al ratio as a function of depth in cores LC21 and LC 25. The shaded area in core LC25 is a small turbidite, and data from this section is omitted to form Figure 6.6b. The lines are regressions of radiocarbon age on depth which yield the accumulation rates shown. In both cores certain data points have been omitted from the regressions and the selected data points are circled.

Figure 6.5c. Uncorrected radiocarbon convention ages for >150 μm planktonic foraminifera fractions and Ba/Al ratio as a function of depth in core MD90-917. The line is the regression of radiocarbon age on depth over the depth range 221-253 cm only to derive the accumulation rate.

Figure 6.6a. Ba/Al ratio as a function of radiocarbon time (uncorrected convention years) in

slowly-accumulated cores MC12, MC07 and T87-26B.

Figure 6.6b. Ba/Al ratio as a function of radiocarbon time (uncorrected convention years) in slowly-accumulated core MD9502 and rapidly-accumulated cores LC21, LC25 and 90-917.

Figure 6.7. Start and finish times of the S1 sapropel as represented by times of increase and decrease of the Ba/Al weight ratio of the studied cores (Figures 6.6a-b) as a function of water depth. The arrows show the expected direction in time of artifacts induced by bioturbation.

Figure 6.8. Maximum Ba/Al weight ratio (filled symbols) and maximum C_{org} content (weight %; open symbols) values of the S1 units in the studied cores as a function of water depth. The lines drawn are regressions of Ba/Al (solid) and C_{org} (dashed) on water depth. This figure is similar to the presentation for maximum S1 C_{org} by Murat *et al.* (1991).

Figure 6.9. Model calculation of the results of constant Ba_{bio} fluxes (500, 1000, 1500 and 2000 ($g.cm^{-2}.ky^{-1}$) superimposed on a variable sediment accumulation which has a constant Al content of 49000 ppm, Ba/Al weight ratio of 0.0035, and density of 0.5 $g.cm^{-3}$. The core data are the means and standard deviations of the increased Ba/Al contents which define S1 in Figure 6.5.

Figure 6.10. Mn/Al (continuous line) and Ba/Al (dotted line) ratio profiles versus depth in cores LC21 and 90-917. Note the logarithmic scale for Mn/Al in core 90-917. In each case a large Mn peak marks the end of high Ba/Al values and the end of S1, but a small Mn peak (arrowed) also occurs in the Ba/Al saddle section, consistent with some degree of oxygenation in the water column at that time. These smaller peaks are expected to be composed of MnO_x, and therefore to be metastable in reducing conditions at the present time and to have been larger in the past.

6.7. References.

Alley, R.B., Mayewski, P.A., Sowers, T., Stuiver, M., Taylor, K.C. and Clark, P.U. (1997) Holocene climatic instability: A prominent, widespread event at 8200 yr ago. *Geology*, **25**, 483-486.

Antoine, D., Morel, A. and Andre, J.-M. (1995). Algal pigment distribution and primary production in the eastern Mediterranean as derived from coastal zone color scanner observations. *J. Geophys. Res.* **100,** 16193-16209.

Azov, Y. (1991). Eastern Mediterranean - a marine desert? *Marine Pollution Bulletin* **23**, 225-232.

Bard, E. (1988). Correction of accelerator mass spectrometry ^{14}C ages measured in planktonic foraminifera: Paleoceanographic implications. *Paleoceanography,* **3,** 635-645.

Bethoux, J.-P. (1989). Oxygen consumption, new production, vertical advection and environmental evolution in the Mediterranean Sea. *Deep-Sea Res.* **36**, 769-781.

Bethoux, J.-P. (1993). Mediterranean sapropel formation, dynamic and climatic viewpoints. *Oceanologica Acta,* **16,** 127-133.

Boudreau, B.P. (1994). Is burial velocity a master parameter for bioturbation? *Geochimica et Cosmochimica Acta,* **58**, 1243-1249.

Boudreau, B.P. (1998). Mean mixed depth of sediments: The wherefore and the why. *Limnology and Oceanography,* **43,** 524-526.

Calvert, S.E. (1983) Geochemistry of Pleistocene sapropels and associated sediments from the Eastern Mediterranean. *Oceanologica Acta,* **6**, 255-267.

Calvert, S.E. and Pedersen, T.F. (1992) Organic carbon accumulation and preservation in marine sediments: How important is anoxia? In *"Productivity, Accumulation and Preservation of Organic Matter in Recent and Ancient Sediments."* (eds. J.K. Whelan and J.W. Farrington) Columbia Univ. Press, New York, pp 231-263.

Calvert, S.E. and Karlin, R.E. (1998) Organic carbon accumulation in the Holocene sapropel of the Black Sea. *Geology*, **26**, 107-110.

Canfield, D.E. (1994). Factors influencing organic carbon preservation in marine sediments. *Chemical Geology*, **114,** 315-329.

Cita, M.B., Beghi, C., Camerlenghi, A., Kastens, K.A., McCoy, F.W., Nosetto, A., Parisis, E., Scolari, F. and Tomadin, L. (1984). Turbidites and megaturbidites from the Herodotus Abyssal Plian (Eastern Mediterranean) unrelated to seismic events. *Mar. Geol.* **55,** 79-101.

Delibrias, G. (1989). Carbon 14. In *Nuclear Methods of Dating*, (Eds. E. Roth and B. Poty), Kluwer, pp. 399-436.

Demaison, G.J. and Moore, G.T. (1980) Anoxic environments and oil source bed genesis. *Bulletin of the American Association of Petroleum Geologists* **64,** 1179-1209.

Dugdale, R.C. and Wilkerson, F.P. (1988). Nutrient sources and primary production in the Eastern Mediterranean. In *Oceanographie pelagique mediteraneenne*, (Eds. H.J Minas and P. Nival), Oceanologica Acta Spec. Vol. no. 9, 179-184.

Dymond, J. and Collier, R. (1996). Particulate barium fluxes and their relationships to biological productivity. *Deep-Sea Research, II,* **43,** 1283-1308.

Dymond, J., Suess, E. and Lyle, M. (1992) Barium in deep-sea sediment: A geochemical proxy for paleoproductivity. *Paleoceanography,* **7,** 163-181.

Emeis, K.-C., and the Shipboard Scientific Party, (1996). Paleoceanography and sapropel introduction. *Proceedings of the Ocean Drilling Program, Initial Reports,* **160,** 21-28.

Fontugne, M.R., Paterne, M., Calvert, S.E., Murat, A., Guichard, F. and Arnold, M. (1989). Adriatic deep water formation during the Holocene: Implication for the reoxygenation of the deep eastern Mediterranean. *Paleoceanography,* **4,** 199-206.

Fontugne, M., Arnold, M., Labeyrie, L., Paterne, M., Calvert, S.E. and Duplessey, J.-C. (1994). Paleoenvironment, sapropel chronology and Nile River discharge during the last 20,000 years as indicated by deep-sea sediment records in the eastern Mediterranean. In *Late Quaternary Chronology and Paaleoclimates of the Eastern Mediterranean*, (Eds. O. Bar-Yosef and R.S. Kra), RADIOCARBON, pp.75-88.

Francois, R., Honjo, S., Manganini, S.J. and Ravizza, G.E. (1995). Biogenic barium fluxes to the deep sea: Implications for paleoproductivity reconstruction. Global Biogechemical Cycles, 9, 289-303.

Guichard, F., Carey, S., Arthur, M.A., Sigurdsson, H. and Arnold, M. (1993). Tephra from the Minoan eruption of Santorini in sediments of the Black Sea. *Nature,* **363,** 610-612.

Hardy, D.A. and Renfrew, A.C. eds. (1990). *Thera and the Aegean World III*, Thera Fdn., London.

Hieke, W. (1976). Problems of Eastern Mediterranean Late Quaternary stratigraphy - a critical evaluation of literature. *Meteor Forschungsergeb., Reihe C,* **24,** 68-88.

Higgs, N.C., Thomson, J., Wilson, T.R.S. and Croudace, I.W.(1994). Modification and complete removal of eastern Mediterranean sapropels by postdepositional oxidation. *Geology*, **22,** 423-426.

Jorissen, F.J., Asioli, A., Borsetti, A.M., Capotiondi, L., de Visser, J.P., Hilgen, F.J., Rohling, E.J., van der Borg, K., Vergnaud Grazzini, C. and Zachariasse, W.J. (1993) Late Quaternary central Mediterranean biochronology. *Mar. Micropaleontol.* **21,** 169-189.

Jung, M., Ilmbeger, J., Mangini, A. and Emeis, K.-C. (1997). Why some Mediterranean sapropels survived burn-down (and others did not). *Marine Geology,* **141,** 51-60.

Kidd, R.B., Cita, M.B. and Ryan, W.B.F. (1978). Stratigraphy of eastern Mediterranean sapropel sequences recovered during DSDP Leg42A and their paleoenvironmental significance. *Initial Reports of the Deep Sea Drilling Project,* **Vol. 42A,** 421-443.

Kromer, B. and Becker, B. (1993). German oak and pine calibration, 7200-9439 BC. *Radiocarbon,* **35,** 125-135.

Kuniholm, P.I., Kromer, B., Manning, S.W., Newton, M., Latini, C.E. and Bruce, M.J. (1996) Anatolian tree rings and the absolute chronology of the eastern Mediterranean, 2200-718 BC. *Nature,* **381,** 780-783.

Legeleux, F., Reyss, J.-L and Schmidt, S. (1994) Particle mixing rates in sediments of the northeast tropical Atlantic: Evidence from $^{210}Pb_{xs}$, ^{137}Cs, $^{228}Th_{xs}$ and $^{234}Th_{xs}$ downcore distributions. *Earth Planet. Sci. Lett.* **128,** 545-562.

Lourens, L.J., Antonarakou, A., Hilgen, F.J., van Hoof, A.A.M., Vergnaud-Grazzini, C. and Zachariasse, W.J. (1996). Evalaution of the Plio-Pleistocene astronomical timescale. *Paleoceanography,* **11,** 391-

Mangini, A. and Schlosser, P. (1986). The formation of Eastern Mediterranean sapropels. *Mar. Geol.* **72,** 115-124.

Malanotte-Rizzoli, P. and Hecht, A. (1988). Large-scale properties of the Eastern Mediterranean: a review. *Oceanologica Acta,* **11,** 323-335.

Murat, A.R., Got, G., Cauwet, G. and Buscail, R. (1990). Facteurs de la variabilite du taux de carbone organique du sapropele holocene de la Mediterranee orientale. *Rapp. P.-v. Reun. Commn. int. Explor. scient. Mer medit.,* **32,** 45.

Passier, H.F., Middelburg, J.J., van Os, B.J.H. and de Lange, G.J. (1996). Diagenetic pyritisation under eastern Mediterranean sapropels caused by downward sulfide diffusion. *Geochim. Cosmochim. Acta,* **60,** 751-763.

Perissoratis, C. and Piper, D.J.W. (1992). Age, regional variation, and shallowest occurrence of S1 sapropel in the Northern Aegean Sea. *Geo-Marine Lett.* **12,** 49-53.

Reeder, M., Rothwell, R.G., Stow, D.A.V., Kahler, G. and Kenyon, N.H. (1998). Turbidite flux, architecture and chemostratigraphy of the Herodotus Basin, Levantine Sea, SE Mediterranean. In *Geological Processes on Continental Margins: Sedimentation, Mass-Wasting and Stability.* (Eds. M.S. Stoker, D. Evans and A. Cramp), Geol. Soc. Lond. Spec. Publ. 129, 19-41.

Roether, W., Manca, B.B., Klein, B., Bregant, D., Georgeopoulos, D., Beitzel, V., Kovacevic, V. and Luchetta, A. (1996). Recent changes in Eastern Mediterranean deep waters. *Science,* **271,** 333-335.

Rohling, E.J. (1994). Review and new aspects concerning the formation of eastern Mediterranean sapropels. *Mar. Geol.* **122,** 1-28.

Rohling, E.J., Jorissen, F.J. and de Stigter, H.C. (1997). 200 year interruption of Holocene sapropel formation in the Adriatic Sea. *J. Micropal.* **16,** 97-108.

Rossignol-Strick, M. (1995). Sea-land correlation of pollen records in the Eastern Mediterranean

for the glacial-interglacial transition: biostratigraphy versus radiometric time-scale. *Quaternary Science Reviews*, **14,** 893-915.

Rossignol-Strick, M., Nesteroff, W., Olive, P. and Vergnaud-Grazzini, C. (1982). After the deluge: Mediterranean stagnation and sapropel formation. *Nature,* **295,** 105-110.

Schlitzer, R., Roether, W., Oster, H., Junghans, H-G., Hausmann, M., Johannsen, H. and Michelato, A. (1991). Chlorofluoromethane and oxygen in the eastern Mediterranean. *Deep-Sea Research,* **38A,** 1531-1551.

Siani, G. *et al.* Radiocarbon (submitted 1999).

Stanley, D.J. (1985) Mud redeposition and problems of assessing microfossil, isotopic and radiocarbon data in the Mediterranean. *Mar. Geol.,* **62,** 381-389.

Stuiver, M. and Becker, B. (1993). High-precision decadal calibration of the radiocarbon time scale, AD 1950-6000 BC. *Radiocarbon,* **35,** 35-65.

Stuiver, M. and Braziunas, T.F. (1993). Modeling atmospheric ^{14}C influences and ^{14}C ages of marine samples to 10,000 BC. *Radiocarbon,* **35,** 137-189.

Strohle, K. and Krom, M.D. (1997). Evidence for the evolution of an oxygen minimum layer at the beginning of S-1 sapropel deposition in the eastern Mediterranean. *Mar. Geol.* **140,** 231-236.

Thomson, J., Higgs, N.C., Wilson, T.R.S., Croudace, I.W., De Lange, G.J. and van Santvoort, P.J.M. (1995). Redistribution and geochemical behaviour of redox-sensitive elements around S1, the most recent eastern Mediterranean sapropel. *Geochim. Cosmochim. Acta,* **59,** 3487-3501.

Thomson, J., Mercone, D., de Lange G.J. and van Santvoort, P.J.M. (1999). Review of recent advances in the interpretation of Eastern Mediterranean sapropel S1 from geochemical evidence. *Mar. Geol.* **153,** 77-89.

Trauth, M.H., Sarnthein, M. and Arnold, M. (1997). Bioturbational mixing depth and carbon flux at the sea floor. *Palaeoceanography,* **12,** 517-526.

Troelstra, S.R., Ganssen, G.M., van der Borg, K. and de Jong, A.F.M. (1991). A Late Quaternary stratigraphic framework for Eastern Mediterranean sapropel S1 based on AMS 14C dates and

stable oxygen isotopes. *Radiocarbon,* **33,** 15-21.

Thunell, R.C. and Williams, D.F. (1989). Glacial-Holocene salinity changes in the Mediterranean sea: hydrographic and depositional effects. *Nature,* **338,** 493-496.

Turekian, K.K. and Wedepohl, K. H. (1961). Distribution of the elements in some major units of the Earth's crust. *Geol. Soc. Amer. Bull.* **72,** 175-192.

van Santvoort , P.J.M., De Lange, G.J., Thomson, J., Cussen, H., Wilson, T.R.S., Krom, M.D. and Strohle, K. (1996). Active post-depositional oxidation of the most recent sapropel (S1) in sediments of the eastern Mediterranean Sea. *Geochim. Cosmochim. Acta,* **60,** 4007-4024.

van Santvoort, P.J.M., De Lange, G.J., Langereis, C.G., Dekkers, M.J. and Paterne, M. (1997). Geochemical and palaeomagnetic evidence for the occurrence of "missing" sapropels in eastern Mediterranean sediments. *Paleoceanography,* **12,** 773-786.

van Straaten, L.M.J.U. (1972). Holocene stages of oxygen depletion in deep waters of the Adsriatic Sea. In *The Mediterranean Sea*, (Ed. D.J. Stanley), Hutchinson and Ross, Stroudsburg, pp 631-643.

Vergnaud Grazzini, C., Devaux, M. and Znaidi, J. (1986) Stable isotope "anomalies" in Mediterranean Pleistocene records. *Marine Micropaleontology* **10,** 35-69.

Wust, G. (1961). On the vertical circulation of the Mediterranean Sea. *J. Geophys. Res.* **66,** 3261-3271.

Core	Latitude °N	Longitude °E	Water Depth (m)	S1 coloration in core (cm)	S1 accumulation rate cm kyr^{-1}	Mean Ba/Al in S1	σ Ba/Al in S1	Maximum Ba/Al in S1	Maximum Corg in S1 wt%
T87-26B	34°44'	16°48'	2415	27-36	4.3	0.014	0.006	0.02	2.30
MC12	33°24'	25°01'	2211	22-28	3.1	0.022	0.01	0.037	2.98
MC07S	34°19'	20°03'	2703	22-24	2.2	0.025	0.012	0.033	3.39
LC21	35°40'	26°35'	1522	140-162, 173-191	14.9	0.0087	0.0029	0.013	2.10
LC25	32°36'	27°23'	3129	69-87, 94-100	8.9	0.015	0.005	0.024	3.42
MDVAL- 9502	34°46'	34°28'	860	28-55	5.4	0.005	0.001	0.007	1.58
MD 90-917	41°18'	17°37'	1010	225-240, 245-255	20.5	0.0058	0.0009	0.007	1.16

Table 6.1. Positions, water depths and miscellaneous data for the cores studied.

Table 6.2. Conventional radiocarbon ages obtained by the Accelerator Mass Spectrometric technique. Depths marked with an asterisk were used in calculation of regression lines in the text.

Core	Depth in core (cm)	Analysis code	^{14}C age (convention years)	$\pm 1\sigma$ years	$\delta^{13}C$ (per mille)
MDVAL 9502	25-26*	AA-28393	5830	55	n.d
	30-31*	AA-28394	6980	60	n.d
	41-42	AA-28395	7940	60	n.d.
	53-54*	AA-28396	7530	60	n.d.
	57-58*	AA-28397	8150	65	n.d.
LC21	49.5-50.5	CAMS-41314	3370	60	-1.0
	95-96	CAMS-41313	4290	60	1.2
	137-138*	CAMS-41311	5590	60	0.4
	161-162*	CAMS-41315	7480	60	0.9
	174-174.5*	CAMS-41312	8120	60	-0.1
	188-191*	AA-30364	9085	65	n.d.
	218.5-219.5	AA-30365	11765	80	n.d.
	252-253	CAMS-41316	14450	60	0.3

LC25	50-51*	AA-30366	4805	50	n.d.
	60-61*	CAMS-43635	6320	60	1.0
	70.5-71.5*	CAMS-43636	7270	50	-0.2
	84.5-85.5*	CAMS-43637	8770	50	-1.0
	92-93	CAMS-43638	8980	60	0.5
	225-226	CAMS-43639	11110	50	1.0
MD90-917	+164-167	GifA-96201	4750	70	
	+175-178	GifA-96202	5000	70	
	+190-192	GifA-96729	5680	70	
	221-222*	CAMS-45865	6500	60	n.d.
	229-230*	CAMS-45866	6990	40	n.d.
	+230-232*	GifA-96730	6920	90	-
	+239-242*	GifA-96203	7930	80	-
	242-243*	CAMS-45867	7750	210	n.d.
	+250-253.5*	GifA-96204	8020	70	
	+250-253.5*	GifA-96205	8170	70	
	251-252*	CAMS-45868	7910	140	n.d.
	+252-253*	GifA-96731	8040	90	-

258-259	CAMS-45869	9750	80	n.d.
+275-278	GifA-96207	10390	90	
+295-297	GifA-96732	10800	90	

+Monospecific samples (*G. bulloides* or *G.ruber*)

Figure 6.1


12°E
16°E
20°E
24°E
28°E
32°E
36°E
46°N
44°N
42°N
40°N
38°N
36°N
34°N
32°N
MD 90-9
T87/26B
MC07S
MC12
MD81-LC21
MD81-LC25
MD81-9502
1000
2000
3000

Figure 6.2

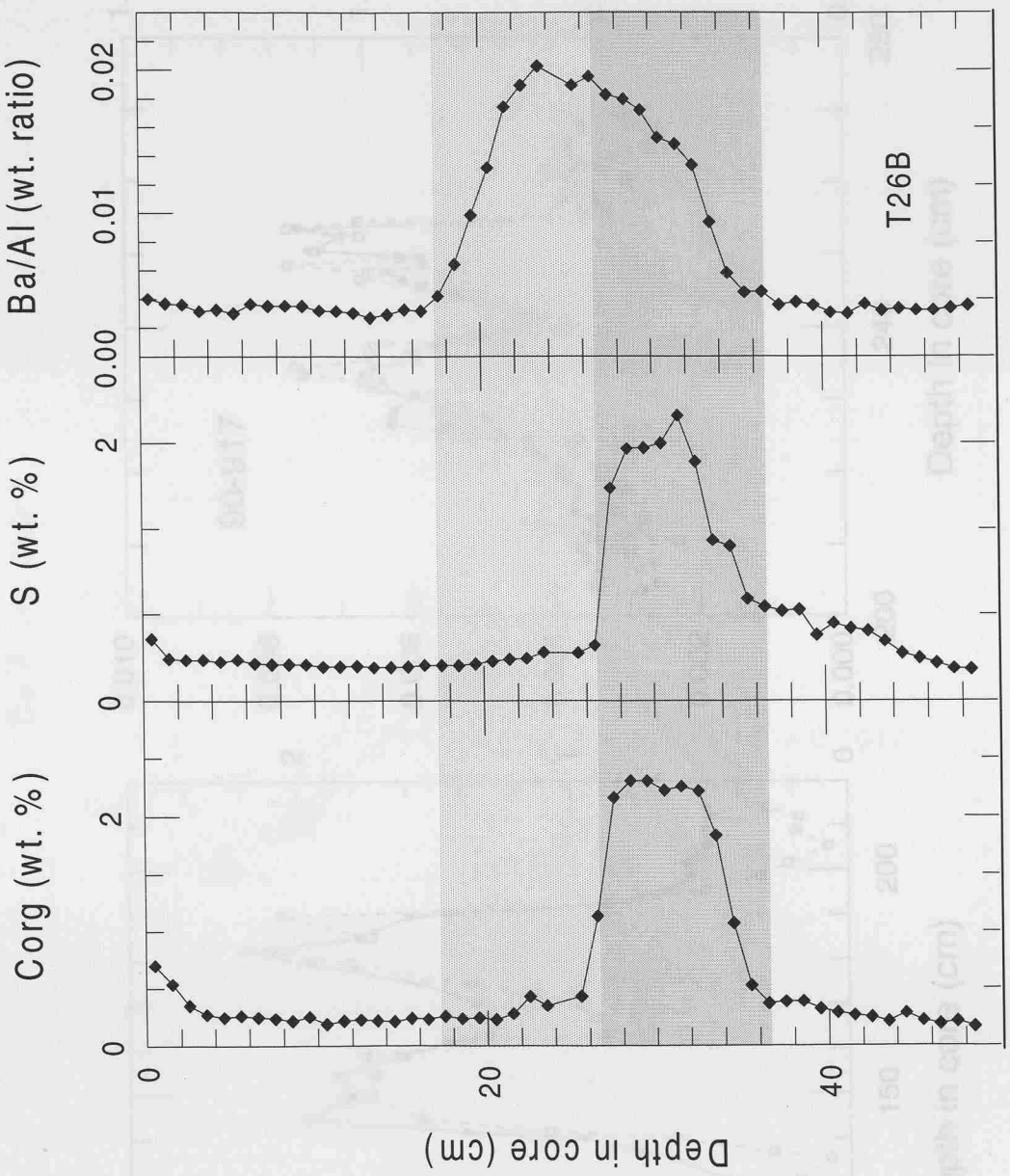
Corg (wt. %)
S (wt. %)
Ba/Al (wt. ratio)
T26B
Depth in core (cm)
0
2
0
2
0
0.00
0.01
0.02
0
20
40

Figure 6.3

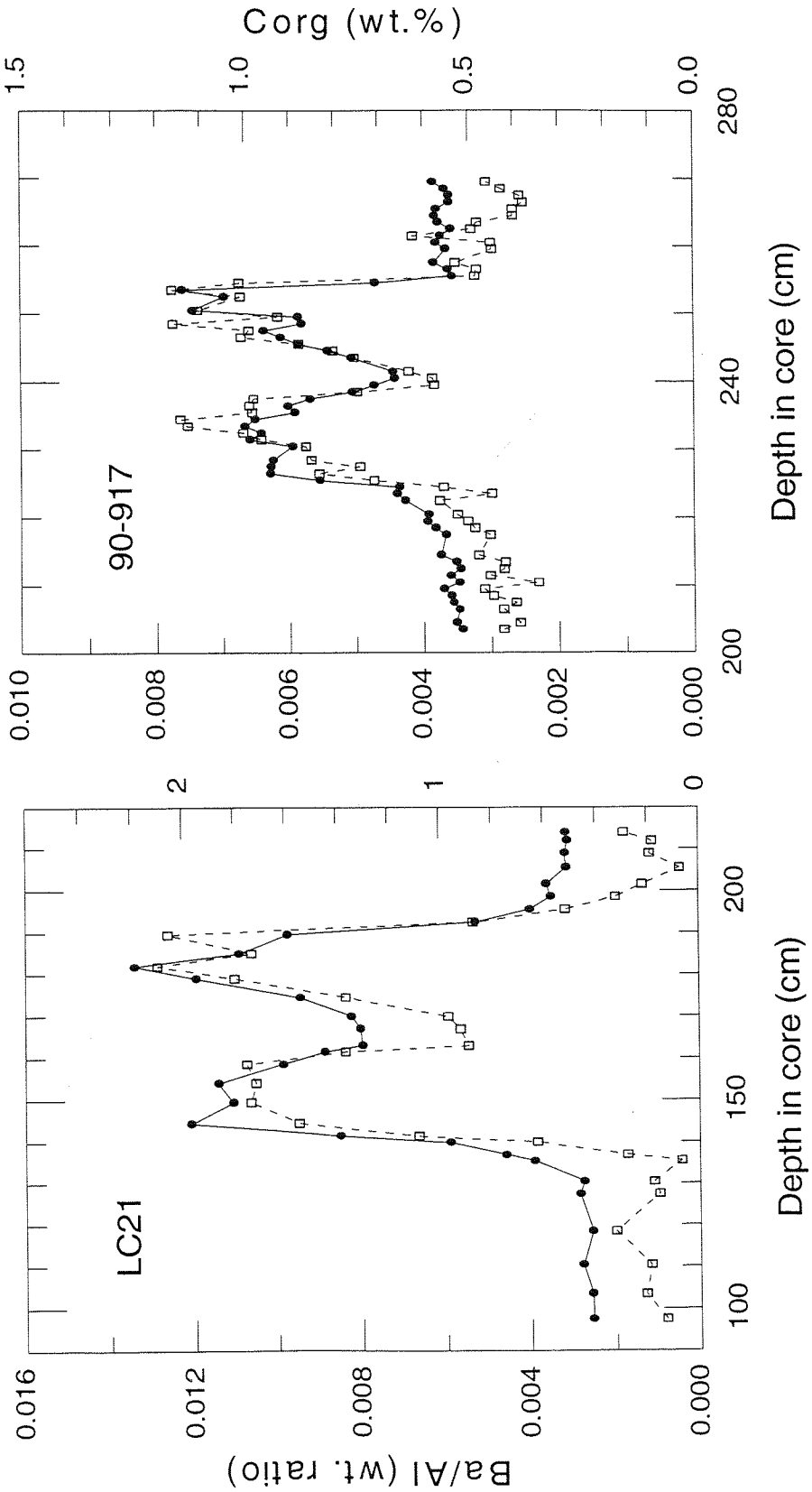
Corg (wt.%)
1.5
1.0
0.5
0.0
90-917
0.010
0.008
0.006
0.004
0.002
0.000
200
240
280
Depth in core (cm)
Ba/Al (wt. ratio)
2
1
0
LC21
0.016
0.012
0.008
0.004
0.000
100
150
200
Depth in core (cm)

Figure 6.4

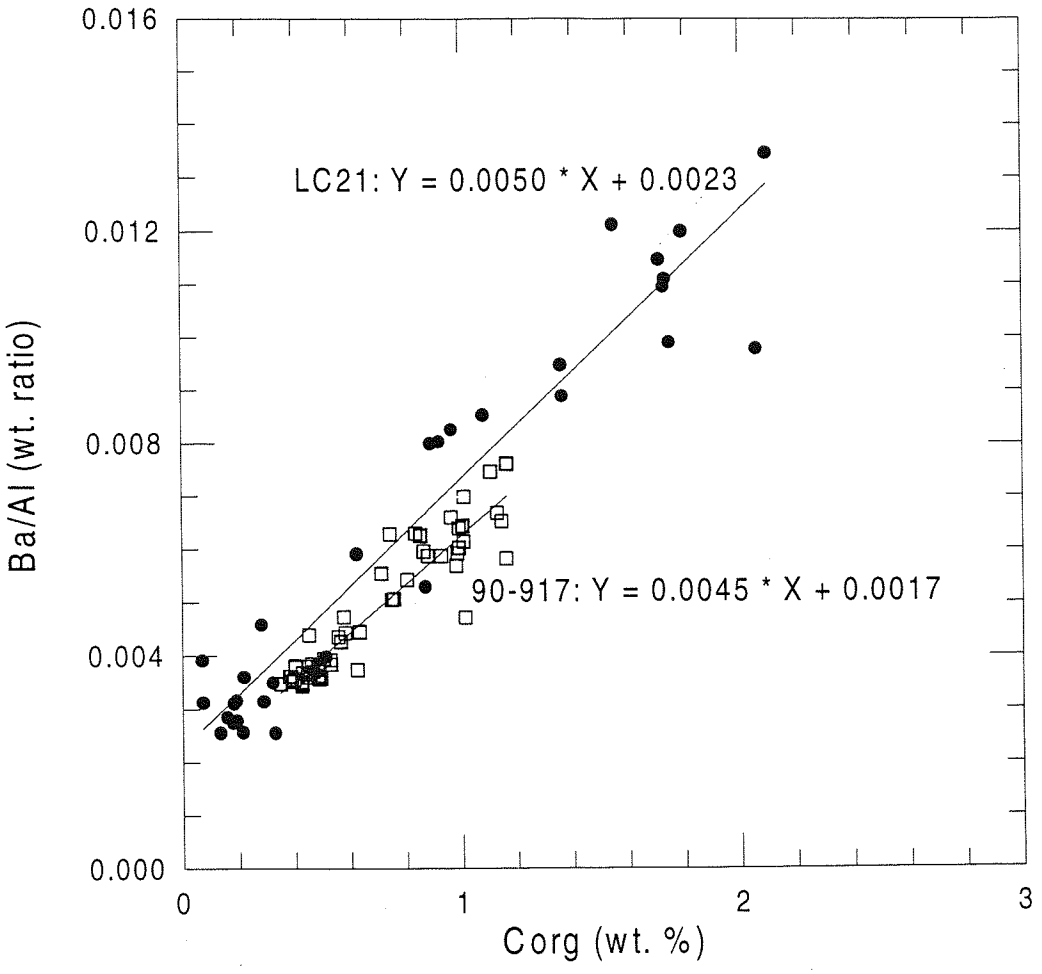
0.016
0.012
0.008
0.004
0.000
Ba/Al (wt. ratio)
LC21: Y = 0.0050 * X + 0.0023
90-917: Y = 0.0045 * X + 0.0017
0
1
2
3
Corg (wt. %)

Figure 6.5a

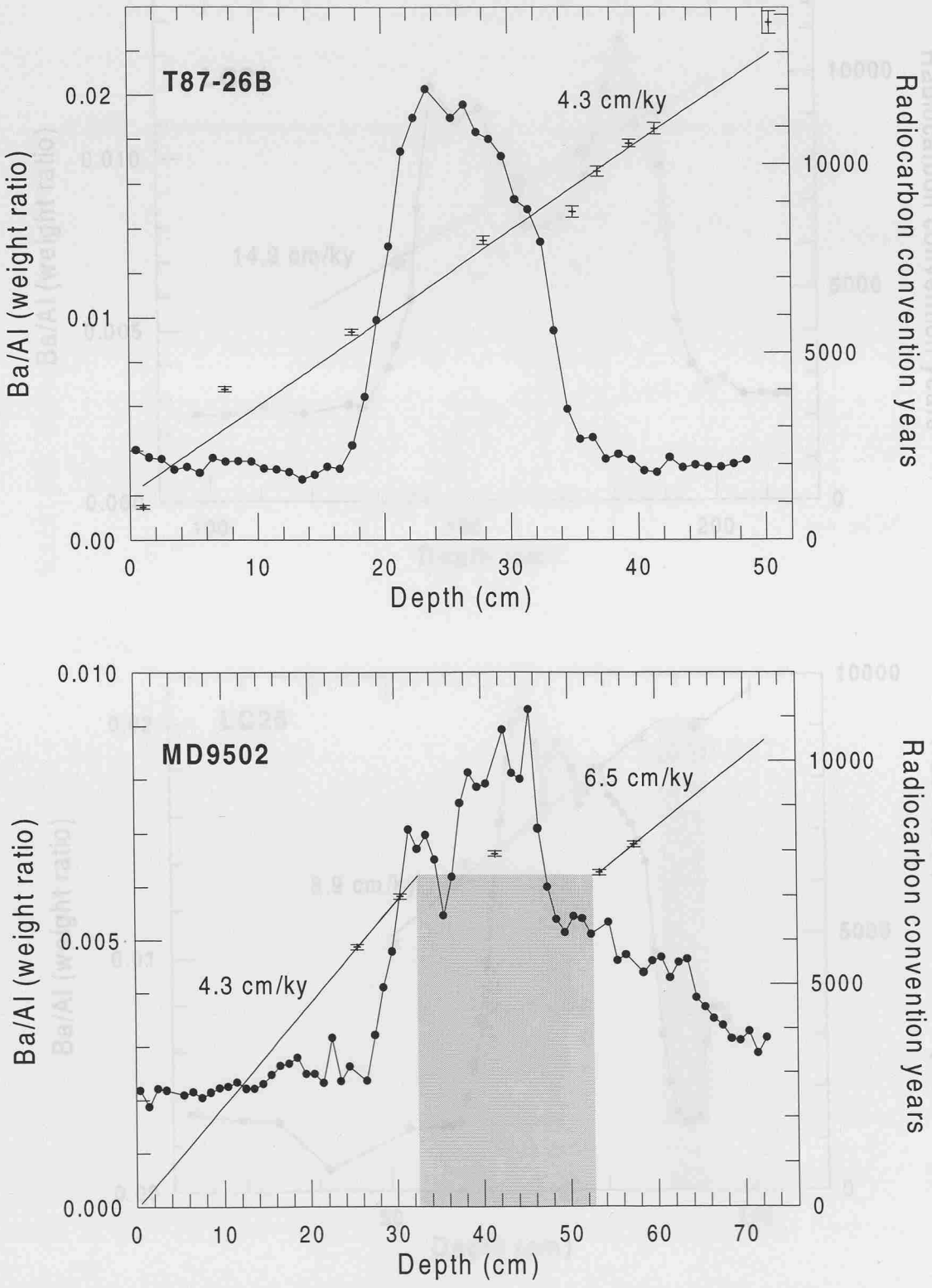
T87-26B
4.3 cm/ky
Ba/Al (weight ratio)
Radiocarbon convention years
Depth (cm)
0.00
0.01
0.02
0
5000
10000
0
10
20
30
40
50
MD9502
6.5 cm/ky
4.3 cm/ky
Ba/Al (weight ratio)
Radiocarbon convention years
Depth (cm)
0.000
0.005
0.010
0
5000
10000
0
10
20
30
40
50
60
70

Figure 6.5b

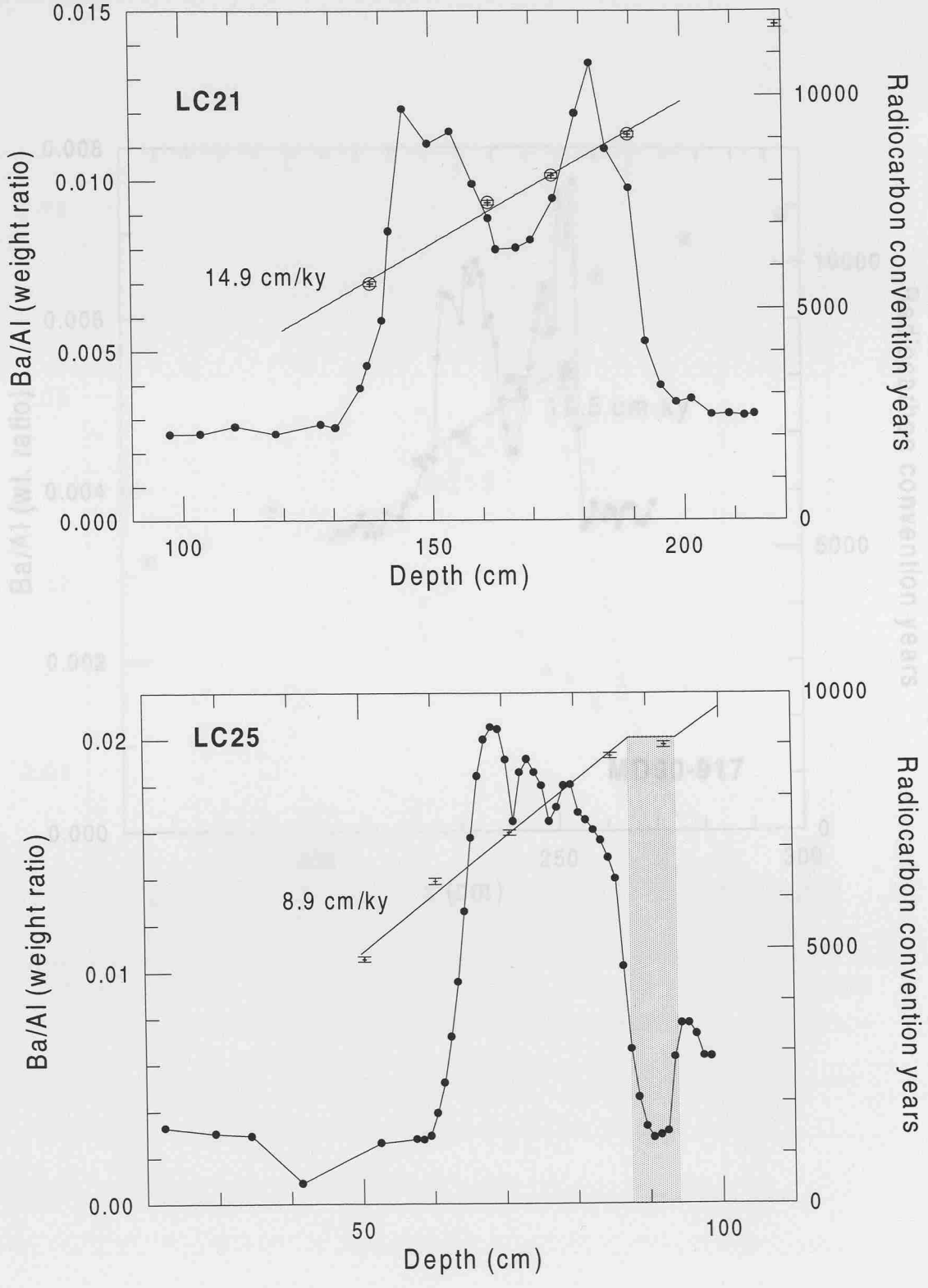
LC21
14.9 cm/ky
Ba/Al (weight ratio)
Radiocarbon convention years
Depth (cm)
0.015
0.010
0.005
0.000
10000
5000
0
100
150
200
LC25
8.9 cm/ky
Ba/Al (weight ratio)
Radiocarbon convention years
Depth (cm)
0.02
0.01
0.00
10000
5000
0
50
100

Figure 6.5c.

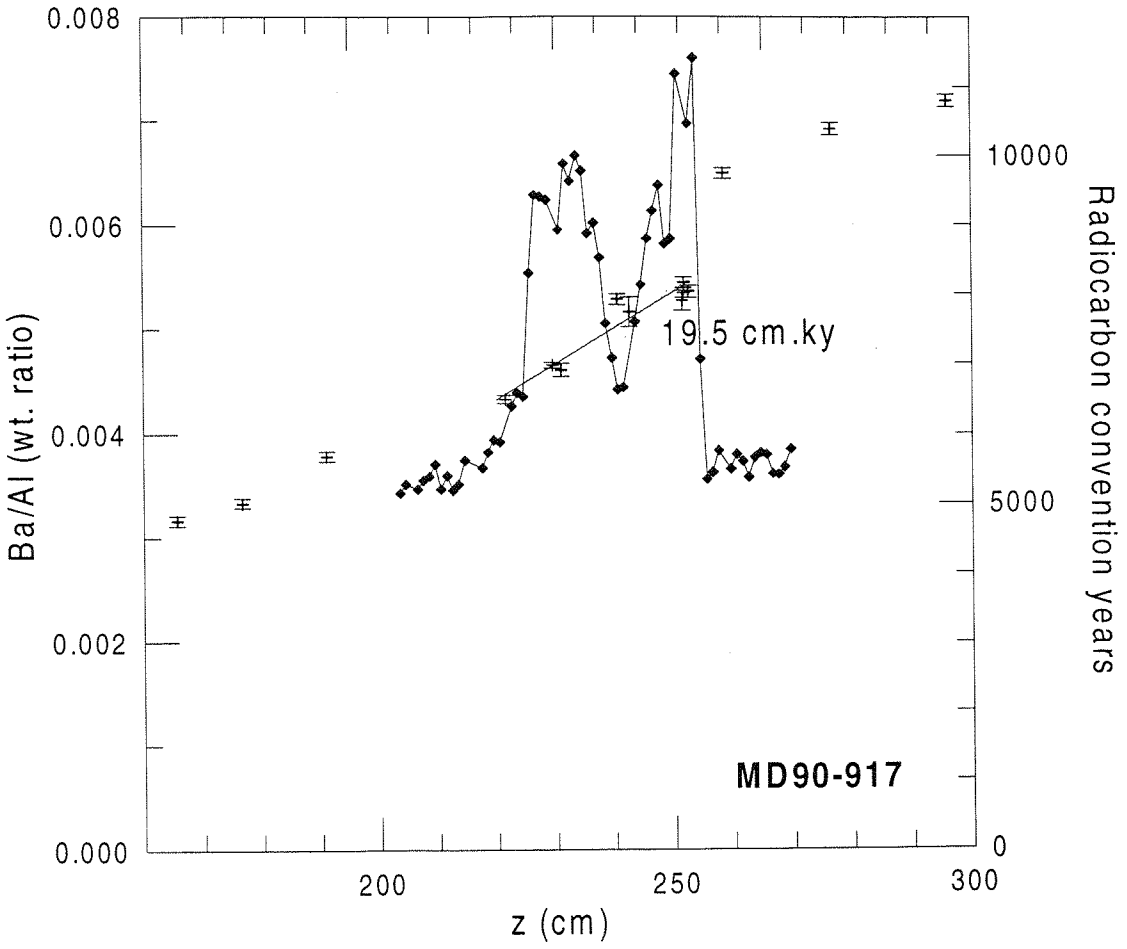
0.008
0.006
0.004
0.002
0.000
Ba/Al (wt. ratio)
200
250
300
z (cm)
10000
5000
0
Radiocarbon convention years
19.5 cm.ky
MD90-917

Figure 6.6a

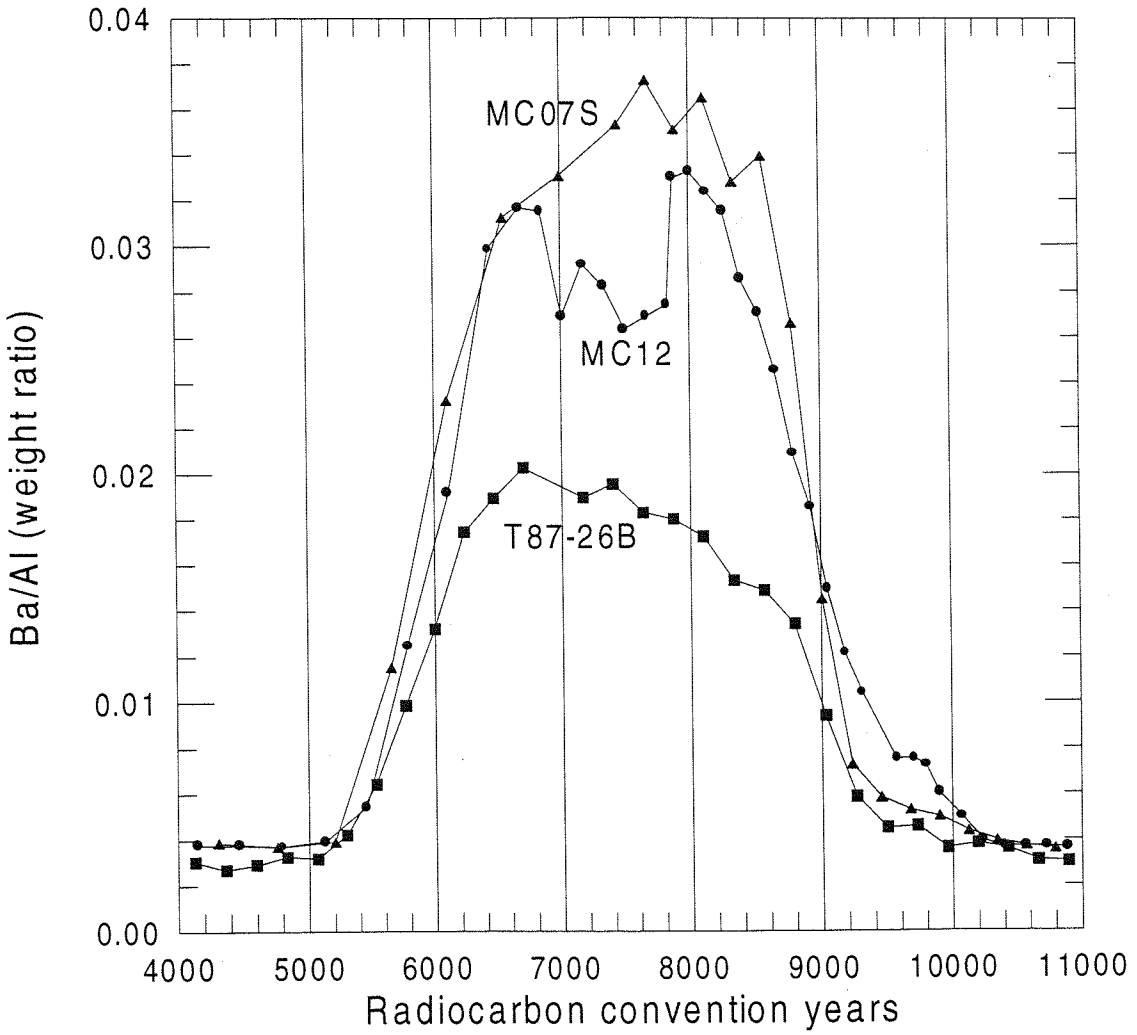
0.04
0.03
0.02
0.01
0.00
Ba/Al (weight ratio)
MC07S
MC12
T87-26B
4000
5000
6000
7000
8000
9000
10000
11000
Radiocarbon convention years

Figure. 6.6b

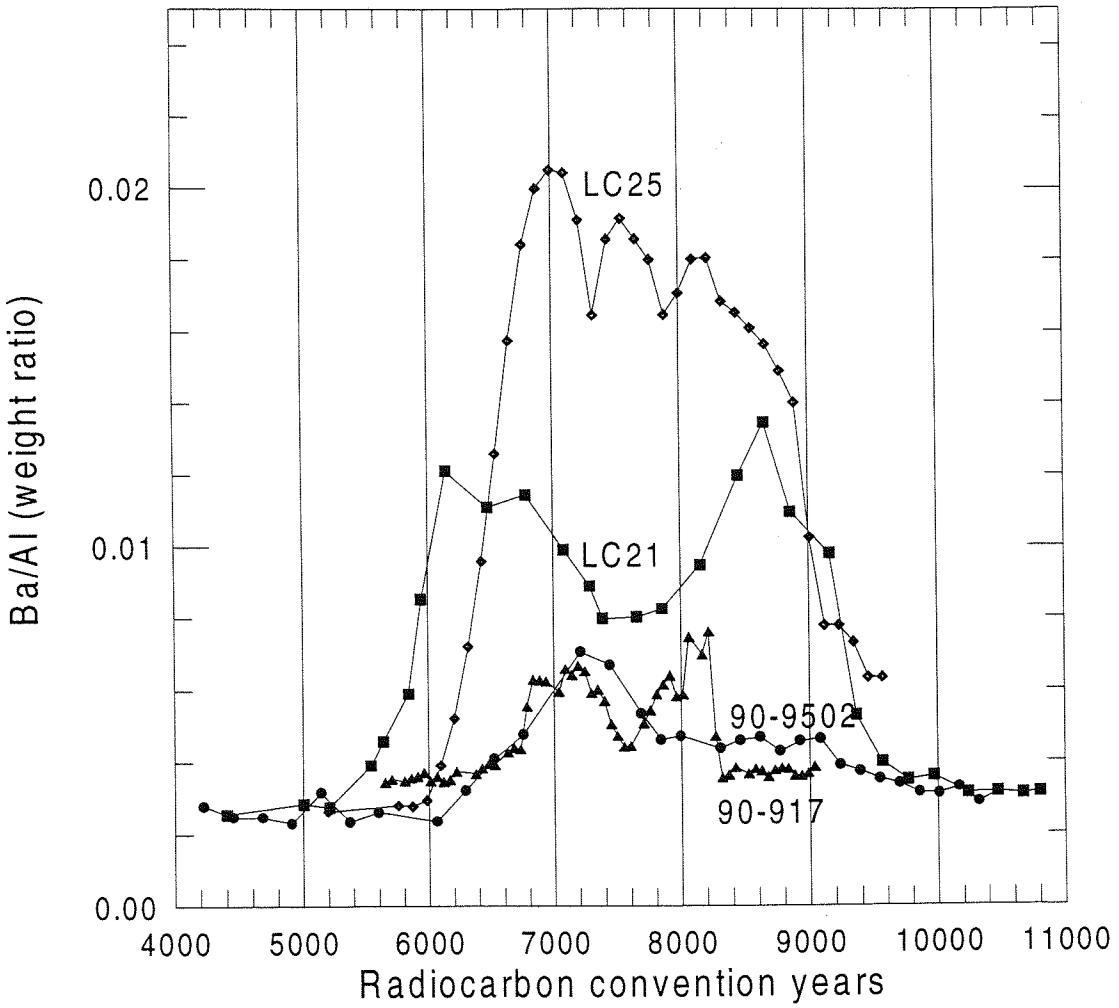
Ba/Al (weight ratio)
0.02
0.01
0.00
LC25
LC21
90-9502
90-917
4000
5000
6000
7000
8000
9000
10000
11000
Radiocarbon convention years

Figure 6.7.

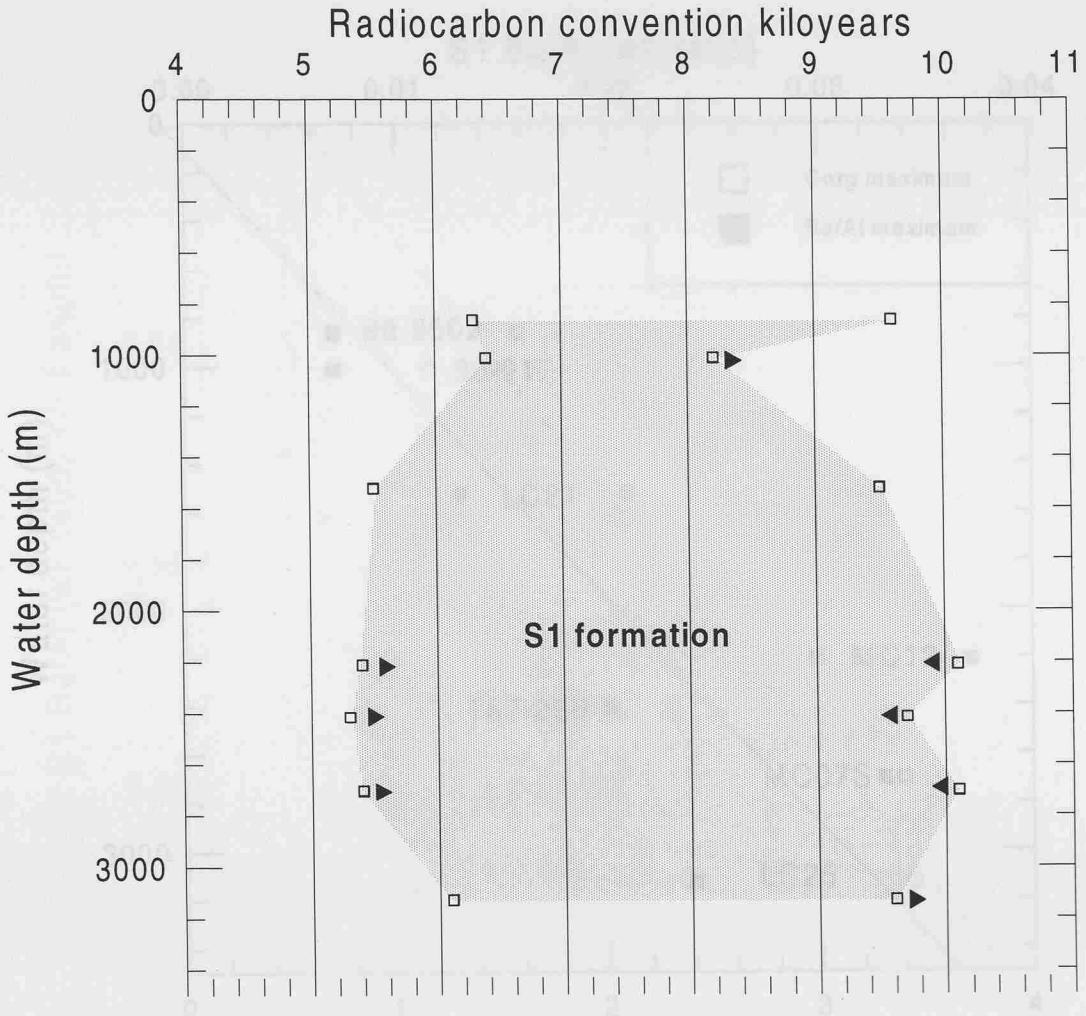
Radiocarbon convention kiloyears
4
5
6
7
8
9
10
11
0
1000
2000
3000
Water depth (m)
S1 formation

Figure 6.8.

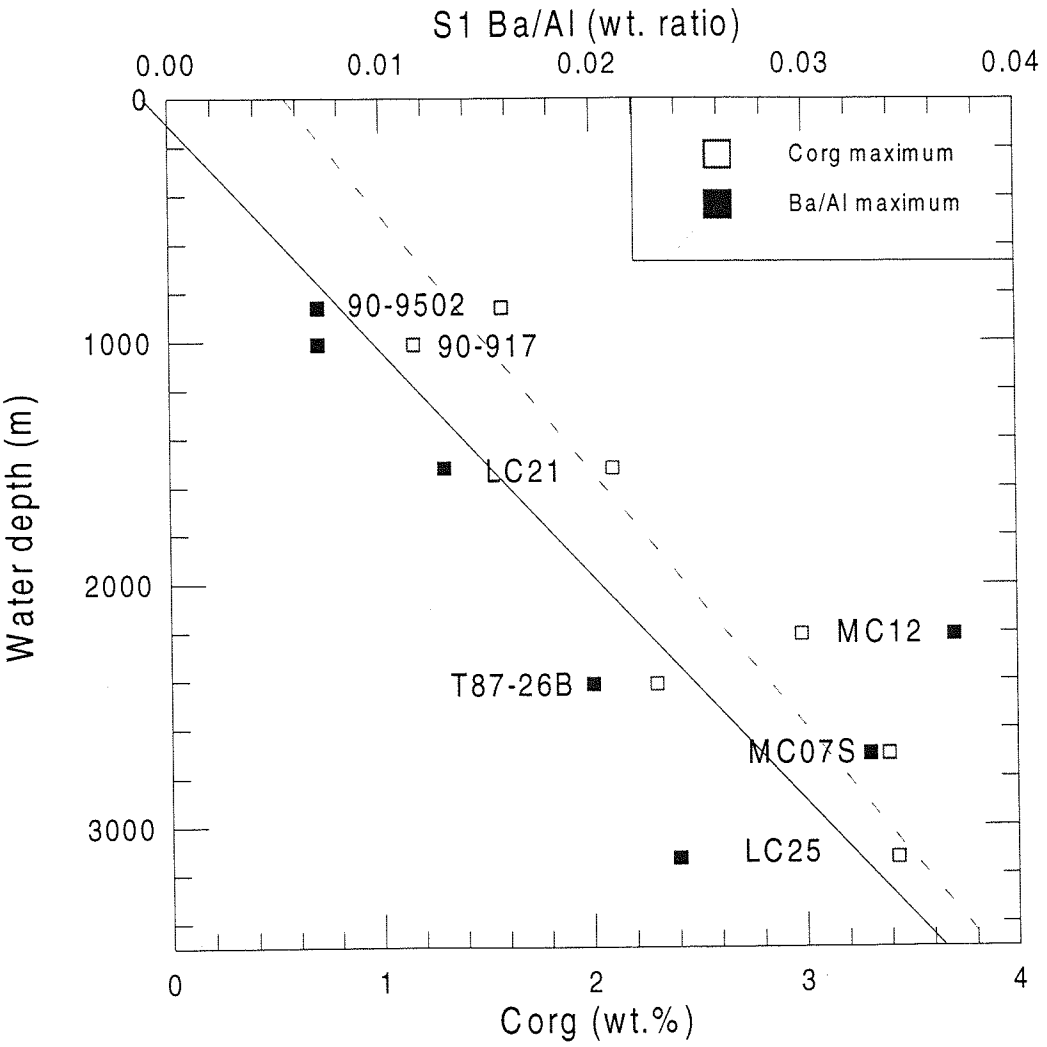
S1 Ba/Al (wt. ratio)
0.00
0.01
0.02
0.03
0.04
0
1000
2000
3000
Water depth (m)
Corg maximum
Ba/Al maximum
90-9502
90-917
LC21
MC12
T87-26B
MC07S
LC25
0
1
2
3
4
Corg (wt.%)

Figure 6.9.

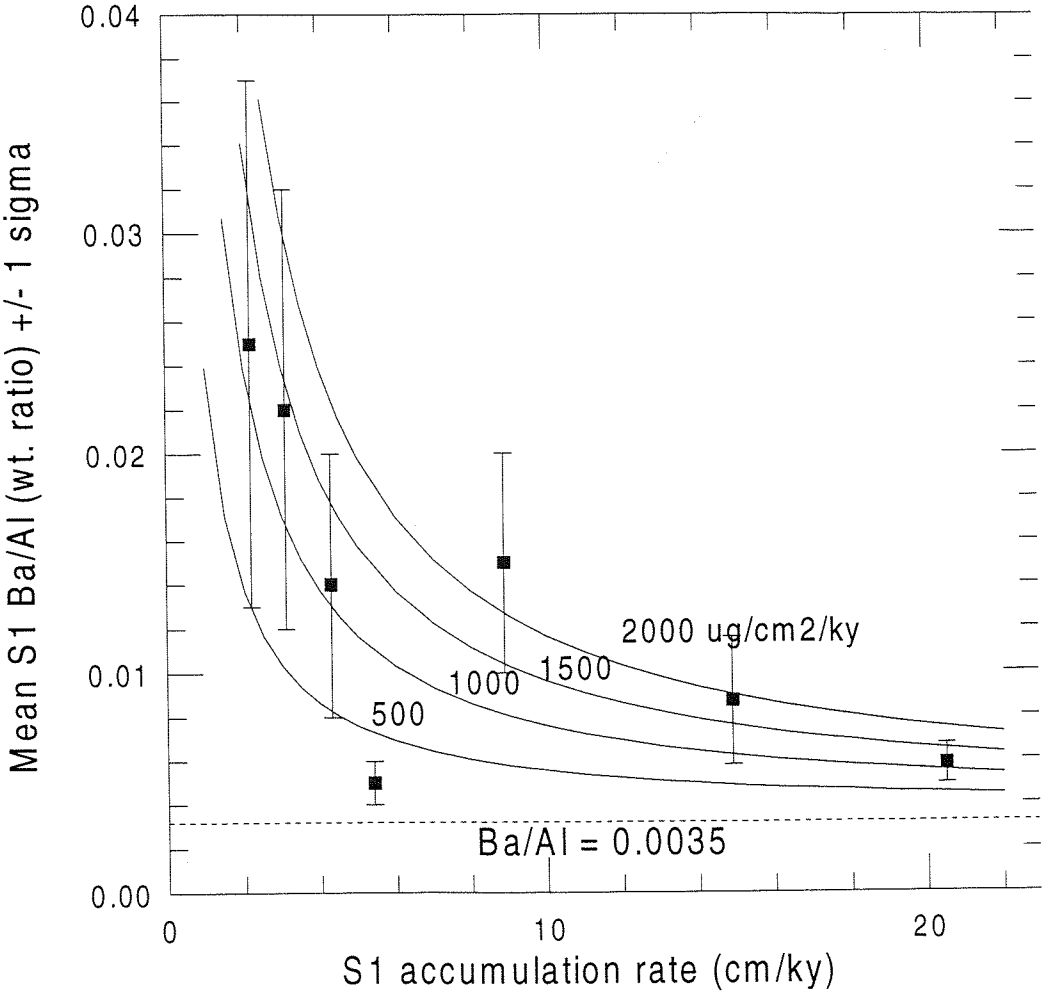
0.04
0.03
0.02
0.01
0.00
Mean S1 Ba/Al (wt. ratio) +/- 1 sigma
2000 ug/cm2/ky
1500
1000
500
Ba/Al = 0.0035
0
10
20
S1 accumulation rate (cm/ky)

Figure 6.10.

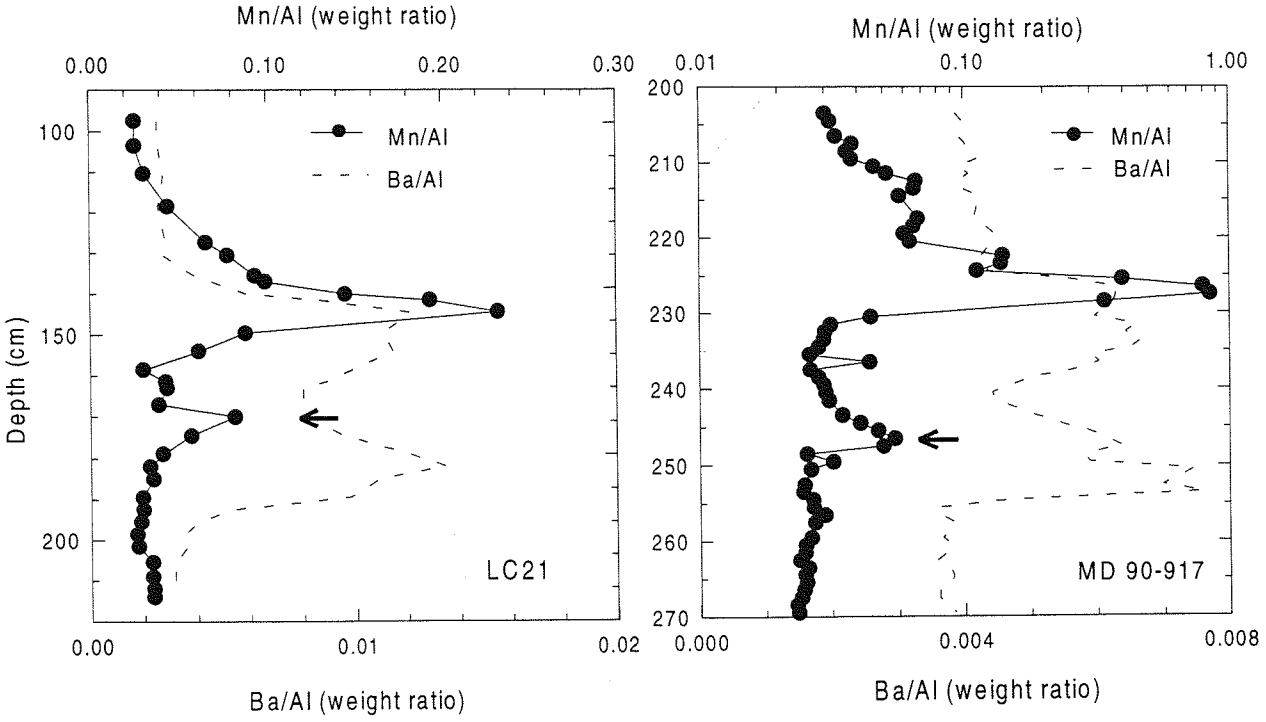
Mn/Al (weight ratio)
0.00
0.10
0.20
0.30
100
150
200
Depth (cm)
Mn/Al
Ba/Al
LC21
0.00
0.01
0.02
Ba/Al (weight ratio)
Mn/Al (weight ratio)
0.01
0.10
1.00
200
210
220
230
240
250
260
270
Mn/Al
Ba/Al
MD 90-917
0.000
0.004
0.008
Ba/Al (weight ratio)

Chapter 7:

Synthesis and Conclusions.

7.1. Trace element geochemistry of slowly-accumulated sapropels.

Investigation of three slowly-accumulated sapropels has revealed that they are extensively affected by post-depositional oxidation through a downward progressing oxidation front. The establishment of an oxidation front in S1-bearing sediments occurs in response to a decrease in the flux of Corg reaching the sea floor combined with an increase in eastern Mediterranean bottom water O_2 concentrations. The effects of an oxidation front on slowly-accumulated S1s have been demonstrated in chapter 3. It has been shown that following formation the oxidation front efficiently remineralises the Corg of S1 (through oxic diagenesis), producing a much thinner sapropel unit than was originally deposited. A close correlation between Corg and Ba has been established in S1 and it has been suggested that Ba/Al profiles may be used as a proxy for visualising the original Corg profile in sapropels. In the three sapropel examples investigated, the Ba/Al profiles exhibit a quasi-Gaussian distribution, with high Ba levels terminating well above the upper interface of the S1 unit. This observation implies that S1 must have originally been much thicker than as suggested by visual evidence alone. The amount of oxidation that S1 has suffered can be inferred from the Mn/Al profiles, and it is estimated that up to 11.5 cm has been lost via oxidation in ~ 6 kyr, which is in close agreement with estimates provided by Jung *et al.* (1997) using a modelling approach. High-resolution geochemical analysis has shown that the redox-sensitive elements are continually remobilised and relocated within and around S1 in response to the advancement of the oxidation front. As a result, the original authigenic geochemical signature of S1 is over-printed by a secondary diagenetic signal, making it difficult to identify the mechanism(s) by which these Corg-rich units are enriched in trace elements. A number of elements show clear partitioning either under oxidising/reducing conditions or both. Partitioning of elements back into the solid phase under oxidising and/or reducing conditions is dependent upon elemental speciation which determines the behaviour of individual elements under different redox conditions. Under oxic conditions, immobilisation of trace elements occurs by co-precipitation with oxides and oxyhydroxides of manganese and iron (e.g. Cr, Mo, As), whilst under more reducing conditions, elements are immobilised via associations with Corg (e.g. Cr, Br, As), co-precipitation with pyrite or formation as sulphide phases (e.g. Zn, Ni, As, Mo). Whilst the elements associated with Mn and Fe oxides are clearly diagenetic in origin, it is difficult to ascertain whether the enrichment found at

depth below the redox boundary is derived from the immobilisation and fixation of trace elements released during oxidation of S and Corg or whether this enrichment occurred at some preferred redox level during S1 formation. It is clear from SEM observations that iron and sulphur are immobilised as framboidal pyrite within the sapropel, although the presence of enhanced Fe and S below S1 (as euhedral pyrite) suggests that during sapropel formation sulphide production exceeded the supply of Fe^{+2} resulting in the downward export of HS^- out of the sapropel. The solid-phase profiles of I and Se are unlike any of the other elements and are present as sharp peaks located at the upper interface of the S1 unit. Whilst Se is fixed in just post-oxic conditions I is immobilised in slightly oxic conditions. The I and Se peaks continually breakdown and reform so as to actively track the movement of an oxidation front, and the presence of an I peak above an Se peak indicates that an oxidation front is currently active within the sediments, with the limit of oxidation located between the two peak maxima.

It has been discovered that like, I and Se, Hg also behaves in a systematic way in sediments affected by oxidation fronts (chapter 4). In turbidite and sapropel examples which have either been affected by or which have active oxidation fronts, well-defined Hg peaks are located in post-oxic conditions at the inferred limit of oxidation in a similar manner to Se. It is believed that the source of Hg and Se for the peaks is derived from the oxidation of trace amounts of pyrite, a process which separates Hg and Se from S. Migration of Se and Hg is inferred to take place through oxidised Se and Hg species which are then immobilised under post-oxic conditions. The formation of Hg and Se peaks in post-oxic environments suggests that the reduced Hg and Se species must be highly insoluble under slightly reducing conditions. It is noted that Hg and Se peaks are closely associated in turbidite and sapropel examples and it is inferred from the data that mercury and selenium are immobilised via the formation of the selenide mineral, tiemannite (HgSe). The persistence of Hg and Se peaks in both recent and ancient sediments (~ 4 My) suggests that Hg and Se peaks can used to define either the location of an active oxidation front in the absence of pore water O_2 measurements, or used to identify if older sediments have undergone any post-depositional oxidation.

7.2. Trace element geochemistry of rapidly-accumulated sapropels.

As discussed in chapter 3, slowly-accumulated sapropels are affected by post-depositional oxidation, so that the original authigenic geochemical signature is over-printed by secondary diagenetic signal. A consequence of this has been that the exact mechanism(s) by which trace elements are enriched in Corg-rich sapropels has remained elusive. Chapter 5 presents high-resolution geochemical data from two rapidly-accumulated sapropels (from the Aegean and Adriatic) in order to assess the importance of sulphide, Corg and sea water as sources for trace

element enrichment in S1. In the rapidly-accumulated sapropel examples, an exceptionally close correlation exists between Corg and Ba*, indicating that these cores have suffered little/no oxidation and so may be reliably used to identify the mechanism(s) for authigenic trace element enrichment. Furthermore, the close correlation between Corg and Ba* profiles in LC21 and MD 90-917 indicates that Ba has not undergone any significant post-depositional migration following S1 formation and so it has been established for the first time that Ba can be used as an accurate and reliable proxy for visualising Corg profiles in both rapidly-accumulated sapropels and those that have been affected by oxidation. The higher-resolution Ba* profile provided by the rapidly-accumulated cores indicates that productivity during S1 was not continuous, but was interrupted by an interval of reduced primary productivity levels. SEM observations clearly indicate that Fe and S are immobilised during S1 formation as framboidal pyrite, although during sapropel deposition an excess of sulphide production over Fe^{+2} supply resulted in the incorporation of HS^- into Corg to produce organically bound sulphur (OBS). Like Corg, Ba and S, many of the redox-sensitive elements exhibit double peaks in their enrichment versus depth profiles through S1 in both LC21 and MD 90-917. Four principal routes by which Corg-rich sediments become enriched in redox-sensitive elements have been identified (Piper, 1994).

(i) pre-concentration in the water column by primary producers followed by deposition of trace elements associated with Corg at the sediment/water interface.

(ii) the precipitation and deposition of individual element sulphide phases in anoxic-sulphidic water columns (e.g. ZnS, NiS) transports elements to the sediment/water interface.

(iii) downward diffusion of trace elements from seawater into post-oxic/anoxic-sulphidic sediments results in the reduction, precipitation and immobilisation of an element at depth.

(iv) combination of mechanisms (i), (ii) and (iii). An element delivered to the sediment water interface is released and is then subsequently reduced and/or complexed with organic matter or sulphides on downward diffusion.

For some elements such as Fe and S, the close correlation between these two elements indicates that they are being immobilised as pyrite in LC21 and MD 90-917, with the S being supplied to the sediments as SO_4^{2-} in the pore waters and Fe^{2+} from anoxic sediments below S1 and from the *in situ* reduction of Fe(III). Two elements that are known to be associated with Corg are I and Br. In the sapropel examples studied, Br enrichment in LC21 or MD 90-917 is limited, with 60-90% of the Br being present in pore water salt. It is not known why Br does not display any significant enrichment, although it is possible that these sapropel-bearing sediments are markedly depleted in Corg relative to examples cited in the literature where positive correlations between Corg and Br have been noted. The I#/Corg ratios for LC21 and MD 90-917 are similar to those found for other sediments deposited under reducing conditions and are within the range of I/Corg ratios found for

modern plankton. It is suggested that the iodine enrichment found in LC21 and MD 90-917 is derived primarily from the uptake and deposition of I associated with plankton since the reducing conditions during S1 deposition would prohibit any further uptake of I from seawater at the sediment/water interface. The amount of excess U within the S1 of LC21 and MD 90-917 is 1-3 ppm and the number of litres of seawater that needs to be quantitatively stripped in order to produce an authigenic enrichment of 1-3 ppm is estimated to be 0.3-1.0 litres. These values suggest that the entire U content of S1 can be supplied from the downward diffusion of U from seawater and is in agreement with the $^{234}U/^{238}U$ ratio of S1 of ~ 1.14 which is the same as seawater (Severman and Thomson, 1998). Similarly, the authigenic enrichment of Mo in LC21 and MD 90-917 amounts to 5-6 ppm which is equivalent to ~0.5 litres of seawater. Again, like U, Mo can be supplied to the sapropels from seawater through downward diffusion of an oxidised Mo species which is then reduced and immobilised either via its association with Corg or co-precipitation with pyrite. Vanadium displays the biggest authigenic enrichment in LC21 and MD 90-917 with excess concentrations of up to 57 ppm. This excess equates to 57 litres of seawater that needs to be quantitatively stripped of its V content in order to explain this degree of enrichment. It is therefore unlikely that the observed enrichment can be derived entirely from the downward diffusion of V from seawater and it is proposed that in addition to this mechanism, V is enriched via associations with Corg (through biological fixation within the photic zone or at the sediment/water interface) or through the reduction of V(V) to VO^{2+}, a highly particle reactive species. The profiles of Cr*, Zn* and Ni* in LC21 display a close similarity to that of S#. It is known that Ni and Zn can be precipitated directly as sulphides within the water column of anoxic-sulphidic water columns. During S1 formation, however, conditions were anoxic-non sulphidic (see later discussion) so that the immobilisation of these elements with an S phase must occur after deposition of Zn and Ni associated with Corg. Calculations suggest that for Ni up to 89 litres of seawater need to be stripped in order to account for an excess Ni concentration in LC21 of 43 ppm, whilst for Zn, 13 litres of seawater are needed to explain contents of 5ppm. Like V, downward diffusion of these trace elements into S1 can not explain the magnitudes of Ni and Zn enrichment in LC21 and MN 90-917, and as explained earlier direct precipitation of ZnS and NiS was thermodynamically excluded within the water column during S1 formation. It is known that certain minor elements, including Ni and Zn, are actively taken up by primary producers and display water concentration-depth profiles similar to those of the nutrient $Si(OH)_4$ (Bruland, 1983). As such, during S1 formation, the excess concentrations of nickel and zinc could be supplied via its association with and deposition of Corg. The similarity between the Corg, Ni* and Zn* profiles may indicate a biological source for these two elements or at least formation of metal-Corg complexes at the sediment/water interface. Chromium is not known to form sulphides, however, Cr enrichment within S1 requires up to 72 litres of seawater in order to explain the Cr enrichments seen within LC21 and MD 90-917. Again, a seawater source for Cr can explain some of the observed

enrichment although it is likely that additional Cr is delivered to the sediment/water interface via association with Corg, considering that Cr is known to be actively taken up by phytoplankton within the euphotic zone (Calvert and Pedersen, 1993). Furthermore, Cr is known to adsorb on to Corg at the sediment/water interface (Francois, 1988) (hence the close correlation between Corg and Cr in LC21), and additionally under reducing conditions the thermodynamically favoured form is Cr(III), a highly particle-reactive species which is removed from solution as $Cr(OH)_2^+$ which can further supply Cr during S1 formation.

It is clear that certain elements are clearly derived from the deposition of Corg (e.g. Ba, I and Br) at the sediment/water interface, whilst others which display minor enrichments in S1 (e.g. Mo and U) can be sourced entirely from seawater. For the remaining trace elements, elemental concentrations within S1 are too great to explain their origins entirely from seawater and so it is proposed that in addition to a seawater source, enrichments are caused either through the formation of metal-Corg complexes at the sediment/water interface or are deposited with Corg during biological fixation within the euphotic zone. The anoxic-non sulphidic water column present during S1 formation prohibits the direct precipitation of metal sulphide complexes as a route by which trace elements such as Zn and Ni become enriched. Within LC21 and MD 90-917 diagenesis proceeded down to sulphate reduction so that free sulphide was present within the pore waters. Elements introduced into S1 through downward diffusion have the possibility of becoming immobilised by forming complexes with Corg, being precipitated directly as sulphide phases or being incorporated/co-precipitated with pyrite. The close correlation between the Corg and S# profiles in LC21 and MD 90-917 makes it difficult to separate the mechanism by which some of the trace elements become immobilised and fixed in S1.

7.3. Productivity *vs* anoxia?

One of the key objectives of this research was to resolve the productivity *vs* preservation debate for the development and formation of S1 within the eastern Mediterranean. As discussed extensively in chapter 5, high-resolution studies on rapidly-accumulated S1 units have shown that Ba/Al weight ratios are reliable and stable geochemical proxies for visualising the Corg profiles of S1 units. As such, the Ba/Al ratios for both slowly- and rapidly-accumulated cores were used to estimate the palaeoproductivity during S1 formation using empirical formulae relating Ba concentrations with surface water productivity levels derived from sediment trap material. Estimates of productivity for both slowly- and rapidly-accumulated sapropel suggest that values reached up to 120 gC m^{-2} yr^{-1} indicating that productivity within the eastern Mediterranean during S1 formation was ~5 times greater than present-day. These palaeoproductivity estimates are in agreement with data presented

in chapter 6, where it has been demonstrated that Ba/Al ratios for slowly-and rapidly-accumulated cores can be modelled to a first approximation as a constant Ba flux of 1000-1500 $\mu g.cm^{-2}.ky^{-1}$, a value that equates to additional export productivity during S1 formation of 0.21-0.38 $gC.cm^{-2}.\ kyr^{-1}$. These results lend further support to the hypothesis that an increase in primary productivity was responsible for S1 development (Calvert, 1983). The problem with increased productivity as a mechanism for explaining S1 development is supplying enough nutrients to the eastern Mediterranean to sustain the estimated levels of palaeoproductivity during S1 deposition. At present, the anti-estuarine circulation of the eastern Mediterranean results in an export of nutrients from the eastern to western basins so that the former is highly oligotrophic. A number of mechanisms have been proposed to explain increased nutrient input into the eastern Mediterranean. It has been recognised that S1 development coincides with intensified monsoonal activity over equatorial Africa and enhanced precipitation over the borderlands. It has been suggested that increased nutrients can be derived from increased river run-off, or more drastically, the increase in freshwater input was sufficient to cause a circulation reversal which would have caused the eastern Mediterranean to have become a nutrient trap (chapter 1). Foraminiferal evidence presented by Zahn and Sarnthein, (1987) from the Straits of Gibraltar, however, suggests that no circulation reversal occurred during S1 formation. A more elegant solution for enhancing nutrient input into the eastern Mediterranean during S1 formation was proposed by Rohling and Giesekes (1989). These authors proposed that during S1 development, the pycnocline (with which the nutricline is closely associated) was shoaled up into the euphotic zone producing a highly productive deep chlorophyll maximum (DCM). The primary production in the DCM is mainly new production which enhances the export Corg from the euphotic zone (Eppley, 1989). Nannoplankton analysis of S1 examples investigated during this research have shown that at the onset of S1 development, there is an increasing abundance of *Florisphaera profunda*, a species which is closely linked to the position of the nutricline and DCM formation (Castradori, 1993). Modelling of the circulation of the eastern Mediterranean has shown that the pycnocline shoaled from its present position of 120-140m in the Levantine to 50-80m during S1 deposition, induced by a decrease in surface water salinities in the region of LIW formation (Myers *et al.*, 1998) and so produced a DCM. Data provided from the Ba/Al ratios and palaeoproductivity estimates are consistent with an increase in productivity during S1 formation. Furthermore, *F.profunda* data and modelling results suggest that S1 formation may have been initiated and sustained by a shoaling of the pycnocline into the euphotic zone with the formation of a highly productive DCM which induced periods of higher primary productivity within the eastern Mediterranean.

Whilst it has been demonstrated that S1 formation is marked by a moderate increase in productivity, according to Nijenhuis (1998), increased productivity alone cannot account for S1 formation, but is there any evidence for anoxia within the eastern Mediterranean during S1

formation? At present $1*10^{13}$ mol O_2 are supplied to the eastern Mediterranean during deep-water formation, however, the accumulation rate of Corg during S1 formation yields an oxygen demand of $3*10^{13}$ mol of O_2, indicating that anoxic bottom waters were present during S1 formation. This mechanism views anoxia as being a consequence of increased productivity rather than indicating circulation changes within the eastern Mediterranean.

There is, however, considerable evidence from $\delta^{18}O$ records of planktonic foraminifera that S1 formation was marked by low salinity surface layer (chapter 1), and so it has been proposed that anoxia (and S1 formation) was induced by circulation changes. Modelling of the eastern Mediterranean circulation formation has shown that production of Eastern Mediterranean Deep Water (EMDW) within the Adriatic ceased during S1 formation, instead forming an intermediate water mass termed Adriatic Intermediate Water (AIW) (Myers *et al.,* 1998). This water mass behaves similarly to EMDW, ventilating the whole of the eastern basin between 200 and 450m and these depths of ventilation are consistent with observations that no S1s are found at depths shallower than 300m in the open eastern Mediterranean (Rohling and Giesekes, 1989). The AIW is separated from the bottom waters by a strong halocline at ~ 450 m, which implies that these bottom waters quickly become anoxic so long as the halocline is maintained.

Geochemical data presented in chapter 5 also indicates that anoxic bottom waters were present during S1 formation. It has long been recognised that relationships between authigenic S and sedimentary Corg can be used as a criteria for establishing the oxidation status of the overlying water column at the time of sediment deposition (Berner and Raiswell, 1984; Morse and Berner, 1995). Based on the S/C criteria, all of the data from cores LC21 and MD 90-917 plot in or just above the normal marine domain, suggesting that during S1 formation, the water column was anoxic-non sulphidic, rather than anoxic-sulphidic (i.e. no free sulphide was present in the water column). These results are consistent with the size distribution of framboidal pyrite found within S1. It was found that the pyrite diameters within S1 ranged from 8-15μm which, according to Wilkin *et al.* (1996;1997) is consistent with the formation of FeS_2 *in situ* within the sediments rather than within the water column which tend to have much smaller diameters. Iodine is also known to be enriched in Corg-rich sediments that have accumulated under oxidising conditions. The lack of I enrichment in either LC21 or MD 90-917 suggests that S1 formation must have occurred primarily under a reducing conditions. Furthermore, the similarity in the I#/Corg ratios for LC21 and MD 90-917 with those found for sediments that have been deposited under reducing conditions further indicates that S1 accumulation occurred during periods of water column anoxia. The V(V+Ni) ratio has also been used to infer the redox state of the water column during sediment deposition (Lewan and Maynard, 1982). For the S1 examples studied in chapter 5, it is clear that

the values of ~0.5 indicate that the water column was primarily anoxic-non sulphidic during S1 formation. The geochemical evidence presented in chapter 5 is consistent with the benthic foraminiferal record of LC21 and MD 90-917 where species diversity and richness is very low (Mercone *et al.* in prep.). Within the two sapropel lobes of LC21, the benthic foraminferal record is dominated by the species *Chilostomella mediterranensis, Rutherfordoides rotundiformis and Globulimina affinis.* All of these species are tolerant to extremely low concentrations of dissolved O_2 so that their presence indicates that the bottom waters of the eastern Mediterranean must have been anoxic-non sulphidic rather than anoxic-sulphidic which would have meant the total absence of these low O_2-tolerant species.

Geochemical and foraminiferal data indicate that increased productivity and bottom water anoxia were present in the eastern Mediterranean during S1 formation. Whilst the benthic foraminiferal record and geochemical data indicates that anoxic-non sulphidic bottom waters were present during S1 development, it is unclear as to whether these reducing conditions were initiated by increased productivity (as shown by increased *F. profunda* abundances) or through circulation changes (as shown by $\delta^{18}O$ of planktonic foraminifera and modelling results). It seems likely that S1 formation was a result of a combination of processes: Increased freshwater input into the eastern Mediterranean resulted in shoaling of the pycnocline into the euphotic zone forming a deep chlorophyll maximum which then initiated high primary productivity. At the same time, the increased freshwater in the eastern Mediterranean, caused circulation changes whereby deep-water formation was reduced (Myers *et al.,* 1998), which reduced the amount of O_2 supplied to the deep-waters. Anoxia was developed within the bottom waters since the flux of Corg exceeded the supply of dissolved O_2 and these periods of anoxia were sustained so long as there was reduced deep-water formation within the eastern Mediterranean.

7.4. Circulation and reventilation during S1.

Within LC21 and MD 90-917, both visual and geochemical evidence suggests that S1 formation was not continuous with the sapropel being present in two distinct layers separated by an interval of lower Corg concentrations. In LC21 and MD 90-917, it is clear that this interval is characterised by a saddle in the Ba/Al ratios corresponding to the double sapropel phenomenon. Double sapropels have been previously reported within the eastern Mediterranean (Fontugne *et al.,* 1989; Perissoratis and Piper, 1992; Rohling *et al.,* 1997), and according to Rohling *et al.* (1997) these interruptions represent the resumption/return of more 'normal' circulation patterns. For LC21 and MD 90-917, the reduction in the Ba/Al ratios suggests that the central section represents a reduction in primary

productivity during S1 development, although the levels of Ba/Al do not indicate that conditions were as oligotrophic as those which preceded and followed S1 formation. The saddle in Ba/Al ratios in LC21 and MD 90-917 corresponds to a calibrated time of ~7900 yr BP, which is close in time to the observed Holocene climatic excursion at 8200 BP (Alley *et al.*, 1997). Palaeoproxy records show that this excursion was characterised by cold, dry and windy conditions and so it is inferred that improved reventilation and increased bottom water O_2 concentrations within the Adriatic and Aegean Seas (both sites of deep-water formation within the eastern Mediterranean) caused the interruption. The Mn/Al profiles in LC21 and MD 90-917 provide further evidence for improved circulation during S1 formation. It has been noted that well-defined Mn peaks are located at the top of the upper and lower S1 lobes in both cores, although the lower Mn peaks in each case are always smaller than the upper ones. The peaks in Mn coincide with the appearance of the benthic foraminifera *G.orbicularis* (see discussion below), a species that requires finite bottom water O_2 concentrations (Jorissen, 1999), and so it is proposed that the Mn peaks form when finite O_2 concentrations permit the precipitation of Mn^{+2} to a Mn oxyhydroxide phase. The lower Mn peaks have been anoxic for at least 7000 years and so must either be metastable as Mn oxyhydroxide or be present in the converted form as Mn (II) carbonate.

Further evidence to suggest that the interruption within S1 is caused through improved ventilation of the eastern Mediterranean comes from the benthic and planktonic foraminiferal record of LC21 and MD 90-917. In LC21, the saddle shows an increased abundance of cold-water planktonic foraminiferal species such as *T. quinqueloba, G. scitula, N. pachyderma* and *G.* (Mercone *et al.*, in prep.), whilst the benthic foraminiferal record indicates that this central section is dominated by the opportunistic species *G. orbicularis*. Within LC21 and MD 90-917, the coincident appearances of *G.orbicularis* in the benthic record along with an increased abundance of cold-water planktonic species is further consistent with the idea that the interruption was caused through increased reventilation and improved bottom water oxygenation.

7.5. Was S1 deposition within the eastern Mediterranean synchronous?

Another fundamental objective of this research was to establish whether the formation of S1 in the eastern Mediterranean was synchronous. Previous estimates for the ages of the onset and termination of S1 has revealed a large degree of variation. This is caused primarily through the fact that the visual base and top of S1 is used for dating purposes and, as demonstrated in chapter 3 slowly-accumulated sapropels are affected by post-depositional oxidation which produces a much thinner S1 unit than was originally deposited. Thomson et al. (1995) initially proposed that Ba/Al

ratios are more reliable than Corg profiles in estimating the original thickness of S1 and so may be used as a proxy in establishing a more accurate chronology for S1 formation. Using the Ba/Al criterion, the onset and termination of S1 in both rapidly- and slowly-accumulated was assessed by way of AMS ^{14}C dating (chapter 6).

AMS ^{14}C dating reveals that there is a discrepancy between the onset and termination ages for the slowly- and rapidly-accumulated sapropels. Dates for the slowly-accumulated cores (< 5 cm kyr^{-1}) consistently reveal that the onset of S1 formation occurred at 10,000 yrs BP whilst the termination ended at 5300 yrs BP. For the rapidly-accumulated examples (>10 cm kyr^{-1}), AMS ^{14}C dating indicates that S1 formation had a somewhat shorter duration with the start of sapropel formation occurring at ~ 9500 yrs BP and ending at ~ 6000 yrs BP. The difference in ages between the rapidly- and slowly-accumulated sapropels is ascribed to bioturbation which affects the Ba/Al index in the more slowly-accumulated cores rather than being the result of a water depth effect. Dating of MD 90-917 indicates that the total S1 duration of this Adriatic core is much shorter (8300-6300 yrs BP) than the other dated S1 examples, but is consistent with the duration of S1 from the Adriatic investigated by Jorissen *et al.*(1993). It is known that the Adriatic Sea is a site of deep-water formation in the eastern Mediterranean and the shorter S1 duration may indicate that ventilation may not have been shut down completely during sapropel formation, but rather it was present at a reduced level which was insufficient to oxygenate the entire eastern Mediterranean. Whilst the best estimates from rapidly-accumulated sapropels places the duration of S1 formation from 9500 to 6000 yrs BP, it is apparent that in LC21, sapropel formation continued for a longer period, terminating at ~ 5590 yrs BP. Like the Adriatic, the Aegean is also known to be a site of deep-water formation in the eastern Mediterranean. The longer duration for the sapropel in LC21 may indicate that the resumption of deep-water formation (and hence improved bottom-water oxygenation) in the Aegean continued for a longer period of time.

It does appear, however, as if the onset of S1 deposition was near-synchronous throughout the eastern Mediterranean i.e. underway by 9500 yrs BP in the Aegean, Levantine and Ionian Seas. The termination of S1 is, however, somewhat more variable, although the end of S1 in a number of rapidly-accumulated cores does occur by 6000 yrs BP (except for LC21). The estimated duration of S1 derived from the Ba/Al criterion and AMS ^{14}C dating is in close agreement with that of 9000-6000 yrs BP proposed by Rossignol-Strick (1995) for the period of high summer moisture and mild winters in the eastern Mediterranean, based on the interpretation of marine and land pollen records with a brief episode of colder winters in the middle.

References.

ABDULLAH, M.I., SHIYA, T. AND MOSGREN, K. (1995). ARSENIC AND SELENIUM SPECIES IN THE OXIC AND ANOXIC WATERS OF THE OSLO FJORD, NORWAY. *MARINE POLLUTION BULLETIN*, **31**, 116-126.

AGGET, J. AND O'BRIEN, G.A. (1985). DETAILED MODEL FOR THE MOBILITY OF ARSENIC IN LACUSTRINE SEDIMENTS BASED ON MEASUREMENTS IN LAKE OHAKURI. *ENVIRONMENTAL SCIENCE AND TECHNOLOGY*, **19**, 231-238.

AGHIB, F.S., BERNOULLI, D. AND WEISSERT, H. (1991). HARDGROUND FORMATION IN THE BANNOCK BASIN, EASTERN MEDITERRANEAN. *MARINE GEOLOGY*, **100**, 103-113.

AKSU, A.E., YASAR, D. AND MUDIE, P.J. (1995) PALEOCLIMATIC AND PALEOCENAOGRAPHIC CONDITIONS LEADING TO DEVELOPMENT OF SAPROPEL LAYER S1 IN THE AEGEAN BASIN. *PALEOGEOGRAPHY, PALEOCLIMATOLOGY AND PALEOECOLOGY*, **116**, 71-101.

ALLER, R.C., MACKIN, J.E., ULLIMAN, W.J., WANG, C., CAI, X, JIANG, J., SUI, Y. AND HANG, J. (1983). EARLY CHEMICAL DIAGENESIS AND SEA WATER SOLUTE EXCHANGE IN THE EAST CHINA SEA. IN: *PROCEEDINGS OF INTERNATIONAL SYMPOSIUM ON THE SEDIMENTATION ON THE CONTINENTAL SHELF WITH SPECIAL REFERENCE TO THE EAST CHINA SEA.* (ED) J. QUINGRUING AND J.D. MILLIMAN, PP 701-717.

ALLEY, R.B., MAYEWSKI, P.A., SOWERS, T., STUVIER, M., TAYLOR, K.C. AND CLARK, P.U. (1997). HOLOCENE CLIMATIC INSTABILITY: A PROMINENT, WIDESPREAD EVENT AT 8200 YR AGO. *GEOLOGY*, **25**, 483-486.

ANASTASKIS, G.C. AND STANLEY, D.J. (1984). SAPROPELS AND ORGANIC RICH VARIANTS IN THE MEDITERRANEAN: SEQUENCE DEVELOPMENT AND CLASSIFICATION. IN: D.A.V. STOW AND D.J.W PIPER (ED) *FINE GRAINED SEDIMENT: DEEP WATER PROCESSES AND FACIES*. BLACKWELL, OXFORD, PP 497-510.

ANASTASAKIS, G.C. AND STANLEY, D.J. (1986). UPPERMOST SAPROPEL, EASTERN MEDITERRANEAN: PALEOCEANOGRAPHY AND STAGNATION. *NATIONAL GEOGRAPHIC RESEARCH*, **2**, 179-197.

ANDERSON, R.F. (1982). CONCENTRATION, VERTICAL FLUX, AND REMINERALISATION OF PARTICULATE URANIUM IN SEAWATER. *GEOCHIMICA ET COSMOCHIMICA ACTA*, **46**, 1293-1299.

ANDERSON, R.F. (1987). REDOX TRANSFORMATIONS OF URANIUM IN AN ANOXIC MARINE BASIN. *URANIUM*, **3**, 145-164.

ANDERSON, R.F., BACON, M.P. AND BREWERM P.G. (1983). REMOVAL OF TH-230 AND PA-231 FROM THE OPEN OCEAN. *EARTH AND PLANETARY SCIENCE LETTERS*, **62**, 7-23.

ANDERSON, R.F., FLEISHER, M.Q. AND LEHURAY, A.P. (1989A). CONCENTRATION, OXIDATION STATE AND PARTICULATE FLUX OF URANIUM IN THE BLACK SEA. *GEOCHIMICA ET COSMOCHIMICA ACTA*, **53**, 2215-2224.

ANDERSON, R.F., LEHURAY, A.P., FLEISHER, M.Q. AND MURRAY, J.W. (1989B). URANIUM DEPOSITION IN SAANICH INLET SEDIMENTS, VANCOUVER ISLAND. *GEOCHIMICA ET COSMOCHIMICA ACTA*, **53**, 2205-2213.

ANDREAE, M.O. (1979). ARSENIC SPECIATION IN SEAWATER AND INTERSTITIAL WATERS. THE INFLUENCE OF BIOLOGICAL-CHEMICAL INTERACTIONS ON THE CHEMISTRY OF A TRACE ELEMENT. *LIMNOLOGY AND OCEANOGRAPHY*, **24**, 440-452.

ANDREAE, M.O. AND FROELICH, P.N. (1984). ARSENIC, ANTIMONY AND GERMANIUM BIOGEOCHEMISTRY IN THE BALTIC SEA. *TELLUS B- CHEMICAL AND PHYSICAL METEOROLOGY*, **36**, 101-117.

ANDREAE, M.O. AND KLUMPP, R. (1979). BIOSYNTHESIS AND RELEASE OF ORGANOARSENIC COMPOUNDS BY MARINE ALGAE. *ENVIRONMENTAL SCIENCE AND TECHNOLOGY*, **13**, 738-741.

APPLEQUIST, M.D., KATZ, A. AND TUREKIAN, K.K. (1972). DISTRIBUTION OF MERCURY IN THE SEDIMENTS OF NEW HAVEN (CONN.) HARBOUR. *ENVIRONMENTAL SCIENCE AND TECHNOLOGY*, **6**, 1123-1124.

ARTEGIANI, A., BREGANT, D., PASCHINI, E., PINARDI, N., RAICICH, F. AND RUSSO, A. (1997). THE ADRIATIC SEA GENERAL CIRCULATION. PART 1: AIR-SEA INTERACTIONS AND WATER MASS STRUCTURES. *JOURNAL OF PHYSICAL OCEANOGRAPHY*, **27**, 1492-1514.

ARTEGIANI, A., GACIC, M., MICHELATO, A., KOVACEVIV V., RUSSO, A., PASCHINI, E., SCARAZZATO, P., SMIRCIC, A. (1993). THE ADRIATIC SEA HYDROGRAPHY AND CIRCULATION IN SPRING AND AUTUMN (1985-1987). *DEEP SEA RESEARCH II*, **40**, 1143-1180.

AYLIFFE, D., WILLIAMS, M.A.J. AND SHELDON, F. (1996). STABLE CARBON AND OXYGEN ISOTOPIC COMPOSITION OF EARLY HOLOCENE GASTROPODS FROM WADI MANSURAB, NORTH-CENTRAL SUDAN. *HOLOCENE*, **6**, 157-169.

BACON, M.P. AND ANDERSON, R.F. (1982). DISTRIBUTION OF THORIUM ISOTOPES BETWEEN DISSOLVED AND PARTICULATE FORMS IN THE DEEP SEA. *JOURNAL OF GEOPHYSICAL RESEARCH*, **87**, 2045-2056.

BAKER, E.W. AND LOUDA, J.W. (1986). PORPHYRINS IN THE GEOLOGICAL RECORD. IN: RB JOHNS (ED). *BIOLOGICAL MARKERS IN THE SEDIMENTARY RECORD*. PP 126-255, ELSEVIER, AMSTERDAM.

BAR-MATTHEWS, M., AYALON, A. AND KAUFMAN, A. (1997). LATE QUATERNARY PALEOCLIMATE IN THE EASTERN MEDITERRANEAN REGION FROM STABLE ISOTOPE ANALYSIS OF SPELEOTHEMS AT SOREQ CAVE, ISRAEL. *QUATERNARY RESEARCH*, **47**, 155-168.

BARNES, C.E. AND COCHRAN, J.K. (1990). URANIUM REMOVAL IN OCEAN SEDIMENTS AND THE OCEANIC URANIUM BUDGET. *EARTH AND PLANETARY SCIENCE LETTERS*, **97**, 94-101.

BARNES, C.E. AND COCHRAN, J.K. (1991). GEOCHEMISTRY OF URANIUM IN BLACK SEA SEDIMENTS. *DEEP-SEA RESEARCH*, **38A**, 1237-1254.

BARNES, C.E. AND COCHRAN, J.K. (1993). URANIUM GEOCHEMISTRY IN ESTUARINE SEDIMENTS- CONTROLS ON REMOVAL AND RELEASE PROCESSES. *GEOCHIMICA ET COSMOCHIMICA ACTA*, **57**, 555-569.

BAUTRIN, G.N., KOCHENOV, A.V. AND SEMIN YU. M. (1971). URANIUM CONCENTRATION IN RECENT OCEANIC SEDIMENTS IN ZONES OF RISING CURRENTS. *GEOCHEMISTRY INTERNATIONAL*, **8**, 281-286.

BEIN, A., ALMOGI-LABIN, A. AND SASS, E. (1990). SULFUR SINKS AND ORGANIC CARBON RELATIONSHIPS IN CRETACEOUS ORGANIC-RICH CARBONATES: IMPLICATIONS FOR THE EVALUATION OF OXYGEN-POOR DEPOSITIONAL ENVIRONMENTS. *AMERICAN JOURNAL OF SCIENCE*, **290**, 882-911.

BELLANCA, A, CLAPS, M., ERBA, E., MASETTI, D., NERI, R., SILVA, I.P. AND VENEZIA, F. (1996). ORBITALLY INDUCED LIMESTONE/MARLSTONE RHYTHMS IN THE ALBIAN-CENOMANIAN CISMAN SCETION (VENETIAN REGION, NORTHERN ITALY): SEDIMENTOLOGY, CALCAREOUS AND SILICEOUS PLANKTON DISTRIBUTION, ELEMENTAL AND ISOTOPE GEOCHEMISTRY. *PALEOGEOGRAPHY, PALEOCLIMATOLOGY AND PALEOECOLOGY*, **126**, 227-260.

BELZILE, N. (1988). THE FATE OF ARSENIC IN SEDIMENTS OF THE LAURENTIAN TROUGH. *GEOCHIMICA ET COSMOCHIMICA ACTA*, **52**, 2293-2302.

BELZILE, N. AND LEBEL, J. (1986). CAPTURE OF ARSENIC BY PYRITE IN NEAR-SHORE MARINE SEDIMENTS. *CHEMICAL GEOLOGY*, **54**, 279-281.

BELZILE, N. AND TESSIER, A. (1990). INTERACTIONS BETWEEN ARSENIC AND IRON OXYHYDROXIDES IN LACUSTRINE SEDIMENTS. *GEOCHIMICA ET COSMOCHIMICA ACTA*, **54**, 103-109.

BENDER, M.L. AND HEGGIE, D.T. (1984). FATE OF ORGANIC CARBON REACHING THE DEEP-SEA FLOOR: A STATUS REPORT. *GEOCHIMICA ET COSMOCHIMICA ACTA*, **48**, 977-986.

BERGER, W.H., FINKEL, R.C., KILLINGLEY, J.S. AND MARCHIG, V. (1983). GLACIAL-HOLOCENE TRANSITION IN DEEP-SEA SEDIMENTS: MANGANESE SPIKE IN THE EASTERN EQUATORIAL PACIFIC. *NATURE*, **303**, 231-233.

BERGER, W.H., SMETACEK, V.S. AND WEFER, G. (1989). OCEAN PRODUCTIVITY AND PALEOPRODUCTIVITY-AN OVERVIEW. IN: *PRODUCTIVITY OF THE OCEAN: PRESENT AND PAST*, WH BERGER, VS SMETACEK AND G WEFER (EDS), 1-34, DAHLEM WORKSHOP REPORTS, WILEY-INTERSCIENCE.

BERNAT, M. AND CHURCH, T.M. (1989). URANIUM AND THORIUM DECAY SERIES IN THE MODERN MARINE ENVIRONMENT. PP 357-383, IN: *HANDBOOK OF ENVIRONMENTAL ISOTOPE GEOCHEMISTRY, VOL 3, MARINE ENVIRONMENT, PART A*, (ED., P. FRITZ AND J.C. FONTES).

BERNER, R.A. (1969). MIGRATION OF IRON AND SULPHUR WITHIN ANAEROBIC SEDIMENTS DURING EARLY DIAGENESIS. *AMERICAN JOURNAL OF SCIENCE*, **267**, 19-42.

BERNER, R.A. (1970). SEDIMENTARY PYRITE FORMATION. *AMERICAN JOURNAL OF SCIENCE*, **268**, 1-23.

BERNER, R.A. (1980). *EARLY DIAGENESIS: A THEORETICAL APPROACH*. PRINCETON, N.J: PRINCETON UNIVERSITY PRESS.

BERNER, R.A. (1984). SEDIMENTARY PYRITE FORMATION: AN UPDATE. *GEOCHIMICA ET COSMOCHIMICA ACTA*, **48**, 605-615.

BERNER, R.A. AND RAISWELL, R. (1983). BURIAL OF ORGANIC CARBON AND PYRITE SULFUR IN SEDIMENTS OVER PHANEROZOIC TIME. *GEOCHIMICA ET COSMOCHIMICA ACTA*, **47**, 855-862.

BERNER, R.A. AND RAISWELL, R. (1984). C/S METHOD FOR DISTINGUISHING FRESHWATER FROM MARINE SEDIMENTARY ROCKS. *GEOLOGY*, **12**, 365-368.

BERNSTEIN, R.E., BYRNE, R.H. AND SCHIJF, B. (1998). ACANTHARIANS: A MISSING LINK IN THE OCEANIC BIOGEOCHEMICAL CYCLE OF BARIUM. *DEEP-SEA RESEARCH*, **45**, 491-505.

BERRANG, P.G. AND GRILL, E.V. (1974). THE EFFECT OF MANGANESE OXIDE SCAVENGING ON MOLYBDENUM IN SAANICH INLET, BRITISH COLUMBIA. *MARINE CHEMISTRY*, **2**, 125-148.

BERTINE, K.K. (1972). THE DEPOSITION OF MOLYBDENUM IN ANOXIC WATERS. *MARINE CHEMISTRY*, **1**, 43-53.

BERTINE, K.K. AND TUREKIAN, K.K. (1973). MOLYBDENUM IN MARINE DEPOSITS. *GEOCHIMICA ET COSMOCHIMICA ACTA*, **37**, 1415-1434.

BERTRAM, M.A. AND COWEN, J.P. (1997). MORPHOLOGICAL AND COMPOSITIONAL EVIDENCE FOR BIOTIC PRECIPITATION OF MARINE BARITE. *JOURNAL OF MARINE RESEARCH*, **55**, 577-593.

BETHOUX, J.P. (1979). BUDGETS OF THE MEDITERRANEAN SEA. THEIR DEPENDENCE ON THE LOCAL CLIMATE AND THE CHARACTERISTICS OF ATLANTIC WATERS. *OCEANOLOGICA ACTA*, **2**, 157-163.

BETHOUX, J.P. (1989). OXYGEN-CONSUMPTION, NEW PRODUCTION, VERTICAL ADVECTION AND ENVIRONMENTAL EVOLUTION IN THE MEDITERRANEAN SEA. *DEEP-SEA RESEARCH*, **36**, 769-781.

BETHOUX, J.P. (1992). MEDITERRANEAN SAPROPEL FORMATION, DYNAMIC AND CLIMATIC VIEW POINTS. *OCEANOLOGICA ACTA*, **16**, 127-133.

BISHOP, A.N., KEARSLEY, A.T. AND PATIENCE, R.L. (1992). ANALYSIS OF SEDIMENTARY ORGANIC MATERIALS BY SCANNING ELECTRON MICROSCOPY: THE APPLICATION OF BACKSCATTERED ELECTRON IMAGERY AND LIGHT ELEMENT X-RAY MICROANALYSIS. *ORGANIC GEOCHEMISTRY*, **18**, 431-446.

BISHOP, J.K.B. (1988). THE BARITE-OPAL-ORGANIC CARBON ASSOCIATION IN OCEANIC PARTICULATE MATTER. *NATURE*, **331**, 341-343.

BOULOUBASSI, I., GUEHENNEUX, G. AND RULLKOTTER, J. (1998). BIOLOGICAL MARKER SIGNIFICANCE OF ORGANIC MATTER ORIGIN IN SAPROPELS FROM THE MEDITERRANEAN RIDGE, SITE 969. *ODP SCIENTIFIC RESULTS*, **160**, 261-270.

BOWEN, H.J.M. (1966). *TRACE ELEMENTS IN BIOCHEMISTRY*. ACADEMIC PRESS.

BOYLE, E.A. AND LEA, D.W. (1989). CD AND BA IN PLANKTONIC FORMAINIFERA FROM THE EASTERN MEDITERRANEAN: EVIDENCE FOR RIVER OUTFLOW AND ENRICHED NUTRIENTS DURING SAPROPEL FORMATION.

BRADLEY, W.H. (1938). MEDITERRANEAN SEDIMENTS AND PLEISTOCENE SEA LEVELS. *SCIENCE*, **88**, 376-379.

BRANNON, J.M. AND PATRICK, W.H. (1987). FIXATION, TRANSFORMATION AND MOBILIZATION OF ARSENIC IN SEDIMENTS. *ENVIRONMENTAL SCIENCE AND TECHNOLOGY*, **21**, 450-459.

BREIT, G.N. AND WANTY, R.B. (1992). VANADIUM ACCUMULATION IN CARBONACEOUS ROCKS- A REVIEW OF GEOCHEMICAL CONTROLS DURING DEPOSITION AND DIAGENESIS. *CHEMICAL GEOLOGY*, **91**, 83-97.

BROOKINS D.G. (1980). *EH-PH DIAGRAMS FOR GEOCHEMISTRY*. SPRINGER-VERLAG.

BRUMSACK, H.J. (1986). THE INORGANIC GEOCHEMISTRY OF CRETACEOUS BLACK SHALES (DSDP LEG 41) IN COMPARISON TO MODERN UPWELLING SEDIMENTS FROM THE GULF OF CALIFORNIA. PP 447-462 IN: *NORTH ATLANTIC PALAEOCEANOGRAPHY*, (ED), C.P. SUMMERHAYES AND N.J. SHACKLETON.

BRUMSACK, H.J. (1989). GEOCHEMISTRY OF RECENT TOC-RICH SEDIMENTS FROM THE GULF OF CALIFORNIA AND BLACK SEA. *GEOLOGISCHE RUNDSCHAU*, **78**, 851-882.

BRUMSACK, H.J. AND GIESEKES, J.M. (1983). INTERSTITIAL WATER TRACE-METAL CHEMISTRY OF LAMINATED SEDIMENTS FROM THE GULF OF CALIFORNIA, MEXICO. *MARINE CHEMISTRY*, **14**, 89-106.

BRUNO, J., CASAS, F. AND PUIGDOMENECH, I. (1988). THE KINETICS AND DISSOLUTION OF $UO_{2(S)}$ UNDER REDUCING CONDITIONS. *RADIOCHIMICA ACTA*, **44/45**, 11-16.

BURDIGE, D.J. (1993). THE BIOGEOCHEMISTRY OF MANGANESE AND IRON REDUCTION IN MARINE SEDIMENTS. *EARTH SCIENCE REVIEWS*, **35**, 249-284.

BURDIGE, D.J. AND GIESEKES, J.M. (1983). A POREWATER/SOLID PHASE DIAGENETIC MODEL FOR MANGANESE IN MARINE SEDIMENTS. *AMERICAN JOURNAL OF SCIENCE*, **283**, 29-47.

BURNS, R.G. AND BURNS, V.M. (1977). MINERALOGY. IN: G P GLASBY (ED), *MARINE MANGANESE DEPOSITS, CHAPTER 7*. ELSEVIER, AMSTERDAM, 185-248.

BURNS, R.G. AND BURNS, V.M. (1981). AUTHIGENIC OXIDES. IN: C.EMILIANI (ED), *THE SEA, 7. THE OCEANIC LIHTOSPHERE*. WILEY-INTERSCIENCE, NY, PP 875-894.

CAGATAY, M.N., GEDIK, A. AND SALTOGLU, T. (1990). GEOCHEMISTRY OF URANIUM IN THE LATE PLEISTOCENE-HOLOCENE SEDIMENTS FROM THE SOUTHERN PART OF THE BLACK SEA. *CHEMICAL GEOLOGY*, **82**, 129-144.

CALVERT, S.E. (1983). GEOCHEMISTRY OF PLEISTOCENE SAPROPELS AND ASSOCIATED SEDIMENTS FROM THE EASTERN MEDITERRANEAN. *OCEANOLOGICA ACTA*, **6**, 255-267.

CALVERT, S.E. AND FONTUGNE, M.R. (1988). GEOCHEMISTRY AND ORIGIN OF MEDITERRANEAN SAPROPELS. *EOS TRANS. AGU*, **69**, 1234.

CALVERT, S.E. AND KARLIN, R.E. (1991). RELATIONSHIPS BETWEEN SULPHUR, ORGANIC CARBON, AND IRON IN THE MODERN SEDIMENTS OF THE BLACK SEA. *GEOCHIMICA ET COSMOCHIMICA ACTA*, **55**, 2483-2490.

CALVERT, S.E. AND MORRIS, R.J. (1977). GEOCHEMICAL STUDIES OF ORGANIC-RICH SEDIMENTS FROM THE NAMIBIAN SHELF. II. METAL-ORGANIC ASSOCIATIONS. IN: M. ANGEL (ED), *A VOYAGE OF DISCOVERY*. PERGAMON, PP 667-680.

CALVERT, S.E. AND PEDERSEN, T.F. (1993). GEOCHEMISTRY OF RECENT OXIC AND ANOXIC MARINE SEDIMENTS: IMPLICATIONS FOR THE GEOLOGICAL RECORD. *MARINE GEOLOGY*, **113**, 67-88.

CALVERT, S.E., MUKHERJEE, S. AND MORRIS, R.J. (1985). TRACE METALS IN FULVIC AND HUMIC ACIDS FROM MODERN ORGANIC0RICH SEDIMENTS. *OCEANOLOGICA ACTA*, **8**, 167-173.

CALVERT, S.E., NIELSEN, B. AND FONTUGNE, M.R. (1992). EVIDENCE FROM NITROGEN ISOTOPE RATIOS FOR ENHANCED PRODUCTIVITY DURING THE FORMATION OF EASTERN MEDITERRANEAN SAPROPELS. *NATURE*, **359**, 223-225.

CALVERT, S.E., PEDERSEN, T.F. AND THUNELL, R.C. (1993). GEOCHEMISTRY OF SURFACE SEDIMENTS OF THE SULU AND SOUTH CHINA SEAS. *MARINE GEOLOGY*, **114**, 207.

CALVERT, S.E., THODE, H.G., YEUNG, D. AND KARLIN, R.E. (1996). A STABLE ISOTOPE STUDY OF PYRITE FORMATION IN THE LATE PLEISTOCENE AND HOLOCENE SEDIMENTS OF THE BLACK SEA. *GEOCHIMICA ET COSMOCHIMICA ACTA*, **60**, 1261-1270.

CALVERT, S.E., VOGEL, J.C. AND SOUTHON, J.R(1987). CARBON ACCUMULATION RATES AND THE ORIGIN OF THE HOLOCENE SAPROPEL IN THE BLACK SEA. *GEOLOGY*, **15**, 918-922.

CAMERLENGHI, A. AND CITA, M.B. (1987). SETTING AND TECTONIC EVOLUTION OF SOME EASTERN MEDITERRANEAN DEEP-SEA BASINS. *MARINE GEOLOGY*, **75**, 31-55.

CANFIELD, D.E. (1994). FACTORS INFLUENCING ORGANIC CARBON PRESERVATION IN MARINE SEDIMENTS. *CHEMICAL GEOLOGY*, **114**, 315-329.

CANFIELD, D.E., JORGENSEN, B.B., FOSSING H., GLUD, R., GUNDERSEN, J., RAMSING, N.B., THAMDRUP, B., HANSEN, T.W., NIELSEN, L.P. AND HALL, P.O.J. (1993). PATHWAYS OF ORGANIC CARBON OXIDATION IN THREE CONTINENTAL MARGIN SEDIMENTS. *MARINE GEOLOGY*, **113**, 27-40.

CANFIELD, D.E., LYONS, T.W. AND RAISWELL, R. (1996). A MODEL FOR IRON DEPOSITION TO EUXINIC BLACK SEA SEDIMENTS. *AMERICAN JOURNAL OF SCIENCE*, **296**, 818-834.

CARTER, T.G., FLANAGAN, J.P., REED JONES, C., MARCHANT, F.L., MURCHISON, R.R., REBMAN, J.H., SYLVESTER J.C. AND WHITNEY, J.C. (1972). A NEW BATHYMETRIC CHART AND PHYSIOGRAPHY OF THE MEDITERRANEAN SEA. IN: *THE MEDITERRANEAN SEA. A NATURAL SEDIMENTATION LABORATORY*, PP 1-23, ED D.J. STANLEY.

CASTRADORI, D. (1993). CALCAREOUS NANNOFOSSILS AND THE ORIGIN OF EASTERN MEDITERRANEAN SAPROPELS. *PALEOCEANOGRAPHY*, **8**, 459-471.

CHAPMAN, P. (1983). CHANGES IN IODINE SPECIATION IN THE BENGUELA CURRENT UPWELLING SYSTEMS. *DEEP-SEA RESEARCH*, **30**, 1247-1259.

CHESTER, R. (1990). *MARINE GEOCHEMISTRY*: UNWIN HYMAN, 698 PP.

CITA, M.B. AND CAMERLENGHI, A. (1990). THE MEDITERRANEAN RIDGE AS AN ACCRETIONARY PRISM IN COLLISIONAL CONTEXT. *MEM. SOC. GEOL. IT.*, **45**, 463-480.

CITA, M.B. AND GRIGNANI, D. (1982). NATURE AND ORIGIN OF LATE NEOGENE MEDITERRANEAN SAPROPELS. IN: S.O SCHLANGER AND M.B. CITA (EDITORS), *NATURE AND ORIGIN OF CRETACEOUS CARBON-RICH FACIES*. ACADEMIC, SAN DIEGO, CA PP 165-196.

CITA, M.B., BEGHI, C., CAMERLENGHI, A., KASTENS, K.A., MCCOY, F.W., NOSELTO, A., PARISI, E., SCOLAN, F. AND TOMADIN, L. (1984). TURBIDITES AND MEGATURBIDITES FROM THE HERODOTUS ABYSSAL PLAIN (EASTTERN MEDITERRANEAN) UNRELATED TO SEISMIC EVENTS. *MARINE GEOLOGY*, **55**, 79-101.

CITA, M.B., VERGNAUD-GRAZZINI, C., ROBERT, C., CHAMLEY H., CIARANFI, N. AND D'ONOFRIO, S. (1977). PALEOCLIMATIC RECORD OF A LONG DEEP SEA CORE FROM THE EASTERN MEDITERRANEAN. *QUATERNARY RESEARCH*, **8**, 205-235.

CLAYPOOL, G.E. AND KAPLAN, I.R. (1974). THE ORIGIN AND DISTRIBUTION OF METHANE IN MARINE SEDIMENTS. PP 99-139 IN: *NATURAL GASES IN MARINE SEDIMENTS*, ED I. R. KAPLAN.

CLIFTON, A.P. AND VIVIAN, C.M.G. (1975). RETENTION OF MERUCRY FROM AN INDUSTRIAL SOURCE IN SWANSEA BAY SEDIMENTS. *NATURE*, **253**, 621-622.

COCHRAN, J.K., CAREY, A.E., SHOLKOVITZ, E.R. AND SURPRENANT, L.D. (1986). THE GEOCHEMISTRY OF URANIUM AND THORIUM IN COASTAL MARINE SEDIMENTS AND SEDIMENT PORE WATERS. *GEOCHIMICA ET COSMOCHIMICA ACTA*, **50**, 663-680.

COLLEY, S, THOMSON, J., WILSON, T.R.S. AND HIGGS, N.C. (1984). POST-DEPOSTIONAL MIGRATION OF ELEMENTS DURING DIAGENESIS IN BROWN CLAY AND TURBITITE SEQUENCES IN THE NORTHEAST ATLANTIC. *GEOCHIMICA ET COSMOCHIMICA ACTA*, **48,** 1223-1235.

COLLEY,S. AND THOMSON, J. (1985). RECURRENT URANIUM RELOCATIONS IN DISTAL TURBIDITES EMPLACED IN PELAGIC CONDITIONS. *GEOCHIMICA ET COSMOCHIMICA ACTA*, **49**, 2339-2348.

COLLEY,S. AND THOMSON, J. AND TOOLE, J. (1989). URANIUM RELOCATIONS AND DEVIATION OF QUASI ISOCHRONS FOR A TURBIDITE/PELAGIC SEQUENCE IN THE NORTH-EAST ATLANTIC. *GEOCHIMICA ET COSMOCHIMICA ACTA*, **53**, 1223-1234.

COLLIER, R. AND EDMOND, J. (1984). THE TRACE ELEMENT GEOCHEMISTRY OF MARINE BIOGENIC PARTICULATE MATTER. *PROGRESS IN OCEANOGRAPHY*, **13**, 113-199.

COLLIER, R.W. (1985). MOLYBDENUM IN THE NORTHEAST PACIFIC OCEAN. *LIMNOLOGY AND OCEANOGRAPHY*, **30**, 1351-1354.

CONTRERAS, R., FOGG, T.R., CHASTEE, N.D., GAUDETTE, H.E. AND LYON, W.B. (1978). MOLYBDENUM IN PORE WATERS OF MARINE SEDIMENTS BY ELECTRON PARAMAGNETIC RESONANCE SPECTROSCOPY. *MARINE CHEMISTRY*, **6**, 365-373.

CORNS, W.T., STOCKWELL, P.B., EBDON, L. AND HILL, S.J. (1993). DEVELOPMENT OF AN ATOMIC FLOURESCENCE SPECTROMETER FOR THE HYDRIDE FORMING ELEMENTS. *JOURNAL OF ANALYTICAL ATOMIC SPECTROMETRY*, **8**, 71-77.

COVENEY, R.M., JR, LEVENTHAL, J.S., GLASSOCK, M.D. AND HATCH, J.R. (1987). ORIGINS OF METALS AND ORGANIC MATTER IN THE MECCA QUARRY SHALE MEMBER AND STRATIGRAPHICALLY EQUIVALENT BEDS ACROSS THE MIDWEST. *ECONOMIC GEOLOGY*, **82**, 915-933.

CRAMP, A., COLLINS, M. AND WEST, R. (1988). LATE PLEISTOCENE-HOLOCENE SEDIMAENTATION IN THE NORTH-WEST AEGEAN SEA: A PALEOCLIMATIC, PALEOCEANOGRAPHIC RECONSTRUCTION. *PALEOGEOGRAPHY, PALEOCLIMATOLOGY AND PALEOECOLOGY*, **68**, 61-77.

CRANSTON, R.E. (1983). CHROMIUM IN CASCADIA BASIN, NORTHEAST PACIFIC OCEAN. *MARINE CHEMISTRY*, **13**, 109-125.

CRANSTON, R.E. AND MURRAY, J.W. (1978). THE DETERMINATION OF CHROMIUM SPECIES IN NATURAL WATERS. *ANALYTICAL CHIMICA ACTA*, **99**, 275-282.

CRECELIUS, E.A. (1975). THE GEOCHEMICAL CYCLE OF ARSENIC IN LAKE WASHINGTON AND ITS RELATION TO OTHER ELEMENTS. *LIMNOLOGY AND OCEANOGRAPHY*, **20**, 441-451.

CRECELIUS, E.A., BOTHNER, M.H. AND CARPENTER, R. (1975). GEOCHEMISTRIES OF ARSENIC, ANTIMONY, MERCURY AND OTHER RELATED ELEMENTS IN SEDIMENTS OF PUGET SOUND. *ENVIRONMENTAL SCIENCE AND TECHNOLOGY*, **9**, 325-333.

CRUSIUS, J., CALVERT, S.E., PEDERSEN, T.F. AND SAGE, D. (1996). RHENIUM AND MOLYBDENUM ENRICHMENT IN SEDIMENTS AS INDICATORS OF OXIC, SUB-OXIC AND SULPHIDIC CONDITIONS OF DEPOSITION. *EARTH AND PLANETARY SCIENCE LETTERS*, **145**, 65-78.

CULLEN, W.R. AND REIMER, K.J. (1989). ARSENIC SPECIATION IN THE ENVIRONMENT. *CHEMICAL REVIEWS*, **89**, 713-764.

CUTTER, G.A. (1991). DISSOLVED ARSENIC AND ANTIMONY IN THE BLACK SEA. *DEEP-SEA RESEARCH*, **38**, S825-S843.

D'ALMEIDA, G.A. (1986). A MODEL FOR SAHARAN DUST TRANSPORT. *JOURNAL OF CLIMATE AND APPLIED METEOROLOGY*, **25**, 903-916.

DE CAPITANI, L. AND CITA, M.B. (1996). THE 'MARKER BED' OF THE MEDITERRANEAN RIDGE DIAPIRIC BELT: GEOCHEMICAL CHARACTERISITICS. *MARINE GEOLOGY*, **132**, 215-225.

DE GROOT, A.J. AND ZSCHUPPE, K.H. (1981). CONTRIBUTION TO THE STANDARDISATION OF THE METHODS FOR HEAVY METAL ANALYSIS IN MARINE SEDIMENTS. *RAPP. P-V. REUN. CONS. INT. EXPLOR. MER.* **181**, 111-122.

DE LANGE, G.J. AND TEN HAVEN H.L. (1983). RECENT SAPROPEL FORMATION IN THE EASTERN MEDITERRANEAN. *NATURE*, **305**, 797-798.

DE LANGE, G.J., MIDDELBURG, J.J., PRUYSERS, P.A. (1989). DISCUSSION: MIDDLE AND LATE QUATERNARY DEPOSITIONAL SEQUENCES AND CYCLES IN THE EASTERN MEDITERRANEAN. *SEDIMENTOLOGY*, **36**, 151-156.

DE LANGE, G.J., MIDDELBURG, J.J., VAN DER WEIJDEN, C.H., CATALANO, G., LUTHER III, G.W., HYDES, D.J. WOITTIEZ, J.R.W. AND KLINKHAMMER, G.P. (1990). COMPOSITION OF ANOXIC HYPERSALINE BRINES IN THE TYRO AND BANNOCK BASINS, EASTERN MEDITERRANEAN. *MARINE CHEMISTRY*, **31**, 63-88.

DEAN, W.E., GARDNER, J.V. AND HEMPHILL-HALEY, E. (1989). CHANGES IN REDOX CONDITIONS IN DEEP-SEA SEDIMENTS OF THE SUBARCTIC NORTH PACIFIC OCEAN: POSSIBLE EVIDENCE FOR THE PRESENCE OF NORTH PACIFIC DEEP WATER. *PALEOCEANOGRAPHY*, **4**, 639-653.

DEGENS, E.T., KHOO, R. AND MICHAELIS, W. (1977). URANIUM ANOMALY IN BLACK SEA SEDIMENTS. *NATURE*, **269**, 566-569.

DEHAIRS, F., CHESSELET, R. AND JEDWAB, J. (1980). DISCRETE SUSPENDED PARTICLES OF BARITE AND THE BARIUM CYCLE IN THE OPEN OCEAN. *EARTH AND PLANETARY SCIENCE LETTERS*, **49**, 528-550.

DEHAIRS, F., GOEYENS, L., STROOBANTS, N., BERNARD, P., GOYET, C. POISSON, A. AND CHESSELET, R, (1990). ON SUPSENDED BARITE AND THE O_2 MINIMUM IN THE SOUTHERN OCEAN. *GLOBAL BIOGEOCHEMICAL CYCLES*, **4**, 85-102.

DEHAIRS, F., STROOBANTS, N. AND GOEYENS, L. (1991). SUSPENDED BARITE AS A TRACER OF BIOLOGICAL ACTIVITY IN THE SOUTHERN OCEAN. *MARINE CHEMISTRY*, **35**, 399-410.

DELLA VEDOVA, B., FOUCHER, J.P., PELLIS, G., HARMEGNIES, F. AND MEDRIFF CONSORTIUM, 1995. HEAT FLOW MEASUREMENTS ON THE MEDITERRANEAN RIDGE INDICATE TRANSIENT PROCESSES OF HEAT TRANSFER BETWEEN THE SEDIMENTS AND THE WATER COLUMN (MAST-II-MEDRIFF PROJECT). *RAPP. COMM. INT. MER MEDIT.*, **34**, 100.

DYMOND, J, (1981). GEOCHEMISTRY OF NAZCA PLATE SURFACE SEDIMENTS: AN EVAULATION OF HYDROTHERMAL, BIOGENIC, DETRITAL AND HYDROGENOUS SOURCES. IN: *NAZCA PLATE: CRUSTAL FORMATION AND ANDEAN CONVERGENCE*, L.D. KULM ET AL. (ED). *GEOLOGICAL SOCIETY OF AMERICA MEMOIRS*, **154**, 133-174.

DYMOND, J. AND COLLIER, R. (1996). PARTICULATE BARIUM FLUXES AND THEIR RELATIONSHIP TO BIOLOGICAL PRODUCTIVITY. *DEEP-SEA RESEARCH II*, **43**, 1283-1308.

DYMOND, J., SUESS, E. AND LYLE, M. (1992). BARIUM IN DEEP SEA SEDIMENTS: A GEOCHEMICAL PROXY FOR PALEOPRODUCTIVITY. *PALEOCEANOGRAPHY*, **7**, 163-181.

EDENBORN, H.M., BELZILE, N, MUCCI, A., LEBEL, J. AND SILVERBERG, N. (1986). OBSERVATIONS ON THE DIAGENETIC BEHAVIOUR OF ARSENIC IN A DEEP COASTAL SEDIMENT. *BIOGEOCHEMISTRY*, **2**, 359-376.

ELDERFIELD, H. (1970). CHROMIUM SPECIATION IN SEAWATER. *EARTH AND PLANETARY SCIENCE LETTERS*, **9**, 10-16.

ELDERFIELD, H. AND TRUESDALE, V.W. (1980). ON THE BIOPHILIC NATURE OF IODINE IN SEAWATER. *EARTH AND PLANETARY SCIENCE LETTERS*, **50**, 105-114.

EMEIS, K-C AND SHIPBOARD SCIENTIFIC PARTY (1996). PALEOCEANOGRAPHY AND SAPROPEL INTRODUCTION. *PROCEEDINGS OF THE OCEAN DRILLING PROGRAM, INITIAL REPORTS*, **160**, 21-26.

EMERSON, S. AND HEDGES, J.I. (1988). PROCESSES CONTROLLING THE ORGANIC CARBON CONTENT OF OPEN OCEAN SEDIMENTS. *PALEOCEANOGRAPHY*, **3**, 621-634.

EMERSON, S. SCRANSTON, R.E. AND LISS, P.S. (1979). REDOX SPECIES IN REDUCING FJORD: EQUILIBRIUM AND KINETIC CONDITIONS. *DEEP-SEA RESEARCH*, **26**, 859-878.

EMERSON, S.R. AND HUESTED, S.S. (1991). OCEAN ANOXIA AND THE CONCENTRATION OF MOLYBDENUM AND VANADIUM IN SEAWATER. *MARINE CHEMISTRY*, **34**, 177-196.

EPPLEY, R.W. (1989). NEW PRODUCTION: HISTORY, METHODS, PROBLEMS. IN: *PRODUCTIVITY OF THE OCEAN: PRESENT AND PAST*, ED., WH BERGER, PP 85-97.

FAIRBANKS, R.G. (1989). A 17,000-YEAR GLACIO-EUSTATIC SEA-LEVEL RECORD: INFLUENCE OF GLACIAL MELTING RATES ON THE YOUNGER DRYAS EVENT AND DEEP OCEAN CIRCULATION. *NATURE*, **342**, 637-642.

FAIRBRIDGE, R.W. (1972). QUATERNARY SEDIMENTATION IN THE MEDITERRANEAN REGION CONTROLLED BY TECTONICS, PALEOCLIMATE AND SEA-LEVEL. IN: *THE MEDITERRANEAN SEA. A NATURAL SEDIMENTATION LABORATORY*, PP 99-114. ED D.J. STANLEY.

FARMER, J.G. AND LOVELL, M.A. (1986). NATURAL ENRICHMENT OF ARSENIC IN LOCH LOMOND SEDIMENTS. *GEOCHIMICA ET COSMOCHIMICA ACTA*, **50**, 2059-2067.

FEELY, R.A., TREFRY, J.H., MASSOTH, G.J. AND METZ, S. (1991). A COMPARISON OF THE SCAVENGING OF PHOSPHOROUS AND ARSENIC FROM SEAWATER BY HYDROTHERMAL IRON OXYHYDROXIDES IN THE ATLANTIC AND PACIFIC OCEANS. *DEEP SEA RESEARCH*, **38**, 617-623.

FINNEY, B.P. AND JOHNSON, R. (1991). SEDIMENTATION IN LAKE MALAWI (EAST AFRICA) DURING THE PAST 10000 YEARS: A CONTINUOUS PALEOCLIMATIC RECORD FROM THE SOUTHERN TROPICS. *PALEOGEOGRAPHY, PALEOCLIMATOLOGY AND PALEOECOLOGY*, **85**, 351-366.

FINNEY, B.P., LYLE, M.W. AND HEATH, G.R. (1988). SEDIMENTATION AT MANOP SITE H (EASTERN EQUATORIAL PACIFIC) OVER THE PAST 400,000 YEARS: CLIMATICALLY INDUCED REDOX VARIATIONS AND THEIR EFFECTS ON TRANSITION METAL CYCLING. *PALEOCEANOGRAPHY*, **3**, 169-189.

FONTUGNE, M., ARNOLD, M., LABEYRIE, L., PATERNE, M., CALVERT, S. AND DUPLESSY, J.C. (1994). PALEOENVIRONMENT, SAPROPEL CHRONOLGY AND NILE RIVER DISCHARGE DURING THE LAST 20,000 YEARS AS INDICATED BY DEEP-SEA SEDIMENT RECORDS IN THE EASTERN MEDITERRANEAN. *RADIOCARBON*, **34**, 75-88.

FONTUGNE, M.R., PATERNE, M., CALVERT, S.E., MURAT, A., GUICHARD, F. AND ARNOLD, M. (1989). ADRIATIC DEEP WATER FORMATION DURING THE HOLOCENE: IMPLICATION FOR THE REOXYGENATION OF THE DEEP EASTEN MEDITERRANEAN. *PALEOCEANOGRAPHY*, **4**, 199-206.

FOWLER, S.W. AND KNAUER, G.A. (1986). ROLE OF LARGE PARTICULATES IN THE TRANSPORT OF ELEMENTS AND ORGANIC COMPOUNDS THROUGH THE OCEANIC WATER COLUMN. *PROGRESS IN OCEANOGRAPHY*, **16**, 147-194.

FRANCOIS, R (1987A). A STUDY OF THE EXTRACTION CONDITIONS OF SEDIMENTARY HUMIC ACIDS TO ESTIMATE THEIR IN SITU SULFUR CONTENT. *LIMNOLOGY AND OCEANOGRAPHY*, **32**, 964-972.

FRANCOIS, R (1987B). A STUDY OF SULFUR ENRICHMENT IN THE HUMIC FRACTION OF MARINE SEDIMENTS DURING EARLY DIAGENESIS. *GEOCHIMICA ET COSMOCHIMICA ACTA*, **51**, 17-27.

FRANCOIS, R. (1987C). THE INFLUENCE OF HUMIC SUBSTANCES ON THE GEOCHEMISTRY OF IODINE IN NEAR-SHORE AND HEMI-PELAGIC MARINE SEDIMENTS. *GEOCHIMICA ET COSMOCHIMICA ACTA*, **51**, 2417-2427

FRANCOIS, R. (1988). A STUDY ON THE REGULATION OF THE CONCENTRATION OF SOME METALS (RB, SR, ZN, PB, CU, V, CR, NI, MN AND MO) IN SAANICH INLET SEDIMENTS, BRITISH COLUMBIA, CANADA. *MARINE GEOLOGY*, **83**, 285-308.

FRANCOIS, R., HONJO, S., MANGANINI, S.J. AND RAVIZZA, G.E. (1995). BIOGENIC BARIUM FLUXES TO THE DEEP SEA: IMPLICATIONS FOR PALEOPRODUCTIVITY RECONSTRUCTIONS. *GLOBAL BIOGEOCHEMICAL CYCLES*, **9**, 289-303.

FROELICH, P.N., KLINKHAMMER, G.P., BENDER, M.L., LUEDTKE, N.A., HEATH, G.R., GULLEN, D., DAUPHIN, P., HAMMOND, D., HARTMAN, B. AND MAYNARD, V. (1979). EARLY OXIDATION OF ORGANIC MATTER IN PELAGIC SEDIMENTS OF THE EASTERN EQUATORIAL ATLANTIC: SUBOXIC DIAGENESIS. *GEOCHIMICA ET COSMOCHIMICA ACTA*, **43**, 1075-1090.

FUSI, N. AND KENYON, N.H. (1996). DISTRIBUTION OF MUD DIAPIRISM AND OTHER GEOLOGICAL STRUCTURES FROM LONG RANGE SIDESCAN SONAR (GLORIA) DAT IN THE EASTERN MEDITERRANEAN SEA. *MARINE GEOLOGY*, **132**, 21-38.

GALOWAY, F. AND BENDER, M. (1982): DIAGENETIC MODELS OF INTERSTITIAL NITRATE PROFILES IN DEEP-SEA SUB-OXIC SEDIMENTS. *LIMNOLOGY AND OCEANOGRAPHY*, **27**, 624-638.

GARDNER, J.V., DEAN, W.E., KLISE, D.H. AND BALDAUF, J.G. (1982). A CLIMATE-RELATED OXIDISING EVENT IN THE DEEP-SEA SEDIMENTS FROM THE BERING SEA. *QUATERNARY RESEARCH*, **107**, 91-107.

GASSE, F AND VAN CAMPO, E. (1994). ABRUPT POSTGLACIAL CLIMATE EVENTS IN WEST ASIA AND NORTH AFRICA MONSOON DOMAINS. *EARTH AND PLANETARY SCIENCE LETTERS*, **126**, 435-456.

GINGELE, F. AND DAHMKE, A. (1994). DISCRETE BARITE PARTICLES AND BARIUM AS TRACERS OF PALEOPRODUCTIVITY IN SOUTH ATLANTIC SEDIMENTS. *PALEOCEANOGRAPHY*, **9**, 151-168.

GLIKSON, M., CHAPPELL, B.W., FREEMAN, R.S. AND WEBBER, E. (1985). TRACE ELEMENTS IN OIL SHALES, THEIR SOURCE AND ORGANIC ASSOCIATION WITH PARTICULAR REFERENCE TO AUSTRALIAN DEPOSITS. *CHEMICAL GEOLOGY*, **53**, 155-174.

GODDEN, R.G. AND STOCKWELL, P.B. (1989). ATOMIC FLUORESCENCE SPECTROMETRIC DETERMINATION OF MERCURY USING A FILTER FLUOROMETER. *JOURNAL OF ANALYTICAL ATOMIC SPECTROMETRY*, **4**, 301-303.

GOLHABER, M.B. AND KAPLAN, I.R. (1974). THE SULFUR CYCLE. IN: *THE SEA*, (ED ED GOLDBERG), VOL 5, CHAPTER 17, 569-655.

GOODAY, A.J. AND NOTT, J.A. (1982). INTRACELLULAR BARITE CRYSTALS IN TWO XENOPHYOPHORES, *ASCHEMONELLA RAMULIFORMIS* AND *GALATHEAMMINA SP.* (PROTOZOA:RHIZOPODA) WITH COMMENTS ON THE TAXONOMY OF *A. RAMIMULIFORMIS*. *JOURNAL OF THE MARINE BIOLOGICAL ASSOCIATION OF THE UK*, **62**, 595-605.

GOODHEW, P. AND HUMPHREYS, F.J. (1988). *ELECTRON MICROSCOPY AND ANALYSIS*. LONDON, TAYLOR AND FRANCIS.

GORBY, Y.A. AND LOVLEY, D.R. (1992). ENZYMATIC URANIUM PRECIPITATION. *ENVIRONMENTAL SCIENCE AND TECHNOLOGY*, **26**, 205-207.

GRAMM-OSIPOVE, L.M. (1997). FORMATION OF SOLID PHASE MANGANESE IN OXYGENATED AQUATIC ENVIRONMENTS. PP 301-368 IN: *MANGANESE MINERALISATION: GEOCHEMISTRY AND MINERALOGY OF TERRESTRIAL AND MARINE DEPOSITS*, ED K. NICHOLSON, J.R. HELM, B. BUHN AND S. DASGUPTA. GEOLOGICAL SOCIETY, 370 PP.

GRATTON, Y., EDENBORN, H.E., SILVERBORG, N. AND SUNDBY, B. (1990). A MATHEMATICAL MODEL FOR MANGANESE DIAGENESIS IN BIOTURBATED SEDIMENTS. *AMERICAN JOURNAL OF SCIENCE*, **290**, 246-262.

GREEN, D.H. (1996). DETERMINATION AND BEHAVIOUR OF PLATINUM GROUP AND ASSOCIATED TRACE ELEMENTS IN OCEAN SEDIMENTS. PHD THESIS, KINGSTON UNIVERSITY.

GUERZONI, S., MOLINAROLI, E. AND CHESTER, R. (1997). SAHARAN DUST INPUTS TO THE WESTERN MEDITERRANEAN SEA: DEPOSITIONAL PATTERNS, GEOCHEMICAL AND SEDIMENTOLOGICAL IMPLICATIONS. *DEEP-SEA RESEARCH II, TOPICAL STUDIES IN OCEANOGRAPHY*, **44**, 631-654.

HAINES, K. AND WU, P. (1995). A MODELLING STUDY OF THE THERMOHALINE CIRCULATION OF THE MEDITERRANEAN SEA: WATER FORMATION AND DISPERSAL. *OCEANOLOGICA ACTA*, **18**, 401-417.

HARALDSSON, C AND WESTERLUND, S (1988). TRACE METALS IN THE WATER COLUMNS OF THE BLACK SEA AND FRAMVAREN FJORD. *MARINE CHEMISTRY*, **23**, 417-424.

HARALDSSON, C AND WESTERLUND, S (1991). TOTAL AND SUSPENDED CADMIUM, COBALT, COPPER, IRON, LEAD, MANGANESE, NICKEL AND ZINC IN THE WATER COLUMN OF THE BLACK SEA. IN: JW MURRAY AND E IZDAR (EDS), *BLACK SEA OCEANOGRAPHY*, 161-172.

HARDY, D.A. AND REFREW, A.C. (1990). THERA AND THE AEGEAN WORLD III, THERA FOUNDATION, LONDON.

HARTGERS, W.A., LOPEZ, J.F., SINNINGHE-DAMSTE, J.S., REISS, C., MAXWELL, J.R. AND GRIMALT, J.O. (1997). SULPHUR-BINDING IN RECENT ENVIRONMENTS: II SPECIATION OF SULPHUR AND IRON AND IMPLICATIONS FOR THE OCCURRENCE OF ORGANO-SULPHUR COMPOUNDS. *GEOCHIMICA ET COSMOCHIMICA ACTA*, **61**, 4769-4788.

HARVEY, G.R. (1980). A STUDY OF THE CHEMISTRY OF IODINE AND BROMINE IN MARINE SEDIMENTS. *MARINE CHEMISTRY*, **8**, 327-332.

HATCH, J.R. AND LEVENTHAL, J.S. (1992). RELATIONSHIP BETWEEN INFERRED REDOX POTENTIAL OF THE DEPOSTITIONAL ENVIRONMENT AND GEOCHEMISTRY OF THE UPPER PENNSYLVANIAN (MISSOURIAN) STARK SHALE MEMBER OF THE DENNIS LIMESTONE, WABAUNSEE COUNTY, KANSAS, USA. *CHEMICAL GEOLOGY*, **99**, 65-82.

HEINRICHS, S.M. AND DOYLE, A.P. (1986). DECOMPOSITION OF ^{14}C LABELLED ORGANIC SUBSTANCES IN MARINE SEDIMENT. *LIMNOLOGY AND OCEANOGRAPHY*, **31**, 765-778.

HELZ, G.R., MILLER, C.V., CHARNOCK, J.M., MOSSELMANS, J.F.W., PATTRICK, R.A.D., GARNER, C.D. AND VAUGHAN, D.J. (1996). MECHANISM OF MOLYBDENUM REMOVAL FROM THE SEA AND ITS CONCENTRATION IN BLACK SHALES: EXAFS EVIDENCE. *GEOCHIMICA ET COSMOCHIMICA ACTA*, **60**, 3631- 3642.

HEM, J.D. (1978). REDOX PROCESSES AT SURFACES OF MANGANESE OXIDES AND THEIR EFFECTS ON AQUEOUS METAL IONS. *CHEMICAL GEOLOGY*, **21**, 199-218.

HEM, J.D., LIND, C.J. AND ROBERSON, C.E. (1989). COPRECIPITATION AND REDOX REACTIONS OF MANGANESE OXIDES WITH COPPER AND NICKEL. *GEOCHIMICA ET COSMOCHIMICA ACTA*, **53**, 2811-2822.

HENNEKE, E., LUTHER, G.W., DE LANGE, G.J. AND HOEFS, J. (1997). SULFUR SPECIATION IN ANOXIC HYPERSALINE SEDIMENTS FROM THE EASTERN MEDITERRANEAN SEA. *GEOCHIMICA ET COSMOCHIMICA ACTA*, **61**, 307-321.

HIGGS, N.C., THOMSON, J., WILSON, T.R.S. AND CROUDACE, I.W. (1994). MODIFICATION AND COMPLETE REMOVAL OF EASTERN MEDITERRANEAN SAPROPELS BY POSTDEPOSITIONAL OXIDATION. *GEOLOGY*, **22**, 423-426.

HILGEN, F.J. (1991). ASTRONOMICAL CALIBRATION OF GAUSS TO MATUYAMA SAPROPELS IN THE EASTERN MEDITERRANEAN AND IMPLICATIONS FOR THE GEOMAGNETIC POLARITY TIMESCALE. *EARTH AND PLANETARY SCIENCE LETTERS*, **104**, 226-244.

HORTON, C., CLIFFORD, M., SCHMITZ, J. AND KANTHA, L.H. (1997). A REAL TIME OCEANOGRAPHIC NOWCAST/FORECAST FOR THE MEDITERRANEAN SEA. *JOURNAL OF GEOPHYSICAL RESEARCH*, **102**, 25123-25156.

HOWELL, M.W. AND THUNELL, R.C (1992). ORGANIC CARBON ACCUMULATION IN THE BANNOCK BASIN: EVALUATING THE ROLE OF PRODUCTIVITY IN THE FORMATION OF EASTERN MEDITERRANEAN SAPROPELS. *MARINE GEOLOGY*, **103**, 461-471.

HSU, K.J. (1977). TECTONIC EVOLUTION OF THE MEDITERRANEAN BASINS. IN: *THE OCEAN BASINS AND MARGINS, VOL 4A*, ED AEM NAIRN, WH KANES AND FG STEHLI, NEW YORK, PLENUM.

HUERTA-DIAZ, M.A. AND MORSE, J.W. (1992). PYRITIZATION OF TRACE METALS IN ANOXIC MARINE SEDIMENTS. *GEOCHIMICA ET COSMOCHIMICA ACTA*, **56**, 2681-2702.

JACOBS, L. AND EMERSON, S. (1982). TRACE METAL SOLUBILITY IN AN ANOXIC FJORD. *EARTH AND PLANETARY SCIENCE LETTERS*, **60**, 237-252.

JACOBS, L. EMERSON, S. AND HUESTED, S.S. (1987). TRACE METAL GEOCHEMISTRY IN THE CARIACO TRENCH. *DEEP-SEA RESEARCH*, **34**, 965-981.

JACOBS, L., EMERSON, S. AND SKEI, J. (1985). PARTITIONING AND TRANSPORT OF METALS ACROSS THE THE O_2/H_2S INTERFACE IN A PERMANENTLY ANOXIC BASIN-FRAMVAREN FJORD, NORWAY. *GEOCHIMICA ET COSMOCHIMICA ACTA*, **49**, 1433-1444.

JARVIS, I. AND HIGGS, N.C. (1987). TRACE ELEMENT MOBILITY DURING EARLY DIAGENESIS IN DISTAL TURBIDITES: LATE QUATERNARY OF THE MADEIRA ABYSSAL PLAIN, NORTH ATLANTIC. IN: PPE WEAVER AND J THOMSON (EDS), *GEOLOGY AND GEOCHEMISTRY OF ABYSSAL PLAINS. GEOLOGICAL SOCIETY SPECIAL PUBLICATIONS*, **31**, 179-213.

JEANDEL, C., CAISSO, M. AND MINSTER, J.F. (1987). VANADIUM BEHAVIOUR IN THE GLOBAL OCEAN AND IN THE MEDITERRANEAN SEA. *MARINE CHEMISTRY*, **21**, 51-74.

JORISSEN, F.J., ASIOLI, A., BORSETTI, A.M., CAPOTONDI, L. DE VISSCHER, J.P., HILGEN, F.J., ROHLING, E.J., VAN DER BORG, K., VERGNAUD-GRAZZINI, C. AND ZACHARISSE, W.J. (1993). LATE QUATERNARY CENTRAL MEDITERRANEAN BIOCHRONOLOGY. *MARINE MICROPALEONTOLOGY*, **21**, 169-189.

JUNG, M., ILMBERGER, J., MANGINI, A. AND EMEIS, K.C. (1997). WHY SOME MEDITERRANEAN SAPROPELS SURVIVED BURN-DOWN (AND OTHERS DID NOT). *MARINE GEOLOGY*, **141**, 51-60.

KALLEL, N., PATERNE, M., DUPLESSY, J.C., VERGNAUD-GRAZZINI, C., PUJOL, C., LABEYRIE, L., ARNOLD, M., FONTUGNE, M. AND PIERRE, C. (1997). ENHANCED RAINFALL IN THE MEDITERRANEAN REGION DURING THE LAST SAPROPEL EVENT. *OCEANOLOGICA ACTA*, **20**, 697-712.

KENNEDY, E.J., RUCH, R.R. AND SHIMP, N.F. (1971). DISTRIBUTION OF MERCURY IN UNCONSOLIDATED SEDIMENTS FROM SOUTHERN LAKE MICHIGAN. *ILLINOIS STATE GEOLOGICAL SURVEY, ENVIRONMENTAL GEOLOGY NOTE*, **44**, 18PP.

KENNEDY, H.A. AND ELDERFIELD, H. (1987A). IODINE DIAGENESIS IN NON-PELAGIC DEEP-SEA SEDIMENTS. *GEOCHIMICA ET COSMOCHIMICA ACTA*, **51**, 2505-2514.

KENNEDY, H.A. AND ELDERFIELD, H. (1987B). IODINE DIAGENESIS IN PELAGIC DEEP-SEA SEDIMENTS. *GEOCHIMICA ET COSMOCHIMICA ACTA*, **51**, 2489-2504.

KENNETT, J. (1982). *MARINE GEOLOGY*. P 392-395. PRENTICE HALL.

KIDD, R., CITA, M.B. AND WILLIAMS, B.F.R. (1978). STRATIGRAPHY OF EASTERN MEDITERRANEAN SAPROPEL SEQUENCES AS RECORDED DURING DSDP LEG 42A AND THEIR ENVIRONMENTAL SIGNIFICANCE. IN: *INITIAL REPORTS OF THE DEEP SEA DRILLING PROJECT*, **VOLUME XLII PART 1**, PP 421-443.

KINNIBURGH, D.G., JACKSON, M.L. AND SEYERS, J.K. (1976). ADSORPTION OF ALKALINE EARTH, TRANSITION AND HEAVY METAL CATIONS BY HYDROUS OXIDE GELS OF IRON AND ALUMINIUM. *SOIL SOCIETY OF AMERICA JOURNAL*, **40**, 796-799.

KLEIN, R., LOYA, Y., GVIRTZMAN, G., ISDALE, P.J. AND SUSIC, M. (1990). SEASONAL RAINFALL IN THE SINAI DESERT DURING THE LATE QUATERNARY INFERRED FROM FLUORESCENT BANDS IN FOSSIL CORALS. *NATURE*, **345**, 145-147.

KLINKHAMMER, G.P. AND LAMBERT, C.E. (1989). PRESERVATION OF ORGANIC MATTER DURING SALINITY EXCURSIONS. *NATURE*, **339**, 271-274.

KLINKHAMMER, G.P. AND PALMER, M.R. (1991). URANIUM IN THE OCEANS: WHERE IT GOES AND WHY. *GEOCHIMICA ET COSMOCHIMICA ACTA*, **55**, 1799-1806.

KNIEWALD, G. AND BRANICA, M (1988). ROLE OF U(V) IN MARINE SEDIMENTARY ENVIRONMENTS: A GEOCHEMICAL POSSIBILITY. *MARINE CHEMISTRY*, **24**, 1-12.

KNIEWALD, G. AND BRANICA, M. (1990). REDOX DISTRIBUTION OF URANIUM SPECIES IN SUB-OXIC MARINE ENVIRONMENTS. *RAPPORTS ET PROCES-VERBAUX DES REUNIONS (CIESM)*, **32**, 52.

KNOWLES, R. (1982). DENITRIFICATION. *MICROBIOL. REV.*, **46**, 43-70.

KOCHENOV, A.V., BAUTRIN, G.N. KOVALEVA, S.A., YEMEL'YANOV YE. M. AND SHIMKUS, K.M. (1965). URANIUM AND ORGANIC MATTTER IN THE SEDIMENTS OF THE BLACK AND MEDITERRANEAN SEAS (ABSTRACT). *GEOCHEMISTRY INTERNATIONAL*, **2**, 212.

KOCHENOV, A.V., KOROLEV, K.G., DUBINCHUK, V.T. AND MEDVEDEV YU. L. (1977). EXPERIMENTAL DARAA ON THE CONDITIONS OF PRECIPITATION OF URANIUM FROM AQUEOUS SOLUTIONS. *GEOCHEMISTRY INTERNATIONAL*, **14**, 82-87.

KOHNEN, M.E.L., SINNINGHE- DAMSTE, J.S., TEN HAVEN, H.L. AND DE LEEUW, J.W. (1989). EARLY INCORPORATION OF POLYSULPHIDES IN SEDIMENTARY ORGANIC MATTER. *NATURE*, **341**, 640-641.

KOLODNY, V. AND KAPLAN, I.R. (1973). DEPOSITION OF URANIUM IN THE SEDIMENTS AND INTERSTITIAL WATERS OF AN ANOXIC FJORD. IN: E INGERSON (ED), *SYMP. HYDROGEOCHEMISTRY AND BIOGEOCHEMISTRY.* CLARKE, WASHINGTON D.C., PP 418-442.

KORNICKER, W.A. AND MORSE, J.W. (1991). INTERACTIONS OF DIVALENT CATIONS WITH THE SURFACE OF PYRITE. *GEOCHIMICA ET COSMOCHIMICA ACTA*, **55**, 2159-2171.

KROM, M.D., MICHARD, A, CLIFF, R.A. AND STROHLE, K. (1999). SOURCES OF SEDIMENT TO THE IONIAN AND WESTERN LEVANTINE BASIN OF THE EASTERN MEDITERRANEAN DURING S-1 SAPROPEL TIMES. *MARINE GEOLOGY*, **160**, 45-61.

KULLENBERG, B. (1952). ON THE SALINITY OF THE WATER CONTAINED IN MARINE SEDIMENT. *MEDD. OCEANOGR. INST. GOTEBORG*, **21**, 1-38.

KUTZBACH, J.E. AND GALLIMORE, R.G. (1988). SENSITIVITY OF A COUPLED ATMOSPHERE/MIXED LAYER OCEAN MODEL TO CHANGES IN ORBITAL FORCING AT 9000 YEARS BP. *JOURNAL OF GEOPHYSICAL RESEARCH*, **93**, 803-821.

KUTZBACH, J.E. AND GUETTER, P.J. (1986A). THE INFLUENCE OF CHANGING ORBITAL PARAMETERS AND SURFACE BOUNDARY CONDITIIONS ON CLIMATE SIMULATIONS FOR THE PAST 18,000 YEARS. *JOURNAL OF ATMOSPHERIC SCIENCES*, **43**, 1726-1759.

KUTZBACH, J.E. AND GUETTER, P.J. (1986B). THE SENSITIVITY OF MONSOON CLIMATES TO ORBITAL PARAMETER CHANGES FOR 9000 YEARS BP: EXPERIMENTS WITH THE NCAR CENTRAL CIRCULATION MODEL. IN: A.L. BERGER, J IMBRIE, J. HAYS, G. KUKLA AND B. SALTZMAN (EDITORS), *MILANKOVITCH AND CLIMATE*, PART 2, PP 801-820, REIDEL.

KUTZBACH, J.E. AND LIU, Z. (1997). RESPONSE OF THE AFRICAN MONSOON TO ORBITAL FORCING AND OCEAN FEEDBACKS IN THE MIDDLE HOLOCENE. *SCIENCE*, **278**, 440-443.

KUTZBACH, J.E. AND STREET-PERROTT, F.A. (1985). MILANKOVITCH FORCING OF FLUCTUATIONS IN THE LEVEL OF TROPICAL LAKES FROM 18 TO 0 KYR. *NATURE*, **317**, 130-134.

KUTZBACH, J.E. AND WEBB, T III. (1993). CONCEPTUAL BASIS FOR UNDERSTANDING LATE QUATERNARY CLIMATES, PP 5-11, IN: H.E.WRIGHT, J.E. KUTZBACH, T.WEBB III, W.F. RUDDIMAN, F.A. STREET-PERROTT, AND P.J. BARTLEIN (EDITORS), *GLOBAL CLIMATES SINCE THE LAST GLACIAL MAXIMUM*, UNIVERSITY OF MINNESOTA PRESS.

LANE-SERFF, G.F., ROHLING, E.J., BRYDEN, H.L. AND CHARNOCK, H. (1997). POSTGLACIAL CONNECTION OF THE BLACK SEA TO THE MEDITERRANEAN AND ITS RELATION TO THE TIMING OF SAPROPEL FORMATION. *PALEOCEANOGRAPHY*, **12**, 169-174.

LANGMUIR, D. (1978). URANIUM SOLUTION-MINERAL EQULIBRIA AT LOW TEMPERATURE WITH APPLICATIONS TO SEDIMENTARY ORE DEPOSITS. *GEOCHIMICA ET COSMOCHIMICA ACTA*, **42**, 547-569.

LASCARATOS, A. AND NITTIS, K. (1998). A HIGH RESOLUTION THREE DIMENSIONAL NUMERICAL STUDY OF INTERMEDIATE WATER FORMATION IN THE LEVANTINE SEA. *JOURNAL OF GEOPHYSICAL RESEARCH*, **103**, 18497-18511.

LASCARATOS, A., WILLIAMS, R.G. AND TRAGOU, E. (1993). A MIXED LAYER STUDY OF THE FORMATION OF LEVANTINE INTERMEDIATE WATER. *JOURNAL OF GEOPHYSICAL RESEARCH*, **98**, 14739-14749.

LEE, C. (1992). CONTROLS ON ORAGNIC CARBON PRESERVATION. THE USE OF STRATIFIED WATER BODIES TO COMPARE INTRINSIC RATES OF DECOMPOSTION IN OXIC AND ANOXIC SYSTEMS. *GEOCHIMICA ET COSMOCHIMICA ACTA*, **56**, 3323-3335.

LEGELEUX, F., REYSS, J-L, BONTE, P. AND ORGANO, C. (1994). CONCOMITANT ENRICHMENTS OF URANIUM, MOLYBDENUM AND ARSENIC IN SUB-OXIC CONTINENTAL MARGIN SEDIMENTS. *OCEANOLOGICA ACTA*, **17**, 417-429.

LEWAN, M.D. (1984). FACTORS CONTROLLING THE PROPORTIONALITY OF VANADIUM AND NICKEL IN CRUDE OILS. *GEOCHIMICA ET COSMOCHIMICA ACTA*, **48**, 2231-2238.

LEWAN, M.D. AND MAYNARD, J.B. (1982). FACTORS CONTROLLING ENRICHMENTS OF VANADIUM AND NICKEL IN THE BITUMEN OF ORGANIC SEDIMENT FACIES. *GEOCHIMICA ET COSMOCHIMICA ACTA*, **46**, 2547-2560.

LEWIS, B.L. AND LANDING, W.M. (1991). THE BIOGEOCHEMISTRY OF MANGANESE AND IRON IN THE BALTIC SEA., **38A**, 773-803.

LIBES, S.M. (1992). *AN INTRODUCTION TO MARINE BIOGEOCHEMISTRY*. JOHN WILEY AND SONS, 734 PP.

LIMONOV, A.F., WOODSIDE, J.M., CITA, M.B. AND IVANOV, M.K. (1996). THE MEDITERRANEAN RIDGE AND RELATED MUD DIAPIRISM: A BACKGROUND. *MARINE GEOLOGY*, **132**, 7-19.

LORING, D.H. (1991). NORMALISATION OF HEAVY METAL DATA FROM ESTUARINE AND COASTAL SEDIMENTS. *ICES JOURNAL OF MARINE SCIENCE*, **48**, 101-115.

LOVELY, D.R. AND PHILLIPS, E.J.P. (1986). ORGANIC MATTER MINERALISATION WITH REDUCTION OF FERRIC IRON IN ANAEROBIC SEDIMENTS. *APPLIED ENVIRONMENTAL MICROBIOLOGY*, **51**, 683-689.

LOVLEY, D.R. AND PHILLIPS, E.J.P. (1992). REDUCTION OF URANIUM BY *DESULFOVIBRIO DESULFURICANS*. *APPLIED ENVIRONMENTAL MICROBIOLOGY*, **58**, 850-856.

LOVLEY, D.R., PHILLIPS, E.J.P., GORBY, Y.A. AND LANDA, E.R. (1991). MICROBIAL REDUCTION OF URANIUM. *NATURE*, **350**, 413-416.

LUCKGE, A., ERCEGORAC, M., STRAUSS, H. AND LITTKE, R. (1999). EARLY DIAGENETIC ALTERATION OF ORGANIC MATTER BY SULPHATE REDUCTION IN QUATERNARY SEDIMENTS FROM THE NORTHEASTERN ARABIAN SEA. *MARINE GEOLOGY*, **158**, 1-14.

LUTHER, G.W. III AND CHURCH, T.M. (1992). AN OVERVIEW OF THE ENVIRONMENTAL CHEMISTRY OF SULPHUR IN WETLAND SEDIMENTS. *IN SULPHUR CYCLING ON THE CONTINENTS* (ED R.W. HOWARTH ET AL.) SCOPE, PP 125-142. JOHN-WILEY AND SONS LTD.

LUTHER, G.W., CHURCH, T.M. AND COSMAN, M. (1986). INORGANIC AND ORGANIC SULFUR CYCLING IN SALTMARSH PORE WATERS. *SCIENCE*, **232**, 746-749.

LYONS, T.W. AND BERNER, R.A. (1992). CARBON-SULFUR-IRON SYSTEMATICS OF THE UPPERMOST DEEP-WATER SEDIMENTS OF THE BLACK SEA. *CHEMICAL GEOLOGY*, **99**, 1-27.

MAHER, W.A. (1984). MODE OF OCCURRENCE AND SPECIATION OF ARSENIC IN SOME PELAGIC AND ESTUARINE SEDIMENTS. *CHEMICAL GEOLOGY*, **47**, 333-345.

MALANOTTE-RIZZOLI, P. AND BERGAMASCO, A. (1989). THE GENERAL CIRCUALTION OF THE EASTERN MEDITERRANEAN, PART 1: THE BAROTROPIC WIND DRIVEN CIRCULATION. *OCEANOLOGICA ACTA*, **12**, 335-35.

MALANOTTE-RIZZOLI, P. AND BERGAMASCO, A. (1991). THE WIND AND THERMALLY DRIVEN CIRCULATION OF THE EASTERN MEDITERRANEAN SEA. *DYNAMICS OF ATMOSPHERES AND OCEANS*, **15**, 355-420.

MALANOTTE-RIZZOLI, P. AND HECHT, A. (1988). LARGE SCALE PROPERTIES OF THE THE EASTERN MEDITERRANEAN: A REVIEW. *OCEANOLOGICA ACTA*, **11**, 323-335.

MALANOTTE-RIZZOLI, P., MANCA, B. D'ALCALA M.R. AND THEOCHARIS, A. (1998). THE EASTERN MEDITERRANEAN IN THE 80'S AND IN THE 90'S: THE BIG TRANISITION EMERGED FROM THE POEM-BC OBSERVATIONAL EVIDENCE. *RAPP.COMM. INT. MER MEDIT.*, **35**, 174-175.

MALANOTTE-RIZZOLI, P., MANCA, B., RIBERA D'ALACALA, M., THEOCHARIS, A., BERGAMASCO, A., BREGANT, D., BUDILLON, G., CIVITARESE, G., GEORGOPOULOS, D., MICHELATO, A., SANSONE, E., SCARAZZATO, P. AND SOUVERMEZOGLOU, E. (1997). A SYNTHESIS OF THE IONIAN SEA HYDROGRAPHY, CIRCULATION AND WATE MASS PATHWAYS DURING POEM PHASE-1. *PROGRESS IN OCEANOGRAPHY*, **39**, 153-204.

MALCOLM, S.J. (1985). EARLY DIAGENESIS OF MOLYBDENUM IN ESTUARINE SEDIMENTS. *MARINE CHEMISTRY*, **16**, 213-225.

MALCOLM, S.J. AND PRICE, N.B. (1984). THE BEHAVIOUR OF IODINE AND BROMINE IN ESTUARINE SURFACE SEDIMENTS. *MARINE CHEMISTRY*, **15**, 263-271.

MANGINI, A. AND DOMINIK, J. (1979). LATE QUATERNARY SAPROPELS ON THE MEDITERRANEAN RIDGE: U-BUDGET AND EVIDENCE FOR LOW SEDIMENTATION RATES. *SEDIMENTARY GEOLOGY*, **23**, 113-125.

MANGINI, A. AND SCHLOSSER, P. (1986). THE FORMATION OF EASTERN MEDITERRANEAN SAPROPELS. *MARINE GEOLOGY*, **72**, 115-124.

MANGINI, A., EISENHAUER, A. AND WALTER, P. (1990). RESPONSE OF MANGANESE IN THE OCEAN TO THE CLIMATIC CYCLES IN THE QUATERNARY. *PALEOCEANOGRAPHY*, **5**, 811-821.

MANGINI, A., EISENHAUER, A. AND WALTER, P. (1991). A SPIKE OF CO_2 IN THE ATMOSPHERS AT GLACIAL-INTERGLACIAL BOUNDARY INDUCED BY RAPID DEPOSITION OF MANGANESE IN THE OCEANS. *TELLUS*, **43B**, 97-105.

McCoy, F.W. (1974). Late Quaternary sedimentation in the eastern Mediterranean Sea. PhD. Dissertation, Harvard University, Massachusetts, 132pp.

McKee, B.A. and Todd, J.F. (1993). Uranium behaviuor in a permanently anoxic fjord-microbial control. *Limnology and Oceanography*, **38**, 408-414.

McManus, J., Berelson, W.M., Klinkhammer, G.P., Kilgore, T.E. and Hammond, D.E. (1994). Remobilisation of barium in continental margin sediments. *Geochimica et Cosmochimica Acta*, **58**, 4899-4907.

Middelburg, J.J. (1991). Organic carbon, sulfur and iron in recent semi-euxinic sediments of Kau Bay, Indonesia. *Geochimica et Cosmochimica Acta*, **55**, 815-828.

Minami, H. and Kato, Y. (1997). Remobilisation of arsenic in sub-oxic sediments from the seafloor of the continental margin. *Journal of Oceanography*, **53**, 553-562.

Mo, T., Suttle, A.D. and Scakett, W.M. (1973). Uranium concentrations in marine sediments. *Geochimica et Cosmochimica Acta*, **37**, 35-52.

Mohagheghi, A., Updegraff, D.M. and Goldhaber, M.B. (1985). The role of sulfate-reducing bacteria in the deposition of sedimentary uranium ores. *Geomicrobiology Journal*, **2**, 153-173.

Moore, J.W., Kicklin, W.H. and Johns, C. (1988). Partitioning of arsenic and metals in reducing sulphidic sediments. *Environmental Science and Technology*, **22**, 432-437.

Morse, J.W. (1994). Interactions of trace metals with authigenic sulphide minerals: implications for their bioavailability. *Marine Chemistry*, **46**, 1-6.

Morse, J.W. and Arakaki, T. (1993). Adsorption and coprecipitation of divalent metals with mackinawite (FeS). *Geochimica et Cosmochimica Acta*, **57**, 3635-3640.

Morse, J.W. and Berner, R.A. (1995). What determines sedimentary C/S ratios? *Geochimica et Cosmochimica Acta*, **59**, 1073-1077.

Mossmann, J-R., Aplin, A.C., Curtis, C.D. and Coleman, M.L. (1991). Geochemistry of inorganic and organic sulfur in organic-rich sediments from the Peru margin. *Geochimica et Cosmochimica Acta*, **55**, 3581-3595.

MUCCI, A. AND EDENBORN, H.M. (1992). INFLUENCE OF AN ORGANIC-POOR LANDSLIDE DEPOSIT ON THE EARLY DIAGENESIS OF IRON AND MANGANESE IN A COASTAL MARINE SEDIMENT. *GEOCHIMICA ET COSMOCHIMICA ACTA*, **56**, 3909-3921.

MULLER, P.J. AND SUESS, E. (1979). PRODUCTIVITY, SEDIMENTATION RATE AND SEDIMENTARY ORGANIC MATTER IN THE OCEANS. I ORGANIC CARBON PRESERVATION. *DEEP-SEA RESEARCH*, **26**, 1347-1362.

MURAT, A. AND GOT, H. (1987). MIDDLE AND LATE QUATERNARY DEPOSITIONAL SEQUENCES AND CYCLES IN THE EASTERN MEDITERRANEAN. *SEDIMENTOLOGY*, **34**, 885-899.

MURAT, A. AND GOT, H. (1987). MIDDLE AND LATE QUATERNARY DEPOSTIONAL SEQUENCES IN THE EASTERN MEDITERRANEAN. *SEDIMENTOLOGY*, **34**, 885-899.

MURAT, A.R., GOT, G., CAUWET, G. AND BUSCALI, R. (1990). FACTEURS DE LA VARIABILITE DE TAUX DE CARBONE ORGANIQUE DU SAPROPEL HOLOCENE DE LA MEDITERRANEE ORIENTALE. *RAPP. P-V. REUN. COMMN. INT. EXPLOR. SCIENT. MAR MEDIT.*, **32**, 45.

MURRAY, J.W. (1979). IRON OXIDES. IN: R.G. BURNS (ED) *MARINE MINERALS.* MSA SHORT COURSE NOTES, 6, 42-98.

MURRAY, J.W., DILLARD, J.G., GIOVANOLI, R., MOERS, H. AND STUMM, W. (1985). OXIDATION OF MN(II): INITIAL MINERALOGY, OXIDATION AND AEGING. *GEOCHIMICA ET COSMOCHIMICA ACTA*, **49**, 463-470.

MURRAY, R.W. AND LEINEN, M. (1993). CHEMICAL TRANSPORT TO THE SEAFLOOR OF THE EQUATORIAL PACIFIC OCEAN ACROSS A LATITUDINAL TRANSECT AT 135W: TRACKING SEDIMENTARY MAJOR, TRACE AND RARE EARTH ELEMENT FLUXES AT THE EQUATOR AND THE INTERTROPICAL CONVERGENCE ZONE. *GEOCHIMICA ET COSMOCHIMICA ACTA*, **57**, 4141-4163.

MYERS, P.G., HAINES, K. AND ROHLING, E.J. (1998). MODELLING THE PALEOCIRCULATION OF THE MEDITERRANEAN: THE LAST GLACIAL MAXIMUM AND THE HOLOCENE WITH EMPHASIS ON THE FORMATION OF SAPROPEL S1. *PALEOCEANOGRAPHY*, **13**, 586-606.

NIHLEN, T., MATTSSON, J.O., RAPP, A., GAGAOUDAKI, C., KORNAROS, G. AND PAPAGEORGIOU, J. (1995). *TELLUS B*, **47**, 365-374.

NIJENHUIS, I.A. (1999). *GEOCHEMISTRY OF EASTERN MEDITERRANEAN SEDIMENTARY CYCLES: ON THE ORIGIN OF MICOCENE TO PLEISTOCENE SAPROPELS, LAMINITES AND DIATOMITES.* UNIVERSITY OF UTRECHT.

NISSENBAUM, A. AND KAPLAN, I.R. (1972). CHEMICAL AND ISOTOPIC EVIDENCE FOR THE *IN SITU* ORIGIN OF MARINE HUMIC SUBSTANCES. *LIMNOLOGY AND OCEANOGRAPHY*, **17**, 570-582.

NISSENBAUM, A. AND SWAINE, D.J. (1976). ORGANIC MATTER-METAL INTERACTIONS IN RECENT SEDIMENTS. THE ROLE OF HUMIC SUBSTANCES. *GEOCHIMICA ET COSMOCHIMICA ACTA*, **40**, 809-816.

OGORELEC, B., MISIC, M. AND FAGANELI, H. (1991). MARINE GEOLOGY OF THE GULF OF TRIESTE (NORTHERN ADRIATIC)- SEDIMENTOLOGICAL ASPECTS. *MARINE GEOLOGY*, **99**, 79-82.

OLAUSSON, E (1961). STUDIES OF DEEP-SEA CORES. *REP. SWED. DEEP SEA EXPED. 1947-1948*, **8**, 353-391.

OZSOY, E., HECHT, A. AND UNLATA, U. (1989). CIRCULATION AND HYDROGRAPHY OF THE LEVANTINE BASIN. RESULTS OF THE POEM CO-ORDINATED EXPERIMENTS, 1985-1986. *PROGRESS IN OCEANOGRAPHY*, **22**, 125-170.

OZSOY, E., HECHT, A., UNLUATA, U., BRENNER, S., SUR, H.I., BISHOP, J., LATIF, M.A., ROZENTRAUB, Z. AND OGUZ, T. (1993). A SYNTHESIS OF THE LEVANTINE BASIN CIRCULATION AND HYDROGRAPHY, 1985-1990. *DEEP SEA RESEARCH II*, **40**, 1075-1119.

PAROPKARI, A.L., BABU, C.P. AND MASCARENHAS, A. (1992). A CRITICAL EVALUATION OF DEPOSITIONAL PARAMETERS CONTROLLING THE VARIABILITY OF ORGANIC CARBON IN ARABIAN SEA SEDIMENTS. *MARINE GEOLOGY*, **107**, 213-226.

PAROPKARI, PRAKASH-BABU, C. AND MASCARENHAS, A. (1993). NEW EVIDENCE FOR ENHANCED PRESERVATION OF ORGANIC CARBON IN CONTACT WITH THE OXYGEN MINIMUM ZONE ON THE WESTERN CONTINENTAL SLOPE OF INDIA. *MARINE GEOLOGY*, **111**, 7-13.

PASSIER, H.F. (1998). *SULPHUR GEOCHEMISTRY AND SAPROPEL FORMATION: SYNGENETIC AND DIAGENETIC SIGNALS IN EASTERN MEDITERRANEAN SEDIMENTS*. UNIVERSITY OF UTRECHT.

PASSIER, H.F. AND DE LANGE, G.J. (1998). SEDIMENTARY SULPHUR AND IRON CHEMISTRY IN RELATION TO THE FORMATION OF EASTERN MEDITERRANEAN SAPROPELS. IN: *PROCEEDINGS OF THE OCEAN DRILLING PROGRAM SCIENTIFIC RESULTS*, **160**.

PASSIER, H.F., MIDDELBURG, J.J., DELANGE, G.J. AND BOTTCHER, M.E. (1997). PYRITE CONTENTS, MICROTEXTURES, AND SULFUR ISOTOPES IN RELATION TO FORMATION OF THE YOUNGEST EASTERN MEDITERRANEAN SAPROPEL. *GEOLOGY*, **25**, 519-522.

PASSIER, H.F., MIDDELBURG, J.J., DELANGE,G.J. AND BOTTCHER, M.E. (1999). MODES OF SAPROPEL FORMATION IN THE EASTERN MEDITERRANEAN: SOME CONSTRAINTS BASED ON PYRITE PROPERTIES. *MARINE GEOLOGY*, **153**, 199-219

PASSIER, H.F., MIDDELBURG, J.J., VAN OS, B.J.H. AND DELANGE, G.J. (1996). DIAGENETIC PYRITISATION UNDER EASTERN MEDITERRANEAN SAPROPELS CAUSED BY DOWNWARD SULPHIDE DIFFUSION. *GEOCHIMICA ET COSMOCHIMICA ACTA*, **60**, 751-763.

PASSIER, H.F., MIDDELBURG, J.J., VAN OS, B.J.H. AND DE LANGE, G.J. (1996). DIAGENETIC PYRITISATION UNDER EASTERN MEDITERRANEAN SAPROPELS CAUSED BY DOWNWARD SULPHIDE DIFFUSION. *GEOCHIMICA ET COSMOCHIMICA ACTA*, **60**, 751-763.

PAYTAN, A., KASTNER, M. AND CHAVEZ, F.P. (1996). GLACIAL TO INTERGLACIAL FLUCTUATIONS IN PRODUCTIVITY IN THE EQUATORIAL PACIFIC AS INDICATED BY MARINE BARITE. *SCIENCE*, **274**, 1355-1357.

PEDERSEN T.F AND CALVERT, S.E. (1990). ANOXIA VS PRODUCTIVITY: WHAT CONTROLS THE FORMATION OF ORGANIC-CARBON RICH SEDIMENTS AND SEDIMENTARY ROCKS? *AAPG BULLETIN*, **74**, 454-471.

PEDERSEN, T.F. AND PRICE, N.B. (1980). THE GEOCHEMISTRY OF IODINE AND BROMINE IN SEDIMENTS OF THE PANAMA BASIN. *JOURNAL OF MARINE RESEARCH*, **38**, 397-411.

PERRISSORATIS, C. AND PIPER, D.J.W. (1992). AGE, REGIONAL VARIATION AND SHALLOWEST OCCURRENCE OF S1 SAPROPEL IN THE NORTHERN AEGEAN SEA. *GEO-MARINE LETTERS*, **12**, 49-53.

PETERSON, M.L AND CARPENTER, R. (1983). BIOGEOCHEMICAL PROCESSES AFFECTING TOTAL ARSENIC AND ARSENIC SPECIES DISTRIBUTIONS IN AN INTERMITTENTLY ANOXIC FJORD. *MARINE CHEMISTRY*, **12**, 295-321.

PIERCE, M.L., AND MOORE, C.B. (1982). I: ADSORPTION OF ARSENITE AND ARSENATE ON AMORPHOUS IRON HYDROXIDE. *WATER RESEARCH*, **16**, 1247-1253.

PILLAY, K.K.S., THOMAS, C.C., SONDEL, J.A. AND HYCHE, C.M. (1971). DETERMINATION OF MERCURY IN BIOLOGICAL AND ENVIRONMENTAL SAMPLES BY NEUTRON ACTIVATION ANALYSIS. *ANALYTICAL CHEMISTRY*, **43**, 1419-1425.

POEM GROUP (1992). THE GENERAL CIRCULATION OF THE EASTERN MEDITERRANEAN. *EARTH SCIENCE REVIEWS*, **32**, 285-309.

PRELL, W.R. AND KUTZBACH, J.E. (1987). MONSOON VARIABILITY OVER THE PAST 150,000 YEARS. *JOURNAL OF GEOPHYSICAL RESEARCH*, **92**, 8411-8425.

PREMOVIC, P.I., PAVLOVIC, N.Z., PAVLOVIC, M.S. AND NIKOLIC, N.D. (1993). PHYSIO-CHEMICAL CONDITIONS OF SEDIMENTATION OF THE FISH CLAY FROM STEVENS KLINT, DENMARK AND ITS DETRITAL NATURE- VANDIUM AND OTHER SUPPORTIVE EVIDENCE. *GEOCHIMICA ET COSMOCHIMICA ACTA*, **57**, 1433-1446.

PRICE, B.A. AND FROELICH, P.N. (1987). LATE HOLOCENE REDOX CHANGES IN EASTERN EQUATORIAL PACIFIC AND ATLANTIC SEDIMENTS: A TIME SCALE FOR RECENT INCREASES IN EQUATORIAL UPWELLING. *TRANS. AM. GEOPHYS. UNION (EOS)*, **68**, 1330 (ABSTR.).

PRICE, N.B. AND CALVERT, S.E. (1973). THE GEOCHEMISTRY OF IODINE IN OXIDISED AND REDUCED RECENT MARINE SEDIMENTS. *GEOCHIMICA ET COSMOCHIMICA ACTA*, **37**, 2149-2158.

PRICE, N.B. AND CALVERT, S.E. (1977). THE CONTRASTING GEOCHEMICAL BEHAVIOURS OF IODINE AND BROMINE IN RECENT SEDIMENTS FROM THE NAMIBIAN SHELF. *GEOCHIMICA ET COSMOCHIMICA ACTA*, **41**, 1769-1775.

PRICE, N.B., CALVERT, S.E. AND JONES, P.G.W. (1970). THE DISTRIBUTION OF IODINE AND BROMINE IN THE SEDIMENTS OF THE SOUTHWEST BARENTS SEA. *JOURNAL OF MARINE RESEARCH*, **28**, 22-34.

PRUYSERS, P.A., DE LANGE, G.J. AND MIDDELBURG, J.J. (1991). GEOCHEMISTRY OF EASTERN MEDITERRANEAN SEDIMENTS: PRIMARY SEDIMENT COMPOSTION AND DIAGENETIC ALTERATIONS. *MARINE GEOLOGY*, **100**, 137-154.

PRUYSERS, P.A., DE LANGE, G.J., MIDDELBURG, J.J. AND HYDES, D.J. (1993). THE DIAGENETIC FORMATION OF METAL-RICH LAYERS IN SAPROPEL CONTAINING SEDIMENTS IN THE EASTERN MEDITERRANEAN. *GEOCHIMICA ET COSMOCHIMICA ACTA*, **57**, 527-536.

QUEDNAU, M, MAGGIULLI, M., RAHDERS, E., HALBACH, P. AND HALBACH, M. (1997). POST-DEPOSITIONAL REALLOCATION PATTERNS IN SAPROPEL-BEARING SEDIMENTS FROM CONTRASTING DIAGENETIC REGIMES, EASTERN MEDITERRANEAN SEA: A COMPARATIVE GEOCHEMICAL STUDY. *CHEMIE DER ERDE- GEOCHEMISTRY*, **57**, 205-230.

QUINBY-HUNT, M.S. AND WILDE, P. (1994). THERMODYNAMIC ZONATION IN BLACK SHALE FACIES BASED ON FE, MN AND V CONTENTS. *CHEMICAL GEOLOGY*, **113**, 297-317.

RABOUILLE, C. AND GAILLARD, J.F. (1991). TOWARDS THE EDGE: EARLY DIAGENESIS GLOBAL EXPLANATION. A MODEL DEPICTING THE EARLY DIAGENESIS OF ORGANIC MATTER, O_2, MN AND PO_4. *GEOCHIMICA ET COSMOCHIMICA ACTA*, **55**, 2511-2525.

RAISWELL, R. AND BERNER, R.A. (1985). PYRITE FORMATION IN EUXINIC AND SEMI-EUXINIC SEDIMENTS. *AMERICAN JOURNAL OF SCIENCE*, **285**, 710-724.

RAISWELL, R., BOTTRELL, S.H., AL-BIATTY, H.J. AND TAN, M.M.D. (1993). THE INFLUENCE OF BOTTOM WATER OXYGENATION AND REACTIVE IRON CONTENT IN SULPHUR INCORPORATION INTO BITUMENS FROM JURASSIC MARINE SHALES. *AMERICAN JOURNAL OF SCIENCE*, **293**, 569-596.

REEDER, M., ROTHWELL, R.G., STOW, D.A.V., KAHLER, G. AND KENYON, N.H. (1998). TURBIDITE FLUX, ARCHITECTURE AND CHEMOSTRATIGRAPHY OF THE HERODOTUS BASIN, LEVANTINE SEA, SE MEDITERRANEAN. IN: *GEOLOGICAL PROCESSES ON CONTINENTAL MARGINS: SEDIMENTATION, MASS WASTING AND STABILITY*. (ED) MS STOKER, D EVANS AND A.CRAMP, GEOLOGICAL SOCIETY OF LONDON SPECIAL PUBLICATION, 129, 19-41.

REIMERS, C.E., JAHNKE, R.A. AND MCCORKLE, D.C. (1992). CARBON FLUXES AND BURIAL RATES OVER THE CONTINENTAL SLOPE AND RISE OFF CENTRAL CALIFORNIA WITH IMPLICATIONS FOR THE GLOBAL CARBON CYCLE. *GLOBAL BIOGEOCHEMICAL CYCLES*, **6**, 199-224.

RICKARD, D. (1997). KINETICS OF PYRITE FORMATION BY THE H2S OXIDATION OF IRON(II) MONOSULPHIDE IN AQUEOUS SOLUTION BETWEEN 25 AND 125°C: THE RATE EQUATION. *GEOCHIMICA ET COSMOCHIMICA ACTA*, **61**, 115-134.

RITCHIE, J.C., EYLES, C.H. AND HAYNE, C.V. (1985). SEDIMENT AND POLLEN EVIDENCE FOR AN EARLY TO MID-HOLOCENE HUMID PERIOD IN THE EASTERN SAHARA. *NATURE*, **314**, 352-355.

ROBERTSON, A.H.F. (1998). MESOZOIC-TERTIARY TECTONIC EVOLUTION OF THE EASTERN MOST MEDITERRANEAN AREA: INTEGRATION OF MARINE AND LAND INFLUENCE. *ODP SCIENTIFIC RESULTS*, **160**, 723-782.

ROBERTSON, A.H.F. AND WOODCOCK, N.H. (1979). MAMONIA COMPLEX SW CYPRUS: EVOLUTION AND EMPLACEMENT OF A MESOZOIC CONTINENTAL MARGIN. *GEOLOGICAL SOCIETY OF AMERICA BULLETIN, PART 1*, **90**, 651-665.

ROBINSON, A.R. AND GOLNARAGHI, M. (1993). CIRCULATION AND DYNAMICS OF THE EASTERN MEDITERRANEAN SEA; QUASI-SYNOPTIC DATA DRIVEN SIMULATIONS. *DEEP SEA RESEARCH II*, **40**, 1202-1246.

ROBINSON, A.R., GOLNARAGHI, M., LESIE, W.G., ARTEGIANAI, A., HECHT, A., LAZZONE, E., MICHELATO, A., SANSONE, E., THEOCHARIS, A. AND UNLUATA, U. (1991). STRUCTURE AND VARIABILITY OF THE EASTERN MEDITERRANEAN GENERAL CIRCULATION. *DYNAMICS OF ATMOSPHERES AND OCEANS*, **12**, 215-240.

ROEHTER, W. AND SCHLITZER, R. (1991). EASTERN MEDITERRANEAN DEEP WATER RENEWAL ON THE BASIS OF CHLOROFLUOROMETHANE AND TRITIUM DATA. *DYNAMICS OF ATMOSPHERES AND OCEANS*, **15**, 333-354.

ROETHER, W., MANCA, B.B., KLEIN, B., BREGANT, D., GEORGOPOULOS D., BEITZEL, V., KOVACEVIC, V. AND LUCHETTA, A. (1996) RECENT CHANGES IN THE EASTERN MEDITERRANEAN DEEP WATER. *SCIENCE*, **271**, 333-335.

ROHLING, E.J. (1991A). A SIMPLE TWO LAYERED MODEL FOR SHOALING OF THE EASTERN MEDITERRANEAN PYCNNOCLINE DUE TO GLACIO-EUSTATIC SEA-LEVEL LOWERING. *PALEOCEANOGRAPHY*, **6**, 537-541.

ROHLING, E.J. (1991B). SHOALING OF THE EASTERN MEDITERRANEAN PYCNOCLINE DUE TO REDUCTION OF EXCESS EVAPORATION : IMPLICATION FOR SAPROPEL FORMATION. *PALEOCEANOGRAPHY*, **6**, 747-753.

ROHLING, E.J. (1994). REVIEW AND NEW ASPECTS CONCERNING THE FORMATION OF EASTERN MEDITERRANEAN SAPROPELS. *MARINE GEOLOGY*, **122**, 1-28.

ROHLING, E.J. AND GIESEKES, W.W.C. (1989). LATE QUATERNARY CHANGES IN MEDITERRANEAN INTERMEDIATE WATER DENSITY AND FORMATION RATE. *PALEOCEANOGRAPHY*, **4**, 531-545.

ROHLING, E.J. AND HILGEN, F.J. (1991). THE EASTERN MEDITERRANEAN CLIMATE AT THE TIMES OF SAPROPEL FORMATION: A REVIEW. *GEOL. MIJNBOUW*, **70**, 253-264.

ROHLING, E.J., JORISSEN, F.J. AND DE STIGER, H.C. (1997). 200 YEAR INTERRUPTION OF HOLOCENE SAPROPEL FORMATION IN THE ADRIATIC SEA. *JOURNAL OF MICROPALEONTOLOGY*, **16**, 97-108.

ROSSIGNOL-STRICK, M. (1983). AFRICAN MONSOONS, AN IMMEDIATE CLIMATE RESPONSE TO ORBITAL INSOLATION. *NATURE*, **304**, 46-49.

ROSSIGNOL-STRICK, M. (1985). MEDITERRANEAN QUATERNARY SAPROPELS, AN IMMEDIATE RESPONSE OF THE AFRICAN MONSOON TO VARIATIONS IN INSOLATION. *PALEOGEOGRAPHY, PALEOCLIMATOLOGY AND PALEOECOLOGY*, **49**, 237-263.

ROSSIGNOL-STRICK, M. (1987). RAINY PERIODS AND BOTTOM WATER STAGNATION INITIATING BRINE ACCUMULATION AND METAL CONCENTRATION 1: THE LATE QUATERNARY. *PALEOCEANOGRAPHY*, **2**, 333-360.

ROSSIGNOL-STRICK, M., NESTEROFF, V., OLIVE, P., AND VERGNAUD-GRAZZINI, C. (1982). AFTER THE DELUGE; MEDITERRANEAN STAGNATION AND SAPROPEL FORMATION. *NATURE*, **295**, 105-110.

ROTHWELL, R.G. (1995). "MARION DUFRESNE" CRUISE 81 CRUISE REPORT: MEDITERRANEAN GIANT PISTON CORING TRANSECT, 17TH JANUARY – 9TH FEBRUARY, 1995, MARSILLE FRANCE-LIMASSOL CYPRUS.

ROUSSENOV, V., STANEV, E., ARTALE, V. AND PINARDI, N. (1995). A SEASONAL MODEL OF THE MEDITERRANEAN SEA GENERAL CIRCULATION. *JOURNAL OF GEOPHYSICAL RESEARCH*, **100**, 13515-13538.

RYAN, W.B.F. (1972). STRATIGRAPHY OF LATE QUATERNARY SEDIMENTS IN THE EASTERN MEDITERRANEAN. IN: STANLEY, D.J. (ED), *THE MEDITERRANEAN SEA*. PP 1-765, DOWDEN, HUTCHISON AND ROSS, STROUDSBURG, PA.

SADIQ, M. (1988). THERMODYNAMIC SOLUBILITY RELATIONSHIPS OF INROGANIC VANADIUM IN THE MARINE ENVIRONMENT. *MARINE CHEMISTRY*, **23**, 87-96.

SADIQ, M. (1990). ARSENIC CHEMISTRY IN MARINE ENVIRONMENTS: A COMPARISON BETWEEN THEORETICAL AND FIELD OBSERVATIONS. *MARINE CHEMISTRY*, **31**, 285-297.

SADIQ, M. (1992). *TOXIC METAL CHEMISTRY IN MARINE ENVIRONMENTS*. NEW YORK: MARCEL DEKKER, 390PP.

SARKAR, A., BHATTACHARYA, S.K. SARIN, M.M. (1993). GEOCHEMICAL EVIDENCE FOR ANOXIC DEEP-WATER IN THE ARABIAN SEA DURING THE LAST GALCIATION. *GEOCHIMICA ET COSMOCHIMICA ACTA*, **57**, 1009-1016.

SARMIENTO, J.L., HERNERT, T. AND TOGGWEILER, J.R. (1988). MEDITERRANEAN NUTRIENT BALANCE AND EPISODES OF ANOXIA. *GLOBAL BIOGEOCHEMICAL CYCLES*, **2**, 427-444.

SARNTHEIN, M., PFLAUMANN.U., ROSS, R., TIEDMANN, R. AND WINN, K. (1992). TRANSFER FUNCTIONS TO RECONSTRUCT PALAEOPRODUCTIVITY: A COMPARISON. PP 411-427 IN: *UPWELLING SYSTEMS: EVOLUTION SINCE THE EARLY MIOCENE*, (ED CP SUMMERHAYES, WC PRELL AND KC EMEIS).

SARNTHEIN, M., THIEDE, J., PFLAUMANN, U., ESLENKEUSER, H., FUTTERER, D., KOOPMAN, B., LANGE, H. AND SEIBOLD, E. (1982). ATMOSPHERIC AND OCEANIC CIRCULATION PATTERNS OFF NORTH WEST AFRICA DURING THE PAST 25 MILLION YEARS, PP 545-604, IN, U. VON RAD, K. HINZ, M. SARNTHEIN AND E. SEIBOLD (EDITORS), *GEOLOGY OF THE NORTH WEST AFRICAN CONTINENTAL MARGIN*: BERLIN, SPRINGER VERLAG.

SCHLITZER R., ROETHER W., OSTER, H., JUNGJANS H-G., HAUSMANN M., JOHANNSEN H., AND MICHELATO, A. (1991). CHLOROFLUORMETHANE AND OXYGEN IN THE EASTERN MEDITERRANEAN. *DEEP-SEA RESEARCH*, **38,** 1531-1551.

SCHMITZ, B. (1987). BARIUM, EQUATORIAL HIGH PRODUCTIVITY AND THE NORTHWARD WANDERING OF THE INDIAN CONTINENT. *PALEOCEANOGRAPHY*, **2**, 63-77.

SCHNEIDER, R.R., PRICE, B., MULLER, P.J., KROON, D. AND ALEXANDER, I. (1997). MONSOON RELATED VARIATIONS IN ZAIRE (CONGO) SEDIMENT LOAD AND INFLUENCE OF FLUVIAL SILICATE SUPPLY ON THE MARINE PRODUCTIVITY IN THE EAST EQUATORIAL ATLANTIC DURING THE LAST 200,000 YEARS. *PALEOCEANOGRAPHY*, **12**, 463-482.

SCHOONEN, M.A.A. AND BARNES, H.L. (1991A). REACTION FORMING PYRITE AND MARCASITE FROM SOLUTION. 1. NUCLEATION OF FeS_2 BELOW 100°C. *GEOCHIMICA ET COSMOCHIMICA ACTA*, **55**, 1495-1504.

SCHOONEN, M.A.A. AND BARNES, H.L. (1991B). REACTIONS FORMING PYRITE AND MARCASITE FROM SOLUTION.2. VIA FES PRECURSORS BELOW 100°C. *GEOCHIMICA ET COSMOCHIMICA ACTA*, **55**, 1505-1514.

SCHRADER, H. AND MATHERNE, A (1981). SAPROPEL FORMATION IN THE EASTERN MEDITERRANEAN SEA: EVIDENCE FROM PRESERVED OPAL ASSEMBLAGES. *MICROPALEONTOLOGY*, **27**, 191-203.

SEVERMANN, S. AND THOMSON, J. (1998). INVESTIGATION OF THE INGROWTH OF RADIOACTIVE DAUGHTERS OF 238U IN MEDITERRANEAN SAPROPELS AS A POTENTIAL DATING TOOL. *CHEMICAL GEOLOGY*, **150**, 317-330.

SEYLER, P. AND MARTIN, J-M. (1989). BIOGEOCHEMICAL PROCESSES AFFECTING ARSENIC SPECIATION DISTRIBUTION IN A PERMANENTLY STRATIFIED LAKE. *ENVIRONMENTAL SCIENCE AND TECHNOLOGY*, **23**, 1258-1263.

SAHW, T.I. (1959). THE MECHANISM OF IODIDE ACCUMULATION BY THE BROWN SEAWEED LAMINARIA DIGITATA. THE UPTAKE OF I-131. *PROCEEDINGS OF THE ROYAL SOCIETY OF LONDON, SERIES B*, **150**, 356-371.

SHAW, H. F. AND EVANS, G. (1984). THE NATURE, DISTRIBUTION AND ORIGIN OF A SAPROPELIC LAYER IN THE SEDIMENTS OF THE CILICIA BASIN, NORTHEASTERN MEDITERRANEAN. *MARINE GEOLOGY*, **61**, 1-12.

SHAW, T.J., GIESKES, J.M. AND JAHNKE, R.A. (1990). EARLY DIAGENESIS IN DEFFERENT DEPOSITIONAL ENVIRONMENTS: THE RESPONSE OF TRANSITION METALS IN PORE WATERS. *GEOCHIMICA ET COSMOCHIMICA ACTA*, **54**, 1233-1246.

SHERRELL, R.M. AND BOYLE, E.A. (1988). ZN, CR, V AND FE IN THE MEDITERRANEAN SEA. *DEEP-SEA RESEARCH*, **35**, 1319-1334.

SHIMKUS, K.M. AND TRIMONIS, E.S. (1974). MODERN SEDIMENTATION IN THE BLACK SEA, IN, E.T. DEGENS AND D. A. ROSS (EDITORS), THE BLACK SEA- GEOLOGY, CHEMISTRY AND BIOLOGY, *AAPG MEMOIR*, **20**, 249-278.

SHIMMIELD, G.B. (1985). THE GEOCHEMSITRY AND MINERALOGY OF PACIFIC SEDIMENTS, BAJA CALIFORNIA, PHD THESIS, UNIVERSITY OF EDINBURGH, EDINBURGH.

SHIMMIELD, G.B. (1992). CAN SEDIMENT GEOCHEMISTRY RECORD CHANGES IN COASTAL UPWELLING PALAEOPRODUCTIVITY? EVIDENCE FROM NORTHWEST AFRICA AND THE ARABIAN SEA. IN: *UPWELLING SYSTEMS: EVOLUTION SINCE THE EARLY MIOCENE*, PP 29-46. (ED) CP SUMMERHAYES, WL PRELL, AND KC EMEIS.

SHIMMIELD, G.B. AND PEDERSEN, T.F. (1990). THE GEOCHEMISTRY OF REACTIVE TRACE METALS AND HALOGENS IN HEMIPELAGIC CONTINENTAL MARGIN SEDIMENTS. *REVIEWS IN AQUATIC SCIENCES*, **3**, 255-279.

SHIMMIELD, G.B. AND PRICE, N.B. (1986). THE BEHAVIOUR OF MOLYBDENUM AND MANGANESE DURING EARLY SEDIMENT DIAGENESIS-OFFSHORE BAJA CALIFORNIA, MEXICO. *MARINE CHEMISTRY*, **19**, 261-280.

SKEI, J.M., LORING, D.H. AND RANTALA, R.T.T. (1988). PARTITIONING AND ENRICHMENT OF TRACE METALS IN A SEDIMENT CORE FROM FRAMVAREN, SOUTHERN NORWAY. *MARINE CHEMISTRY*, **23**, 269-281.

STANLEY AND F. C. WEZEL (EDITORS), *GEOLOGICAL EVOLUTION OF THE MEDITERRANEAN BASIN*. SPRINGER, NEW YORK, PP 413-451.

STANLEY, D.J. (ED) (1972). *THE MEDITERRANEAN SEA: A NATURAL SEDIMENTATION LABORATORY.* 765PP.

STANLEY, D.J. AND MALDONADO, A. (1979): LEVANTINE SEA- NILE CONE LITHOSTRATIGRAPHIC EVOLUTION: QUANTITATIVE ANALYSIS AND CORRELATION WITH PALEOCLIMATIC AND EUSTATIC OSCILLATIONS IN THE LATE QUATERNARY. *SEDIMENTARY GEOLOGY*, **23**, 37-65.

STRATFORD, K. AND WILLIAMS, R.G. (1997). A TRACER STUDY OF THE FORMATION, DISPERSAL AND RENEWAL OF LEVANTINE INTERMEDIATE WATER. *JOURNAL OF GEOPHYSICAL RESEARCH*, **102**, 12534-12549.

STREET, A.F. AND GROVE, A.T. (1979). GLOBAL MAPS OF LAKE LEVEL FLUCTUATIONS SINCE 30,000 YEARS BP. *QUATERNARY RESEARCH*, **12**, 83-118.

STREET-PERROT, F.A. AND PERROT, R.A. (1993). HOLOCENE VEGETATION, LAKE LEVELS AND CLIMATE OF AFRICA. IN: H.E.WRIGHT, J.E. KUTZBACH, T.WEBB III, W.F. RUDDIMAN, F.A. STREET-PERROTT, AND P.J. BARTLEIN (EDITORS), *GLOBAL CLIMATES SINCE THE LAST GLACIAL MAXIMUM*, PP 318-356, UNIVERSITY OF MINNESOTA PRESS.

STREET-PERROTT, F.A., MITCHELL, J.F.B., MARCHAND, D.S. AND BRUNNER, J.S. (1990). MILANKOVITCH AND ALBEDO FORCING OF THE TROPICAL MONSOONS: A COMPARISON OF GEOLOGICAL EVIDENCE AND NUMERICAL SIMULATIONS FOR 9000 YEARS BP. *TRANSACTIONS OF THE ROYAL SOCIETY OF EDINBURGH- EARTH SCIENCES*, **81**, 407-427.

STROHLE, K. AND KROM, M.D. (1997). EVIDENCE FOR THE EVOLUTION OF AN OXYGEN MINIMUM LAYER AT THE BEGINNING OF S-1 SAPROPEL DEPOSITION IN THE EASTERN MEDITERRANEAN. *MARINE GEOLOGY*, **140**, 231-236.

STUMM, W. AND MORGAN, J.J. (1981). *AQUATIC CHEMISTRY*. 2 ED. WILEY-INTERSCIENCE, NEW YORK, 780 PP.

SULLIVAN, K.A. AND ALLER, R.C. (1996). DIAGENETIC CYCLING OF ARSENIC IN AMAZON SHELF SEDIMENTS. *GEOCHIMICA ET COSMOCHIMICA ACTA*, **60**, 1465-1477.

SUN, M.Y., LEE, C. AND ALLER, R.C. (1993). LABORATORY STUDIES OF OXIC AND ANOXIC DEGRADATION OF CHLOROPHYLL–A IN LONG ISLAND SEDIMENTS. *GEOCHIMICA ET COSMOCHIMICA ACTA*, **57**, 147-157.

SUTHERLAND, H.E., CALVERT, S.E. AND MORRIS, R.J. (1984). GEOCHEMICAL STUDIES OF THE RECENT SAPROPEL AND ASSOCIATED SEDIMENT FROM THE HELLENIC OUTER RIDGE, EASTERN MEDITERRANEAN SEA, I. MINERALOGY AND CHEMICAL COMPOSITION. *MARINE GEOLOGY*, 56, 79-92.

SWEENY, R.E. AND KAPLAN, I.R. (1973). PYRITE FRAMBOID FORMATION: LABORATORY SYNTHESIS AND MARINE SEDIMENTS. *ECONOMIC GEOLOGY*, **68**, 618-634.

SZALAY, A AND SZILAGYI, M. (1967). THE ASSOCIATION OF VANADIUM WITH HUMIC SUBSTANCES. *GEOCHIMICA ET COSMOCHIMICA ACTA*, **31**, 1-6.

SZILAGYI, M. (1967). SORPTION OF MOLYBDENUM BY HUMUS PREPARATIONS. *GEOKHIMYA*, **12**, 1489-1492.

TAKEMATSU, N., SATO, Y., OKABE, S. AND NAKAYAMA, E. (1985). THE PARTITIONING OF VANADIUM AND MOLYBDENUM BETWEEN MANGANESE OXIDES AND SEAWATER. *GEOCHIMICA ET COSMOCHIMICA ACTA*, **49**, 2395-2399.

TANG, C.M. AND STOTT, L.D. (1993). SEASONAL SALINITY CHANGES DURING MEDITERRANEAN SAPROPEL DEPOSITION 900 YEARS BP, EVIDENCE FROM ISOTOPIC ANALYSIS OF INDIVIDUAL PLANKTONIC FORAMINFERA. *PALEOCEANOGRAPHY*, **8**, 473-493.

TEMPLETON, G.D. III AND CHASTEEN, N.D. (1980). VANADIUM FULVIC ACID CHEMISTRY: CONFORMATIONAL AND BINDING STUDIES BY ELECTRON SPIN TECHNIQUES. *GEOCHIMICA ET COSMOCHIMICA ACTA*, *44*, 741-752.

TEN HAVEN, H.L. DE LEEUW, J.W., SCHENK, P.A. AND KLAVER, G.T. (1987). GEOCHEMISTRY OF MEDITERRANEAN SEDIMENTS. BROMINE/ORGANIC CARBON AND URANIUM/ORGANIC CARBON RATIOS AS INDICATORS FOR DIFFERENT SOURCES OF INPUT AND POST-DEPOSITIONAL OXIDATION, RESPECTIVELY. *ORGANIC GEOCHEMISTRY*, 13, 255-261.

TEN HAVEN, H.L., DE LANGE, G.J. AND MCDUFF, R.E. (1991). INTERSTITIAL WATER STUDIES OF LATE QUATERNARY EASTERN MEDITERRANEAN SEDIMENTS WITH EMPHASIS ON EARLY DIAGENETIC REACTIONS AND EVAPORITIC SALT INFLUENCES. *MARINE GEOLOGY*, **75**, 119-136.

TEN HAVEN, H.L., DE LEEUW, J.W., SCHENK, P. AND KLAVER, G.T. (1987). GEOCHEMISTRY OF MEDITERRANEAN SEDIMENTS. BROMINE/ORGANIC CARBON AND URANIUM/ORGANIC CARBON RATIOS AS

INDICATORS FOR DIFFERENT SOURCES OF INPUT AND POST-DEPOSITIONAL OXIDATION, RESPECTIVELY. *ORGANIC GEOCHEMISTRY*, **13**, 255-261.

TERTIAN R. AND CLAISSE, F. (1982). *PRINCIPLES OF QUANTITATIVE X-RAY FLUORESCENCE ANALYSIS*. CHICHESTER, WILEY, 355PP.

TESSIER, A., CAMPBELL, P.G.C. AND BISSON, M. (1979). A SEQUENTIAL EXTRACTION PROCEDURE FOR THE SPECIATION OF PARTICULATE TRACE METALS. *ANALYTICAL CHEMISTRY*, **51**, 844-851.

TESSIER, A., FORTIN, D., BELZILE, N., DEVITRE, R.R. AND LEPPARD, G.G. (1996). METAL SORPTION TO DIAGENETIC IRON AND MANGANESE OXYHYDROXIDES AND ASSOCIATED ORGANIC MATTER: NARROWING THE GAP BETWEEN FIELD AND LABORATORY MEASUREMENTS. *GEOCHIMICA ET COSMOCHIMICA ACTA*, **60**, 387-404.

TESSIER, A., RAPIN, F. AND CARIGNAN, R. (1985). TRACE METALS IN OXIC LAKE SEDIMENTS-POSSIBLE ADSORPTION ONTO IRON OXYHYDROXIDES. *GEOCHIMICA ET COSMOCHIMICA ACTA*, **49**, 183-194.

THEOCHARIS, A., GEORGOPOULOS, D., LASCARATOS, A. AND NITTIS, K. (1993). WATER MASSES AND CIRCULATION IN THE CENTRAL REGION OF THE EASTERN MEDITERRANEAN: EASTERN IONIAN, SOUTH AEGEAN AND NORTWEST LEVANTINE, 1986-1987. *DEEP SEA RESEARCH II*, **40**, 1121-1142.

THEOCHARIS, A., PAPAGEORGIOU, E., KONTOYANNI, H., NITTIS, K. AND BALOPOLO, S.E. (1998). THE EVOLUTION OF THE AEGEAN WATER'S INFLUENCE IN THE DEEP THERMOHALINE CIRCULATION OF THE EASTERN MEDITERRANEAN (1986-1995). *RAPP. COMM. INT. MER MEDIT.*, **35**, 200-201.

THOMPSON, K.C. AND REYNOLDS, G.D. (1971). THE ATOMIC FLUORESCENCE DETERMINATION OF MERCURY BY THE COLD VAPOUR TECHNIQUE. *ANALYST*, **96**, 771-775.

THOMSON, J., HIGGS, N.C. WILSON, T.R.S., CROUDACE, I.W., DE LANGE, G.J. AND VAN SANTVOORT, P.J.M. (1995). DISTRIBUTION AND GEOCHEMICAL BEHAVIOUR OF REDOX-SENSITIVE ELEMENTS AROUND S1, THE MOST RECENT EASTERN MEDITERRANEAN SAPROPEL. *GEOCHIMICA ET COSMOCHIMICA ACTA*, **59**, 3487-3501.

THOMSON, J., HIGGS, N.C., CROUDACE, I.W., COLLEY, S. AND HYDES, D.J. (1993). REDOX ZONATION OF ELEMENTS AT AN OXIC/POST-OXIC BOUNDARY IN DEEP-SEA SEDIMENTS. *GEOCHIMICA ET COSMOCHIMICA ACTA*, **57**, 579-595.

THOMSON, J., HIGGS, N.C., WILSON, T.R.S., CROUDACE, I.W., DE LANGE, G.J. AND VAN SANTVOORT, P.J.M. (1995). REDISTRIBUTION AND GEOCHEMICAL BEHAVIOUR OF REDOX-SENSITIVE ELEMENTS AROUND S1, THE MOST RECENT EASTERN MEDITERRANEAN SAPROPEL. *GEOCHIMICA ET COSMOCHIMICA ACTA*, **59**, 3487-3501.

THOMSON, J., JARVIS, I., GREEN, D.R.H., GREEN, D.A. AND CLAYTON, T. (1998). MOBILITY AND IMMOBILITY OF REDOX-SENSITIVE ELEMENTS IN DEEP-SEA TURBIDITES DURING SHALLOW BURIAL. *GEOCHIMICA ET COSMOCHIMICA ACTA*, **62**, 643-656.

THOMSON, J., MERCONE, D., DE LANGE, G.J. AND VAN SANTVOORT, P.J.M. (1999). REVIEW OF RECENT ADVANCES IN THE INTERPRETATION OF EASTERN MEDITERRANEAN SAPROPEL S1 FROM GEOCHEMICAL EVIDENCE. *MARINE GEOLOGY*, 153, 77-89.

THOMSON, J., WALLACE, H.E., COLLEY, S. AND TOOLE, J. (1990). AUTHIGENIC URANIUM IN ATLANTIC SEDIMENTS OF THE LAST GLACIAL STAGE- A DIAGENETIC PHENOMENON. *EARTH AND PLANETARY SCIENCE LETTERS*, **98**, 222-232.

THOMSON, J., MERCONE, D., DE LANGE, G.J. AND VAN SANTVOORT P.J.M. (1999). REVIEW OF RECENT ADVANCES IN THE INTERPRETAION OF EASTERN MEDITERRANEAN SAPROPEL S1 FROM GEOCHEMICAL EVIDENCE. *MARINE GEOLOGY*, **153**, 77-89.

THUNELL, R.C. AND WILLIAMS, D. F. (1983). PALEOTEMPERATURE AND PALEOSALINITY HISTORY OF THE EASTERN MEDITERRANEAN DURING THE LATE QUATERNARY. *PALEOGEOGRAPHY, PALEOCLIMATOLOGY AND PALEOECOLOGY*, **44**, 23-39.

THUNELL, R.C. AND WILLIAMS, D.F. (1982). PALEOCEANOGRAPHIC EVENTS ASSOCIATED WITH TERMINATION II IN THE EASTERN MEDITERRANEAN. *OCEANOLOGICA ACTA*, 5, 229-233.

THUNELL, R.C., AND WILLIAMS, D.F. (1989). GLACIAL HOLOCENE SALINITY CHANGES IN THE MEDITERRANEAN SEA: HYDROGRAPHIC AND DEPOSITIONAL EFFECTS. *NATURE*, **338**, 493-496.

THUNELL, R.C., WILLIAMS, D.F. AND BELYEA, P.R. (1984). ANOXIC EVENTS IN THE MEDITERRANEAN SEA IN RELATION TO THE EVOLUTIOIN OF LATE NEOGENE CLIAMTES. *MARINE GEOLOGY*, **59**, 105-134.

THUNELL, R.C., WILLIAMS, D.F. AND CITA, M.B. (1983). GLACIAL ANOXIA IN THE EASTERN MEDITERRANEAN. *JOURNAL OF FORAMINIFERAL RESEARCH*, **13**, 283-290.

THUNELL, R.C., WILLIAMS, D.F. AND HOWELL, M. (1987). ATLANTIC-MEDITERRANEAN EXCHANGE DURING THE LATE NEOGENE. *PALEOCEANOGRAPHY*, **2**, 661-678.

THUNELL, R.C., WILLIAMS, D.F. AND KENNETT, J. P. (1977) LATE QUATERNARY PALEOCLIMATOLOGY, STRATIGRAPHY AND SAPROPEL HISTORY IN EASTERN MEDITERRANEAN DEEP-SEA SEDIMENTS. *MARINE MICROPALEONTOLOGY*, **2**, 371-388.

TOMADIN, L., LENOZ, R, LANDUZZI, V., MAZZUCATEKKI, A. AND VANNUCCI, R. (1984). WIND BLOWN DUSTS OVER THE CENTRAL MEDITERRANEAN. *OCEANOLOGICA ACTA*, **7**, 13-23.

TORRES, M.E., BRUMSACK, H.J., BOHRMANN, G. AND EMEIS, K.C. (1996). BARITE FRONTS IN CONTINENTAL MARGIN SEDIMENTS: A NEW LOOK AT BARIUM REMOBILISATION IN THE ZONE OF SULPHATE REDUCTION AND FORMATION OF HEAVY BARITES IN DIAGENETIC FRONTS. *CHEMICAL GEOLOGY*, **127**, 125-139.

TREFY, J.H. AND METZ, S. (1989). ROLE OF HYDROTHERMAL PRECIPITATES IN THE GEOCHEMICAL CYCLING OF VANADIUM. *NATURE*, **342**, 531-533.

TROELSTRA, S.R., GANSSEN, G.M., VAN DER BORG, K AND DE JONG, A.F.M. (1991). A LATE QUATERNARY STRATIGRAPHICAL FRAMEWORK FOR EASTERN MEDITERRANEAN SAPROPEL S1 BASED ON AMS 14C DATES AND STABLE OXYGEN ISOTOPES. *RADIOCARBON*, **33**, 15-21.

TROMP, T.K., VAN CAPPELLEN, P. AND KEY, R.M. (1995). A GLOBAL MODEL FOR THE EARLY DIAGENESIS OF ORGANIC CARBON AND ORGANIC PHOSPHOROUS IN MARINE SEDIMENTS. *GEOCHIMICA ET COSMOCHIMICA ACTA*, **59**, 1284.

TURNER, D.R., WHITFIELD, M. AND DICKSON, A.G. (1981). THE EQUILIBRIUM SPECIATION OF DISSOLVED COMPONENTS IN FRESHWATER AND SEAWATER AT 25°C AND 1 ATM PRESSURE. *GEOCHIMICA ET COSMOCHIMICA ACTA*, **45**, 855-881.

ULLMAN, W.J. AND ALLER, R.C. (1985). THE GEOCHEMISTRY OF IODINE IN NEAR-SHORE CARBONATE SEDIMENTS. *GEOCHIMICA ET COSMOCHIMICA ACTA*, **49**, 967-978.

UPSILL-GODDARD, R.C. AND ELDERFIELD, H. (1988). THE ROLE OF DIAGENESIS IN THE ESTUARINE BUDGETS OF IODINE AND BROMINE. *CONTINENTAL SHELF RESEARCH*, **8**, 405-430.

VAIRAVAMURTHY, A. AND MOPPER, K. (1987). GEOCHEMICAL FORMATION OF ORGANOSULFUR COMPOUNDS (THIOLS) BY ADDITION OF H_2S TO SEDIMENTARY ORGANIC MATTER. *NATURE*, **329**, 623-625.

VAN DER SLOOT, H.A., HOEDE, D., HAMBURG, G. AND WOITTIEZ, J.R.W. (1990). TRACE ELEMENTS IN SUSPENDED MATTER FROM THE ANOXIC HYPERSALINE TYRO AND BANNOCK BASINS (EASTERN MEDITERRANEAN). *MARINE CHEMISTRY*, **31**, 187-203.

VAN DER SLOOT, H.A., HOEDE, D., WIJKSTRA, J., DUINKER, J.C. AND NOLTING, R.F. (1985). ANIONIC SPECIES OF V, AS, SE, MO, SB, AND TE IN THE SCHELDT AND RHINE ESTUARIES AND THE SOUTHER BIGHT (NORTH SEA). *ESTUARINE AND COASTAL SHELF SCIENCE*, **21**, 633-651.

VAN DER WEIJDEN, C. (1992). EARLY DIAGENESIS AND MARINE PORE WATER, IN: *DIAGENESIS III*, ED BY K.H. WOLF AND G.V. CHILLINGHAM, PP 13-134.

VAN DER WEIJDEN, C.H., MIDDELBURG, J.J., DE LANGE, G.J., VAN DER SLOOT, H.A., HOEDE, D. AND WOIFFIEZ, J.R.W. (1990). PROFILES OF REDOX-SENSITIVE ELEMENTS AS, SB, V, MO AND U IN THE TYRO AND BANNOCK BASINS (EASTERN MEDITERRANEAN). *MARINE CHEMISTRY*, **31**, 171-186.

VAN OS, B.J.H., MIDDELBURG, J.J. AND DE LANGE, G.J. (1991). POSSIBLE DIAGENETIC MOBILISATION OF BARIUM IN SPAROPELIC SEDIMENT FROM THE EASTERN MEDITERRANEAN. *MARINE GEOLOGY*, **100**, 125-136.

VAN SANTVOORT P.J.M., DE LANGE, G.J., LANGEREIS, C.G., DEKKERS, M.J. AND PATERNE, M. (1997). GEOCHEMICAL AND PALEOMAGNETIC EVIDENCE FOR THE OCCURRENCE OF "MISSING" SAPROPELS IN EASTERN MEDITERRANEAN SEDIMENTS. *PALEOCEANOGRAPHY*, **12**, 773-786.

VAN SANTVOORT, P.J.M. AND DE LANGE, G.J. (1996). MESSINIAN SALT FLUXES INTO THE PRESENT DAY EASTERN MEDITERRANEAN: IMPLICATIONS FOR BUDGET CALCULATIONS AND STAGNATION. *MARINE GEOLOGY*, 132, 241-251.

VAN SANTVOORT, P.J.M., DE LANGE, G.J., LANGEREIS, C.G. DEKKERS, M.J AND PATERNE, M. (1997). GEOCHEMICAL AND PALEOMAGNETIC EVIDENCE FOR THE OCCURRENCE OF "MISSING" SAPROPELS IN THE EASTERN MEDITERRANEAN. *PALEOCEANOGRAPHY*, **12**, 773-786.

VAN SANTVOORT, P.J.M., DE LANGE, G.J., THOMSON, J., CUSSEN, H., WILSON, T.R.S., KROM, M.D. AND STROHLE, K. (1996). ACTIVE POSTDEPOSTIONAL OXIDATION OF THE MOST RECENT SAPROPEL (S1) IN SEDIMENTS OF THE EASTERN MEDITERRANEAN SEA. *GEOCHIMICA ET COSMOCHIMICA ACTA*, **60**, 4007-4024.

VAN SANTVOORT, P.J.M., DE LANGE, G.J., THOMSON, J., CUSSEN, H., WILSON, T.R.S., KROM, M.D. AND STROHLE, K. (1996). ACTIVE POST-DEPOSITIONAL OXIDATION OF THE MOST RECENT SAPROPEL (S1) IN SEDIMENTS OF THE EASTERN MEDITERRANEAN SEA. *GEOCHIMICA ET COSMOCHIMICA ACTA*, **60**, 4007-4024.

VARNANVAS, S.P., PAPAIOANNOU, J. AND CATANI, J. (1988). A HYDROTHERMAL MANGANESE DEPOSIT FROM THE ERATOSTHENES SEAMOUNT, EASTERN MEDITERRANEAN SEA. *MARINE GEOLOGY*, **81**, 205- 214.

VERGNAUD-GRAZZINI, C. (1985). MEDITERRANEAN LATE CENOZOIC STABLE ISOTOPE RECORD: STRATIGRAPHIC AND PALEOCLIMATIC IMPLICATIONS. IN: D.J.

VERGNAUD-GRAZZINI, C., BORSETTI, A.M., CATI, F., COLANTONI, P., D'ONOFRIO, S., SALIEGE, J.F., SARTORI, R. AND TAMPIERI, R. (1988). PALEOCEANOGRAPHIC RECORD OF THE LAST DEGLACIATION IN THE STRAITS OF SICILY. *MARINE MICROPALEONTOLOGY*, 13, 1-21.

VERGNAUD-GRAZZINI, C., CARALP, M., FALLGERES, J-C., GONTHIER, E., GROUSSET, F., PUJOL, C. AND SALIEGE, J-F.(1989). MEDITERRANEAN OUTFLOW THROUGH THE STRAITS OF GIBRALTAR SINCE 18,000 YEARS BP. *OCEANOLOGICA ACTA*, **12**, 305-324.

VERGNAUD-GRAZZINI, C., DEVAUX, M. AND ZNAIDI, J. (1986). STABLE ISOTOPE 'ANOMALIES' IN MEDITERRANEAN PLEISTOCENE RECORDS. *MARINE MICROPALEONTOLOGY*, **10**, 35-69.

VERGNAUD-GRAZZINI, C., RYAN W.B.F AND CITA, M.B. (1977). STABLE ISOTOPE FRACTIONATION, CLIMATIC CHANGE AND EPISODIC STAGNATION IN THE EASTERN MEDITERRANEAN DURING THE LATE QUATERNARY. *MARINE MICROPALEONTOLOGY*, **2**, 353-370.

WAKEFIELD, S.J. AND ELDERFIELD, H. (1985). INTERSTITIAL WATER IODINE ENRICHMENTS IN SEDIMENTS FROM THE EASTERN PACIFIC. *JOURNAL OF MARINE RESEARCH*, **43**, 951-961.

WALLACE, H.E., THOMSON, J., WILSON, T.R.S., WEAVER, P.P.E, HIGGS, N.C. AND HYDES, D.J. (1988). ACTIVE DIAGENETIC FORMATION OF METAL-RICH LAYERS IN NORTHEAST ATLANTIC SEDIMENTS. *GEOCHIMICA ET COSMOCHIMICA ACTA*, **52**, 1557-1569.

WANG, Q. AND MORSE, J.W. (1996). PYRITE FORMATION UNDER CONDITIONS APPROXIMATING THOSE IN ANOXIC SEDIMENTS. I. PATHWAY AND MORPHOLOGY. *MARINE CHEMISTRY*, **52**, 99-121.

WANTY, R.B. AND GOLDHABER, M.B. (1992). THERMODYNAMICS AND KINETICS OF REACTIONS INVOLVING VANADIUM IN NATURAL SYSTEMS. ACCUMULATION OF VANADIUM IN SEDIMENTARY ROCKS. *GEOCHIMICA ET COSMOCHIMICA ACTA*, **56**, 1471-1483.

WEHRLI, B. AND STUMM, W. (1989). VANADYL IN NATURAL WATERS: ADSORPTION AND HYDROLYSIS PROMOTE OXYGENATION. *GEOCHIMICA ET COSMOCHIMICA ACTA*, **53**, 69-77.

WESTRICH, J.T. AND BERNER, R.A. (1984). THE ROLE OF SEDIMENTARY ORGANIC MATTER IN BACTERIAL SULPHATE REDUCTION: THE G MODEL TESTED. *LIMNOLOGY AND OCEANOGRAPHY*, **29**, 236-249.

WIGNALL, P.B.(1993) *BLACK SHALES*. OXFORD SCIENCE PUBLICATIONS.

WILKIN, R.T. AND BARNES, H.L. (1996). PYRITE FORMATION BY REACTIONS OF IRON MONOSULFIDES WITH DISSOLVED INORGANIC AND ORGANIC SULFUR SPECIES. *GEOCHIMICA ET COSMOCHIMICA ACTA*, **60**, 4167-4179.

WILKIN, R.T. AND BARNES, H.L. (1997). FORMATION PROCESSES OF FRAMBOIDAL PYRITE. *GEOCHIMICA ET COSMOCHIMICA ACTA*, **61**, 323-339.

WILKIN, R.T., ARTHUR, M.A. AND DEAN, W.E. (1997). HISTORY OF WATER COLUMN ANOXIA IN THE BLACK SEA INDICATED BY PYRITE FRAMBOID SIZE DISTRIBUTION. *EARTH AND PLANETARY SCIENCE LETTERS*, **148**, 517-525.

WILKIN, R.T., BARNES, H.L. AND BRANTLEY, S.L. (1996). THE SIZE DISTRIBUTION OF FRAMBOIDAL PYRITE IN MODERN SEDIMENTS: AN INDICATOR OF REDOC CONDITIONS. *GEOCHIMICA ET COSMOCHIMICA ACTA*, **60**, 3897-3912.

WILLIAMS, D.F., THUNELL, R.C. AND KENNETT, J.P. (1978). PERIODIC FRESHWATER FLOODING AND STAGNATION OF THE EASTERN MEDITERRANEAN DURING THE LATE QUATERNARY. *SCIENCE*, **201,** 252-254.

WILSON, T.A. AND WEBER, J.H. (1979). AN EPR STUDY OF THE REDUCTION OF V(V) TO V(IV) BY FULVIC ACIDS. *CHEMICAL GEOLOGY*, **26**, 345-354.

WILSON, T.R.S., THOMSON, J., COLLEY, S., HYDES, D.J. AND HIGGS, N.C. (1985). EARLY ORGANIC DIAGENESIS: THE SIGNIFICANCE OF PROGRESSIVE SUBSURFACE OXIDATION FRONTS IN MARINE SEDIMENTS. *GEOCHIMICA ET COSMOCHIMICA ACTA*, **49**, 811-822.

WILSON, T.R.S., THOMSON, J., HYDES, D.J., COLLEY, S., CULKIN, F. AND SORENSON, J. (1986). OXIDATION FRONTS IN PELAGIC SEDIMENTS: DIAGENETIC FORMATION OF METAL RICH LAYERS. *SCIENCE*, **232**, 972-975.

WONG, G.T.F. (1991). THE MARINE GEOCHEMISTRY OF IODINE. *REVIEWS IN AQUATIC SCIENCES*, **4**, 45-73.

WONG, G.T.F. AND BREWER, P.G. (1977). THE MARINE GEOCHEMISTRY OF IODINE IN ANOXIC BASINS. *GEOCHIMICA ET COSMOCHIMICA ACTA*, **41**, 151-159.

WONG, G.T.F., TAKAYANAGI, K. AND TODD, J.F. (1985). DISSOLVED IODINE IN WATERS OVERLYING AND IN THE ORCA BASIN, GULF OF MEXICO. *MARINE CHEMISTRY*, **17**, 177-183.

WOODSIDE, J.M. (1977). TECTONIC ELEMENTS AND CRUST OF THE EASTERN MEDITERRANEAN SEA. *MARINE GEOPHYSICAL RESEARCHES*, **3**, 317-354.

WOOLNOUGH, W.G. (1937). SEDIMENTATION IN BARRED BASINS, SOURCE ROCKS OF OIL. *AAPG BULLETIN*, **21**, 1101-1157.

WU, P. AND HAINES, K. (1996). MODELLING THE DISPERSAL OF LEVANTINE INTERMEDIATE WATER AND ITS ROLE IN MEDITERRANEAN DEEP WATER FORMATION. *JOURNAL OF GEOPHYSICAL RESEARCH*, **101**, 6591-6607.

YOUNG, L.B. AND HARVEY, H.H. (1992). THE RELATIVE IMPORTANCE OF MANGANESE AND IRON OXIDES AND ORGANIC MATTER IN THE SORPTION OF TRACE METALS BY SURFICIAL LAKE SEDIMENTS. *GEOCHIMICA ET COSMOCHIMICA ACTA*, **56**, 1175-1186.

ZAHN, R., SARTHEIN, M. AND ERLENKEUSER, H. (1987). BENTHIC ISOTOPE EVIDENCE FOR CHANGES OF THE MEDITERRANEAN OUTFLOW DURING THE LATE QUATERNARY. *PALEOCEANOGRAPHY*, **2**, 543-539.

Appendices:

Appendix 1: Major and trace element data for core MD81-LC25.

Depth in core (cm)	SiO_2 wt%	TiO_2 wt%	Al_2O_3 wt%	Fe_2O_3 wt%	MnO wt%	MgO wt%	CaO wt%	Na_2O wt%	K_2O wt%	P_2O_5 wt%	As ppm	Ba ppm	Br ppm	Cr ppm	Hg ppb	I ppm	MnO ppm	Mo ppm	Ni ppm	Se ppm	U ppm	V ppm	Zn ppm	Zr ppm	Cl wt%	S wt%	Corg wt%	$CaCO_3$ wt%
22.5	27.77	0.4527	7.272	3.282	0.078	3.212	27.53	0.814	0.248	0.099	0	126	72.9	54.7	n.d.	15.6	1241	2.09	38	n.d.	0.87	57.9	51.8	116	1.71	0.187	0.47	49.868
29.5	26.24	0.4402	7.162	3.158	0.084	3.249	28.73	0.734	0.161	0.105	0	115	77.7	49.2	n.d.	27.1	1252	1.39	39	n.d.	0.83	58.9	53.8	93	1.99	0.218	0.367	51.92
34.5	24.12	0.4089	6.964	3.121	0.102	3.216	29.38	0.627	0.095	0.109	0	108	80	46.7	n.d.	23.8	1424	1.52	34	n.d.	0.43	56.9	48.3	84	2.08	0.222	0.323	53.294
41.5	20.41	0.3378	5.711	2.653	0.117	2.917	28.39	0.356	0.086	0.098	0	27.3	96.8	26.5	n.d.	45.9	1658	1.32	26	n.d.	2.46	35.6	33.2	0	1.99	0.295	0.366	73.357
52.5	21.58	0.3717	6.014	2.872	0.176	3.237	32.96	0.162	0.088	0.108	0	84	71	49.8	n.d.	29.2	2200	2.36	42	n.d.	0	53.2	51.1	65	2.11	0.228	0.325	58.475
57.5	21.27	0.3782	6.206	3.113	0.324	2.978	32.88	0.155	0.122	0.115	0	91.7	82.6	53.2	n.d.	31.1	3614	4.7	53	n.d.	0.27	61.3	50.3	55	1.76	0.235	0.327	57.876
58.5	21.35	0.3788	6.338	3.233	0.406	2.909	32.73	0.108	0.074	0.115	7.66	92.8	84.7	52.8	n.d.	33.5	4348	4.51	57	n.d.	0.71	60.1	56	52	2.17	0.258	0.288	57.019
59.5	21.28	0.3775	6.275	3.249	0.371	2.871	32.63	0.162	0.081	0.115	7.73	97.7	83.6	60	16.5	27.8	4013	3.88	57	0.0412	1.32	62.9	53.9	53	2.14	0.267	0.367	56.889
60.5	21.06	0.3772	6.331	3.388	0.37	2.815	32.67	0.155	0.067	0.121	0	131	90.5	54.5	19	33.1	4002	5.35	59	0.0426	1.34	67.3	53.8	47	2.18	0.275	0.296	56.267
61.5	21.11	0.3708	6.29	3.485	0.33	2.73	32.57	0.303	0.108	0.121	0	174	98.1	62.8	30	37	3620	5.42	58	0.0326	0.1	68.7	56.4	45	2.07	0.282	0.303	56.04
62.5	20.35	0.3709	6.147	3.636	0.265	2.59	32.3	0.411	0.331	0.119	2.41	235	106	62.1	28	36.1	3098	4.22	58	0.0255	0.3	69.3	53.2	43	2.41	0.296	0.345	56.287
63.5	19.71	0.3752	6.056	3.739	0.23	2.508	32.22	0.428	0.132	0.125	14.7	307	111	58.3	32	42.9	2859	5.68	55	0.0325	0.38	74.2	57	40	2.92	0.305	0.35	56.537
64.5	19.68	0.3426	6.009	4.138	0.211	2.471	32.41	0.448	0.046	0.138	15.5	400	123	62.4	32.5	52.5	2533	4.39	53	0.0417	1.16	72.2	55	38	3.08	0.324	0.305	55.76
65.5	19.69	0.3483	5.974	4.39	0.171	2.451	32.2	0.315	0.039	0.151	17.4	498	125	65.7	33	43.4	2112	4.21	52	0.0299	0.56	76.4	50.8	36	2.76	0.285	0.313	55.512
66.5	19.63	0.355	6.015	4.516	0.158	2.419	31.92	0.447	0.039	0.151	17.3	586	136	59.9	29.5	55	1915	4.48	53	0.0297	2.52	75.2	53.9	38	2.95	0.356	0.326	55.792
67.5	19.53	0.342	6.031	4.69	0.151	2.407	31.78	0.638	0.046	0.158	16.3	638	142	67.3	37.5	72.3	1878	4.39	52	0.0399	0.85	75.2	49.8	39	2.71	0.373	0.426	54.137
68.5	20.2	0.363	6.304	5.083	0.191	2.422	30.55	0.62	0.092	0.178	13.9	684	146	69.1	39.5	115	2307	5.87	55	0.0359	0.13	80.3	59.1	42	3.51	0.393	0.524	51.6
69.5	21.08	0.378	6.685	5.021	0.172	2.494	29.69	0.597	0.04	0.166	22.2	723	165	72.3	95.5	198	2113	7.18	56	0.0458	1.14	78.3	74.3	45	3.85	0.436	1.342	49.887
70.5	22.26	0.4006	7.043	5	0.154	2.443	32.41	0.34	0.047	0.147	16.5	712	181	81.5	146	182	1887	8.87	62	1.5698	2.04	83.4	85.4	48	4.1	0.504	2.081	46.997
71.5	23.7	0.4372	7.897	4.951	0.081	2.744	26.25	1.238	0.215	0.155	18.6	688	202	81.5	201 5	119	1210	17.7	70	5.237	4.92	100	79.4	54	5.33	0.757	2.639	43.512
72.5	23.03	0.4223	7.331	4.692	0.046	2.725	26.06	1.346	0.172	0.158	17	720	214	78.2	151	59.8	900.4	26.9	84	29.237	5.74	136	75.6	52	4.04	1.38	2.975	43.177
73.5	21.99	0.4047	7.151	4.568	0.045	2.602	26.36	0.899	0.116	0.109	14	724	236	75.1	104	56	858.2	31.3	89	8.6986	7.94	180	72.6	44	3.55	1.842	3.007	43.62
74.5	22.1	0.4168	7.387	4.777	0.045	2.597	25.73	0.93	0.064	0.109	14.3	726	238	80.2	85.5	35.7	863.4	34.4	99	2.2369	8.67	205	74.9	43	4.12	2.04	3.152	43.822
75.5	22.02	0.4411	7.448	4.929	0.045	2.583	25.37	0.946	0.051	0.102	18.9	709	252	80.6	81.5	30.1	834	34.7	95	1.9847	9.5	228	75.9	47	4.62	1.613	3.228	42.126
76.5	22.35	0.4535	7.422	5.084	0.045	2.523	24.72	1.009	0.153	0.102	21.6	647	254	70.4	75.5	31.6	831.2	33.8	91	0.9569	7.44	217	76.3	45	5.94	1.871	3.257	39.64
77.5	23.18	0.4535	7.467	5.206	0.038	2.459	24.88	1.035	0.16	0.153	34.4	674	247	73.1	59.5	29.3	831.6	36.8	88	0.8424	11.1	199	68.8	46	4.03	2.167	3.173	38.639
78.5	23.42	0.4474	7.184	5.133	0.037	2.361	25	1.088	0.174	0.18	34	685	248	63.7	59.5	38.9	884.5	33.7	84	0.8024	12.3	153	65.7	43	5.07	2.506	3.424	38.859
79.5	20.13	0.424	7.067	5.156	0.043	2.311	24.81	1.131	0.178	0.203	23.8	675	253	62.2	58	32.6	861.2	40.6	88	0.757	19.7	128	64.2	33	3.28	2.281	3.413	41.27
80.5	19.94	0.4155	7.045	5.301	0.038	2.386	26.69	0.888	0.138	0.113	27	628	253	56.6	59.5	29.9	819.9	41.6	89	0.747	17	109	64.9	31	4.4	2.374	3.26	43.524
81.5	21.39	0.4318	7.313	5.741	0.04	2.537	27.77	1.518	0.573	0.148	35	640	249	63.1	57.3	27	887.1	40.3	86	0.7015	17.9	106	66.9	27	4.89	2.763	3.089	44.048
82.5	21.73	0.4331	7.391	5.94	0.034	2.578	28.59	1.684	0.564	0.144	43.8	630	248	53	56.5	27.9	822.8	39.2	85	0.6981	14.7	112	62.5	27	5.69	2.865	3.167	43.701
83.5	21	0.4269	7.175	6.108	0.048	2.569	28.78	1.784	0.551	0.138	57.7	594	246	60.5	61.5	36.3	913.1	37.4	85	0.2365	3.04	112	64.5	19	7.7	2.932	2.987	44.567
84.5	20.82	0.423	7.065	6.317	0.042	2.572	29.36	2.115	0.499	0.125	69.5	557	242	55.9	36.5	24.6	890.7	35.9	90	0.1237	1.74	122	62.7	17	7.68	3.196	2.856	44.838
85.5	20.91	0.4386	7.188	6.434	0.041	2.542	28.8	1.583	0.473	0.13	86.3	532	236	52	48.5	9.14	808.1	34.2	87	0.0857	2.16	125	62.4	20	7.74	3.232	2.742	43.444
86.5	23.24	0.546	8.138	6.829	0.039	2.46	21.91	1.737	0.763	0.125	91.3	441	270	64.5	42.5	77.9	886.8	27.5	93	0.0759	2.51	142	72.9	50	5.26	2.23	2.52	37.072
87.5	29.7	0.7699	10.68	7.81	0.052	2.754	18.98	2.288	0.851	0.141	71.7	376	197	75.2	35	14.4	920.5	25.2	85	0.0746	2.99	150	80.8	87	3.36	2.768	2.366	29.11
88.5	33.52	0.9257	11.75	7.983	0.052	2.755	11.58	2.466	1.296	0.141	53.8	284	172	86.4	44.5	18.3	930	21.5	77	0.0689	3.03	166	91.1	139	4.31	2.103	1.793	18.551
89.5	39.88	1.1627	14.34	8.927	0.065	3.057	9.009	2.87	1.837	0.154	39.9	251	154	95	36.5	8.83	964.1	18.2	73	0.0457	4.68	171	110	165	3.98	1.851	1.663	12.961
90.5	42.33	1.2714	15.34	9.133	0.066	3.125	6.548	3.183	1.945	0.158	31	231	145	104	35.5	11.1	960.4	14	70	0.0499	5.54	180	97.4	188	4.26	1.568	1.537	8.5127
91.5	41.91	1.2627	15.09	9.119	0.066	3.128	6.825	3.062	1.898	0.165	20.4	237	141	97.6	34	5.03	987.6	13.9	71	0.0359	3.78	189	102	182	4.07	1.543	1.897	8.8995
92.5	40.86	1.2262	14.76	8.809	0.065	3.001	7.018	2.864	1.912	0.153	32.3	242	146	101	43	3.8	879.9	16.1	74	0.0326	2.41	183	104	184	4.23	1.564	2.082	9.4502
93.5	32.96	0.8903	11.84	9.471	0.054	2.84	14.62	2.725	1.213	0.138	88.4	395	189	78.3	42.5	19.4	888.2	27.3	88	0.03	4.54	207	92.8	112	3.29	3.716	2.215	22.297
94.5	28.85	0.7032	10.34	8.069	0.044	2.783	19.86	2.398	0.836	0.133	79.7	426	210	74.9	37.5	10.2	816.6	20.6	91	0.0296	3.45	227	76.5	75	4.41	3.278	2.382	30.998
95.5	27.73	0.6592	9.889	7.838	0.044	2.762	21.2	2.241	0.762	0.125	82.8	407	212	79	38	19.3	799.8	21.5	82	0.0325	3.84	230	75.5	64	6.05	2.865	2.425	32.563
96.5	28.36	0.6634	10.12	7.581	0.044	2.777	20.4	2.15	0.678	0.131	47.1	391	207	83.1	39.5	28.5	862.8	21.2	78	0.0376	3.98	242	80.5	70	6.45	2.465	2.432	31.777
97.5	28.84	0.6556	10.09	7.432	0.044	2.88	20.56	2.151	0.877	0.125	19.6	339	198	92	41	22.7	884.3	22	70	0.0426	4.24	231	75.7	68	5.4	2.014	2.221	31.702
98.5	30.42	0.6934	10.25	7.745	0.052	2.987	18.58	2.213	0.612	0.148	17	343	198	120	36.5	23.8	850	19.3	64	0.043	4.35	204	82.9	86	5.84	1.71	2.28	29.099

Appendix 2: Major and trace element data for core T87/26B.

Depth in core (cm)	SiO_2 wt%	TiO_2 wt%	Al_2O_3 wt%	Fe_2O_3 wt%	MnO wt%	MgO wt%	CaO wt%	Na_2O wt%	K_2O wt%	P_2O_5 wt%	As ppm	Ba ppm	Br ppm	Cr ppm	Hg ppb	I ppm	MnO ppm	Mo ppm	Ni ppm	Se ppm	U ppm	V ppm	Zn ppm	Cl wt%	S wt%	Corg wt%	$CaCO_3$ wt%
0.5	30.39	0.564	9.469	4.537	0.161	3.115	22.822	1.51	0.608	0.103	5.39	202	111	80.1	n.d.	46.6	1679	3	39.6	n.d.	0.19	114.2	68.26	2.635	0.3584	0.7	37.9898
1.5	30.76	0.58	9.991	4.739	0.179	3.348	22.46	1.585	0.647	0.104	5.16	195	107	84.6	n.d.	42.9	1751	3.55	40.2	n.d.	0.75	113.5	65.4	2.748	0.2435	0.54	37.1606
2.5	27.01	0.512	8.693	4.125	0.143	3.121	22.707	1.427	0.458	0.096	10.7	167	110	72.4	n.d.	38.4	1566	3.4	38.3	n.d.	2.06	101.2	58.44	2.531	0.2373	0.35	40.4807
3.5	29.86	0.47	9.991	3.778	0.123	3.128	23.269	1.466	0.383	0.108	3.62	167	101	77	n.d.	27.3	1449	2.72	37	n.d.	0	93.74	55.08	2.598	0.2378	0.27	42.6139
4.5	28.98	0.461	9.462	3.749	0.122	3.166	24.098	1.454	0.367	0.108	0	165	99	71.1	n.d.	17.6	1426	3.71	35.7	n.d.	0	95.11	53.58	3.139	0.2264	0.24	44.1003
5.5	29.27	0.46	9.648	3.777	0.137	3.158	23.691	1.302	0.381	0.108	0	154	96.1	73.7	n.d.	21.7	1570	3.91	35.3	n.d.	0.77	89.74	56.66	2.908	0.2374	0.26	43.2825
6.5	28	0.475	9.567	3.92	0.187	3.158	24.493	1.59	0.439	0.108	2.84	186	92.7	69.4	n.d.	26.9	2058	3.26	39.3	n.d.	0	99.44	61.35	2.695	0.2165	0.24	44.6575
7.5	29.27	0.496	9.678	4.03	0.226	3.134	23.861	1.581	0.488	0.117	5.31	180	91.1	70.6	n.d.	31	2419	2.64	38.4	n.d.	1.04	99.17	60.08	2.626	0.2111	0.23	42.8322
8.5	30.29	0.481	9.533	3.797	0.175	3.134	23.512	1.37	0.466	0.117	5.14	179	85.9	72.3	n.d.	30	2061	2.14	35.6	n.d.	1.15	96.1	56.94	2.51	0.2119	0.22	42.9645
9.5	29.09	0.462	9.323	3.68	0.144	3.168	24.816	0.981	0.39	0.115	3.28	174	80.4	73.2	n.d.	23.4	1659	3.47	32.8	n.d.	0	98.34	55.08	2.127	0.2081	0.25	45.0311
10.5	26.72	0.448	8.813	3.621	0.128	3.094	26.454	1.316	0.434	0.107	0	149	77.8	67.6	n.d.	18.2	1433	3.82	35.2	n.d.	0.95	92.51	52.49	1.852	0.1956	0.19	48.2674
11.5	26.21	0.415	8.535	3.366	0.127	3.049	27.745	0.599	0.268	0.106	0	143	73.3	68.3	n.d.	30.4	1512	3.38	35.2	n.d.	1.89	90.5	55.66	2.196	0.1963	0.22	50.7053
12.5	26.72	0.441	8.913	3.699	0.156	2.966	26.46	1.28	0.391	0.107	3.66	144	75.2	72.5	n.d.	22.3	1705	4	36.6	n.d.	1.73	96.56	56.11	1.984	0.1992	0.22	47.6642
13.5	27.39	0.434	9.29	3.639	0.192	2.936	25.631	1.137	0.327	0.107	3.66	133	78.4	73.8	n.d.	27.6	2175	4.25	37.7	n.d.	0.88	92.25	56.59	1.889	0.1918	0.21	46.5359
14.5	27.67	0.437	9.561	3.717	0.315	2.908	25.387	1.239	0.272	0.107	5.32	148	82.5	76	n.d.	18.8	3568	6.99	42.7	n.d.	0.01	94.7	59.26	2.65	0.1921	0.21	45.6608
15.5	28.08	0.444	9.707	3.797	0.544	2.787	24.508	1.368	0.301	0.107	1.71	168	93.5	79.6	n.d.	26.5	6101	9.5	50.2	n.d.	0	102.1	61.54	1.836	0.1964	0.24	43.8009
16.5	29.22	0.465	10.15	3.968	0.792	2.718	23.181	1.722	0.334	0.109	0	171	99.6	85	n.d.	16.5	9015	11.6	56.5	n.d.	1.41	104	68.34	2.887	0.2052	0.23	40.8663
17.5	29.35	0.484	10.17	4.242	0.925	2.598	22.996	2.011	0.506	0.117	0	227	102	85.4	n.d.	21.4	9707	12.4	58	n.d.	0	112.4	71.06	3.111	0.2042	0.25	39.6875
18.5	27.77	0.496	9.635	4.365	0.971	2.752	24.568	2.007	0.299	0.124	3.17	328	106	94.1	25.5	24.5	10029	12.5	67	0.041	0.07	110.3	70.82	3.113	0.2043	0.23	39.7433
19.5	27	0.477	9.201	4.196	0.556	2.643	25.854	1.87	0.303	0.13	5.95	481	111	81.1	28.5	31.7	5844	7.41	60.8	0.036	0.17	110.5	64.21	3.133	0.2143	0.24	41.7914
20.5	27.27	0.404	9.319	3.716	0.255	2.298	26.183	1.184	0.177	0.113	5.99	651	116	87.8	35	33.1	3025	4.47	46.4	0.028	0.71	108.6	56.53	3.737	0.2294	0.23	44.8484
21.5	27.21	0.429	9.33	4.172	0.364	2.265	25.519	1.722	0.3	0.129	9.27	862	122	86.6	39.5	25.8	3892	5.13	53.3	0.033	2.41	116.3	58.35	3.248	0.2405	0.28	43.5317
22.5	27.5	0.406	9.353	4.099	0.442	2.317	25.607	1.233	0.171	0.157	11	938	129	93.2	36	39.2	5164	6.51	66.3	0.037	0.56	120.6	90.63	2.441	0.244	0.42	42.8731
23.5	28	0.408	9.544	4.4	0.659	2.343	24.133	1.799	0.236	0.143	21.8	1024	135	98.6	47	59.2	7792	9.44	73.3	0.052	1.42	130.9	67.43	3.07	0.281	0.35	41.0974
25.5	30.19	0.48	10.32	5.093	0.672	2.584	22.455	1.609	0.251	0.162	22.8	1035	147	103	139	110	7103	10.1	64.4	0.09	0.97	130.2	71.77	3.729	0.2768	0.43	37.5241
26.5	27.92	0.442	9.381	5.756	0.648	2.472	22.652	1.574	0.207	0.185	39.3	971	176	94	182	267	6706	9.95	63.2	0.715	1.87	136.4	74.96	3.841	0.3206	1.13	38.4689
27.5	27.86	0.439	9.431	5.841	0.042	2.4	22.026	2.159	0.439	0.156	32.7	914	197	85.3	78.5	41.1	648.2	17.7	54.9	26.17	2.19	143.6	77.45	4.417	1.2367	2.16	37.9298
28.5	28.94	0.462	9.771	5.358	0.043	2.47	22.661	1.892	0.484	0.137	22.4	931	215	86.9	72	42.3	665.3	21.7	58.7	10.5	3.44	172	72.29	3.933	1.465	2.3	37.7644
29.5	29.57	0.476	10.08	4.734	0.043	2.555	22.464	1.689	0.426	0.123	20.3	920	208	88.7	81	18.2	692	20.5	61.8	7.875	4.23	206.8	73.26	3.699	1.4692	2.3	37.3833
30.5	29.43	0.476	10	4.54	0.043	2.548	22.807	1.783	0.433	0.115	16.5	810	185	82.4	64.5	17.2	637.5	16.9	62.2	2.1	4.57	204.3	66.86	3.945	1.4993	2.22	38.3131
31.5	28.85	0.458	9.768	4.544	0.043	2.555	22.977	1.782	0.422	0.143	32.2	768	190	87.8	73.5	28.7	691.3	16.3	74	1	10	182.5	65.71	3.943	1.6584	2.26	38.8492
32.5	29.9	0.484	10.16	4.481	0.043	2.659	21.933	1.966	0.535	0.108	31.5	720	191	94.8	64.5	29.3	678.1	18.2	69.9	0.9	8.8	239.4	71.57	3.695	1.3926	2.22	37.6535
33.5	29.95	0.478	10.19	4.305	0.043	2.616	22.314	1.971	0.428	0.109	19.3	507	178	111	65.5	29.2	676.5	13.4	57.5	0.8	7.92	199.1	69.93	3.472	0.9319	1.83	38.1631
34.5	30.03	0.474	10.17	4.377	0.044	2.619	22.719	1.933	0.489	0.102	13.4	315	135	94.4	58	30.7	709.2	6.96	53.3	0.621	6.89	119.6	68.55	3.349	0.8985	1.07	39.4756
35.5	31.73	0.502	10.71	4.394	0.052	2.725	22.436	1.744	0.472	0.097	5.33	255	113	92.6	59.5	24.8	720.5	7.93	50.2	0.617	6.34	103.9	67.23	1.797	0.5886	0.52	38.81
36.5	32.2	0.51	10.76	4.426	0.053	2.768	21.769	1.838	0.6	0.098	7.55	260	107	95.2	52	10.4	772.1	7.92	52.7	0.185	6.69	113	69.48	1.984	0.5439	0.37	38.2204
37.5	33.1	0.524	10.81	4.656	0.053	2.932	21.617	1.679	0.486	0.099	12.9	207	92.6	89.3	45.5	10.8	798.3	31.8	47.4	0.123	5.96	114.9	68.77	1.502	0.5181	0.38	37.5888
38.5	33.51	0.535	10.94	4.768	0.053	2.988	21.327	1.574	0.619	0.099	6.87	222	88.6	89.3	42.5	15.6	802.9	28.3	46.7	0.098	6.52	111.1	66.07	1.662	0.5256	0.38	36.2317
39.5	33.8	0.533	10.79	4.259	0.061	3.009	21.675	1.425	0.533	0.107	1.48	205	77.3	91.3	38.5	17	833.5	16.9	43.1	0.081	4.51	115.9	66.95	3.74	0.3794	0.32	38.0481
40.5	33.42	0.519	10.67	4.865	0.061	2.944	21.414	1.518	0.747	0.099	11.2	174	86.8	88.8	40.5	8.69	889.7	19.2	44.3	0.084	5.67	109.8	62.43	2.602	0.4486	0.28	38.0043
41.5	33.81	0.527	10.58	4.745	0.069	3.011	21.411	1.521	0.642	0.107	8.48	169	89.2	87.1	39.5	12.1	946.2	14.1	46.8	0.079	5.06	109.3	61.82	1.901	0.4188	0.26	37.9589
42.5	34.17	0.529	10.51	4.537	0.069	3.058	21.1	1.724	0.843	0.1	13.5	205	78.7	88.7	34.5	14.8	921.1	8.93	45.4	0.067	5.45	108	62.98	1.919	0.4043	0.25	37.7284
43.5	32.91	0.514	10.12	4.198	0.076	3.048	22.629	1.498	0.537	0.106	8.99	172	68.7	80.7	29	16.4	1020	3.6	44.2	0.067	4.73	111.3	60.93	2.473	0.3448	0.21	40.1879
44.5	32.64	0.505	10.17	3.777	0.083	3.068	23.092	1.432	0.528	0.106	0	180	72.8	85.6	24.5	4.8	1084	0.97	41.5	0.06	5.07	102	60.82	2.023	0.2741	0.28	41.2166
45.5	31.65	0.493	9.884	3.613	0.09	3.001	23.731	1.396	0.687	0.105	0	170	68.8	85.8	27	11.5	1148	1.17	43.7	0.053	3.31	98.61	57.39	0.961	0.2469	0.22	42.7463
46.5	32.22	0.485	9.753	3.592	0.097	3.084	22.986	1.479	0.881	0.105	0	168	66.6	84.2	18.5	17.6	1206	1.37	43	0.048	3.47	107.5	59.04	1.021	0.2189	0.19	42.1629
47.5	34.49	0.51	10.06	3.735	0.084	3.233	21.157	1.522	1.179	0.107	0	181	64.1	87	17	18.6	1057	1.66	47.1	0.05	1.45	106.1	63.64	1.442	0.1873	0.21	38.8132
48.5	36.57	0.536	10.55	3.989	0.078	3.258	19.29	2.115	1.26	0.109	0	199	63.7	91.8	16.5	14.8	1017	1.84	50.5	0.049	2.37	110.6	63.81	1.374	0.1823	0.17	35.7715

Appendix 3: Major and trace element data for core MD 90-917.

Depth in core (cm)	SiO_2 wt%	TiO_2 wt%	Al_2O_3 wt%	Fe_2O_3 wt%	MnO wt%	MgO wt%	CaO wt%	Na_2O wt%	K_2O wt%	P_2O_5 wt%	As ppm	Ba ppm	Br ppm	Cr ppm	Hg ppm	I ppm	MnO ppm	Mo ppm	Ni ppm	Se ppm	U ppm	V ppm	Zn ppm	Zr ppm	Cl Wt%	S Wt%	Corg Wt%	$CaCO_3$ Wt%
203.5	36.699	0.4792	11.201	5.137	0.1414	4.532	17.109	1.767	1.28	0.1021	0	203.8	98	177.8	n.d.	30	1572.7	0.96	153.2	n.d.	0.84	112.9	80.2	73.6	2.272	0.2152	0.42	27.469
204.5	35.694	0.4749	10.914	4.873	0.1401	4.422	16.909	1.822	1.23	0.0934	0	203.4	93	192.3	n.d.	21	1607.9	1.69	152	n.d.	1.03	111.98	82.1	73.6	2.293	0.2019	0.39	27.584
206.5	36.344	0.4836	11.262	5.015	0.1638	4.508	17.104	1.685	1.217	0.1014	0	207	96	176.5	n.d.	19	1737.9	2.78	151.7	n.d.	0.87	111.96	80.5	72.3	2.614	0.212	0.42	27.678
207.5	36.765	0.4863	11.319	5.044	0.1883	4.495	16.904	1.726	1.31	0.102	3.89	213.2	97	182	n.d.	21	2019.3	2.38	153.6	n.d.	0	117.74	82.7	73.7	2.446	0.2139	0.4	27.57
208.5	36.335	0.4768	11.192	5.049	0.1719	4.486	17.156	1.766	1.313	0.1016	2.51	213.2	97	179	n.d.	25	1903.2	2.01	153.9	n.d.	0	121.45	82.3	71.5	2.342	0.2463	0.45	27.698
209.5	36.312	0.4816	11.123	5.033	0.1864	4.521	17.166	1.647	1.087	0.101	0.39	218.5	97	177.8	n.d.	25	1971.1	1.88	152	n.d.	0	120.89	82.9	71.3	2.39	0.2279	0.47	27.848
210.5	36.478	0.4781	11.318	5.024	0.2273	4.491	16.969	1.709	1.301	0.0941	0	208.1	97	179.3	n.d.	23	2437.1	1.89	152.8	n.d.	0	118.8	82	74.3	2.361	0.2238	0.35	27.894
211.5	36.54	0.4786	11.22	5.124	0.2589	4.488	17.05	1.71	1.326	0.102	0	213.8	103	176.3	n.d.	21	2701.7	1.94	154.8	n.d.	0	116.25	82.4	70.9	2.463	0.4021	0.45	27.986
212.5	36.153	0.4699	11.161	5.107	0.3368	4.417	16.447	1.801	1.331	0.1018	0	204.5	98	174.8	n.d.	21	3456.6	1.98	152.3	n.d.	0.8	115.97	82.1	71.9	2.403	0.2449	0.42	28.013
213.5	37.194	0.4897	11.54	5.173	0.3396	4.486	16.444	1.722	1.43	0.0948	0	214.9	101	178.6	n.d.	21	3523.8	2.03	154	n.d.	0.15	116.52	83.5	73.5	2.461	0.2048	0.42	28.379
214.5	36.908	0.4876	11.333	5.143	0.2831	4.506	16.413	1.769	1.361	0.1022	0	224.8	106	181.1	n.d.	18	3049.7	2.21	156.6	n.d.	0	113.45	84.9	74.7	2.653	0.2261	0.48	28.49
215.5	36.23	0.4858	11.189	4.952	0.3369	4.45	16.548	1.685	1.34	0.1019	1.04	217.6	101	175.8	n.d.	25	3534.2	1.52	151.5	n.d.	0.55	115.18	81.5	74.1	2.282	0.2113	0.45	28.459
216.5	36.891	0.4876	11.285	5.025	0.3303	4.498	16.688	1.683	1.353	0.1022	1.83	228.6	100	178.1	n.d.	23	3432.1	2.14	151.5	n.d.	0.1	109.31	83.3	74.2	2.485	0.2206	0.49	28.759
219.5	36.861	0.4793	11.158	5.021	0.2907	4.487	16.533	1.807	1.289	0.1022	0	233.1	97	181.8	n.d.	23	3116.2	2.19	154.7	n.d.	1.02	119.98	80.9	74.9	2.353	0.2361	0.5	29.37
220.5	36.18	0.4768	10.896	4.869	0.3048	4.447	16.75	1.688	1.344	0.0938	0	226.3	96	181	n.d.	30	3207.1	1.57	153.3	n.d.	0.56	117.35	82.1	71.6	2.261	0.2194	0.53	29.259
222.5	35.768	0.4699	10.878	4.93	0.7858	4.43	16.486	1.579	1.079	0.1001	0.9	245.7	95	174.1	34.5	38	8079.6	2.18	148.4	2.2	0.92	118.35	81.4	69.8	2.984	0.2794	0.56	30.298
223.5	35.564	0.467	10.773	4.862	0.7281	4.425	16.538	1.593	0.965	0.1072	2.97	250.6	95	171.5	32.5	34	7987.1	3.11	143.9	2.6	0.29	112.21	76.4	68.5	5.882	0.2912	0.45	30.032
224.5	36.51	0.481	11.056	5.051	0.6517	4.585	17.13	1.629	0.97	0.1086	1.57	255.1	96	176.2	47.5	39	6543.4	2.7	147.3	3.1	0.31	116.21	81.6	70.9	2.973	0.3154	0.56	30.665
225.5	33.582	0.4351	10.222	4.733	2.0612	4.519	17.288	1.733	0.832	0.1145	0	300	106	162.3	38	39	21372	3.5	142.7	3.3	1.44	120.47	78	62.8	3.059	0.3648	0.71	33.084
226.5	30.772	0.3918	9.491	4.435	3.6885	4.465	17.452	1.693	0.591	0.1257	0	316.3	120	155.5	33	38	40002	9.54	132.8	3.5	1.91	125.6	71.8	54.9	4.355	0.4089	0.83	36.486
227.5	30.51	0.3927	9.4833	4.364	3.9415	4.371	17.574	1.697	0.541	0.126	0	315.3	111	155.2	32.5	34	42542	21	127.5	3.1	1.64	127.8	72.9	54.1	3.737	0.3827	0.74	36.56
228.5	32.616	0.4227	10.326	4.944	1.7663	4.212	16.908	1.804	0.921	0.1132	1.74	341.6	120	160.4	39.5	37	18451	17.9	142.5	4.1	2.39	137.3	78.7	59	3.754	0.5598	0.85	32.67
230.5	35.263	0.4636	11.226	5.316	0.2472	4.28	16.117	1.661	1.167	0.1004	3.57	354	108	169.5	34.5	35	2650.2	6.39	146.4	4	1.94	145.9	86.3	66.1	3.396	0.5728	0.86	28.916
231.5	35.662	0.464	11.261	5.306	0.1701	4.269	15.723	1.694	1.253	0.1005	1.38	393.1	121	180.9	35.5	23	1872.8	6.39	157.2	4.3	1.78	148.97	89.1	69.7	4.01	0.5628	0.96	27.987
232.5	36.588	0.4743	11.507	5.38	0.1633	4.346	15.62	1.617	1.322	0.1011	4.08	391.5	116	177	29.5	28	1821.1	7.14	157.7	4.2	2.32	141.42	88.9	72.1	4.458	0.5359	1.01	27.578
233.5	36.283	0.4809	11.479	5.483	0.1629	4.382	15.403	1.807	1.295	0.1008	4.16	405.4	119	178.7	26	36	1795.5	10.1	156.5	4.2	3.01	138.82	86.5	70.2	2.995	0.651	1.13	26.4
234.5	35.702	0.4717	11.367	5.382	0.1469	4.23	15.736	1.709	1.206	0.1005	6.85	392.5	121	176.1	28	35	1701.8	8.62	151.6	3.9	3.1	142.78	85.4	69.4	2.895	0.6846	1.15	27.368
235.5	35.982	0.4719	11.442	5.346	0.1393	4.263	15.605	1.617	1.122	0.1006	3.82	358.7	117	169.7	29.5	34	1585.5	8.28	149.5	3.8	2.74	144.61	87.5	68.6	2.919	0.639	0.99	27.248
236.5	36.111	0.4679	11.33	5.302	0.2495	4.538	16.04	1.801	1.177	0.1092	0	361	117	173.8	26.5	36	2642.7	5.9	142.7	3.6	1.54	119.72	82.9	75	3.511	0.5777	0.99	28.195
237.5	34.517	0.4566	11.102	5.038	0.137	4.178	16.368	1.72	1.164	0.0913	1.44	334.4	111	171.1	27.5	28	1547.5	7.26	142.5	3.7	2.02	151.79	82.9	66.6	3.524	0.5412	0.98	29.262
238.5	35.784	0.467	11.308	5.183	0.1479	4.319	16.094	1.774	1.191	0.0934	0	302.8	101	177.6	24.5	36	1698	5.03	149.9	3.5	1.67	125.48	84.1	71.6	2.88	0.4957	0.75	28.642
239.5	36.474	0.4733	11.235	5.222	0.1552	4.469	15.937	1.816	1.28	0.0931	0	281.2	106	180.7	30.5	25	1765.5	5.07	149.9	3.2	1.32	121.33	85.7	77.8	4.541	0.439	0.58	28.51
240.5	37.044	0.4774	11.208	5.197	0.1565	4.602	15.904	1.769	1.182	0.1017	0	262.6	107	175.1	31	29	1785.8	3.89	140.9	2.5	1.29	119.12	84.4	80.9	3.988	0.397	0.58	28.243
241.5	36.961	0.4753	11.071	5.127	0.1636	4.675	15.683	2.002	1.208	0.0935	0	260.7	116	183	30.2	25	1812.1	5.56	147.7	2.1	0.52	111.19	82.3	84.9	4.716	0.4127	0.63	27.848
243.5	36.615	0.4822	11.052	4.977	0.1789	4.62	15.842	1.929	1.19	0.0933	0	296.6	117	187.7	31.2	29	2035.9	4.47	140.3	1.9	1.42	107.97	83.1	81.3	4.627	0.4121	0.75	28.034
244.5	36.088	0.4734	11.137	5.091	0.2251	4.61	15.7	1.894	1.218	0.1009	0	319.8	118	176.3	30.5	36	2388.4	6.15	139.7	2.1	2.33	114.15	82.4	78.5	3.979	0.4625	0.8	28.051
245.5	35.752	0.4664	10.984	5.045	0.2565	4.54	15.625	1.85	1.158	0.1011	0	341.4	118	179.8	n.d.	38	2756.8	5.84	142.7	n.d.	2.21	114.73	82.4	80.3	3.749	0.4658	0.88	28.404
246.5	35.729	0.4693	11.11	5.132	0.3077	4.516	15.849	1.723	1.039	0.1077	5.87	360.8	123	170.6	n.d.	32	3224.1	6.41	141.7	n.d.	0.62	114.84	82.2	75.2	3.847	0.5124	1.01	28.128
247.5	35.992	0.4655	11.219	5.299	0.2716	4.547	16.293	1.916	1.109	0.1009	5.51	379.1	123	176.8	n.d.	38	2945.1	7.04	143.4	n.d.	1.33	127.08	84.7	74.9	3.298	0.5741	0.99	28.68
248.5	35.506	0.4704	11.437	5.275	0.1465	4.319	16.45	1.82	1.064	0.108	5.37	362.4	113	167.4	n.d.	32	1547.5	8.42	149.2	n.d.	2.29	144.94	86.4	67.2	2.803	0.6156	1.16	28.473
249.5	36.176	0.4766	11.454	5.337	0.1797	4.469	15.978	1.774	1.344	0.1016	1.27	355.8	106	166.6	n.d.	26	1937.4	6.6	143.9	n.d.	1.49	126.64	85.9	75.3	2.192	0.5935	0.93	28.271
250.5	35.726	0.4634	11.383	5.414	0.139	4.417	15.585	1.869	1.251	0.1004	3.26	449.3	133	180.8	n.d.	21	1588.8	7.42	161.1	n.d.	1.05	142.11	90.6	77.7	4.971	0.655	1.11	27.194
252.5	35.664	0.4535	11.252	5.265	0.1307	4.32	16.018	1.914	1.122	0.0999	2.08	415.7	130	181.9	n.d.	19	1489.9	7.18	151.9	n.d.	0.94	124.68	100	71.8	3.744	0.6284	1.01	27.663
253.5	33.882	0.4375	10.79	5.221	0.1186	4.249	15.113	1.906	1.105	0.0964	10.4	434.5	129	180.2	n.d.	18	1408.8	6.56	153.9	n.d.	0.9	128.65	98.4	74.7	3.401	0.7119	1.16	27.66
254.5	35.649	0.4652	11.382	5.427	0.1473	4.497	15.398	2	1.14	0.1008	7.95	284.1	113	159.9	n.d.	21	1617.6	5.58	131.6	n.d.	2.04	119.92	82.6	78.6	3.46	0.6998	1.01	27.856
255.5	35.907	0.4841	11.196	5.231	0.1483	4.606	16.528	1.561	1.156	0.0937	0	211.3	81	165.7	n.d.	23	1594.9	4.21	137.1	n.d.	1.34	122.47	85.5	76.6	2.115	0.5489	0.48	30.374
256.5	35.975	0.486	11.14	5.331	0.1568	4.563	16.424	1.568	1.325	0.1019	0	214.1	81	169.4	n.d.	16	1759.5	4.56	137.7	n.d.	0.73	119.76	84.3	72.9	2.64	0.5184	0.48	30.035
257.5	36.042	0.4847	11.219	5.113	0.1485	4.566	16.559	1.478	1.274	0.0938	0	228.2	80	179.4	n.d.	14	1618.4	3.58	136	n.d.	1.48	120.95	83.4	73.3	2.859	0.4089	0.53	30.027
258.5	36.557	0.5011	11.353	4.894	0.1468	4.721	17.226	1.402	1.331	0.1096	0	220.1	72	169.9	n.d.	23	1589	1.72	129.9	n.d.	1.15	118.7	79.6	74.2	1.8	0.2936	0.45	30.904
260.5	36.039	0.4893	11.192	4.823	0.132	4.614	17.157	1.561	1.111	0.101	2.26	225.5	77	161.7	n.d.	21	1483.6	1.31	131.2	n.d.	1.37	119.79	79	74.9	1.973	0.2846	0.45	30.987
261.5	36.016	0.4883	11.091	4.736	0.1318	4.643	16.997	1.659	1.24	0.1085	0	219.2	72	164.9	n.d.	28	1468.7	1.2	130.6	n.d.	1.9	116.99	80.7	76.2	1.648	0.2595	0.62	31.398
262.5	36.91	0.5049	11.399	4.891	0.1341	4.78	17.252	1.649	1.231	0.1104	0	216.2	72	169.4	n.d.	23	1442.5	1.45	132.8	n.d.	1.46	114.9	78.8	74.6	1.251	0.2126	0.49	30.801
263.5	35.36	0.4771	10.997	4.864	0.1308	4.586	16.707	1.547	1.039	0.1	0	219.6	72	170.7	n.d.	23	1495.1	1.16	132.9	n.d.	1.26	114.53	80.7	74.1	1.753	0.2786	0.48	30.469
264.5	36.565	0.4926	11.292	4.961	0.1408	4.707	17.07	1.658	1.282	0.1095	0	228.3	72	172.8	n.d.	25	1489.9	1.73	131.3	n.d.	1.1	117.96	80.2	74.6	1.609	0.2947	0.4	30.935
265.5	36.205	0.4907	11.185	4.884	0.1324	4.666	16.856	1.566	1.176	0.1013	0	225	77	167.4	n.d.	25	1490.9	0.78	133.2	n.d.	1.28	119.84	81.7	74.7	1.778	0.2597	0.4	30.815
266.5	36.297	0.4926	11.166	4.856	0.1329	4.715	17.077	1.587	1.29	0.1095	0	213.7	72	172.5	n.d.	21	1461.4	1.45	132.7	n.d.	1	113.27	78.6	76.6	1.92	0.2571	0.38	31.093
267.5	36.419	0.4902	11.266	4.886	0.1245	4.66	16.93	1.587	1.222	0.1089	0	215.4	72	168.5	n.d.	26	1439.6	1.61	133.6	n.d.	0.86	123.55	79.4	76.9	1.671	0.2516	0.38	30.652
268.5	36.748	0.4972	11.25	4.879	0.1243	4.685	16.564	1.499	1.111	0.1088	0	219.1	70	175.4	n.d.	26	1381.8	1.08	135.7	n.d.	1.73	116.88	79	79.3	1.69	0.2503	0.43	29.895
269.5	36.886	0.4995	11.184	4.94	0.1249	4.8	16.757	1.592	1.116	0.1093	0	228.1	70	169.7	n.d.	19	1390.1	1.08	132.5	n.d.	1.27	111.5	79.9	80.3	2.466	0.2509	0.46	30.472

Appendix 4: Major and trace element data for core MD81-LC21.

Depth in core (cm)	SiO_2 wt%	TiO_2 wt%	Al_2O_3 wt%	Fe_2O_3 wt%	MnO wt%	MgO wt%	CaO wt%	Na_2O wt%	K_2O wt%	P_2O_5 wt%	As ppm	Ba ppm	Br ppm	Cr ppm	Hg ppb	I ppm	MnO ppm	Mo ppm	Ni ppm	Se ppm	U ppm	V ppm	Zn ppm	Zr ppm	Cl wt%	S wt%	Corg wt%	$CaCO_3$ wt%
97.5	48.817	0.3422	10.4	2.769	0.4841	0.93	2.84	3.32	1.17	0.0641	0	103	55	153	56	4.67	1038.7	1.2	143	0.4959	2.86	79.2	59.6	75	1.35	0.1612	0.44	49.297
103.5	25.474	0.3701	7.63	3.219	0.0628	4.63	27.7	0.51	0.17	0.0838	0	97.8	58	149	54.5	10.9	970.7	0.6	139	0.1406	2.36	81.4	55.1	74	1.25	0.1642	0.61	51.432
110.5	24.754	0.3532	7.22	3.207	0.0693	4.58	28.5	0.33	0.17	0.09	0	106	63	157	51	20.2	1169.7	0.9	143	0.0529	1.87	83.7	53.5	71	1.41	0.1746	0.5	49.577
118.5	24.778	0.3438	7.2	3.259	0.0894	4.59	28.1	0.23	0.08	0.0963	0	94.1	65	154	18.5	15.6	1614.6	0.3	157	0.0027	1.97	75.3	56.7	73	1.56	0.1671	0.83	47.268
127.5	25.129	0.3439	6.97	3.371	0.1307	4.63	27.6	0.36	0.19	0.0963	0	109	79	168	22	12.5	2528.2	1.1	165	-0.022	1.36	69.8	60	72	1.52	0.1738	0.39	52.851
130.5	25.304	0.3537	7.28	3.53	0.2219	4.74	27.2	0.52	0.12	0.0901	0	99.4	75	161	33.5	9.34	2822.5	1.7	162	-0.022	1.55	67.6	54.7	68	1.43	0.1741	0.42	49.521
135.5	24.611	0.3287	6.85	3.403	0.2534	4.5	28	0.31	0.1	0.089	0	155	69	179	26.5	15.6	3680.4	1.3	195	0.0965	0.97	80.1	59.7	72	1.62	0.169	0.47	48.264
137	26.553	0.3555	7.47	3.747	0.3484	4.85	26.6	0.87	0.19	0.0995	0	167	66	179	43	23.4	3605.6	1.2	199	0.0988	1.24	80.6	62.1	73	1.59	0.1823	0.47	47.22
140	25.86	0.3603	6.88	3.95	0.2719	4.56	25.1	0.75	0.2	0.0952	0	237	91	190	60.5	34.3	5792	0.9	203	1.0851	2.89	91.9	62.5	74	1.61	0.183	1.22	46.021
141.5	26.869	0.3619	7.59	3.732	0.5747	4.92	25.7	0.87	0.21	0.1064	0	331	108	192	92.5	38.9	7504.7	2.9	206	2.9992	2.89	96.2	67.1	71	1.92	0.2918	2.14	44.743
144.5	26.271	0.3512	7.34	3.746	0.7299	4.73	24.6	0.83	0.15	0.0964	6.27	461	141	203	83.5	24.9	8833.6	6.6	226	4.3951	3.07	145.8	67.4	73	2.57	0.4099	3.14	43.289
149.5	26.623	0.357	7.19	3.796	0.8787	4.61	24	0.89	0.16	0.103	7.34	452	146	204	57	32.7	3574.5	6.2	218	2.8948	4.28	208.6	65.7	72	2.99	0.3989	3.11	42.584
154	26.956	0.3699	7.71	3.748	0.335	4.74	24.4	1.23	0.17	0.1047	11.6	463	133	204	72	31.1	2476.2	10	220	3.2082	7.23	191.2	68	73	2.87	0.487	2.99	42.537
158.5	26.668	0.3692	7.64	3.908	0.1602	4.67	24.8	1.21	0.18	0.1045	28.7	399	135	200	73	26.5	1205.1	8.6	210	3.6261	7.76	192.3	64.6	73	3.45	0.6271	3.15	41.667
161.5	27.093	0.3748	7.61	4.082	0.0972	4.77	23.8	1.24	0.26	0.0972	19.4	374	123	201	62	29.6	1780.4	9.4	229	3.1288	6.93	157.5	70.4	74	2.79	0.6324	2.49	40.771
163	27.972	0.3751	7.95	4.176	0.1486	4.98	23.4	1.35	0.38	0.092	9.41	355	102	210	49	40.5	1920.8	3.6	243	1.1813	6.58	116.6	70.5	81	2.03	0.46	1.61	39.026
167	30.307	0.3944	8.4	4.338	0.168	5.21	22.5	1.31	0.34	0.0876	2.12	356	98	207	59	31.1	1716.4	1.8	237	1.3108	6.78	96.4	69.4	83	1.93	0.3945	1.56	38.983
170	29.882	0.3966	8.39	4.319	0.1514	5.13	22	1.35	0.39	0.101	1.15	372	112	204	51.5	29.6	3689.1	3.4	223	1.0057	6.05	103.2	70.3	82	2.62	0.3986	1.85	38.801
174.5	30.316	0.4014	8.52	4.247	0.2262	5.23	22.4	1.32	0.23	0.0949	5.5	414	113	202	47.5	38.9	2475.2	5.6	225	1.8708	7.29	114.7	67.4	83	3.07	0.4578	2.23	38.206
179	29.158	0.3856	8.25	4.149	0.2214	5.04	22.4	1.41	0.35	0.1	17.4	494	135	203	68	21.8	1680.3	8.7	225	2.8404	6.56	135.7	67.5	77	3.03	0.5684	3.56	39.8
182	28.191	0.3705	7.79	3.984	0.1398	4.87	22.7	1.38	0.34	0.0979	23.6	519	145	195	53.5	29.6	1286.5	15	211	3.0745	6.69	152.2	62	71	3.64	0.7313	4.21	42.18
185	26.228	0.3512	7.29	3.863	0.1033	4.75	24.9	1.07	0.16	0.1102	19.7	440	129	204	68.5	21.8	1420	10	222	3.0995	6.92	146.6	67.8	73	2.45	0.745	3.53	42.198
189.5	27.758	0.37	7.6	4.161	0.1117	4.85	23	1.39	0.47	0.0977	40.9	371	154	195	64	23.4	1102.8	17	212	5.8119	6.36	252.9	63.4	65	2.79	0.9159	4.13	43.53
192.5	25.474	0.338	7.16	4.408	0.0759	5.03	24.7	1.39	0.26	0.1035	33.7	224	98	203	65.5	17.1	1244.9	4.6	221	1.5616	5.28	112	63.1	77	1.64	0.8338	1.65	41.549
195.5	28.098	0.3775	8.01	5.097	0.0871	5.18	24.1	1.3	0.26	0.0871	14.3	172	66	196	67.5	21.8	1204.8	2	210	0.6171	3.76	85.4	63.7	82	1.46	0.4087	0.74	42.192
198.5	28.742	0.4067	8.13	4.677	0.0871	5.16	23.6	1.28	0.42	0.0871	0	157	70	193	59.5	18.7	1164.4	1.3	197	0.1573	4.79	90.3	64.4	86	1.37	0.2438	0.6	42.434
201.5	29.644	0.4031	8.52	4.075	0.1026	5.23	23.8	1.1	0.31	0.0879	0	161	67	202	42	18.7	1189.5	1.3	199	0.0738	3.85	92.7	64	86	1.35	0.1881	0.53	42.98
205.5	30.056	0.4197	8.43	3.991	0.1031	5.18	23.9	1.07	0.38	0.0884	0	123	61	175	34	20.2	1361.5	0.3	176	0.0445	3.44	94.2	57.5	79	1.45	0.1698	0.38	48.536
209	27.527	0.3663	7.45	3.404	0.1005	4.55	27.1	0.85	0.35	0.0862	0	135	58	181	40.5	15.6	1485.9	0.3	189	0.0027	2.91	89.4	65.4	86	1.29	0.1611	0.36	44.076
212	29.647	0.4024	8.11	3.768	0.1244	5.01	24.7	0.91	0.39	0.0951	0	134	55	186	63	14	1534	0.3	180	0.0194	2.39	94.4	62.4	87	1.81	0.1414	0.41	44.582
214	30.064	0.4114	8.17	3.894	0.1249	5	24.5	0.9	0.28	0.0955	0	135	54	177	26	14	1499.7	1.2	176	0.0019	2.29	93.5	62.1	87	1.81	0.1412	0.45	43.642

Appendix 5: Major and trace element data for core UM41.

Depth in core (cm)	SiO_2 wt %	TiO_2 wt %	Al_2O_3 wt %	Fe_2O_3 wt %	MnO wt %	MgO wt %	CaO wt %	Na_2O wt %	K_2O wt %	P_2O_5 wt %	As ppm	Ba ppm	Br ppm	Cr ppm	Hg ppb	I ppm	Mn ppm	Mo ppm	Ni ppm	Se ppm	U ppm	V ppm	Zn ppm	Zr ppm	S wt%	Cl wt%	Corg ppm	$CaCO_3$ wt%
1	18.188	0.289	5.4	2.12	0.0638	3.82	36.235	0.68	0.32	0.0957	0	132	55.4	57.4	47.231	46.32	1235.2	1.9	28.2	0.2836	1.7	65.8	48.6	87.6	0.22	1.5447	0.27	69.226
2	24.005	0.3839	7.41	2.86	0.1023	3.55	30.529	1.11	0.51	0.1073	3.6	123	49.3	62	45.181	56.38	1341.5	2.7	30.1	0.2942	1.1	74.1	49.6	87.3	0.21	1.2364	0.2	58.603
3	24.637	0.3952	7.66	3.04	0.1084	3.54	30.157	1.19	0.51	0.1041	1.7	141	51.6	71.6	37.771	19.2	1467.5	2.8	31.9	0.1275	1.5	77.3	52.5	92.3	0.21	1.1649	0.16	57.698
4	26.976	0.4976	9.42	3.79	0.1277	4.07	27.586	1.4	0.5	0.1313	3.7	170	56.8	69.6	38.962	40.42	1551.8	2.4	36.1	0.2783	0.6	91	55.6	105	0.24	1.3894	0.18	51.216
5	19.883	0.4402	7.38	3.07	0.1206	4.36	32.938	1.18	0.37	0.1352	18.1	178	54.1	53.3	40.153	18.82	1606.2	3.2	33.5	0.2356	1.8	107.5	53.4	101	0.53	1.5967	0.15	60.627
6	17.393	0.3371	6.1	2.37	0.101	4.02	34.582	0.67	0.31	0.1157	13.7	160	39.6	57.4	33.868	29.08	1312.4	3.6	36.2	0.1986	2.2	136.3	59.1	111	0.61	1.079	0.1	68.681
7	21.641	0.3581	6.97	2.71	0.1159	3.65	32.721	0.79	0.46	0.1103	0	139	40	54.9	36.051	17.9	1408.5	2.9	30.9	0.1705	2.1	73.7	48.6	83.7	0.19	0.9495	0.12	64.002
8	22.722	0.3746	7.42	2.87	0.1536	3.61	31.667	1.52	0.42	0.1101	0.3	134	38.9	61.3	31.222	15.29	1749.5	4	32.7	0.0715	1.2	74.3	50.5	86.5	0.19	0.9529	0.12	62.017
9	20.801	0.3498	6.85	2.66	0.2282	3.42	31.245	0.75	0.36	0.1039	0	132	40.8	62.1	29.965	17.51	2714.9	5	35.3	0.2112	0.9	73.5	48.3	78.3	0.18	0.9709	0.2	61.072
10	18.349	0.3088	6.42	2.41	0.4871	3.36	33.598	0.71	0.33	0.0989	0	97.6	44.4	81.3	23.416	40.08	5464.4	7.6	51.4	0.2147	0.6	68.7	48.9	67.9	0.18	1.1295	0.11	64.929
10.5	20.378	0.3322	6.98	2.65	0.701	3.17	33.382	0.59	0.31	0.1034	0	128	49.6	76.6	23.019	13.27	7408.1	10.3	63.1	0.0553	1.5	78.3	56.2	69.1	0.17	1.2254	0.15	61.169
11	20.772	0.3453	7.1	2.76	0.635	3.04	31.779	0.65	0.32	0.1062	2.7	138	50.3	65.3	23.548	24.69	6952.1	11.3	49.5	0.1822	2.5	74.7	54.9	70.4	0.18	1.4361	0.14	60.007
11.5	21.567	0.3545	7.29	2.77	0.6157	3.04	31.6	0.84	0.38	0.1092	0	148	53.6	66.5	22.358	27.61	6668.2	9.7	48.5	0.1847	1.7	78.1	55	72.2	0.18	1.6795	0.17	55.524
12	21.469	0.3526	7.35	2.8	0.5667	3.14	32.116	0.96	0.37	0.1085	0.2	158	54.4	72.8	25.202	23	6128.2	9.1	46.9	0.2764	0.8	79.1	55.1	70.8	0.18	1.7251	0.13	59.723
12.5	21.409	0.3487	7.24	2.77	0.62	3.07	32.095	0.92	0.32	0.1056	0	213	56	66.6	23.813	15.33	6393.5	8.9	51.8	0.1684	1.3	77	54.5	67.6	0.19	1.7999	0.24	58.844
13	21.783	0.3554	7.64	2.96	0.6153	3.1	31.764	0.68	0.23	0.1092	0.8	272	53.8	69.3	24.145	25.62	6628.5	9.1	58.2	0.1676	2.9	80.2	57.5	68.7	0.2	1.8653	0.17	59.015
13.5	22.053	0.3584	7.72	2.94	0.5971	2.83	30.605	0.85	0.29	0.1031	1.7	308	57.1	88.6	23.615	19.77	6392.1	9.4	61.2	0.1654	1.8	80.2	55.8	69.6	0.18	1.8064	0.2	55.718
14	22.834	0.3648	7.86	3.01	0.533	2.79	30.216	0.9	0.32	0.114	0.3	345	65.7	200	30.296	29.45	5621.3	8.5	86.3	0.3251	2.1	83.6	56.1	71	0.21	1.9806	0.16	55.726
14.5	23.551	0.3734	8.14	3.09	0.4764	2.7	30.555	1.27	0.33	0.1156	2.6	522	63	86.3	26.922	21.97	4929.2	7.5	63	0.2963	2.9	90.7	56.5	70.2	0.21	2.2991	0.17	55.142
15	23.985	0.3718	8.32	3.14	0.4154	2.58	30.397	1.38	0.34	0.1153	2.1	683	74	80.5	40.881	22.03	4593.9	5.3	62.9	0.0858	1.4	95.2	57.9	72.2	0.21	2.7808	0.2	52.912
15.5	24.213	0.3679	8.22	3.15	0.304	2.43	30.266	1.3	0.31	0.1109	0.2	765	74.7	77.8	42.005	14.36	3435.9	3	56.2	0.1658	1.8	95.6	56.5	72.8	0.2	3.156	0.1	54.269
16	23.394	0.3604	7.99	3.03	0.2363	2.28	30.578	0.91	0.34	0.0997	1.7	804	74.7	77	41.41	21.29	2682.3	2.4	50.1	0.1592	1.9	95.3	53	69.7	0.2	2.5574	0.15	55.363
16.5	24.356	0.3766	8.35	3.21	0.2902	2.45	29.719	1.23	0.34	0.1068	2.7	904	69.2	82.2	39.756	14.71	3372.7	3.5	58.6	0.0917	1.4	97.7	56.1	75.4	0.21	3.0443	0.22	53.738
17	25.377	0.5032	8.54	3.38	0.3144	2.49	28.958	1.2	0.39	0.1121	9.8	974	75.8	84.4	65.093	32.09	3533.2	3.8	61.4	0.1708	2.2	104.5	59.4	76.6	0.21	3.5407	0.23	51.135
17.5	23.051	0.3575	7.96	3.25	0.2771	2.26	26.152	1.38	0.4	0.1071	8.9	1026	74	86.7	50.076	23.96	3449.7	3	61.3	0.1504	2.3	112.2	59.5	79.5	0.21	2.3081	0.25	50.66
18	26.364	0.4046	8.92	3.78	0.3758	2.59	26.561	2.09	0.5	0.1267	15.4	1029	77.8	89	40.55	33.45	4460.2	4.9	75.1	0.4191	1.6	123.5	62.4	86.1	0.22	2.6613	0.24	48.978
18.5	27.169	0.4271	9.26	4.04	0.4532	2.71	25.883	2.26	0.48	0.1302	14.5	990	76.6	88.6	36.118	42.1	5151.2	4.3	84.6	0.3262	2.5	128.4	66.9	90.8	0.22	3.117	0.25	48.043
19	27.573	0.4651	9.32	3.99	0.4644	2.64	25.52	2.72	0.58	0.13	16.6	891	82.1	83.3	38.83	41.12	5509.6	5	80.1	0.3772	2.1	129.7	66.4	95.2	0.22	3.4611	0.24	46.159
19.5	29.172	0.5785	9.64	4.21	0.3741	2.27	25.421	2.05	0.52	0.138	14.7	858	74.2	136	40.682	45.64	4349	4.9	92.8	0.1924	1.9	135.6	66	98	0.21	2.4788	0.25	44.763
20	28.486	0.4547	9.4	4.35	0.3496	2.73	24.656	1.97	0.59	0.1359	18.4	834	71.7	167	52.59	50.61	4004.9	4.2	102.5	0.449	2.5	144.8	66.6	99.6	0.2	1.938	0.3	44.709
20.5	29.054	0.4706	9.7	4.55	0.3258	2.81	24.945	2.07	0.52	0.1403	24.1	761	72.2	86.9	58.147	53.2	3740.9	4.9	61	0.4996	1.1	167.7	65.8	100	0.2	2.1081	0.28	43.092
21	29.36	0.4683	9.92	4.51	0.3778	2.92	24.408	1.5	0.55	0.1395	23.4	706	73.1	89.4	56.824	76.7	4200.7	5.7	64.7	0.9253	2.5	175.5	70.6	99.3	0.2	1.8645	0.32	43.901
21.5	28.71	0.456	9.72	4.52	0.3579	2.86	24.004	1.53	0.61	0.138	24.5	622	85.8	100	140.22	124.5	4137.4	6.5	69.8	2.4807	2.1	194.3	70.4	99.4	0.2	2.4582	0.41	44.114
22	29.232	0.4508	9.55	4.56	0.3108	2.87	24.09	1.59	0.53	0.1305	23.8	526	101	188	338.02	235.7	3408.3	5.9	85.9	6.1294	1.6	139.8	72.3	99	0.22	2.4112	0.99	41.141
22.5	29.951	0.4655	9.85	4.51	0.2075	2.98	23.95	1.67	0.46	0.1301	20.7	473	115	155	185.87	217.4	2430.9	3.6	62.9	7.4625	2.7	129.3	82.9	94.8	0.23	2.357	1.23	42.377
23	30.228	0.4594	9.93	4.54	0.0496	2.94	23.474	1.84	0.51	0.1304	23	452	115	101	66.615	45.41	751.2	1.8	44.7	10.972	2.5	134.2	84.3	94.3	0.27	2.1646	1.48	41.513
23.5	28.529	0.4386	9.41	4.15	0.0256	2.94	25.392	1.71	0.52	0.1164	17.4	364	92.7	84	57.221	23.49	579	3.6	46	20.81	2.9	134.8	69.7	94.4	0.39	2	0.97	45.421
24	27.385	0.4231	8.65	3.68	0.0241	2.93	27.156	1.33	0.49	0.1065	12.5	272	62.9	79.9	55.104	29.02	586.3	5.9	41.7	7.1603	2.6	139.7	60.4	95.5	0.36	1.3662	0.42	50.309
24.5	26.668	0.4176	8.72	3.54	0.0285	3.06	27.058	1.35	0.49	0.1029	6.6	208	53.1	78.4	54.442	21.98	631.2	12.2	40.6	1.4064	2.6	140.1	57.1	98.2	0.33	1.4271	0.3	50.494
25	26.427	0.4113	8.31	3.35	0.04	3.15	28.483	1.11	0.45	0.1032	5.3	157	50.7	75	41.675	21.95	747.2	12.8	35.8	0.6134	6	106	55.9	102	0.33	1.2023	0.23	53.154
25.5	24.435	0.3778	7.67	2.81	0.0475	3.26	29.945	1.04	0.43	0.0978	0	131	48.4	72.8	39.888	7.892	843.6	2.7	38.3	0.189	8.7	78.2	54	91	0.27	1.0963	0.17	57.607
26	23.606	0.3553	7.13	2.67	0.0528	3.4	30.982	0.88	0.36	0.1027	0.4	132	45.8	111	41.013	37.81	905.4	3.3	49.2	0.313	10	73.9	51.4	90.7	0.25	1.2213	0.14	60.066
26.5	23.017	0.3387	6.9	2.28	0.0527	3.51	31.435	0.77	0.41	0.0979	0	123	45.3	87.4	34.861	35.76	873.8	1	41.5	0.2701	6.1	71.6	49.9	88	0.22	1.1177	0.12	59.904
27	23.706	0.3545	7.24	2.34	0.0497	3.52	31.257	0.96	0.42	0.0972	0	148	44.4	76.2	34.067	28.21	877	1.2	37	0.3181	4.2	75.9	52	89.4	0.19	1.2406	0.08	60.007
27.5	22.975	0.3377	6.99	2.26	0.0527	3.54	31.455	0.7	0.38	0.0936	0	145	41.9	104	31.884	16.27	899.9	2	47.5	0.2592	5.3	70	47.7	90.5	0.19	1.1764	0.06	59.988

Appendix 6: Major element data for core MDVAL-9502.

Depth in core (cm)	SiO_2 wt%	TiO_2 wt%	Al_2O_3 wt%	Fe_2O_3 wt%	MnO wt%	MgO wt%	CaO wt%	Na_2O wt%	K_2O wt%	P_2O_5 wt%
0.5	28.17	0.6117	9.33	5.87	0.1943	3.807	22.998	1.19	0.17	0.1223
1.5	28.81	0.6267	9.65	5.68	0.1991	3.9	23.505	1.29	0.2	0.1253
2.5	29.41	0.632	9.83	5.77	0.2008	3.904	23.481	1.37	0.22	0.1264
3.5	29.05	0.6187	9.46	5.6	0.221	3.852	23.592	1.26	0.2	0.1252
5.5	29.22	0.6205	9.6	5.64	0.2216	3.834	23.475	1.28	0.21	0.1256
6.5	29.31	0.6292	9.71	5.7	0.2073	3.827	23.111	1.31	0.21	0.1258
7.5	29.43	0.6305	9.74	5.82	0.2151	3.902	23.656	1.36	0.21	0.1261
8.5	29.04	0.6281	9.61	5.75	0.2217	3.776	23.099	1.46	0.26	0.1256
9.5	29.67	0.6405	9.8	5.76	0.283	3.746	22.739	1.44	0.25	0.1266
10.5	29.8	0.6399	9.81	5.76	0.2902	3.75	22.612	1.4	0.26	0.119
11.5	27.98	0.6049	9.31	5.44	0.299	3.469	20.99	1.27	0.23	0.1182
12.5	30.37	0.6592	10.1	5.93	0.4869	3.775	22.643	1.42	0.24	0.1273
13.5	30.37	0.6521	10	5.87	0.5396	3.777	22.5	1.48	0.24	0.1274
14.5	30.19	0.6429	9.94	5.88	0.6205	3.768	21.986	1.55	0.25	0.1271
15.5	29.36	0.6217	9.69	5.61	0.5551	3.686	21.458	1.5	0.23	0.1184
16.5	27.83	0.5926	9.15	5.28	0.6355	3.427	20.45	1.41	0.22	0.1142
17.5	29.77	0.6475	9.73	5.86	0.7963	3.55	22.282	1.42	0.21	0.1265
18.5	29.02	0.63	9.66	5.58	1.0154	3.484	21.798	1.42	0.23	0.1186
19.5	30.25	0.682	10.1	5.88	1.0642	3.695	22.048	1.36	0.22	0.1274
20.5	29.36	0.6448	9.85	5.72	0.6086	3.594	21.229	1.43	0.28	0.1232
21.5	29.62	0.6534	9.87	5.67	0.5123	3.608	22.266	1.43	0.23	0.1262
22.5	22.9	0.5045	7.61	4.49	0.5857	2.737	17.582	1.1	0.17	0.0986
23.5	30.04	0.6628	9.94	5.92	0.3575	3.523	22.289	1.47	0.27	0.1266
24.5	29.45	0.6348	9.58	5.88	0.0664	3.432	22.58	1.46	0.22	0.1255
26.5	29.79	0.6297	9.42	6.49	0.0667	3.393	21.824	1.47	0.26	0.1259
27.5	29.67	0.606	9.27	6.47	0.0739	3.326	22.328	1.33	0.22	0.1256
28.5	30.98	0.6119	9.44	6.87	0.0895	3.358	22.775	1.42	0.24	0.1269
29.5	31.92	0.633	9.81	6.93	0.0904	3.542	21.056	1.37	0.32	0.1356
31.5	31.16	0.6076	9.65	5.91	0.0963	3.586	20.583	1.72	0.27	0.126
32.5	31.38	0.6253	9.86	5.85	0.0893	3.707	21.282	1.77	0.26	0.1265
33.5	31.36	0.6153	9.9	5.68	0.0964	3.595	20.712	1.8	0.27	0.1186
34.5	30.23	0.6101	9.64	5.46	0.0882	3.624	21.361	1.68	0.22	0.1176
35.5	30.24	0.6109	9.69	5.48	0.0883	3.695	22.08	1.73	0.22	0.1251
36.5	30.11	0.6111	9.66	5.29	0.0884	3.608	21.691	1.79	0.21	0.1252
37.5	31.04	0.6215	9.89	5.4	0.0962	3.655	21.537	1.72	0.24	0.1258
38.5	30.05	0.5914	9.58	5.17	0.1022	3.49	20.596	1.61	0.26	0.1241
39.5	30.61	0.6181	9.8	5.31	0.103	3.532	21.759	1.6	0.26	0.1251
40.5	30.14	0.6084	9.65	5.05	0.1026	3.489	22.299	1.66	0.25	0.1246
42.5	26.33	0.5271	8.47	4.43	0.0791	3.176	21.531	1.5	0.18	0.1186
43.5	31.56	0.5614	9.89	5.12	0.0886	3.442	20.638	1.71	0.4	0.1256
44.5	36.94	0.5315	10.5	4.72	0.0847	3.058	17.315	1.79	0.9	0.1232
45.5	30	0.5918	9.62	5.32	0.095	3.595	21.415	1.72	0.26	0.1315
46.5	29.39	0.5965	9.36	5.26	0.0946	3.564	22.311	1.65	0.25	0.1237
47.5	29.91	0.6164	9.58	5.42	0.1027	3.581	22.563	1.81	0.22	0.1394
48.5	30.33	0.6107	9.7	5.36	0.103	3.576	22.337	1.66	0.25	0.1251
49.5	30.32	0.6173	9.66	5.42	0.1029	3.52	22.106	1.73	0.26	0.1249
50.5	28.66	0.5903	9.14	5.26	0.102	3.505	22.744	1.6	0.21	0.1239
51.5	29.83	0.6255	9.46	5.5	0.1104	3.576	22.665	1.72	0.24	0.1325
52.5	29.98	0.6187	9.49	5.74	0.1031	3.602	22.811	1.66	0.28	0.1326
54.5	29.33	0.5882	9.04	5.95	0.0882	3.536	22.226	1.83	0.38	0.1176
55.5	29.56	0.605	9.2	5.73	0.1033	3.697	22.792	1.7	0.33	0.1181
56.5	29.9	0.6204	9.18	5.54	0.1256	3.781	22.947	1.67	0.32	0.1256
58.5	29.89	0.6346	9.11	5.33	0.1254	3.756	22.447	1.71	0.3	0.1254
59.5	30.6	0.6449	9.33	5.37	0.1334	3.795	22.401	1.6	0.31	0.126
60.5	30.75	0.6446	9.32	5.25	0.1334	3.823	22.108	1.64	0.28	0.1259
61.5	30.65	0.6434	9.33	5.2	0.1331	3.853	22.726	1.43	0.27	0.1331
62.5	29.21	0.6166	8.87	4.9	0.1205	3.615	21.327	1.74	0.28	0.1205
63.5	30.51	0.6365	9.13	5.03	0.1258	3.878	22.603	1.91	0.41	0.1258
64.5	30.44	0.6455	9.13	5.14	0.1261	3.918	22.504	1.83	0.48	0.1261
65.5	30.25	0.6516	9	4.96	0.1111	3.939	22.851	1.98	0.42	0.1259
66.5	31.12	0.67	9.39	5.28	0.1117	3.901	22.005	1.85	0.48	0.1414
67.5	31.12	0.6575	9.34	5.12	0.1121	3.922	22.309	1.81	0.47	0.127
68.5	31.32	0.6729	9.42	5.3	0.1122	3.97	22.102	1.91	0.45	0.1346
69.5	31.58	0.6671	9.68	5.28	0.1199	4.002	22.006	1.93	0.51	0.1349
70.5	31.05	0.6617	9.26	5.23	0.119	3.948	21.805	1.75	0.44	0.1264
71.5	30.45	0.6545	9.06	5.28	0.119	3.964	22.44	1.84	0.42	0.1264
72.5	30.32	0.6541	9.11	5.29	0.1115	3.925	22.308	1.87	0.52	0.1264

Appendix 6 continued: Trace element data for MDVAL-9502.

Depth in core (cm)	As ppm	Ba ppm	Br ppm	Cr ppm	I ppm	MnO ppm	Mo ppm	Ni ppm	U ppm	V ppm	Zn ppm	Zr ppm	Cl wt%	S wt%	Corg wt%	$CaCO_3$ wt%
0.5	3.08	107	63.6	95.5	42.1	2169.8	5.19	83.2	0	99.55	85.81	82.5	1.95	0.1981	0.68	40.373
1.5	4.63	95.4	63.3	91.4	51.6	2096.5	3.83	82.7	0	92.52	65.37	83.6	1.75	0.2025	0.33	41.311
2.5	2.87	115	64.8	94.2	48.8	2151.1	3.53	82.6	0.3	98.51	67.03	85.4	1.72	0.1949	0.27	41.311
3.5	0.78	109	61	99.1	52.5	2337	3.94	83.2	0.06	92.83	62.47	81.9	1.85	0.1876	0.29	41.68
5.5	3.69	106	61.3	96.4	47.6	2367.4	4.62	84.6	0.55	95.75	62.98	84.7	1.81	0.1921	0.31	41.245
6.5	1.84	110	63.5	96.1	50.6	2171.2	5.06	83.4	0	90.32	63.12	85.4	1.73	0.1898	0.3	40.696
7.5	0	105	63.7	99.4	48.4	2221	4.23	84.7	0	97.63	63.6	85.6	1.79	0.1891	0.39	40.395
8.5	0	108	60	91.5	50.7	2383.9	4.45	82.6	0.29	90.59	64.48	83.1	1.81	0.1826	0.32	40.765
9.5	1.83	115	60.4	97.4	53.2	2984.4	4.68	87.9	0	93.94	67.87	84.3	1.63	0.1862	0.29	40.066
10.5	1.51	117	61.4	96.6	47.9	3076.7	5.46	92.7	0.07	96.54	63.65	85.3	1.88	0.1847	0.14	39.837
11.5	0	115	63.6	91.5	54.2	3313.3	6.17	96.7	0.44	90.62	65.35	87.6	1.85	0.1797	0.33	39.152
12.5	0.07	118	63.6	96	55.6	4959.4	6.75	101	0.13	96.46	64.93	85.9	1.91	0.185	0.29	39.061
13.5	1.53	117	64.5	95.4	51.7	6183.5	7.07	98.1	0	94.99	65.61	87	1.99	0.1851	0.31	38.694
14.5	0	121	63.8	97.4	54.7	6344.5	5.63	95.6	0	89.54	66.59	87.3	1.94	0.1805	0.33	38.458
15.5	1.22	126	63.8	95.6	60.4	5778.2	4.74	87.4	0.77	90.09	65.62	87	1.83	0.183	0.28	38.71
16.5	0	127	66.9	98.5	59.6	6737.1	3.77	81.4	0.13	93.05	64.53	87.7	1.9	0.186	0.35	38.354
17.5	0.4	138	66.4	93.3	54.7	7960.9	6.02	83.3	0	88.91	62.75	86.7	1.87	0.1813	0.32	38.648
18.5	0	142	65.9	89.1	55.9	10562	5.12	87.1	0	87.3	62.12	87.9	1.85	0.1832	0.3	39.019
19.5	3	132	65.5	93.4	54.8	10605	4.87	90.8	0.62	91.99	66.07	88.9	1.93	0.1813	0.23	38.903
20.5	2.97	129	64.7	98.5	57.7	6217.3	3.4	78.5	0.18	94.2	69.51	91.3	1.79	0.1852	0.36	38.162
21.5	0	120	65.5	95.4	64.4	5011.9	3.38	76.8	0.2	84.33	63.31	88.5	1.81	0.1818	0.44	38.505
22.5	0.67	127	66.5	96.9	58.3	7582.1	4.07	84.2	0	83.75	62.64	87.7	1.73	0.1707	0.29	39.32
23.5	3.56	123	70.5	88.9	57.9	3658.6	3.7	76.3	0.39	81.89	63	88.7	2.04	0.1865	0.37	38.66
24.5	6.56	133	69.3	95.7	50.5	834.95	1.78	68.1	0.18	82.95	63.69	87.7	1.95	0.1961	0.35	39.888
26.5	16.5	117	71	104	35.3	916.96	1.61	67.4	0	90.13	60.45	86.9	1.87	0.1875	0.35	38.716
27.5	6.13	157	71.1	97.1	46.4	776.01	2.16	68.8	0	103.8	61.64	83.1	2.06	0.1916	0.41	38.991
28.5	5.21	205	71.7	97.9	49.1	776.44	2.16	73.3	0.5	106.4	63.46	88.6	2.06	0.1888	0.32	37.266
29.5	0	248	79.3	106	71.2	1010.9	2.13	77.2	0	104.3	65.26	88.1	1.88	0.2069	0.46	35.909
31.5	0	361	113	110	29.5	1051.9	1.84	88.6	0.6	111.1	70.31	87.4	2.83	0.2796	1.04	35.419
32.5	0	350	113	110	28.2	999.5	0.94	88.6	0.77	115.9	70.16	89.1	2.83	0.2816	1.55	35.762
33.5	0	365	116	113	28.4	1077.7	2.83	92.2	1.6	120.3	74.07	90.2	2.92	0.2826	1.23	33.791
34.5	0	332	108	109	24.2	1049.3	2.63	90.2	1.19	128	73.66	88.9	2.71	0.2762	0.92	37.123
35.5	0	280	103	103	29.8	991.9	2.75	83.4	2.18	126.4	68.19	86	2.73	0.2707	0.85	37.825
36.5	0	316	110	104	28.3	1030.9	2.92	86.1	2.4	138.4	71.79	86	2.92	0.2886	0.98	36.771
37.5	2.89	395	113	116	29.5	1078.6	2.79	89.5	2.8	140.5	71.4	88.2	2.8	0.2981	1.08	36.281
38.5	0	411	109	106	29.5	1169.3	2.65	90.6	4.15	126.3	71.4	88.1	2.5	0.2987	1.16	36.046
39.5	0	407	108	100	29.6	1195.3	2.91	88.9	4.12	117	72.45	88.1	2.37	0.3422	1.18	36.692
40.5	0.75	404	106	109	34.7	1134	2.64	86.8	4.8	113.8	69.51	86.1	2.5	0.3503	1.14	37.982
42.5	5.12	400	119	105	21	959.73	4.43	90.9	4.74	145.9	67.27	79.6	2.59	0.4585	1.43	39.835
43.5	3.33	424	119	106	21.7	1043.6	5.27	89.7	5.24	135.7	66.52	90.2	2.6	0.4236	1.28	35.161
44.5	10.8	443	114	91.9	17.1	992.45	4.82	91.7	5.15	127.5	65.45	110	2.64	0.4165	1.23	29.218
45.5	10	474	125	111	25.6	1064.4	5.18	96.1	4.73	145.6	72.02	87.9	2.85	0.5013	1.58	36.459
46.5	7.14	351	112	101	23.6	1075.7	3.48	86.7	3.13	132.6	69.03	85.2	2.64	0.4522	1.24	38.435
47.5	4.18	304	103	103	25	1137.2	3.27	83.4	2.17	123.7	68.15	88.5	2.71	0.3807	1.06	38.481
48.5	2.34	277	100	97.6	29.9	1127.2	3.4	80	2.24	112.1	63.09	89.5	2.71	0.36	0.91	38.067
49.5	5.89	263	99.4	106	26.4	1175.8	3.86	80.8	2.37	113	61.72	90.1	2.72	0.3653	0.25	38.056
50.5	0.69	263	99.9	95.6	20.2	1171.5	3.26	79.1	1.18	117.1	66.06	88.1	2.5	0.3813	0.84	40.021
51.5	0.06	271	101	97.8	25.7	1226.2	4.04	79.2	1.76	122	64.59	87.6	2.65	0.3827	0.88	38.861
52.5	14.5	257	101	99.7	28.7	1108.8	4.29	83.6	1.81	157.9	65.97	87.8	2.66	0.5226	0.91	38.976
54.5	12.2	256	106	106	20.7	1041	4.35	88.2	3.73	110.7	77.59	84.1	2.14	0.7494	0.99	37.988
55.5	22.3	225	93.3	105	28.2	1174.8	5.16	89.8	3.12	96.48	65.15	89.9	2.5	0.6415	0.77	39.428
56.5	16.7	230	90.1	107	28.3	1363.2	3.01	86.5	2.07	93.71	64.93	94.2	2.62	0.545	0.73	39.701
58.5	11.5	211	85.4	98.1	28.5	1411.1	3.11	83.6	1.98	96.26	64.31	99.2	2.5	0.4365	0.6	39.576
59.5	6.3	227	86.2	104	26.1	1469.1	3.35	83.3	1.91	94.46	66.7	105	2.49	0.4101	0.61	39.158
60.5	3.34	231	87.2	103	25.3	1481.3	2.42	85.6	1.36	102.3	66.18	106	2.52	0.3558	0.65	38.543
61.5	0	212	86.4	103	28.6	1437.2	1.95	83.2	1.45	100.3	65.54	103	2.44	0.2957	0.6	39.737
62.5	0	215	90.6	98.4	31.1	1436.7	2.64	86.2	1.79	102.9	66.47	105	2.5	0.2819	0.59	39.138
63.5	0	224	83.3	111	25.5	1424.9	3.04	90.3	2.77	107.3	68.69	104	2.29	0.2677	0.53	39.737
64.5	0	189	79.8	106	22.4	1384.5	2.1	87.9	2.14	95.95	63.19	106	2.3	0.2407	0.42	40.013
65.5	0	178	78	98.4	22.4	1264	2.41	83.3	1.09	95.89	64.18	104	2.37	0.2462	0.41	41.091
66.5	0	175	77.3	104	17.9	1211.8	2.41	83.9	0.88	100.8	75.51	105	2.05	0.212	0.41	39.566
67.5	0	167	75.2	104	17.7	1216.6	2.65	78.4	2.32	95.1	78.07	103	2.06	0.2048	0.39	39.076
68.5	0	156	78.7	104	24	1251.5	2.89	76.6	1.27	96.71	75.87	108	2.18	0.2075	0.37	38.972
69.5	0	159	76.4	107	21.6	1312.3	2.65	75.9	1.82	97.7	73.06	105	2.22	0.2095	0.39	38.946
70.5	0	160	74.1	105	19.5	1297.9	2.54	77.6	1.52	94.44	74.28	104	1.96	0.2016	0.38	38.47
71.5	0	137	75.2	98.2	17.8	1280.9	2.24	78.9	2.29	96.8	78.79	99.8	2.13	0.211	0.32	40.161
72.5	0	152	72	100	24.9	1275.3	2.36	75.1	1.4	92.48	71.88	97.8	1.86	0.1993	0.33	40.314

Appendix 7: AMS ^{14}C dates for the cores used in this research.

Core	Depth in core (cm)	Analysis code	^{14}C age (convention yrs)	$\pm 1\ \sigma$ years	^{13}C (per mille)
MDVAL - 9502	25-26	AA-28393	5830	55	n.d.
	30-31	AA-28394	6980	60	n.d.
	41-42	AA-28395	7940	60	n.d.
	53-54	AA-28396	7530	60	n.d.
	57-58	AA-28397	8150	65	n.d.
LC21	49.5-50.5	CAMS-41314	3370	60	-1.0
	95-96	CAMS-41313	4290	60	1.2
	137-138	CAMS-41311	5590	60	0.4
	161-162	CAMS-41315	7480	60	0.9
	174-174.5	CAMS-41312	8120	60	-0.1
	188-191	AA-30364	9085	65	n.d.
	218-219.5	AA-30365	11765	80	n.d.
	252-253	CAMS-41316	14450	60	0.3
LC25	50-51	AA-30366	4805	50	n.d.
	60-61	CAMS-43635	6320	60	1.0
	70.5-71.5	CAMS-43636	7270	50	-0.2
	84.5-85.5	CAMS-43637	8770	50	-1.0
	92-93	CAMS-43638	8980	60	0.5
	225-226	CAMS-43639	11110	50	1.0

Appendix 7.

MD 90-917	+164-167	GifA-96201	4750	70	
	+175-178	GifA-96202	5000	70	
	+190-192	GifA-96729	5680	70	
	221-222	CAMS-45865	6500	60	n.d.
	229-230	CAMS-45866	6990	40	n.d.
	+230-232	GifA-96730	6920	90	-
	+239-242	GifA-96203	7930	80	-
	242-243	CAMS-45687	7750	210	n.d.
	+250-253.5	GifA-96204	8020	70	
	+250-253.5	GifA-96205	8170	70	
	251-252	CAMS-45868	7910	140	n.d.
	+252-253	GifA-96731	8040	90	-
	258-259	CAMS-45869	9750	80	n.d.
	+275-278	GifA-96207	10390	90	
	+295-297	GifA-96732	10800	90	

SOUTHAMPTON UNIVERSITY LIBRARY

USER'S DECLARATION

AUTHOR: Meecoo, K.C. TITLE: Lipid peroxidation geochemical studies on the most recently accumulated sapropel S1 in the eastern Mediterranean

DATE: 1999

I undertake not to reproduce this thesis, or any substantial portion of it, or to quote extensively from it without first obtaining the permission, in writing, of the Librarian of the University of Southampton.

To be signed by each user of this thesis

DATE	SIGNATURE	ADDRESS